JOURNAL OF POLYMER SCIENCE: PART A VOL. 3, PP. 833-846 (1965)

Preparation and Hyperfiltration Properties of a Polyacrylate–Cellophane Membrane

W. H. BALDWIN, D. L. HOLCOMB, and J. S. JOHNSON,
Chemistry Division, Oak Ridge National Laboratory,
*Oak Ridge, Tennessee**

Synopsis

Preparation of a carboxylic ion-exchange membrane by grafting poly(acrylic acid) onto cellophane is described. This membrane filters appreciable fractions of dissolved salt from solutions $1M$ and less in NaCl; flow rates through the membrane at 2500 psi are 0.5 cm./hr. and higher. Comparison is made of salt rejection properties and flow rates with a film of cellulose acetate in which rejection does not depend on fixed ionizable groups. Rejections of salts having ions of different charges are presented. Experimental apparatus for hyperfiltration is described.

It has been realized for some time that if a salt solution is forced by pressure through a membrane having fixed ionic groups, the solution passing through the membrane may have a higher ratio of water to solute than the feed, i.e., some of the salt may be rejected. This occurs if charged groups are uniformly distributed through the membrane and if their density is high enough, in which case equations[1,2] based on what we shall call (perhaps inaccurately) a Donnan approach are useful. Even if charge departs substantially from a homogeneous distribution, rejection may occur. Recently two examples, one of them a membrane having cylindrical pores with charge distributed along the walls, have been treated[3] theoretically; rejection depends on pore size and the charge density of the barrier and on the concentrations and charges of the solute ions. In this treatment, the equations apply only for the case of good exclusion of coions; in a more recent study, this condition is relaxed.[4] In dealing with actual membranes one must remember of course that there are other mechanisms which may contribute to observed rejection besides those resulting from ionized groups in the matrix.

Observations in which dependence on solute concentration suggests at least a contribution to rejection of membrane charge have been made with several materials. Erschler,[5] for example, studied the rejection of KIO_3 by collodion, and cellophane has been tested with KIO_3,[6,7] and with several

---

* Work performed for the Office of Saline Water, U. S. Department of the Interior, at the Oak Ridge National Laboratory, Oak Ridge, Tennessee, operated by Union Carbide Corporation for the U. S. Atomic Energy Commission.

other salts.[7] In general, appreciable rejections were found only at low feed concentration; above $0.1M$, rejection was less than 10% in all cases. Flow rates, on the other hand, were high, at least when the membranes had been chemically swollen.

With the increasing interest in desalination of recent years, membranes have begun to receive attention for use in the hyperfiltration, or reverse osmosis, process. Of materials tried, cellulose acetate has appeared to have very interesting properties, both with respect to rejection and to permeability;[8,9] the mechanism of the rejection in this material appears not to result from fixed ionizable groups. With commercial ion-exchange films, McKelvey, Spiegler, and Wyllie[10] found rejections almost as high as with cellulose acetate, but flow rates were only 0.002–0.02 cm./hr. under 1000 psi.

We have prepared a charged membrane by grafting poly(acrylic acid) onto cellophane, which has properties intermediate between those earlier studied. Rejection is considerably higher than those of the cellophane and collodion types, though flow is much slower than with collodion or swollen cellophane. Rejection is not so high as with the ion exchange membranes tested by McKelvey et al.,[14] but flow through our membrane is from twenty to a hundred times the rate through their samples. It is less favorable on both counts than the Loeb cellulose acetate membranes, but the possibilities of future improvement make it an interesting material, especially for brackish waters. In addition the combination of substantial flow rate and appreciable rejection make it a more convenient material than any heretofore tested (to our knowledge) for study of hyperfiltration by a charged membrane. We report here some preliminary observations of salt rejection by this material.

EXPERIMENTAL

Membranes

The preparative method used for the polyacrylic cellophane is based on a technique of Bridgeford[11] for grafting polymers onto films and fabrics. The loci of the initiation of polymerization are controlled by utilizing the small (~0.02 meq./g.) ion exchange capacity of cellulose to retain Fe(II) ions. Addition of H_2O_2 to the film results in formation of radicals, which in turn initiate the polymerization of olefins. Details of a particular procedure follow.

Visking dialysis tubing (1.5 in. wide, 5 in. long, and 1 mil thick) was weighed, washed with distilled water (five times; softener was effectively eliminated in the process) and slit to form sheets. The wet sheets were soaked for 5 min. in $0.02M$ ferrous ammonium sulfate at pH 5 (200 ml./g. film) and the excess solution washed out with three portions of distilled water, 15 min. each. The film was then placed in a refluxing aqueous solution of 10% freshly distilled acrylonitrile (100 ml./g. film) that was then made 0.02% in hydrogen peroxide. Refluxing was continued for 30 min. to graft polyacrylonitrile onto the cellulose. After the film was washed with three portions of distilled water, it was hydrolyzed in refluxing 5% sodium hydroxide solution (200 ml./g. film) for 1 hr., and then it was washed with distilled water until neutral. The exchange capacity of the resulting product was 3.6–3.9 meq./g. of dry film. The sodium form of the polymer was soaked for 4 hr. in distilled water, blotted between filter paper and the water was removed under vacuum (1 mm. Hg) at room temperature over Drierite. The water content was four times the weight of the dry film. From qualitative observation, the water content is less for the membrane in the hydrogen form. For the base cellophane, water content was estimated to be ca. 32%, from weight loss at 100°C. of the film blotted after water washing.

For both base cellophane and the polyacrylic material, capacity was determined by conversion to the acid form by treatment with HCl, equilibration with excess NaOH in 0.5M NaCl solution, and back-titration of the equilibrating solutions combined with solutions from subsequent washing of the membrane.

Cellulose acetate membranes, which were used for some comparison experiments, were of an improved variety,[10] kindly supplied by S. Loeb of the University of California at Los Angeles.

Hyperfiltration Equipment

The equipment used in this study is shown in Figure 1. Solution from a reservoir at atmospheric pressure (1) is pumped to the desired pressure by a Sprague S-216CS pump (2). From here it goes to the membrane cell (4), past a dampener (3), which reduces pressure pulses on the pump backstroke to a tolerable level. Two filters of glass wool are located just before and after the cell to remove from the stream corrosion products and traces of grease from the pump and dampener piston. Liquid passing through the membrane is taken by the tube coming from the top of the cell into a receiver, here a graduated cylinder, for analysis. Most of the solution goes by the membrane and is bled through a let-down valve (5) back to atmospheric pressure and to the reservoir. A float in the reservoir actuates a microswitch should the reservoir level fall too low for any reason and in turn a solenoid shuts off the drive air from the impeller section of the pump. The system can be used at pressures up to ca. 4000 psi.

The system is constructed of material resistant to corrosion. The pump piston and other parts in contact with solution were replaced by titanium elements; for hardness, Stellite balls were substituted for those of stainless steel in the check valve. The rest of the system was made of titanium or of 347 stainless steel. Porous frits to support the membrane have been of several different materials; titanium appears to be the most satisfactory. Modifications of the system shown were carried out in shops of this laboratory, but a similar pump for a second assembly was constructed for us by the manufacturer (Sprague Engineering Corp., Gardena, Cal.).

The dampener shown operates by compression of a spring; its pressure range can be adjusted within limits by the screw on top. Dampeners based on compression of gas, separated from solution by a piston with O-ring seal, have also been constructed; one of them has a smaller area of piston exposed to solution than to gas, so that relatively low gas pressures may be used with higher solution pressures. Usually the pressure surges in the pumping cycle are less than 15%. The pressure gauge in Figure 1 is filled

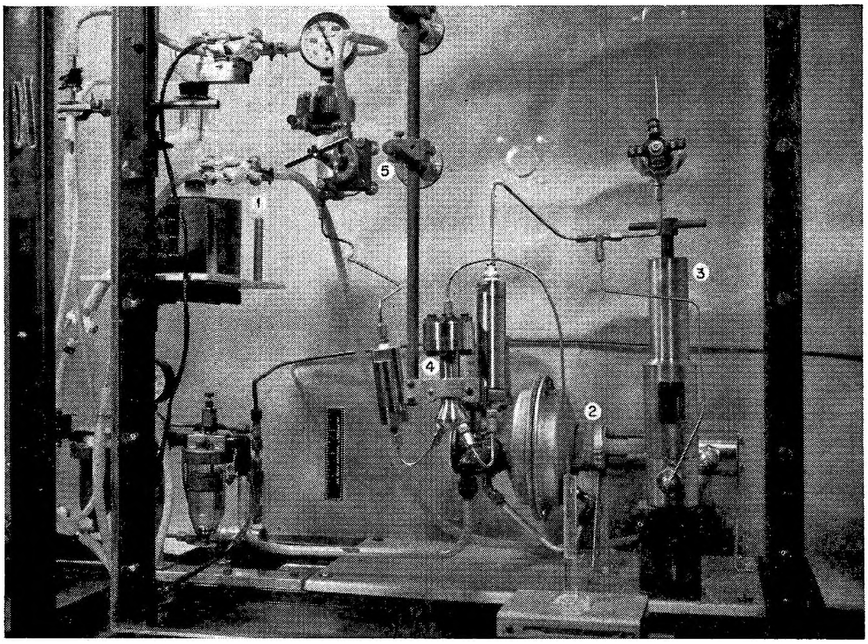

Fig. 1. Hyperfiltration apparatus.

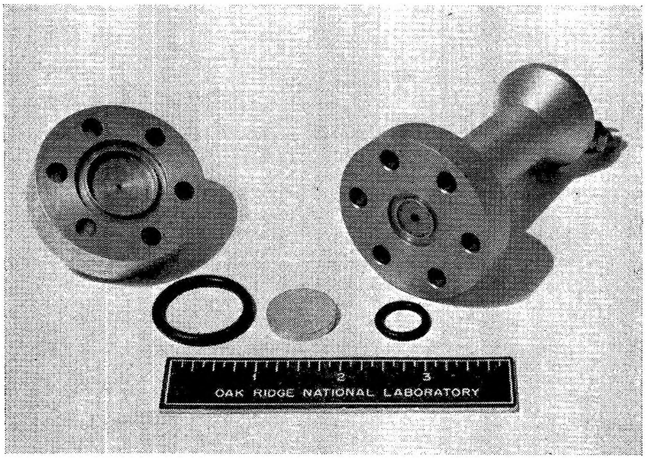

Fig. 2. Membrane cell disassembled. Membrane and backing not shown.

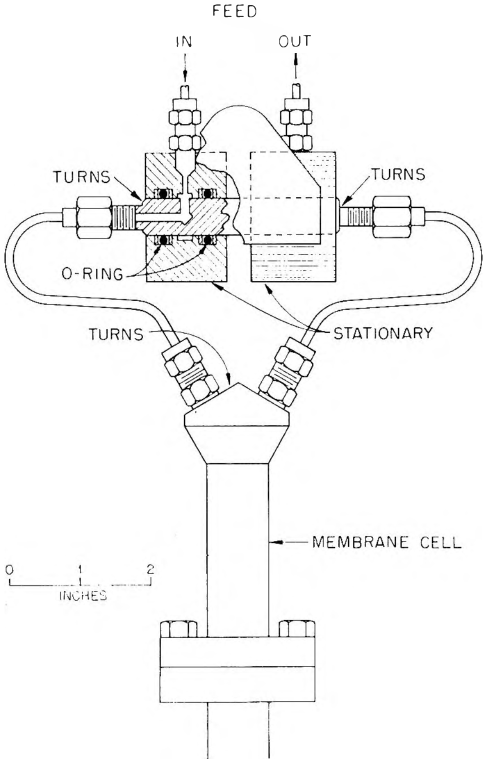

Fig. 3. Cell with rotation device allowing positioning of membrane in up or down position.

with distilled water and isolated from the rest of the system by an elastic diaphragm.

The membrane cell is shown in more detail in Figure 2. Inflowing solution is discharged through the center of a disk placed close (ca. 0.5 mm.) to the membrane and flows out through small openings in the periphery of the disk. The membrane (not shown in Fig. 2) is supported by a metal frit; a cushion of millipore (HAWP) or filter paper (Whatman 41H) is placed between the membrane and the frit. Seals are made with O-rings. The area of the membrane exposed to the solution is ca. 1.5 cm.^{2}.

With rejection of solute, salt will be concentrated in the boundary layer. This concentration polarization will lower the apparent rejection, computed from the bulk feed concentration and the effluent, and will decrease the pressure difference effective in driving solution through the membrane. With membranes for which per cent rejection is concentration-dependent, the actual rejection for the solution at the interface will be different from that of bulk solution. It is therefore important to minimize concentration buildup at the interface. In our equipment, rate of flow over the membrane surface can be adjusted over a wide range with the bleed valve; usually in this study, no further effect of concentration polarization was seen on increasing the flow rate above 20 cc./min., which corresponds to changing the solution in contact with the membrane ca. 3 times/sec. In addition, the cell is normally oriented with the membrane at the upper end, to take advantage of gravity mixing by density gradients when desalination occurs.

In another modification of the cell (Fig. 3), a double O-ring arrangement allows the cell to be turned so that the membrane is in the up or down position with relation to the feed, and the position can be easily changed during an experiment. The effect of gravity on mixing can be illustrated by some results with a cellulose acetate membrane and a 0.5*M* NaCl solution; rejection was 97.5% if the solution in contact with the membrane was changed once a second or more, whether the membrane was up or down. If flow was decreased so that the solution in contact with the membrane was changed ca. every 40 sec., rejection with the membrane up was about 90%, and down about 73%. An even more striking effect is seen if the flow-promoting disk is not oriented parallel to the membrane. With it skewed and with the solution changed every 2 sec., rejection was 94% with membrane up and 55% with membrane down.

Analysis

Analysis of feed and effluent for NaCl or for total chloride were by Mohr titrations; of sulfate, by $Pb(NO_3)_2$ with dithizone indicator;[12] and for magnesium and calcium, by EDTA titrations. With the more concentrated solutions of a single solute, some analyses were made by measurement of the refractive indices of the solutions with a Brice-Phoenix differential refractometer.

RESULTS

Rejection of Salt from Air-Equilibrated Solutions

Salt rejection behavior of the polyacrylate membrane is illustrated for NaCl in Figure 4.* (Salt rejection is defined as the per cent of the solute present in the feed not found in the effluent from the membrane.) Solutions were air-equilibrated i.e., at a pH determined by atmospheric CO_2. Rejection of 0.5*M* NaCl (at 170 atm. applied pressure) is about 35% and rises with decrease in feed concentration to ca. 80% at 0.01*M*. Results for independent preparations of the membrane are differentiated by symbols, and it appears that the preparative procedure yields films of reproducible properties. Rejection is clearly much higher than for the base cellophane, for which the results are given at the same applied pressure. The grafting of polyacrylate onto the cellophane decreased the permeability, or the flow per atmosphere of "effective" pressure (applied pressure

---

* The abscissas of Figures 4 and 5 are in terms of square roots of concentration. We used this scale simply to spread out the points at the low concentration end, and do not imply any theoretical significance.

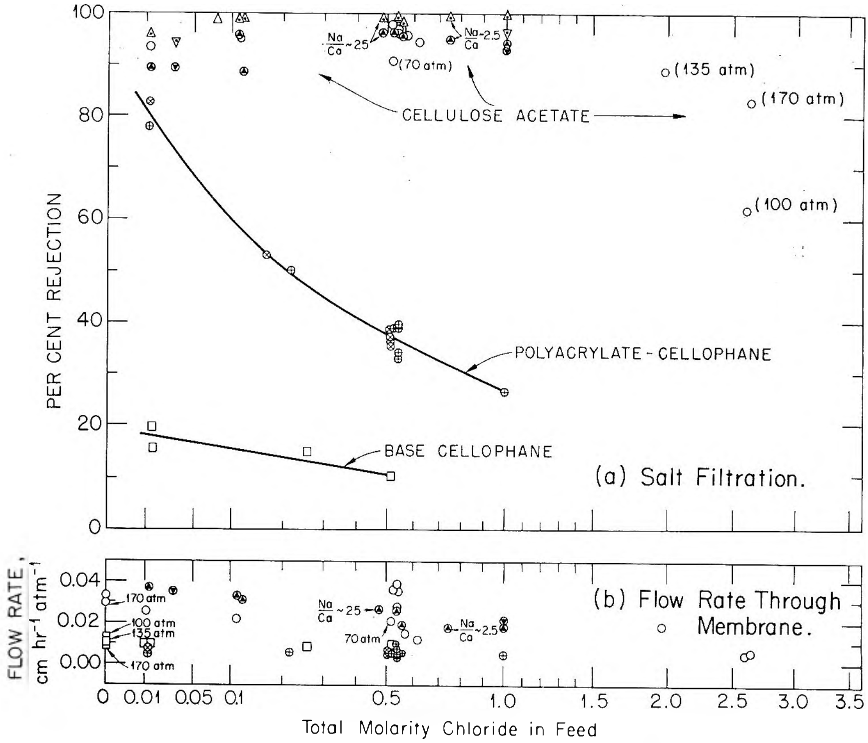

Fig. 4. Comparison of hyperfiltration of cellulose acetate (100 atm.) and of polyacrylate–cellophane ion-exchange membrane (170 atm.) (rate of flow given per atmosphere of applied pressure less osmotic pressure across membrane): (○) cellulose acetate (CA), NaCl from NaCl soln.; (◉) CA, NaCl from NaCl–$CaCl_2$ soln. (moles Na^+/moles $Ca^{+2} \simeq 8$ unless indicated); (⊛) CA, NaCl from $MgCl_2$ soln.; (△) CA, $CaCl_2$ from $CaCl_2$ soln.; (⟁) CA, $CaCl_2$ from NaCl soln.; (▽) CA, $MgCl_2$ from NaCl soln. (moles Na^+/moles $Mg^{+2} \simeq 8$); (⊗, ⊕) polyacrylate–cellophane NaCl, different membrane preparations; (□) base cellophane, NaCl.

minus the difference in osmotic pressure of the feed and effluent) through the membrane by less than a factor of two.

The contrast with rejection by a process not dependent on fixed charges in the membrane[9] is illustrated in Figure 4 by some observations with cellulose acetate. Rejection by the latter is not very dependent on concentration in this range and falls off only well above 1*M* (at these higher concentrations, rejection becomes strongly pressure-dependent, and prolonged exposure leads to deterioration of the membrane; with the points shown here, repetition of measurements at lower concentrations carried out afterwards indicated that only small irreversible changes had occurred).

The rates of flow through the membranes, though somewhat less reproducible for both materials than the rejections, are nevertheless significantly different. Flow through cellulose acetate per effective atmosphere is considerably higher than through cellophane, whether or not polyacrylate groups have been grafted. It should be noted that, if the two membranes are compared under the same applied pressure, 100 atm., the difference in permeability is diminished, the flow for $0.5M$ NaCl for cellulose acetate being about 2 cm./hr. (or cc./cm.^{2} hr.) through the membrane compared to 0.8 cm./hr. for the polyacrylate–cellophane. (Multiply by 5.9 to convert to gal./ft.^{2}-day.) The flow through the charged membrane is thus not linear with pressure. However the rejection is substantially less at 100 than at 170 atm, i.e., ca. 25% rather than 35%.

Further aspects of the behavior of the polyacrylate membrane are shown in Figure 5; the curve for NaCl drawn through the points of Figure 4 is repeated here, and curves are also drawn through points for Na_2SO_4 and $La(NO_3)_3$, which were studied over substantial concentration ranges. It is apparent that salts having highly charged ions, either negative or positive, tend to be rejected from two-component solutions more strongly than salts of monovalent ions only, at least at high salt concentrations. The direction here is similar to what is observed with cellulose acetate, but the effect of the presence of NaCl on the rejection of divalent counterions is sharply different with the two materials. With cellulose acetate the rejection of $CaCl_2$ and $MgCl_2$ is scarcely affected by the presence of NaCl; no effect was

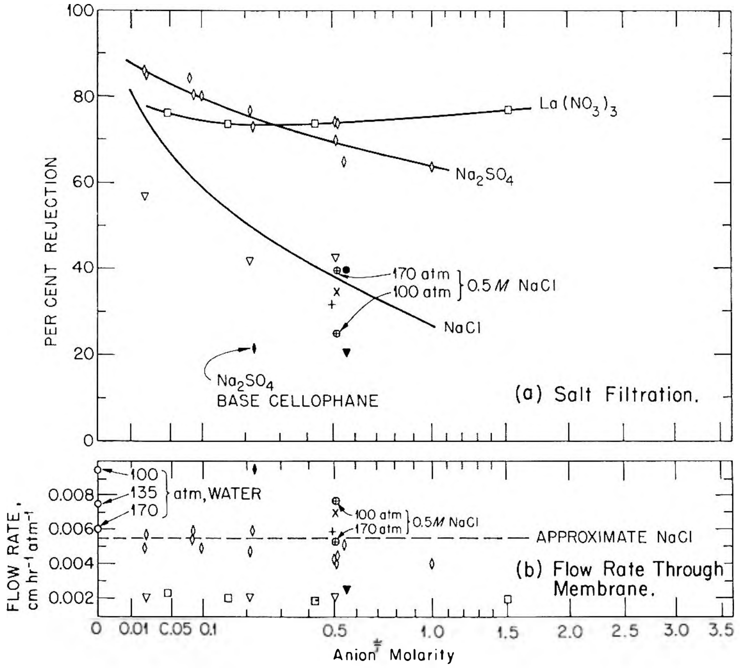

Fig. 5. Hyperfiltration by polyacrylate–cellophane membrane (170 atm.), (with Na_2SO_4, cation molarity): (◇) Na_2SO_4; (□) $La(NO_3)_3$; (▽) $MgCl_2$; (+) $NaNO_3$; (×) KCl; (——) NaCl, Fig. 4; (●, ▼) NaCl, $MgCl_2$ in same solution (moles Na^+/moles Mg^{++}) ~ 10.

seen at the highest ratio measured (25 moles Na^+/mole Ca^{++}). In Figure 5, it is apparent that Mg^{+2} rejection by the charged membrane is drastically reduced by excess NaCl. Permeability of this membrane for solutions containing multivalent positive ions (whether alone or with NaCl) is also much lower than with NaCl alone; the presence of $MgCl_2$ in predominantly NaCl solutions lowers the flow rate by more than a factor or two. The divalent coion, sulfate, does not slow the flow to any great extent.

Concentration dependence of rejection is not so sharp for salts of multivalent ions as for NaCl; for $La(NO_3)_3$ there is essentially no variation of rejection with concentration in the range studied, and with two component solutions of $MgCl_2$, rejections at the low concentration end arc less than those of NaCl.

Effect of pH

As we mentioned, these experiments were carried out with air equilibrated solutions. The pH was thus not high enough for the polyacrylic groups to be altogether in the salt form,[13] and the charge was therefore not the maximum possible. That part of rejection arising from a Donnan or other mechanism depending on concentration of fixed charge in the membrane would (other things being equal) be expected to increase with an increase of charge density. One would predict on this basis an increased rejection with increase of pH, though increased swelling of the membrane with conversion to salt form would counteract this somewhat.

We have attempted to investigate the effect of solution acidity (pH 3–11) on rejection and flow of NaCl. The results have not been reproducible; exposure to either acidic or basic media seems to affect the membrane irreversibly. In addition, corrosion of certain elements of the apparatus was accelerated, and as we have discussed above, multivalent ions which might be introduced in this way can, even at low concentrations, profoundly affect the characteristics of the membrane. Corrosion products were found deposited in the form of hydrous oxides on the membranes, and results may have also been influenced by such layers. Control of pH was difficult.

Usually, though not always, when the pH was increased, the rejection became greater. We observed, for example, with $0.5M$ NaCl feed, pH 9–10, as high as 57% rejection, in comparison with the normal 35%, and with $0.01M$ NaCl, rejections of 90%, compared to ca. 80% shown in Figure 4. Rates of flow through the membrane were usually less at higher pH, by as much as a factor of two when high rejections were observed.

In acid solutions (pH 3–4), scatter of results was even greater. Rejection of acidified 0.01–$0.1M$ NaCl appeared to be lower; from $0.01M$, for example, 55–65% was observed in comparison with the "normal" (ca. 80%). However, for $0.5M$ NaCl, no clear decrease in rejection occurred on acidification, and in some cases there was, contrary to expectation, even an increase over the normal 35%, once even to 45%. Permeation rates were lower with acidified solutions, again by as much as a factor of two.

Effect of Temperature

A few measurements were carried out with the polyacrylate–cellophane membrane as a function of temperature. Between 25 and 65°C., there was no significant effect on rejection of salt from 0.5M NaCl. Permeation rates increased with temperature roughly as one would predict from viscosity changes; the product of water viscosity and rate was constant within ±10% at 25, 45, and 65°C. Exposure of the membrane to 45°C. for about 3 hr. had little effect on rejection and permeation rate on return to room temperature, but after a similar period at 65°C., the rejection at 25°C. dropped to 29% (from 34%).

Effect of Capacity

A series of membranes of differing capacities was prepared, and their hyperfiltration properties (air equilibrated solutions) are summarized in Table I. The results are somewhat erratic, but the expected trend to higher rejection for higher capacity is obtained. The apparent minimum in permeation rate, if real, may indicate an effect of higher water content at higher capacity.

TABLE I

Rejection[a] of Polyacrylate–Cellophane Membranes as a Function of Capacity

Capacity, meq./g. dry	Weight % water[b]	Permeation rate, cm./hr.	Rejection, %
Base Cellophane		1.9	10
0.33	64	1.2	12
0.53	66	0.9	18
1.2	63	0.7	30
1.3	67	1	22
1.6	67	0.5	25–35
2.0	71	0.5	40–45
3.7	80	0.7	35
4.8	83	1	50

[a] 0.5 M NaCl feed, 2500 psi.

[b] At atmospheric pressure.

DISCUSSION

The marked dependence of rejection on concentration, in contrast to the lack of concentration dependence with cellulose acetate, identifies at least part of the rejection with the presence of ionizable groups. The dependence on the charge of coion (sulfate versus chloride) is another indication. It is of interest to see if any other inferences concerning the structure of the membrane may be drawn from the data presently available.

The fact that substantial rejection is obtained indicates immediately that the solution passing through the membrane must be brought into fairly intimate contact with the substance of the film. Permeation rates (Figs. 4 and 5) confirm this. A detailed model for the membrane is of course not available, but a rough estimate of the distances over which solution interacts with the barrier can be made by assuming that the solution passes through pores; these may not be real, but are convenient for computational purposes on a Poiseuille basis.[14] If it is further assumed that the volume available for pores is given by the water content, one obtains an average pore radius of ca. 5 A. Here the pores are assumed to go straight through the membrane, i.e., the length is taken to be the thickness of the membrane. A more realistic model would postulate some tortuosity, and the radius computed would increase approximately linearly with the length taken for the pores. For any reasonable allowance for this however, the effective pore radius would remain small.

Interpretation of the permeation rate with a diffusional equation[14] leads to a similar conclusion. For assumption of fraction of total membrane weight as water of 0.5–0.8, one obtains from permeation rates values of the water diffusion coefficient of $2\text{–}3 \times 10^{-5}$, a number close to the self diffusion coefficient of water.[15] If there were large gaps in the structure, an unreasonably high value of $\mathfrak{D}$ should have been obtained. Permeation rates, in agreement with the fact that substantial rejection is observed, thus indicate that the membranes have a basically homogeneous structure. The apparent pore size is in the region where, even if one assumed a Dresner[3,4] pore model, it would not be greatly different from a homogeneous charge distribution, and a homogeneous distribution would appear to be a better first approximation for this membrane.

It is of interest to compare the dependence of rejection on feed concentration of the polyacrylate cellophane with related observations made on standard electrodialysis (ion-exchange) membranes. A convenient procedure is to assume* that the effluent solution has the molality of the solution in the membrane in equilibrium with the feed concentration under the conditions of the experiment. Activity of the salt at the high pressure side will be the same in the feed and membrane phases, if they are referred to the same standard state. Thus

$$m^2_{\mathrm{NaCl}}\gamma_{\pm}^2 = m_{\mathrm{Na}(r)}m_{\mathrm{Cl}(r)}\gamma_{\pm}{}^2{}_{(r)} = [C + m_{\mathrm{Cl}(r)}]m_{\mathrm{Cl}(r)}\gamma_{\pm}{}^2{}_{(r)}$$

where C is concentration of fixed ionizable groups; subscript r indicates the membrane phase; m is concentration in moles/kilogram H_2O; and $\gamma_{\pm}$

---

* Although we intend to discuss transport properties of membranes in hyperfiltration in more detail later, a few words concerning two main assumptions involved may be helpful. The first, which seems reasonable here, is that the flow of solute and solvent is closely coupled, i.e., that the salt permeation (moles/cm.^{2}-sec.) is given by its concentration (moles/kg. water) in the membrane times water flow rate (kg./cm.^{2}-sec.), plus a diffusive term dependent on the salt concentration gradient. The second, which is perhaps more doubtful, is that the product of water permeation rate and thickness of membrane, divided by the diffusion coefficient of the salt, has a value so large that asymptotic rejection is attained. Computations with estimated diffusion coefficients of the salt indicate that this condition is likely, but by no means certainly, met here. It is ununfortunately not feasible in this case to confirm that limiting rejection is attained from measurements of rejection as a function of pressure, since the nonlinear dependence of permeation rate on pressure indicates changes in the membrane.

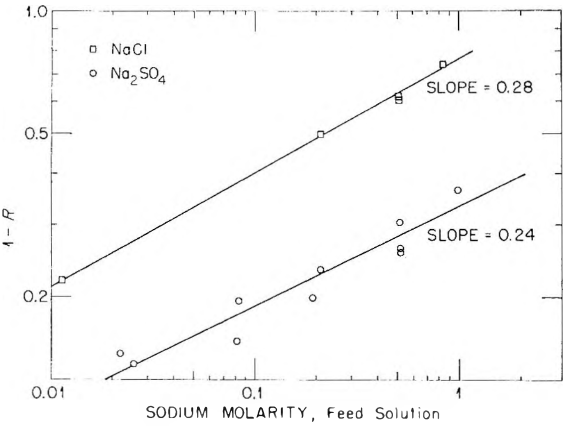

Fig. 6. Logarithmic plot of membrane rejection.

is the mean activity coefficient. The coion uptake, $m_{Cl(r)}$, is equal to $m_{NaCl}(1 - R)$, where R is rejection (expressed as fraction). If the ratio of the activity coefficients in the membrane to those in solution is assumed independent of m_{NaCl}

$$d \log m_{NaCl} \approx d \log (1 - R)$$

since $m_{Cl(r)}$ is, except at the high concentration end of the range, much less than C, and the term involving C is therefore neglected. A plot of log $(1 - R)$ versus the logarithm of NaCl feed concentration should thus give a straight line of unit slope. For Na_2SO_4, the slope should be 2.

In Figure 6, results are plotted in this manner for a series of NaCl and Na_2SO_4 solutions, all carried out on a single sample of membrane (concentrations in the figure are in moles/liter rather than molality, but the difference is not important for present purposes). It can be seen that approximate straight lines are obtained, with slopes 0.28 for NaCl and 0.24 for Na_2SO_4. The slopes for magnesium and lanthanum solutions are 0.1 or less. While the slopes, even in absence of multivalent counterions, are not those expected for a mechanism purely of the Donnan type, neither are slopes obtained with commercial ion-exchange membranes, which are reported to be between ca. 0.4 and 0.7.[16] Glueckauf explains departure from the expected slope by postulating nonhomogeneity in the membranes.[16,17] The behavior of the polyacrylate–cellophane, in absence of multivalent counterions, is qualitatively similar to standard ion-exchange membranes, though if nonhomogeneity is the correct explanation for departures from ideality, the nonhomogeneity is greater with this material. From a practical point of view, the nonideality is bothersome, since it indicates that the improvement of rejection of brackish waters over rejection of sea water will not be as great as one might hope.

The strong pressure dependence of rejection and permeation rate could be taken to indicate a compression of the membrane, with an accompanying increase in charge density. It could, on the other hand, indicate the presence of large channels, containing solution essentially at feed level and numerous enough to contribute substantially to flow; these gaps might tend to be closed more by pressure than the regions in which proximate fixed charged groups exert an influence. The present data do not allow a choice between these possibilities.

The effect of multivalent counterions on the membrane appears complicated. Their presence reduces permeation rates sharply, whether alone or in presence of excess NaCl. It seems likely that there may be specific interactions between these ions and the carboxylic sites, and in view of complications which may be incurred from such complexing reactions and the limited data at present available, further speculation on the observations with multivalent ions does not seem profitable.

There would appear to be several possibilities for practical improvement of the present membrane. Grafting polyacrylate groups onto a more porous base cellophane might increase permeation rates without unacceptable loss of rejection; our attempts to obtain improved membranes in this way however have so far been disappointing. Use of a polyelectrolyte with more strongly acidic functional groups than carboxyls (or with strongly basic groups) might increase charge density in neutral solutions.[13] It is probable that the charged layer actually doing the rejection need not be nearly so thick as in the present membrane (100 A. in good contact with the feed should be ample, if asymptotic rejection is maintained by an inverse dependence of permeation rate on rejecting layer thickness). If methods could be found of preparing this kind of membrane with such a thin active layer over a porous mass, analogous to what has been accomplished with cellulose acetate,[9] permeation rates should be greatly increased without sacrifice of rejection.

We are indebted to Donna Michelson and John Csurny for carrying out hyperfiltration measurements, to K. A. Kraus and G. Scatchard for discussions, and to Neva Harrison for technical assistance.

References

1. Teorell, T., *Trans. Faraday Soc.*, **33,** 1053 (1937).
2. Meyer, K. H., and J.-F. Sievers, *Helv. Chim. Acta,* **19,** 649 (1936).
3. Dresner, L., and K. A. Kraus, *J. Phys. Chem.*, **67,** 990 (1963).
4. Dresner, L., *J. Phys. Chem.*, submitted.
5. Erschler, B., *Kolloid-Z.*, **68,** 289 (1934).
6. McBain, J. W., and R. F. Stuewer, *J. Phys. Chem.*, **40,** 1157 (1936).
7. Trautmann, S., and L. Ambard, *J. Chim Phys.*, **49,** 220 (1952).
8. Reid, C. E., and E. J. Breton, *J. Appl. Polymer Sci.*, **1,** 133 (1959).
9. Loeb, S., and S. Sourirajan, *Advances in Chemistry Series,* **38,** 117 (1963).
10. McKelvey, J. G., K. S. Spiegler, and M. R. Wyllie, *Chemical Engineering Progress Symposium Series,* **55,** 199 (1959).
11. Bridgeford, D. J., *Ind. Eng. Chem., Prod. Res. Dev.*, **1,** 45 (1962).
12. Archer, E. E., *Analyst,* **82,** 208 (1957).
13. Gregor, H. P., and M. Frederick, *J. Polymer Sci.*, **23,** 451 (1957).
14. Ticknor, L. B., *J. Phys. Chem.*, **62,** 1483 (1958).

15. Wang, J. H., C. V. Robinson, and I. S. Edelman, *J. Am. Chem. Soc.*, **75,** 466 (1953).
16. Glueckauf, E., and R. E. Watts, *Proc. Roy. Soc.* (*London*), **A268,** 339 (1962).
17. Crabtree, J. M., and E. Glueckauf, *Trans. Faraday Soc.*, **59,** 2639 (1963).

Résumé

On décrit la préparation d'une membrane échangeuse d'ions par greffage d'acide polyacrylique sur la cellophane. Cette membrane filtre des fractions appréciables de sels dissous au départ de solutions $1M$ et de concentration inférieure en NaCl; les vitesses d'écoulement à travers la membrane à 2500 psi sont 0.5 cm/h et plus. On a fait la comparison des propriétés de rejet de sel et des vitesses d'écoulement avec un film d'acétate de cellulose, dans lequel le rejet ne dépend pas des groupements fixés et ionisables. Des rejets de sel avec des ions de charges différentes sont présentés. Un appareil expérimental d'hyperfiltration est décrit.

Zusammenfassung

Die Darstellung einer Carbonsäure-Ionenaustauschmembran durch Aufpfropfung von Polyacrylsäure auf Zellophan wird beschrieben. Diese Membran filtriert beträchtliche Bruchteile des gelösten Salzes aus $1M$ und geringer konzentrierter NaCl-Lösung; die Fliessgeschwindigkeit durch die Membran bei 2500 psi ist 0,5 cm/h und höher. Ein Vergleich der Salzabweisungseigenschaften und Fliessgeschwindigkeiten mit einem Zelluloseacetatfilm, bei welchem die Abweisung nicht von fixierten ionisierbaren Gruppen abhängt, wird durchgeführt. Die Abweisung von Salzen mit Ionen verschiedener Ladung wird angegeben. Die Versuchseinrichtung für die Hyperfiltration wird beschrieben.

Received March 19, 1964
Revised May 11, 1964

JOURNAL OF POLYMER SCIENCE: PART A VOL. 3, PP. 847-857 (1965)

Preparation and Characterization of Some Cellulose Graft Copolymers. Part III. The Role of Concurrent Degradation during Radiation Grafting

J. D. WELLONS and V. STANNETT, *Camille Dreyfus Laboratory, Research Triangle Institute, Durham, North Carolina*

Synopsis

The radiation degradation of cellulose acetate has been studied both in the dry state and in solution. The rate of degradation was greater in the solid state and was unaffected by oxygen. Conjugated solvents such as pyridine, toluene, and α-methylstyrene were shown to exert considerable protection against the radiation degradation of cellulose acetate when in solution or as swollen films. α-Methylstyrene has been used as a model for styrene to study the amount of degradation accompanying the grafting process. Matching experiments have been carried out by using both the mutual and the preirradiation methods of grafting. Considerably greater chain cleavage was found to accompany the grafting in the preirradiation case. With both methods the number of chain cleavages has been measured when α-methylstyrene was present in the "grafting" solution and the number of grafted side chains when styrene was used. It was shown that at least twice as many grafted chains as cleavages occur with the mutual technique, but in the case of preirradiation the number of cleavages is comparable to the number of grafted chains. The *G* (grafted chain) value for cellulose acetate with styrene was determined and was about 1.1 in all cases. The *G* (chain cleavage) values varied, however, from 0.2 to 1.3, approximately. The proportion of grafted chains attached to the ester groups was determined by extraction with benzene after cold alkaline hydrolysis. About half of the grafts were found to be attached in each case, including the preirradiation product. In general, it can be said that in every case at least 50% of the graft copolymers are side-chain grafts; this figure is probably considerably higher in the case of the mutual radiation preparations.

Polymers can degrade or crosslink when subjected to ionizing radiation in the absence of monomer. In some cases measurable degradation and crosslinking occurs, and the ratio can be found by sol–gel analysis. In the presence of a vinyl monomer, however, graft polymerization takes place, normally with complete absence of gel formation. With polymers which predominantly crosslink with radiation it is easy to visualize that monomer adds to the active centers before they can combine to form crosslinks. In the case of polymers which mainly degrade, the situation may be more complex; monomer may add to broken chain ends and form block copolymers. Alternately, radicals formed from the elimination of atoms or side groups may add monomer and form graft copolymers. Such side chain radicals might, in the absence of monomer, disproportionate, and this leads to chain scission. Since cellulose and its derivatives are polymers which degrade with radiation, it was thought of interest to study more closely the effects on the degradation of the monomer and solvents used in the grafting reaction. It is known from the work of Leavitt[1] that cellulose derivatives can be made to crosslink under suitable conditions, but under the conditions used in the present work it will be seen that degradation was the only noticeable reaction. All the work to be reported is concerned with the cellulose acetate–styrene system.

Normally it is extremely difficult to follow the changes in the cellulosic backbone during the grafting process due to the complexities introduced by the simultaneous graft polymerization. The graft copolymer can be separated from the homopolymers and its composition and the molecular weight of the side chains determined. However, little knowledge can be gained about the cellulose acetate backbone itself, since it is destroyed during the isolation of the polystyrene side chains by acid hydrolysis. It was thought that one way of closely simulating the conditions encountered during radiation grafting would be to use α-methylstyrene in place of styrene. This monomer cannot propagate by radical polymerization due mainly to steric hindrance; however, it has a radical affinity close to styrene itself. For example, the rates of addition of methyl and polystyryl radicals to α-methylstyrene are, respectively, 1.2 and 1.4 times those found with styrene.[2] The solvent properties are also quite comparable; for example, the intrinsic viscosity in a 70:30 dimethylformamide–monomer solution was identical within the experimental error when α-methylstyrene was substituted for the styrene. A number of parallel studies have been carried out, therefore, with the use of styrene for the grafting experiments and α-methylstyrene to follow the behavior of the cellulose acetate under what is hoped are conditions very close to those obtained in the grafting experiments themselves.

EXPERIMENTAL

The degradation experiments were conducted with the use of a cellulose acetate having a degree of substitution (D.S.) of 2.25 and viscosity-average molecular weight of about 120,000 obtained from the Celanese Corporation. A cellulose acetate of D.S. = 1.75 and viscosity-average molecular weight of about 55,000, obtained from the Eastman Kodak Company, was used for some of the grafting experiments. The lower degree of substitution makes for somewhat easier separations owing to the wider solubility differences between the polystyrene and the cellulose acetate. For the matching experiments the cellulose acetate was freed from low molecular weight material by dissolving in dimethylformamide and adding methanol until the precipitation point was reached. About two-thirds of the cellulose acetate was recovered in this operation.

The degradation experiments were carried out in sealed tubes after thoroughly degassing at 10^{-5} torr. The intrinsic viscosities were determined in appropriate solvents in an Ubbelohde viscometer. The viscosity-average molecular weights were calculated by the relationship $[\eta] = K[\bar{M}_v]^\alpha$; the parameters used were as follows:

Cellulose acetate in acetone at 25°C.:[3]

$$K = 1.32 \times 10^{-4},\ \alpha = 0.85$$

Polystyrene in toluene at 30°C.:[4]

$$K = 0.98 \times 10^{-4},\ \alpha = 0.73$$

Polyisobutylene in toluene at 30°C.:[5]

$$K = 2.0 \times 10^{-4},\ \alpha = 0.67$$

The number-average molecular weights were determined by osmometry in acetone, dimethylformamide, and dioxane in the case of the cellulose acetate and in toluene and dimethylformamide in the case of polystyrene. A Meyerhoff steel block osmometer was used at 25°C. Duplicate measurements in two solvents were in good agreement. The preparation and separation of the graft copolymers were as previously described.[6,7] All the irradiations were carried out in a Co^{60} source at 25°C. at a dose rate of about 300,000 rad/hr.

The removal of the ester side groups of the cellulose acetate by alkaline hydrolysis was carried out in the following manner. A 1-g. portion of graft was dissolved in 40 ml. of pyridine and precipitated in an equal quantity of ethanol. Then 50 ml. of 5% aqueous sodium hydroxide solution was added and the mixture warmed for 4 hr. and then stirred at room temperature for 2 days, filtered, and freeze-dried. The polystyrene was then extracted with dimethylformamide. Infrared examination of the extract showed no contamination with cellulose or cellulose acetate. An earlier method[6] was found to give incomplete hydrolyses leading to somewhat lower values.

RESULTS AND DISCUSSION

Degradation in Solution

The results of the degradation experiments carried out in solution are shown graphically in Figure 1. The data have been plotted in the familiar way of reciprocal of the viscosity-average molecular weight versus radiation dose. A linear relationship is seen to be followed, and from the slopes the G (cleavage) values can be calculated. These calculations involve transforming the viscosity-average molecular weights to number-averages by using the relationship developed by Flory for the most probable distribution, i.e., $\bar{M}_v = 1.93\ \bar{M}_n$ for the particular molecular weight–intrinsic viscosity relationship used. This is probably reasonable since, after a few cleavages have taken place, a random distribution is approached; however, G values calculated from viscosity data must obviously be treated with reserve. For example, the sharpness of the fractions used for establishing

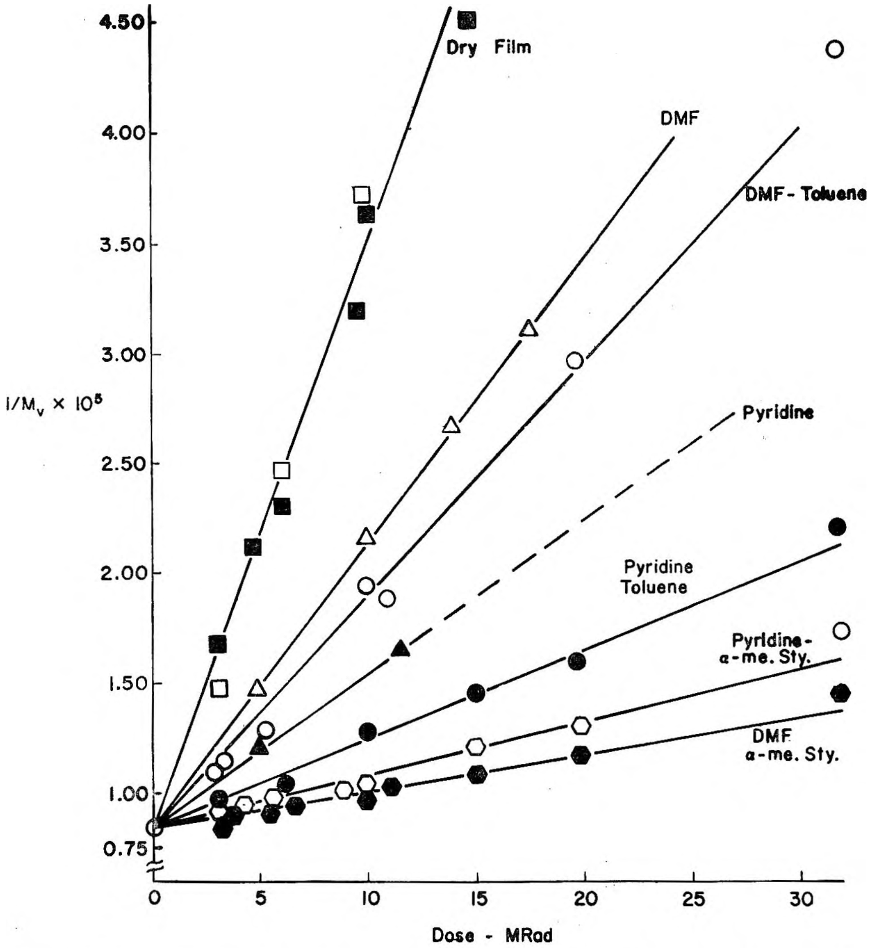

Fig. 1. Reciprocal molecular weight vs. radiation dose for solutions of cellulose acetate.

the original molecular weight–viscosity relationship and the possibility of some degree of branching occurring during the radiation would interfere with the validity of the calculation of number-average molecular weights. The calculated *G* values are summarized in Table I. In spite of the large *G* (radical) value for dimethylformamide, the degradation in solution is less than that of the dry film. This is in contrast to the results of Henglein and Schneider[8] with polyisobutylene and of Henglein et al.[9] and Okamura et al.[10] with poly(methyl methacrylate), who found much higher degradation in a number of unconjugated solvents than in dry film. This behavior was attributed to the increased probability of self-healing (radical recombination) reactions in the solid state. This explanation is reasonable in the case of these α-substituted vinyl polymers since the chains may cleave mainly by direct excitation. In the case of cellulose acetate, chain scission may be preceded, in part, by the loss of a hydrogen atom followed

TABLE I
Calculated G (cleavage) Values for Cellulose Acetate (D.S. = 2.25) in Solution at 25°C. Under High Vacuum

Solvent	G (cleavage)
None (dry film)	5.24[a]
Dimethylformamide (DMF)	2.48
DMF–toluene (70:30)	2.04
DMF–α-methylstyrene (70:30)	0.33
Pyridine	1.45
Pyridine–toluene (70:30)	0.77
Pyridine–α-methylstyrene (70:30)	0.49
Pyridine–α-methylstyrene (50:50)	0.19
Pyridine–α-methylstyrene (10:90)[b]	0.24

[a] As can be seen from Figure 1, similar values are obtained from the degradation experiments in air or vacuum.
[b] Swollen film.

by carbonyl formation and chain fracture. Hydrogen removal at the 1, 4, or 5 positions could easily result in chain cleavage and carbonyl formation, as shown in eq. (1). Recombination reactions are therefore far less likely with this polymer. The detailed reasons for the lower degradation rate in solution must await more definitive work with simpler systems.

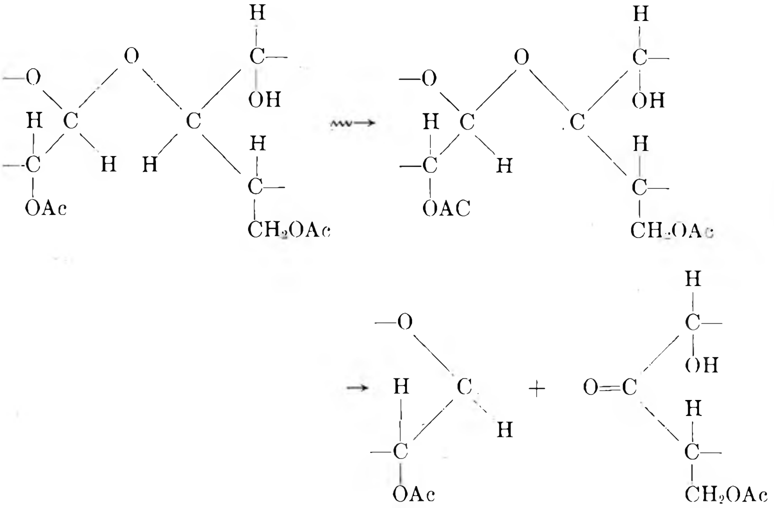
(1)

When the polymer is irradiated in solution, the cleavage reaction could be forestalled by chain transfer to solvent molecules, leading to a lower G (cleavage) value than in the case of the solid polymer. When a monomer such as α-methylstyrene is present, a similar protective effect can be postulated but by addition to the chain before cleavage. The lack of effect of oxygen on the solid-state degradation of cellulose acetate is explainable since the resulting peroxy adduct would also cleave, leading eventually to terminal carboxylic acid groups. Such groups were actually

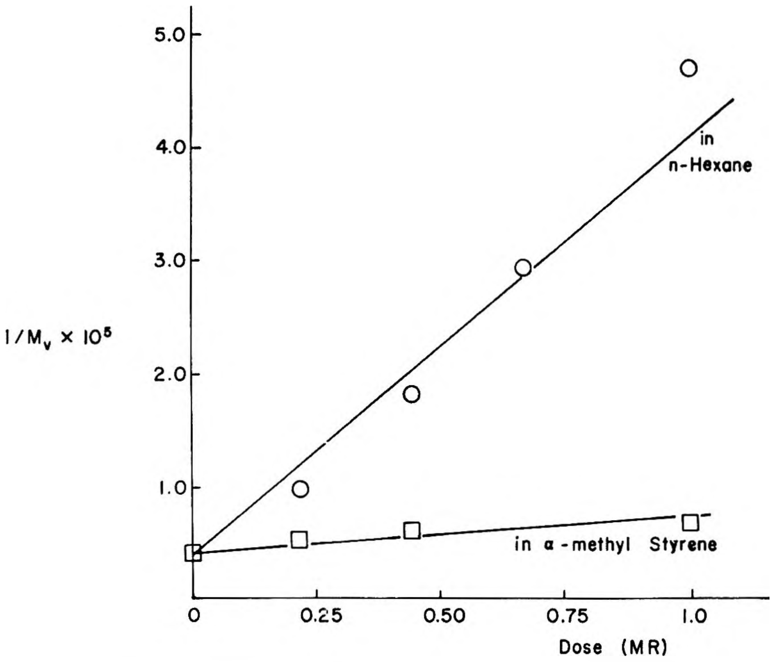

Fig. 2. Degradation of polyisobutylene in 1% solution *in vacuo* at 25°C.

found by Arthur et al.[11] in the case of the radiation degradation of cotton cellulose in air.

With the dry films in high vacuum it was observed that if the tubes were opened immediately the viscosities were somewhat higher than if left for some time after irradiation. The samples irradiated in air, on the other hand, were not sensitive to the time of standing after irradiation. This observation was only qualitative in nature but also indicated cleavage reactions of the type outlined above. The values shown in Figure 1 were all for samples left overnight before analysis.

The aromatic solvents reduced the G (cleavage) values considerably. It is interesting that with mixtures of aromatics with dimethylformamide, α-methylstyrene exerted a powerful protective effect compared with toluene. This suggests that a great deal of the degradation is from dimethylformamide radicals attacking the cellulose acetate. In the presence of the α-methylstyrene these will add and form stable substituted benzyl radicals. In the case of pyridine the radiolysis produces few radicals, and so the addition of α-methylstyrene confers much less additional protection than in the case of dimethylformamide. The net effect is that a mixture of pyridine and α-methylstyrene is similar in its protective effect to dimethylformamide and α-methylstyrene.

The G (radical) value for cellulose acetate has been determined by electron spin resonance by Florin and Wall.[12] At 6.5 Mrad at 20°C. the value was 1.76; this compares with the G (cleavage) value of 5.24. The corresponding values for cellulose are 2.88 and about 10.0 for the G (radical) and G (cleavage), respectively, and are in a similar ratio. The G (radical) value of 1.76 for cellulose acetate at 6.5 Mrad is quite consistent with the G (grafted side chains) value of about 1.0 found in the present study.

A comparable set of degradation experiments was conducted with polyisobutylene in 1% solution in *n*-hexane and in α-methylstyrene, both under high vacuum. The strong protective effect of the α-methyl styrene was again shown. The plots of reciprocal molecular weight versus dose are presented in Figure 2, and the slopes can be used to determine approximate G (cleavage) values. These slopes are calculated to be 7.3 for *n*-hexane and 0.62 for α-methylstyrene. The value for *n*-hexane is somewhat lower than the value of 11.0 calculated by Chapiro[13] from the results of Henglein and Schneider[8] in *n*-heptane, and the value for α-methylstyrene is lower than the value of 1.1 reported for cyclohexene. Since cyclohexene has only a very limited affinity for free radicals, it appears from these results that the α-methylstyrene may, in the case of polyisobutylene, exert mainly the normal protective effect usually attributed to energy transfer. The lack of degradation, in the case of polyisobutylene, by attack of solvent radicals in a manner leading to chain cleavage compared with the apparent efficiency in the case of cellulose acetate is also quite compatible with these results.

Heterogeneous Degradation

In addition to the degradation experiments in solution, a number of heterogeneous degradation experiments were conducted. These included studies on dry film without additives and films immersed and swollen in mixtures of solvents and nonsolvents. The results of these experiments are summarized in Table II. More extensive experiments were made with

TABLE II
Degradation Experiments with Cellulose Acetate Films

	Intrinsic viscosity[a]	
	4.95 mrad	11.50 mrad
Direct irradiation		
Dry film, 25°C.	1.36	0.84
Dry film, −78°C.	1.89	1.42
Film swollen in 90:10 α-methylstyrene–DMF solution, 25°C.	2.33	2.13
Film swollen in 90:10 α-methylstyrene–DMF solution, −78°C.	2.48	2.18
Irradiation followed by admitting swelling solution *in vacuo*		
90:10 α-methylstyrene–DMF, 25°C.	1.24	0.92
90:10 α-methylstyrene–DMF, −78°C.	2.10	1.53
90:10 toluene–DMF, −78°C.	1.83	1.48

[a] Initial intrinsic viscosity = *3.06*.

dry film, both under high vacuum and in air, and these results are also included in Figure 1 and Table I. A few experiments were made in which the dry film was irradiated and then the solvent–nonsolvent mixture added in an exactly similar manner to that used with preirradiation grafting experiments. The results of these experiments are included in Table II. A number of the heterogeneous experiments were carried out both at 25 and −78°C.

The results presented in Table II show that the protective effect of the α-methylstyrene is also found with swollen films and that there is a strong temperature effect with the dry film degradations which is not, however, found with the swollen film experiments. The preirradiation experiments at 25°C. show that the degradation has taken place before the addition of monomer. At −78°C. some minor amount of protection is still afforded by the α-methylstyrene but none at all by toluene. This suggests that in the preirradiation case the "protection" is by the addition of monomer to some few macroradicals which otherwise would cleave on warming and isolating the polymer in the normal way. The *G* (cleavage) value for the dry film is 5.2 at 25°C. and 2.1 at −78°C.; the corresponding values for polyisobutylene are 5.4 and 3.7, respectively. The temperature dependence and lack of effect of oxygen on the degradation is similar for both polymers, but the solvent effect is quite different, as has been discussed above.

Much more work is necessary in order to arrive at any conclusion regarding the true mechanism of degradation of cellulose acetate. The work reported here has been aimed more directly at observing the degradation which might be expected to accompany the radiation grafting process under various conditions. Although the monomer protects the polymer from radiation degradation there is still considerable chain cleavage, particularly with the preirradiation method. There is, then, a high probability that polymerization is initiated, to some extent at least, from broken chain ends leading to block polymers rather than graft. In an attempt to estimate this probability, a number of matching experiments were carried out by grafting with styrene and with degradation in the presence of α-methylstyrene.

Matching Grafting and Degradation Experiments

Three series of experiments were conducted: one in solution and one with swollen film by the direct (mutual) radiation method, and one by means of preirradiation grafting. The preparation and other details are described in the experimental section and elsewhere.[6,7] The results of the three experiments are summarized in Table III. In the case of the solution grafting, there were 6.5 times as many side chains as chain cleavages and 4.0 times for the mutual heterogeneous grafting. Chain cleavage can result in 1 or 2 free radical ends according to the mechanism, but even with two radicals there are at least twice as many chains as live chain ends, showing

TABLE III
Matching Grafting and Degradation Experiments

	Grafting (styrene)			Degradation (α-methyl styrene)			
Conditions of preparation	M_n side chains	No. chains/g. $\times 10^{18}$	G (side chains)	M_n (initial)	M_n (final)	No. cleavages/g. $\times 10^{18}$	G (cleavages)
50:50 monomer–pyridine Sol.	21,600	7.8	1.24	115,000	93,900	1.2	0.19
80:20 monomer–pyridine (mutual)	90,400	6.0	1.04	39,780	36,240	1.5	0.24
80:20 monomer–pyridine (preirrad.)	59,000	6.6	1.12	39,780	26,285	7.8	1.15

that the products are at least 50% graft and probably considerably more. In the case of the preirradiation, there are more cleavages than side chains, and the grafted product could be mainly block copolymer. It is interesting that the G value for grafting is almost the same for all three experiments, although the G value for chain cleavage varies by nearly sevenfold. It is tempting to speculate that the graft copolymers are mainly initiated by the radicals resulting from the removal of hydrogen atoms or groups from the chain situated in such a way that they cannot lead to chain cleavage. The cleavage reaction, on the other hand, may proceed mainly from another process such as direct excitation leading to an intramolecular reaction. Contributions to the cleavage by radical formation followed by carbonyl formation, as discussed earlier, could lead to block polymer formation and would be still included in the grafting yield. It should be noted that attack of solvent radicals leading to cleavage (as noted earlier in the case of

TABLE IV
Loss of Grafted Polystyrene Side Chains by Alkaline Hydrolysis

Sample preparation			Composition of graft		M_v		PS removable after alkaline hydrolysis, %
Pyridine, %	Dose, mrads	Conditions	PS	CA	PS	CA	
50	5.0	Mutual 8,300 rad/hr.	45	55	130,000	55,000	49.3
50	10.0	" 340,000 rad/hr.	27	73	30,000	55,000	44.4
50	10.0	" "	18	82	32,000	120,000	47.4
20	10.0	Preirradiation 340,000 rad/hr.	57	43	1,400,000	55,000	47.7
20	10.0	Mutual 340,000 rad/hr.	57	43	810,000	55,000	48.1

dimethylformamide solutions) will be absent in the matching experiments owing to the presence of monomer and the use of pyridine as the solvent.

The graft copolymers have been subjected to alkaline hydrolysis and extracted with benzene to remove the polystyrene previously attached to the ester groups. Infrared examination of the products showed that all the acetate groups were removed and that the benzene-soluble portions were essentially pure polystyrene. The results of this study are presented in Table IV; it can be seen that nearly 50% of the grafted side chains were attached to the ester groups in every case. Only one half of the side chains could therefore be grown from chain ends in the best case and probably, of course, considerably less as the parallel degradation studies have shown. It was of interest in the preirradiation grafting experiments that essentially no homopolymer was produced, showing that any hydrogen atoms or small radical fragments produced during the radiation were lost by combination or chain transfer. Since the G (graft) value was similar to the mutual radiation values, presumably combination of radicals was favored. An analysis of any gaseous products from the radiation would be necessary, however, to establish this fact more definitely.

We would like to thank Mrs. Jane Graper for her help with the experimental work and the School of Textiles, N. C. State College, Raleigh, N. C. for allowing the use of their radiation facilities.

This work was supported, in part, by the U. S. Army Research Office, Durham, and by the Celanese Corporation of America.

References

1. Leavitt, F. C., *J. Polymer Sci.*, **45**, 436 (1960); *ibid.*, **51**, 349 (1961).
2. Leavitt, F. C., V. Stannett, and M. Szwarc, *J. Polymer Sci.*, **31**, 193 (1958).
3. Guzman, G. M., and J. M. G. Fatow, *Quimica*, **B53**, 669 (1957).
4. Fox, T. G, and P. J. Flory, *J. Am. Chem. Soc.*, **73**, 1915 (1951).
5. Fox, T. G, and P. J. Flory, *J. Phys. Colloid Chem.*, **53**, 197 (1949).
6. Stannett, V., J. D. Wellons, and H. Yasuda, *J. Polymer Sci.*, **C4**, 551 (1964).
7. Wellons, J. D., A. Schindler, and V. Stannett, *Polymer*, **5**, 499 (1964).
8. Henglein, A., and C. Schneider, *Z. Physik. Chem. (Frankfurt)*, **19**, 367 (1959).
9. Henglein, A., C. Schneider, and W. Schnabel, *Z. Physik. Chem. (Frankfurt)*, **12**, 339 (1957).
10. S. Okamura et al., *Proc. Second Intern. Conf. Atomic Energy, Geneva,* **1958,** United Nations, Vol. 29, p. 176.
11. Blouin, F. A., and J. C. Arthur, *Textile Res. J.*, **28**, 108 (1958).
12. Florin, R. E., and L. A. Wall, *J. Polymer Sci.*, **A1**, 1163 (1963).
13. Chapiro, A., *Radiation Chemistry of Polymeric Systems*, Interscience (Wiley), New York, 1962, p. 566.

Résumé

La dégradation par irradiation de l'acétate de cellulose a été étudiée tant à l'état solide qu'en solution. La vitesse de dégradation plus grande à l'état solide n'est pas affectée par la présence d'oxygène. Il est apparu que les solvants conjugués tels que la pyridine, le toluène, l'α-méthyl-styrène, exercent une protection considérable vis-à-vis de la dégradation par irradiation de l'acétate de cellulose en solution ou en films gonflés. α-Me-styrène a été utilisé comme modèle pour le styrène en vue d'étudier l'importance de la dégradation qui accompagne le processus de greffage. Des expériences comparatives ont été effectuées en utilisant à la fois les méthodes de greffage mutuelles et de pré-irradiation. Il s'est avéré qu'un nombre considérablement plus grand de ruptures de chaîne accompagne le greffage dans le cas de la pré-irradiation. Pour les 2 méthodes, le nombre de ruptures de chaîne a été mesuré lorsque l'α-Me-styrène était présent dans la solution greffante de mêmeque le nombre de chaînes latérales greffées lorsque le styrène était utilisé. Il a été montré qu'au moins 2 fois plus de greffage de chaîne que de rupture ont lieu dans le cas de la méthode mutuelle, mais dans le cas de la préirradiation le nombre de ruptures est comparable au nombre de chaînes greffées. La valeur de G (chaine greffée) dans le cas de l'acétate de cellulose avec le styrène a été déterminée et était de 1.1 dans tous les cas. La valeur de G (rupture de chaîne) variait cependant de 0.2 à 13 approximativement. La proportion de chaînes greffées, attachées aux groupements esters, a été déterminée par extraction au benzène après hydrolyse alcaline à froid. Environ la moitié des greffons étaient attachés dans chaque cas en y incluant les produits de préirradiation. En général on peut dire que dans tous les cas 50% des copolymères greffés le sont par chaînes latérales et probablement beaucoup plus encore dans les cas de préparation par irradiation mutuelle.

Zusammenfassung

Der Strahlungsabbau von Zelluloseacetat wurde im trockenen Zustand und in Lösung untersucht. Die Abbaugeschwindigkeit war im festen Zustand grösser und wurde durch Sauerstoff nicht beeinflusst. Konjugierte Lösungsmittel wie Pyridin, Toluol, und α-Methylstyrol übten auf Zelluloseacetat in Lösung oder als gequollener Film einen beträchtlichen Schutz gegen den Strahlungsabbau aus. α-Methylstyrol wurde als Modell für Styrol bei der Untersuchung des Batrages des Abbaus, der den Aufpfropfungsprozess begleitet, verwendet. Vergleichsversuche wurden sowohl nach der wechselweisen als auch nach der Vorbestrohlungsmethode für die Aufpfropfung ausgeführt. Im Fall der Vorbestrahlung trat eine beträchtlich grössere Kettenspaltung während der Aufpfropfung ein. Nach beiden Methoden wurde die Anzahl der Kettenspaltungen bei Anwesenheit von α-Methylstyrol in der Aufpfropflösung und die Anzahl der aufgepfropften Seitenketten bei Verwendung von Styrol gemessen. Es wurde gezeigt, dass beim Wechselverfahren mindestens doppelt soviele aufgepfropfte Ketten als Spaltungen auftreten und dass hingegen im Fall der Vorbestrahlung die Anzahl der Spaltungen derjenigen der aufgepfropften Ketten vergleichbar ist. Der G (aufgepfropfte Kette)-Wert wurde für Zelluloseacetat mit Styrol bestimmt und betrug in allen Fällen etwa 1,1. Die G (Kettenspaltung)-Werte hingegen variierten etwa zwischen 0,2 und 1,3. Der Anteil der an den Estergruppen gebundenen aufgepfropften Ketten wurde durch Extraktion mit Benzol nach kalter alkalischer Hydrolyse bestimmt. Etwa die Hälfte der Aufpfropfungen waren in jedem Fall einschliesslich des Vorbestrahlungsproduktes gebunden. Im allgemeinen kann gesagt werden, dass in allen Fällen zumindest 50% des Pfropfcopolymeren Seitenkettenpfropfungen waren und wahrscheinlich ein beträchtlich höherer Anteil im Fall der Reaktionsprodukte bei wechselweiser Bestrahlung.

Received June 10, 1964

JOURNAL OF POLYMER SCIENCE: PART A VOL. 3, PP. 859-882 (1965)

Mechanisms of Thermal Degradation of Phenolic Condensation Polymers. II. Thermal Stability and Degradation Schemes of Epoxy Resins*

LIENG-HUANG LEE, *Polymer and Chemicals Research Laboratory, The Dow Chemical Company, Midland, Michigan*

Synopsis

The thermal degradation of uncured and cured epoxy resins was studied. By the use of the thermogravimetric analysis, the thermal stability of the cured epoxy resins, D.E.N. 438 and D.E.R. 331 resins, was compared with those of polycarbonate and polyphenylene sulfide. The resins, including novolac resin and D.E.R. 669 resins, were pyrolyzed, and their volatiles were determined with a mass spectrometer. The experimental results showed that the phenolic compounds were the major volatile products. Thus, the data do not support the degradation scheme proposed by Neiman and co-workers. Several degradation schemes for epoxides are proposed based on the principles of the cleavage of simple ethers and the products obtained from the pyrolysis study.

INTRODUCTION

The thermal degradation of phenol-formaldehyde condensation polymers has been widely studied.[1-4] Several hypotheses have been proposed regarding the degradation mechanisms of these polymers. However, other phenolic condensation polymers, thermoplastic and thermosetting, have not been fully investigated with reference to their mechanisms of degradation. The studies conducted in our laboratories have been aimed towards the mechanisms of thermal degradation up to 600°C. for polycarbonate, epoxy resins, polyphenylene sulfide and other phenolic condensation polymers. The study on the thermal stability and degradation mechanisms of polycarbonate[5] has been previously reported. In this paper, the degradation schemes of epoxy resins are discussed.

Anderson[6] first applied differential thermal analysis (DTA) to the study of the thermal stability of epoxy resins. Neiman[7] and co-workers studied the degradation mechanism of the cured epoxy resins with the aid of thermogravimetric analysis (TGA) and electron spin resonance (ESR). Anderson[8] proposed a different isomerization scheme based on his DTA findings, and further[9] studied the kinetics of pyrolysis of epoxide polymers. Madorsky and Straus[10] reported their results on the thermal stability of

---

* Paper presented at the Battelle Symposium on Thermal Stability of Polymers, Battelle Memorial Institute, Columbus, Ohio, December 5, 1963.

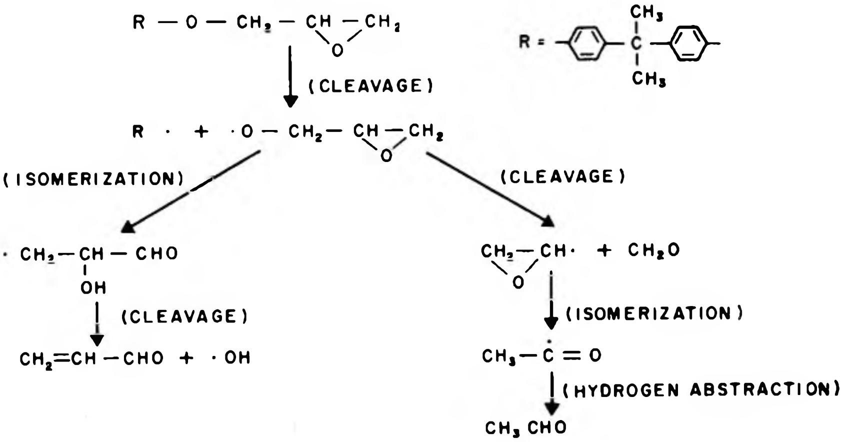

Fig. 1. Degradation of epoxide by Neiman's scheme.

phenolic, polyester, and epoxy resin up to 1200°C. The mechanism of oxidative degradation was reported by Park and Blount.[11] This study is limited to nonoxidative thermal degradation schemes.

The degradation scheme (Fig. 1) proposed by Neiman and co-workers was found to be inadequate to explain the presence of the predominant phenolic compounds obtained during the thermal degradation of epoxy resins. A careful study of the proposed scheme which was based on the cleavage between the phenyl ring and the phenoxy oxygen revealed that this situation is rarely encountered in the cleavage of simple ethers. Our study was therefore focused on establishing plausible schemes other than the one proposed by Neiman and co-workers.

In the following sections, we discuss the thermal stability of epoxy resins, the results of the thermal degradation of the uncured and the cured epoxy resins, and the degradation schemes. A detailed study of the degradation mechanisms of various epoxy resins will be published with a study of model compounds. It was hoped that this type of fundamental study could aid in improving the thermal stability of current epoxy resins and in designing better resins for specialty uses, such as the ablative plastics.

EXPERIMENTAL

Materials

The epoxy resins were produced by The Dow Chemical Company. D.E.R. resins (Fig. 2) were the epoxylated bisphenol-A resins, while D.E.N. resins were the epoxylated novolac resins. D.E.R. 669 resin was a solid resin with an epoxide equivalent weight between 3,500 and 5,500 (total chlorine: 0.24%). D.E.R. 331 resin was a liquid resin with an epoxide equivalent between 186 and 192 (total chlorine: 0.35%). D.E.N. 438 resin was a viscous semisolid with an epoxide equivalent between 175 and 182 (total chlorine: 0.30%). The *n* value for the center unit (Figure

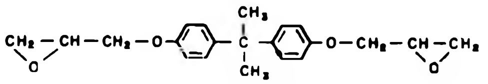

D.E.R. 331 RESIN

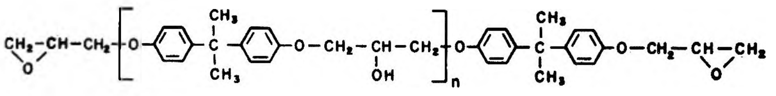

D.E.R. 669 RESIN

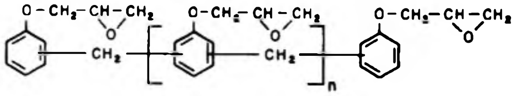

D.E.N. 438 RESIN

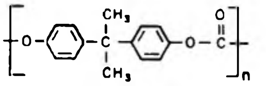

POLYCARBONATE

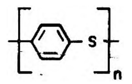

POLYPHENYLENE SULFIDE

Fig. 2. Phenolic condensation polymers.

2) had an average value of 1.5. A novolac resin of higher *n* value also prepared in the presence of an acid catalyst was used as a reference for the degradation study. It should be noted that D.E.R. 669 resin, D.E.R. 331 resin, and D.E.N. 438 resin contained small amounts of residual toluene.

The epoxy resins were cured according to the formulations described in the technical bulletins. D.E.N. 438 resin was cured with methylenedianiline (D.E.H. 50 manufactured by The Dow Chemical Company) according to formulation 43.[12] The catalyst (MDA, 28 parts) was mixed with the preheated resin (100 parts) at 90°C., and the mixture was cured for 16 hr. at 55°C., 2 hr. at 125°C., and 2 hr. at 175°C. The cured resin contained 1.92% of nitrogen and 0.195% of total chlorine.

Methyl Nadic anhydride, methylbicyclo[2.2.1]hept-5-ene-2,3-dicarboxylic anhydride (manufactured by National Aniline Division of Allied Chemical Company) was used as the anhydride catalyst with the addition of benzyldimethylamine (BDMA, 1.5 part per 100 parts of resin) as an accelerator. D.E.N. 438 resin (100 parts) was cured with the catalyst (MNA, 87.5 parts) according to formulation 45, e.g., 2 hr. at 90°C., 4 hr. at 165°C., and 16 hr. at 200°C. The cured resin contained 0.134% total chlorine.

D.E.R. 331 resin was reacted with methylenedianiline according to formulation 10.[13] The catalyst (26 parts) was mixed with the preheated resin (100 parts) at 90°C., and the mixture was cured with the same schedule used for the curing of D.E.N. 438 resin with the same catalyst (MDA). The amine-cured D.E.R. 331 resin contained 2.60% nitrogen and 0.209% total chlorine. The anhydride-cured D.E.R. 331 resin was prepared according to formulation 18.[12] The catalyst (MNA, 87.5 parts) was mixed with the resin (100 parts). The curing schedule was identical to that used for the curing of D.E.N. 438 resin with the same catalyst (MNA). The anhydride-cured D.E.R. 331 resin contained 0.148% total chlorine.

The reference materials used for the thermogravimetric analysis were polyphenylene sulfide, polycarbonate, and polytetrafluoroethylene. Polyphenylene sulfide[14] was supplied by the Polymer Research Laboratory of The Dow Chemical Company. The polymer (softening point 250°C., melting point 269–273°C.) was soluble in diphenyl ether. The molecular weight of the polymer as determined from the melt viscosity measurement was between 45,000 and 50,000. Other reference materials were obtained from commercial sources. The Lexan polycarbonate (Lot 2076) was one of the latest production materials manufactured by the General Electric Company.

Thermogravimetric Analysis (TGA)

A simple thermogravimetric balance was used.[15] The sample holder was attached to the quartz spring balance by a fine quartz fiber and centered in a furnace, the temperature of which was measured with a thermocouple situated directly beneath the sample holder. The weight of the remaining sample was recorded continuously versus temperature by use of an X-Y recorder. A heating rate of 9–10°C./min. was used for the study.

Differential Thermal Analysis (DTA)

The differential thermal analysis equipment was described by Cobler and Miller.[16] When a phase change or a reaction occurs involving absorption or evolution of heat, the temperature difference between the sample and the reference material increases. In general, phase transformations and depolymerization are endothermic, whereas oxidation and polymerization are exothermic. A heating rate of 10°C./min. was used for the analyses.

Vapor-Phase Chromatography

The direct pyrolysis was conducted directly in the injector inlet of the chromatography unit (HY-FI Model 600 manufactured by Wilkens Instrument and Research Inc.). The material was pyrolyzed on a hot filament. A sorbitol column (6 ft.) was used for the separation of phenolic compounds.

Mass Spectrometric Analysis of the Pyrolyzed Products

Low-Boiling Volatiles (below 120°C.). The pyrolysis was conducted in a Vycor flask (25 ml.) heated with a heating mantle. The vapor evolved during pyrolysis at 350 or 450°C. was conducted directly to the mass spectrometer. (Consolidated Model 21-103.) The ionization was carried out using an electron energy of 70 e.v. and ion source pressure of 10^{-7}

mm. Hg. The injector temperature was maintained at room temperature.

High-Boiling Fractions (Mostly Phenolic Compounds). The pyrolysis tube consisted of an 8-in. glass tube sealed at one end. There was a 90° bend 5 in. from the sealed end. This tube was connected to a U-tube, and the other end of the latter was connected to a vacuum pump. The pyrolysis tube was filled with about 1 in. of polymer, enclosed in a furnace, and heated at ~475°C. under vacuum for 3 hr. During pyrolysis the U-tube was immersed in liquid nitrogen. Samples for mass spectrometer analysis were collected from various parts of the pyrolysis tube and U-tubes to determine if fractionation of the products had occurred. For the analyses of the high-boiling fractions, the mass spectrometer with a 90° sector magnetic scanning spectrometer built by the Chemical Physics Research Laboratory was used. The sample inlet temperature was 200°C. The ionization was carried out by using an electron energy of 75 e.v. and an ion source pressure of 10^{-7} mm. Hg.

RESULTS AND DISCUSSION

Thermal Stability

The thermal stability of epoxy resins is chiefly affected by the structure of the particular epoxy resin under study,[17] the type of curing agent,[18] the chlorine content[19] and the curing schedule. It is generally known that the epoxylated novolac resins are more stable than the epoxylated bisphenol-A resins because the methylene linkages in the former are more stable than the isopropylidene linkages in the latter. It is also recognized that the anhydrides are generally better curing agents than the amines. It was reported that the presence of the residual chlorine adversely affected the thermal stability, especially when an amine was used as a curing agent. Undoubtedly there are other variables, such as curing schedules, which can affect the thermal stability of epoxy resins. Most studies on thermal stability have been correlated with the physical properties of the cured resins. In order to understand the basic stability problems, we prefer to correlate the above-mentioned variables with the chemical structure of the resins.

Madorsky and Straus[9] found that the epoxy resin used in their study was less stable than the polyester used and the polyester was less stable than the phenolic resin used. In Figure 3, the cured epoxy resins used in this study are compared with polycarbonate and polyphenylene sulfide. The stability decreases in the order: polyphenylene sulfide > polycarbonate > epoxy resins. All these phenolic condensation polymers seem to be inferior to Teflon, but once Teflon starts to decompose, the weight loss is linear as a result of unzipping of the polymer chain to form monomers. Therefore at temperatures higher than 600°C., the phenolic condensation polymers generally have a small nonvolatile portion remaining.

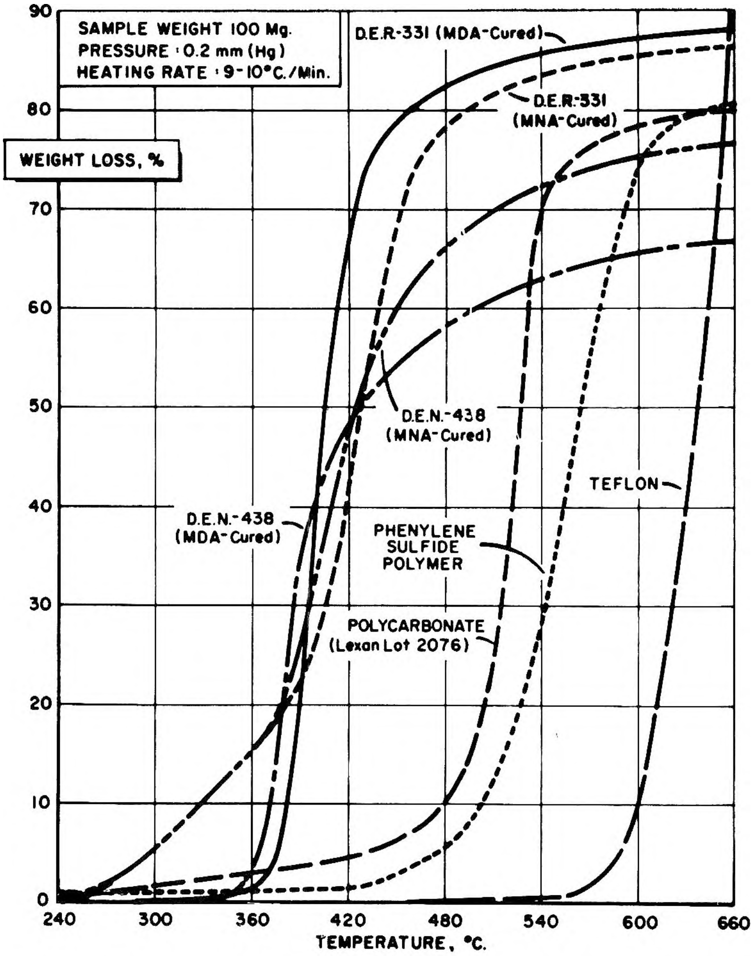

Fig. 3. Thermogravimetric curves of phenolic condensation polymers.

The effects of curing agents and the structure of epoxy resins on the weight loss are shown in Figure 3. For the samples prepared according to the procedures described in the experimental part, we found that the anhydride-cured samples started to lose weight in the range of 260–268°C. This was also previously reported by Anderson.[20] However, the differences in the weight losses are slight after 25% of the original weight of the sample has been lost during the degradation. The weight loss curves cross over at 50% weight loss (40–428°C.) for D.E.R. 331 and D.E.N. 438 resins. Beyond this point, the rate of weight loss for D.E.N. 438 resins seems to be lower than the rate for D.E.R. 331 resins.

The second part of the thermal stability study was to determine what kind of reactions took place during the exothermic portion of the experiment. Anderson[8] proposed that it was the isomerization of epoxide into aldehydes on the side-chains which caused the characteristic exothermic reaction. Initially we decided to determine whether oxidation was the major cause of the exothermic reaction. Two epoxy resins, D.E.R. 331 resin (Fig. 4) and D.E.R. 669 resin (Fig. 5), were both analyzed by differential thermal analysis in the presence of air and nitrogen, respectively. We found that nitrogen did not inhibit the exothermic reaction. We also found that the intensity of the exothermic peak seems to be stronger in the case of D.E.R. 331 resin than in the case of D.E.R. 669 resin which had less epoxy terminal groups than D.E.R. 331 resin.

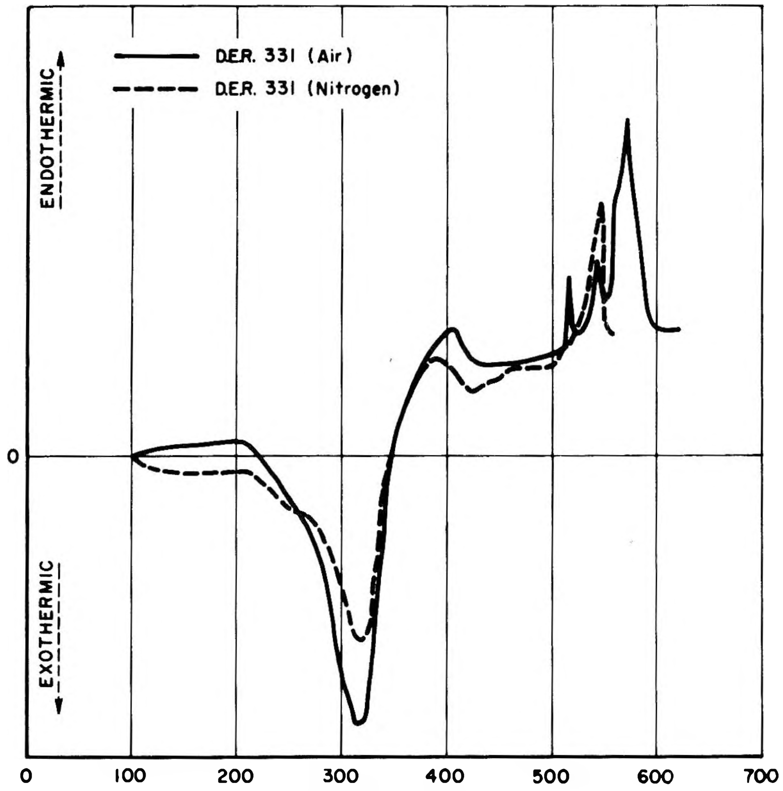

Fig. 4. Differential thermogram of D.E.R. 331.

Furthermore, the addition of curing agents to the uncured resins seems to reduce the intensity of this characteristic peak for more than one reason. In the case of D.E.N. 438 resin, the amine-cured resin (Fig. 6) seems to have a longer exothermic reaction than the uncured resin. The characteristic exothermic peak shifts to the right at 370°C. In the case of the anhydride-cured resin (MNA), an early exothermic reaction took place at 260°C., as shown also in the TGA curve (Fig. 3). The endothermic reaction was mainly caused by the volatilization of the decomposed products. The major volatile has been shown by Anderson[20] to be carbon dioxide. This endothermic reaction occurs simultaneously with the characteristic exothermic reaction at 320°C. The resultant weak exothermic peak is then shifted to 355°C.

In the case of D.E.R. 331 resin (Fig. 7), the decrease of the intensity of the exothermic peaks of the cured resins is more obvious. For the amine-cured resin, the exothermic peak is at 300°C. instead of 315°C. for the uncured resin. The reason for this shift to the left is not yet clear. For the anhydride-cured resin, the second exothermic peak is at 360°C., which

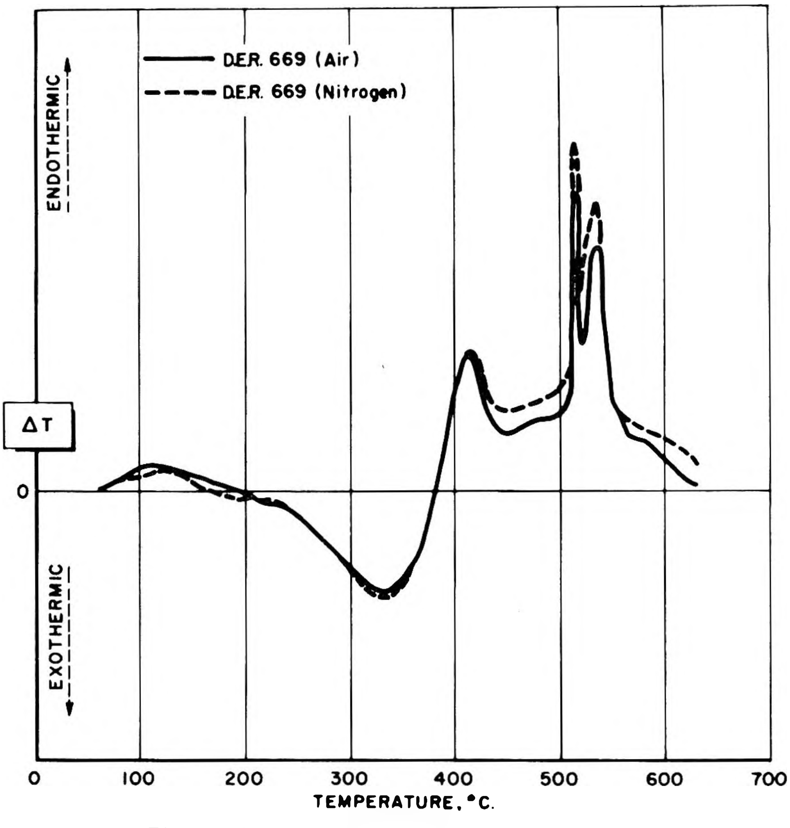

Fig. 5. Differential thermogram of D.E.R. 669.

is close to that of the anhydride-cured D.E.N. 438 resin. In both cases, the anhydride-cured resins had two exothermic peaks.

The differential thermal analysis results indicate that the characteristic exothermic peak between 300–380°C. is at least partially caused by some reaction (or reactions) of the epoxide. Presumably, the nature of the reaction is either the isomerization or the etherification (or polymerization) of the epoxide with the hydroxy groups on the side chains or both. The following experimental results from pyrolysis experiments are used to verify this basic reaction during the degradation of epoxy resins.

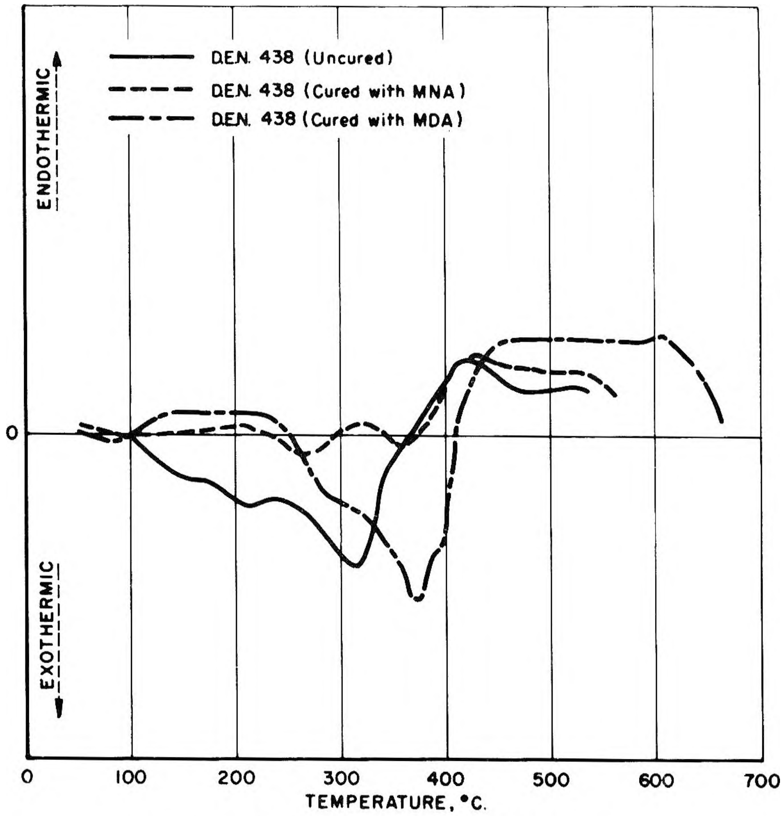

Fig. 6. Differential thermogram of D.E.N. 438.

Pyrolysis of Novolac and Uncured Epoxy Resins

The pyrolysis of the epoxy resins for the determination of low-boiling volatile products was conducted at two temperatures: 350 and 450°C.; the pyrolysis for the determination of high boiling volatiles was conducted at 475°C. Generally the low-boiling volatiles were only a small portion of the total pyrolyzed products, and the major pyrolyzed products were the tarry residues.

Novolac Resin. The unepoxylated novolac resin is the backbone of D.E.N. 438 resin except that the latter has a lower molecular weight. Therefore, the results of pyrolysis of novolac resin should give some insight into the degradation scheme of D.E.N. 438 resin. The low boiling volatile at 350°C. (Table I) yielded water (87.40 mole-%), CO_2 (5.84 mole-%), and CO (2.95 mole-%). At 450°C. the pyrolysis yielded chiefly CO (40.20 mole-%), CO_2 (30.60 mole-%) water (10.50 mole-%), and formaldehyde (10.10 mole-%). The high-boiling fraction obtained at 475°C. contained mostly cresols, phenol, and $(HOC_6H_4)_2CH_2$ (Table V). These results show that the degradation scheme seemed to involve the cleavage of the methylene linkage and the removal of water.

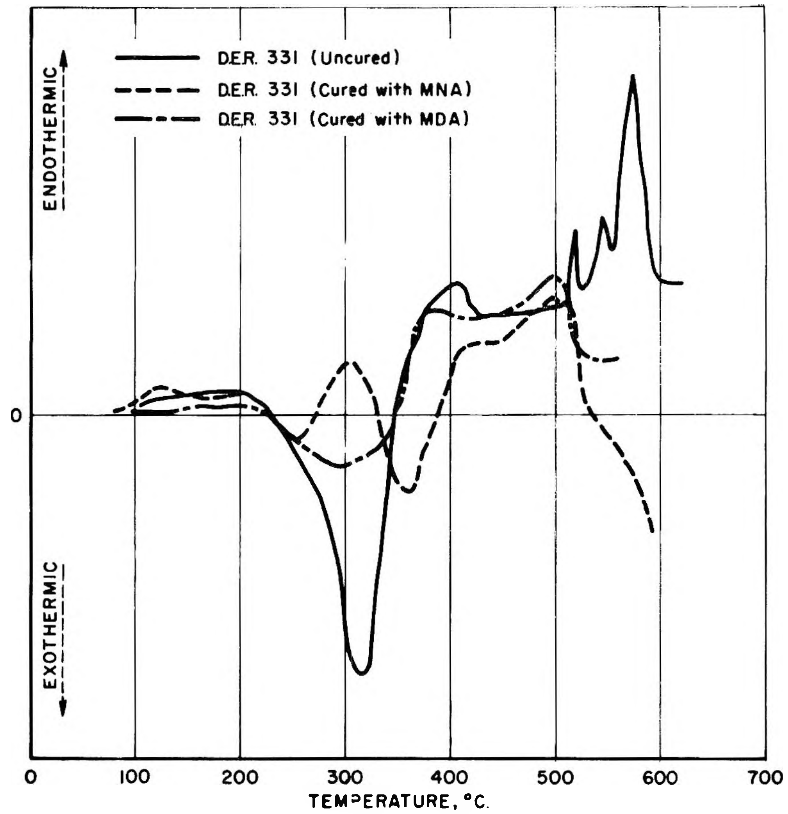

Fig. 7. Differential thermogram of uncured and cured D.E.R. 331.

D.E.N. 438 Resin. At 350°C. the pyrolysis yielded the low-boiling volatiles (Table I): toluene (68.30 mole-%) and water (25.80 mole-%). The main constituents of the volatiles obtained at 450°C. were toluene (32.40 mole-%), ethane (13.40 mole-%), allyl chloride (9.19 mole-%) and water (7.42 mole-%). The high-boiling fractions obtained at 475°C. were the phenolic mixture (Table V) similar to that obtained from the degradation of the novolac resin.

The differences were found in the low-boiling volatiles obtained from the two resins. Due to the presence of ethane, it was assumed that scheme I, given in a later section, could be one of the degradation schemes. The presence of aldehydes indicated that scheme III could also be one of the many other possibilities. Toluene was known to be the solvent retained in the resin, therefore the presence of toluene in the volatiles was expected.

D.E.R. 331 Resin. The major volatile constituents for D.E.R. 331 resin pyrolyzed at 350°C. (Table II) were toluene (57.20 mole-%) and water (34.10 mole-%). At 450°C., the pyrolysis yielded toluene (57.20 mole-%), methylcyclopentadiene (16.50 mole-%), and water (11.10 mole-%). The high-boiling fractions at 475°C. contained mainly phenol, cresols,

TABLE I
Volatile Products from Pyrolysis of Novolac and D.E.N. 438 Epoxy Resin

		Novolac		D.E.N. 438	
Compounds	*m/e*	At 350°C. (mole-%)	At 450°C. (mole-%)	At 350°C. (mole-%)	At 450°C. (mole-%)
Hydrogen	2	—	0.47	0.39	1.49
Methane	16	0.45	0.75	1.05	—
Water	18	87.40	10.50	25.80	7.42
Acetylene	26	—	—	—	1.47
Ethylene	28	0.14	0.51	—	—
Carbon monoxide	28	2.95	40.20	—	—
Ethane	30	—	—	0.40	13.40
Formaldehyde	30	0.38	10.10	—	8.52
$—CH_2OH$	31	0.26	—	0.22	2.52
Allene	40	—	0.20	—	0.55
Propylene	42	0.05	1.66	—	—
Acetaldehyde	44	0.19	0.96	—	5.32
Propane	44	—	—	—	2.42
Carbon dioxide	44	5.84	30.60	0.35	—
Methyl chloride	50, 52	—	—	—	1.08
Acrolein	56	—	—	0.11	4.24
$—CH_3CH_2CO$	57	—	—	1.12	6.75
Acetone	58	0.12	—	—	0.49
Propionaldehyde	58	—	0.30	—	1.41
$HCOOCH_3$	60	0.64	1.71	—	—
Vinyl chloride	62, 64	—	—	0.95	—
$—COCl$	63, 65	—	—	1.12	—
$—(CH_2)_3Cl$	76, 78	—	—	—	0.94
Allyl Chloride	76, 78	—	—	—	9.19
Methylcyclopentadiene	80	0.16	0.46	0.26	0.38
Toluene	92	1.44	1.46	68.30	32.40
Phenol	94	—	0.12	—	—

C_2H_5 phenols, isopropylphenol (or C_3H_7 phenol), isopropenylphenol, $C_6H_4OC_3H_4$, and bisphenol-A (Table VI).

A large quantity of water was obtained at 350°C. among the low-boiling volatiles. This could suggest that the epoxide groups were mostly opened and formed ethers. The subsequent dehydration of the hydroxy ether yielded the unsaturated ether on the side chains. The unsaturated ether may cleave and rearrange into various unsaturated phenols; these phenols might polymerize (or crosslink) in the residue. The small concentration of either carbon monoxide or carbon dioxide in the volatile may suggest scheme IIC given in a later section to be one of the degradation schemes, besides the major cleavage of the bisphenol-A unit.

The source of methylcyclopentadiene is not clearly known. We hope that a study with a model compound, such as phenyl glycidyl ether, could throw some light into the degradation mechanism. However, the problem with the low-boiling epoxide and the uncured resin is the tendency for the compound to distill off before the pyrolysis takes place.

D.E.R. 669 Resin. D.E.R. 669 resin (Table II) differed from D.E.R. 331 resin in that the former contained less terminal epoxide than the latter. There are at least ten times as many free hydroxy groups as there are terminal epoxide groups. It was expected that dehydration would be one of the major reactions. The major low-boiling volatiles obtained at 350°C. were water (40.70 mole-%), toluene (38.00 mole-%), carbon dioxide (9.38 mole-%), and acetaldehyde (4.34 mole-%). Those obtained at 450°C. were toluene (39.50 mole-%), water (20.50 mole-%), methyl chloride (14.80 mole-%), acetaldehyde (12.90 mole-%) and carbon dioxide (4.6 mole-%). The presence of acetaldehyde suggests that the degradation may also follow scheme III. The high-boiling fractions obtained at 475°C. (Table VI) were identical to those obtained from D.E.R. 331 resin.

TABLE II
Volatile Products from Pyrolysis of D.E.R. 331 and D.E.R. 669 Epoxy Resins

Compounds	*m/e*	D.E.R. 331		D.E.R. 669	
		At 350°C. (mole-%)	At 450°C. (mole-%)	At 350°C. (mole-%)	At 450°C. (mole-%)
Hydrogen	2	—	—	—	—
Methane	16	0.73	1.87	—	0.56
Water	18	34.10	11.10	40.70	20.50
Acetylene	26	—	—	—	—
Ethylene	28	—	1.09	0.88	1.41
Carbon monoxide	28	—	1.30	—	1.60
Ethane	30	0.49	1.50	0.44	0.54
Formaldehyde	30	—	—	—	—
—CH_2OH	31	1.21	1.24	0.88	0.91
Allene	40	—	0.15	0.93	0.34
Propylene	42	—	—	0.35	0.42
Acetaldehyde	44	—	—	4.34	12.90
Propane	44	—	—	—	—
Carbon dioxide	44	0.16	1.27	9.38	4.60
Methyl chloride	50, 52	—	0.60	2.93	14.80
Acrolein	56	0.07	0.57	—	0.09
—CH_3CH_2CO	57	3.89	3.75	—	—
Acetone	58	—	—	0.77	1.32
Propionaldehyde	58	0.13	0.22	—	—
Vinyl chloride	62, 64	0.92	0.51	—	—
—COCl	63, 65	0.66	0.80	—	—
Mass 70 (and 97)	70, 97	—	—	0.16	0.31
Cyclopentadiene	66	—	0.25	—	—
Benzene	78	—	0.16	—	—
Methylcyclopentadiene	80	0.38	16.50	0.22	0.20
Toluene	92	57.20	57.20	38.00	39.50

Pyrolysis of Methylenedianiline-Cured Resins

The amine-cured epoxy resins[21,22] generally contain more free hydroxy groups in the cured network than the anhydride-cured resins. As the thermal curing proceeds, a number of the hydroxy groups may form ether linkages. The presence of these free hydroxy groups may be one of the causes for the thermal instability of the amine-cured resins. One example is the initial fast dehydration of the MDA-cured epoxy resins. The second cause of the thermal instability of the amine-cured resin was postulated to be the formation of a small amount of amine hydrochloride. Upon the decomposition of the amine hydrochloride, a catalytic amount of HCl could initiate the cleavage of the epoxy resin, especially D.E.R. resins containing a bisphenol-A unit. (The cleavage of bisphenol-A was described in the previous paper.[5])

D.E.N. 438 Resin (Cured with MDA). The major low-boiling volatile obtained from the pyrolysis of D.E.N. 438 resin at 350°C. (Table III) was water (97.70%). At 450°C., the pyrolysis yielded carbon dioxide (25.40 mole-%), methylcyclopentadiene (21.00 mole-%), water (17.00 mole-%), carbon dioxide (13.90 mole-%), methyl chloride (6.19 mole-%),

TABLE III
Volatile Products from Pyrolysis of Epoxy Resins Cured with Methylenedianiline (MDA)

		D.E.N. 438		D.E.R. 331	
Compounds	*m/e*	At 350°C. (mole-%)	At 450°C. (mole-%)	At 350°C. (mole-%)	At 450°C. (mole-%)
Hydrogen	2	—	1.02	—	1.12
Methane	16	—	3.59	0.14	2.59
Water	18	97.70	17.00	96.70	15.40
Carbon monoxide	28	—	25.40	—	16.80
Ethylene	28	—	0.77	0.13	1.58
Ethane (or HCHO)	30	—	0.37	—	—
$-CH_2OH$	31	—	0.63	0.13	0.66
Allene (or methylacetylene)	40	—	0.70	0.10	0.79
Propylene	42	—	0.97	—	0.76
Acetaldehyde	44	—	4.85	—	7.71
Carbon dioxide	44	1.70	13.90	0.79	9.95
Methyl chloride	50, 52	—	6.19	—	6.92
Acrolein	56	—	0.11	—	0.22
Acetone	58	—	0.93	—	0.81
Propionaldehyde	58	—	0.41	—	0.23
Vinyl chloride	62, 64	—	0.21	—	0.26
Ethyl chloride	64, 66	—	0.21	—	0.26
Cyclopentadiene	66	—	0.79	0.03	1.26
Benzene	78	—	0.33	—	0.54
Methylcyclopentadiene	80	—	21.00	1.44	31.50
Toluene	92	0.56	0.56	0.58	0.62

acetaldehyde (4.85 mole-%), and methane (3.59 mole-%). The phenolic compounds (Table V) were similar to those obtained from the uncured resin.

Due to the presence of a high concentration of carbon monoxide we could assume scheme III to be one of the major schemes. Other possibilities may include scheme IIA and scheme IV. A small amount of allene could indicate that there was a small amount of decomposition following scheme IIC. However, the blocking of a part of *ortho* positions by the methylene linkages might reduce the possibility of the Claisen rearrangement.

The remaining volatiles did not show any identifiable fragments decomposed from the MDA unit. Other decomposition products containing the residual chlorine were methyl chloride, ethyl chloride, and vinyl chloride. Thus methylenedianiline might exist in the form of a di-tertiary amine in the polymer network:

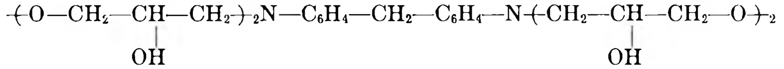

$$(O-CH_2-\underset{\displaystyle OH}{\underset{|}{CH}}-CH_2)_2N-C_6H_4-CH_2-C_6H_4-N(CH_2-\underset{\displaystyle OH}{\underset{|}{CH}}-CH_2-O)_2$$

A detailed study on the fate of the MDA unit will be discussed in a future paper.

D.E.R. 331 (Cured with MDA). The amine-cured D.E.R. 331 resin decomposed similarly to the amine-cured D.E.N. 438 resin. At 350°C., the major low-boiling volatile (Table III) was water (96.70 mole-%). At 450°C., the major constituents were methylcyclopentadiene (31.50 mole-%), carbon monoxide (16.80 mole-%), water (15.40 mole-%), carbon dioxide (9.95 mole-%), acetaldehyde (7.71 mole-%), methyl chloride (6.92 mole-%), and methane (2.59 mole-%). The high-boiling fractions obtained at 475°C. are shown in Table VI. Based on these results, we could assume that the degradation schemes were similar to those for the preceding resin, except that scheme IIC might be important in this case, when the *ortho* positions of the phenolic units are open. It should be noted that the presence of methylcyclopentadiene in the two amine-cured resins might serve as a clue to unlock one of the degradation schemes.

Pyrolysis of Methyl Nadic Anhydride-Cured Resins

The anhydride-cured resins[23] generally contain predominantly the diester and some monoester of the compound used as the curing agent. At elevated temperatures, the monoester can convert into the diester and the anhydride. Generally, the diester can undergo *cis*-elimination to release an olefin and carbon dioxide:

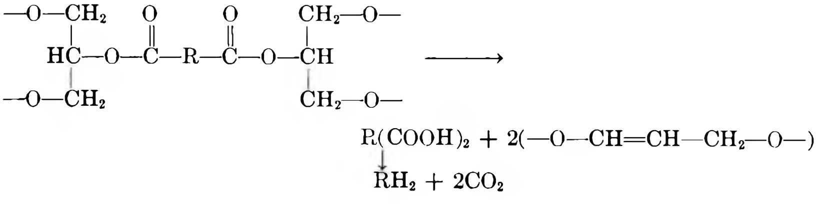

$$\begin{array}{c}-O-CH_2\\ |\\ HC\\ |\\ -O-CH_2\end{array}\!-O-\overset{\overset{\displaystyle O}{\|}}{C}-R-\overset{\overset{\displaystyle O}{\|}}{C}-O-\!\begin{array}{c}CH_2-O-\\ |\\ CH\\ |\\ CH_2-O-\end{array}\longrightarrow$$

$$\begin{array}{l}R(COOH)_2 + 2(-O-CH{=}CH-CH_2-O-)\\ \downarrow\\ RH_2 + 2CO_2\end{array} \qquad (1)$$

This decomposition was previously anticipated by Anderson[20] based on the amount of carbon dioxide evolved. For instance, methyl Nadic acid may decompose according to eq. (2) into methylcyclopentadiene:

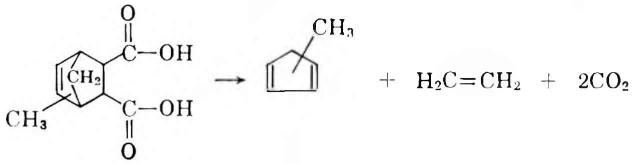

(2)

Therefore in the case of MNA-cured resins, the presence of methylcyclopentadiene in the low-boiling volatiles is somewhat expected. A portion of methylcyclopentadiene could come from the same source as in the case of amine-cured epoxy resins. However the appearance of a large quantity of methylcyclopentadiene at 350°C. in the anhydride-cured cases could support the above assumption.

D.E.N. 438 Resin (Cured with MNA). At 350°C., the MNA-cured resins (Table IV) yielded more low-boiling volatiles than the MDA-cured resins. For D.E.N. 438 resin the major constituents were water (38.40 mole-%), carbon dioxide (21.90 mole-%), methylcyclopentadiene (19.10

TABLE IV
Volatile Products from Pyrolysis of Epoxy Resins Cured with Methyl Nadic Anhydride (MNA)

		D.E.N. 438		D.E.R. 331	
Compounds	*m/e*	At 350°C. (mole-%)	At 450°C. (mole-%)	At 350°C. (mole-%)	At 450°C. (mole-%)
Hydrogen	2	6.06	1.30	4.21	0.55
Methane	16	0.59	1.11	1.12	1.63
Water	18	38.40	4.32	19.00	5.78
Carbon monoxide	28	8.89	7.48	5.16	6.38
Ethylene	28	0.85	1.22	1.11	1.24
Ethane (or HCHO)	30	—	—	—	—
—CH_2OH	31	0.33	0.57	0.37	0.64
Allene (or methylacetylene)	40	0.91	0.52	0.79	0.69
Propylene	42	—	0.22	—	0.22
Acetaldehyde	44	—	—	—	—
Carbon dioxide	44	21.90	40.80	23.40	30.50
Methyl chloride	50, 52	0.71	1.52	1.41	1.58
Acrolein	56	—	0.09	—	0.07
Acetone	58	—	0.27	0.25	0.25
Propionaldehyde	58	—	—	—	—
Vinyl chloride	62, 64	—	0.19	0.26	0.33
Ethyl chloride	64, 66	—	0.56	0.24	0.69
Cyclopentadiene	66	1.05	4.12	2.52	5.41
Benzene	78	0.23	0.49	0.50	0.54
Methylcyclopentadiene	80	19.10	35.00	38.90	43.20
Toluene	92	1.03	0.27	0.76	0.30

TABLE V
High-Boiling Products from Pyrolysis of Novolac and D.E.N. Epoxy Resins (475°C. under Vacuum)

Compounds	m/e	Novolac resin (acid-catalyzed)	D.E.N. 438 (epoxy equiv. 175–182)	D.E.N. 438 (cured with MDA)	D.E.N. 438 (cured with MNA)
Cresols	108	Largest	Largest	Largest	Largest
Phenol	94	Major	Major	Major	Major
$(HOC_6H_4)_2CH_2$	200	Major	Major	Major	Major
C_2H_5 Phenols	122	Minor	Minor	Minor	Minor
$(HOC_6H_4)_2(CH_2)_2$	214	Minor	Minor	Minor	Minor
C_3H_5 Phenol	134	—	—	Minor	Minor
C_3H_7 Phenol	136	—	—	Minor	Minor
Unidentified Masses (small amounts)		100, 128, 152, 178, 180, 182, 190, 196, 208	120, 150, 164, 181, 196, 197, 256	118, 120, 130, 132, 144, 152, 158, 166, 168, 170, 172, 178, 182, 184, 194, 196, 198, 205, 210, 224, 226, 228, 238, 240, 248, 252, 254, 262, 266, 276	128, 146, 160 and others similar as shown left

TABLE VI
High-Boiling Products from Pyrolysis of D.E.R. Epoxy Resins (475°C. under Vacuum)

Compounds	m/e	D.E.R. 669 (epoxy equiv. 3,500–5,500)	D.E.R. 331 (epoxy equiv. 186–192)	D.E.R. 331 (cured with MDA)	D.E.R. 331 (cured with MNA)
Phenol	94	Largest	Largest	Largest	Largest
Cresols	108	Major	Major	Major	Major
C_2H_5 Phenols	122	Major	Major	Major	Major
Isopropylphenol	136	Major	Major	Major	Major
Isopropenylphenol	134	Major	Major	Major	Major
$C_6H_4OC_3H_4$	132	—	Major	Major	Major
Bisphenol-A	228	Minor	Minor	Minor	Major
Unidentified masses (small amounts)		148, 150, 199, 200, 211, 223, 237, 242, 251, 269	146, 150, 160, 174, 211, 213, 264, 278, 292	106, 118, 120, 158, 160, 178, 180, 182, 194, 196, 198, 210, 222, 224, 242, 250, 252, 254, 266	146, 150, 160, 174, 240, 242, 266, 268

mole-%), carbon monoxide (8.89 mole-%), and hydrogen (6.06 mole-%). The presence of CO and H_2 in a similar mole ratio may indicate that formaldehyde was one of the intermediates. As expected, at a higher temperature (450°C.) more carbon dioxide (40.80 mole-%) and methylcyclopentadiene (35.0 mole-%) were obtained. Other major volatiles were carbon monoxide (7.48 mole-%), water (4.32 mole-%), and cyclopentadiene (4.12 mole-%). The phenolic components (Table V) were similar to those obtained from the amine-cured resin. These results suggest that the major decomposition scheme could be the *cis*-elimination of the ester as shown previously. Other schemes related to the evolution of carbon monoxide might be plausible (scheme IIA, IIB, and III).

D.E.R. 331 Resin (Cured with MNA). In general, the MNA-cured D.E.R. 331 resin (Table IV) decomposed to yield similar products obtained from the decomposition of the MNA-cured D.E.N. 438 resin. At 350°C., the major volatile components were methylcyclopentadiene (38.90 mole-%), carbon dioxide (23.40 mole-%), water (19.00 mole-%), carbon monoxide (5.16 mole-%), and hydrogen (4.21 mole-%). At 450°C., the major volatiles were methylcyclopentadiene (43.20 mole-%), carbon dioxide (30.50 mole-%), carbon monoxide (5.38 mole-%), and cyclopentadiene (5.41 mole-%). The phenolic compounds (Table VI) obtained from the decomposition at 475°C. were similar to those obtained from the uncured resin pyrolyzed under the same conditions.

DEGRADATION SCHEMES OF EPOXIDES

The fact that the degradation products of epoxy resins were mostly phenolic compounds was further confirmed by carrying out the direct pyrolysis in the vapor-phase chromatography unit. A pyrogram for D.E.R. 669 resin and D.E.N. 438 resin is shown in Figure 8. This result and the previous pyrolysis results do not support the scheme proposed by Neiman as shown in Figure 1. It is possible that there might be a small fraction of the complex degradation which could follow Neiman's scheme, but the main course of degradation as demonstrated in the previous sections may follow several concurrent, competitive schemes proposed in this section.

The basis of the proposed scheme is the ether cleavage reactions occurring in the simple organic compounds. In 1929, Hurd[24] summarized in his book, *The Pyrolysis of Carbon Compounds*, about the cleavage of ethers as follows: (*1*) aliphatic ethers, R—CH_2—O—CH_2—R, etc., from which aldehydes and hydrocarbons are formed; (*2*) aromatic ethers, Ar—O—R, or Ar—O—Ar, from which phenols are produced; (*3*) unsaturated ethers, which rearrange on heating (these especially possess the vinyl type of unsaturation or the allyl type of unsaturation); (*4*) complex ethers, from which alcohols are frequently eliminated by heat.

Based on the principles of the simple ether cleavage and the results obtained in the previous sections, we would propose the following schemes for the thermal degradation of epoxides.

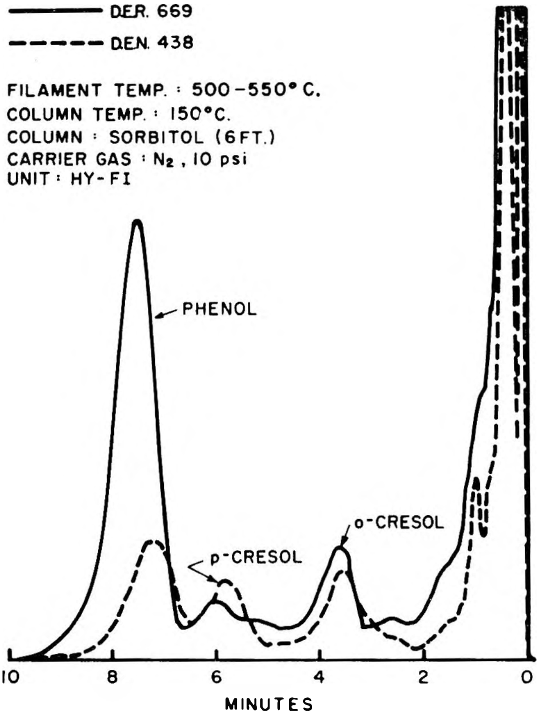

Fig. 8. Pyrogram of epoxy resins.

Scheme I

The residual epoxide (Fig. 9) isomerizes into an aldehyde. Then, the volatiles in the pyrolyzed products should contain propionaldehyde and/or ethane and carbon monoxide. This scheme is similar to the one proposed by Anderson.[20]

Scheme II

The residual epoxide undergoes etherification or polymerization to form 1,3-diethers; the ether may cleave according to the type of groups attached to the ether oxygens. There are three possible routes.

Scheme IIA. When one of the two groups (Fig. 10) attached to the ether oxygens is phenyl, the cleavage of the ether may take place in two different routes. The first route is the cleavage of the unsaturated ether between one of the ether oxygens and the R group (IIA).

$$\mathrm{Ar{-}O{-}CH{=}CH{-}CH_2{-}O\,\vdots\,{-}R}$$

Thus, the major volatile should be carbon monoxide. At the same time, the vinyl phenyl ether obtained from the cleavage may undergo Claisen-type rearrangement to yield vinylphenol which may further readily polymerize or crosslink.

Scheme IIB. The second route (Fig. 11) is the cleavage of the unsaturated ether between the phenoxy oxygen and the allylic carbon.

$$\mathrm{Ar{-}O{-}}\vdots\mathrm{{-}CH_2{-}CH{=}CH{-}O{-}R}$$

For this case, the major volatile products should be acrolein and/or ethylene and carbon monoxide.

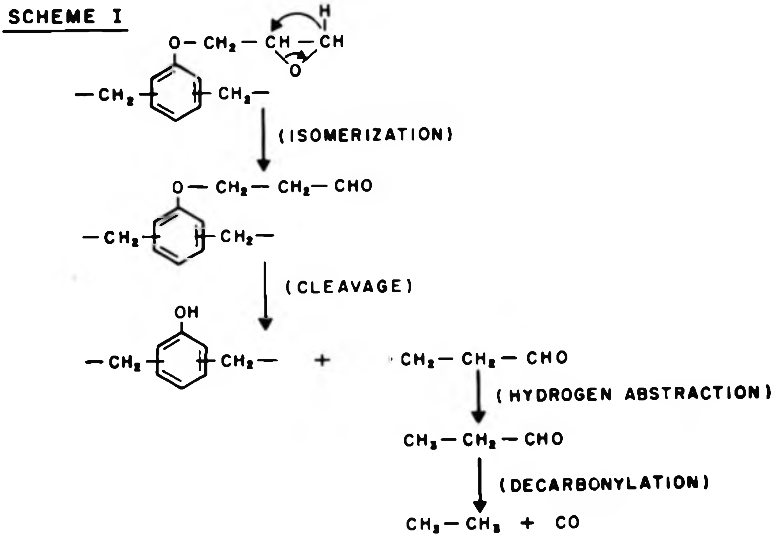

Fig. 9. Degradation of epoxide, scheme I.

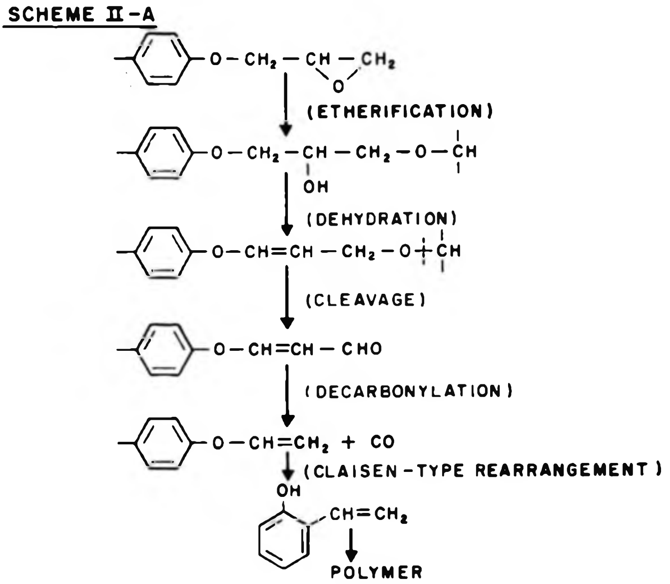

Fig. 10. Degradation of epoxide, scheme IIA.

Scheme IIC. When both of the two groups (Fig. 12) attached to ether oxygens are phenyl, the result of the cleavage could yield allylphenols and for isopropenylphenols via the Claisen rearrangement. These phenols may further polymerize or decompose. Therefore, in the volatile mixtures,

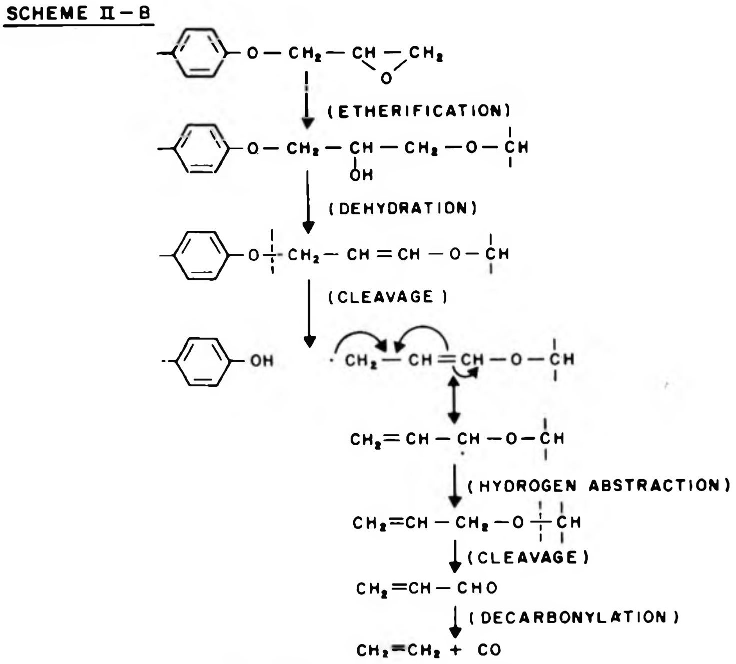

Fig. 11. Degradation of epoxide, scheme IIB.

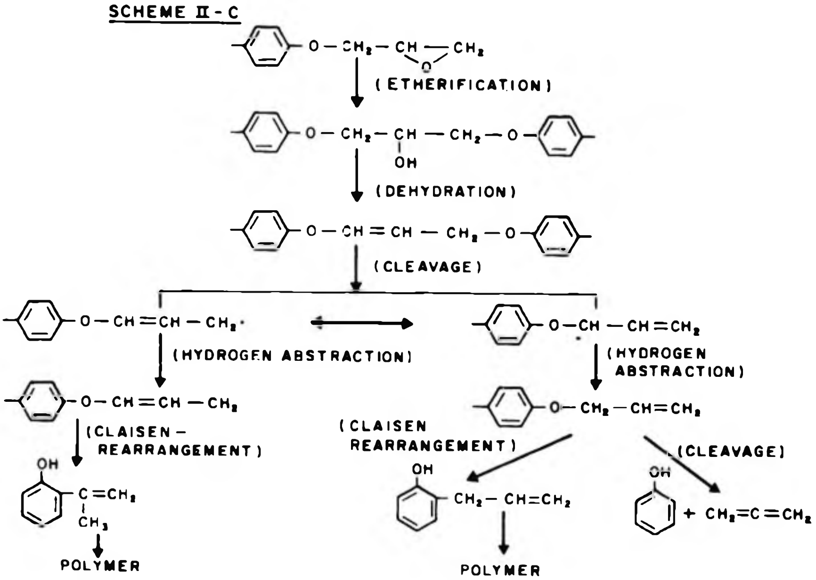

Fig. 12. Degradation of epoxide, scheme IIC.

a small amount of allene should be detected. Allene may also dimerize and cyclize into methylcyclopentadiene. This could be one of the major sources of methylcyclopentadiene.

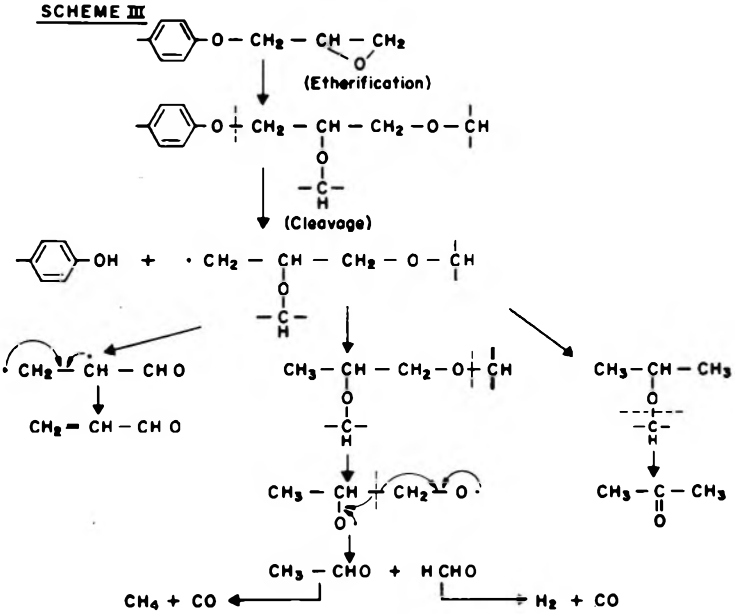

Fig. 13. Degradation of epoxide, scheme III.

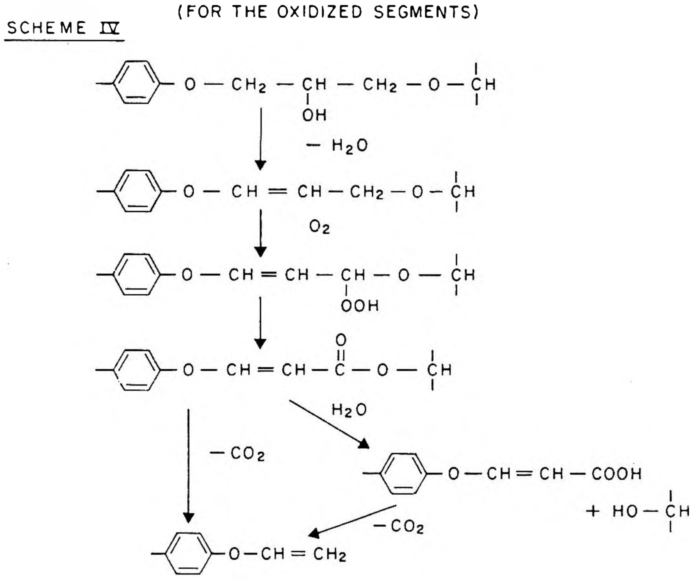

Fig. 14. Degradation of epoxide, scheme IV.

Scheme III

The residual epoxide (Fig. 13) may form a 1,2,3-triether which is the most predominant species in the cured epoxy resins.

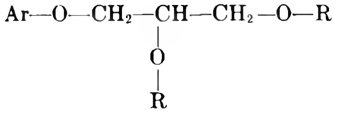

$$\mathrm{Ar{-}O{-}CH_2{-}\underset{\underset{\displaystyle R}{|}}{\underset{\displaystyle O}{\underset{|}{CH}}}{-}CH_2{-}O{-}R}$$

The result of the cleavage should yield acrolein, acetaldehyde, formaldehyde, acetone, or propylene in the volatiles. These compounds may further decompose to yield methane, ethylene, or hydrogen.

Scheme IV

If the epoxy resin (Fig. 14) is oxidized[25] during curing, the oxidized segments may decompose differently to yield an unsaturated acid and/or vinylphenols. Then, carbon dioxide should be the main constituent in the volatile mixtures.

CONCLUSIONS

The thermal degradation of epoxy resins was found to proceed along several concurrent schemes. During curing the opening of the epoxide groups was shown to be one of the major exothermic reactions. Presumably, the isomerization of the epoxide group could also be one of the exothermic reactions, but the experimental results do not support the isomerization and the cleavage scheme proposed by Neiman and coworkers. The isomerization scheme proposed by Anderson seemed to be one of the degradation schemes. Several additional schemes were proposed for the degradation of epoxides and the possible routes for the cleavage of the unsaturated ether formed after the subsequent dehydration of the cured resins.

The author gratefully acknowledges Messrs. J. G. Cobler and E. T. Wagonner of the Polymer Analysis Laboratory for the differential and the thermogravimetric analyses, Mrs. W. Dilling and Mr. L. B. Westover of the Chemical Physics Research Laboratory for the mass spectrometric analysis of the pyrolyzed products, Mr. E. O. Camehl of the Analytical Laboratory for the mass spectrometric analysis of the low-boiling volatiles.

References

1. Heron, G. F., *High Temperature Resistance and Thermal Degradation of Polymers*, Soc. Chem. Ind., Monograph 13, London, 1961, pp. 475-498.

2. Levine, H. H., *S.P.E. Technical Papers*, Vol. 7, 17th ANTEC, Washington, D. C., 1961.

3. Jeffrey, K. D., *Brit. Plastics*, **36,** 188 (April 1963).

4. Friedman, H. L., paper presented at 145th American Chemical Society Meeting, New York, Sept. 1963; *Preprints Div. Poly. Chem.*, 662 (Sept. 1963).

5. Lee, L. H., paper presented at 142nd American Chemical Society, Atlantic City, N. J., Sept. 1962; *Preprints Div. Org. Coatings Plastics*, **22,** No. 2, 131 (Sept. 1962); *J. Polymer Sci.*, **A2,** 2859 (1964).

6. Anderson, H. C., paper presented at 136th American Chemical Society Meeting, Atlantic City, N. J., Sept. 1959; *Preprints Div. Paint, Plastics Printing Ink Chem.*, **19,** No. 2, 104 (Sept. 1959).

7. Neiman, M. B., B. M. Kovarskaya, A. S. Strizhkova, I. I. Levanotoskaya, and M. S. Akutin, *Dokl. Akad. Sci. SSSR*, **135,** 1419 (1960).

8. Anderson, H. C., *Polymer*, **2,** 451 (1961).

9. Anderson, H. C., *Kolloid-Z.*, **184,** 26 (1962).

10. Madorsky, S. L., and S. Straus, *Mod. Plastics*, **36,** No. 8, 134 (Feb. 1961).

11. Park, W. R. R., and J. Blount, Jr., paper presented at 130th American Chemical Society Meeting, Atlantic City, N. J., Sept. 1956; *Preprints Div. Paint, Plastics Printing Ink Chem.*, **16,** No. 2, 56 (Sept. 1956).

12. Technical Bulletin: *D.E.N. 438 Dow Epoxy Novolac Resin*, Plastics Department, The Dow Chemical Company.

13. Technical Bulletin: *Dow Liquid Epoxy Resins*, Plastics Department, The Dow Chemical Company.

14. Lenz, R. W., C. E. Handlovits, and H. A. Smith, *J. Polymer Sci.*, **58,** 351 (1962).

15. Cobler, J. G., D. L. Miller, and E. P. Samsel, "Thermal Stability of Polymers," unpublished (1960).

16. Cobler, J. G., and D. L. Miller, paper presented to Div. Polymer Chem., 136th American Chemical Society Meeting, Atlantic City, N. J., Sept. 1959.

17. Wynstra, J., A. G. Farnham, N. H. Reinking, and J. S. Fry, paper presented at 136th American Chemical Society Meeting, Atlantic City, N. J., Sept. 1959; *Preprints, Div. Paint, Plastics Printing Ink Chem.*, **19,** No. 2 (Sept. 1959).

18. Delmonte, J., *Chem. Eng. Progr.*, **58,** No. 10, 51 (1962).

19. Belanger, W. J., and S. A. Schulte, *Mod. Plastics*, **37,** No. 3, 154 (1959).

20. Anderson, H. C., *J. Appl. Polymer Sci.*, **6,** 484 (1962).

21. Damusis, A., paper presented at 136th American Chemical Society Meeting, Atlantic City, N. J., Sept. 1956; *Preprints Div. Paint, Plastics Printing Ink Chem.*, **16,** No. 2, 217 (Sept. 1956).

22. Lee, H., and K. Neville, *Epoxy Resins*, McGraw-Hill, New York, 1957.

23. Fisch, W., and W. Hofmann, paper presented at 136th American Chemical Society Meetings, Atlantic City, N. J., Sept. 1959; *Preprints Div. Paint, Plastics Printing Ink Chem.*, **19,** No. 2 (Sept. 1959).

24. Hurd, C. D., *The Pyrolysis of Carbon Compounds*, ACS Monograph Series, 1929, p. 198.

25. Shelton, J. R., and H. Winn, *Ind. Eng. Chem.*, **38,** 71 (1946).

Résumé

On a étudié la dégradation thermique des résines d'époxyde non-vulcanisées et vulcanisées. En employant l'analyse thermogravimétrique, la stabilité thermique des résines époxydes vulcanisées, D.E.N. 438 et D.E.R. 331, est comparée avec celle du polycarbonate et du polysulfure de phénylène. On a pyrolysé ces résines, y compris la résine novolaque et la D.E.R. 669, et on a déterminé les produits volatils au moyen d'un spectromètre de masse. Les résultats expérimentaux montrent que la plupart des produits volatils sont des composés phénoliques. Ainsi, ces résultats ne sont pas en accord avec le schéma de dégradation proposé par Neiman et ses collaborateurs. Plusieurs schémas de dégradation d'époxydes sont proposés sur la base de principes de rupture des éthers ordinaires et sur la base des produits obtenus par l'étude de la pyrolyse.

Zusammenfassung

Der thermische Abbau nicht gehärteter und gehärteter Epoxyharze wurde untersucht. Mittels der thermogravimetrischen Analyse wurde die thermische Stabilität der gehärteten Epoxyharze, D.E.N. 438 und D.E.R. 331 mit derjenigen von Polycarbonat und Polyphenylensulfid verglichen. Die Harze, darunter auch Novolakharz und D.E.R.

669-Harze wurden pyrolysiert und die flüchtigen Produkte mit einem Massenspektrometer bestimmt. Die Versuchsergebnisse liessen die phenolischen Verbindungen als flüchtige Hauptprodukte erkennen. Die vorliegenden Ergebnisse liefern keine Stütze für das von Neiman und Mitarbeitern vorgeschlagene Abbauschema. Es werden einige Abbauschemen für Epoxyde vorgeschlagen, welche auf dem Prinzip der Spaltung einfacher Äther und den bei der Pyrolyseuntersuchung erhaltenen Produkten beruhen.

Received April 24, 1964
Revised June 25, 1964

JOURNAL OF POLYMER SCIENCE: PART A VOL. 3, PP. 883–894 (1965)

Diffusion-Controlled Termination in Free Radical Polymerizations[*]

R. D. BURKHART, *University of Oregon, Eugene, Oregon*[†]

Synopsis

The theory of Kuhn and Kuhn for the diffusion of polymer chain ends has been applied to the termination mechanism for free radical polymerizations, proposed by Benson and North. By using the dimensions for a Gaussian chain, an expression for this diffusion-controlled termination rate constant in terms of solvent viscosity, polymer chain flexibility, and chain length has been derived. The theory predicts that the termination rate constant is inversely proportional to solvent viscosity for flexible polymer chains and independent of solvent viscosity for very stiff polymer chains. Several previously reported effects of solvent viscosity on the termination rate constant may be explained with the present theory. The effect of polymer chain length on the termination rate constant depends upon the range of chain lengths considered and upon the relative chain stiffness. The necessity of taking into account the frequency distribution of radicals which exists during polymerization is discussed. Calculated values of the termination rate constant have been carried out with the use of values for the various parameters which are believed to be typical of vinyl polymers in solution. These calculated values are in general agreement with those which are usually obtained experimentally.

INTRODUCTION

A great deal of experimental evidence is being accumulated in support of a mechanism of diffusion control for the bimolecular (radical coupling or disproportionation) termination step in certain free radical polymerizations. Notably, the studies of Nicholson and Norrish,[1] Benson and North,[2] and North and Reed[3,4] all indicate that for several monomers the termination rate constant is inversely proportional to solvent viscosity even at very low conversions. It has long been thought, of course, that the familiar Trommsdorff effect[5] which is observed only at relatively high conversions was due to a decreased mobility of polymer chain radicals with increasing viscosity of the medium.

In a theoretical study of this problem, Benson and North[6] visualized the termination reaction as a two-step process:

$$\mathrm{V} + \mathrm{W} \underset{k_2}{\overset{k_1}{\rightleftarrows}} [\mathrm{V}\text{------}\mathrm{W}] \tag{1}$$

---

[*] The major part of this work was carried out at Research and Development of the Chemicals Division of Union Carbide Corp., South Charleston, West Virginia.

[†] Presented in part at the 146th meeting of the American Chemical Society, Denver, Colorado, January 1964.

$$[\mathrm{V}\text{-----}\mathrm{W}] \xrightarrow{k_3} \mathrm{V{-}W} \qquad (2)$$

In step (1), two polymer chain radicals diffuse together to form a proximate pair. Once the proximate pair has been formed, the two chain radicals may diffuse apart with no termination occurring or termination may occur as shown in step (2) leading to the formation of a dead polymer molecule (two molecules in the case of disproportionation). They concluded that step (2) was the rate-controlling process, that is, diffusion of the active centers belonging to the two chain radicals. Further progress of the theory along these lines was hampered by the lack of an expression for the effective diffusion constant for the active centers of the proximate pair and an assumed form for this equation was used to complete the analysis.

Actually Kuhn and Kuhn, in a somewhat different context have considered the motion of a polymer chain end in certain specific directions.[7] In their work the concept of the inner viscosity of polymer chains was invoked in order to analyze the forces which restrict the motion of these chain ends. The use of the Kuhn and Kuhn relations is, therefore, one avenue of approach for obtaining the effective diffusion constant of active centers which are located at the ends of polymer molecules.

Utilizing the Smoluchowsky equation to obtain expressions for k_1 and k_3 and expressing the ratio k_1/k_2 as $4\pi R_{\mathrm{VW}}^3/3$, where R_{VW} is the radius of the sink into which two polymer chain radicals are diffusing, Benson and North[6] find the expression for the overall termination rate constant, k_t, to be

$$k_t = 4\pi R_{\mathrm{E}} D_{\mathrm{E}} R_{\mathrm{VW}} D_{\mathrm{VW}}/(D_{\mathrm{VW}} R_{\mathrm{VW}} + R_{\mathrm{E}} D_{\mathrm{E}}) \qquad (3)$$

where D_{VW} is the diffusion coefficient of chain radical V with respect to chain radical W, D_{E} is the effective diffusion coefficient of the active centers, and R_{E} is the distance between the active centers at termination. The rate constant k_t is defined by the expression,

$$d\,[\mathrm{V} - \mathrm{W}]/dt = k_t[\mathrm{V}][\mathrm{W}] \qquad (4)$$

We shall want to express eq. (3) in terms of the frictional forces involved and therefore need to define the following terms.

$f_{\mathrm{V}}, f_{\mathrm{W}}, \ldots$, (the subscript denoting the particular polymer chain radical to which one refers) is the frictional force acting on a diffusing polymeric species. The frictional force is that which is required to impart unit velocity to the diffusing species.

$f_{1\mathrm{V}}, f_{1\mathrm{W}}, \ldots$, is the frictional force acting at a polymer chain end as a result of the motion of a fraction of the chain segments. It will be shown below that this force is related to the distance of separation of the centers of gravity of the two chain radicals involved in the proximate pair.

$f_{2\mathrm{V}}, f_{2\mathrm{W}}, \ldots$, is a force restricting chain end mobility having its source in the energy barrier to rotation about adjacent bonds in the backbone of the polymer chain radical. This force is related to the inner viscosity of the polymer chain radical and it will also be seen to depend upon the distance of separation of the centers of gravity of the proximate pair.

Following the theory of Kuhn and Kuhn we have thus decomposed the total force acting at the chain end into two subforces, f_1 and f_2. The former is dependent upon the interaction between polymer and solvent and the latter is independent of the nature of the solvent but is quite dependent upon the nature of the polymer molecule.

If we now apply Einstein's equation to the diffusion coefficients D_E and D_{VW}, eq. (3) may be rewritten as

$$k_t(x) = \frac{4\pi R_E kT}{\dfrac{f_{1V} + f_{2V}}{1 + (f_{1V} + f_{2V})/(f_{1W} + f_{2W})} + \dfrac{f_V R_E}{(1 + f_V/f_W)R_{VW}}} \tag{5}$$

where k is Boltzmann's constant, T is the absolute temperature, and x is a parameter which is related to the separation of the centers of gravity of the two chain radicals in the proximate pair. For brevity we shall symbolize the first term in the denominator of eq. (5) as γ_{12} and the second term as γ_{VW}. We see, therefore, that when diffusion of the active centers is involved in the rate-controlling process then $\gamma_{12} \gg \gamma_{VW}$ and we shall restrict further considerations to this limiting case.

In their analysis of this limiting case Benson and North[6] derived expressions in which were included two parameters, a probability factor which is related to steric hindrance and chain entanglements, and a characteristic segmental length the physical origin of which is not clear. It is the aim of the present work to obtain an expression for the termination rate constant in terms of parameters whose numerical values can be obtained by a study of the solution properties of polymer molecules and, hopefully, to obtain further insight into the complexities of these diffusion-controlled processes.

THEORY

Development of a Model for the Proximate Pair

The model for a proximate pair to be used here is that of two polymer chains, V and W, whose centers of gravity are at such a distance that it is possible for the reactive ends to approach each other to within a distance R_E which is about 4 A. It is necessary to be more precise, however, by defining the distance, R, between the centers of gravity of the two chains when they are in proximate pair position. One recognizes that termination occurs at more than just one specific value of R and so we use the general definition

$$R^2 = x(\overline{h_V^2} + \overline{h_W^2}) \tag{6}$$

where $\overline{h_V^2}$ and $\overline{h_W^2}$ are the mean-square end-to-end distances of chain radicals V and W, respectively. It will become apparent below that x is a variable which has physical significance only for $0 \leqslant x \leqslant 2/3$.

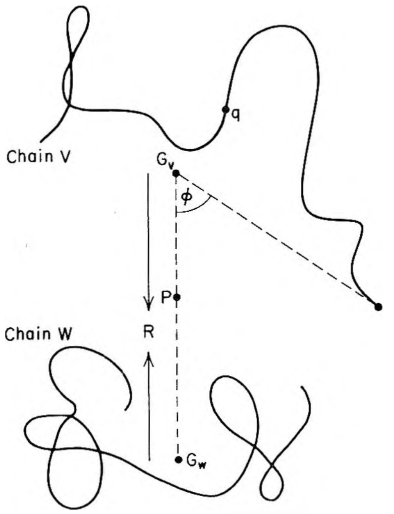

Fig. 1. A model for the proximate pair. The point q is a chain located reference point and p is a reference point for the pair of radicals.

We now must establish a convenient reference point for the proximate pair. Since we assume that the unpaired electron (i.e., the active center) lies at one end of the polymer molecule, then we must find the diffusion coefficient for one end of each of the chain radicals with respect to the reference point. The sum of these two diffusion coefficients will then yield the desired expression for D_E of eq. (3). Let us choose for this reference point the point p the square of whose distance from the center of gravity of chain V is $x\overline{h_V^2}$ and the square of whose distance from the center of gravity of chain W is $x\overline{h_W^2}$ and which lies along a line joining the centers of gravity of the two chains.

It will be recognized that at any chosen time the reference point will not necessarily coincide with a point on either of the polymer molecules. On the other hand, the relations derived by Kuhn and Kuhn give the diffusion coefficient of a chain end with respect to some point fixed on the polymer molecule. We must demonstrate, therefore, that the diffusion coefficient of a chain end with respect to the point p is equivalent to the diffusion coefficient of the chain end with respect to a point on chain V (or chain W) which is a mean square distance of $F(x)\overline{h_V^2}$ [or $F(x)\overline{h_W^2}$] from the chain end where $F(x)$ is a fractional quantity defined in eq. (7). Let us imagine that an infinite number of random flights may be generated from the end of the polymer chain containing the active center and that each flight not only contains the same number of steps but also each step is the same length. Suppose that one of these flights corresponds to the polymer chain. The locus of points corresponding to the root-mean-square distance of each flight describes a sphere about the chain end. If each step of each flight is equivalent to the length of a statistical chain element and if the number of steps in each flight is $F(x)Z_V'$, where Z_V' is the number of statistical chain elements in chain V, then the radius of our imaginary sphere is $[F(x)\overline{h_V^2}]^{1/2}$. Therefore, one point on the surface of our sphere corresponds to the reference point p, and another point coincides with a chain element; let us call this latter point q as shown in Figure 1.

During a time τ there will occur a number of displacements of the chain end with respect to the point q resulting in a mean square displacement of $\overline{\Delta r^2}$. Since these displacements are randomly oriented it is equally likely that in time τ the mean square displacement of the chain end with respect to the point p is also $\overline{\Delta r^2}$. From the theory of random flights the diffusion coefficient D is given by $D = \overline{\Delta r^2}/6\tau$, thus the diffusion coefficient with respect to the point p is equal to the diffusion coefficient with respect to the point q. In order to retain a one-to-one correspondence between the diffusion coefficients with respect to the points p and q the quantity $F(x)$ must be restricted in such a way that $0 \leqslant F(x) \leqslant 1$.

We now must find an expression for the mean square distance between the reference point p and the chain end; let us call this distance $\overline{g_V^2}$. If the most probable positions of the reference point and the chain end are distributed spherically about the center of gravity of the polymer chain then

$$\begin{aligned}\overline{g_V^2} &= x\overline{h_V^2} + \overline{h_V^2}/3 - \langle(2\overline{h_V^2}\sqrt{x/3})\cos\phi\rangle_{\text{avg. over all}\,\phi} \\ &= F(x)\overline{h_V^2} \qquad (7)\end{aligned}$$

where $F(x) = (3x + 1)/3$ and ϕ is the angle between the vectors joining the center of gravity with the point p and the chain end. The requirement that $0 \leqslant x \leqslant {}^2/_3$ is now clear.

Forces Involved in the Brownian Motion of the Ends of a Polymer Chain

Let us focus attention on just one of the chain radicals for the moment, say chain radical V. According to the arguments of Kuhn and Kuhn,[7] the diffusive motion of a polymer chain end with respect to some given point on the molecule involves the concentration at the chain end of one-half of the mass of the molecule lying between the given point and the end of the chain. If the contour length of chain radical V is L_V, the viscosity of the solvent is η_0, and if the solvent is flowing past the stationary chain with a velocity u, then according to Kuhn and Kuhn the effective force K_1 exerted at the chain end is

$$K_1 = -\lambda\eta_0 uF(x)L_V/2 \qquad (8)$$

where $F(x)$ is the fraction of chain elements lying between the given reference point and the chain end and λ is the shape resistance factor.[8,9] This equation assumes that the length and mass of all chain elements is the same. If we now suppose that the chain end is moving with a root-mean-square velocity $\dot{s}$, then the work performed when the chain end moves a distance ds is

$$dW_1 = \lambda\eta_0\dot{s}F(x)L_V ds/2 \qquad (9)$$

and the force required to achieve the velocity $\dot{s}$ is

$$dW_1/ds = \lambda \eta_0 \dot{s} F(x) L_V/2 \tag{10}$$

When $\dot{s}$ is equal to unity, this force satisfies the definition for f_1 given above.

In order to find f_2 one must consider the force which opposes any rapid change in the end-to-end distance of the polymer molecule. This force is associated with what Kuhn and Kuhn called the inner viscosity. This concept has been discussed extensively,[10,11] and no repetition is necessary here.

If κ_2 is the component of force arising from the inner viscosity and is directed along the end-to-end vector of the polymer chain, then according to Kuhn and Kuhn,

$$\kappa_2 = -B\dot{h} \tag{11}$$

where $\dot{h}$ is the time rate of change of the end-to-end distance of the chain and B is a constant for a given polymer and a given molecular weight. If we consider the motion of the polymer chain end in three dimensions and suppose that at some time it is moving with a velocity $\dot{s}$, then the force K_2 acting at the chain end as a result of the inner viscosity is

$$K_2 = -B'\dot{s} \tag{12}$$

We shall attempt to relate B' to B of eq. (11).

Kuhn and Kuhn derived the expression

$$\Delta r^2 = \sqrt{2} L_V C \tau \tag{13}$$

for the mean square displacement of one chain end with respect to the opposite end in a solvent of vanishingly small viscosity in a time τ, where C is a collection of constants including the molecular weight of the monomer units and the energy barrier to rotation about adjacent atoms in the backbone of the polymer chain. Since $F(x)$ can be viewed as the fraction of statistical chain elements between the chain end and a point $F(x)L_V$ distant from the chain end as measured along the contour of the chain, then from the above arguments and eq. (13)

$$\Delta \overline{r^2} = \sqrt{2} F(x) L_V C \tau \tag{14}$$

is the mean square displacement of the chain end with respect to the reference point in a solvent of vanishingly small viscosity. Using the random flight expression for the diffusion coefficient we have

$$D' = \sqrt{2} F(x) L_V C/6 \tag{15}$$

D' can also be written in terms of the Einstein equation as

$$D' = u'kT \tag{16}$$

where u' is the velocity of the diffusing species under a force of 1 dyne. Thus we have

$$\dot{s} = u'K_2 \tag{17}$$

and, combining eqs. (15), (16), and (17) we obtain,

$$K_2 = 6kT\dot{s}/\sqrt{2}F(x)L_{\mathrm{V}}C \tag{18}$$

Kuhn and Kuhn find the analogous equation for κ_2, i.e.,

$$\kappa_2 = 6kT\dot{h}/\sqrt{2}L_VC \tag{19}$$

From eqs. (11), (12), (18), and (19) we find

$$B_{\mathrm{V}}' = B_{\mathrm{V}}/F(x) \tag{20}$$

The work performed per second, dW_2/dt, as a result of the inner viscosity when the chain end is moving with a velocity $\dot{s}$ relative to the point p is

$$dW_2/dt = B_{\mathrm{V}}\dot{s}^2/F(x) \tag{21}$$

and the force necessary to achieve the velocity $\dot{s}$ is then

$$dW_2/ds = B_{\mathrm{V}}\dot{s}/F(x) \tag{22}$$

This force satisfies our definition for f_2 when $\dot{s}$ is unity. Thus for the limiting case $\gamma_{12} \gg \gamma_{\mathrm{VW}}$ we obtain from eqs. (5), (10), and (22), setting $\dot{s}$ equal to unity,

$$k_t(x) = 4\pi R_{\mathrm{E}}kT\left[\frac{1}{\lambda\eta_0F(x)L_{\mathrm{V}}/2 + B_{\mathrm{V}}/F(x)} + \frac{1}{\lambda\eta_0F(x)L_{\mathrm{W}}/2 + B_{\mathrm{W}}/F(x)}\right] \tag{23}$$

Equation (23) gives the rate constant for a bimolecular chain termination reaction involving two polymer chain radicals which have approached each other to within a specified distance under the assumption that the rate is controlled by the diffusion of the active centers of the two chain radicals.

The magnitude of the parameter λ, the shape resistance factor, depends upon the nature of the solvent and the polymer. In carrying out experiments with macroscopic models Kuhn and Kuhn[8] and Kuhn, Kuhn, and Silberberg[9] have found that for a Gaussian chain having a sufficiently large value of Z'

$$\lambda = 19.2/\sqrt{Z'} \tag{24}$$

where Z' is the number of statistical chain elements in the polymer chain. In the numerical calculations carried out below, eq. (24) was used without modification.

In a detailed analysis of the molecular quantities which affect the inner viscosity of polymer chains Kuhn and Kuhn[10] have found that for a chain having Z links

$$\mathrm{B} = \beta/Z \tag{25}$$

In principle, β may be calculated if the rotational barrier about the chain bonds is known.

Relations have been derived[7,10] which allow the numerical evaluation of the parameters λ and β from measurements of the viscosity and flow birefringence of polymer solutions when the polymer molecular weights are known. Cerf has also derived an expression which relates the inner viscosity to flow birefringence.[11]

DISCUSSION

The calculation of numerical values for $k_t(x)$ has been carried out by use of the values $T = 298°\text{K.}$, $R_E = 4 \times 10^{-8}$ cm., $\eta_0 = 5 \times 10^{-3}$ poise, $\beta = 2 \times 10^{-3}$ dyne-sec./cm., $L = Z \times 1.25 \times 10^{-8}$ cm., and λ as given by eq. (24). It was assumed that the two chain radicals involved in the proximate pair are identical and that $Z = Z'$. The results are presented in graphical form in Figure 2. Here log $k_t(x)$ is plotted against the parameter x for values of Z ranging from 200 to 200,000. It will be noted that all of the values of $k_t(x)$ fall within the range of termination rate constants usually found experimentally.[12]

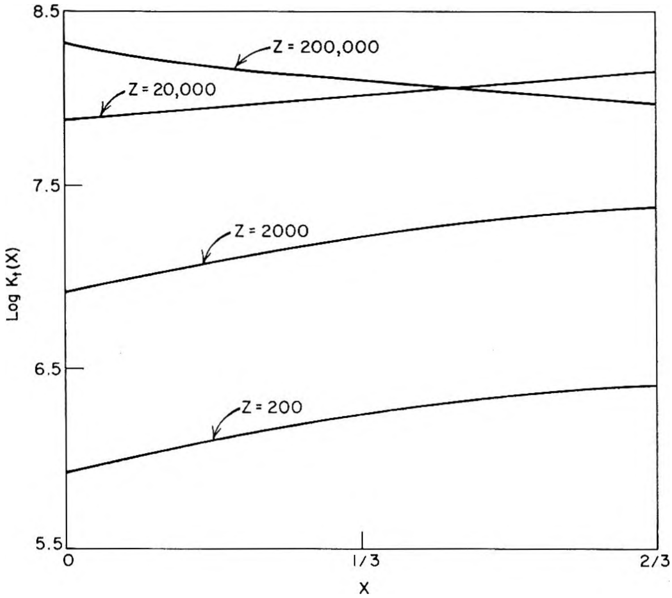

Fig. 2. Calculated values of $k_t(x)$ plotted against the parameter x for $Z = 200$, 2000, 20,000, 200,000.

It is interesting to note that, within a given molecular weight range, the calculated termination rate constants are dependent on x to only a small extent. If the polymer chains are viewed as spheres having a Gaussian distribution of chain elements,[13] eq. (23) predicts that the degree to which interpenetration of adjacent spheres occurs only slightly affects the expected termination rate constant. It will be immediately recognized that for a given monomer–polymer system not all values of x will be equally probable. The extent to which this effect must be taken into account depends upon the extent to which excluded volume effects are important, however, in the present work no attempt has been made to account for excluded volume. Using the assumption that all separations of the centers of mass of the proximate pair are equally probable, a value of k_t averaged over all values of x from zero to two-thirds may be found. Thus for the case where the two radicals of the proximate pair are identical we have

$$k_t = 3/2 \int_0^{2/3} k_t(x)dx$$
$$= (12\pi R_E kT/\lambda\eta_0 L)\ln[(9\lambda\eta_0 L + 18B)/(\lambda\eta_0 L + 18B)] \quad (26)$$

The calculations on $\bar{k}_t$ at three different values of the parameter β and at four different values of Z are presented in Table I.

TABLE I

Calculated Values of k_t from Eq. (26). Experimental Values of k_t for Styrene, Methyl Methacrylate, and Vinyl Acetate Are Also Given for Comparison

β	Z	$\bar{k}_t$, liter/mole sec.
10^{-3}	200	3.29×10^6
	2000	3.23×10^7
	20,000	1.80×10^8
	200,000	1.43×10^8
10^{-4}	200	3.27×10^7
	2000	2.58×10^8
	20,000	4.02×10^8
	200,000	1.86×10^8
10^{-5}	200	3.03×10^8
	2000	9.62×10^8
	20,000	5.70×10^8
	200,000	1.53×10^8
	Polystyrene[a]	$0.14–2.4 \times 10^7$
	Poly(methyl methacrylate)[a]	$1.2–3.2 \times 10^7$
	Poly(vinyl acetate)[a]	$0.3–2.0 \times 10^8$

[a] Data of Bamford et al.[12]

Again it is seen that the calculated values of $\bar{k}_t$ are of the correct order of magnitude. The results of Table I further show that, for any given β, there is a particular value of Z for which $\bar{k}_t$ exhibits a maximum. Also the dependence of $\bar{k}_t$ on Z seems to become less marked as β decreases. The increase in $\bar{k}_t$ at the lower range of Z means that the effects of the inner viscosity are dominant in this range. When the inner viscosity is dominant, the mobility of the chain end is controlled by the rotational energy barrier about the bonds of the chain backbone, the mobility increasing as the number of bonds increases. As the number of bonds increases, however, the effects of hydrodynamic resistance increase with f_2 eventually giving way to f_1 as the dominant factor in controlling the

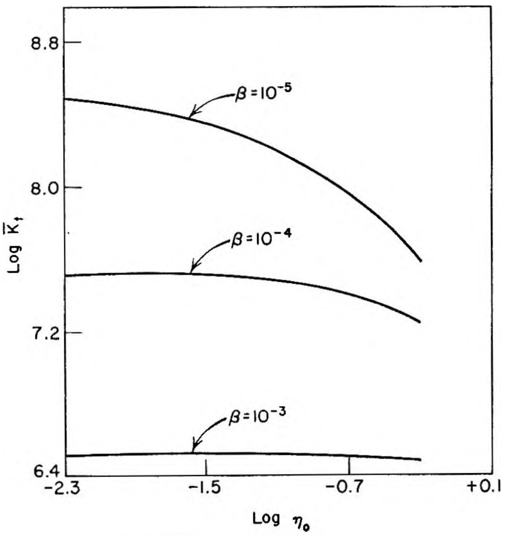

Fig. 3. Calculated values of log $\bar{k}_t$($\bar{k}_t$ in liter/mole sec.) versus log η_0(η_0 in poise) for $Z = 200$.

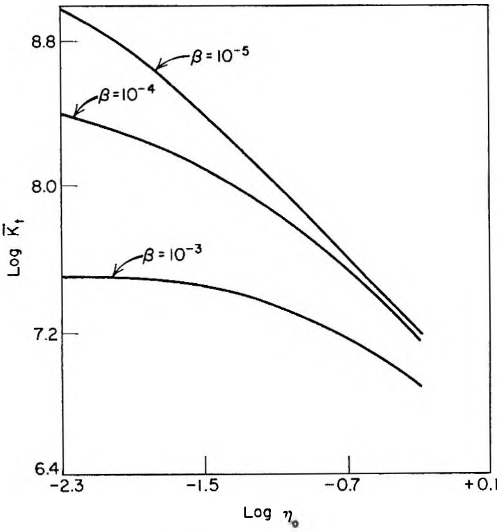

Fig. 4. Calculated values of log $\bar{k}_t$($\bar{k}_t$ in liter/mole sec.) versus log η_0(η_0 in poise) for $Z = 2000$.

mobility of the chain end. When this occurs, $\bar{k}_t$ becomes inversely proportional to the square root of the number of bonds in the backbone if λ is accurately given by eq. (24).

Equations (23) and (26) seem to predict a reasonable dependence of the termination rate constant on solvent viscosity. In Figures 3 and 4 are plotted log $\bar{k}_t$ versus log η_0 for solvent viscosities ranging from 5×10^{-3} to 0.5 poise. It will be noted that for sufficiently small β and sufficiently large Z, $\bar{k}_t$ is proportional to $1/\eta_0$ consistent with the findings of Benson and North[2] for methyl methacrylate polymerization. Further, if the inner viscosity is relatively large, the effect of solvent viscosity on $\bar{k}_t$ would begin to deviate from a strictly inverse linear relation. This behavior was recently observed by North and Reed[4] in a study of the polymerization of a series of alkyl methacrylates, and Benson and North[2] report a similar effect for butyl acrylate. Of course, if the chains are extremely stiff, i.e., if the inner viscosity is extremely large, no effect of solution viscosity on $\bar{k}_t$ is noticed, even though the reaction is diffusion-controlled. To distinguish between this situation and a chemically controlled termination would be difficult indeed.

One further point should be emphasized. The calculations of $k_t(x)$ and $\bar{k}_t$ which were carried out above assumed that identical chains were involved in the termination process. It is well known that a free radical polymerization carried out to give a number-average degree of polymerization of, say 1000, involves termination reactions which are primarily between radicals which are much shorter than the number average. Thus, the termination constant which would be predicted for a process yielding some particular number-average degree of polymerization must take account of the frequency distribution of radicals which exists during polymerization. Although the details have yet to be worked out, the following may be said. If the termination rate constant between two radicals, one of which contains i bonds while the other contains j bonds in the chain backbone, is $k_{t_{ij}}$ and if the fraction of radicals containing i and j bonds is w_i and w_j, respectively, then the rate of termination between these species is $k_{t_{ij}}w_iw_jN_0^2$ where N_0 is the total concentration of radicals present. The total rate of termination would then be $N_0^2\Sigma_i\Sigma_{j\geq i}k_{t_{ij}}w_iw_j$ and the effective termination constant is then $\Sigma_i\Sigma_{j\geq i}k_{t_{ij}}w_iw_j$.

The author would like to thank Drs. J. A. Faucher and N. L. Zutty for many helpful discussions and Prof. John D. Ferry who first suggested an examination of the work of Kuhn and Kuhn in relation to this problem.

References

1. Nicholson, A. E., and R. G. W. Norrish, *Discussions Faraday Soc.*, **22,** 104 (1956).
2. Benson, S. W., and A. M. North, *J. Am. Chem. Soc.*, **81,** 1339 (1959).
3. North, A. M., and G. A. Reed, *Trans. Faraday Soc.*, **57,** 859 (1961).
4. North, A. M., and G. A. Reed, *J. Polymer Sci.*, **A1,** 1311 (1963).
5. Trommsdorff, E., Colloquium on High Polymers, Freiburg (1944); see B.I.O.S. Report No. 363, Item 22.
6. Benson, S. W., and A. M. North, *J. Am. Chem. Soc.*, **84,** 935 (1962).
7. Kuhn, W., and H. Kuhn, *Helv. Chim. Acta,* **29,** 1533 (1945).
8. Kuhn, H., and W. Kuhn, *J. Polymer Sci.*, **9,** 1 (1952).
9. Kuhn, H., W. Kuhn, and A. Silberberg, *J. Polymer Sci.*, **14,** 193 (1954).
10. Kuhn, W., and H. Kuhn, *Helv. Chim. Acta,* **29,** 609 (1946).
11. Cerf, R., *Fortschr. Hochpolymer. Forsch.*, **1,** 382 (1959).
12. Bamford, C. H., W. A. Barb, A. D. Jenkins, and P. F. Onyon, *The Kinetics of Vinyl Polymerization by Radical Mechanisms,* Academic Press, New York, 1958, pp. 71, 92, 87.
13. Flory, P. J., *Principles of Polymer Chemistry,* Cornell Univ. Press, Ithaca, N. Y., 1953, p. 525.

Résumé

On a appliqué la théorie de Kuhn et Kuhn concernant la diffusion des fins de chaînes de polymères au mécanisme de terminaison des polymérisations par radicaux libres, proposé par Benson et North. En employant les dimensions d'une chaîne gaussienne, on a déduit une expression pour la constante de vitesse de terminaison contrôlée par diffusion faisant intervenir la viscosité du solvant, la flexibilité de la chaîne polymérique et la longueur de la chaîne. La théorie prévoit que la constante de vitesse de la terminaison est inversément proportionnelle à la viscosité du solvant pour des chaînes polymériques flexibles et est indépendante de la viscosité du solvant pour des chaînes rigides. Plusieurs effets de la viscosité du solvant sur la constante de vitesse de la terminaison décrits antérieurement peuvent être expliqués par cette théorie. L'influence de la longueur de la chaîne sur la constante de vitesse de terminaison dépend des longueurs de chaînes considérées et de la rigidité relative de la chaîne. On discute de la nécessité de tenir compte de la fréquence de distribution des radicaux existant pendant la polymérisation. Les valeurs de la constante de vitesse de terminaison sont calculées à partir des valeurs de différents paramètres caractéristiques des polymères vinyliques en solution. Ces valeurs calculées sont en accord avec celles obtenues expérimentalement.

Zusammenfassung

Die Theorie von Kuhn und Kuhn für die Diffusion von Polymerkettenenden wurde auf den von Benson und North vorgeschlagenen Abbruchmechanismus bei der radikalischen Polymerisation angewendet. Unter Benützung der Dimensionen einer Gauss'schen Kette wurde ein Ausdruck für diese diffusionskontrollierte Abbruchsgeschwindigkeitskonstante als Funktion der Lösungsmittelviskosität, der Polymerkettenflexibilität und der Kettenlänge abgeleitet. Die Theorie liefert eine umgekehrte Proportionalität der Abbruchsgeschwindigkeitskonstanten zur Lösungsmittelviskosität für flexible Polymerketten und eine Unabhängigkeit von der Lösungsmittelviskosität für sehr steife Polymerketten. Einige schon früher gefundene Effekte der Lösungsmittelviskosität auf die Abbruchsgeschwindigkeitskonstante können mit der vorliegenden Theorie erklärt werden. Der Einfluss der kettenlänge des Polymeren auf die Abbruchsgeschwindigkeitskonstante hängt vom betrachteten Kettenlängenbereich und von der relativen Kettensteifigkeit ab. Die Notwendigkeit, die Häufigkeitsverteilung der Radikale während der Polymerisation in Betracht zu ziehen, wird diskutiert. Unter Verwendung für Vinylpolymere in Lösung typisch scheinender Werte der verschiedenen Parameter berechnete Werte der Abbruchsgeschwindigkeitskonstanten werden angegeben. Diese berechneten Werte stimmen im allgemeinen mit den üblicherweise experimentell erhaltenen überein.

Received June 8, 1964
Revised July 23, 1964

JOURNAL OF POLYMER SCIENCE: PART A VOL. 3, PP. 895–905 (1965)

Coordinated Polymerization of the Bicyclo-[2.2.1]-heptene-2 Ring System (Norbornene) in Polar Media

FRANCIS W. MICHELOTTI and WILLIAM P. KEAVENEY, *Interchemical Corporation, Central Research Laboratories, Clifton, New Jersey*

Synopsis

Norbornene and a derivative have been polymerized to high molecular weight materials by use of the hydrated trichlorides of ruthenium, osmium, and iridium in alcoholic solvents. Structural studies on these polymers indicate that a major portion of the polymer repeating unit consists of cyclopentane rings linked in *cis*-1,3 configuration with a predominance of *trans* double bonds.

INTRODUCTION

The polymerization of butadiene in polar solvents by means of Rh^{3+} and related transition metal salts has recently been reported.[1,2] Depending on the catalyst system employed, broad steric control from high 1,4-*cis*- to high 1,4-*trans*-polybutadiene was described. This paper reports a predominantly stereospecific polymerization of the bicyclo-[2.2.1]-heptene-2 ring system by use of the hydrated trichlorides of ruthenium, osmium, and iridium as catalysts in refluxing Synasol (special denatured anhydrous alcohol, Union Carbide), anhydrous ethyl alcohol or 95% ethanol to high molecular weight polymers in good conversions.

DISCUSSION AND RESULTS

By use of Ziegler-type catalysts derived from 100% excess lithium aluminum tetraheptyl over titanium tetrachloride, Truett et al.[3,4] first polymerized norbornene (Ia) to a crystalline high melting polymer in about 31% conversion. An inherent viscosity of 0.66 was reported for this type of polymer when measured in a 0.1% solution in α-chloronaphthalene at 125°C. Characterization of this material indicated the presence of a repeating unit composed of cyclopentane rings linked in a *cis*-1,3 configuration with *trans* double bonds (II, X = H) as the major constituent.

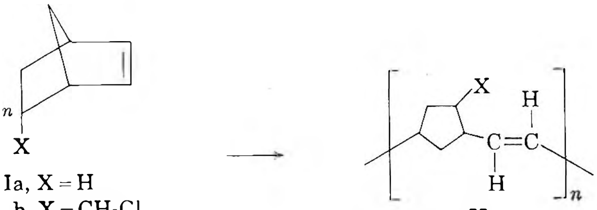

Ia, X = H
b, X = CH_2Cl
c, X = CN

II

TABLE I

Catalyst	Monomer	Polymer softening range, °C.[a]	Polymerization temp., °C.	Time	Conversion, %[b]
Ru^{3+}	Ia	72–90	80	6.5 hr.	60
Os^{3+}	Ia	58–90	80	4 hr.	55
Ir^{3+}	Ia	90–115	80	7 min.	73
Ir^{3+}	Ib	45–70	80	4.5 hr.	69
Ir^{3+}	Ia	90–115	24	48 hr.	53

[a] Determined on a Fisher-Johns melting point apparatus.
[b] Based on analytically pure polymer.

In our study, it has been found that Ia and Ib can be polymerized to a similar polymeric structure in refluxing ethanolic solvents containing catalytic quantities (2% by weight based on monomer concentration) of the hydrated trichlorides of Ru^{3+}, Os^{3+}, and Ir^{3+}. The solvent/monomer ratios were in all cases 4/1. The polymerizations, though initially homogeneous, became heterogeneous as the reactions progressed as a result of polymer insolubility. The rates of polymerization were found to be markedly dependent on the catalyst and temperature employed. These and related data are summarized in Table I.

From Table I, it is seen that Ru^{3+} is the most sluggish and Ir^{3+}, the most active catalyst for the polymerization of Ia, Os^{3+} being of intermediate activity. Because of the marked reactivity of the Ir^{3+} catalyst, it was also possible to polymerize Ia at room temperature. Characterization of the polymers was based upon elementary analysis, infrared and nuclear magnetic resonance spectroscopy, ozonolysis, bromination, and intrinsic viscosity measurements. An x-ray diffraction pattern of the polymer II (X = H) prepared by ruthenium catalysis indicated that this material was essentially amorphous. Ozonolysis of this polymer resulted in the isolation of only *cis*-1,3-cyclopentane dicarboxylic acid, characterized as the di-*p*-bromophenacyl ester.

The infrared spectra of these polymers have been reproduced in Figures 1–4. The common spectral features are the strong to moderate absorption bands at 2900 and 2840 cm.$^{-1}$ and the moderate to weak absorptions at 1440 and 1460 cm.$^{-1}$, indicative of C–H and CH_2 deformations. The outstanding characteristic of these spectra is the band at 963 cm.$^{-1}$, indicative of olefinic C–H deformations such as found in *trans* olefinic structures.[3] There are also present broader (weaker) bands at 742 cm.$^{-1}$, of moderate intensity in the polymer prepared by Os^{3+} catalysis, attributable to C–H olefinic deformations found in *cis* olefinic compounds.[5] Bromination of these polymers according to the procedure described by Truett[3] resulted in the complete disappearance of absorption at 963 and 742 cm.$^{-1}$. It is noteworthy that the spectrum of the polymer (not shown) prepared by Ir^{3+} catalysis at room temperature did not indicate any

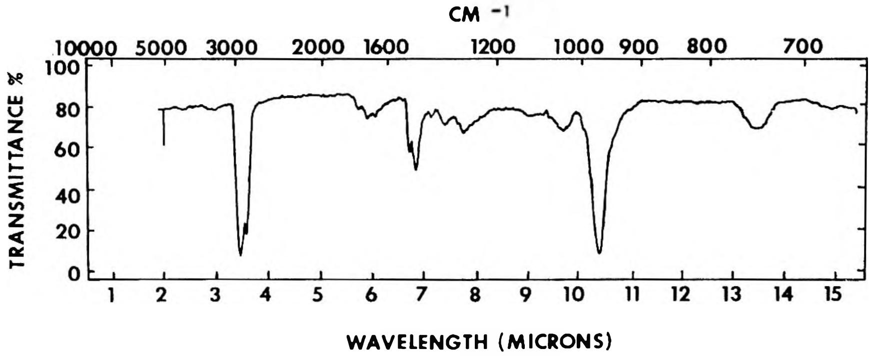

Fig. 1. Infrared spectrum of polynorbornene, Ru^{3+}-catalyzed.

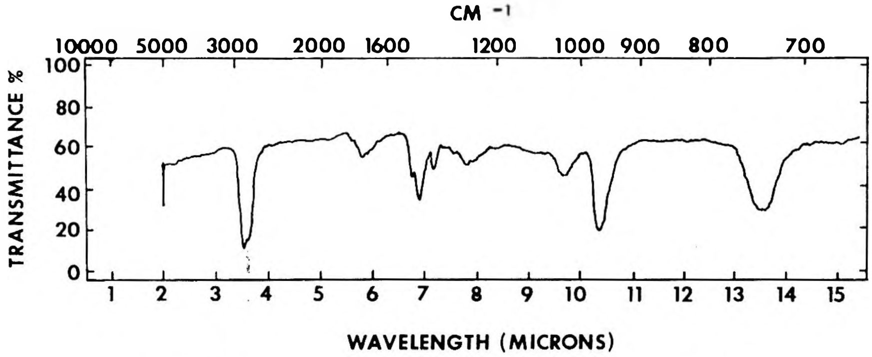

Fig. 2. Infrared spectrum of polynorbornene, Os^{3+}-catalyzed.

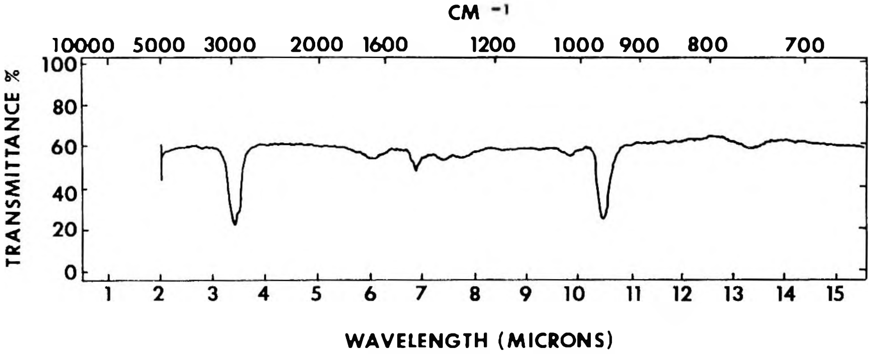

Fig. 3. Infrared spectrum of polynorbornene, Ir^{3+}-catalyzed.

increase in the *trans* absorption band and concomitant rise in softening range (Table I) as one might have expected from a drop in polymerization temperature. The spectrum of the polymer prepared by Ru^{3+} catalysis (Fig. 1) is very similar to that reported by Truett[3] for the polymer obtained from Ia using excess lithium aluminum tetraheptyl over titanium tetrachloride. However, the spectrum of the latter polymer showed no absorption in the *cis*-C-H olefinic region. These data may explain the relatively low softening ranges (Table I) and lack of crystallinity of our polymers in contrast to a polymer sample prepared with the Ziegler-type catalyst which was reported to have a melting point of 202°C. and 20% crystallinity was determined by x-ray diffraction. The polymer prepared by Os^{3+} catalysis (lowest softening range) apparently contained the largest fraction of *cis* double bonds (Fig. 2) while polynorbornene prepared by Ir^{3+} catalysis (highest softening range) contained the least *cis* absorption.

The NMR spectra of the polymer prepared by Ru^{3+} catalysis were determined at 60 Mcycle/sec. (70°C.) and at 100 Mcycle/sec. (30°C.), and have been reproduced in Figures 5 and 6, respectively. For comparative purposes, the spectrum (60 Mcycle/sec. 70°C.) of the polymer prepared by Os^{3+} catalysis has also been reproduced (Fig. 7). All spectra were determined in CCl_4 as solvent with tetramethylsilane (TMS) as internal standard. The spectra appear to be in general agreement with the proposed structure II (X = H). They exhibit a quartet at $\delta = 5.3$ assigned to the chemically equivalent olefinic protons with a 5-cycle coupling to the α-allylic protons and a smaller coupling through the double bond to the other allylic protons on the β-carbon atom. Though the signal/noise ratio is poor so that an unequivocal assignment is not possible, a small satellite peak indicative of *trans* olefinic protons at about 14 cycles downfield in the 60 Mcycle spectrum of the polymer prepared by Ru^{3+} catalysis appears to be present. The 100 Mcycle spectrum of the same material also shows satellite peaks just upfield from the quartet which have been assigned to the presence of *cis* olefinic protons in the polymer. The NMR spectrum of the polymer prepared by Os^{3+} catalysis (the infrared spectrum of which indicated increased *cis* content) clearly shows increased absorption in this region. The complex broad absorptions between $\delta = 2$–3 and $\delta = 0.7$–2 have been assigned to the allylic and ring protons, respectively.

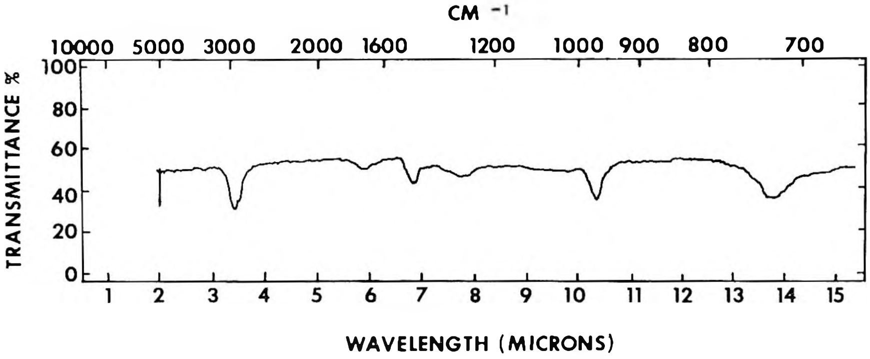

Fig. 4. Infrared spectrum of poly-2-chloromethyl-5-norbornene, Ir^{3+}-catalyzed.

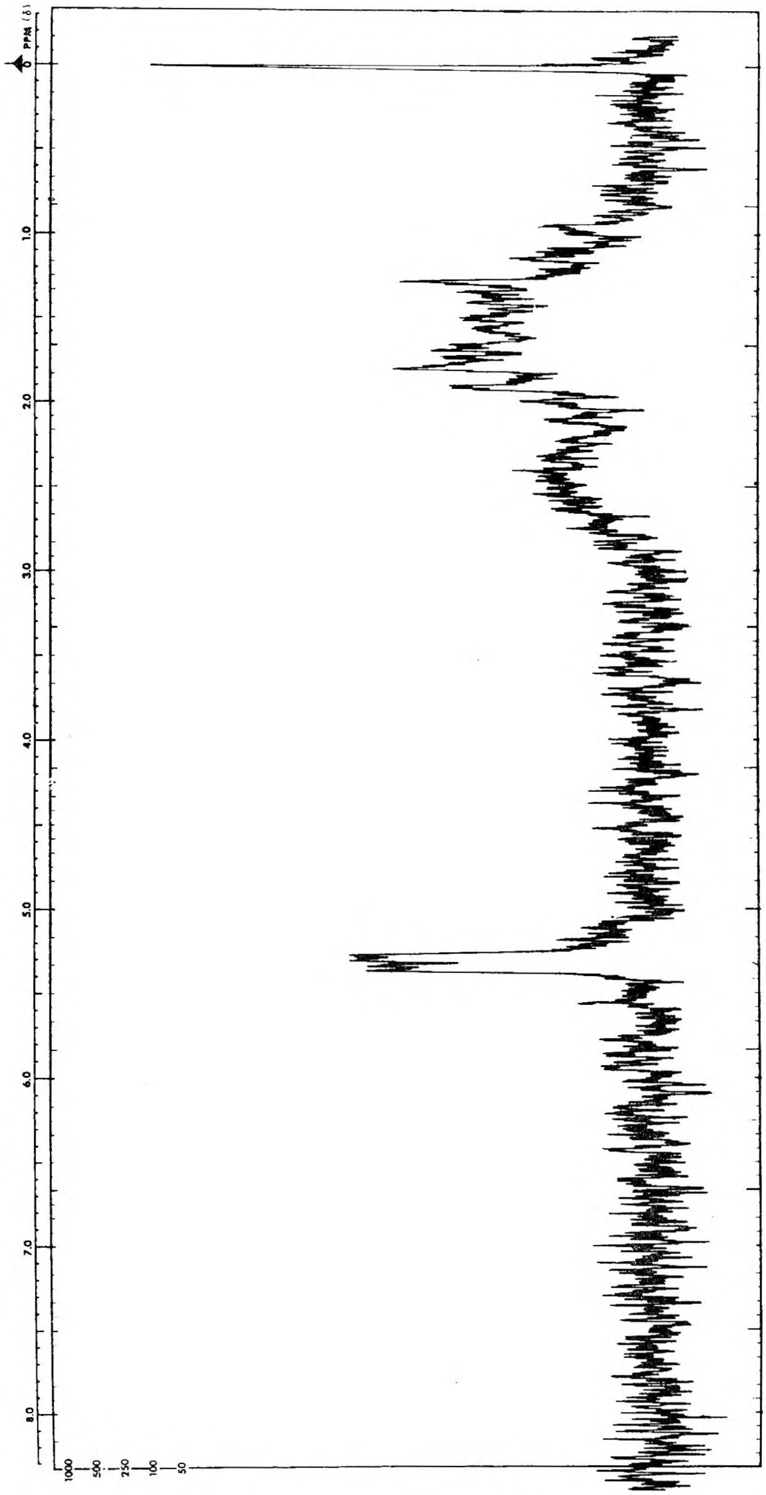

Figure 5.

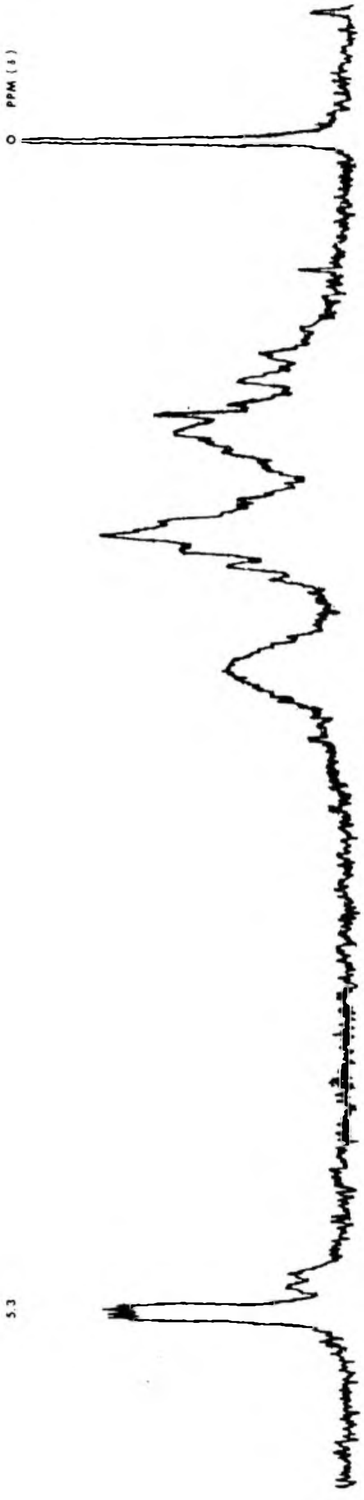

Figure 6.

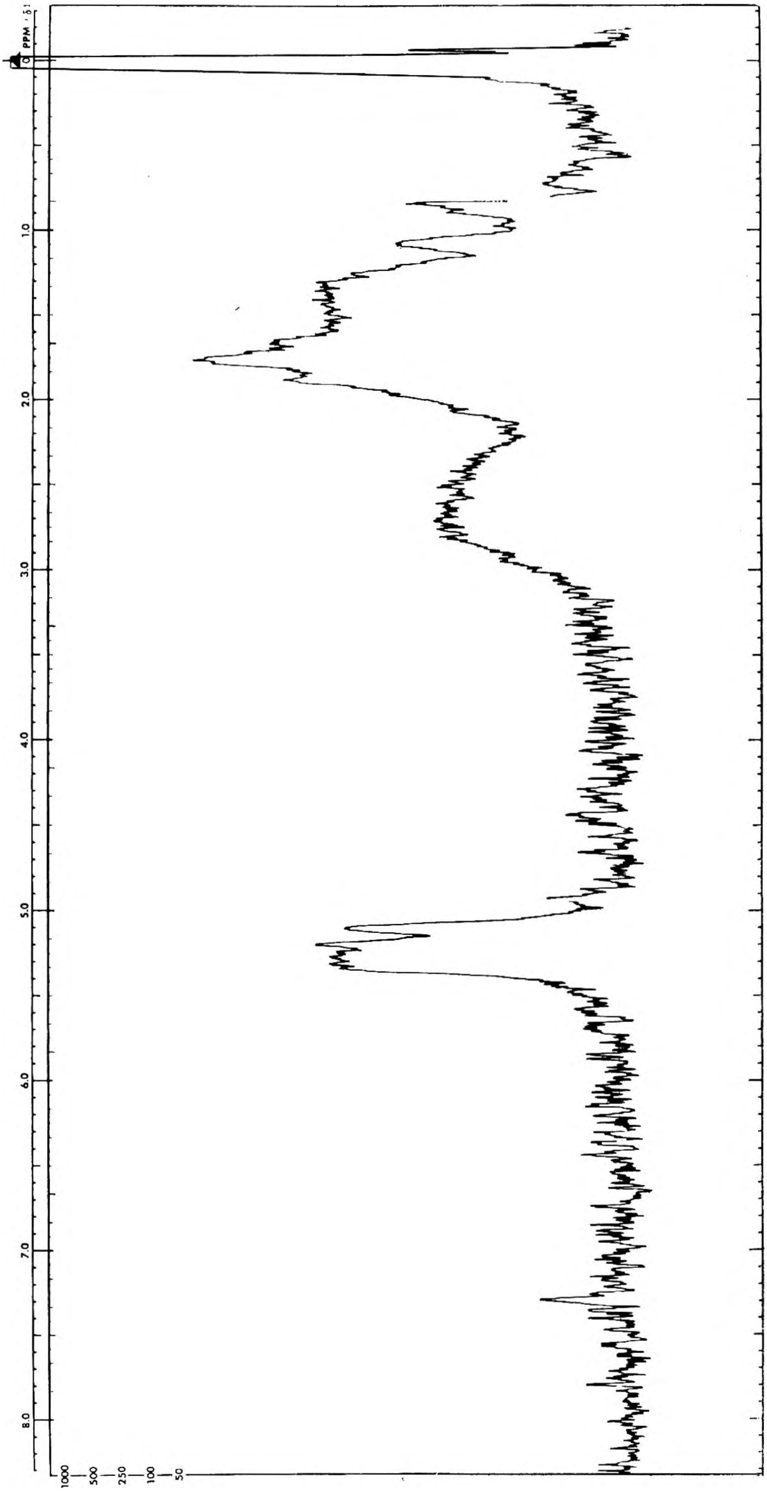

Figure 7.

Integration of the assigned absorptions in the case of the polymer prepared by Os^{3+} catalysis is consistent with the proposed structure of one olefinic proton per four aliphatic protons. However, a corresponding integration of the assigned peaks in the polymer prepared by Ru^{3+} catalysis resulted in a ratio of 1/5.3. The latter result may purport a polymerization occurring to some extent through the bicyclic double bond without ring opening.

The intrinsic viscosities of these polymers were determined at 25°C. in benzene with the use of a Cannon-Fenske viscometer. The following values were obtained: for polymer II, X = H (Ru^{3+} catalysis), = 0.69 dl./g.; (Os^{3+} catalysis), = 0.15 dl./g.; (Ir^{3+} catalysis), = 0.57 dl./g.; for polymer II, X = CH_2Cl (Ir^{3+} catalysis), = 0.19 dl./g.

The lower intrinsic viscosity measurements for II, X = CH_2Cl as compared to II, X = H prepared by Ir^{3+} catalysis can perhaps best be explained by the steric hindrance posed by the chloromethyl group in the chain propagation step.

PROPOSED MECHANISM OF POLYMERIZATION

Evidence that these polymerizations are probably not free radical chain in character stems from the absence of inhibition of polymerization when these reactions were carried out in the presence of 0.5% hydroquinone based on monomer concentration. The following mechanism appears consistent with the data available thus far. Initially, monomer is activated through π-complex formation [eq. (1)] with perhaps a simultaneous concerted ring opening displacement on the bridgehead carbon by solvent (or water) [eq. (2)], to regenerate the active metal center (III) in a reduced oxidation state. Metal–olefin complex formation is often accompanied by a reduction in the valence state of the metal.[6]

It is interesting to note that when Ic is the monomer, no polymerization ensues. This inhibition may be due to preferential complex formation between the nitrile group and the catalyst,

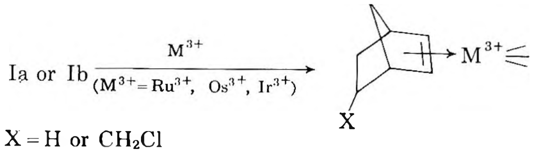

(1)

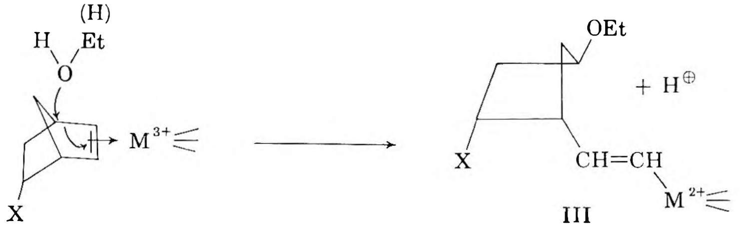

(2)

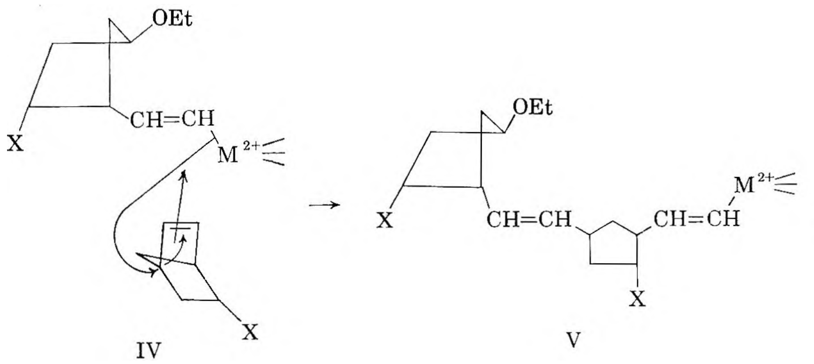

thereby depleting the availability of the latter for polymerization. The powerful ligand field associated with the cyanide ion is attributed, at least in part, to $d\pi$–$p\pi$ bonding between the metal ion and this ligand.[7] It is also worthy of note that little polymer was obtained when this reaction was attempted in commercial tetrahydrofuran in which these catalysts have some solubility. The intermediate (III) may now activate (coordinate) another monomer (IV) followed by another concerted rearrangement to V. Repetition of this process [eq. (3)] would constitute the propagation step, and appears to be consistent with the presence of *cis*-1,3-cyclopentane rings in the polymer backbone. Termination may occur by the solvolysis of the metal carbon possibly involving oxidation of the metal to a higher valence state thereby regenerating the catalyst.

The unusual character of this type of polymerization was already pointed out by Truett,[3] in that it was the first known instance of an addition polymerization of a monomer containing only one double bond leading to a polymer having more than trace amounts of unsaturation. Consequently, a considerable part of the driving force or heat of polymerization for this largely stereospecific polymerization cannot arise from the usual cascading from π to σ bonds, but must originate from the high degree of strain present in these bicyclic monomers. It has been estimated,[8] for example, that the bicyclo-[2.2.1]-heptane ring system is perhaps strained to the extent of 20 kcal./mole and that the strain in the double bond of Ia is about 6 kcal./mole relative to that of cyclohexene.[9]

EXPERIMENTAL

Materials

Norbornene was obtained from the Aldrich Chemical Company and was distilled prior to use. Ruthenium, osmium, and iridium trichloride trihydrates were obtained from Engelhard Industries and were used without further purification. The monomer, 2-chloromethyl-5-norbornene (Ib) was prepared according to the procedure of Alder and Windermuth,[10] b.p. 55–56°C./11–12 mm. (lit.: 54–57°C./11 mm.)

The infrared spectra were determined on a Model 21 Perkin-Elmer double-beam infrared spectrophotometer using NaCl optics from films cast from benzene solutions of the respective polymers. All films were dried *in vacuo* at 0.05 mm. for 2 hr. at 100°C. prior to analysis.

The NMR spectra of the polymers were determined on a Varian A-60 Spectrometer (60 Mcycle, 14,092 gauss) and a Varian HR-100 Spectrometer (100 Moycle, 23,490 gauss).

Polynorbornene (II, X = H)

The following is a typical example of the procedure employed. Ruthenium trichloride trihydrate (1.0 g.) and 50 g. (0.53 mole) of Ia were dissolved in 200 ml. of Synasol. The solution was heated to reflux and after 6.5 hr. an 86% conversion to an alcohol-insoluble, dark polymer was obtained. The crude polymer was washed with acetone and dissolved in hot benzene. The solution was filtered and the polymer precipitated by pouring into methanol. After two additional precipitations followed by vacuum drying, a grayish-white fibrous polymer (30 g., 60%) was obtained, softening range, 72–90°C.

ANAL. Calcd. for $(C_7H_{10})_n$: C, 89.29%; H, 10.71%. Found: C, 89.95%; H, 9.78%.

In a similar manner, Ib was converted to polymer (Table I).

ANAL. Calcd. for $(C_8H_{11}Cl)_n$: C, 67.37%; H, 7.72%. Found: C, 67.21%; H, 7.69%.

Some care should be exercised in carrying out the Ir^{3+}-catalyzed polymerization of Ia in refluxing ethanol because of its almost explosive character, particularly at high monomer/solvent ratios.

Ozonolysis of II, X = H (Prepared by Ru^{3+} Catalysis)

A Welsbach ozonator, Model T-23, was used as the source of ozone in this experiment. The procedure employed is essentially that of Truett.[3] The only isolable product was *cis*-1,3-cyclopentane dicarboxylic acid in 10% yield, characterized as the di-*p*-bromophenacyl ester, m.p. 172–174°C. (lit.:[3] 166–168°C.).

The authors are grateful to Mr. Jerome Holcomb of Varian Associates for the determination and assistance in interpretation of the NMR spectra. We also wish to thank Mr. M. Lambropoulos of our Laboratories for the determination and discussions concerning the infrared spectra described in this paper.

References

1. Rinehart, R. E., H. P. Smith, H. S. Witt, and H. Romeyn, Jr., *J. Am. Chem. Soc.*, **83**, 4864 (1961); *ibid.*, **84**, 4145 (1962).

2. Canale, A. J., W. A. Hewett, T. M. Shryne, and E. A. Youngman, *Chem. Ind. (London)*, **1962**, 1054.

3. Truett, W. L., D. R. Johnson, I. M. Robinson, and B. A. Montague, *J. Am. Chem. Soc.*, **82**, 2337 (1960).

4. Robinson, I. M., and W. L. Truett, U. S. Pat. 2,932,630, (1960).
5. Golub, M., *J. Am. Chem. Soc.*, **80**, 1794 (1958).
6. Bennett, M. A., *Chem. Rev.*, **62**, 612 (1962).
7. Gould, E. S., *Inorganic Reactions and Structures*, Revised Ed., Holt, Rinehart, and Winston, 1962, p. 359.
8. Schleyer, P., *J. Am. Chem. Soc.*, **80**, 1700 (1958).
9. Turner, R. B., W. R. Meador, and R. E. Winkler, *J. Am. Chem. Soc.*, **79**, 4117 (1957).
10. Alder, K., and E. Windermuth, *Ber.*, **B71**, 1939 (1938).

Résumé

On a fait polymériser le norbornène et un de ses dérivés en substances de hauts poids moléculaires à l'aide de trichlorures hydratés de ruthénium, osmium et irridium dans des solvants alcooliques. Des études structurales indiquent qu'une partie importante de l'unité périodique du polymère consiste en cycles cyclopentaniques associés en configuration *cis*-1,3 avec une prédominance de doubles liaisons *trans*.

Zusammenfassung

Norbornen und ein Derivat wurden mit dem hydratisierten Trichloriden von Ruthenium, Osmium, und Iridium in alkoholischen Lösungsmitteln zu hochmolekularen Produkten polymerisiert. Strukturuntersuchungen an diesen Polymeren zeigen, dass ein Grossteil der Polymerbausteine aus in *cis*-1,3-Konfiguration verbundenen Cyklopentanringen mit vorherrschender *trans*-Doppelbindung besteht.

Received January 31, 1964
Revised August 6, 1964

JOURNAL OF POLYMER SCIENCE: PART A VOL. 3, PP. 907-916 (1965)

Distribution of Short-Chain Branching in Low-Density Polyethylene

KENZO SHIRAYAMA, TAKAYUKI OKADA, and SHIN-ICHIRO KITA, *Sumitomo Chemical Company, Ohe Works, Niihama, Japan*

Synopsis

The distributions of short-chain branching in some commercial low-density polyethylenes have been investigated by measuring the degree of short-chain branching of their fractionated samples. The results obtained on the fractions which were fractionated with respect to molecular weight showed that some polyethylenes have broad distributions and others have narrow distributions, and these results have been considered to depend mainly on the polymerization conditions. These fractions of which the molecular weight is considered to be approximately uniform were further refractionated with respect to degree of short-chain branching, and thus cross-fractionations were accomplished. The distributions of short-chain branching in those parent fractions were also examined, and it was found out that the parent fractions have fairly broad distributions, and the distribution is broader when the molecular weight is lower, but the difference of distribution is not so great in the different samples. The distributions in those parent fractions showed close agreement with the theoretical distributions which were calculated on the basis of statistical branch formation.

INTRODUCTION

In the studies of physical properties of polyethylenes, molecular weight and degree of short-chain branching have been considered to be the principal factors.[1-4] However, commercial low-density polyethylene should be considered as the mixture of aliphatic hydrocarbons of varied molecular size and structure, so it would appear to be important to investigate these distributions for further study.

Investigation of the distribution is of interest in connection not only with physical properties of the polymer but also with polymerization conditions.

Recently, the molecular weight distribution has been studied by several workers,[5-10] but very few studies on the distribution of molecular structure have been reported in the literature.[11]

In this paper, the distribution of the molecule having different degrees of short-chain branching (hereafter referred to as branching distribution) in some commercial low-density polyethylenes has been examined by measurement of the degree of short-chain branching in fractionated samples.

For this purpose, it was necessary to fractionate polyethylene into a number of fractions which are uniform in molecular weight and degree of short-chain branching.

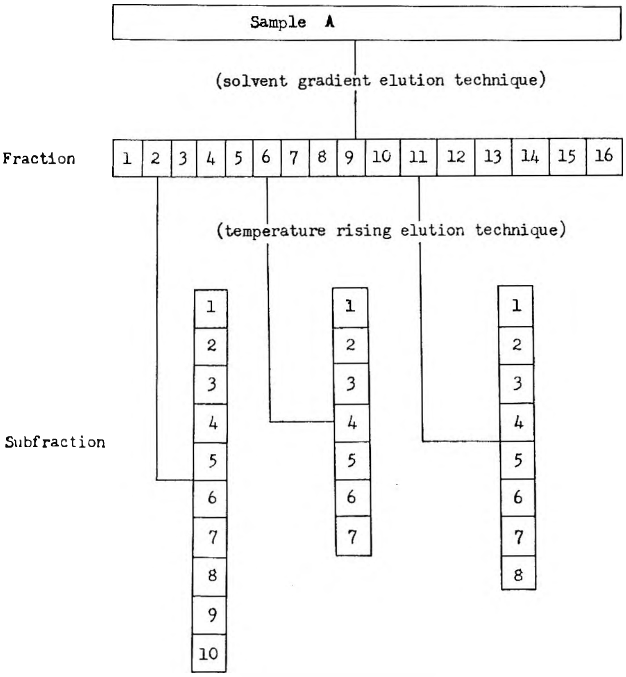

Fig. 1. Fractionation scheme.

Although it is difficult to divide polyethylene into fractions which are exactly uniform with respect to both molecular weight and degree of short-chain branching, it is known that the fractionation can take place only on the basis of molecular weight if a sand column solvent gradient elution technique at a temperature above the melting point is used, while the fractionation takes place mainly on the basis of degree of short-chain branching if a sand column temperature rising elution technique is used. As these results have been confirmed also in our laboratory, cross fractionation was performed by means of a combination of these techniques according to the scheme shown in Figure 1.

TABLE I
Characteristics of the Samples

Sample	Melt index[a]	$[\eta]$[b]	Degree of branching (CH_3/100C)	Density, g./cc.[c]
A	7	0.930	2.77	0.920
B	4	0.935	2.00	0.926
C	2	0.900	2.31	0.924
D	4	0.863	2.69	0.919
E	2	0.888	2.55	0.924
F	0.3	1.020	2.86	0.921

[a] ASTM D1238-57T Condition E.

[b] In xylene, 75°C.

[c] The densities were determined at 20°C. on compression-molded sheets after 1 hr. annealing in boiling water in a density-gradient tube.

EXPERIMENTAL

Samples

The specific characteristics of the samples used in this investigation are listed in Table I.

Fractionation

Solvent Gradient Elution Technique.[12] This procedure is similar to that described by Francis et al.[8] The experimental arrangement used is shown in Figure 2.[12] About 1400 g. of sea sand coated with 10 g. of precipitated polymer was introduced into column 70 mm. in diameter and 380 mm. in length. The polymer was precipitated from xylene solution on the sand by gradually lowering the temperature. A preheated solvent (xylene)–nonsolvent (ethyl Cellosolve) mixture was continuously dropped into the sand column at 125 ± 0.1°C., and the overflow effluent was collected in a beaker. The xylene content of the mixture employed was varied from about 37 to 60 vol.-%. In general, 500 cc. of extraction mixture for each fraction was added during 60 min., and about 16 fractions were obtained for each run. To prevent oxidative degradation during the course of fractionation, 0.2% Nonox WSP (Imperial Chemical Industries, Ltd.) was added to the extraction mixture, and all operations were carried out under nitrogen. The polymer was precipitated with cold methanol, filtered, washed, and dried in a vacuum oven at 50°C.

The samples used for refractionation were prepared in a similar apparatus holding about ten times the volume of polymer-coated sand in order to

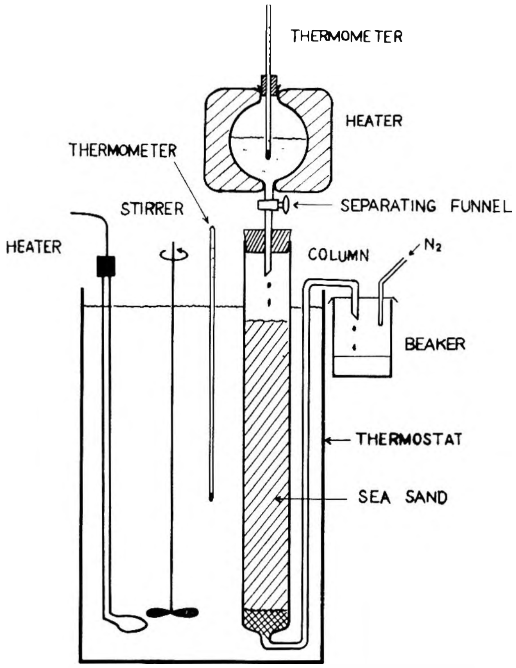

Fig. 2. Sand column elution fractionation apparatus.

obtain sufficient amount of material for subsequent fractionation. The column dimensions were 100 mm. (diameter) × 2200 mm., and temperature was maintained by recycling Dowtherm through the outer jacket. The fractionation efficiency of this large apparatus was the same as that of the smaller one.

Temperature Rising Elution Technique.[11] Using the same apparatus as described before, 4 g. of the above fraction was refractionated by the Desreux and Spiegels technique[13] with xylene as extracting solvent. The extraction temperature was raised stepwise in small intervals over the range of 50–80°C. In order to assure temperature equilibrium, the temperature was kept constant at each level for 30 min. before the next extraction started. A 350-cc. portion of preheated xylene was added dropwise during 60 min. at each level of temperature, and about ten subfractions were obtained for each run.

Determination of Degree of Short-Chain Branching

The degree of short-chain branching was determined by infrared analysis with the use of a Shimadzu Model AR-275IIS infrared spectrophotometer. The measurements were performed on film samples or carbon tetrachloride solutions, and the methyl content was determined from the 1378 cm.^{-1} absorption by the method of Bryant et al.[14] and Willbourn,[4] except that the corrections for the methylene absorptions at 1368, 1352, and 1303 cm.^{-1} were made by using eq. (1):

$$(K'_{1378})_{\text{corr.}} = (K'_{1378})_{\text{app.}} - 0.741\,K'_{1303} - 2.6 \qquad (1)$$

where

$$K' = \text{Optical density}/(\text{density} \times \text{thickness}) \qquad (2)$$

For the samples having molecular weight above 20,000, compression-molded films 0.1 mm. thick were used as the specimen. For the samples having molecular weight below 20,000, 3% solutions of carbon tetrachloride were used, and the measurement was carried out at 70°C. The number of methyl groups per hundred carbon atoms was calculated from the value of $(K'_{1378})_{\text{corr.}}$ by comparing with the standard specimens which were calibrated with *n*-octadecane.

The value thus obtained includes the number of methyl groups attached to the end of the main chain. Since the proportion of these methyl end-groups is quite large for small molecules, it is necessary to do some correction in order to have "true" degree of short-chain branching. As almost all the endgroups of the main chain of low-density polyethylene are considered to be methyl groups, the correction was made by subtracting two methyl groups per polymer molecule.

Determination of Molecular Weight

Intrinsic viscosities were determined in xylene at 75°C. with an Ubbelohde viscometer. Then, assuming monodispersity of the fraction, number-average molecular weight of the individual fraction $\bar{M}_\eta$ was calculated from this intrinsic viscosity by using eq. (3):[7]

$$[\eta] = 0.88 \times 10^{-3}\bar{M}_\eta^{0.635} \tag{3}$$

RESULTS AND DISCUSSION

Figure 3 shows the branching distribution related to whole samples, where the degree of short-chain branching of the fractions by solvent gradient technique is plotted against their molecular weight. From these data, it can readily be seen that samples A and B have narrow distributions, while samples C, D, and E have broader distributions, and sample F has the broadest distribution.

As is well known, the degree of short-chain branching of polyethylene depends markedly on polymerization temperature and pressure.[14,15] But, in this situation, the broad branching distribution must be ascribed to the wide range of reaction temperature in the reactor, because unless these polymers are blended, polymerization pressure is uniform and has no effect on the branching distribution. Inasmuch as the molecules of lower molecular weight are produced in the higher temperature region, the general trend

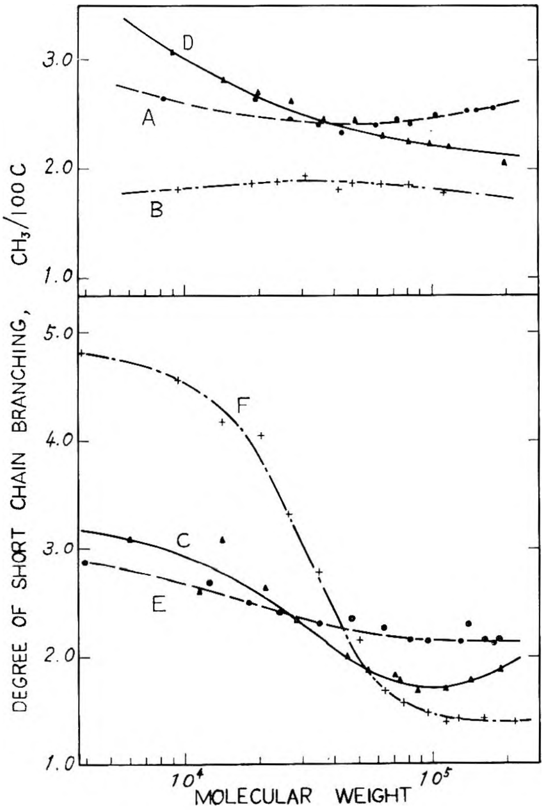

Fig. 3. Branching distribution in commercial low-density polyethylene.

that the degree of short-chain branching increases with decreasing molecular weight would be a reasonable result. There are exceptions, however; e.g., samples A and C, in which the degree of short-chain branching increases once again at a very high molecular weight region (referred to as a "tailing-up" phenomenon).

In conjunction with the results of the refractionation study to be mentioned later, the most reasonable explanation of this deviation would be that an intermolecular chain transfer might have occurred at the "hot spots" in the polymerization reactor and that long-chain branches having many short-chain branches might have been grafted to the primary molecules. Since this would be considered to take place near the entrance of the reactor, where the temperature would be generally low and unstable, it seems also reasonable that the deviation occurs only at very high molecular weights. (In fact, the presence of low polymer with side branches of about 20 CH_3/100°C has been detected in benzene extracts of commercial polyethylene.)

In order to study the internal branching distribution within these fractionated samples, three fractions of low, medium, and high molecular weight, respectively, were chosen from the 16 fractions of samples A and E and refractionated by the temperature rising technique. A typical example of the data on the refractionation is given in Table II, and the cumulative and differential distribution curves are shown in Figures 4 and 5, respectively.

These results show that there is a considerably broad branching distribution within the fractionated samples, particularly in the low molecular weight fractions, and this tendency is common to samples A and E. In case of sample E, such a broad distribution might be reasonable, since this sample might be polymerized over a broad temperature distribution and would be a mixture of various kinds of molecules produced at different temperatures. In case of sample A, however, the broad branching distribu-

TABLE II
Results of Refractionation by Temperature Rising Method (A Fraction of Sample E, MW = 35,000)

Subfraction no.	Extraction temperature, °C.	Weight, %	Cumulative weight, %	Molecular weight	Degree of branching (CH_3/100C)
1	58°C	9.41	95.24	30,500	3.00
2	62	11.40	84.84	33,300	2.68
3	64	9.34	74.47	33,900	2.52
4	66	12.13	63.73	37,000	2.43
5	68	13.18	51.08	37,700	2.26
6	70	13.74	37.62	39,100	2.20
7	72	12.28	24.61	37,100	1.90
8	73	5.05	15.94	38,400	1.67
9	74	6.61	10.11	35,300	1.65
10	80	6.81	3.40	37,600	1.70

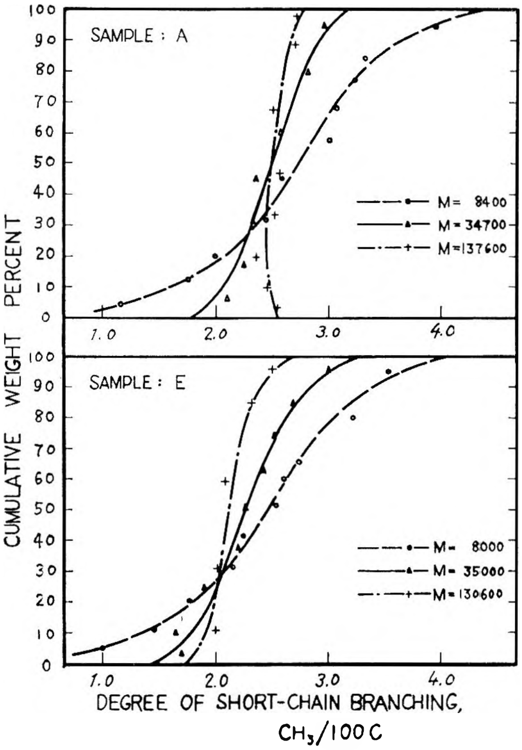

Fig. 4. Distribution of degree of short-chain branching in fraction (cumulative curve).

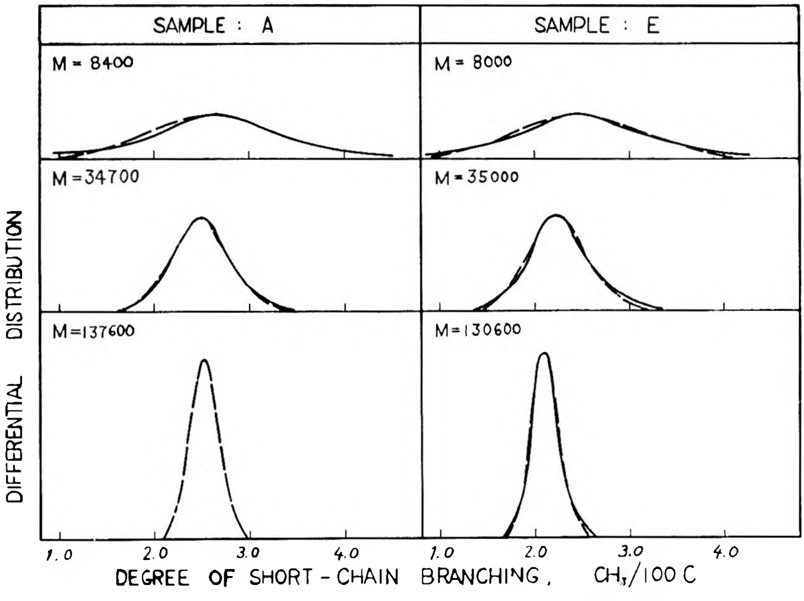

Fig. 5. Distribution of degree of short-chain branching in fraction (differential curve): (——) observed curve; (- - -) theoretical curve.

tion is a rather unexpected result, because the distribution of polymerization temperature is considered to be narrow.

This suggests that this internal branching distribution in the fractionated sample arises from statistical reasons not from the polymerization conditions, and we tried to arrive at a statistical calculation for the branching distribution.

For the sake of simplicity, it was assumed that every carbon atom of the main chain has equal probability for branch formation, then the probability P_{nk} that a molecule of n carbon atoms has k branches, is given by eq. (4)

$$P_{nk} = {}_nC_k p^k q^{n-k} \tag{4}$$

where p is the probability of branch formation at each carbon atom and corresponds to the average degree of short-chain branching (CH_3/CH_2), and $q = (1 - p)$ is the probability that branching does not occur.

If the molecular weight of the fraction is assumed to be uniform, the statistical branching distribution within the fraction can be easily calculated according to the above binomial function, using the average degree of branching of each fraction as p. When n is large and p is small ($n > 100$, $p < 0.1$), eq. (4) can be approximated by Poisson's function and the calculation is simplified.

$$P_{nk} = {}_nC_k p^k q^{n-k} \doteqdot e^{-\lambda}(\lambda^k/k!) \tag{5}$$

where $\lambda = np$.

The probability thus obtained is the value for each branching number k, and in order to convert this to a value in terms of branching degree units of $CH_3/100C$, it must be normalized by multiplying by $n/100$. An example of this calculation is shown in Table III, and the calculated differential distribution curves for each fraction are shown in Figure 5 (broken lines).

In comparison with observed distribution curves, the agreement is excellent. Consequently, it seems to be a quite reasonable conclusion that the

TABLE III
Statistical Calculation of Branching Distribution in a Fraction with M.W. = 35,000, $CH_3/100C = 2.24$; $n = 2{,}500$, $p = 0.0224$

k	P_{nk}	Degree of branching ($CH_3/100C$)[a]	Probability/CH_3/100C[b]
35	7.1098×10^{-4}	1.40	1.7775×10^{-2}
40	4.9588×10^{-3}	1.60	1.2397×10^{-1}
45	1.8628×10^{-2}	1.80	4.6570×10^{-1}
49	3.6026×10^{-2}	1.96	9.0065×10^{-1}
53	5.0414×10^{-2}	2.12	1.2604
56	5.3231×10^{-2}	2.24	1.3308
59	4.7927×10^{-2}	2.36	1.1982
63	3.2970×10^{-2}	2.52	8.2425×10^{-1}
67	1.7626×10^{-2}	2.68	4.4065×10^{-1}
72	5.7816×10^{-3}	2.88	1.4454×10^{-1}
77	1.3430×10^{-3}	3.08	3.3575×10^{-2}

[a] $100k/n$.

[b] $P_{nk}n/100$.

branching distribution within the fraction is mainly caused by a statistical effect. Even in sample E, which has a fairly broad polymerization temperature distribution, the agreement is as good as in other cases, so that the effect of temperature distribution in this regard is considered to be comparatively small.

Now it must be pointed out that in case of the high molecular weight fraction of sample A, the observed distribution curve deviates from the calculated one (its observed distribution is not given in Fig. 5). In this case, the refractionation with respect to degree of short-chain branching seems to be unsuccessful, as the degree of short-chain branching of the fractions extracted at higher temperature was higher than that extracted at lower temperature (Fig. 4). This deviation is considered to be closely connected with the "tailing-up" phenomenon mentioned before, and to be also ascribed to the complicated molecular structure with long-chain branches having many short-chain branchings. This complicated structure seems to affect the solubility differently in the temperature rising fractionation.

On the above statistical calculation, it was assumed that each carbon atom has equal probability for branch formation. The same result can be obtained even if a different assumption is employed, however. For instance, according to Roedel's mechanism,[17] chain branching can occur only at one carbon atom of each ethylene unit. In this case, eq. (4) has the form:

$$P_{nk} = {}_{n/2}C_k(2p)^k(1 - 2p)^{n/2-k} \doteqdot e^{-\lambda}(\lambda^k/k!) \qquad (6)$$

where, as before, $\lambda = np$.

When n is large and p is small, this function can also be approximated by Poisson's function to be identical with eq. (5).

Thus, although the statistical calculation curves on the basis of this simple theory showed good agreement with the observed distribution curves in many cases, this result gives no evidence as to the mechanism for branching. It should be emphasized, however, that as far as the formation of short-chain branching takes place statistically, branching distribution exists even if the polymerization conditions are constant, and the distribution calculated from eq. (5) was in good agreement with the experimental data. Since p is assumed constant in this calculation, this cannot be applied as such to blends of polymers produced under very different polymerization conditions. Conversely speaking, when this cannot be applied, one might be able to infer inhomogeneity of polymerization conditions.

In conclusion, the characteristic features of the distribution of short-chain branching (distribution of molecular species) in various kinds of low-density polyethylenes are expressed well enough by the variation of the degree of short-chain branching among the fractions divided with respect to molecular weight (Fig. 3), and within these fractions the molecules with different degree of short-chain branching are considered to be distributed statistically in the manner mentioned above, regardless of the sample source.

The authors are grateful to Dr. O. Saheki and Dr. I. Taniguchi for their interest in this work. The authors also wish to thank the Sumitomo Chemical Company for permission to publish this paper.

References

1. Richard, R. B., *J. Appl. Chem.*, **1**, 370 (1951).
2. Sperati, C. A., W. A. Franta, and H. W. Starkweather, Jr., *J. Am. Chem. Soc.*, **75**, 6127 (1953).
3. Peticolas, W. L., and J. M. Watkins, *J. Am. Chem. Soc.*, **79**, 5083 (1957).
4. Willbourn, A. H., *J. Polymer Sci.*, **34**, 569 (1959).
5. Tung, L. H., *J. Polymer Sci.*, **20**, 495 (1956).
6. Nasini, A., and C. Mussa, *Makromol. Chem.*, **22**, 59 (1957).
7. Nicolas, L., *Makromol. Chem.*, **24**, 173 (1957).
8. Francis, P. S., R. C. Cooke, Jr., and J. H. Elliott, *J. Polymer Sci.*, **31**, 453 (1958).
9. Henry, P. M., *J. Polymer Sci.*, **36**, 3 (1959).
10. Guillet, J. E., R. L. Combs, D. F. Slonaker, and H. W. Coover, *J. Polymer Sci.*, **47**, 307 (1960).
11. Hawkins, S. W., and H. Smith, *J. Polymer Sci.*, **28**, 341 (1958).
12. Kita, S., K. Shirayama, I. Taniguchi, and O. Saheki, paper presented at Informal Meeting on Molecular Weight Distribution, Kyoto University, Japan, Nov. 11, 1960.
13. Desreux, V., and M. C. Spiegels, *Bull. Soc. Chim. Belges.*, **59**, 476 (1950).
14. Bryant, W. M. D., and R. C. Voter, *J. Am. Chem. Soc.*, **75**, 6113 (1953).
15. Woodbrey, J. C., and P. Ehrlich, *J. Am. Chem. Soc.*, **85**, 1580 (1963).
16. Mortimer, G. A., and W. F. Hamner, *J. Polymer Sci.*, **A2**, 1301 (1964).
17. Roedel, M. J., *J. Am. Chem. Soc.*, **75**, 6110 (1953).

Résumé

On a étudié les distributions des ramifications à courtes chaînes de quelques polyéthylènes commerciaux de faible densité en mesurant le degré de ramification de ces courtes chaînes sur leurs échantillons fractionnés. Les résultats obtenus à partir des fractions qui ont été fractionnées par rapport au poids moléculaire, ont montré que certains polyéthylènes ont des distributions larges et d'autres des distributions étroites, et on considère que ces résultats dépendent principalement des conditions de polymérisation. Ces fractions, dont le poids moléculaire est considéré comme étant approximativement uniforme, sont refractionnées par rapport au degré de ramification à chaînes courtes; de ce fait on a effectué des fractionnements croisés. Les distributions des ramifications à courtes chaînes dans ces fractions-mères ont aussi été examinées, et on a trouvé que les fractions-mères ont des distributions raisonnablement larges et que la distribution est plus large quand le poids moléculaire est plus faible, mais que la différence de distribution n'est pas aussi grande que dans les échantillons différents. Les distributions de ces fractions-mères sont en accord parfait avec les distributions théoriques, calculées sur la base de la formation statistique des ramifications.

Zusammenfassung

Die Verteilung der Kurzkettenverzweigung in einigen handelsüblichen Polyäthylenen niedriger Dichte wurde durch Messung des Kurzkettenverzweigungsgrades an fraktionierten Proben bestimmt. Die an bezüglich des Molekulargewichtes fraktionierten Fraktionen erhaltenen Ergebnisse zeigen, dass manche Polyäthylene eine breite und andere eine enge Verteilung besitzen, wobei in der Hauptsache eine Abhängigkeit von den Polymerisationsbedingungen besteht. Die Fraktionen, deren Molekulargewicht angenähert als einheitlich betrachtet wird, wurde weiter bezüglich des Grades an Kurzkettenverzweigung refraktioniert und auf diese Weise eine gekreuzte Fraktionierung erreicht. Die Kurzkettenverzweigungsverteilung in den Ausgangsfraktionen wurde ebenfalls untersucht, und es zeigte sich, dass die Ausgangsfraktionen ziemlich weite Verteilungen besitzen und die Verteilung bei niedrigerem Molekulargewicht breiter ist, wobei jedoch der Unterschied in der Verteilung nicht so gross ist wie bei verschiedenen Proben. Die Verteilung in den Ausgangsfraktionen stimmt gut mit der theoretischen, auf Grundlage der statistischen Verzweigungbildung berechneten Verteilung überein.

Received March 24, 1964
Revised August 8, 1964

JOURNAL OF POLYMER SCIENCE: PART A VOL. 3, PP. 917-932 (1965)

Elastic, Strength, and Viscous Properties of Polymer (Polyethylene and Polystyrene) Melts

G. V. VINOGRADOV and I. M. BELKIN, *Institute of Petrochemical Synthesis of the USSR Academy of Sciences, Moscow, U.S.S.R.*

Synopsis

A description is given of a rotational elastoviscometer with a very rigid dynamometer designed for the investigation of the rheological properties of polymer melts and concentrated polymer solutions by the constant deformation rate method. Alkathene-2 and polystyrene were studied over a wide range of temperatures. The deformation dependences of the shear stress obtained for these polymers became non-monotonic with rising deformation rates. This was characteristic of the reversible destruction of the polymer structure which increased with growing rates of shear. The maximum on the shear stress vs. deformation curve enabled the ultimate shear strength to be determined as a specific point on this curve. The ultimate shear strengths were reached at a deformations of several hundred per cent, while steady flow conditions were attained at deformations of several thousand per cent. With rising deformation rates, the time for attaining the ultimate strength decreased, as did, to some extent, the time of attainment of steady flow conditions. The deformation corresponding to the ultimate strength increased slightly, and the deformation corresponding to the attainment of steady flow conditions increased greatly with growing deformation rates. The activation energies of steady flow and of the passage through the ultimate strength were close in value. The dependence of the modulus of highly elastic deformation in a polymer of intact structure on the deformation rate is expressed by a function of saturation. The saturation corresponds to the deformation rates at which viscous flow cannot develop without breakdown of the melt structure (without passage through the ultimate strength).

INTRODUCTION

Though the viscous properties of polymer melts have been dealt with in numerous publications, little is known about their elastic characteristics and the specific features of the transition from elastic deformation to steady flow. Nevertheless, these characteristics are of considerable theoretical and practical interest.

Dienes[1] studied the elastic properties of polyethylene melts by compressing cylindrical specimens on a parallel-plate type plastometer by a constant load method. The experimental results were treated on the Voigt model. Dienes' tests showed poor reproducibility, and the technique used for measuring small deformations was not very satisfactory. For that reason the tests are largely of a qualitative character.

Buchdahl[2] was the first to employ a Stormer-type rotational falling weights viscometer for studies of the elastic properties of polystyrenes at temperatures of 135–230°C. He found that the fluidity of polystyrene melts changed with time at constant shear stress and temperature. However, Buchdahl failed to study the processes occurring in the initial period of the polymer deformation and the transition from elastic deformation to steady viscous flow.

Hoff[3] investigated melts of several commercial high-pressure polyethylenes of different molecular weights on a coaxial-cylinder apparatus by the dynamic method. The outer cylinder of the apparatus vibrated at a frequency of 0.5–50 cycles/sec.; the amplitude and frequency of the vibration of the inner cylinder suspended on a torsion wire were determined. Hoff managed to measure the shear modulus and calculate the viscosity and the activation energy of the viscous flow of the polymers studied.

Dexter[4] investigated polyethylene melts on a coaxial-cylinder apparatus by the constant shear stress method. The elastic deformations were calculated on the basis of the Voigt model in combination with a piston moving in viscous fluid liquid. The mechanical recorder used by Dexter did not permit reliable control of the processes occurring during the initial period of deformation.

A series of investigations of the elastic properties of polyisobutylenes was carried out by Rebinder and Ivanova-Chumakova.[5]

Melts of several polymers were studied on a cone-plane rotational apparatus by Kepes.[6] In his tests the shear stresses were set and recorded by the twisting of torsion wires connected to the cone. Visual control of the torsion wire deformation permitted a reliable estimation of only the steady flow conditions. He showed that these conditions were set in time.

Pohl and Gogos[7] carried out tests with polyisobutylenes on a double-cone rotational rheometer which recorded the time dependence of shear stress, as characterized by a sharp rise in stress at the initial period of the test then by a similar sharp drop (at constant rotor speed). It should be pointed out that these authors presented the results of their tests in terms of time dependence of viscosity, assuming the rate of deformation to be constant. The use of the concept of viscosity, however, cannot be considered valid in the case of unsteady deformation conditions. Moreover, they did not give the rigidity of the dynamometer, and therefore it is not known whether the deformation rate remained constant on passing from elastic deformations to steady flow.[8]

McCord and Maxwell[9] made a comparative investigation of the elastic properties of several polyolefin melts on a rotational apparatus with coaxial cylinders. After being subjected to a definite deformation, the specimen under study was unloaded and its elastic recovery observed. Interesting qualitative results were obtained in this study. The relative elastic recovery was found to decrease with increasing initial deformation. The temperature dependence of the elastic recovery for linear polyethylene was less than that for low-density polyethylene or for polypropylene. The elasticity of polyolefin melts became most apparent at temperatures close to the melting points.

Glukhov and co-workers[10,11] studied the rheological properties of a high-pressure polyethylene melt. However, they failed to determine the course of the time versus shear stress curves at the initial period of deformation. These authors, as well as Kepes,[6] reported the occurrence of a maximum stress a short time after the start of the tests (at high deformation rates), followed by a decrease in the stress.

In many papers which will not be cited in detail here, the existence and manifestation of elastic properties in polymers in flow were judged indirectly by entrance effects in their flow through capillaries, by swelling of extrudate, etc. This emphasizes the timeliness of direct studies of the elastic and strength properties of polymer melts.

The object of the present work was to develop a method for studying the transition from elastic deformations to steady viscous flow in polymer systems and for characterizing the main features of this process in such widely known polymers as Alkathene-2 and polystyrene.

EXPERIMENTAL

Equipment and Procedure

Figure 1 shows a schematic diagram of a rotational elastoviscometer which can be employed for studying polymers at temperatures of −30 to +300°C. and at reduced air pressures of the order of 10^{-4} torr.

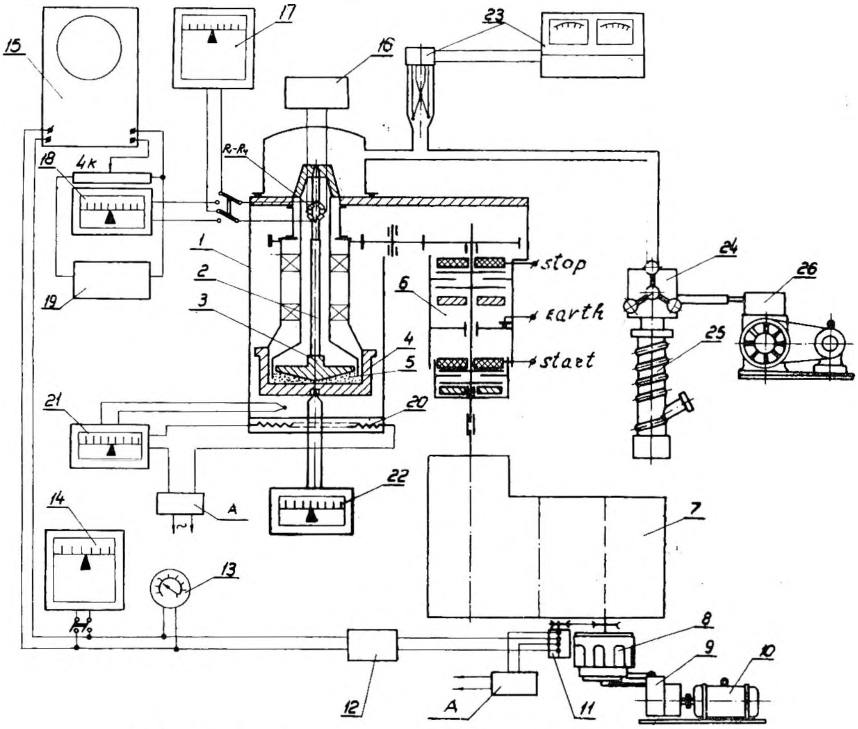

Fig. 1. Schematic diagram of a rotational elastoviscometer.

A rigid torsion rod (*2*) is fixed in a measuring unit (*1*) (the modulus of the rod being 140 kg./radian). Interchangeable cones (*3*) with apex angles of 179–174°, are set on the free end of the torsion rod. Arranged coaxially with the cone is a flat-bottomed cup (*4*) in which a form (*5*) of the polymer to be studied is placed. The thermostatted cup with the molten polymer can be rotated at a constant rate of 1.5×10^3–1.5×10^{-5} rpm. An assembly (*6*) consisting of two electromagnetic clutches is installed between the drive and the revolving parts of the measuring unit, enabling rapid connection and disconnection of the drive and the viscometer cup, as well as stopping of the latter. The drive includes an eight-step reducing gear box (*7*) connected to a hydraulic transmission assembly consisting of a hydraulic motor (*8*), a hydraulic pump (*9*), and an electric motor (*10*). The hydraulic transmission permits reversing and stepless tenfold variation of the rotation speed of the cup containing the polymer. Connected to the reducing gear driving shaft is a tachometer (*11*), the output voltage of which is proportional to the rate of deformation of the polymer. This voltage is rectified by rectifier (*12*), measured by a meter (*13*), and registered by an electronic potentiometer (*14*) or a cathode oscillograph (*15*). The torque (shear stress) transmitted through the polymer to the torsion rod is measured tensimetrically. For this purpose four tensimetric pick-ups R_1–R_4 are attached to the torsion rod and included in a bridge circuit fed by a current source (*16*). The shear stresses are registered on an electronic potentiometer (*17*). When the shear stresses are registered on the screen of an oscillograph (*15*), a potentiometer (*18*) with an additional 4-Kohm rheochord fed by a rectifier unit (*19*) is connected to the tensimetric pick-ups.

The polymer under study is heated by a removable electric heater (*20*). The cup temperature is kept constant automatically with a potentiometer (*21*) and registered by a potentiometer (*22*) with a thermocouple. The electric heater (*20*) can be replaced by a tank with a liquid circulating at a constant temperature. The reduced air pressure in the measuring unit is measured by a vacuum gauge (*23*). The vacuum system also comprises a distributing cock (*24*), a diffusion pump (*25*), and mechanical vacuum pump (*26*). Voltage regulators in the system are denoted in Figure 1 by A.

The tachometer and the torque-measuring system were calibrated, respectively, by a pulse counter and a special device enabling preset torques to be applied to the cone (*3*). The rotational elastoviscometer was checked on high-viscosity Newtonian fluids (polysiloxanes).

The primary results of the tests made on the rotational elastoviscometer were obtained as automatically recorded shear stress τ versus time t curves equivalent to shear stress versus deformation (γ) dependences. The time dependences of shear stresses are noted for high reproducibility.

Materials

The work was carried out with widely known polymers of highly stable properties, namely, Alkathene-2, a polyethylene produced by ICI, and Dbrand polystyrene manufactured according to the U.S.S.R. State Standard 9440–60. Alkathene-2 and polystyrene were studied at 114–195°C. and at 160–210°C., respectively, over a range of deformation rates of 0.02–21 sec.$^{-1}$

RESULTS AND DISCUSSION

Typical shear stress–time and shear stress–deformation curves for polyethylene and polystyrene are shown in Figures 2 and 3, respectively. Table I indicates the conditions of deformation used. The time co-ordinate in the left-hand part of Figures 2 and 3 is given in two scales, the break in the τ versus t curves corresponding to the transition from one scale to the other. Steady flow conditions were achieved in all the tests described herein, as indicated by the points marked × on the τ versus t and τ versus γ curves.

TABLE I
Conditions of Polymer Deformation Represented in Figures 2 and 3

Alkathene-2			Polystyrene		
Temp., °C.	Rate of deformation, sec.$^{-1}$	Curve number in Fig. 2	Temp., °C.	Rate of deformation, sec.$^{-1}$	Curve number in Fig. 3
114	0.028	1	160	0.056	1
	0.056	2		0.075	2
	0.075	3		0.21	3
	0.21	4		0.28	4
	0.28	5			
	0.56	6			
	0.75	7	210	0.056	1
	2.1	8		0.28	2
				0.56	3
195	0.56	1		2.1	4
	0.75	2		2.8	5
	2.1	3		5.6	6
	2.8	4		7.5	7
	5.6	5		21	8
	21	6			

As can be seen from Figures 2 and 3, the τ versus t dependences increase monotonically at low deformation rates. Deformation results in elastic strains and growth of the stresses, which accelerates stress relaxation. Hence, the rate of the stress growth gradually decreases. This decrease continues at constant $\dot{\gamma}$ until the rate of the stress growth becomes equal to the rate of stress relaxation which corresponds to the limiting value of elastic strain and to the steady flow conditions.

Irreversible deformation occurs simultaneously with the development of reversible elastic strain. The closer the development of elastic strain (at constant $\dot{\gamma}$) comes to its completion, the more the deformation increment

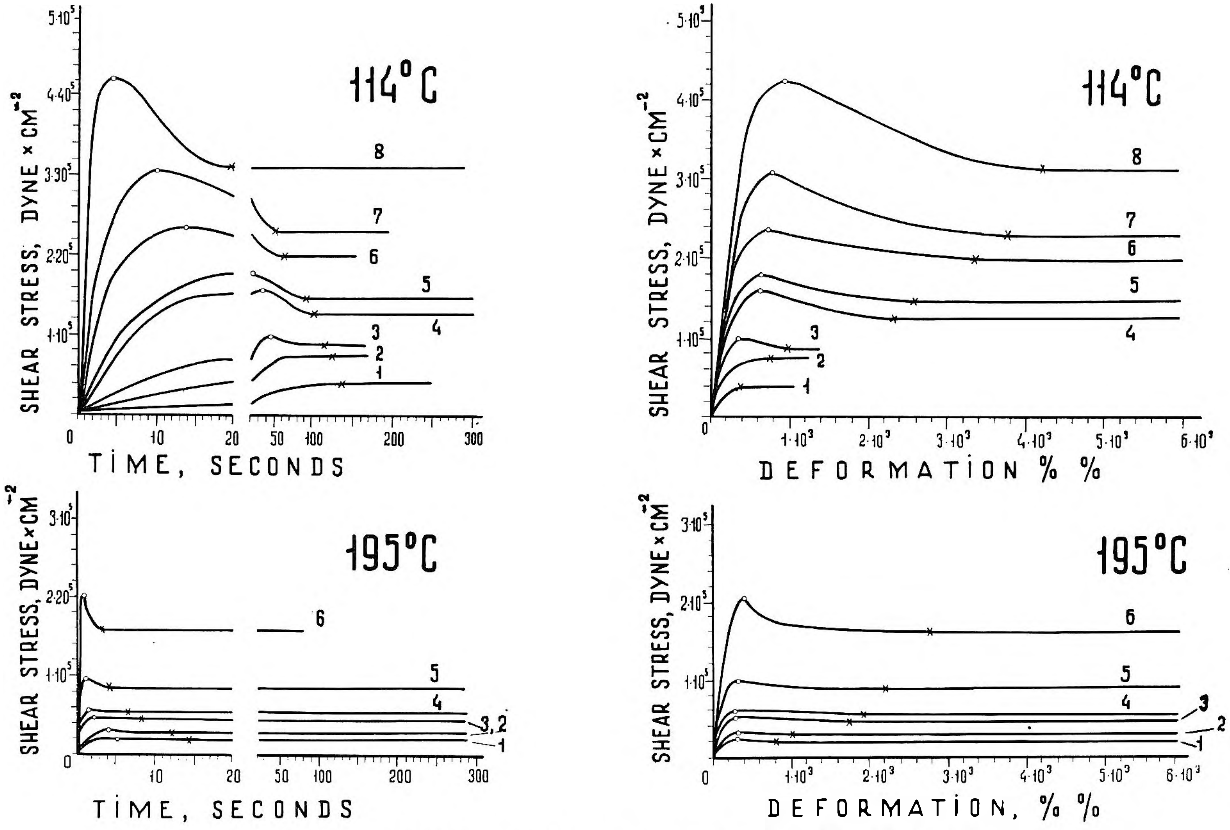

Fig. 2. Time and deformation dependences of shear stress for Alkathene-2.

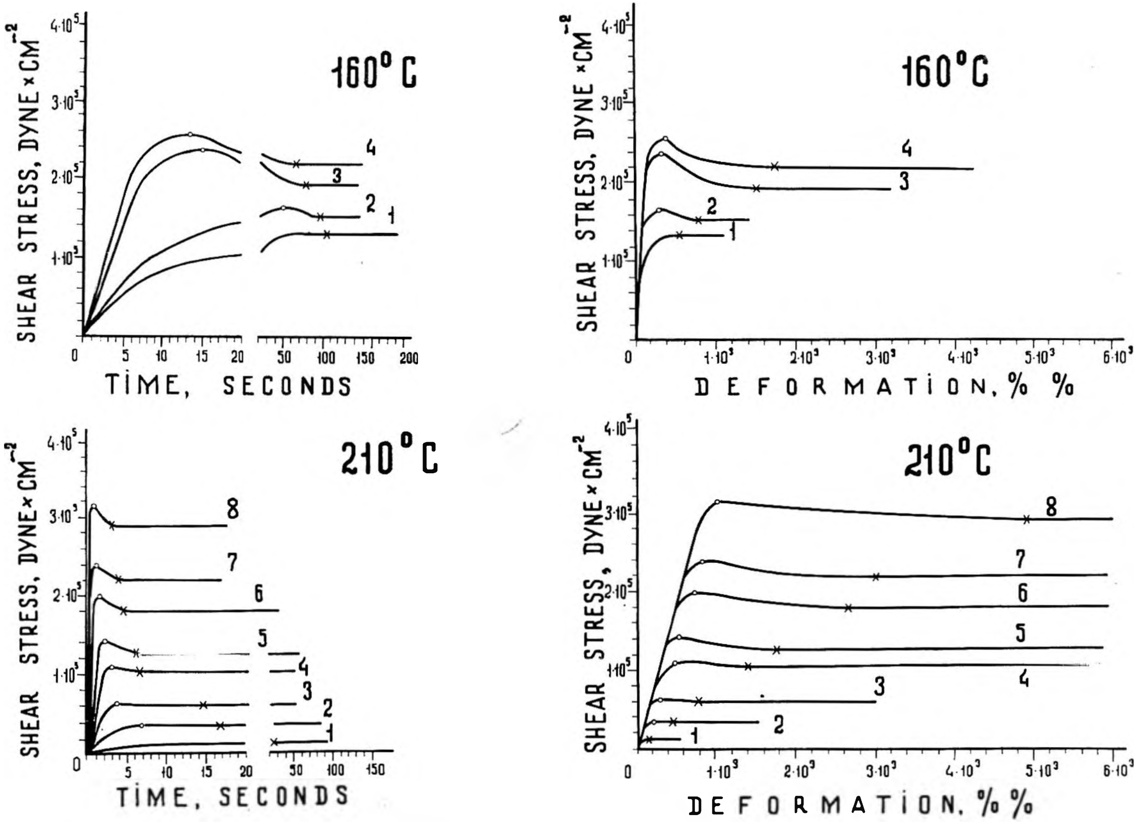

Fig. 3. Time and deformation dependences of shear stress for polystyrene.

is due to the irreversible component. At the initial stage of deformation the contribution of the elastic strain to the total strain increases with increasing deformation rates.

Under these conditions the attainment of steady flow occurs in time and is accompanied by a monotonic increase in shear stress. The duration of this transitional process depends on the relation of the deformation rate to the rate of stress relaxation. The deformation of polyethylene melts at higher rates causes the appearance on the τ versus t curves of maxima indicated by circles. These maxima divide the τ versus t curves into two parts: left-hand branches of rising stresses and mainly highly elastic strains, and right-hand branches which, owing to destruction of the polymer network and subsequent rapid stress relaxation, drop abruptly at first, and then more and more slowly, until steady flow conditions are reached. Therefore, the right-hand branches of the τ versus t curves having a maximum correspond to the development of viscous flow.

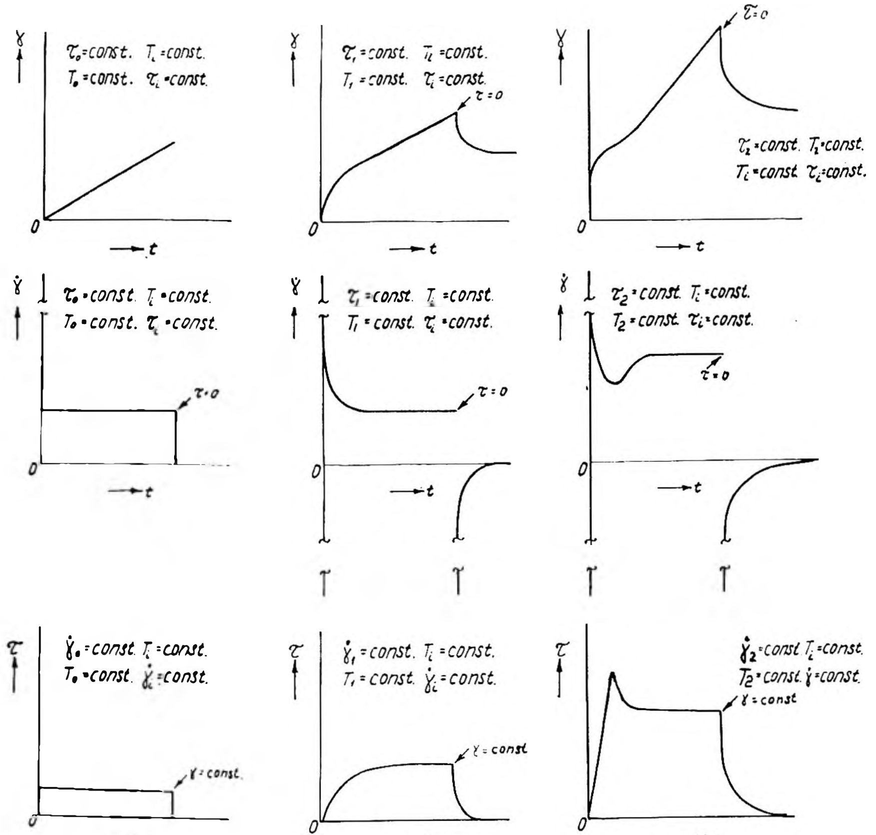

Fig. 4. Time dependence of deformations and deformation rates obtained by the constant shear stress method; time and deformation dependences of shear stress by the constant deformation rate method; stress relaxation vs. time at constant shear.

The use of a very rigid dynamometer makes it possible to pass from the τ versus t curves to τ versus γ curves corresponding to strictly constant deformation rates. The sense of the maxima on the τ versus t and τ versus γ curves for polymer melts is similar to that of the ultimate shear strength τ_{sh} for plastic disperse systems.[12] The point is that in systems where there is a three-dimensional network of macromolecules with a sufficiently high concentration of junction points existing under the action of intermolecular forces, the possibilities of an accelerating of the stress relaxation rate with increasing highly elastic strain and stress acting within the polymer are limited. This results in the multiple breaking of the tie points of the macromolecules (and in the breaking of the macromolecules themselves at extremely high $\dot{\gamma}$) and then in the lowering of the shear stresses. At a given rate of deformation the character of the curves under consideration, if estimated by the ratio of the maximum shear stress to the shear stress at steady flow τ_s, is more pronounced at lower temperatures. The τ_{sh}/τ_s ratio did not exceed 1.4 in our tests.

The transition from highly elastic strains to viscous flow is most conveniently studied by the above described constant deformation rate method; however, a constant shear stress method may also be used. A generalization of the most important cases of the shear deformation of the polymers displaying highly elastic strain and viscous flow is presented in Figure 4. It is based on the data obtained in the present work and described earlier by Bartenev.[13] It is assumed in Figure 4 that $\tau_0 < \tau_1 < \tau_2$ and $T_0 > T_1 > T_2$ (T being the absolute temperature).

The two top rows of curves in Figure 4 are the γ versus t and $\dot{\gamma}$ versus dependences obtained by the constant shear stress method. The arrows at the curves indicate the moment of removal of the load from the specimens, after which a reverse elastic aftereffect may be observed.

The three lower curves are the time or deformation dependences of the shear stresses obtained by the constant deformation rate method. The arrows at these curves show the moment at which deformation is stopped and stress relaxation begins at constant strain.

The curves in the left-hand column in Figure 4 were obtained at low shear stresses or high temperatures when the deformation rate of the polymers was small compared with the rate of the relaxation processes. Under these conditions the polymers behave like Newtonian fluids. After the deformations begin at the constant τ or the constant $\dot{\gamma}$, steady deformation conditions are set practically instantly. The shear stresses and the rate of deformation also drop quickly to zero after the deformation of specimens stops (at the constant deformation or upon unloading, respectively). In the case of Alkathene-2 and polystyrene, the polymers studied in this work, curves similar to those in the lower left-hand corner of the Figure 4 were obtained at rather high temperatures.

The curves in the middle vertical column describe the cases where the rates of deformation and relaxation processes are commensurable. The transition to steady flow conditions corresponds to attainment of limiting (equilibrium) highly elastic strain when the rate of its development becomes zero. As indicated above, the duration and nature of the transitional process (up to the steady flow conditions) depend on the relation between the rates of deformation and stress relaxation. In the case of highly elastic polymer melts the appearance of retarded elastic deformations corresponds to the nonlinear dependence of shear stresses on the rate of deformation at steady flow conditions. With increasing shear stress and deformation rates a monotonic transition takes place from the steady flow conditions at constant viscosity to the flow conditions under which the polymer systems behave as non-Newtonian fluids.

The graphs in the right-hand column in Figure 4 show the course of the deformation of the polymer melts at rather low temperatures and at high shear stresses and high deformation rates. In these cases there appears a point of inflection on the γ versus t curve corresponding to a minimum on the $\dot{\gamma}$ versus t curve. This fact can be accounted for in the following way. After applying the load at a rate decreasing in time, highly elastic deformation develops. At the same time the stresses inside the system are redistributed, being resolved in the zones containing rapidly relaxing structural elements and concentrated on the slowly relaxing elements which retard irreversible deformation. Since the effective stress in polymer increases steadily, the total deformation should develop at a considerable rate. If the rate of relaxation processes in the stress concentration zones is not high enough, the destruction of the structural elements retarding the development of deformation is enhanced. At a certain moment this breakdown of the structure becomes avalanchelike and results in acceleration of the irreversible deformation (viscous flow). Therefore, on the one hand, the possibility of the development of highly elastic deformation (always limited by its nature) is exhausted; on the other, the accumulation of plastic deformations is accelerated, which results in a point of inflection on the γ versus t curve and in a minimum on the $\dot{\gamma}$ versus t curve. After the sudden breakdown of the polymer structure there begins a restoration of the network, which retards the development of plastic deformation (viscous flow). When dynamic equilibrium is reached between the breakdown and restoration processes, a steady flow occurs in the polymer.

As to the τ versus γ and τ versus t dependences obtained at high deformation rates and shown in the lower right-hand plot in Figure 4 the following is of importance. In readily relaxing polymer systems the rigidity of the structural framework consisting of a network of macromolecules and bearing the load is strongly dependent on the rate of deformation. At high deformation rates the stress growth may exceed the rate of stress relaxation. This is due to the high concentration of crosslink points in the three dimensional network of macromolecules. The tying points begin to break at the same time as the deformation of the polymer does. The breakdown becomes very intensive at high stresses. Multiple ruptures of the macromolecule junction points correspond to the attainment of the ultimate strength of the three-dimensional macromolecular network or to the max-

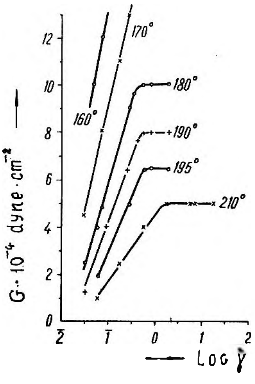

Fig. 5. Dependence of shear modulus for highly elastic deformation on the deformation rate for polystyrene.

ima on the τ versus γ and τ versus t curves. This was proved just recently by direct experiments.[14] After the ultimate strength is surpassed, the shear stresses begin to diminish, since the destruction of the macromolecules network facilitates the relaxation process. A rapid drop in stresses right after passing through the maximum on the τ versus t curve is due to the high stress attained at the point where the destruction of the network became most intensive (in the maximum zone). The destruction of the supermolecular structures in the polymer occurs with steadily decreasing intensity until steady flow conditions are attained. Recently a quantitative description was given[15] of the transition through the ultimate shear strength for the case where the relaxation time spectrum and the τ versus $\dot{\gamma}$ dependence were known.

We should like to conclude our examination of the two main methods of studying the elastic-strength properties of polymer melts and the transition from elastic deformations to steady viscous flow with the following note. The advantage of the constant shear stress method lies in the fact that it permits the magnitude of highly elastic deformation to be determined for various τ and total deformation values and enables study of the effect of various factors on this magnitude. The method is not very convenient for determining the ultimate shear strength and in general the transition from elastic deformation to steady viscous flow. The constant deformation rate method is applicable not only to studying this transition; it can be readily combined with the measurement of stress relaxation at constant deformations. However, the constant deformation rate method permits the quantitative estimation of polymer properties only when very rigid dynamometers are employed.[8]

After a qualitative analysis of the various cases of attainment of steady flow conditions, it should be reasonable to return to a more detailed examination of the data given in Figures 2 and 3.

The angular factors of the tangents of the τ versus γ curves at zero shear stresses can be used to find the shear modulus G for highly elastic deforma-

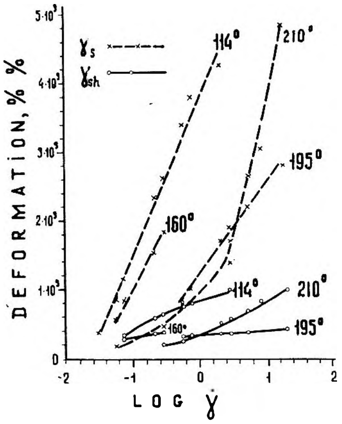

Fig. 6. Dependence of the deformations corresponding to the ultimate shear strength and attainment of steady flow on the rate of deformation for Alkathene-2 and polystyrene.

tion. This procedure is reliable only in the case of very rigid dynamometers, since otherwise the inertia factor[8] has a great effect on the initial parts of the τ versus γ curves. The G versus $\dot{\gamma}$ dependences for polystyrene are shown in Figure 5. After a certain critical $\dot{\gamma}$ value is reached, G no longer depends on $\dot{\gamma}$. This occurs in the range of the $\dot{\gamma}$ values where the τ versus γ curves become markedly extreme in shape and their ascending branch becomes linear over a considerable τ interval. It may be assumed that the saturation region of the $G(\dot{\gamma})$ function corresponds to the plateau—the middle part of the horizontal section characterizing high elasticity on the thermomechanical curve or to the part adjacent to the horizontal section. A transition to the saturation region of the $G(\dot{\gamma})$ function signifies that the deformation rates become so high that under these conditions the macromolecules do not move, on the whole with respect to one another, i.e., coordinated movements of their segments have no time to develop. However, these rates remain much lower than the rates of the change in macromolecular conformations responsible for the mobility of separate segments and the high elasticity of a polymer. This means that it is in the range of deformation rates where G is independent of $\dot{\gamma}$ that the high elasticity of a polymer melt becomes apparent in pure form. The polymer melt network formed by intermolecular bonds plays an important part in the processes under consideration. A sharp transition to the region of saturation of the $G(\dot{\gamma})$ function indicates that the rates of the change in macromolecular conformations on the sections of separate segments may be much higher than those of the coordinated movements of these segments.

The τ versus t and τ versus γ curves obtained at various deformation rates which are constant for each given test enable a determination of the conditions for attaining ultimate shear strength and steady flow. It is evident from Figures 2 and 3 that as the deformation rate rises the ultimate shear strength and steady deformation conditions are reached

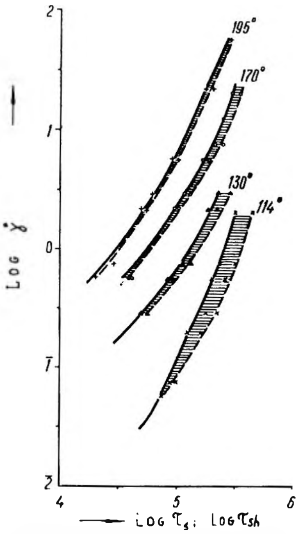

Fig. 7. Dependence of the ultimate shear strength and shear stress in steady flow on the deformation rate for Alkathene-2.

much faster. These processes are much accelerated with increasing temperature. At lower temperatures the time of the attainment of the ultimate strength depends more strongly on the rate of deformation. It is noteworthy that even at rather high temperatures and deformation rates the time of the attainment of ultimate strength and steady flow takes several seconds.

Figure 6 gives typical curves characterizing the dependence between the rate of deformation and the magnitudes of deformation corresponding to the ultimate shear strength (γ_{sh}) and to the attainment of steady flow conditions (γ_s). The 114 and 195°C. curves are for Alkathene-2 and the 160 and 210°C. curves are for polystyrene. The dotted lines show the γ_s versus γ dependence, whereas the continuous ones show the γ_{sh} versus $\dot{\gamma}$ dependence.

It follows from the data discussed above that the ultimate strength of polymer melts is reached at deformations of several hundred per cent, while the attainment of steady flow conditions corresponds to deformations of several thousand per cent. This is of prime importance for determining deformation conditions and the state of polymers as to their structure in various cases of processing. It may be supposed that the passage of a polymer through short nozzles and pinpoint pouring channels at very high rates occurs under conditions of highly elastic deformation (before passing the ultimate strength). On passage of a polymer melt from a reservoir into a nozzle the rate of deformation may increase abruptly, which is followed by a change in structure and properties. Very great deformations are required for the development and completion of the change. Under the conditions of a nonhomogeneous deformation rate field this may result in a very complicated state pattern of the polymer.

Figures 2, 3, and 6 show that increasing deformation rate results in a sharp rise in the γ_s values and in a slight increase in γ_{sh}.

Figures 7 and 8 give the dependences of the ultimate shear strength and shear stress at steady flow conditions on the rates of deformation at various temperatures for Alkathene-2 and polystyrene, respectively. The continuous curves represent the τ_s versus $\dot{\gamma}$ dependences and the dotted ones show the τ_{sh} versus $\dot{\gamma}$ dependences. The horizontal lines connecting the τ_s versus $\dot{\gamma}$ and τ_{sh} versus $\dot{\gamma}$ curves characterize the transitional regimes and changes in the polymer structure on passing from highly elastic deformation to viscous flow. The calculation of the activation energy for the passage through the ultimate strength and for steady viscous flow revealed that for the deformation rates used the values of the activation energy are practically identical (as would be expected, the activation energy of the passage through the ultimate shear strength is a little higher). Hence, it may be concluded that the passage through the ultimate shear strength and the viscous flow are processes of similar molecular mechanism.

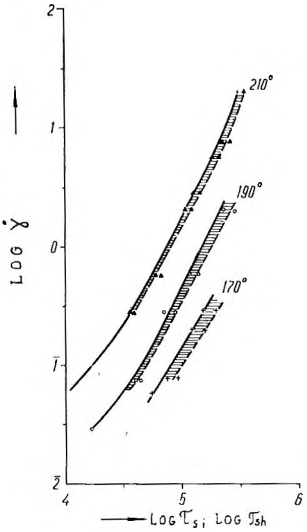

Fig. 8. Dependence of the ultimate shear strength and shear stress in steady flow on the deformation rate for polystyrene.

It follows from a comparison of the τ_s versus $\dot{\gamma}$ and τ versus γ curves obtained at different deformation rates that the maxima on the τ versus γ curves can be recorded practically only at the rates corresponding to the very marked non-Newtonian behavior of polymer systems. However, the theory of this question shows[15] that changes in the polymer structure and the maxima on the τ versus γ curves should appear parallel with the nonlinear relationship of τ_s and $\dot{\gamma}$. It follows from this, that the lower value of the ultimate strength corresponds to the critical value of shear stress at which on the flow curves there is a transition from the Newtonian to the non-Newtonian branch. As this transition is smooth for polymer melts, the experimental determination of the lower ultimate strength present some difficulties.

The margin by which τ_{sh} exceeds τ_s increases with growing deformation rates. The resistance to the development of highly elastic deformations cannot grow boundlessly, while an increase in the resistance to viscous flow as the deformation rate increases is theoretically infinite. Therefore, it is to be expected that the contribution of the resistance to deformation corresponding to the change in the polymer structure on passing through the ultimate strength, i.e., the value $(\tau_{sh} - \tau_s)/\tau_s$, will fall off at high deformation rates. It should tend to zero on reaching the upper value of the ultimate strength corresponding to the transition to the upper Newtonian branch on the flow curves. Thus, in general the τ_{sh} versus $\dot{\gamma}$ and τ_s versus $\dot{\gamma}$ curves should form a closed loop. Its area can serve as an energy measure of the possible structure changes in polymer systems on their deformation.

At the deformation rates used there were only reversible changes in the mechanical properties and structure of polymer melts observed. Under higher rates the polymers may undergo mechanical degradation.

All the regularities described for Alkathene polyethylene and polystyrene are common to many polymer melts, as has been demonstrated by tests with polypropylene, polyisobutylene, and some other thermoplastics and elastomers. It remains to add that at lower temperatures the recovery of the structure and properties of polymers after their deformation may take a long time at lower temperatures.[14]

References

1. Dienes, G. J., *J. Colloid Sci.*, **2**, 131 (1947).
2. Buchdahl, R., *J. Colloid Sci.*, **3**, 87 (1948).
3. Hoff, E. A. W., *J. Polymer Sci.*, **9**, 41 (1952).
4. Dexter, F. D., *J. Appl. Phys.*, **25**, 1124 (1954).
5. Rebinder, P. A., and L. V. Ivanova-Chumakova, in *Collection Uspekhi Khimii i Tekhnologii Polimerov*, Coll. 2, Goskhimizdat, Moscow, 1957, p. 146.
6. Kepes, A., "Contribution a l'étude rhéologique des hauts polymères a l'état fondu," Dissertation, Strasbourg, 1958.
7. Pohl, A., and C. G. Gogos, *J. Appl. Polymer Sci.*, **5**, 67 (1961).
8. Leonov, A. I., A. Ya. Malkin, and G. V. Vinogradov, *Kolloid. Zh.*, **26**, 335 (1964).
9. McCord, R. A., and B. Maxwell, *Modern Plastics*, **39**, 116 (1961).
10. Klaz, S. I., and E. E. Glukhov, *Plasticheskie Massy*, **1961**, No. 3, 28.
11. Glukhov, E. E., G. V. Vinogradov, and S. I. Klaz, *Vysokomolekul. Soedin.*, **5**, 1953 (1963).
12. Vinogradov, G. V., and V. P. Pavlov, *Rheol. Acta*, **1**, 455 (1961).
13. Bartenev, G. M., *Dokl. Akad. Nauk SSSR*, **133**, 88 (1960).
14. Vinogradov, G. V., et al., *Dokl. Akad. Nauk SSSR*, **154**, 1421 (1964).
15. Leonov, A. I., and G. V. Vinogradov, *Dokl. Akad. Nauk SSSR*, **155**, 406 (1964).

Résumé

Ce mémoire décrit un élastoviscosimètre rotatif avec un dynanomètre extrêmement rigidedestiné à étudier les propriétés rhéologiques des polymères visco-fluides à l'état condensé ainsi que des solutions concentrées de polymères par le procédé des vitesses de déformation constantes. Dans un large domaine de températures on a étudié l'Alkathene-2 et le polystyrène. On a obtenu pour ces corps les relations entre les contraintes de cisaillement et la déformation qui deviennent non-monotones lorsque la vitesse augmente. Ce fait caractérise la désintégration réversible de leur structure qui s'accroît avec la vitesse et permet de déterminer la résistance à la rupture par cisaillement comme un point singulier sur les courbes contrainte–déformation. La rupture par cisaillement est atteinte pour des déformations qui se chiffrent par des centaines de pour cent, alors que les régimes d'écoulement stationnaires s'établissent pour des déformations de plusieurs milliers de pour cent. A mesure que la vitesse de déformation croît, le temps nécessaire pour atteindre la résistance à la rupture par cisaillement diminue, et la durée requise pour l'établissement de l'écoulement stationnaire baisse elle aussi. Lorsque la vitesse de déformation s'élève, la déformation pour laquelle la résistance à la rupture par cisaillement est atteinte, augmente légèrement, tandis que la déformation correspondant au début de l'écoulement stationnaire s'accroît trés fortement. Les énergies d'activation du passage par la résistance à la rupture par cisaillement et du début de l'ecoulement stationnaire ont des valeurs voisines. La relation entre le module de la déformation hautement élastique dans un polymère à structure intacte et la vitesse de déformation s'exprime sous la forme d'une fonction à saturation, le domaine de saturation correspondant à des vitesses de déformation pour lesquelles les progrès de l'écoulement visqueux s'avèrent impossibles sans que la structure du bain de fusion soit désintégrée (sans passage par la résistance à la rupture par cisaillement).

Zusammenfassung

Ein Rotations-Elastoviskosimeter mit sehr hartem Dynamometer wird beschrieben, das für die Untersuchung rheologischer Eigenschaften an zähflüssigen Polymeren in kondensiertem Zustand und in konzentrierten Lösungen der Polymeren nach der Methode der stationären Deformationsgechswidigkeit bestimmt ist. Alkathen-2 und Polystyrol wurden in einem grossen Temperaturbereich untersucht. Die Abhängig keit der Schubspannung von der Deformation ermittelt, die bei erhöhter Deformations geschwindigkeit nicht mehr monoton ist. Das charakterisiert die mit der vergrösserten Geschwindigkeit zunehmende reversible Zerstörung der Struktur und erlaubt die Schubfestigketsgrenze als besonderen Punkt auf den Kurven Schubspannung–Deformation zu bestimmen. Die Schubfestigkeitsgrenze ereicht man bei Deformationen, welche Hunderte von Prozenten ausmachen, Bereiche konstanten Fliess stellen sich bei Deformationen ein, welche Tausende von Prozenten betragen. Bei vergrösserter Schergeschwindig keit wird die Zeit für das Erreichen der Festigkeitsgrenze vermindert, etwas vermindert wird auch die Zeit zum Erreichen eines konstanten Fliessregime. Bei vergrösserters Schergeschwindigkeit wird eine Deformation entsprechend der Schubfestigkeitsgrenze etwas erhöht; sehr stark vergrössert sich die Deformation, welche dem Erreichen des konstanten Fliessens entspricht. Die Aktivierungsenergie des Übergangs über die Schubfestigkeitsgrenze und die des konstanten Fliessens haben sehr ähnliche Beträge. Die Abhängigkeit des Moduls der hochelastischen Deformation im Polymeren mit einer nicht zerstörten Struktur von der Schergeschwindigkeit wird durch eine Funktion mit Sättigungsbereich ausgedrückt, wobei das Gebiet der Sättigung solchen Schergeschwindigkeiten entspricht, dei denen die Entwicklung des zahflüssigen Fliessens ohne Zerstörung der Struktur des Schmelzens unmöglich ist (ohne Ubergang über die Festigkeitsgrenze).

Received April 29, 1964
Revised August 31, 1964

JOURNAL OF POLYMER SCIENCE: PART A VOL. 3, PP. 933–948 (1965)

Chain Stiffness in Polyisocyanates*

N. S. SCHNEIDER† and S. FURUSAKI, *Department of Chemical Engineering, Massachusetts Institute of Technology, Cambridge, Massachusetts,* and R. W. LENZ, *Fabric Research Laboratories, Dedham, Massachusetts*

Synopsis

Light-scattering measurements of the molecular conformation of *n*-hexyl polyisocyanate (PIC) in tetrahydrofuran (THF) show that the ratio of the root-mean-square end-to-end distance to the maximum extension exceeds 25% even at a molecular weight of 3×10^5 and that the effective bond length in the equivalent freely linked chain is 23 A., corresponding to about 17 links per statistical segment. These results are at least twice as high as the values of cellulose trinitrate in acetone at a comparable degree of polymerization. Although a significant variation in intrinsic viscosity occurs in different solvents, the recently reported viscosity- and sedimentation coefficient–molecular weight exponents of 1.18 and 0.16 for *n*-butyl PIC in THF indicate that the polymer behavior lies outside the Gaussian region and must result from the short range structure rather than from strong interactions with the solvent. In fact, by using a form of the Kirkwood-Riseman theory, modified to take account of the expansion factor, a viscosity–molecular weight exponent of 0.9 is calculated for theta conditions. It is proposed that the chain is stiffened by restrictions to rotation imposed by resonance effects in the peptide bonds that make up the polymer backbone.

INTRODUCTION

The low temperature anionic polymerization of a variety of N-substituted monoisocyanates to high molecular weight polyisocyanates (PIC) was reported by Shashoua and co-workers in 1960.[1] The polymerization system of choice was NaCN in *N,N*-dimethylformamide which gave polymer yields of about 70% with isocyanates carrying linear aliphatic substituents. Conceivably polymerization might take place either through the carbon–nitrogen double bond to yield the repeating structure I:

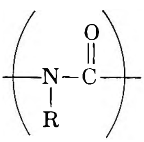

$$\left(-\underset{\substack{| \\ R}}{N}-\overset{\substack{O \\ \|}}{C}- \right)$$

I

---

* Taken in part from the M.S. Thesis of S. Furusaki, Department of Chemical Engineering, Massachusetts Institute of Technology, January 1964.

† Present address: Clothing and Organic Materials Division, U. S. Army Natick Labs., Natick, Massachusetts.

or through the carbon–oxygen double bond resulting in a polyacetalic structure II:

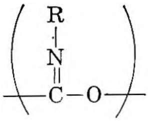

$$\left(\overset{\overset{\displaystyle R}{|}}{\underset{}{\overset{\displaystyle N}{\|}}} \!\!\!\! -\text{C}-\text{O}- \right)$$

II

The intense carbonyl adsorption of 5.9 μ indicates that the first structure predominates, but this does not exclude the possibility that some addition occurs through the carbon–oxygen double bond. In a later study of the polymerization of *n*-butyl isocyanate with a variety of catalysts Natta's group[2] found that a polymer with a far higher degree of crystallinity could be obtained using the catalyst system, ethyllithium in benzene. As with the polymer of lower crystallinity from NaCN–DMF, this sample also showed the strong carbonyl adsorption typical of the substituted amide structure.

The properties of this class of polymers which are especially provocative are those which call attention to the possibility that the polyisocyanates possess an unusually extended chain structure. This was suggested by two items of the properties reported by Shashoua; first, an *n*-heptyl polymer of molecular weight 69,000 had an inherent viscosity in benzene of 2.4 dl./g., equivalent to the intrinsic viscosity of polystyrene of molecular weight 1×10^6 in toluene and, second, in spite of the absence of hydrogen bonding the melting points of the polymers were unusually high, 250°C. for the *n*-ethyl and *n*-propyl homologs, which is comparable to the melting temperature of nylon 66. The more highly crystalline *n*-butyl PIC prepared by Natta's group also had an unusually high intrinsic viscosity. These inferences regarding chain extension have recently been substantiated by the results published by Buchard[3] on *n*-butyl PIC samples polymerized with the NaCN–DMF system to cover the molecular weight range of 18,000–210,000. His measurements on the solution properties of these samples showed that both the viscosity–molecular weight exponent and the sedimentation coefficient–molecular weight exponent appear to lie outside the range expected for Gaussian behavior.

This paper reports on a limited light scattering and viscosity study of a higher N-substituted homolog, the *n*-hexyl PIC, which furnishes additional information on the nature of the chain conformation in these polymers. When taken together with the work on the *n*-butyl polymer, the data suggest that the PIC molecules deviate from random-flight statistics as a result of inherent chain stiffness rather than strong interactions with the solvent and therefore, should exhibit partial draining even in a theta solvent. Many of the problems of interpretation that arise in the present work are similar to those which have been dealt with in the several extensive studies cellulose trinitrate (CTN),[4–7] and the behavior of the PIC may be viewed profitably by comparison with results obtained on this classical stiff chain polymer. In the interests of brevity, concepts and equations found in the group of papers just cited will be used without full development. The papers by Holtzer, Benoit, and Doty,[4] and by Hunt, Newman, Scheraga, and Flory[5] are especially pertinent, while the recent review by Kurata and Stockmayer[8] was indispensible to the authors in preparation of this paper.

EXPERIMENTAL

The sample was prepared following the directions given by Shashoua[1] as a single run performed to test the method of polymerization. Since only 5 g. of polymer was available a conservative approach to the experimental work was necessary. A number of measurements were first made to characterize the original sample. A little more than 1 g. of the sample was then fractionated from a 0.5% benzene solution by titration with acetone to the cloud point. The separation was poor with the fractions covering less than a threefold range of molecular weight. Since the ratio of the weight-average to number-average molecular weight in the sample was close to two, this limited resolution either reflects the poor choice and control of the fractionation conditions or the interference of some crystallization during phase separation. Consideration of the latter possibility raised the question as to whether association of molecules through polar interactions might occur in solution. As a check on possible aggregation a sample was dissolved with slow stirring in tetrahydrofuran and the viscosity first determined 30 min. after the addition of the solvent. No changes in viscosity were detected, either shortly after solution or over the following 96 hr. period. This suggests that aggregation does not occur in tetrahydrofuran and that the polymer in solution is stable at room temperature. Equivalent results were obtained in benzene.

Light-scattering determinations were made in cylindrical cells with plane entrance and exit windows at ambient temperature and at a wavelength of 436 A. The Brice-Phoenix light-scattering photometer was calibrated against benzene, a value of 48.9×10^{-6} cm.$^{-1}$ being adopted for Rayleigh's ratio. The solutions were clarified by filtration through solvent-resistant microporous membranes of 0.45 μ pore diameter. Tetrahydrofuran was used as solvent, since it provided a relatively large refractive index increment $dn/dc = 0.0978$ cm.^{3}/g., in comparison to the value of 0.054 cm.^{3}/g. in chloroform, the solvent used for this purpose by Shashoua.

Viscosity measurements were made in an Ubbelohde suspended-level viscometer on the three fractions f_1, f_2, and f_3 and on the reprecipitated but unfractionated sample 4, in tetrahydrofuran and in chloroform. In addition, a survey was made on the viscosity of the unfractionated sample in a number of other solvents as well. The intrinsic viscosity, $[\eta]$, was determined as the common intercept of linear plots of η_{sp}/c and $\ln \eta_{rel}/c$ against concentration. No corrections were made for shear rate dependence, but judging from the results reported by Hunt[4] this would increase values of the intrinsic viscosity above 8 by about 6%, with a smaller effect on the samples of lower viscosity.

RESULTS

The Zimm plot for the lowest molecular weight fraction shown in Figure 1 has the appearance of a normal rectilinear grid. The plot for the unfractionated sample, shown in Figure 2, displays curvature in the zero angle line. There is also some evidence of curvature in the angular data at high angles but this was ignored, and the angular data at each concentration were fitted with a straight line. The graphs for the other two fractions showed no curvature in the angular data and the concentration dependence showed curvature only for the highest molecular weight fraction. Molecular weights and values of the second virial coefficient A_2 were actually determined by plotting the data at zero angle according to the equation

$$Kc/R(\theta = 0°, c)^{1/2} = Kc/R(\theta = 0°, c = 0)^{1/2}(1 + \Gamma_2 c)$$

where $\Gamma_2 = A_2 M$. This is analogous to the recommended procedure for plotting osmotic pressure data, and was used for the light-scattering measurements as a result of the large values of Γ_2. Compared to the direct method of plotting the data, the molecular weights so determined for the PIC samples were lower by about 6% and the virial coefficients lower by about 10% for f_1 and f_2, while for the two samples f_3 and 4, where the zero angle line showed curvature, the differences were far less.

If the data were assumed to lie in the initial angular region of the particle-scattering factor, then, as is well known, the intercept determines the weight-average molecular weight:

$$Kc/R(0°, 0) = 1/M_w$$

The z-average of the root-mean-square end-to-end distance, $(\overline{R_z^2})^{1/2}$ is calculated from the initial slope of the zero concentration line:

$$(\overline{R_z^2})^{1/2} = [3\lambda'/2(2\pi)^{1/2}](SM_w)^{1/2}$$

where λ' is the wavelength of light in the medium and S is the slope. These values and the second virial coefficients from the implementation of the first equation are collected in Table I along with some derived parameters.

TABLE I
Light-Scattering Results

Sample	$\bar{M}_w \times 10^{-5}$	$A_2 \times 10^4$	$(\overline{R_z^2})^{1/2}$ A. $\times 10^{-3}$	$\dfrac{(\overline{R_w^2})^{1/2}}{L_w}$	$b = \left(\dfrac{\overline{R_w^2}}{2N_w}\right)^{1/2}$, A.	$\Phi_0 \times 10^{21}$
f_1	1.46	7.6	1390	0.44	24	0.63
f_2	2.80	8.2	1800	0.29	22	0.97
f_3	3.20	7.8	1920	0.27	22	1.07
4	3.55	6.9	2040	0.26	23	0.92

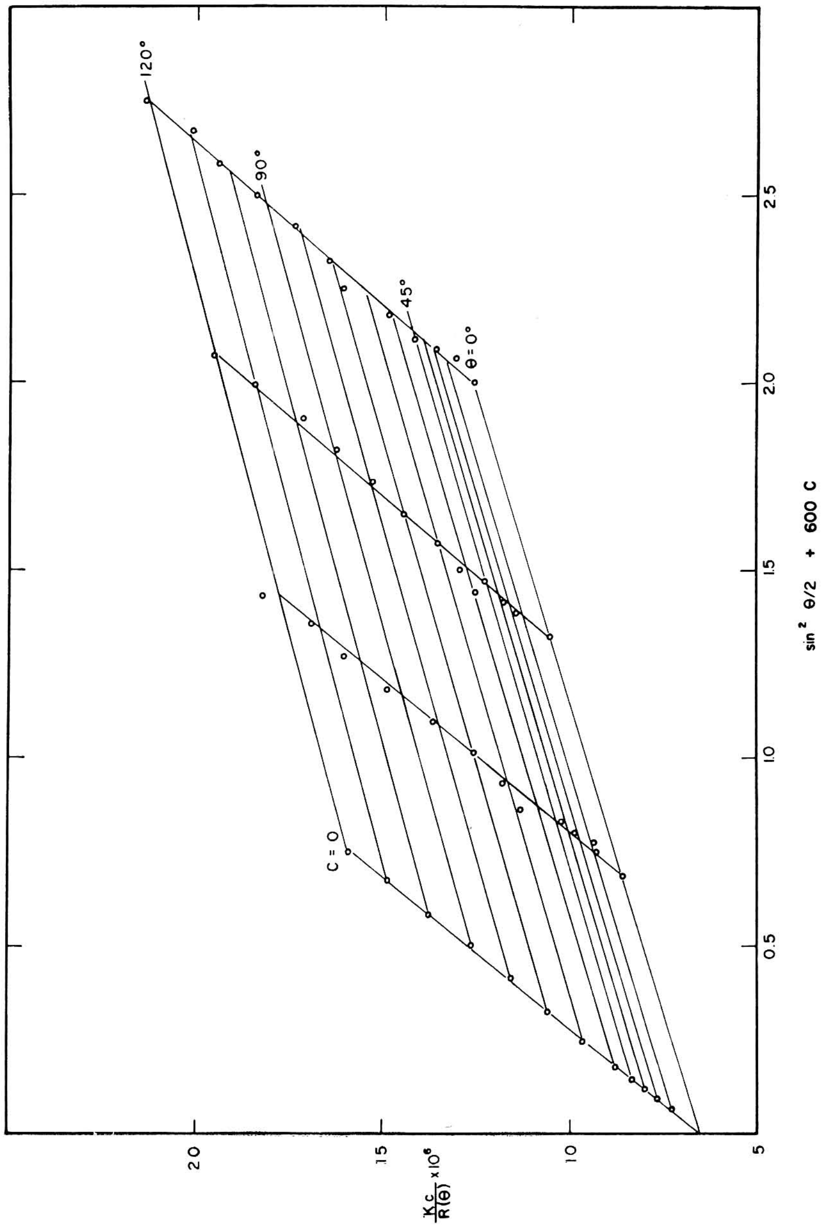

Fig. 1. Zimm plot for *n*-hexyl polyisocyanate, $\bar{M}_W = 1.46 \times 10^5$, in tetrahydrofuran.

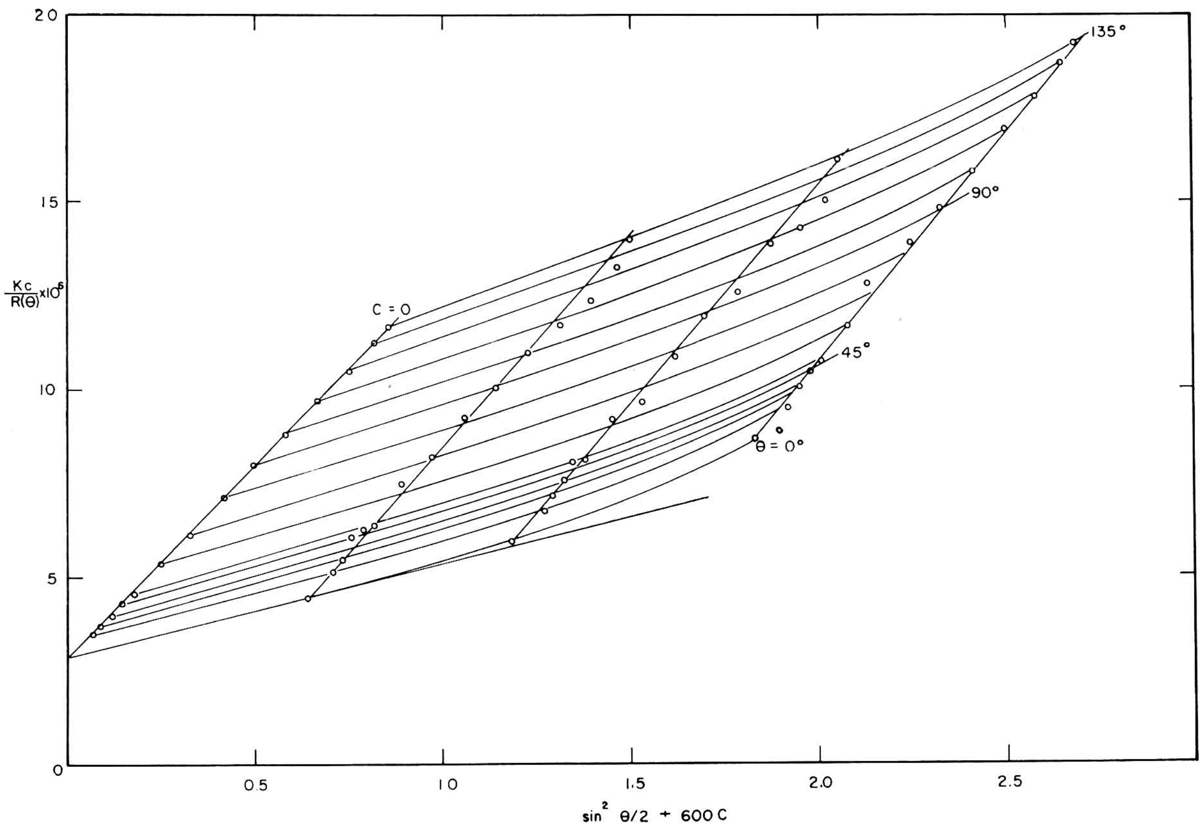

Fig. 2. Zimm plot for *n*-hexyl polyisocyanate, $\bar{M}_W = 3.20 \times 10^5$, in tetrahydrofuran.

TABLE II
Viscosity Results

Sample	Tetrahydrofuran $[\eta]$	Tetrahydrofuran k	Chloroform $[\eta]$	Chloroform k	$[\eta]_{\text{thf}}/[\eta]_{\text{CHCl}_3}$
f_1	5.9	0.49	4.5	0.81	1.31
f_2	10.3	0.60	7.0	0.61	1.47
f_3	12.1	0.57	8.3	0.78	1.55
4	11.2	0.75	7.8	0.90	1.43

TABLE III
Intrinsic Viscosity in Various Solvents[a]

Solvent	$[\eta]$	k	$[\eta]/[\eta]_{\text{CHCl}_3}$
Carbon tetrachloride	12.1	0.56	1.65
Benzene	11.5	0.51	1.57
Tetrahydrofuran	10.0	0.43	1.37
Tetrahydrofuran–dimethylformamide (4:1)	7.8	0.75	1.07
Chloroform	7.3	1.10	1.00

[a] Unfractionated sample.

Viscosities were determined over the concentration range of 0.01–0.06% and in some cases up to 0.08%. The values of η_{sp}/c or $\ln \eta_{\text{rel}}/c$ followed a strictly linear dependence on concentration. Intrinsic viscosities in tetrahydrofuran and carbon tetrachloride are listed in Table II together with values of the Huggins constant k which occurs in the concentration dependence of η_{sp}/c. Results from the viscosity survey on the unfractionated sample appear in Table III.

DISCUSSION OF RESULTS

Light-Scattering Behavior

Application of the light-scattering results to the specification of chain conformation is complicated by a number of effects. Nonetheless, it will be shown that it is possible to develop a significant if qualitative measure of the magnitude of chain stiffness which provides a clear demonstration of the unique behavior of the polyisocyanates. To take account of the effects of polydispersity the corrections appropriate to the random distribution with $\overline{M}_n:\overline{M}_w:\overline{M}_z = 1:2:3$ are invoked for the fractions as well as the unfractionated sample. If the fractions are significantly less polydispersed this procedure will underestimate the magnitude of the chain extension. On this basis the relative extension of the chain, $(\overline{R_w^2})^{1/2}/L_w$, equal to the ratio of the end-to-end distance to the length of the fully extended chain, L, and values of the effective bond length, $b = (\overline{R_w^2}/2N_w)^{1/2}$, where N_w is the weight-average degree of polymerization, have been calculated and appear in columns 5 and 6 of Table I. In these calculations it was assumed that $(\overline{R^2})^{1/2}$ is proportional to $M^{1/2}$ and that the projection of a PIC monomer unit in the direction of the chain is 2.27 A. in accord with the structure to be discussed in the last section of the paper. The value of b signifies the bond length in the equivalent freely linked chain having the same number of bonds, $2N_w$, as the real chain.

Even after correction for heterogeneity the values of the relative extension and the effective bond length are enormous. The extraordinary nature of these values is even more apparent when the results for CTN are used as a yardstick. The difference in monomer molecular weight, 127 for PIC and 297 for CTN, must be taken into account so that the characteristic parameters are compared at the same degree of polymerization. For CTN the values of $(\overline{R_w^2})^{1/2}/L_w$ drop rapidly in the appropriate molecular weight range from about 0.20 at $M_w = 3.5 \times 10^5$ to 0.13 at $M_w = 8 \times 10^5$, according to values calculated on a weight-average basis from the results of Holtzer et al.[4] These are only one-half the corresponding values for PIC. The value of b is 34 A. for CTN, about 40% larger than the values for PIC. However, the length of the projection of the rigid glucose unit in the chain direction is 5.15 A. for CTN and the bond length is 1.32 A. for PIC. Therefore, the respective values of b correspond to 6.6 links per statistical segment in the cellulose polymer compared to 17.4 links per statistical segment in the PIC chain. A comparison on this basis rather than in terms of the effective bond length appears to be a more satisfactory expression of chain stiffness since it relates directly to the rotational freedom above the bonds in the chain backbone.

The foregoing comparisons were based on values calculated under the assumption that the data for PIC lie in the initial angular region. Reference to Table I shows that the values of $(\overline{R_z^2})^{1/2}$ are well above 800 A., which is the approximate upper limit for the region in which the initial linear behavior of $p^{-1}(\theta)$ can be observed for Gaussian coils,[9] and, therefore, the angular data for the highest molecular weight samples or possibly for all the samples may lie on the high angle asymptote of the reciprocal particle scattering factor, $p^{-1}(\theta)$. If this condition holds, the intercept $Kc/R(0°, 0) = 1/2M_n$. In turn, the slope defines the number-average end-to-end distance, $(\overline{R_n^2})^{1/2}$, which would be lower than the tabulated values of $(\overline{R_z^2})^{1/2}$ by a factor of $(^1/_3)^{1/2}$. This would leave the values for b unaltered but the values of $(\overline{R_n^2})^{1/2}/L_n$ would be increased by 40%. It would then be necessary to make the comparison with values ranging from about 40 to 20 for CTN over the appropriate range of M_n values.

Interpretation of the asymptotic data in this form presumes that the sample is a polydisperse collection of Gaussian coils whereas deviations from Gaussian behavior can also decrease the slope of the asymptote. From the particle scattering factors calculated for stiff chains in terms of the Porod-Kratky wormlike chain model,[9] it can be shown that the values of $(\overline{R_z^2})^{1/2}$ and of the relative extension should lead to some reduction in the slope of the asymptotic data. In view of the uncertainties about the angular region under observation and the polydispersity of the fractions it hardly seems worthwhile to attempt a more detailed examination of this effect at the present time.

The preceding discussion has sketched some of the issues that arise in any attempt to establish a definitive statement of the molecular conformation of the polyisocyanates on the basis of light-scattering data alone. However, the basic conclusion that the polyisocyanates are extraordinary stiff chain polymers appears to be clearly established by these results beyond the uncertainties in the precise values introduced by the various complications.

Viscosity Results

In view of the evidence which has just been assembled to establish the unusual stiff chain nature of PIC one might be surprised in turning to the

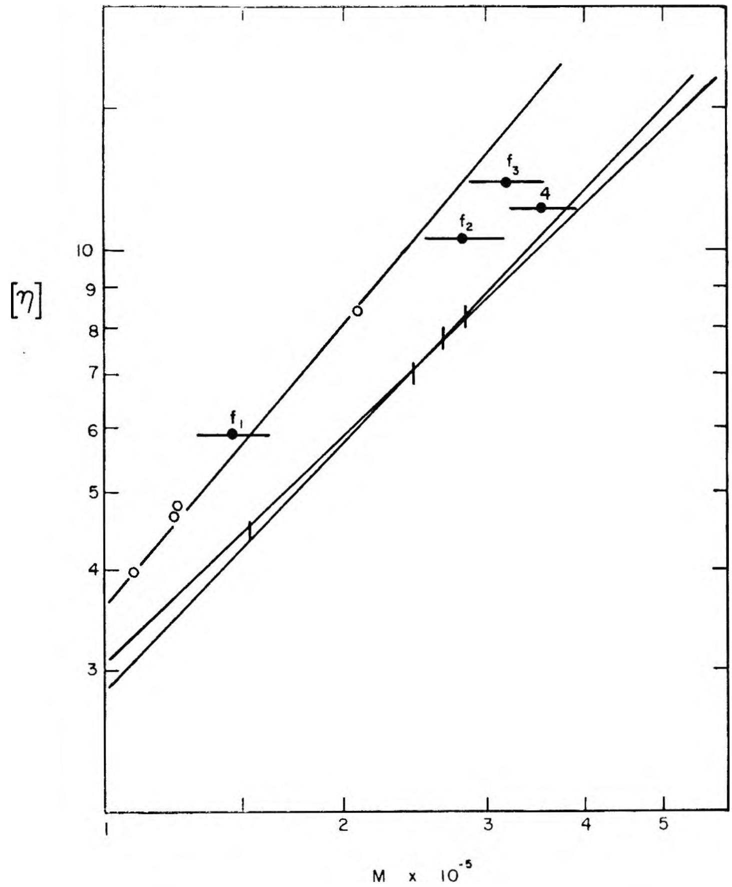

Fig. 3. Viscosity–molecular weight curve for *n*-hexyl polyisocyanate in chloroform (lower curves); vertical segments represent intrinsic viscosities in chloroform plotted at the molecular weights estimated from viscosities in THF using the calibration curve (upper line) based on Burchard's results[3] for *n*-butyl PIC in THF.

viscosity data in Table II to find that there is a difference of 30% to 50% for the viscosities in tetrahydrofuran and chloroform while a somewhat larger viscosity change can be observed by including other solvents as shown by the results on the unfractionated sample in Table III. These viscosity differences may arise from solvent effects on the short range interactions or from the resulting changes in the long range interactions. In general, the unperturbed dimensions of polymers are insensitive to the nature of the solvent except when there are strong polar interactions within the polymer chain. In the PIC molecule there is good reason to believe that the carbonyl oxygen and the amide nitrogen are strongly polarized (see the final section). However, there seems to be little interaction of these groups with the solvent since the polymer is soluble in liquids of low polarity. Therefore, it is tentatively suggested that the variation in viscosity is primarily the result of long range interactions.

On this assumption the viscosity changes provide a measure of the contribution of the excluded volume and it becomes of interest to test the viscosity-molecular weight exponent in chloroform, the solvent in which the polymer shows the lowest viscosity. To compensate for the limited molecular weight range covered by the samples and the uncertainties raised by the problems of molecular weight characterization discussed above, Burchard's viscosity data were used as a molecular weight calibration curve based on the viscosities in tetrahydrofuran. A portion of his data in the required range is plotted in Figure 3 as the open circles, and the solid line is drawn through the points with the slope of 1.18 deduced from the full set of data. When the present results are plotted against this curve (filled circles), the fractions can just be accommodated by horizontal lines representing an error of ±10% in molecular weight, but the point for the unfractionated sample 4 deviates by a larger amount. With the use of the molecular weights estimated from the viscosities in tetrahydrofuran, the viscosities in chloroform have been plotted with vertical segments representing ±2% error in viscosity. Two lines can be put through these data permitting a variation in slope from 0.96 to 1.04. Thus, the limited viscosity data in chloroform also appear to reside at the extreme limit of Gaussian behavior.

Implications of the Viscosity– and Sedimentation–Coefficient Molecular Weight Exponents

The problem which remains to be considered is to what extent the highly extended conformation of PIC is due to intrinsic chain stiffness (perhaps involving short-range interactions with the solvent) or to favorable long-range solvent interactions which swell the chain. In the case of CTN it was long believed that the various results argued for departure from random-flight behavior even in the unperturbed conformation, since the expansion factor α in ethyl acetate or acetone was estimated to be quite small and the parameters determined under these conditions were considered to differ little from the values in a theta solvent. However, it has recently been shown that these conclusions may be incorrect, and that strong interactions with the solvent may account for the very large values of the expansion factor, as high as 2.7 in acetone and 3.0 in ethyl acetate at a molecular weight of 3×10^5, while under theta conditions the chain would deswell to the dimensions of a normal Gaussian coil.[8] In connection with the estimate of α, we note that values of the quantity $A_2M_w/[\eta]$ for PIC are in the range of 20–25, close to the values of 20–30 for CTN in ethyl acetate. In the case of CTN, interpretation of these values according to a theory for the second virial coefficient was responsible for the small estimated values of α. However, Kurata and Stockmayer[8] have concluded that present theories of A_2 are untrustworthy in the range of large α or for polymers deviating from Gaussian statistics.

The viscosity–molecular weight and sedimentation–molecular weight exponents obtained by Burchard for the n-butyl PIC in tetrahydrofuran were $\nu_v = 1.18$ and $\nu_s = 0.16$. Burchard pointed out that both of these molecular weight exponents fall beyond the limiting values expected for Gaussian behavior. The Flory theory[10] for the excluded volume effect predicts the limiting values $\nu_v = 0.8$ and $\nu_s = 0.4$ for a Gaussian chain swollen by strong interactions with solvent. The theory of Kurata, Stockmayer, and Roig[11] yields a stronger dependence of the expansion factor on molecular weight and leads to the limiting values $\nu_v = 1.00$ and $\nu_s = 0.33$ for nondraining molecules in a good solvent. While Burchard's conclusion was predicated on the limiting values $\nu_v = 0.91$ and $\nu_s = 0.40$ derived from still another theory, clearly the n-butyl PIC passes even the more stringent requirements posed by the Kurata-Stockmayer-Roig theory. Thus the values of the exponents constitute definitive evidence that the observed non-Gaussian behavior cannot arise solely from the swelling of the polymer chain by interactions with the solvent.

The trend of the viscosity data in Table III also suggests that the expanded coil dimensions are not the result of a large value for α. Here the viscosity is seen to decrease in solvents of increasing polarity, and it has been found that the polymer is insoluble in ethyl acetate, methyl ethyl ketone, or in solvents such as dimethylformamide which are noted for their ability to solubilize polymers having strong polar interactions. The highest viscosities appear in carbon tetrachloride and benzene, where exothermic heats of mixing could hardly occur. The n-hexyl PIC is soluble even in aliphatic hydrocarbons such as cyclohexane and n-hexane, revealing a surprisingly non-polar character.

The plot of $[\eta]^{2/3}/M^{1/3}$ versus $M^{2/3}/[\eta]^{1/3}$ follows from the Kurata-Stockmayer-Roig theory as a means of extrapolating to an intercept on the ordinate which characterizes the unperturbed polymer chain dimensions. A necessary consequence of the fact that ν_v exceeds unity for the n-butyl PIC is that this plot cannot make a positive intercept as it does for all polymers thus far examined, including CTN,[8] with but one exception, the polypeptides in the helical form. When Burchard's data are plotted in the recommended form (not shown) the line through the data strikes a negative intercept without any ambiguity. The fit of the data serves to demonstrate the precision of Burchard's results and the reliability of the values for ν_v and presumably also ν_s.

From the pair of values, ν_v and ν_s, it is possible to estimate the level of polymer–solvent interactions and the molecular weight dependence of the viscosity and sedimentation coefficients in a theta solvent by application of the Kirkwood-Riseman relations for partially draining coils[12] in the form suggested by Kurata and Stockmayer.[8] Assuming an exponential form for the molecular weight dependence of the expansion factor,

$$\alpha = kM^{\nu_\alpha}$$

the draining parameter may be modified from $X = \lambda_0 N^{1/2}$ to $X = (\lambda_0 N^{1/2})/\alpha$ for nontheta conditions, where N is the degree of polymerization and λ_0 the parameter defined by Kirkwood and Riseman. This leads to the following results:[8]

$$\nu_v = \epsilon_v + (4 - 2\epsilon_v)\nu_\alpha$$

$$\nu_s = (1 - 2\nu_\alpha)\epsilon_s$$

Here ϵ_v is the value of ν_v for the free-draining case, tabulated by Kirkwood and Riseman, and ϵ_s is the corresponding value of ν_s, which may be calculated from their equation for the friction constant. Inserting the values for PIC leads to the following results: $X = 0.28$, $\nu_\alpha = 0.122$, $\epsilon_v = 0.91$, and $\epsilon_s = 0.21$. Thus tetrahydrofuran corresponds to a moderately good solvent, the limiting value of ν_α for an extremely good solvent being 0.167. The predicted viscosity–molecular weight exponent in a theta solvent, $\epsilon_v = 0.91$, indicates that the chain is abnormally expanded even in the absence of excluded volume effects. Further, from the value of X, the constant Φ_0 in the Flory-Fox equation:

$$[\eta] = \Phi_0(\overline{R^2})^{3/2}/M$$

is estimated to be 0.42×10^{21} under theta conditions. Values of Φ_z calculated directly from the results $(\overline{R_z^2})^{1/2}$, M_w, $[\eta]$, in Tables I and II are in the range 0.33×10^{21}–0.55×10^{21}. When the correction for the assumed random distribution is applied, $\Phi_0 = \Phi_z/0.51$, the approximately twofold higher values listed in the final column of Table I are obtained.

Consider the approximations involved in the data the correspondence between the calculated value of Φ_0 and that derived from the Kirkwood-Riseman relations is probably as good as could be expected and adds confidence to the conclusions on PIC conformation developed earlier from the light-scattering data. Thus we arrive at a reasonably consistent picture of the abnormally expanded conformation of the polyisocyanate chain. Further, it has been possible to show that the observed chain dimensions must be a consequence of short-range restrictions to rotation modified in only a secondary way by long-range excluded volume effects.

STRUCTURE OF THE POLYISOCYANATES

In seeking an explanation for the abnormal chain stiffness of PIC the structural feature which immediately commands attention is the repeated peptide linkage which forms the chain backbone structure. It is well known that resonance between the nitrogen and carbonyl of the peptide group endows the carbon–nitrogen bond with partial double bond character, imposing rigorous coplanarity on the participating atoms: N, H, C, O, all lying in the same plane. In fact, coplanarity of the atoms in the peptide link represents one of the canonical principles observed in formulating the structure of crystalline proteins. In polypeptides an α-methylene group separates each pair of peptide linkages. However in PIC there is the possibility of interaction between pairs of peptide groups involving resonance with the carbonyl groups on both sides of a given nitrogen in the fashion shown in eq. (1):

$$-\overset{\overset{\delta^-}{O}}{\overset{\|}{C}}-\underset{R}{\underset{|}{\overset{\delta^+}{N}}}-\overset{O}{\overset{\|}{C}}- \quad \text{———} \quad -\overset{O}{\overset{\|}{C}}-\underset{R}{\underset{|}{\overset{\delta^+}{N}}}-\overset{\overset{\delta^-}{O}}{\overset{\|}{C}}- \qquad (1)$$

This would impose partial double bond character on all the atoms of the chain backbone and could furnish a simple explanation of the unique conformational behavior of PIC. There are two possible arrangements for such a regular planar structure, the *trans* conformation III, and the *cis* conformation IV:

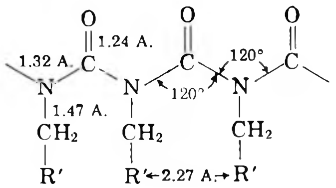

III

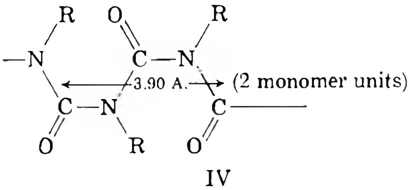

IV

Both planar structures suffer from severe steric crowding. In structure III the combined van der Waal's radii of the two carbonyl groups is 2.8 A., which is not incompatible with the calculated 2.27 A. separation, but the corresponding value for the two methylene groups is 4.0 A., which exceeds the center-to-center distance of the methylene carbons by 1.73 A. This is about 20% greater than the overlap of the substituents on the alternate carbons in polyisobutylene for which a strain energy of about 6 kcal./mole[13] has been estimated from the heat of polymerization. For the planar PIC conformation the strain energy should be somewhat higher due to the more severe crowding and the fact that the polyisobutylene chain spirals to relieve the steric interference. A further unfavorable aspect of structure III is the repulsive interaction between pairs of negatively polarized carbonyl groups and between the pairs of positively polarized nitrogens. In polyoxymethylene interaction between the oxygen atoms of the chain backbone favors the *gauche* over the *trans* conformation by about 1.8 kcal./-mole.[14] The repulsive energy in the planar PIC conformation must be larger than twice this value owing to the doubling of the number of interacting groups, as well as the increase in polarity and the decrease in interatomic distances which results from resonance. While these estimates lead to a rather large increase in internal energy arising from steric and electronic interactions, it seems likely that the total remains below the value of 21 kcal./mole resonance energy of the peptide bond.[15] Values for the contour length of the chain, L_w, used in Table I are based on this *trans* structure.

Turning now to structure IV, the calculated center-to-center distance between the carbonyl oxygen and methylene carbon is 1.29 A., which is 2.1 A. less than the combined van der Waal's radii of these opposing groups. Thus, steric interference is greater than that operating between the pairs of methylene groups in the previous conformation. However, the present arrangement achieves a greater separation of the carbonyl groups virtually eliminating this contribution to the internal energy. Therefore, the *cis* conformation is probably not any less acceptable than the first model. Furthermore, shielding of the carbonyl group by the aliphatic substituent provides an explanation for the surprising lack of polar interactions that might have been expected on the basis of the trans structure.

Some relief from steric interference in either structure could be achieved by slight departures from coplanarity, or by the distortion of bond angles. In the accepted structure for the *trans* polypeptide conformation the C—N—C bond angle in the chain backbone is opened to 123° and the O—C—N angle to 125° to provide greater separation between the carbonyl oxygen and the substituent on the α-carbon. Either or both types of modifications could be applied to structure IV and the first type to structure III. Further, it is possible that there is a distribution of monomer units between the two conformations. The infrared spectra for the polymer sample used in this study was virtually identical with that shown by Natta for the more crystalline polymer, the only strong difference being the presence of an adsorption peak of medium intensity at 1000 cm.$^{-1}$ which was not present in Natta's sample. The similarity of the spectra indicates that the primary structure of the two samples are essentially identical. Since there are also no asymmetric centers in the molecule the only remaining cause for the difference in crystallinity would appear to be configurational differences such as that between *cis* and *trans* arrangement or, possibly, an increased number of units enchained through the carbon–oxygen bond in the polymer prepared with NaCN-DMF system.

The preceding suggestions about the chain structure are clearly provisional. A more detailed study of the properties of polymers prepared from the two catalyst systems would hold much interest while, hopefully, x-ray diffraction studies could provide a test of the proposed planar structures.

Note added in proof: Measurements of the dielectric relaxation which are being carried out on solutions of *n*-butyl PIC at the National Bureau of Standards provide further information about PIC structure. There is observed only a single loss peak which occurs at a low and strongly molecular weight dependent frequency. Both the values and the molecular weight dependence of these long relaxation times are consistent with virtually rod like behavior of the molecule involving rotation about an axis transverse to the rod length. The absence of dispersion peaks at higher frequencies indicates that no flexible chain bonds are present. Furthermore, the large magnitude of the dielectric increment and the fact that it increases almost in proportion to molecular weight, indicates that there is an additive dipole moment along the chain. This suggests that the dominant configuration is the *cis* arrangement of units in Model IV.

The authors wish to express their appreciation to Drs. Hyuk Yu, Anthony Bur, and Lewis Fetters of the National Bureau of Standards for permission to report this summary of conclusions from their work.

We wish to express our appreciation to Professor W. H. Stockmayer for his helpful comments in the preparation of the manuscript and to Professor R. C. Lord for assistance in interpretation of the infrared spectra.

References

1. Shashoua, V. E., W. Sweeny, and R. F. Tietz, *J. Am. Chem. Soc.*, **82**, 866 (1960).
2. Natta, G., J. DiPietro, and M. Cambini, *Makromol. Chem.*, **56**, 200 (1962).
3. Burchard, W., *Makromol. Chem.*, **67**, 182 (1963).
4. Holtzer, A. M., H. Benoit, and P. Doty, *J. Phys. Chem.*, **58**, 624 (1954).
5. Hunt, M. L., S. Newman, H. A. Scheraga, and P. J. Flory, *J. Phys. Chem.*, **60**, 1278 (1956).
6. Huque, M. M., D. A. I. Goring, and S. G. Mason, *Can. J. Chem.*, **36**, 952 (1958).
7. Marrinan, H. J., and J. J. Hermans, *J. Phys. Chem.*, **65**, 385 (1961).
8. Kurata, M., and W. H. Stockmayer, *Fortschr. Hochpolymer. Forsch.*, **3**, 196 (1963).
9. Benoit, H., A. M. Holtzer, and P. Doty, *J. Phys. Chem.*, **58**, 635 (1954).
10. Flory, P. J., *J. Chem. Phys.*, **17**, 303 (1949).
11. Kurata, M., W. H. Stockmayer, and A. Roig, *J. Chem. Phys.*, **33**, 151 (1960).
12. Kirkwood, J. G., and J. Riseman, *J. Chem. Phys.*, **16**, 565 (1948).
13. Flory, P. J., *Principles of Polymer Chemistry*, Cornell Univ. Press, 1953, Ithaca, N. Y., p. 246.
14. Uchida, T., Y. Kurata, and M. Kubo, *J. Polymer Sci.*, **19**, 365 (1956).
15. Pauling, L., *Nature of the Chemical Bond*, 3rd Ed., Cornell Univ. Press, 1960, Ithaca, N. Y., p. 281.

Résumé

Des mesures de diffusion de lumière sur la conformation moléculaire du polyisocyanate (PIC) de *n*-hexyle dans le tétrahydrofuranne (THF) montrent que le rapport entre la distance quadratique moyenne entre extrémités de chaînes et celle de l'extension maximale, dépasse 25% même pour un poids moléculaire de 3×10^5 et que la distance effective d'une liaison dans la chaîne équivalente liée librement est de 23 Å, ce qui correspond à environ 17 liaisons par segment statistique. Ces résultats sont au moins deux fois aussi élevés que les valeurs pour le trinitrate de cellulose dans l'acétone à un degré de polymérisation comparable. Bien qu'il y ait une variation importante de viscosité intrinsèque dans différents solvants, les exposants du poids moléculaire déterminés récemment par viscosité et sédimentation, de valeur 1.18 et 0.16 pour le PIC de *n*-butyle dans le THF montrent que le comportement du polymère est situé en dehors de la région gaussiène et doit résulter de la structure à courte distance plutôt que de fortes interactions avec le solvant. En fait, en se basant sur la théorie de Kirkwood-Riseman, modifiée pour tenir compte du facteur d'expansion, on a calculé dans des conditions thèta un exposant viscosimétrique du poids moléculaire de 0.9. On propose que la chaîne est rendue moins mobile à cause des empêchements de rotation imposées par des effets de résonance dans les liaisons peptidiques qui constituent le squelette du polymère.

Zusammenfassung

Lichtstreuungsmessungen der Molekülkonformation von *n*-Hexylpolyisocyanat (PIC) in Tetrahydrofuran (THF) zeigen, dass das Verhältnis der Wurzel aus den mittleren End-zu-End Abstandsquadrat zur maximalen Ausdehnung sogar bei einem Molekulargewicht von 3×10^5 25% übersteigt und dass die effektive Bindungslänge in der äquivalenten frei verknüpften Kette 23Å beträgt, was etwa 17 Gliedern pro statistischem Segment entspricht. Diese Ergebnisse liegen mindestes doppelt so hoch als die Werte für Zellulosetrinitrat in Aceton bei einem vergleichbaren Polymerisationsgrad. Obgleich eine signifikante Änderung der Viskositätszahl in verschiedenen Lösungsmitteln auftritt, zeigen die neuerdings mitgeteilten Viskositäts- und Sedimentationskoeffizienten und Molekulargewichtsexponenten von 1,18 und 0,16 für *n*-Butyl PIC in THF, dass das Polymerverhalten ausserhalb des Gauss- Bereiches liegt und durch die Nahstruktur und nicht durch starke Wechselwirkung mit dem Lösungsmittel bedingt sein muss. Tatsächlich kann mit Hilfe der zur Berücksichtigung des Expansionsfaktors modifizierten Kirkwood- Riseman-Theorie für Theta- Bedingungen ein Viskosität- Molekulargewichtsexponent von 0,9 berechnet werden. Es wird angenommen, dass die Kette durch Rotationsbewegungen welche durch Resonanzeffekte in den die Polymerkette bildenden Peptidbindungen bedingt sind, versteift wird.

Received May 12, 1964
Revised July 28, 1964

JOURNAL OF POLYMER SCIENCE: PART A VOL. 3, PP. 949-960 (1965)

Some Low Molecular Weight Polymers of *d*-Limonene and Related Terpenes Obtained by Ziegler-Type Catalysts*

MARIO MODENA,† R. B. BATES, and C. S. MARVEL, *Department of Chemistry, University of Arizona, Tucson, Arizona*

Synopsis

d-Limonene has been polymerized by use of Ziegler-type catalysts to give a low molecular weight polymer which is identical in structure with those prepared by cationic initiation. The evidence indicates that the polymer has more than one type of recurring unit, at least one of which is bicyclic. α- and β-pinene have also been polymerized by these catalysts. Data on optical activity and NMR spectra for all of the polymers are reported.

d-Limonene (I) polymers have been obtained by Roberts and Day[1] using Friedel-Crafts catalysts while studying β-pinene (II) and α-pinene (III) polymers. These authors suggested that the recurring unit in poly-β-pinene is (IV) and that α-pinene is isomerized to limonene before polymerizing because they obtained polymers having very similar properties for these two monomers. However, they were not able to prove the structure of the poly-*d*-limonene because the expected recurring unit (V) does not ex-

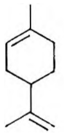
I


II


III

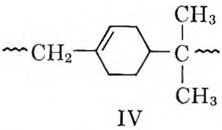

$$\sim\!\!\sim CH_2-C_6H_8-\underset{CH_3}{\overset{CH_3}{C}}\sim\!\!\sim$$

IV

---

* This is a partial report of work done under contract with four Utilization Research and Development Divisions, Agricultural Research Service, U. S. Department of Agriculture, and authorized by the Research and Marketing Act. The contract was supervised by Dr. J. C. Cowan of the Northern Division.

† M. M. is grateful to Societa Edison for a G. Motta Fellowship. Present address: Sicedison SPA, Laboratorio Ricerche, Bollate, Milan, Italy.

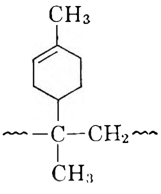

V

plain the fact that according to ozone absorption data, the polymer has only 0.4–0.5 double bonds per recurring unit.

It was the intent of this work to prepare polymers from *d*-limonene using Ziegler-type catalysts and to study their structure. Our results indicate that this catalytic system leads to polymers having the same properties as those obtained with titanium tetrachloride or boron trifluoride etherate, but that the structure of the product is not that expected from a propagation mechanism involving only the isopropenyl double bond. The molecular weights of the polymers are low.

Dipentene, α-pinene, and β-pinene polymers have been prepared by the same catalysts and their properties compared with those of poly-*d*-limonene.

EXPERIMENTAL

Materials

d-Limonene and the other monomers were distilled from sodium hydride under reduced pressure and stored under a nitrogen atmosphere. Their purity, as determined by vapor-phase chromatography, was at least 98%.

The solvent employed was *n*-heptane which had been refluxed with sulfuric acid and distilled over sodium in a nitrogen atmosphere.

Boron trifluoride etherate was distilled under reduced pressure, while the other catalysts were used without further purification.

General Procedure

The polymerizations were usually carried out by adding 10 ml. of monomer to the catalyst prepared by adding the required amount of cocatalyst to 10 ml. of *n*-heptane and 1.5 mmole of triisobutylaluminum or 1 mmole of diisobutylaluminum monochloride in a 50-ml. bottle. The reaction mixture was prepared in a dry box filled with nitrogen and the bottles sealed with rubber serum caps. When cooling the catalyst before the addition of the monomer was required, the latter was injected with a syringe.

The use of 50-ml. flasks with ground-glass stoppers or the changing from occasional to continuous shaking led to only slight changes in yields.

The polymers were isolated by pouring the polymerization mixtures in reagent grade methanol and reprecipitating twice from benzene–methanol. The low molecular weight products, soluble in methanol, were recovered by pouring the methanol solution in water, extracting with ethyl ether and distilling the organic layer. In every case the monomer was the main compo-

TABLE I
d-Limonene Polymerization

Run No.	Al(i-Bu)$_3$, mmole	Al(i-Bu)$_2$Cl, mmole	TiCl$_4$, mmole	TiI$_4$, mmole	VOCl$_3$, mmole	Temp., °C.	Time, days	Conversion, %[a]	M.p., °C.[b]	Inherent viscosity[c]
L6	1.5		0.5			30	11	<0.1	79–91	
L7	1.5		0.3			30	11	0		
L28		1	1.5			30	5	49	73–78	0.07
L59		1	1.5			0	5	67.5	90–100	0.026
L29		1	0.5			30	5	<0.1		
L11	1.5			1.5		30	11	33	80–94	
L12	1.5			0.3		30	11	0		
L32		1		1.5		30	5	45		0.02
L33		1		0.5		30	5	<0.1		
L8	1.5				1.5	30	11	29	58–65	0.02
L9	1.5				0.5	30	11	<0.1		
L10	1.5				0.3	30	11	<0.1		
L30		1			1.5	30	6	10	80–90	0.02
L31		1			0.5	30	6	<0.1	89–99	
L17			1.5			30	4	1.6	112–120	0.04
L69		$BF_3 \cdot OEt_2$ 1.2				25	4	9.2		0.01

[a] Conversion is based on amounts of monomer used and of polymer recovered after three reprecipitations from benzene–methanol.

[b] Melting points determined in a capillary tube.

[c] Determined with an Ostwald-type viscometer with solution of 0.4 g. of polymer in 100 ml. of benzene.

TABLE II
Dipentene Polymerization

Run no.	Al(i-Bu)$_3$, mmole	Al(i-Bu)$_2$Cl, mmole	TiCl$_4$, mmole	VOCl$_3$, mmole	Temp., °C.	Time, days	Conversion, %	M.p., °C.	Inherent viscosity
L47	1.5		1.5		25	7	<0.1		
L48	1.5		0.5		25	7	<0.1		
L51		1	1.5		25	7	80	65–70	0.012
L52		1	0.5		25	7	1.2	96–97	
L49	1.5			1.5	25	7	6.1	66–76	
L50	1.5			0.5	25	7	<0.1		
L53		1		1.5	25	7	21.7	56	
L54		1		0.5	25	7	6.4	65–70	

TABLE III
α-Pinene Polymerization

Run no.	Al(i-Bu)$_3$, mmole	Al(i-Bu)$_2$Cl, mmole	TiCl$_4$, mmole	VOCl$_3$, mmole	Temp., °C.	Time, days	Conversion, %	M.p., °C.	Inherent viscosity
L37	1.5		1.5		25	7	<0.1		
L38	1.5		0.5		25	7	<0.1		
L40		1	1.5		25	7	2.3	114–119	0.02
L57		1	1.5		35	5	2.3	120–125	
L39	1.5			1.5	25	7	1.2	102–105	0.02
L63		1		1.5	25	7	19	58–60	0.02

TABLE IV

β-Pinene Polymerization

Run no.	Al(i-Bu)$_3$, mmole	Al(i-Bu)$_2$Cl, mmole	TiCl$_4$, mmole	VOCl$_3$, mmole	Temp., °C.	Time., days	Conversion, %	M.p., °C.	Inherent viscosity
L42	1.5		1.5		−80, +25	7	18.3	109–119	0.036
L55	1.5		1.5		−80	4	3.5	91–93	
L45		1	1.5		+25	7	68.2	69–74	
L56		1	1.5		−80	4	36.1	87–125	0.06
L44	1.5			1.5	−80, +25	7	70	76–85	0.025
L46		1		1.5	+25	7	53.6	69–73	0.03

nent recovered, and it was identified by vapor-phase chromatography. From dipentene and α-pinene polymerizations, small amounts of products boiling in the range of diterpenes (150°C./1 mm. Hg and 140°C./1 mm. Hg) were isolated.

RESULTS

The results are summarized in Tables I–IV. In each run 10 ml. of *n*-heptane and 10 ml. of monomer were used.

Infrared Spectra

The infrared spectra of the polymers have been recorded on a Perkin-Elmer Infracord spectrophotometer. The positions of the absorption maxima are given in Table V.

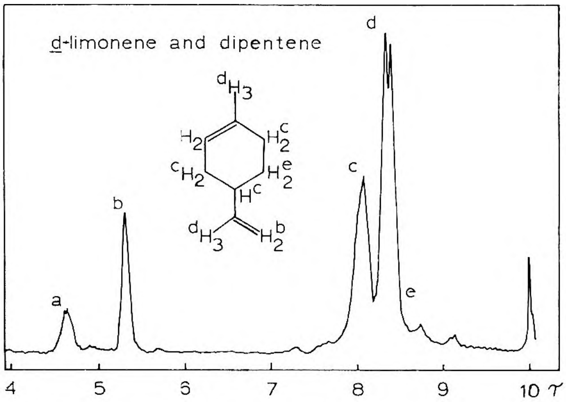

Fig. 1. NMR spectrum of *d*-limonene and dipentene (no solvent).

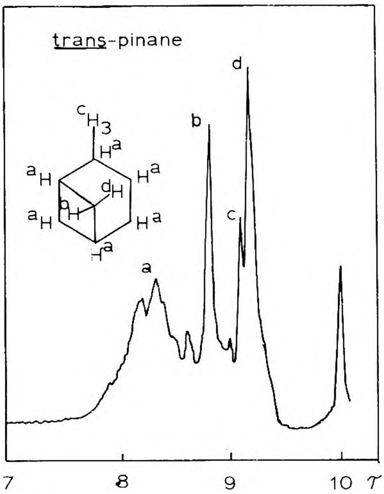

Fig. 2. NMR spectrum of *trans*-pinane (no solvent).

In all the spectra the bands with maxima at about 3000, 1475, 1380, 1160 cm.$^{-1}$ are characteristic C—H bands;[2] the first is assignable to the stretching vibration, the second and the third to the deformation vibrations, and the last to the in-plane rocking vibration. A 1700 cm.$^{-1}$ band is characteristic of the C=C stretching vibration.

The spectra of the dipentene and α-pinene dimers are very similar to those of the respective polymers, the main difference being a slightly stronger absorption in the 1670 cm.$^{-1}$ region.

Nuclear Magnetic Resonance Spectra

The NMR spectra of polymers, monomers, and a few model compounds have been determined with a Varian A-60 spectrometer; tetramethyl-

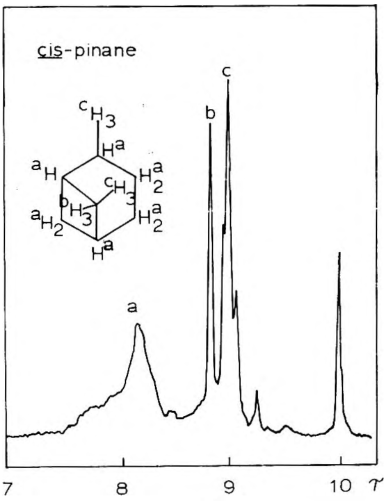

Fig. 3. NMR spectrum of *cis*-pinane (20% in CCl_4).

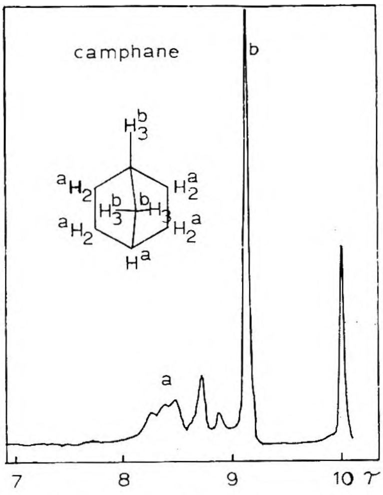

Fig. 4. NMR spectrum of camphane (14% in CCl_4).

silane was added as an internal standard. The spectra taken at room temperature (25–30°C.) are reported in Figures 1–8. The α- and β-pinene spectra have been previously published.[3] The spectra of poly-*d*-limonene and polydipentene show a very small absorption, having an area indicating

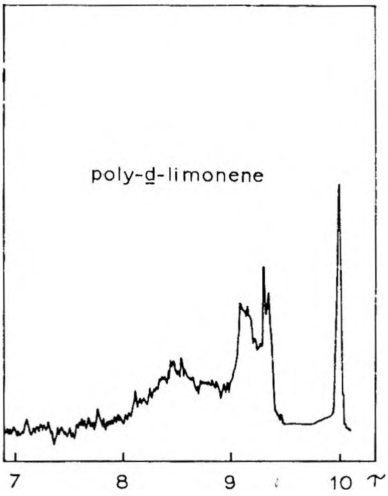

Fig. 5. NMR spectrum of poly-*d*-limonene (1% in CCl_4).

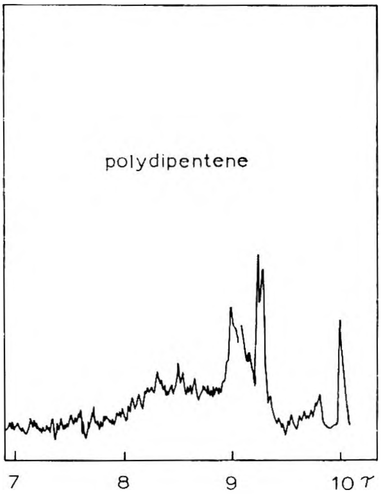

Fig. 6. NMR spectrum of polydipentene (1% in CCl_4).

0.3 of a proton per recurring unit assuming 16 protons per recurring unit in the 4–6 τ region (not shown in the figures), where the peaks due to vinyl hydrogens usually appear. In the poly-α-pinene spectrum no such absorption has been detected.

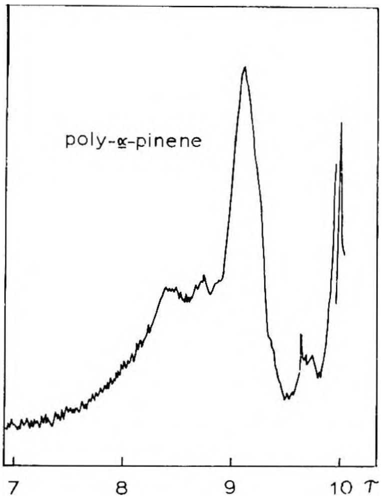

Fig. 7. NMR spectrum of poly-α-pinene (5% in CCl_4).

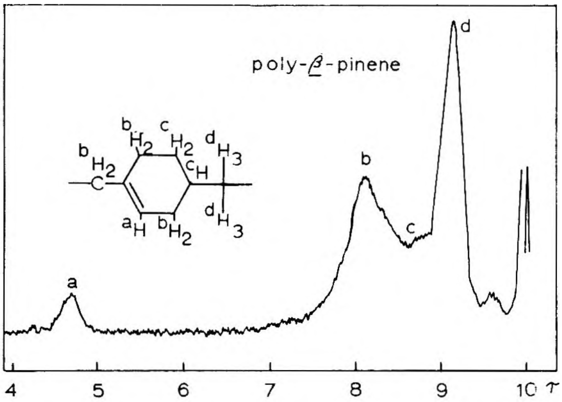

Fig. 8. NMR spectrum of poly-β-pinene (1.6% in CCl_4).

Optical Activity

The optical activities of monomers and polymers measured with a Rudolph Polarimeter Model 80 are collected in Table VI.

Perbenzoic Acid Oxidation

Perbenzoic acid has been prepared following Braun's[4] method with the modifications suggested by Kolthoff,[5] and the stock benzene solution diluted to about 0.2*M*. A 10-ml. portion of this solution was added to samples of polymers (0.15–0.2 g.) dissolved in purified chloroform[5] in a 100-ml. volumetric flask and allowed to react at room temperature (19.5–21.5°C.) in the dark. Samples of the reaction mixture were transferred in 0.4*N* acetic

TABLE V
Ifrared Spectra

Poly-*d*-limonene and poly-dipentene, cm.$^{-1}$	Poly-α-pinene, cm.$^{-1}$	Poly-β-pinene, cm.$^{-1}$
3000 (s)	3000 (s)	3000 (s)
1700–1650 (w)	1700–1650 (w)	1670 (w)
1475 (m)	1475 (m)	1480–1450 (m)
1380 (m)	1380 (m)	1400–1380 (m)
1160 (w)	1260 (w)	1160 (w)
1030 (w)	1160 (w)	1020 (w)
1000 (w)	1100 (w)	920 (w)
970 (w)	1040–970 (w)	725 (w)
880–890 (w)	885 (w)	
805 (w)	720 (w)	
720–735 (w)	670 (w)	
670 (w)		

acid containing potassium iodide after about 3, 6, and 24 hr. and the liberated iodine titrated with 0.1N thiosulfate solution. The titer of a blank run was determined in the same way. The results expressed in number of double bonds per monomeric unit oxidized after a given time are collected in Table VII.

TABLE VI
Optical Activities

Monomer	$[\alpha]_D$ of monomer	Run	$[\alpha]_D$ of polymer[a]
d-Limonene	+126[b]	L11	+0.6
		L23	+2.2
		L28	+1.2
		L32	+1.3
		L59[c]	+0.8
Dipentene	−1.7[d]	L51	0
α-Pinene	+44.9[b]	L39	−7.1
		L40	−11.2
		L57[e]	−9.2
		L63	−8.2
β-Pinene	−28.8[a]	L42	−52.6
		L44	−20.2
		L46	−6.2
		L56[f]	−53.7

[a] Benzene, $C = 10$.

[b] Benzene, $C = 7$.

[c] Recovered monomer $[\alpha]_D = +50$ (benzene, $C = 50$).

[d] Neat.

[e] Recovered monomer $[\alpha]_D = +36.3$ (benzene, $C = 12$); dimer $[\alpha]_D = -30$ (CCl_4, $C = 20$).

[f] Recovered monomer $[\alpha]_D = -27.9$ (benzene, $C = 10$).

TABLE VII
Perbenzoic Acid Oxidation

Polymer	Time, hr.	Double bonds reacted per $C_{10}H_{16}$ unit
Poly-*d*-limonene (L59)	4	0.36
	6.8	0.41
	24.6	0.44
Polydipentene (L51)	3.6	0.30
	6.5	0.31
	24.3	0.37
Poly-β-pinene (L56)	3.5	0.64
	6.4	0.86
	24.5	0.93
Poly-α-pinene (L63)	4.2	0.31
	9.5	0.33
	24.3	0.45

DISCUSSION

The use of Ziegler-type catalysts in the polymerization of *d*-limonene leads to the formation of a polymer having the same properties as those prepared by cationic initiation. Since the best conversions have been obtained with a 1:1 aluminum alkyl–metal halide molar ratio also these complex catalysts probably acted by a cationic mechanism.

The low values of unsaturation found by perbenzoic acid oxidation, and the low ratio of vinyl hydrogen and high ratio of methyls at about 9.1 τ in the NMR spectra of the polymers suggest a polymerization mechanism leading predominantly to bicyclic saturated units of the camphane-type (VII) and/or pinane-type (VIII).

In the plausible mechanism shown, the bicyclic type structure VII and/or VIII is favored by a 1.5–2 factor over the monocyclic structure VI.

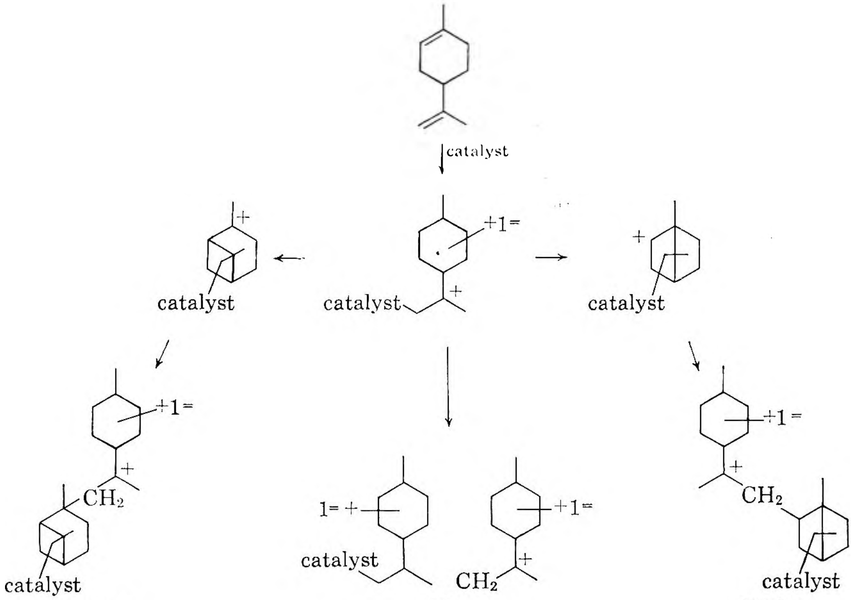

VII VI VIII

The almost complete racemization of the polymer while the monomer recovered after the reaction still has about 50% of the original activity may be linked to the fact the asymmetry of the monomer depends upon the position of the ring double bond and this must be shifted by a cationic catalyst during polymerization.

The optical activity measurements on poly-α-pinene show that this polymer is different from poly-*d*-limonene. The double bond content is too high for a single type of bicyclic recurring unit.

Our results with poly-β-pinene are in accord with the structure previously reported;[1,6] the high optical activity of the polymer prepared in mild conditions shows that the reaction proceeds without extensive racemization.

References

1. Roberts, W. J., and A. R. Day, *J. Am. Chem. Soc.*, **72,** 1226 (1950).
2. O'Connor, R. T., and L. A. Goldblatt, *Anal. Chem.*, **26,** 1726 (1954).
3. Bhacca, N. S., L. F. Johnson, and J. N. Shoolery, *NMR Spectra Catalog,* Varian Associates, 1962.
4. Braun, G., Organic Syntheses, Coll. Vol. I., Wiley, New York, 1941, p. 431.
5. Kolthoff, I. M., T. S. Lee, and M. A. Mairs, *J. Polymer Sci.*, **2,** 199 (1947); *ibid.*, **2,** 206 (1947).
6. Marvel, C. S., J. R. Hanley, Jr., and D. T. Longone, *J. Polymer Sci.,* **11,** 551 (1959).

Résumé

Par polymérisation du *d*-limonène au moyen de catalyseurs du type Ziegler, on a obtenu un polymère de faible poids moléculaire, structurellement identique à celui préparé par initiation cationique. Il est évident que le polymère possède plus d'un type d'unite sont un au moins est bicyclique. L'α et le β-pinène ont également été polymérisés au moyen de ces catalyseurs. L'activité optique et les spectres N.M.R. de tous ces polymères sont donnés.

Zusammenfassung

d-Limonen wurde mit Katalysatoren vom Ziegler- Typ zu einem niedermolekularen Polymeren mit identischer Struktur wie das bei kationischer Anregung erhaltene polymerisiert. Die Befunde sprechen dafür, dass das Polymere mehr als einen Bausteintyp besitzt und dass zumindest einer davon bizyklisch ist. Auch α- und β-Pinene wurden mit diesen Katalysatoren polymerisiert. Angaben über die optische Aktivität und die NMR-Spektren der Polymeren wurden gemacht.

Received June 17, 1964
Revised August 14, 1964

JOURNAL OF POLYMER SCIENCE: PART A VOL. 3, PP. 961-969 (1965)

Homopolymerization of Hydronopyl Vinyl Ether and 2-Hydronopoxyethyl Vinyl Ether[*]

C. S. MARVEL, R. A. MALZAHN,[†] and J. L. COMP,[‡] *Department of Chemistry, University of Arizona, Tucson, Arizona*

Synopsis

The effectiveness of several free radical, cationic, and coordination initiators for the polymerization of hydronopyl vinyl ether and 2-hydronopoxyethyl vinyl ether has been examined. The most effective initiator found for polymerization of hydronopyl vinyl ether is a coordination catalyst prepared from triisobutylaluminum and titanium tetrachloride. Generally, cationic initiators are less effective and free radical initiators much less effective with this monomer. Of the initiators investigated for polymerization of 2-hydronopoxyethyl vinyl ether, only one, boron fluoride etherate, proved to be effective. This initiator yielded a rubbery polymer of high molecular weight.

DISCUSSION

The work reported in this paper was undertaken to determine the optimum conditions for polymerizing hydronopyl vinyl ether (Ia) and 2-hydronopoxyethyl vinyl ether (Ib) and to investigate the properties of the resulting polymers.

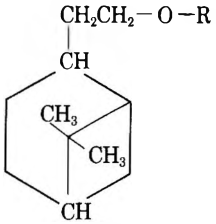

Ia $R = -CH{=}CH_2$
Ib $R = -CH_2CH_2-O-CH{=}CH_2$

Samples of hydronopyl vinyl ether (HVE) and 2-hydronopoxyethyl vinyl ether (HEVE) were provided by the Naval Stores Division of the

---

[*] This is a partial report of work done under contract with the four Utilization Research and Development Divisions, Agricultural Research Service, U. S. Department of Agriculture, and authorized by the Research and Marketing Act. The contract was supervised by Dr. J. C. Cowan of the Northern Division.

[†] Research Associate, 1961–63. Present address: Department of Chemistry, West Texas State College, Canyon, Texas.

[‡] Research Associate, 1963–64. Present address: Department of Chemistry, Southwest Texas State College, San Marcos, Texas.

Southern Utilization Research and Development Division of the Agricultural Research Service and were prepared by published methods.[1,2] During the course of the investigation, the preparation of additional HEVE became necessary. Bissel[2] reported a yield of 38% (based on sodium) for the preparation of HEVE. He allowed sodium to react with a large excess of hydronopol and then treated the resulting suspension with 2-chloroethyl vinyl ether. We have found that HEVE can be prepared in 93% yield (based on hydronopol) by mixing hydronopol and sodium hydride in an excess of 2-chloroethyl vinyl ether.

The polymerization of HVE and HEVE by initiation with free radical, cationic, and coordination catalysts was investigated. In accord with the report[3] that most vinyl ethers do not polymerize well by free radical initiation, neither HVE nor HEVE polymerized appreciably by free radical initiation in bulk or emulsion systems.

Under the conditions studied, the order of effectiveness of cationic initiation of the polymerization of HVE is stannic chloride > boron fluoride etherate > titanium tetrachloride > vanadium oxychloride. Vanadium trichloride does not catalyze the polymerization of HVE. For polymerization of HEVE the order of effectiveness is boron fluoride etherate >>> stannic chloride. Titanium tetrachloride, vanadium oxychloride, and vanadium trichloride do not catalyze the polymerization.

Polymerization of HEVE by initiation with boron fluoride etherate at -78°C. produces the highest conversion and molecular weight of any method investigated. The poly(HEVE) is a tough, slightly tacky rubber with a specific rotation of $[\alpha]_D^{25} = -20.1°$. It is soluble in petroleum ether, benzene, toluene, carbon tetrachloride, and tetrahydrofuran but insoluble in methanol, acetone, and 2-butanone.

Okamura and Higashimura[4] report that poly(isobutyl vinyl ether) can be separated into crystalline and noncrystalline fractions because the crystalline fraction is less soluble in 2-butanone. The insolubility of poly(HEVE) in 2-butanone may indicate the presence of some crystalline portions.

At best, coordination catalysts prepared by mixing triisobutylaluminum with titanium tetrachloride or vanadium oxychloride or vanadium trichloride produce poor yields of poly(HEVE). Poor results were also obtained when attempts were made to polymerize HVE with catalysts prepared by mixing triisobutylaluminum with vanadium oxychloride or vanadium trichloride. Conversely, catalyst prepared by mixing triisobutylaluminum and titanium tetrachloride in a mole ratio of 2.7:1 produces poly(HVE) in the highest conversion and with the highest molecular weight of any catalyst investigated by us.

The poly(HVE) prepared with triisobutylaluminum–titanium tetrachloride catalyst is hard and brittle, but becomes rubbery at temperatures above 45°C. It has a specific rotation of $[\alpha]_D^{25} = -26.2$ and is soluble and insoluble in the same solvents as poly(HEVE). An x-ray diffraction pattern indicates considerable crystallinity in this polymer.

EXPERIMENTAL

Materials

Hydronopyl vinyl ether (HVE), b.p. 80–81°C./2 mm., n_D^{25} 1.4788; $[\alpha]_D^{25}$ −2.3.8° (0.3882 g. in 25 ml. of benzene); 2-hydronopoxyethyl vinyl ether (HEVE), b.p. 87–88°C./0.5 mm., n_D^{25} 1.4760, $[\alpha]_D^{25}$ −18.1° (0.418 g. in 25 ml. of benzene), and hydronopol, b.p. 126–128°C./10 mm., n_D^{25} 1.488 were provided by the USDA Naval Stores Laboratory, Olustee, Florida. The vinyl ethers contained 0.2% of hydroquinone and were purified by the method described by Schildknecht, Zosc, and McKinley[5] and passed through alumina (Merck's chromatographic grade) just before they were used. 2-Chloroethyl vinyl ether was obtained from Monomer-Polymer Laboratories and distilled before use. Hexane (Phillips 99%) was refluxed over sulfuric acid, washed, dried with potassium carbonate, and distilled from over sodium. A dispersion of sodium hydride (50.6% by weight) in mineral oil was procured from Metal Hydrides, Inc. The boron fluoride etherate was obtained from Eastman Organic Chemicals, stannic chloride from Baker Chemical Company, triisobutylaluminum from Texas Alkyls, titanium tetrachloride (99.5%) from Matheson, Coleman, and Bell, and vanadium trichloride and vanadium oxychloride from Anderson Chemical Company.

Preparation of 2-Hydronopoxyethyl Vinyl Ether

Into a 5-liter four-necked flask fitted with a stirrer, reflux condenser that was protected with a calcium chloride drying tube, addition funnel, and nitrogen inlet tube were placed 321 g. (6.68 moles) of NaH in mineral oil (50.6% dispersion by weight) and 650 g. (6.1 moles) of 2-chloroethyl vinyl ether. While the mixture was stirred rapidly, 460 g. (2.7 moles) of hydronopol was added over a period of 1 hr. Stirring was continued for 2 hr. at room temperature and for 48 hours at reflux temperature. The reaction mixture was allowed to cool to room temperature and 500 ml. of methanol followed by 1500 ml. of water was added slowly. Six 250-ml. portions of ether were used to extract the organic material. The portions were combined, washed with 500 ml. of water, and dried over anhydrous magnesium sulfate. The ether and methanol were removed by distillation and the residue was distilled under reduced pressure through a 100 × 1 cm. spinning band column. A total of 580 g. (93% yield based on hydronopol) of 2-hydronopoxy-ethyl vinyl ether, b.p. 109°C./0.75 mm., n_D^{30} 1.4730, was collected.

Polymerization of HVE and HEVE

Attempted Free Radical Initiation in Bulk. A 6 × 1 in. polymerization tube was charged with 2.0 g. of HVE and 0.02 g. of α,α'-azodiisobutyronitrile. To purge the reaction mixture of oxygen the pressure in the tube was reduced to 0.1 mm. Hg with a vacuum pump, and then nitrogen was admitted to the tube. Then the pressure was reduced to 0.1 mm. Hg and the tube was sealed and heated in an oil bath at 65°C. At the end of 40 hr. the contents of the tube was a thin liquid that was completely soluble in methanol. Similar results were obtained when 2.0 g. of HEVE was substituted for HVE.

Attempted Free Radical Initiation in Emulsion. Into a 2-oz. screw-topped bottle were placed 0.2 g. of Triton X-301 (a 20% aqueous dispersion of Rohm and Haas sodium alkylaryl polyether sulfate), 1.0 g. of HVE, 5 ml. of distilled water, and 0.5 ml. of 2.5% potassium persulfate solution. The bottle was flushed with nitrogen, capped, and tumbled in a water bath at 55°C. for 36 hr. After the emulsion had been broken with saturated sodium chloride solution, two layers formed. The organic layer was a free-flowing liquid completely soluble in methanol. The same results were obtained when 2.0 g. of HEVE was substituted for HVE.

Initiation with Boron Fluoride Etherate. A method similar to the one reported by Sorenson and Campbell[6] was used. A 250-ml., three-necked flask was fitted with a stirrer, nitrogen inlet tube, and rubber, serum-bottle cap and charged with 10 g. of vinyl ether in 40 ml. of *n*-hexane. While the solution was kept under a nitrogen atmosphere and stirred, it was cooled in Dry Ice–acetone to −78°C. A hypodermic needle was inserted through the serum cap and four drops of boron fluoride etherate were added to the solution. After 30 min. another four drops were added and the mixture was stirred for the desired length of time. A 10-ml. portion of methanol was poured into the reaction mixture, which was allowed to warm to room temperature. The resulting solution was poured into 800 ml. of methanol that was being rapidly stirred. The polymer that precipitated was removed from the supernatant liquid. Further purification of the polymer was effected by dissolving it in benzene and repeating the precipitation step. Finally the polymer was dissolved in 200 ml. of benzene. The solution was filtered and the polymer isolated by freeze drying. Inherent viscosities were calculated from flow times of the benzene solution taken

TABLE I
Cationic Polymerization of HVE

Catalyst	Temperature, °C.	Reaction time, hr.	Conversion, %	Inherent viscosity
$BF_3 \cdot OEt_2$	−78	2	39	0.43
$BF_3 \cdot OEt_2$[a]	−78	0.5	88	0.47
$SnCl_4$	−78	2	48	0.25
$SnCl_4$	0	2	93	0.50
$SnCl_4$	30	2	93	0.35
$TiCl_4$	−78	24	80	0.14
$TiCl_4$	0	24	85	0.12
VCl_3	−78	24	0	—
$VOCl_3$	−78	24	90	0.19

[a] "Flash" polymerization.

TABLE II
Cationic Polymerization of HEVE

Catalyst	Temperature, °C.	Reaction time, hr.	Conversion, %	Inherent viscosity
$BF_3 \cdot OEt_2$	−78	2	93	1.87
$BF_3 \cdot OEt_2$	−78	19	96	2.14[a]
$BF_3 \cdot OEt_2$[b]	−78	0.5	86	0.63
$SnCl_4$	−78	2	10	—
$SnCl_4$	0	2	87	0.37
$SnCl_4$	30	2	0	—
$SnCl_4$[c]	0	2	93	0.13
$TiCl_4$	0	24	0	—
VCl_3	−78	24	0	—
$VOCl_3$	−78	24	0	—

[a] $[\alpha]^{25}_{D} = -20.10$ (0.383 g. in 25 ml. of benzene).

[b] "Flash" polymerization.

[c] One drop of water was added to reaction mixture before the stannic chloride was added.

at 30°C. in a number 50 Cannon-Fenske viscometer. Data for polymerization of HVE and HEVE are collected in Tables I and II.

Initiation with Boron Fluoride Etherate (Flash Polymerization). Into a 250-ml., four-necked flask fitted with a stirrer, nitrogen inlet tube, Dry Ice–acetone cooled dropping funnel and Dry Ice–acetone cooled condenser was placed 30 ml. of *n*-hexane and eight drops of boron fluoride etherate. While a nitrogen atmosphere was maintained, the solution was cooled to −78°C. and a solution of 10 g. of vinyl ether in 20 ml. of *n*-hexane that was also at −78°C. was added rapidly. After the reaction mixture had been stirred for 30 min., 10 ml. of methanol was added and the resulting solution was allowed to warm to room temperature. The poly(vinyl ether) was purified and isolated by the same method described in the preceding section. Data for the polymerization of HVE and HEVE are collected in Tables I and II.

Initiation with Stannic Chloride, Titanium Tetrachloride, and Vanadium Oxychloride. Inside a dry box that was continually flushed with nitrogen, a 4-oz. screw-topped bottle was charged with a weighed amount of vinyl ether and 15 ml. of *n*-hexane. The bottle was sealed with a screw cap that had a hole punched in it and had been lined with a neoprene gasket. When the bottle had been cooled to the desired temperature, a measured volume of *n*-hexane solution containing a known amount of metal chloride or oxychloride was injected through the gasket into the bottle. Cooling was continued until polymerization was terminated by addition of 10 ml. of methanol. The poly(vinyl ether) was purified by the same method described previously. Data concerning the polymerization of HVE and HEVE with cationic initiators are collected in Tables I and II.

Attempted Initiation with Vanadium Trichloride. In general the procedure was the same as described in the preceding section, although the order in which the reagents were added was different. The vanadium trichloride was weighed directly into the polymerization bottle and mixed with *n*-hexane. Then after the bottle was sealed and cooled, the vinyl ether was injected into the bottle. Tables I and II contain data for the attempted polymerization of HVE and HEVE with vanadium trichloride.

Initiation with "Coordination Type" Catalysts. A 4-oz. screw-topped bottle was charged, in a dry box and under nitrogen, with hexane (10 ml./g. of monomer), a measured volume of a hexane solution of triisobutylaluminum (0.1 g. i-Bu_3Al/ml.) and a measured volume of hexane solution of titanium tetrachloride (0.084 g. $TiCl_4$/ml.) or vanadium oxychloride (0.03 g. $VOCl_3$/ml.) or a weighed amount of vanadium trichloride. The bottle was sealed with a neoprene-gasketed cap and the catalyst mixture was allowed to age.

If the polymerization were to be performed at room temperature, a measured volume of vinyl ether was injected into the polymerization bottle which was shaken occasionally while it stood for 24 hr. For polymerization at −78°C. the catalyst mixture, after aging, was cooled in a Dry Ice–acetone bath for 30 min. and a measured volume of vinyl ether was injected slowly into the bottle. Cooling was maintained for 24 hr., during which time the reaction mixture was swirled occasionally. Then

TABLE III
Polymerization with Catalysts Prepared from Triisobutylaluminum and Titanium Tetrachloride

Monomer	Wt. monomer, g.	Wt. i-Bu_3Al, g.	Wt. $TiCl_4$, g.	Temp., °C.	Aging time, hr.	Conversion, %	Inherent viscosity
HVE	1.0	0.1	—	−78	0.5	0	—
HVE	2.0	0.2	0.2	−78	0.5	98	0.50
HVE	2.0	0.2	0.1	−78	0.5	70	0.55
HVE	2.0	0.2	0.07	−78	0.5	90	1.17
HVE	2.0	0.2	0.05	−78	0.5	35	0.58
HVE	3.0	0.3	0.05	−78	0.5	7	—
HVE	2.0	0.2	0.07	−78	0.5	5	—
HVE	2.0	0.2	0.07	−78	0[a]	70	0.29
HVE	2.0	0.2	0.07	−78	2	90	1.25[b]
HVE	2.0	0.2	0.07	−78	8	80	0.79
HVE	2.0	0.2	0.07	−78	24	80	0.89
HVE[c]	2.0	0.2	0.07	−78	0.5	0	—
HEVE	1.0	0.1	—	−78	0.5	0	—
HEVE	2.0	0.2	0.2	−78	0.5	30	0.26
HEVE	2.0	0.2	0.07	−78	0.5	0	—
HEVE	2.0	0.2	0.07	−78	0.5	0	—
HEVE	2.0	0.6	0.2	−78	0.5	0	—

[a] Triisobutylaluminum and HVE were mixed, aged, cooled and then the titanium tetrachloride was added.

[b] This sample of poly(HVE) is hard and brittle, has a softening range of 45–200°C., and $[\alpha]_D^{25} = -26.2$ (0.338 g. in 25 ml. of benzene).

[c] Ether was substituted for hexane as solvent.

TABLE IV
Polymerization with Catalysts Prepared from Triisobutylaluminum and Vanadium Oxychloride

Monomer	Wt. monomer, g.	Wt. *i*-Bu_3Al, g.	Wt. $VOCl_3$, g.	Temp., °C.	Aging time, hr.	Conversion, %	Inherent viscosity
HVE	2.0	0.2	0.06	−78	0.5	15	0.53
HVE	2.0	0.2	0.03	−78	0.5	25	0.82
HEVE	2.0	0.2	0.06	−78	0.5	25	0.98
HEVE	2.0	0.2	0.03	−78	0.5	0	—

TABLE V
Attempted Polymerization with Catalyst Prepared from Triisobutylaluminum and Vanadium Trichloride

Monomer	Wt. monomer, g.	Wt. *i*-Bu_3Al, g.	Wt. VCl_3, g.	Temp., °C.	Aging time, hr.	Conversion, %
HVE	2.0	0.2	0.16	−78	0.5	0
HVE	4.0	0.4	0.1	−78	0.5	0
HEVE	2.0	0.2	0.16	−78	0.5	0
HEVE	4.0	0.4	0.1	−78	0.5	0

the contents of the bottle were poured into rapidly stirred methanol. The precipitated polymer was purified by the same method previously described. Data for the polymerization of HVE and HEVE are collected in Tables III–V.

X-Ray Analysis of Poly(HVE)

A thick film was obtained by repeated casting of thin layers of a benzene solution of the poly(HVE). After the portions had dried over water, the film was removed from the water and allowed to remain at room temperature for two weeks to remove residual solvent.

A Phillips x-ray diffraction instrument (operated by Dr. M. L. Corrin) was used. The major machine settings were: 35 Kv., 20 ma., Bl 200, SF 16, TC 4, and M 0.8.

The scan of diffracted x-rays (Fig. 1) indicates two maxima ($2\theta = 13.5$ and 19.0). Using $\lambda = 1.54$ and Bragg's Law $\lambda = 2d \sin \theta$ the spacing distances are 6.55 and 4.66 A. The sharpness of the recorded scan and the short distance (*d*) indicate considerable crystalline polymer structure.

Evaluation of Poly(HEVE)

Preparation of Sample. A 150-g. sample for evaluation was prepared by polymerizing 10–30-g. lots of 2-hydronopoxyethyl vinyl ether in dry *n*-hexane solution by boron fluoride initiation in a Dry Ice–acetone cooling bath. The polymerization mixture was stirred for the first 4 hr. and then allowed

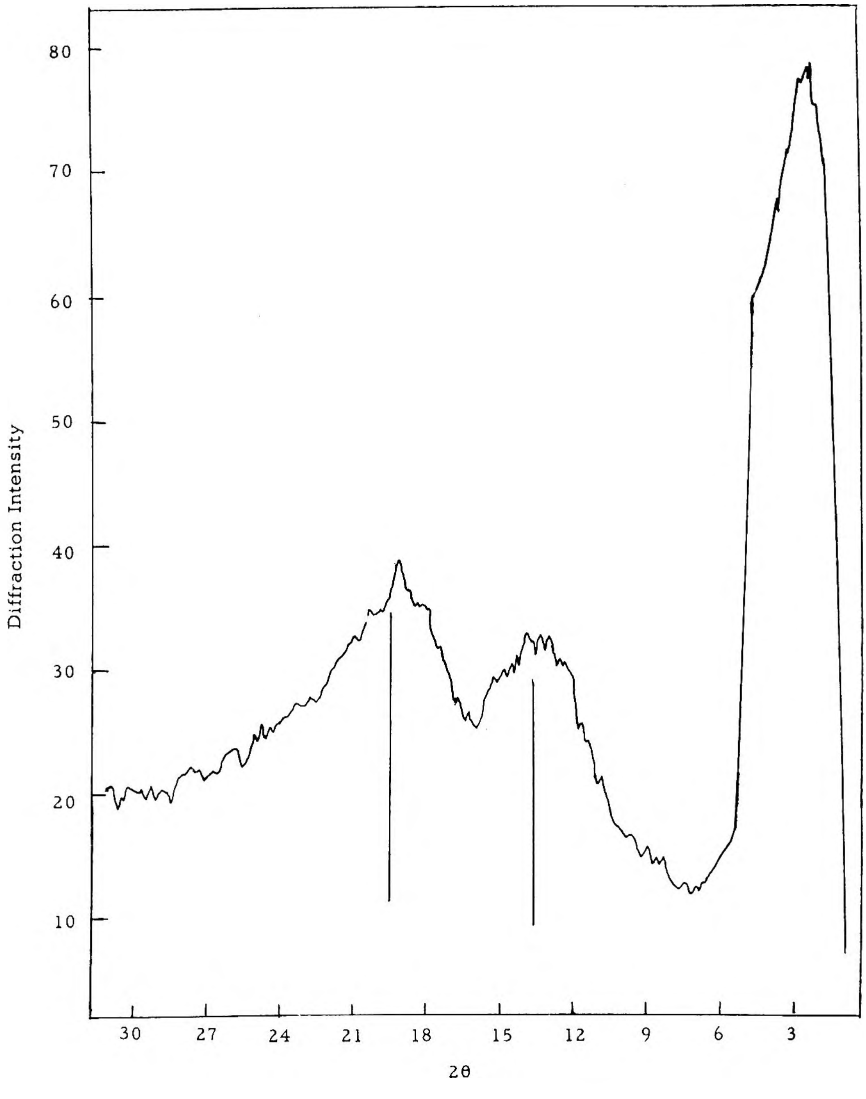

Fig. 1. X-ray diffraction pattern of poly(HVE).

to stand for 14 hr. Then, methanol was added, the mixture stirred well and then allowed to warm to room temperature. The polymer was dissolved in benzene, the solution was filtered, and then the polymer precipitated by adding this solution to excess methanol with stirring. Solution in benzene and reprecipitation in methanol was repeated two more times and then the polymer was dried under reduced pressure. On the average conversion was 96% and the inherent viscosity of the polymer varied from 1.5 to 2.1 with the average for the 150-g. sample being 1.8.

It should be noted that when this procedure was carried out during the season when the relative humidity in the laboratory was very low, the operations could be carried out in the open laboratory without difficulty. However, when the humidity in the laboratory had increased due to operation of the evaporative cooling system, only very low molecular weight polymers could be prepared unless the preparation of the polymerization charge was carried out in a dry box.

Evaluation. Mr. Frank C. Magne, Southern Utilization Research and Development Division, Agricultural Research Service, New Orleans, La., examined the above polymer as a possible plasticizer for poly(vinyl chloride). He found the two polymers were not completely compatible over the range of 10–30% of the polyether and 90–70% of poly(vinyl chloride). Attempts to work the polyether on a rubber mill were unsuccessful because the polymer adhered to the rolls too tenaciously. Further evaluation tests on this material as a rubbery adhesive appear to be desirable.

References

1. Teeter, H. M., E. J. Durkef, C. B. Coleman, C. A. Glass, H. Melvin, and J. C. Cowan, *J. Am. Oil Chemists Soc.*, **33**, 399 (1956).
2. Bissel, R. E., M. S. Thesis, University of Mississippi, 1961, p. 41.
3. Schildknecht, C. E., *Vinyl and Related Polymers*, Wiley, New York, 1952, p. 593.
4. Okamura, S., and T. Higashimura, Japanese Pat. 14,938 (1960).
5. Schildknecht, C. E., A. O. Zose, and C. McKinley, *Ind. Eng. Chem.*, **39**, 180 (1947).
6. Sorenson, W., and T. W. Campbell, *Preparative Methods of Polymer Chemistry*, Interscience, New York, 1961, p. 194.

Résumé

On a examiné l'efficacité de divers initiateurs radicalaires, cationiques et de coordination, pour la polymérisation de l'éther hydronopyl-vinylique et de l'éther 2-hydronopoxyéthyl-vinylique. L'initiateur le plus efficace pour la polymérisation de l'éther hydronopyl-vinylique est un catalyseur de coordination, préparé à partir de triisobutylaluminium et de tétrachlorure de titane. Généralement, les initiateurs cationiques sont moins efficaces et les initiateurs radicalaires beaucoup moins efficaces avec ce monomére. Parmi les initiateurs étudiés pour la polymérisation de l'éther 2-hydronopoxyéthylvinylique, il n'y en a qu'un, l'éthérate du fluorure de bore, qui se trouve être efficace. Cet initiateur a produit un polymére caoutchouteux de haut poids moléculaire.

Zusammenfassung

Die Wirksamkeit einiger radikalischer, kationischer und koordinativer Starter bei der Polymerisation von Hydronopylvinyläther und 2-Hydronopoxyäthylvinyläther wurde untersucht. Als wirksamster Starter für die Polymerisation von Hydronopylvinyläther erwies sich ein aus Triisobutylaluminium und Titantetrachlorid dargestellter Koordinationskatalysator. Im allgemeinen besitzen bei diesen Monomeren kationische Starter eine geringere und radikalischer Starter eine viel geringere Wirksamkeit. Von den für die Polymerisation von 2-Hydronopoxyäthylvinyläther untersuchten Startern erwies sich nur Borfluoridätherat als wirksam. Dieser Starter lieferte eine hochmolekulares kautschukartiges Polymeres.

Received September 2, 1964

JOURNAL OF POLYMER SCIENCE: PART A VOL. 3, PP. 971-981 (1965)

Cyclic Distribution in Dimethylsiloxanes

JACK B. CARMICHAEL and ROBERT WINGER,
Dow Corning Corporation, Midland, Michigan

Synopsis

Gas–liquid chromatography was used to determine the amounts of cyclic molecules present in an equilibrium polymerization mixture of high polymer and cyclic dimethylsiloxane molecules. The study was carried out as a function of polymerization temperature. For $[(CH_3)_2SiO]_{4-10}$ the equilibrium concentration is shown to be independent of temperature. The change in cyclic concentration as a function of n for $[(CH_3)_2SiO]_{4-10}$ does not follow the theoretical Stockmayer-Jacobson distribution. The concentrations of $[(CH_3)_2SiO]_{3,4}$ are qualitatively predictable by the Stockmayer-Jacobson theory and by the model proposed by Carmichael and Kinsinger. For $[(CH_3)_2SiO]_4$, $K_{\text{exp}} = 0.74$ mole —SiO—/l. The model calculations yield 0.12 (Stockmayer-Jacobson) and 0.36 Carmichael-Kinsinger. For $[(CH_3)_2SiO]_3$, $K_{\text{exp}} = 0.024$ mole —SiO—/l. Model calculations yield 0.017–0.16 (Stockmayer-Jacobson) and 0.056–0.52 (Carmichael-Kinsinger). The range of values rises because of uncertainty in the cyclic strain energy.

INTRODUCTION

In all equilibrium polymerizations of disubstituted siloxanes substantial quantities of cyclic molecules are found to be present. These cyclics are of the general formula $(RR'SiO)_n$, where R and R′ are alkyl or aryl groups and $n = 3, 4, 5, \ldots$ The polydimethylsiloxane equilibrium is the only system reported in the literature. The first work reported was that by Scott.[1] Scott's investigations were carried out on two low molecular weight dimethylsiloxane polymers equilibrated with sulfuric acid catalyst at 25°C. The distributions of cyclic and linear molecules were obtained by fractional distillation. The only cyclic molecules identified were $[(CH_3)_2SiO]_{4,5}$. Hartung and Camiolo[2] prepared high molecular weight dimethylsiloxane polymers equilibrated in refluxing xylene at solvent amounts in the range of 25–75% by weight. The catalyst used was $KO[(CH_3)_2SiO]_xK$. Gas–liquid chromatography was used to determine the quantities of $[(CH_3)_2SiO]_{3-9}$. The data from solvent polymerizations were extrapolated by us to indicate the cyclic concentrations which would be present in a neat polymerization.

In this study $[(CH_3)_2SiO]_4$ was equilibrated to high molecular weight polymer plus cyclics by using $KO[(CH_3)_2SiO]xK$ or H_2SO_4 as catalyst. The polymerizations were carried out at several temperatures to establish the cyclic concentrations as a function of temperature. $(CH_2{=}CH)(CH_3)_2SiO[(CH_3)_2SiO]xSi(CH_3)_2(CH_2{=}CH)$ was used as a chain terminator to control the average degree of polymerization of the chain portion. The cyclic concentrations were plotted as a function of n to determine the fit of the data to the theoretical distribution developed by Stockmayer and Jacobson.[3]

EXPERIMENTAL

Starting Materials

For all but one of the polymerization reactions $[(CH_3)_2SiO]_4$ was used as the monomer. A large quantity of this monomer was distilled with individual cuts taken for each polymerization. Chromatographic analysis of each cut indicated no other cyclic or linear materials present. Refractive indices (n_D^{25}) were in the range of 1.3943–1.3937. Hunter, Hyde, Warrick, and Fletcher[4] report $n_D^{25} = 1.3935$ for $[(CH_3)_2SiO]_4$. In one case a mixture of cyclic dimethylsiloxanes was used. The mixture had the composition 4% $[(CH_3)_2SiO]_3$, 67% $[(CH_3)_2SiO]_5$, 28% $[(CH_3)_2SiO]_5$, 0.5% $[(CH_3)_2SiO]_6$, 0.1% $[(CH_3)_2SiO]_7$.

Polymerization Reaction

The polymerization reaction is as follows:

$$[(CH_3)_2SiO]_4 \xrightarrow[T,\ t]{K^+} [(CH_3)_2SiO]_x + \text{Cyclics}$$

A 100-g. portion of $[(CH_3)_2SiO]_4$ was used. The ratio of chain terminating groups to Si atoms in the chain was 1 $(CH_3)_2(CH_3{=}CH)Si/2500$ Si; the ratio of potassium as $KO[(CH_3)_2SiO]_xK$ to Si atoms in the chain was 1 K/5000 Si. The conditions of time and temperature were 72 hr. at 110°C., 24 hr. at 150°C., 24 hr. at 165°C., or 3.5 hr. at 178°C. One polymer was prepared at room temperature in the presence of 5% by weight concentrated sulfuric acid as catalyst. The polymerization was carried out for 48 hr.[5]

The times necessary to reach equilibrium for the potassium-catalyzed polymers were determined from the temperature dependence of the rate constant as measured by Grubb and Osthoff.[6]

The polymers were dissolved to a concentration of 10% by weight in benzene and neutralized with an amount of acetic acid equivalent to the polymerization catalyst. To the neutralized polymer solution Super-Cel (4% by weight) was added to act as a filtering cake. The solutions were then filtered through pressure filtration equipment to insure that no material was lost during the filtration step.

Establishing the neutrality of the filtered polymer solutions was important to insure that no catalyst was present that could cause thermal rearrangement of the polymers during the chromatographic analyses. Potassium analyses of the solutions and weight losses of the polymers are reported in Table I.

TABLE I
Neutrality of Polymers

Polymer	K^+, ppm[a]	Weight loss (24 hr./250°C.), %[b]
1	(H_2SO_4 catalyst)	4.9
2	1.0	9.4
3	1.0	17.0
4	1.0	8.2
5	2.4	10.7
6	1.0	13.2
7	1.0	6.2

[a] Parts per million potassium as measured by flame photometry.

[b] Per cent weight loss =

$$\left(\frac{\text{wt. after 24 hr./80°C.} - \text{wt. after 24 hr./250°C.}}{\text{wt. after 24 hr./80°C.}}\right) \times 100.$$

To further establish the lack of catalyst in the polymers, polymer 3 was stripped for 8 hr. at 150°C. Chromatographic analysis indicated no cyclics present up to $[(CH_3)_2SiO]_{10}$. This indicated that no cyclic molecules were being generated during the chromatographic analyses of the polymers.

Gas–Liquid Chromatography Experiments

The F and M Model 500 linear temperature-programmed gas–liquid chromatograph was used. The 0–1 mv. Brown recorder was equipped with a model 201 Disc integrator. Columns used were: (*1*) 8 ft × $^3/_{16}$ in. stainless steel packed with 15% Dow Corning 400 (dimethylsiloxane) gum on 42–80 mesh Chromosorb P, nontreated, and (*2*) 4 ft. × $^1/_8$ in. stainless steel packed with 20% Dow Corning 560 silicone fluid on 80–100 mesh Chromosorb P, treated with Dow Corning Z-6030. Column temperatures were programmed from 70 to 150°C. at 7.9°C./min., then 15°C./min. to 325°C. The detector temperature was 300°C. The injector temperature was 325–350°C. The bridge current was 150 ma. The He column flow rate

TABLE II
Standard Solution for Cyclic Analysis

Compound	Weight-%	Weight response factor, R[a]	Purity (GLC), %
Benzene	89.914	—	99.9
$[(CH_3)_2SiO]_3$	0.3718	1.523	100
$[(CH_3)_2SiO]_4$	0.6803	1.186	100
$[(CH_3)_2SiO]_5$	0.3624	1.155	100
$(CH_3)_3SiO[(CH_3)_2SiO]_3Si(CH_3)_3$	0.3448	1.0000	99.8
$(CH_3)_3SiO[(CH_3)_2SiO]_8Si(CH_3)_3$	8.326	—	99

[a] $$\left(\frac{\text{Area of } 5-}{\text{Wt.-\% of } 5-}\right) = \left(\frac{\text{Area of } n}{\text{Wt.-\% of } n}\right) \times R,$$

where n denotes a cyclic of n units.

was 82 ± 2 ml./min. The He reference flow rate was 20 ± 1 ml./min. A standard solution was prepared for quantitative cyclic analysis. The solution was made up to simulate the actual polymer solutions. Its composition is given in Table II.

Quantitative determination of solvent with the chromatograph was not possible due to column overloading. Therefore the amount of solvent was determined by evaporation. The boiling point of benzene is 90°C. lower than that of $[(CH_3)_2SiO]_4$, and the benzene could thus be evaporated with very little loss of siloxane. Both $[(CH_3)_2SiO]_4$ and $[(CH_3)_2SiO]_5$ were used as controls during the evaporation of benzene from the polymers. A correction was then made to account for the loss of siloxane. In a typical solution the weight per cent of $[(CH_3)_2SiO]_4$ lost was only about 0.1%, so the correction due to evaporation represented a very small per cent of the total amount of material evaporated. Weight loss data of the polymers and cyclic siloxane controls are given in Table III.

TABLE III
Determination of Benzene in Polymer Solutions

Solution	Weight loss, %[a]	Weight loss due to benzene, %
1	90.54	90.46
2	90.31	90.23
3	90.42	90.34
4	90.26	90.18
5	91.25	91.17
6	90.52	90.44
7	90.51	90.43
$[(CH_3)_2SiO]_4$	10.04	
$[(CH_3)_2SiO]_5$	3.12	

[a] Weight loss determined after 72 hr. at 25°C. The polymers were analyzed by ultraviolet spectroscopy to prove that all but a trace of benzene had evaporated after the 72 hr. at 25°C.

Molecular Weight of the Polymers

The polymer solutions were allowed to evaporate to dryness at room temperature, then were stripped to 8 hr. at 150°C. to remove the cyclic portion

TABLE IV
Polymer Molecular Weights

Polymer	Molecular weight, g./mole
1	1.74×10^5
2	1.00×10^6
3	1.23×10^6
4	1.60×10^6
6	7.3×10^6
7	1.03×10^6

TABLE V
Cyclic Distribution of $[(CH_3)_2SiO]_n$

Polymer	Temperature, °C.	Cyclic distribution, wt.-%									
		$n = 3$	$n = 4$	$n = 5$	$n = 6$	$n = 7$	$n = 8$	$n = 9$	$n = 10$	$n = 11$	total
1	Room	n.d.[a]	5.62	4.22	1.59	0.46	0.16	0.10	0.47	Trace	12.6
2	110	n.d.	5.88	4.41	1.55	0.40	0.15	0.09	Tr.	Trace	12.5
3	150	n.d.	6.94	4.78	1.54	0.43	0.17	0.11	0.07	Trace	14.0
4	150	n.d.	6.55	4.69	1.51	0.45	0.18	0.13	0.06	Trace	13.6
5	150	n.d.	6.32	4.80	1.90	0.83	0.21	0.08	n.d.	n.d.	14.1
6	165	n.d.	6.63	4.71	1.69	0.44	0.17	0.09	0.07	Trace	13.8
7	178	0.21	6.40	4.88	1.73	0.41	0.19	0.11	0.08	Trace	14.0
Scott[1]		n.d.	3.1	0.8	n.d.	n.d.	n.d.	n.d.	n.d.	n.d.	3.9
Hartung, et al.[2] (extrap.)[b]		0.17	10.0	6.10	1.85	0.38	0.25	0.17	n.d.	n.d.	20.0

[a] n.d. = not detectable.

[b] Our extrapolation to zero solvent of Hartung's solution polymerization data.

of the mixture prior to molecular weight determination. Molecular weights were determined from intrinsic viscosity measurements by using Barry's relation:[7]

$$[\eta] = 2.00 \times 10^{-4} M^{0.66}$$

The average molecular weights so calculated are listed in Table IV.

The molecular weights of polymers 2–4, 6, and 7 are the same order of magnitude. This is certainly to be expected since the amount of chain terminator was the same in all these polymers. The molecular weight of polymer 1 is an order of magnitude below the rest. This polymer was the one catalyzed with sulfuric acid. No end-blocker was added to this polymer, but the water present in the sulfuric acid was sufficient to lower the molecular weight below those of the base-catalyzed polymers.

RESULTS

The cyclic distribution in weight per cent is given in Table V for the polymers studied.

From these data a trend of increasing weight per cent with increasing polymerization temperature is noted for each cyclic.

These data must be converted into concentration units to permit calculation of the equilibrium constant for the formation of a particular cyclic.

Due to the difficulties in accurately measuring the densities of the high molecular weight polymers at elevated temperature, a simpler approach was used for determining densities. The polymer was assumed to consist of a

TABLE VI
Density vs. Temperature for Dimethylsiloxanes

Temperature, °C.	Density, g./ml.		
	$[(CH_3)_2SiO]_4$	$[(CH_3)_2SiO]_5$	$[(CH_3)_2SiO]$, DP = 230[a]
20	0.9558[b]	0.9584[b]	
	0.9561[c]		
25	0.9498	0.9536[d]	0.970
	0.9498[e]	0.9531	
28.1		0.9500[b]	
29.3	0.9451[b]		
80	0.8878	0.8988	
110	0.8528	0.8664	0.898
136	0.8197	0.8355	
150			0.868
165			0.855
178			0.850

[a] Data of Polmanteer.[8]

[b] Data of Mills and MacKenzie.[9]

[c] Data of Solbodin et al.[10]

[d] Data of Hunter et al.[4]

[e] Data of Hildebrand and Shinoda.[11]

high molecular weight linear portion plus $[(CH_3)_2SiO]_{4,5}$. The densities of $[(CH_3)_2SiO]_{4,5}$ were measured at various temperatures, and a plot of density versus temperature was constructed for each cyclic. The density versus temperature relation for the linear portion was assumed to follow that a 1000 cstoke ($\bar{M}$ = 26,400) dimethylsiloxane fluid polymer. The weight fractions of $[(CH_3)_2SiO]_{4,5}$ at each temperature are given in Table V. Assuming the remaining weight fraction to be polymer, the density of the equilibrated polymer could be calculated. Since the densities of the larger cyclic molecules undoubtedly approach the density of a high polymer, and since the total weight fraction of cyclics with six and more $[(CH_3)_2SiO]$ units is less than 0.03, the approximate density calculation should be quite accurate. The densities obtained and values from the literature are listed in Table VI for the cyclics and the linear fluid polymer. Density versus temperature plots for $[(CH_3)_2SiO]_{4,5}$ are given in Figures 1 and 2, respectively.

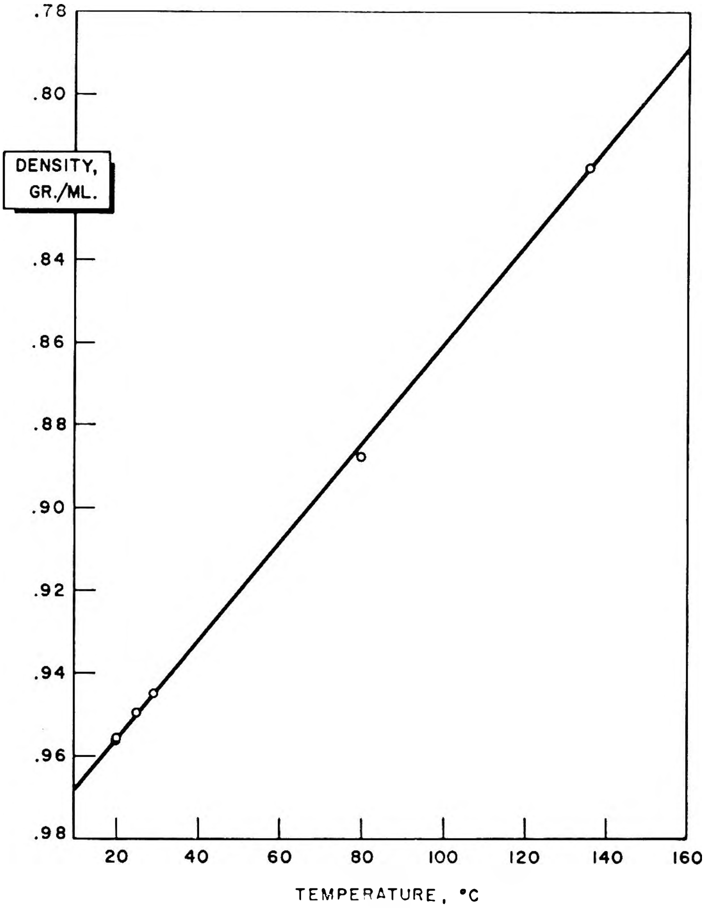

Fig. 1. Density of $[(CH_3)_2SiO]_4$ vs. temperature.

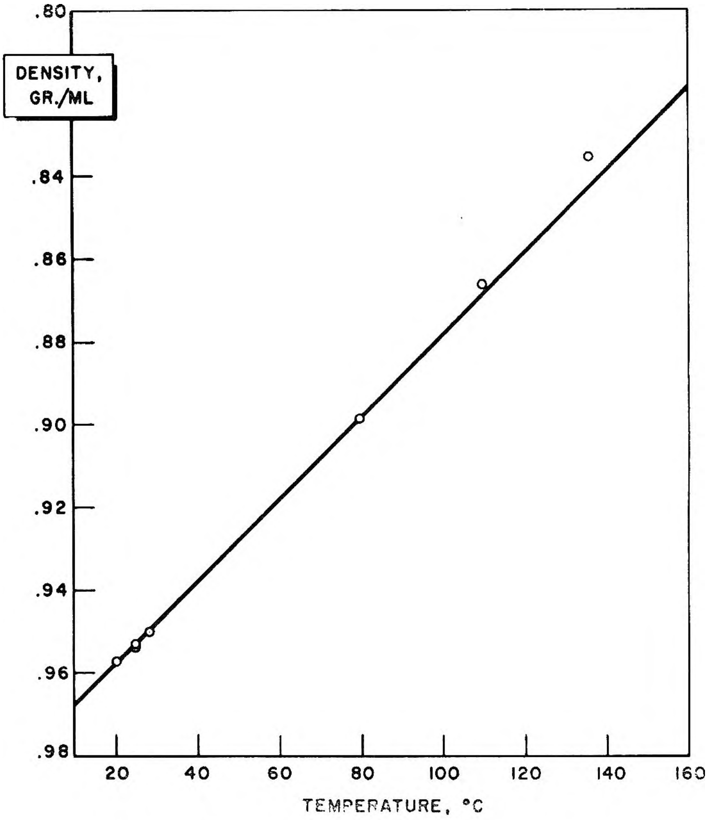

Fig. 2. Density of $[(CH_3)_2SiO]_5$ vs. temperature.

The densities of the polymer mixture thus calculated are listed in Table VII.

TABLE VII
Calculated Density of Equilibrated Polymers at the Polymerization Temperature

Polymer	Temperature, °C.	Density, g./ml.
1	25	0.9681
2	110	0.8937
3, 4, 5	150	0.8618
6	165	0.8482
7	178	0.8425

From the density data in Table VII and the weight per cent of cyclic molecules in Table V, the cyclic concentrations in moles per liter have been calculated. Concentrations of $[(CH_3)_2SiO]_{4-10}$ in the polymers are given in Table VIII.

TABLE VIII

Cyclic Concentration at Various Polymerization Temperatures for $[(CH_3)_2SiO]_n$

Polymer	Temperature, °C.	Cyclic concentration, mole/l.						
		$n = 4$	$n = 5$	$n = 6$	$n = 8$	$n = 9$	$n = 9$	$n = 10$
1	25	0.183	0.110	0.035	0.0086	0.0026	0.0015	
2	110	0.177	0.106	0.031	0.0069	0.0023	0.0012	
3, 4, 5	150	0.192	0.111	0.037	0.0073	0.0028	0.0014	0.0008
6	165	0.190	0.108	0.032	0.0072	0.0024	0.0011	0.0008
7	178	0.182	0.111	0.033	0.0067	0.0027	0.0014	0.0009
Average		0.185	0.091	0.034	0.0073	0.0026	0.0013	0.0008
Standard deviation		0.005	0.002	0.002	0.0006	0.0002	0.0001	0.0001

Treatment of the Experimental Data

From the data in Table VIII the concentrations of cyclics are seen to be independent of temperature. This result and the cyclic distribution in Table IX will be considered in terms of the thermodynamics of the polymer–cyclic equilibrium.

TABLE IX

Average Cyclic Distribution

Cyclic, $[(CH_3)_2SiO]_n$	Cyclics concentration, mole $[(CH_3)_2SiO]$/l.
$n = 4$	0.740
$n = 5$	0.545
$n = 6$	0.204
$n = 7$	0.051
$n = 8$	0.021
$n = 9$	0.012
$n = 10$	0.008

Consider the equilibrium between a chain of $n + x$ siloxane units in equilibrium with a chain of n units and a cyclic of x units:[3,12]

$$C_{n+x} \rightleftharpoons C_n + R_x \tag{1}$$

Assuming activity coefficients equal to unity,

$$K = [C_n][R_x]/[C_{n+x}] \tag{2}$$

If the cyclics are present in a high molecular weight polymer, then $[C_n] \cong [C_{n+x}]$* and

$$K \cong [R_x] \tag{3}$$

---

* The exact expression is $K = [R_x]/p^x$, where p is the fraction of reacted endgroups. The average degree of polymerization P equals $1/(1 - p)$. For the cases studied here the calculated P equals 5000. When corrected for an equilibrium cyclic content of about 14%, $P = 4300$. Then $p = 0.99976$; $p^{10} = 0.9976$. We therefore assume $p^x = 1$.

The change in free energy, ΔF°, may be expressed as

$$\Delta F^\circ = -RT \ln K \tag{4}$$

For reaction (1) then

$$\Delta F^\circ = -RT \ln [R_x] \tag{5}$$

Also,

$$\Delta F^\circ = \Delta H^\circ - T\Delta S^\circ \tag{6}$$

Combining eqs. (5) and (6) yields

$$\ln [R_x] = \Delta S^\circ/R - \Delta H^\circ/RT \tag{7}$$

From Table VIII, $[R_x]$ is independent of temperature. Therefore, $\Delta H^\circ = 0$. This assumption was made earlier by Stockmayer and Jacobson[3] in their development of a theoretical expression for the cyclic distribution in the dimethylsiloxane equilibrium.

For the dimethylsiloxane equilibrium,

$$\ln [R_x] = \Delta S^\circ/R \tag{8}$$

Calculated values of ΔS° for the cyclics are given in Table X.

TABLE X

Cyclic, $[(CH_3)_2SiO]_n$	ΔS°, cal./mole °K.[a]	ΔS°, cal./mole SiO °K.
$n = 4$	−3.35	−0.84
$n = 5$	−4.40	−0.88
$n = 6$	−6.7	−1.1
$n = 7$	−9.8	−1.4
$n = 8$	−11.8	−1.5
$n = 9$	−13	−1.5
$n = 10$	−14	−1.4

[a] Here the activity coefficients were assumed to equal one in every case for internal consistency.

ΔS° appears to converge to a value of about −1.4 cal./mole —SiO— °K. for the heptamer and higher cyclics.

Theoretical Predictions of the Cyclic Distribution

We rewrite K as

$$K = e^{\Delta S^\circ/R} e^{-\Delta H^\circ/RT} \tag{9}$$

From eq. (8) for rings of four and more siloxane units, $\Delta H^\circ = 0$. We consider this case now and later treat the formation of $[(CH_3)_2SiO]_3$.

From a statistical mechanics treatment it has been shown that for the ring-chain equilibrium in polymers[3,13]

$$e^{\Delta S/R} = PV/2xv_sN \tag{10}$$

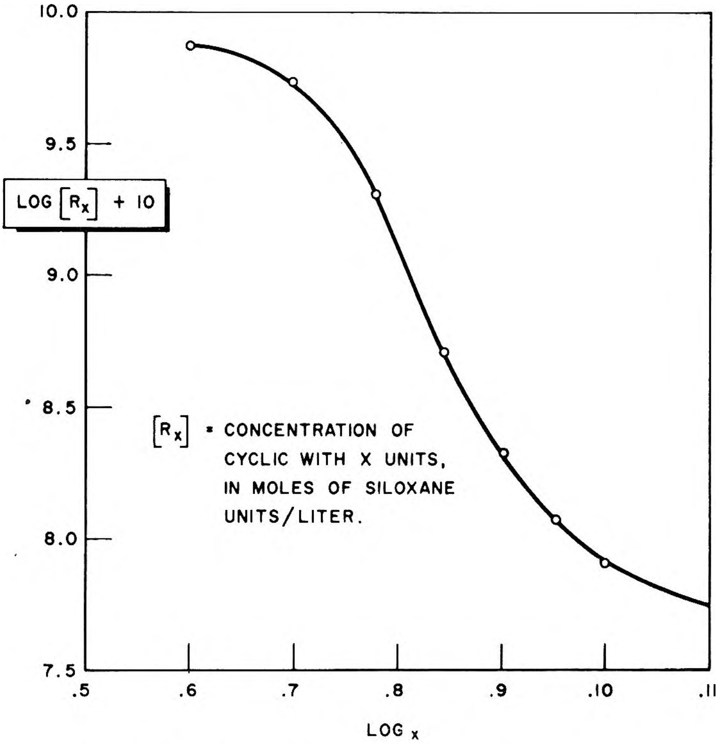

Fig. 3. Cyclic distribution in polydimethylsiloxane.

where P is the probability of ring closure, i.e., the fraction of chains that will close to form ring structures, V is the total volume of the system, v_s is the volume of a constrained skeletal atom prior to bond breaking, x is the number of —SiO— units in the ring, and N is Avogadro's number.

Two approaches have been followed for calculating P: (*1*) assume Gaussian distribution of end-to-end distances (Stockmayer-Jacobson model);[3] (*2*) assume detailed structural model for the chain with fixed bond length, fixed bond angles, and fixed rotational states. Thus, for dimethylsiloxanes $\angle$OSiO = 110°, $\angle$SiOSi = 140°; *gauche* ($\phi = 60°, 300°$), *trans* ($\phi = 180°$) rotational states, equally probable; ring closure is assumed to occur when the end-to-end distance is less than one bond length (Carmichael-Kinsinger model).[13]

From approach (*1*),

$$e^{\Delta S/R} = (3/2\pi\nu)^{3/2}(V/2b^3)x^{-5/2} \tag{11a}$$

where x and V were defined in eq. (10), ν is the number of bonds per monomer unit, b is the effective link length defined by $\langle \bar{R}^2\rangle = \nu n b^2$, $\langle R^2\rangle$ being the mean square end-to-end distance.

For $n \geq 4$,

$$\ln\,[R_x] = 5/2 \ln x + \ln C \tag{11b}$$

where

$$C = (3/2\pi\nu)^{3/2}(V/2b^3)$$

Thus a plot of the log of the concentration versus the log of the number of SiO units in the ring, according to the Stockmayer-Jacobson theory, should be a straight line with a slope of $-5/2$.

A plot of the averaged data from Table IX appears in Figure 3. The data do not lie on a straight line, indicating that the Stockmayer-Jacobson theory is not obeyed over the entire range of cyclics studied in this work. However, it is interesting to note that a straight line drawn through the values of $[R_x]$ at $x = 4$ and 5 has a slope of -2.46, in excellent agreement with the predicted slope of -2.5. Even so, the value of K for $[R_4]$ calculated from the Stockmayer-Jacobson theory is 0.12. From Table XI this is far lower than the amount experimentally observed. Therefore we conclude that the Stockmayer-Jacobson theory cannot quantitatively account for the experimentally observed cyclic distribution in polydimethylsiloxane.

TABLE XI
Comparison of Theory and Experiment

	$[(CH_3)_2SiO]_3$	$[(CH_3)_2SiO]_4$
K_{exp}	0.024	0.74[a]
K_{theor}		
Carmichael-Kinsinger	0.056[b]–0.52[c]	0.36
Stockmayer-Jacobson[d]	0.017[b]–0.16[c]	0.12

[a] With $\gamma = 3$, $K_{exp} = 2.2$. Activity coefficient calculated γ from data of Grubb and Osthoff.[14]

[b] Calculated assuming strain energy of 9 kcal./mole (upper limit).

[c] Calculated assuming strain energy of 3 kcal./mole (lower limit).

[d] All calculations based on Stockmayer-Jacobson theory assume freely rotating chain; $<r_0{}^2{}_f>/nl^2 = 3.2$.[15] A calculation based on dimensions of the real chain,[15] $\langle r_0{}^2\rangle/nl^2 = 6.3$, yields K_{exp} for $[(CH_3)_2SiO]_4 = 0.042$.

From approach (*2*),

$$e^{\Delta S/R} = PV/25.6N \qquad (12a)$$

For $n = 4$, $P = 0.00548$, and

$$e^{\Delta S/R} = 0.36 = K \qquad (12b)$$

To account quantitatively for the formation of $[(CH_3)_2SiO]_3$, the strain energy of this ring must be considered. The strain has been measured by Merker et al.[16] by heat of polymerization and reported to be 3–4 kcal./mole. Tanaka[17] employed calorimetry and reports a strain energy of <9 kcal./mole.

We assume that the cyclic strain energy can be equated with $\Delta H°$ of formation. Therefore K is calculated from eqs. (9) and (11a) by the Stockmayer-Jacobson distribution and from eqs. (9) and (12a) by the Carmichael-Kinsinger model, assuming $T = 423°K$. The range of values in Table XI represents the range of strain energies of 3–9 kcal./mole.

The Stockmayer-Jacobson model appears best to represent the formation of R_3, while the Carmichael-Kinsinger model best fits the experimental determination of R_4. Both models fail to account quantitatively for the experimental results.

The chief advantage of the Stockmayer-Jacobson formulation is that K is predicted as a function of ring size. In the discrete state model the ring closure probability must be calculated separately for each ring size. The probability of ring closure, P, must be evaluated for each model. In the evaluation of P the Carmichael-Kinsinger model invokes the arbitrary assumption that ring closure occurs when the end-to-end distance is less than one bond length. Further, the volume occupied by a chain atom, v_s, must be calculated. The need for calculating this additional parameter adds much uncertainty to the method.

References

1. Scott, D. W., *J. Am. Chem. Soc.*, **68**, 2294 (1946).
2. Hartung, H. A., and S. M. Camiolo, papers presented to the Division of Polymer Chemistry, 141st National Meeting, American Chemical Society, Washington, D. C., March 1962.
3. Jacobson, H., and W. H. Stockmayer, *J. Chem. Phys.*, **18**, 1600 (1950).
4. Hunter, M. J., J. F. Hyde, E. L. Warrick, and H. J. Fletcher, *J. Am. Chem. Soc.*, **68**, 667 (1946).
5. Hyde, J. F., private communication.
6. Grubb, W. T., and R. C. Osthoff, *J. Am. Chem. Soc.*, **77**, 1405 (1955).
7. Barry, A. J., *J. Appl. Phys.*, **17**, 1020 (1946).
8. Polmanteer, K. E., private communication.
9. Mills, A. P., and C. A. MacKenzie, *J. Am. Chem. Soc.*, **76**, 2672 (1954).
10. Slobodin, Y. M., Y. E. Shmulyakovskiĭ, and K. H. Rzhedzinskaya, *Dokl. Akad. Nauk SSSR*, **105**, 958 (1955).
11. Hildebrand, J. H., and K. Shinoda, *J. Phys. Chem.*, **65**, 183 (1961).
12. Gee, G., *Inorganic Polymers*, The Chemical Society, London, 1961, pp. 67–77.
13. Carmichael, J., and J. Kinsinger, *Can. J. Chem*, **42**, 1996 (1964).
14. Osthoff, R. C., and W. T. Grubb, *J. Am. Chem. Soc.*, **76**, 399 (1954).
15. Flory, P. J., V. Crescenzi, and J. E. Mark, *J. Am. Chem. Soc.*, **86**, 146 (1964).
16. W. A. Piccoli, G. G. Haberland, and R. L. Merker, *J. Am. Chem. Soc.*, **82**, 1883 (1960).
17. T. Tanaka, *Bull. Chem. Soc. Japan*, **32**, 1258 (1959).

Résumé

Pour déterminer les quantités de molécules cycliques présentes à l'équilibre dans une polymérisation d'un mélange de polymère et de molécules cycliques de diméthylsiloxane, on a employé la chromatographie gaz–liquide. L'étude chromatographique a été effectuée en fonction de la température de polymérisation. On montre que la concentration à l'équilibre est indépendante de la température pour $[(CH_3)_2SiO]_{4-10}$. Le changement de concentration des molécules cycliques en fonction de n pour $[(CH_3)_2SiO]_{4-10}$ ne suit pas la distribution théorique de Stockmayer-Jacobson. Il est possible de calculer qualitativement les concentrations de $[(CH_3)_2SiO]_{3,4}$ par la théorie de Stockmayer-Jacobson et par le modèle proposé par Carmichael et Kinsinger. Pour $[(CH_3)_2SiO]_4$, $K_{\exp} = 0.74$ moles-SiO–/litre. Les calculs à partir du modèle nous donnent 0.12 (Stockmayer-Jacobsen) et 0.36 (Carmichael et Kinsinger). Pour $[(CH_3)_2SiO]_3$, $K_{\exp} = 0.24$ moles–SiO–/litre, les calculs par le modèle nous donnent 0.017–0.16 (Stockmayer-Jacobsen) et

0.056–0.52 (Carmichael et Kinsinger). Le domaine des valeurs augmente parce qu'on est incertain des énergies de tension cyclique.

Zusammenfassung

Gas-Flüssigchromatographie wurde zur Bestimmung der in einer Gleichgewichtspolymerisationsmischung von Hochpolymeren und zyklischen Dimethylsiloxanmolekülen vorhandenen zyklischen Moleküle verwendet. Es wurde die Abhängigkeit von der Polymerisationstemperatur untersucht. Für $[(CH_3)_2SiO]_{4-10}$ erweist sich die Gleichgewichtskonzentration als unabhängig von der Temperatur. Die Konzentration an zyklischen Verbindungen als Funktion von n befolgt für $[(CH_3)_2SiO]_{4-10}$ nicht die theoretische Verteilung von Stockmayer-Jakobson. Die Konzentration an $[(CH_3)_2SiO]_{3,4}$ kann nach der Stockmayer-Jakobson-Theorie und nach dem von Carmichael und Kinsinger vorgeschlagenen Modell qualitativ vorausgesagt werden. Für $[(CH_3)_2SiO]_4$, beträgt K_{exp} = 0.74 Mole–SiO–/l. Die Modellberechnunger gibt 0,12 (Stockmayer-Jacobsen) und 0,36 (Carmichael et Kinsinger). Für $[(CH_3)_2SiO]_3$ beträgt K_{exp} = 0,024 Mole–SiO–/l. Die Modellberechnung ergibt 0,017–0,16 (Stockmayer-Jakobson) und 0,056–0,52 (Carmichael et Kinsinger). Der Wertebereich nimmt wegen der Ungenauigkeit bei der zyklischen Spannungsenergie zu.

Received June 26, 1964
Revised July 30, 1964

JOURNAL OF POLYMER SCIENCE: PART A VOL. 3. PP. 985-994 (1965)

Unperturbed Dimensions of Polystyrene Derivatives

NOBUHIRO KUWAHARA, KAZUYOSHI OGINO, AKIRA KASAI, SUSUMU UENO, and MOTOZO KANEKO, *Department of Polymer Science, Faculty of Science, Hokkaido University, Sapporo, Japan*

Synopsis

Several methods have been developed for estimating the unperturbed dimensions of polymer chains without measurements under theta conditions. Osmotic pressure and viscosity measurements have been performed to test the applicability of the methods of estimating the unperturbed dimensions. It has been observed that the Kurata-Stockmayer and Stockmayer-Fixman methods are applicable to poly-*p*-methylstyrene and poly-*p*-chlorostyrene in nonpolar and polar solvents. The effect of halogenation at the *para* position to internal rotation has been given by a comparison of the unperturbed dimensions for poly-*p*-methylstyrene and poly-*p*-chlorostyrene.

INTRODUCTION

The excluded volume effect vanishes under a special condition of temperature or solvent, which is usually known as the Flory theta temperature or solvent. Light-scattering and viscosity measurements under such theta conditions furnish direct knowledge of the unperturbed dimensions of polymer chains. However, theta conditions can rarely be attained, even among amorphous polymers. This limitation becomes especially serious for the investigations of crystalline polymers. Several methods have been developed to estimate the unperturbed dimensions without measurements under theta conditions. Flory and Fox have shown the possibility that the unperturbed dimensions may be estimated from intrinsic viscosity-molecular weight data in usual solvents.[1] Krigbaum has proposed a semiempirical relation correlating osmotic second virial coefficients with intrinsic viscosities.[2,3] Kurata et al. have refined the Flory-Fox theory of the excluded volume effect of a single chain[4] and developed a new method of estimating the unperturbed dimensions of chain molecules from viscosity measurements in any solvent, good or poor.[5] Recently, Stockmayer and Fixman have proposed a very simple equation for obtaining the unperturbed dimensions.[6] The present work was done to test the applicability of the methods of estimating the unperturbed chain dimensions from viscosity measurements.

Poly-*p*-methylstyrene and poly-*p*-chlorostyrene were used as solutes in this work. It is possible to test the applicability of the viscosity methods for polar and the nonpolar polymer in various solvents. Since the van der

Waals radius of the chlorine atom is almost the same as that of the methyl group, the difference between Cl and CH_3 may contribute only a minor effect on the steric hindrance to internal rotation. Therefore, it is expected that the effect of halogenation at the *para* position to internal rotation may be determined by a comparison of the unperturbed dimensions for the two polymers.

EXPERIMENTAL

Materials

Two *p*-substituted derivatives of styrene, *p*-methylstyrene (I) and *p*-chlorostyrene (II)

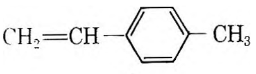

I

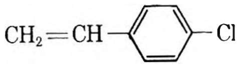

II

were synthesized and polymerized. Synthesis of the monomers was effected through the following processes: ketone synthesis by Friedel-Crafts reaction [eq. (1)],

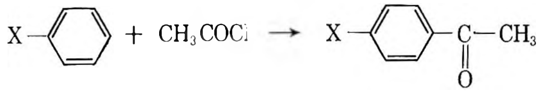

(1)

reduction of the ketones by the Meerwein-Ponndorf method [eq. (2)],

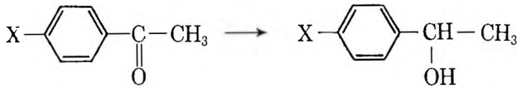

(2)

and dehydration of the alcohols by $KHSO_4$ [eq. (3)].

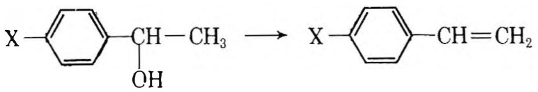

(3)

Poly-*p*-methylstyrene and poly-*p*-chlorostyrene were fractionated from dilute benzene solutions by the addition of methanol. Nine fractions of poly-*p*-methylstyrene and eight fractions of poly-*p*-chlorostyrene were prepared by the successive precipitation method. The separated fractions were redissolved and reprecipitated. Seven fractions for each polymer were chosen in this work.

The solvents employed were reagent grade. Toluene and methyl ethyl ketone were dried over anhydrous calcium chloride before use.

Measurements

Osmotic pressure measurements were performed in a modified Fuoss-Mead type osmometer with a collodion membrane. Tests for diffusion of polymer were always negative. A water bath was controlled within 30 ± 0.003°C. The osmotic pressures were determined by the static method.

The solution viscosities were measured with Ubbelohde-type viscometers calibrated for kinetic energy corrections. Those viscometers were so designed that rate of shear corrections was negligible. Measurements were carried out at 30 ± 0.01 °C.

All solutions were stirred by magnetic stirrer for at least 25 hr. before measurement and filtered into the osmometers or the viscometers through a medium glass filter. The concentrations of all solutions were determined by dry weights.

RESULTS

The osmotic pressure data were fitted to the equation

$$(\pi/c)^{1/2} = (\pi/c)_0^{1/2}[1 + (\Gamma_2/2)c]$$

according to the procedure used by Krigbaum and Flory.[7] Plots of $(\pi/c)^{1/2}$ versus c for the present data are in all cases linear, as illustrated in Figure 1. Number-average molecular weights $\bar{M}_n$ and second virial coefficients A_2 were determined by using the intercepts and the slopes of the straight lines. Values of $\bar{M}_n$ and A_2 are given in Tables I and II.

Intrinsic viscosities were determined by plotting η_{sp}/c against concentration and extrapolating to zero concentration, as shown in Figure 2. Values obtained are also given in Tables I and II.

As illustrated in Figure 3*a*, plots of $[\eta]$ versus $\bar{M}_n$ on a log-log scale are represented in all cases by a straight line conforming to the Mark-Houwink relation

$$[\eta] = K'\bar{M}_n^{\nu}$$

Comparison of the result for poly-*p*-chlorostyrene in toluene at 30°C. with comparable results of earlier workers is afforded by Figure 3*b*.[8,9] The

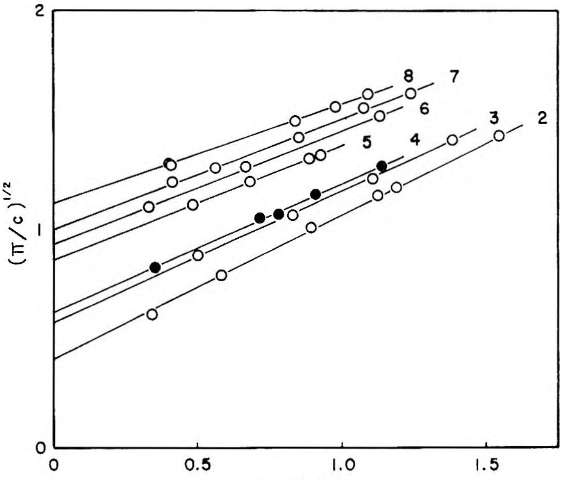

Fig. 1. $(\pi/c)^{1/2}$ plotted against concentration for poly-*p*-methylstyrene fractions in toluene at 30°C.

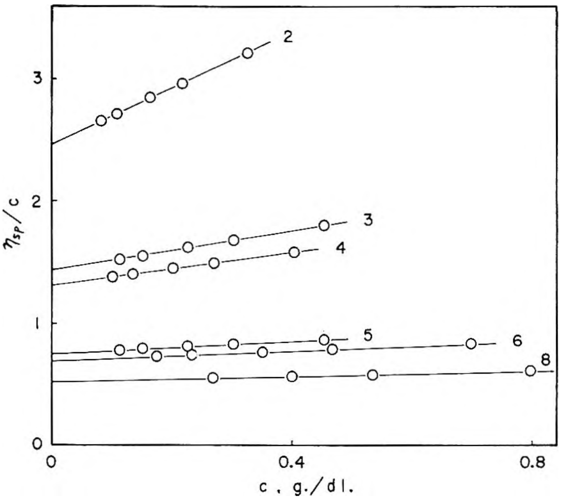

Fig. 2. Relations between η_{sp}/c and concentration for poly-*p*-methylstyrene fractions in cyclohexane at 30°C.

TABLE I

Results for Poly-*p*-methylstyrene Fractions

Fraction	$\bar{M}_n \times 10^{-4}$	$A_2 \times 10^4$, cm.³-mole/g.²	[η], dl./g. Toluene	Cyclohexane	Methyl ethyl ketone
MS 2	154	2.10	3.52	2.46	1.72
MS 3	79.1	2.69	2.10	1.44	1.05
MS 4	67.3	2.84	1.92	1.31	0.980
MS 5	34.0	3.47	1.09	0.752	0.580
MS 6	29.9	3.78	0.992	0.695	0.540
MS 7	25.7	3.89			
MS 8	20.6	3.97	0.696	0.518	0.414

TABLE II

Results for Poly-*p*-chlorostyrene Fractions

Fraction	$\bar{M}_n \times 10^{-4}$	$A_2 \times 10^4$, cm.³-mole/g.²	[η], dl./g. Chlorobenzene	Methyl ethyl ketone	Toluene
CS 1	268	0.56	3.18	2.40	2.06
CS 2	107	0.77	1.53	1.22	1.07
CS 3	59.0	0.86	0.888	0.760	0.676
CS 4	59.0	0.86		0.758	0.676
CS 5	46.9	0.86	0.756	0.623	0.550
CS 6	28.4	0.77	0.486		0.406
CS 7	17.0	0.74	0.327	0.296	0.274

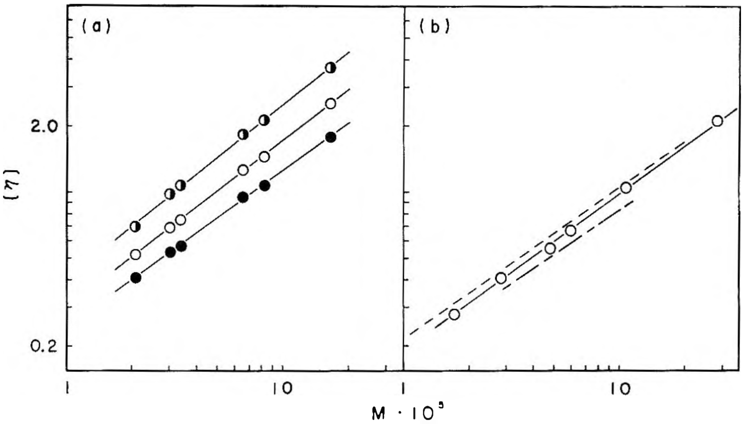

Fig. 3. (*a*) Double logarithmic plots of $[\eta]$ vs. $\bar{M}_n$ for poly-*p*-methylstyrene at 30°C.: (◑) in toluene; (○) in cyclohexane; (●) in methyl ethyl ketone. (*b*) Relations of $[\eta]$ vs. $\bar{M}_w$ for poly-*p*-chlorostyrene in toluene: (○) 30°C., this work; (– –) 25°C., data of Davis;[8] (– –) 30°C., data of Saito.[9]

present data lie between the results of Davis and that of Saito. Values of the parameters K' and ν corresponding to straight lines of the present results are given in Table III.

TABLE III
Parameters of Intrinsic Viscosity–Molecular Weight Relations for Poly-*p*-methylstyrene and Poly-*p*-chlorostyrene in Various solvents at 30°C.; $[\eta] = K'\bar{M}_n^{\nu}$

Polymer	Solvent	$K' \times 10^5$	ν	Range $M \times 10^{-4}$
Poly-*p*-methylstyrene	Toluene	6.88	0.76	20–155
	Cyclohexane	8.07	0.72	
	Methyl ethyl ketone	10.3	0.68	
Poly-*p*-chlorostyrene	Chlorobenzene	2.19	0.80	18–250
	Methyl ethyl ketone	3.52	0.75	
	Toluene	5.37	0.71	

DISCUSSION

It is well known that the quantities A_2, $[\eta]$, and ν depend on the chain conformations in solutions. As shown by the values of $[\eta]$ and ν, poly-*p*-methylstyrene molecule reaches its largest dimension in toluene. For poly-*p*-chlorostyrene, chlorobenzene is the best of three solvents. It may be said that solvents with the structure similar to the substituent of a given polymer act as better solvents. Some investigators have found that the theta temperature of the polystyrene–cyclohexane system is 34.5°C., and that the parameter ν is equal to 0.5 under such a theta temperature.[10–13] Cyclohexane is a good solvent for poly-*p*-methylstyrene, and the ν value of this system at 30°C. is 0.72. The large difference between the ν values of polystyrene and poly-*p*-methylstyrene in cyclohexane at approximately equal temperatures may be taken as an indication that the solution properties are remarkably affected by the methyl group in the *para* position. Similar effects of the substituent in the *para* position on the solution properties may be also observed by a comparison of the values of A_2, $[\eta]$, and ν for poly-*p*-methylstyrene in toluene with those for poly-*p*-chlorostyrene in the same solvent. The values for poly-*p*-chlorostyrene in toluene are consistently smaller than those for poly-*p*-methylstyrene in toluene.

Flory and Fox have tried to estimate the unperturbed dimensions without the aid of theta solvent experiments. The method is based on the combination of Flory and Fox's viscosity equation and Flory's excluded volume equation:[14,15]

$$[\eta]^{2/3}/M^{1/3} = K^{2/3} + 0.857\Phi_0 BK^{2/3}M/[\eta] \qquad (4)$$

where B is related to Flory's interaction parameter χ_1 by

$$B = \bar{v}^2(1 - 2\chi_1)/V_1N_A$$

where v is the specific volume of the polymer, V_1 is the molar volume of the solvent, and N_A is the Avogadro's number. The unperturbed dimensions of chain polymers are calculated from

$$K = \Phi_0(<L^2>_0/M)^{3/2} \qquad (6)$$

where $\langle L^2\rangle_0$ is the mean-square end-to-end length for the unperturbed chain and Φ_0 is the universal viscosity constant for all chain polymers in theta solvents. Equation (4) implies that the two quantities K and B can be determined simultaneously from the intercept and the slope of a straight line which should be obtained by plotting $[\eta]^{2/3}/M^{1/3}$ against $M/[\eta]$. However, its application was observed to give unreasonably small values for K in better solvents even for the nonpolar polymer, as suggested by Kurata and Stockmayer.[5] This becomes especially serious for poly-*p*-chlorostyrene.

Kurata, Stockmayer, and Roig have calculated the excluded volume effect of linear polymer molecules with the use of an ellipsoid model.[4] Kurata and Stockmayer have used it to obtain unperturbed dimensions of a large number of polymers from their intrinsic viscosities.[5] Their results are presented by eqs. (7)–(9):

$$[\eta]^{2/3}M^{1/3} = K^{2/3} + 0.363\Phi_0 B[g(\alpha_\eta)M^{2/3}/[\eta]^{1/3}] \qquad (7)$$

$$g(\alpha_\eta) = 8\alpha_\eta{}^3/(3\alpha_\eta{}^2 + 1)^{3/2} \qquad (8)$$

$$\alpha_\eta{}^3 = [\eta]/KM^{1/2} \qquad (9)$$

where α_η is the viscosity expansion factor. These equations provide the possibility for separate estimation of the short-range and long-range interactions. An approximate value of K is estimated from the first plots of $[\eta]^{2/3}/M^{1/3}$ against $M^{2/3}/[\eta]^{1/3}$. The value of $g(\alpha_\eta)$ can easily be calculated from eqs. (8) and (9) by using the approximate value of K. Kurata-Stockmayer plots for poly-*p*-methylstyrene and poly-*p*-chlorostyrene in

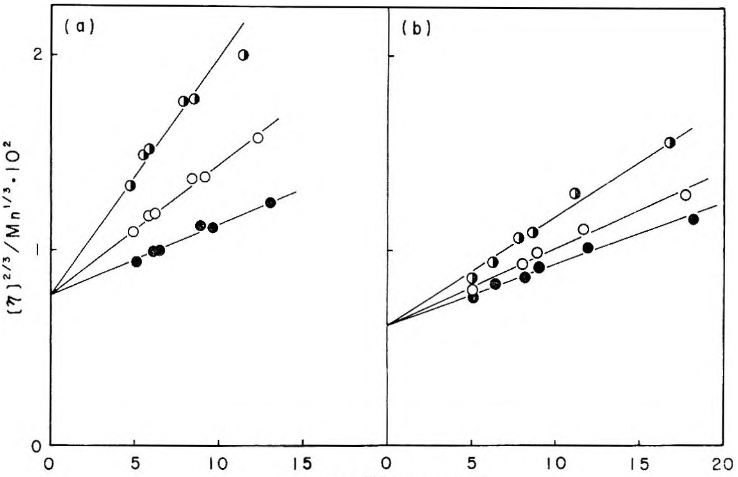

Fig. 4. (*a*) Kurata-Stockmayer plots for poly-*p*-methylstyrene at 30°C.: (◑) in toluene; (○) in cyclohexane; (●) in methyl ethyl ketone. (*b*) Kurata-Stockmayer plots for poly-*p*-chlorostyrene at 30°C.: (◑) in chlorobenzene; (○) in methyl ethyl ketone; (●) in toluene.

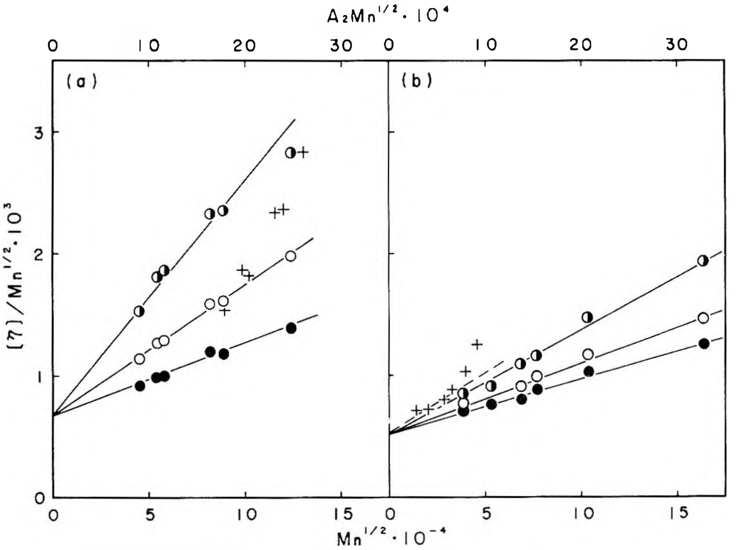

Fig. 5. (*a*) Stockmayer-Fixman plots for poly-*p*-methylstyrene at 30°C. (◑) in toluene, (○) in cyclohexane, and (●) in methyl ethyl ketone; (+) Krigbaum plot for poly-*p*-methylstyrene in toluene at 30°C. (*b*) Stockmayer-Fixman plots for poly-*p*-chlorostyrene at 30°C. (◑)in chlorobenzene, (○) in methyl ethyl ketone, and (●) in toluene; (+) Krigbaum plot for poly-*p*-chlorostyrene in toluene at 30°C.

several solvents are given in Figure 4. The straight lines drawn through the three sets of points have a common intercept, leading to a single value of *K* independent of solvent. It is seen that Kurata-Stockmayer method is applicable even to poly-*p*-chlorostyrene in polar solvents.

TABLE IV

Unperturbed Chain Dimensions Calculated from K Values

Polymer	Method	$K \times 10^5$	$(\langle L^2\rangle/M)^{1/2} \times 10^{11}$	$(\langle L^2\rangle_0 \text{ of}/M)^{1/2} \times 10^{11}$	σ
Poly-*p*-methylstyrene	Kurata-Stockmayer	68 ± 5	620 ± 15	284	2.18 ± 0.05
	Stockmayer-Fixman	66 ± 5	615 ± 15		2.17 ± 0.05
Poly-*p*-chlorostyrene	Kurata-Stockmayer	50 ± 5	560 ± 20	261	2.15 ± 0.07
	Stockmayer-Fixman	52 ± 5	565 ± 20		2.16 ± 0.07
	Krigbaum	53 ± 5	570 ± 20		2.18 ± 0.07
Polystyrene[a]	Kurata-Stockmayer	82 ± 5	670 ± 15	302	2.22 ± 0.05

[a] Value of Kurata and Stockmayer.[5]

The perturbation theory of the excluded volume effect now is well established,[16-20] although its application is limited to a very narrow range near the theta temperature. Recently, Stockmayer and Fixman have used it to develop a method for estimating the unperturbed dimensions and obtained the very simple equation[6]

$$[\eta]/M^{1/2} = K + 0.51\Phi_0 B M^{1/2} \tag{10}$$

As shown by Figure 5, Stockmayer-Fixman plots give a set of lines with a common intercept, which is practically independent of solvent. Values of K obtained through this method agree well with those of Kurata-Stockmayer as shown in Table IV. It may be considered that the Stockmayer-Fixman method has as wide an applicability for the nonpolar and polar polymers in usual solvents as the Kurata-Stockmayer method.

Krigbaum has proposed a semiempirical relation correlating osmotic second virial coefficients with intrinsic viscosities:[2,3]

$$[\eta]/M^{1/2} = K + 0.50 A_2 M^{1/2} \tag{11}$$

Krigbaum plots for the two polymers in toluene at 30°C. are included in Figure 5. The K value of poly-*p*-chlorostyrene obtained through this method is in fairly good agreement with that obtained by the Stockmayer-Fixman method. This indicates that Krigbaum method is applicable to poor solvent systems.

Values of K and the resulting values of the unperturbed dimensions calculated with the use of the theoretical number, 2.87×10^{21}, for Φ_0 are tabulated in Table IV; the values for polystyrene[5] are also included. The factor, which is used as a measure of the hindrance to internal rotation about the single bonds of the chain, is defined in the general manner

$$\sigma^2 = \langle L^2 \rangle_0 / \langle L^2 \rangle_{0f}$$

The quantity $\langle L^2 \rangle_{0f}$ is the mean-square end-to-end length corresponding to completely free internal rotations.

The σ value of poly-*p*-methylstyrene is of the same order of magnitude as that for polystyrene. This indicates that the methyl group at the *para* position has only a minor effect on the hindering potential for rotation about the C—C bond. The difference between the σ values of poly-*p*-methylstyrene and poly-*p*-chlorostyrene is less than the probable experimental error. The present value for poly-*p*-chlorostyrene is in good agreement with $\sigma = 2.18$ deduced by Kurata and Stockmayer.[5] It has been pointed out that electrostatic interactions between polar groups in a series of polymethacrylates stabilize the *trans* conformation relative to *gauche* conformations.[5,21,22] This may not be the case with polar derivatives of polystyrene. The agreement of the σ values of the two polymers, poly-*p*-methylstyrene and poly-*p*-chlorostyrene, may be taken as an indication that the effect of interaction between polar groups at the *para* position on the hindering potential for rotation is small.

The authors are indebted to Prof. J. Furuichi for encouragement throughout the present investigation and to Prof. T. Nakagawa and members of Department of Polymer Science in this University for useful discussions.

References

1. Fox, T. G, and P. J. Flory, *J. Am. Chem. Soc.*, **73**, 1915 (1951).
2. Krigbaum, W. R., *J. Polymer Sci.*, **18**, 315 (1955).
3. Krigbaum, W. R., *J. Polymer Sci.*, **28**, 213 (1958).
4. Kurata, M., W. H. Stockmayer, and A. Roig, *J. Chem. Phys.*, **33**, 151 (1960).
5. Kurata, M., and W. H. Stockmayer, *Fortschr. Hochpolymer. Forsch.*, **3**, 196 (1963).
6. Stockmayer, W. H., and M. Fixman, *J. Polymer Sci.*, **C1**, 137 (1963).
7. Krigbaum, W. R., and P. J. Flory, *J. Am. Chem. Soc.*, **75**, 1775 (1953).
8. Davis, J. E., Ph.D. Thesis, M.I.T. Cambridge, Mass., May 1960.
9. Saito, T., *Bull. Chem. Soc. Japan*, **35**, 1580 (1962).
10. Outer, P., C. I. Carr, and B. H. Zimm, *J. Chem. Phys.*, **18**, 830 (1950).
11. Krigbaum, W. R., *J. Am. Chem. Soc.*, **76**, 3758 (1954).
12. Krigbaum, W. R., and D. K. Carpenter, *J. Phys. Chem.*, **59**, 1166 (1955).
13. Fujita, H., A. M. Linklater, and J. W. Williams, *J. Am. Chem. Soc.*, **82**, 379 (1960).
14. Flory, P. J., and T. G Fox, *J. Am. Chem. Soc.*, **73**, 1904 (1951).
15. Flory, P. J., *J. Chem. Phys.*, **17**, 303 (1949).
16. Fixman, M., *J. Chem. Phys.*, **23**, 1656 (1955).
17. Yamakawa, H., and M. Kurata, *J. Phys. Soc. Japan*, **13**, 78 (1958).
18. Kurata, M., and H. Yamakawa, *J. Chem. Phys.*, **29**, 311 (1958).
19. Kurata, M., and H. Utiyama, *Makromol. Chem.*, **34**, 139 (1959).
20. Fixman, M., *J. Chem. Phys.*, **36**, 3123 (1962).
21. Chinai, S. N., *J. Polymer Sci.*, **25**, 413 (1957).
22. Chinai, S. N., and R. J. Valles, *J. Polymer Sci.*, **39**, 363 (1959).

Résumé

On expose plusieurs méthodes pour estimer les dimensions non perturbées des chaînes polymériques sans effectuer de mesures dans des conditions thèta. On a employé des mesures de pression osmotique et de viscosité pour contrôler l'applicabilité de ces méthodes à l'estimation des dimensions non-perturbées. On a observé que les méthodes de Kurata-Stockmayer et Stockmayer-Fixman sont applicables au poly-*p*-méthylstyrène et au poly-*p*-chlorostyrène dans les solvants non-polaires et polaires. On montre l'influence de l'halogénation en position *para* sur la rotation interne en comparant les dimensions non-perturbées du poly-*p*-méthylstyrène et du poly-*p*-chlorostyrène.

Zusammenfassung

Einige Methoden wurden zur Bestimmung der ungestörten Dimension von Polymerketten ohne Messung unter Theta-Bedingungen entwickelt. Zur Überprüfung der Anwendbarkeit der Methoden zur Bestimmung der ungestörten Dimensionen wurden Messungen des osmotischen Druckes und der Viskosität ausgeführt. Es zeigte sich, dass die Methoden von Kurata-Stockmayer und Stockmayer-Fixman auf Poly-*p*-Methylstyrol und Poly-*p*-Chlorstyrol in unpolaren und polaren Lösungsmitteln angewendet werden können. Der Einfluss der Halogenierung in *para*-Stellung auf die innere Rotation wurde durch einen Vergleich der ungestörten Dimensionen von Poly-*p*-Methylstyrol und Poly-*p*-Chlorstyrol ersichtlich.

Received July 8, 1964

JOURNAL OF POLYMER SCIENCE: PART A VOL. 3, PP. 995-1012 (1965)

Ziegler Polymerization of Olefins. V. Site Removal and Site Activation by Electron Donors

J. BOOR, JR., *Emeryville Research Center, Shell Development Company, Emeryville, California*

Synopsis

Electron donors having different structures have been incorporated into the Ziegler catalyst, $ZnEt_2$ + γ-$Al_xTi_yCl_z$-160, in order to understand the site removal and the site activation processes. Donors which were studied in the present work include: azulenes, unsaturated compounds, aromatics, substituted pyridines and quinolines, cyclopentadienyl compounds of V, Cr, Ni, and Co, $(C_6H_6)_2Cr$, and PF_3. Their effect on the polymerization of propylene was determined. It was found that the site removal and the site activation processes could be brought about by many different donors. Variations were noted among the donor types. This finding shows that a variety of isolated sites with different abilities to coordinate and orient the α-olefin are found on the crystal surface of the titanium chloride cocatalyst.

INTRODUCTION

In previous papers it was shown that both components of the heterogeneous Ziegler catalyst determine the number and type of sites which are formed.[1-4] By using the polymerization of propylene as an analytical tool, the effect of aliphatic amines on the catalyst was studied. In the process of interacting with the titanium chloride component, these amines changed not only the polymerization rate but also the isotacticity and the molecular weight of the polypropylene which was formed. This afforded an opportunity to study the nature of the active sites of the catalyst.

Two important processes were brought about by the amine: (*1*) site removal and (*2*) site activation. Site removal was said to occur because the amine molecules coordinated with the active sites and thereby inactivated them. This results in decreased conversion of monomer. It was speculated that site activation (increased conversion) was caused by amine molecules which were absorbed in the vicinity of the uncoordinated active sites.

The present work shows that the site removal and the site activation processes can be obtained with donors other than the Lewis base type. The degree to which each of these processes occurs depends markedly on the particular donor and its concentration. The present findings have been described briefly in an earlier paper.[5]

Studies of this type are valuable because by understanding what happens when different donors are present in the Ziegler catalyst, we can begin to formulate a picture of the orienting process which occurs when the α-olefin coordinates with the same sites. These concepts can be utilized within the framework of both mono- and bimetallic mechanisms.[6]

RESULTS

Polymerizations: Metal Alkyl-Based Catalysts

The assessment of donor effect on the titanium chloride component of the catalyst was simplified by using $ZnEt_2$ since the donors do not coordinate with this weak acceptor. The more complicated situation which occurs when the donor complexes with the metal alkyl is shown in Figure 1. Here the strong acceptors are $AlEt_3$ and $AlEt_2Cl$. Over a wide Et_3N concentration range, the amine had a small effect when $AlEt_3$ was used. But with $AlEt_2Cl$ pronounced increases in catalyst activity and polymer molecular weight as reflected by intrinsic viscosity (I.V.) were observed. The different effects were probably due to the adsorption of $AlEt_3 \cdot Et_3N$ and $AlEt_2Cl \cdot Et_3N$ complexes on the crystal surface.[7] These results are more difficult to interpret than those where the donor coordinates only with the titanium chloride component.

Another advantage of $ZnEt_2$ is that it reacts with γ-$Al_xTi_yCl_z$-160 to

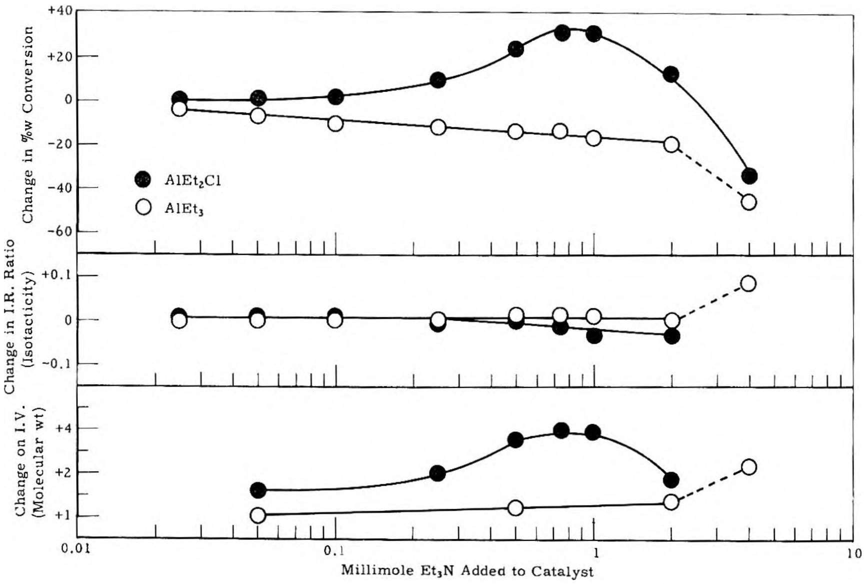

Fig. 1. Effect of Et_3N on aluminum alkyl-based catalysts. The system consisted of 100 ml. heptane, 2.1 mmole $AlEt_3$ or $AlEt_2Cl$, and 0.5 mmole γ-$Al_xTi_yCl_z$-160. Propylene (20–22 g.) was polymerized for 2 hr. ($AlEt_2Cl$) or 1 hr. ($AlEt_3$) at 22°C. In amine-free polymerizations, polypropylene was obtained in 36 wt.-% conversion (I.R. = 0.92, I.V. = 10 dl./g.) when $AlEt_2Cl$ was used, and in 52 wt.-% conversion (I.R. = 0.65, I.V. = 4.4 dl./g.) with $AlEt_3$.

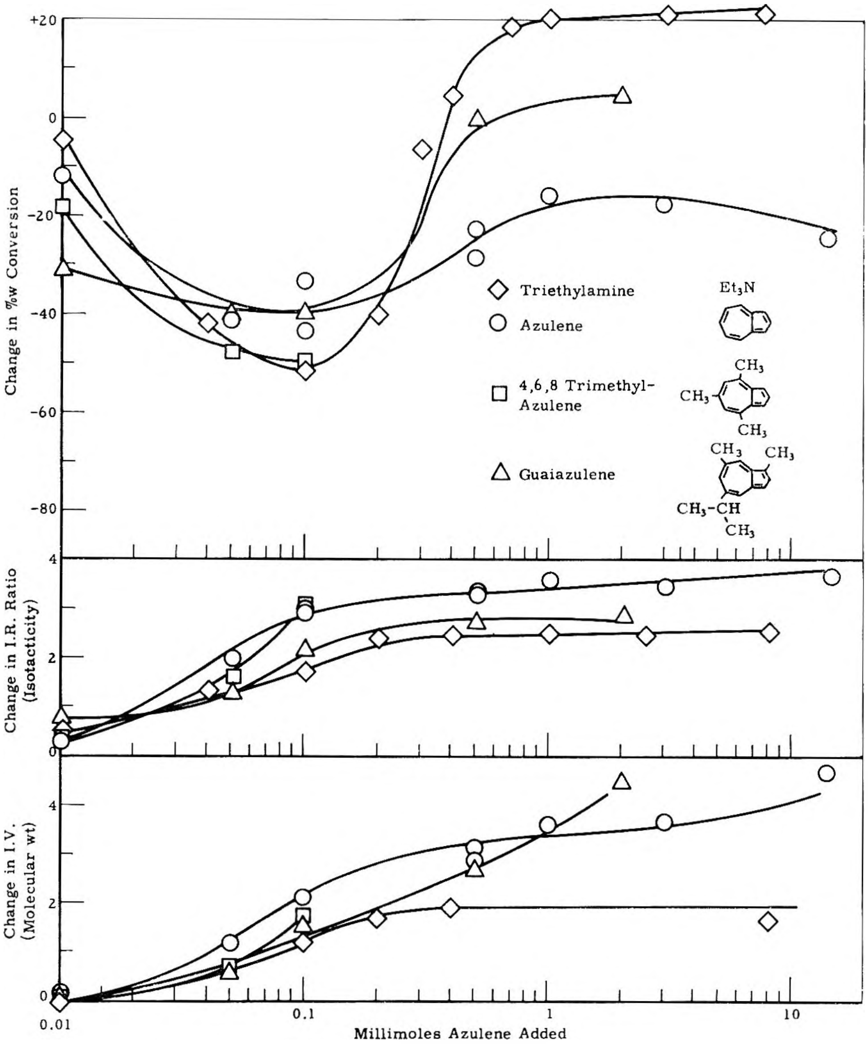

Fig. 2. Azulenes and Et$_3$N compared as donors. The system consisted of 100 ml. heptane, 4.2 mmole ZnEt$_2$, and 1.0 mole γ-Al$_x$Ti$_y$Cl$_z$-160 mixed in this order. Propylene (20–22 g.) was polymerized for 20 hr. at 50°C. The donor-free catalyst gave about 75 ± 7 wt.-% conversion to polymer having an $A_{10.02\mu}/A_{10.28\mu}$ ratio (I.R. ratio) of 0.63 ± 0.03 and an I.V. of 1.3 ± 0.3 dl./g.

form only a moderately specific catalyst. Presumably, sites having a wide range of stereoregulating abilities are made available for coordination.

Infrared techniques were used to measure relative isotactic contents of these polymers. The $A_{10.02}$ $\mu/A_{10.28}$ μ band ratio (I.R. ratio) was taken as an index of isotacticity.[8] The detailed procedure has been described previously.[2]

The donor effect of a variety of compounds is described in Figures 2–4 and Tables I–VI. The different donors are compared for both site removal

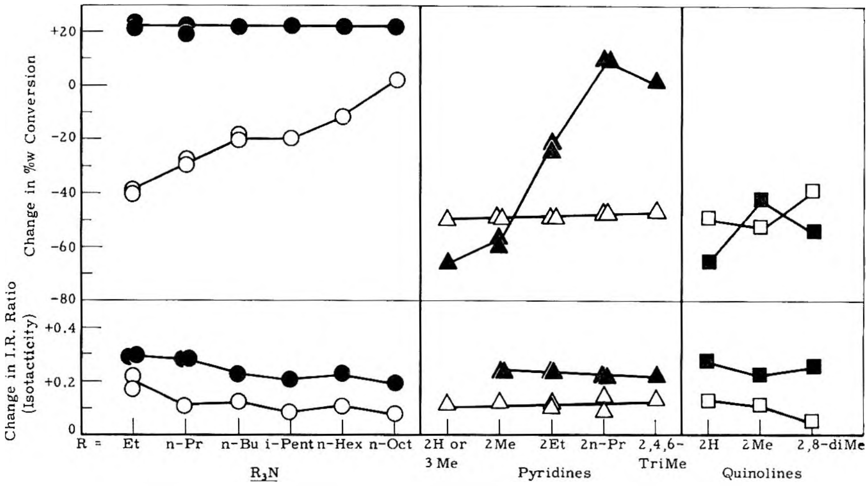

Fig. 3. Aliphatic and aromatic heterocyclic amines as donors (see Figure 2 for catalyst description): (○, △, □) 0.07 mmole amine in 100 ml. heptane; (●, ▲, ■) 3.3 mmole amine in 100 ml. heptane. Greater increases in polymer activity than shown in the curves for aliphatic amines have been obtained at lower catalyst concentrations.

and site activation in Table VIII. In the following, the results are discussed according to donor structure.

Azulenes. Both site removal and site activation occurred when azulene was incorporated into the catalyst at different concentrations (Fig. 2). At low concentrations (0.001*M*) azulene was a very good site remover. At higher donor concentrations (0.03*M*), azulene became a moderate site ac-

TABLE I
Aromatic Compounds as Donors

Donor	Amt. donor, mmole	Change effected by donor[a,b] Conversion, wt.-%	I.R. $(A_{10.02\mu}/A_{10.28\mu})$	I.V., dl./g.
Acenaphthylene[c]	14	−16	+0.11	—
Fluoranthene	"	−6	+0.05	—
Mesitylene[d]	10	−6	+0.06	—
Durene	"	−11	+0.04	—
Pentamethylbenzene	"	−21	+0.10	+0.5
Hexamethylbenzene	"	−15	+0.10	+0.5

[a] See Figure 2 for description of catalyst and system.

[b] Donor-free catalyst gave 75 wt.-%conversion, I.R. ratio = 0.63, and an I.V. = 1.3 dl./g. To get the absolute values in Tables I–V and Figures 1–4, the appropriate addition or subtraction must be made, e.g., with hexamethylbenzene as donor a 60 wt.-% conversion of polypropylene having an I.R. band ratio of 0.73 and an I.V. of 1.8 dl./g. was obtained.

[c] Naphthalene, anthracene, pyrene, acenaphthene, and fluorene were inert; higher polynuclears were only sparsely soluble.

[d] Benzene, toluene, hexaethylbenzene, and chlorobenzene were inert.

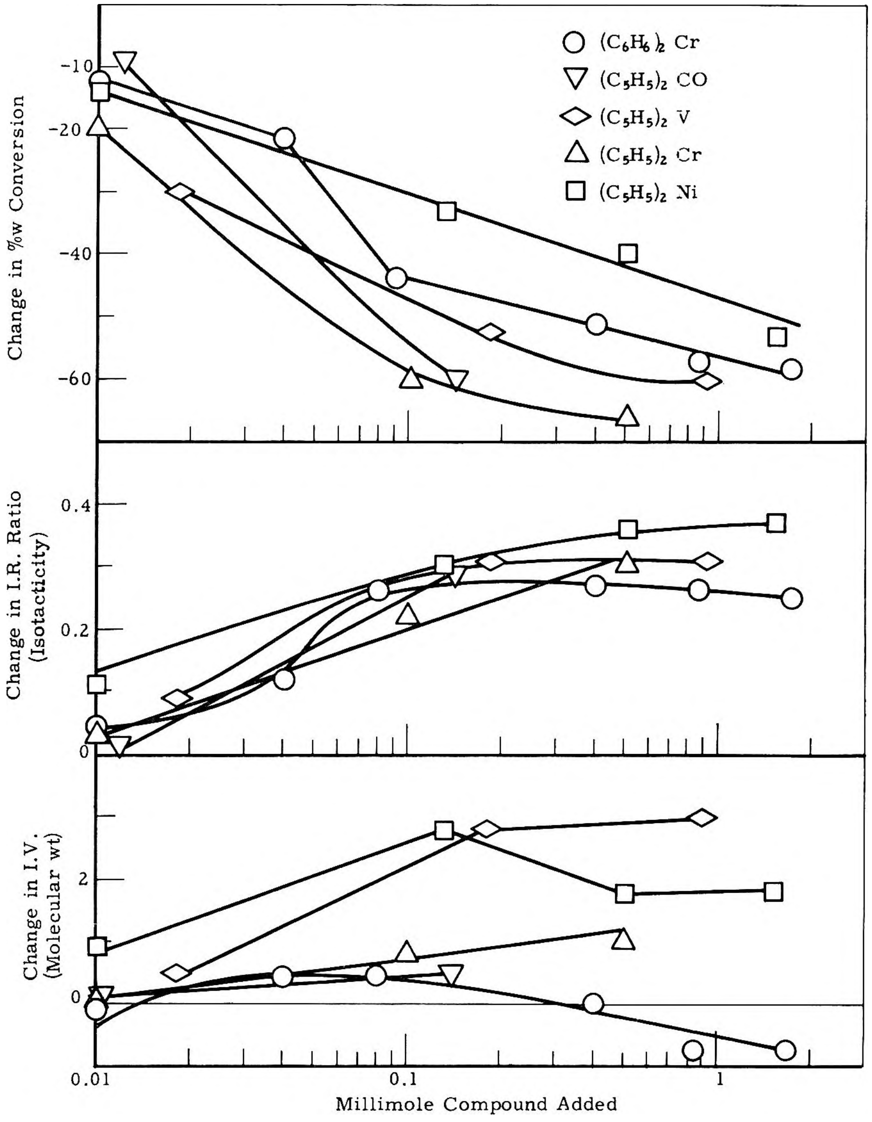

Fig. 4. $(C_6H_6)_2Cr$ and cyclopentadienyl compounds of transition metals as donors. (see Figure 2 for description of system). Toluene used as solvent in place of heptane.

tivator. Except for a lower activating ability, the polymer conversion-donor curves (Fig. 2) were similar for azulene and Et_3N. The substituted azulenes, guaiazulene and 4,6,8-trimethylazulene, were also found very effective for both site removal and site activation.

Substituted Pyridine and Quinoline Compounds. The bulky aromatic heterocyclic amines were more effective in site removal relative to Et_3N than might have been predicted (Fig. 3). Even though there is a variation in the bulkiness of these heterocyclic amines, they caused site inactivation

TABLE II
Olefinic Compounds as Donors

Donor	Amt. donor, mmole	Change effected by donor[a,b]		
		Conversion, wt.-%	I.R. ($A_{10.02\mu}/A_{10.28\mu}$)	I.V., dl./g.
1,3-Butadiene	10	−35	+0.15	+0.3
1,4-Pentadiene	10	−67	+0.09	−0.3
1,5-Hexadiene	10	−5	−0.03	+0.1
1,6-Heptadiene	10	−4	−0.01	0
Isoprene	10	−46	+0.09	+0.2
1,3-Cyclooctadiene	2–10	−3	0	−0.1
1,5-Cyclooctadiene	2–10	−17–−30	+0.04–0.22	−0.3–−1.3
Bicyclo[2,2,1]hepta-2,5-diene	0.2–10	−25–−65	+0.06–0.16	—
Cyclooctene (*trans*)	2–10	−9–−45	+0.10–0.19	—
Cyclooctatetraene	0.1–10	−15–−37	+0.26–0.30	+1.6–4.0
Bicyclo[2,2,1]hepta-2-ene	2–10	−6–−23	0	0
2-Butyne	10	−67	0.35	+1.1
Tetramethylethylene	10	−13	+0.07	—
Dimethylfulvene	0.1	−13	−0.14	—
Diphenylfulvene	0.1	−15	+0.13	—

[a] See Figure 2 for catalyst description.

[b] Donor-free catalyst gave 75 wt.-% conversion, I.R. ratio = 0.63, and an I.V. = 1.3 dl./g.

TABLE III[a]
Weak Donors

Donor	Amt. donor, mmole	Change effected by donor		
		Conversion, wt.-%	I.R. ($A_{10.02\mu}/A_{10.28\mu}$)	I.V., dl./g.
PF_3[b]	0.6–4.9	−42 to −54	+0.30	+1.3–2.1
Tetracyanoethylene[c,d]	0.02–0.53	−8 to −75	+0.06–0.33	+0.5–2.2
SO_2[d,e]	0.01–0.10	−3 to −11	+0.02–0.26	−0.1 to 2.1

[a] See Table I for description of catalyst and system.

[b] PF_3 was condensed into the heptane solvent before the catalyst components were added. Attempts to add it in solution form by syringe techniques always gave lower values for changes in conversion.

[c] These polymerizations were carried out in chlorobenzene; 0.2 mmole CH_3CN killed the polymerization if added under similar conditions.

[d] SO_2 and tetracyanoethylene react vigorously with $ZnEt_2$, in molar ratios of about 3:1 and 2.4:1, respectively.

[e] Dispensed in a heptane solution.

about equally well when present in 0.001M concentrations. The amines included: pyridine, 2-methyl-, 2-ethyl-, and 2-propylpyridine, 2,4,6-trimethylpyridine, quinoline, 2-methylquinoline, and 2,8-dimethylquinoline. Despite extensive site removal by these amines, the attendant increases in isotacticities (higher $A_{10.02}\ \mu/A_{10.28}\ \mu$ band ratios) at 0.001M concentrations were not large. It appeared that under these conditions the heterocyclic

TABLE IV
Polymerizations: Metal Alkyl-Free Catalysts[a]

Donor	Amt. donor, mmole	Isotactic polymer formed		
		Conversion, wt.-%	I.R., ($A_{10.02\mu}/A_{10.28\mu}$)	I.V., dl./g.
None[b,d]	—	80	Cationic oil	
$(C_6H_5)_2PH$[b,d]	6.6	1	0.91	—
Et_3N[b,c,e]	3.3	8	0.89	12
$(C_6H_5)_3P$[c,e]	6.2	4	0.92	13
$(C_6H_5)_3N$[c,e]	3.3	Only cationic oil formed		
Azulene[b,c]	2.5	Trace solid but no oil was formed		

[a] System consisted of 100 ml. heptane or toluene, 20 mmole $Al_xTi_yCl_z$-AA and donor. About 20 g. propylene was reacted for five or seven days at 50°C.

[b] Heptane solvent.

[c] Toluene solvent.

[d] Polymerized for five days.

[e] Polymerized for seven days.

[f] The activity of the $Al_xTi_yCl_z$-AA composition decreased with use. A freshly opened sample was about 5 times more active under similar conditions. All of the experiments above were done concurrently.

TABLE V
Miscellaneous Polymerizations

Donor	Amt. donor, mmoles	Change effected by donor[a,b]	
		Conversion, wt.-%	I.R. ($A_{10.02\mu}/A_{10.28\mu}$)
$(C_6H_5)_2PH$	3.3	+4	+0.31
$(C_6H_5)_3P$	"	+52	+0.08
Et_3N	"	+62	+0.31

[a] Polymerization system consisted of 100 ml. heptane, 1.4 mmole $ZnEt_2$, and 0.5 mmole γ-$Al_xTi_yCl_z$-160. Propylene (20–22 g.) was polymerized for 16 hr., at 50°C.

[b] Donor-free catalyst gave 35 wt.-% conversion, I.R. ratio = 0.68, and an I.V. = 2.1 dl./g.

amines showed only a slightly higher preference for less specific sites than for the more specific sites.

Site activation at higher amine concentrations (Fig. 3) was observed with 2-ethylpyridine, 2-propylpyridine, and 2,4,6-trimethylpyridine but not with the other amines. These three amines, which were more activating in the order given, resembled azulene more than Et_3N in their ability to function as site activators.

Aromatic Compounds. Substituted benzenes and polynuclear compounds were examined (Table I). It was necessary to add substituted benzenes in much higher concentrations ($0.1M$) to produce even a small degree of site removal. Of the compounds examined, only the tri-, tetra-, penta-, and hexamethylbenzenes were effective. Only small increases in polymer isotacticities were produced, i.e., the increase in the I.R. band ratio was 0.10, at best, compared to an increase of 0.30 obtained with azulene or Et_3N. Hexaethylbenzene, toluene, benzene, and chlorobenzene had no effect. In fact, the polymerizations could be carried out in toluene or chlorobenzene without any noticeable departure from the catalyst activity or specificity experienced in heptane solvent.

Of the polynuclear compounds examined, only acenaphthylene acted as a site remover. Furthermore, it was necessary to add the latter in very high concentrations to cause even a small decrease in catalyst activity. Concentrations up to nine times those used with amines or azulene were necessary to get approximately one third as great a loss in catalyst activity. The presence of acenaphthylene increased the polymer isotacticity about as much as hexamethylbenzene.

TABLE VI

Correlation of pK_a and Heats of Mixing Values of Donors with Their Ability to Act as Site Removers and Site Activators

Donor	pK_a	ΔH, gcal./mmole[a]	Ability of donor for	
			Site removal[b]	Site activation[c]
Et_3N	10.65	2.96	Strong	Strong
n-$Octyl_3N$	—	3.06	Weak	Strong
n-$Butyl_3P$	8.43	—	Strong	Strong
$(C_6H_5)_3P$	2.73	2.18	Moderate	Strong
$(C_6H_5)_2PH$	0.03	—	Strong	Moderate
2,8-Dimethylquinoline	—	1.68	Strong	None
Azulene	−1.7	0.59	Strong	Moderate
$(C_6H_5)_3N$	Very small	0	Inert	Inert
Cyclooctatetraene	—	0	Moderate	Inert
1,4-Pentadiene	—	0	Moderate	Inert
Hexamethylbenzene	—	0	Weak	Inert
Naphthalene	—	0	Inert	Inert
Anthracene	—	0	Inert	Inert
Pyrene	—	—	Weak	Inert

[a] Heat liberated when 1.0 mmole γ-$Al_xTi_yCl_z$-160 was titrated with donor until no further interactions between the components took place.

[b] The site removal character was determined with the $ZnEt_2$–γ-$Al_xTi_yCl_z$-160 catalyst.

[c] The site-activating character was determined with both the $ZnEt_2$–γ-$Al_xTi_yCl_z$-160 catalyst and the $Al_xTi_yCl_z$-AA catalyst.

In contrast, fluoranthene had a marginal effect; naphthalene, acenaphthene, anthracene, pyrene, and fluorene were inert.

None of the aromatic compounds brought about site activation in the concentration range examined. It has been reported[9] that such compounds as benzene and naphthalene increase catalyst activity for the $AlEt_3$–$TiCl_3$ catalyst. We did not observe this phenomena with the $ZnEt_2$-γ-$Al_xTi_yCl_z$-160 catalyst.

Olefinic Compounds. A number of unsaturated compounds were examined (Table II). These included monoolefins, conjugated and nonconjugated diolefins, and fulvenes.

None of these compounds caused site activation in the concentration range examined. However, many were effective site removers in the 0.001–0.1*M* concentration range. As found before, whenever sites were removed, higher isotactic polymer was formed; also, the increase in isotacticity per site loss was dependent upon the particular olefin. Some of these compounds may have been copolymerized in small amounts. Infrared measurements, however, failed to show this. Their effect on the polymer molecular weight suggests strongly that some of these, e.g., 1,4-pentadiene, functioned in part as chain terminators.

Olefins which were observed to be effective site removers include: 1,4-pentadiene, bicyclo[2,2,1]hepta-2,5-diene, *trans*-cyclooctene, dimethyl- and diphenylfulvenes, cyclooctatetraene, 1,3-butadiene, isoprene, and 1,5-cyclooctadiene.

Cyclopentadienyl and Benzene Compounds of Transition Metals. In addition to $(C_6H_6)_2Cr$ the cyclopentadienyl compounds of V, Co, Cr, and Ni were examined (Fig. 4). None of these effected site activation. However, all functioned to remove sites and increase polymer isotacticities. As with many of the other donors, the relative improvement in isotacticity per site loss varied with the specific compounds used.

Weak Donors. Three such compounds were examined: PF_3, tetracyanoethylene (TCNE) and SO_2 (Table III). With all three compounds, site removal but not site activation was noted. Polymer isotacticity was simultaneously increased. The obtained data are ambiguous because SO_2 and TCNE react with $ZnEt_2$. PF_3 may also react with $ZnEt_2$ but this was not examined.

Polymerizations: Methyl Alkyl-Free Catalysts

Previous work[4] which reported the polymerization of propylene with metal alkyl-free catalysts has now been extended (Table IV). These catalysts consisted of a titanium chloride and certain amine or phosphine donors. In the present work, several other donors have been examined with the object of comparing the effect of the donors in the two types of catalyst, i.e., the Ziegler catalyst consisting of $ZnEt_2$ and a titanium chloride and the metal alkyl-free catalyst consisting of only a titanium chloride and the donor.

In the present work, the latter catalyst[4] consisted of an aluminum reduced titanium chloride ($Al_xTi_yCl_zAA$) and the following donors: $(C_6H_5)_3P$, $(C_6H_5)_2PH$, $(C_6H_5)_3N$, Et_3N, and azulene. Of these only Et_3N, $(C_6H_5)_3P$, and $(C_6H_5)_2PH$ removed cationic sites effectively while simultaneously activating specific sites. Et_3N was about twice as effective as $(C_6H_5)_3P$ as a site activator; in contrast, $(C_6H_5)_2PH$ was only a weak site activator. Azulene also acted as a cationic site remover but did not bring about site activation at the concentration level examined. $(C_6H_5)_3N$ was inert; in its presence only a cationic oil was formed.

For comparison some of these compounds were also tested in the $ZnEt_2$-γ-$Al_xTi_yCl_z$-160 catalyst (Table V).

Heats of Interaction of Catalyst Components

The heat evolved on mixing the titanium chloride and a donor compound should tell us something about the interaction between the two components. Thermometric titration techniques offered a simple way to obtain such heats of interaction. The sensitivity of the apparatus used was sufficient to detect and measure as little as 1 kcal./mole of titrant. This sensitivity is adequate to measure the heat evolved in the interaction of $AlEt_3$ for example, with bases weaker than anisole. The heat of interaction of the latter components is 2.3 kcal./mole $AlEt_3$. The heats of interaction between various donors and the γ-$Al_xTi_yCl_z$-160 cocatalyst component are summarized in Table VII. We might also note that there was no heat evolved when all but a few of these donors were titrated with $ZnEt_2$ under similar conditions. Aliphatic amines do not coordinate $ZnEt_2$.[10]

These thermometric titration results are discussed in detail in a later section.

TABLE VII
Heats of Interaction of Catalyst Components

Compound[a,b,c]	Heat liberated, gcal./mmole catalyst	
	γ-$Al_xTi_yCl_z$-160[d]	$ZnEt_2$
Azulene	0.59	0
TCNE	0.29	ca. 95
Trioctylamine	3.06	—
2,8-Dimethylquinoline	1.68	0
Triphenylphosphine	2.18	0
Triethylamine	2.96	0
Pyridine	2.96	0
$AlEt_2Cl$	0.88	—
$ZnEt_2$	2.40	—
$(C_6H_5)_2Ni$	—	0
Acenaphthylene	—	0
Dimethylfulvene	—	0

[a] The compounds 1,4-pentadiene, naphthalene, cyclooctatetraene, hexamethylbenzene, and triphenylamine did not react with γ-$Al_xTi_yCl_z$-160 to give measurable heats.

[b] Excess of these components added to $ZnEt_2$ or γ-$Al_xTi_yCl_z$-160.

[c] The thermometric titrations were performed at ambient temperatures; the polymerizations in which the effect of these compounds was studied were performed at 50°C.

[d] Because the reaction of the donor takes place on a surface stoichiometry is not possible.

DISCUSSION

The relative abilities of different compounds to act as site removers or site activators are summarized in Table VIII. The comparison should be

TABLE VIII

Site Removal and Site Activation by Donors at Low and High Donor Concentration, Respectively[a]

Strong	Moderate-weak	Ineffective
Relative Abilities of Donors to Remote Sites		
Azulene	n-Octyl$_3$N	Benzene
Et$_3$N	Acenaphthylene	Naphthalene
n-Pr$_3$N	Mesitylene	Acenaphthene
Pyridine and quinoline compounds	Durene	Anthracene
$(C_6H_6)_2Cr$	Pentamethylbenzene	Pyrene
Cyclopentadienyl compounds of V, Cr, Ni, and Co	Hexamethylbenzene Tetramethylethylene	Fluorene Hexaethylbenzene
Butadiene		1,3-Cyclooctadiene
Isoprene		$(C_6H_5)_3N$
1,4-Pentadiene		
2-Butyne		
Cyclooctatetraene		
Dimethylfulvene		
Diphenylfulvene		
2,5-Norbornadiene		
trans-Cyclooctene		
PF$_3$		
1,5-Cyclooctadiene		
n-Bu$_3$N		
Relative Abilities of Donors to Activate Sites		
R$_3$N (R = Et to n-octyl)	Azulene	
	Diphenylphosphine	Benzene
$(C_6H_5)_3P$	2-Ethylpyridine	Naphthalene
n-Bu$_3$P	2-Propylpyridine	Acenaphthene
	2,4,6-Trimethylpyridine	Anthracene Pyrene
		Fluorene
		Hexaethylbenzene
		1,3-Cyclooctadiene
		$(C_6H_5)_3N$

[a] Under the conditions examined in this investigation. At much higher donor concentrations different results might be obtained.

considered qualitative only; because of differing solubilities as well as different donating abilities, all compounds could not be examined over identical concentration ranges.

Site Removal by Donors

A variety of donors have been shown to remove sites. This shows clearly that the coordination chemistry of the active site is similar to the coordination chemistry of other transition metal compounds. Therefore, the effects of amines, noted in our earlier work, cannot be attributed to some unique interaction of amines and titanium chloride.

A basic difference in the acceptor character of the active Ziegler catalyst sites and that of soluble transition metal compounds is worth emphasizing. All of the acceptor molecules are identical in solutions of transition metal compounds. However, the acceptor sites of the Ziegler catalyst are located on the cocatalyst crystal surface. These sites are postulated to be pentacoordinated, partially exposed titanium atoms. Exposed titaniums, being buried in the second layer of the crystal and having different numbers of adjacent chlorine atoms, are expected to present different steric fronts to the donor molecule. In other words, all sites are not identical and will show different acceptor abilities. In our view, polymerization most probably occurs at edge sites. The work of Hargitay and his co-workers suggests that polymerization occurs at crystal edges.[11]

The preferential removal (coordination) of the less specific sites by amine molecules which has been found supports the view that the sites are different; furthermore, all donors which acted as site removers in the present work also showed some preference to coordinate with the less specific sites. Thus with all donors, site removal was always accompanied by an increase in the isotacticity of the polymer product. However, the specific increase in polymer isotacticity per site loss varied according to the donor structure.

Site removal was accompanied by an increase in polymer molecular weight for most donors, e.g., amines, azulenes, aromatic heterocyclic amines, the cyclopentadienyl compounds of Cr, V, Ni, and Co, cyclooctatetraene, and hexamethylbenzene. This suggests that higher molecular weight polymer is formed at the more specific sites, i.e., the least exposed sites which are most difficult to remove by the donor molecules. Put another way, low molecular weight polymer is formed at the most exposed sites at which less isotactic polymer is formed. Whenever the donor molecules show preference toward the different sites, the most exposed, less specific sites at which low molecular weight polymer is formed are removed first.

A few donors which caused site removal (and higher isotactic polymer) did not produce polymer having higher molecular weight. We attribute this atypical result to the ability of these donors to act as chain terminators. This was observed with $(C_6H_6)_2Cr$, isoprene, and 1,4-pentadiene.

Site removal probably occurs through a variety of bonding modes. All of the donors which were found to be effective site removers in this work have been reported to coordinate with other transition metal compounds, especially those in groups five to eight.[12] The literature on the coordination chemistry of trivalent titanium is scant.

If the proposed model[3] is accepted, then donors take the position left vacant by chlorine removal. Thus one octahedral position is available for coordination. The following possible bonding types are suggested:

(*1*) Nonbonding electrons of a Lewis base are donated to the vacant *d* orbitals, e.g., Et_3N, n-Bu_3P, etc.

(*2*) The π-bond electrons of the double bond are donated to the vacant *d* orbitals, e.g., *trans*-cyclooctenes, the α-olefins, norbornene.

(*3*) The delocalized π electrons rather than the localized π electrons of a double bond are donated to the vacant *d* orbital, e.g., azulene, 1,8-di-

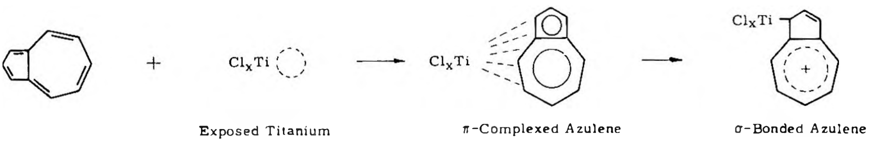

Fig. 5. Possible bonding of azulene and the exposed pentacoordinate titanium.

methylquinoline, polysubstituted benzenes, isoprene, cyclooctatetraene, 2,4,6-trimethylpyridine, etc.

(*4*) Strong bonds are formed because back donation of electrons from a filled *d* orbital of Ti to the antibonding orbital or an empty orbital of the donor occurs. This may be the case with PF_3 ($d\pi$–$d\pi$).

(*5*) Electron transfer to the exposed titanium occurs, e.g. $(C_6H_6)_2Cr$ and cyclopentadienyl compounds of V, Cr, Ni, and Co.

In support of (*5*) is the reported observation that organic halides such as benzyl chloride are reduced by $(C_6H_6)_2Cr$ and $(C_5H_5)_2V$ to yield $(C_6H_6)_2CrCl$ and $(C_5H_5)_2VCl$, respectively.[13,14] The reduction of the trivalent exposed titanium could yield an ion pair, e.g., Cl_xTi^- $(C_6H_6)_2Cr^+$, in which the bivalent titanium site is inactive for polymerization.

In addition to bonding type (*3*), azulene can coordinate by first forming a π complex with the exposed titanium which then collapses into a σ-bonded adduct, (Fig. 5). The strong stabilizing effect of the cycloheptatrienyl cation favors a σ-bonded azulene. This type of bonding has been suggested for the proton adduct of azulene.[15]

Site Activation by Donors

Site removal occurs when donors coordinate with the exposed titaniums. Site activation, on the other hand, is attributed to the surface adsorption of the same donor molecules in the vicinity of the exposed titanium sites. The donor molecules are presumed to be chemisorbed extensively to the surface chlorine atoms. The results obtained with amines are in agreement with this view. For example, the adsorption of the amine on the chlorine surface was not sensitive to amine bulk such as was found when amines coordinated with the exposed titaniums. Such bulky amines as *n*-octyl$_3$N were as effective as less bulky amines, e.g., Et_3N, as site activators. For site removal *n*-octyl$_3$N was almost ineffective, while Et_3N was very effective under similar conditions.

Supplementary evidence comes from thermometric titration measurements in the present work. We have made the following observations.

No heat was evolved when those donors which caused site removal but not site activation e.g., cyclooctatetraene, were added to γ-$Al_xTi_yCl_z$-160.

Those donors which acted as site activators e.g. *n*-octyl$_3$N, Et_3N, $(C_6H_5)_3P$, and azulene, always produced heat when mixed with γ-$Al_xTi_yCl_z$-160.

Those donors which produced the highest heats of interaction were the most efficient activators, e.g., $Et_3N \gg$ azulene (Table VI).

It is clear that the heat of interaction is not associated with site removal. Because the number of sites is very small;[16] the number of site–donor interactions must be small. A more plausible explanation is that the activator donors are adsorbed on the crystal surface in relatively high concentration.

The results obtained with pyridine and 2,8-dimethylquinoline appear anomalous. These donors produced a heat of mixing with γ-$Al_xTi_yCl_z$-160 but were not activators. We attributed this apparent anomaly to the ability of these donors to remove readily all sites rather indiscriminately at all concentrations. To be effective, activator donors must not coordinate readily with the less exposed (but more specific) sites.

The present evidence suggests that potentially active or sluggishly active sites are being activated by these donors. The observation has been made that donors which were site activators when propylene was polymerized with the Ziegler-type catalyst, $ZnEt_2$ + γ-$Al_xTi_yCl_z$-160, were also activators for propylene polymerization when a metal alkyl-free $Al_xTi_yCl_zAA$ composition was used as catalyst. Donors which activated both catalyst types include Et_3N, $(C_6H_5)_3P$, $(C_6H_5)_2PH$, and n-Bu_3P. However, the $Al_xTi_yCl_zAA$ catalyst alone (no donor present) yielded only a cationic oil and no isotactic polymer. This suggested strongly that the donor activated either potentially active sites or those sites which were only very sluggishly active under the conditions investigated.

An attempt was made to correlate site activation ability with some fundamental property of the donor. We realized that such a correlation should take into account the differing bulk of the donors. In general, we found that donors having pK_a values over a wide range were effective, e.g. pk_a's between -2 and 10 were examined. Also, donors having at least a moderate bulkiness were the best site activators. Further attempts to correlate site activation with other donor parameters failed, e.g., with ionization potentials, I_p or the (calculated) energy of the highest filled molecular orbital, m_m.*

Since many factors such as rehybridization and resonance stabilization energies are probably important, a unique correlation with the varied structured compounds perhaps is too much to expect.

It was suggested by Coppinger that the donors which are activators form charge transfer complexes with the crystal surface.[18] We tried to obtain some evidence in support of this suggestion by correlating I_p and m_m values against the activating ability of the donor. Although no correlation was found, the charge transfer complex idea cannot be ruled out. The charge transfer mechanism appears plausible on the basis of observations of Stevenson and Coppinger.[19] They showed that CCl_4 forms contact charge transfer complexes with Et_3N. It would not be unreasonable to expect that the more highly electropositive titanium (compared to carbon in CCl_4) should be more effective in imparting acceptor properties to the surface chlorines of the titanium chloride.

---

* For definitions of I_p and m_m see Streitwieser.[17]

The observation that only those donors which activate the $ZnEt_2$–γ-$Al_xTi_yCl_z$-160 system also activate the metal alkyl-free ($Al_xTi_yCl_zAA$) catalyst for propylene polymerization most certainly has a bearing on the mechanism by which this catalyst operates. Since in the $Al_xTi_yCl_zAA$–donor catalyst, no metal alkyl was present, it would seem necessary to invoke a monometallic mechanism to explain the very similar site activating effect of the donor in both systems. However, because several alternate explanations are possible, further evidence is necessary to make a convincing case. Because hydrogen was shown to function as a transfer agent in the latter catalyst also,[4] a metal–carbon bond and a metal–hydrogen bond are presumed to be active for monomer insertion in the metal alkyl-free catalyst.

Although we have no direct experimental evidence we feel that the donor alters the ligand field of the titanium atom. Such alteration would account readily for changes in the activity of both mono- and bimetallic sites.

EXPERIMENTAL PROCEDURE AND MATERIALS

Polymerization Technique

The polymerizations were carried out in 8-oz. bottles. These were charged with the solvent, catalyst, and propylene and subsequently rotated in polymerization baths at times and temperatures indicated in the appropriate tables or figures. The detailed procedure has been already discussed in a previous paper.[2]

Evaluation of Polymers

The per cent conversion was taken as the weight fraction of propylene converted to polymer times 100. The infrared band ratio $A_{10.02\mu}/A_{10.28\mu}$ (I.R. ratio) was taken as an index of isotacticity. The measurement was made on compression-molded films (about 0.002 in. thick) which were annealed at 100°C. for 16 hr. and conditioned at 25°C. for 20 hr. An average of four sample specimens were determined for each polymer. Intrinsic viscosities (I.V.) were determined in decalin at 150°C.

Catalyst Components

$ZnEt_2$ was purchased from Orgmet (Hampstead, New Hampshire). A 25% heptane solution was heated over molten sodium (5% based on $ZnEt_2$) for 10 min. under refluxing conditions. The alkyl and solvent were then flash distilled, and transferred into bottles in 100 ml. lots. These were stored below 0°C. when not in use.

Two titanium chloride compositions were used in this work. The γ-$Al_xTi_yCl_z$-160 composition was prepared by mixing 1 mole $AlEt_3$ with 3 mole $TiCl_4$ in heptane at room temperature and then heating the product to 160°C. for about $^1/_2$ hr. (when it turns purple).[2] This form is usually referred to in the literature as γ-$TiCl_3$. The composition $Al_xTi_yCl_zAA$ was purchased from Stauffer Chemical Company. It is reported to be prepared by heating $TiCl_4$ with aluminum at high temperature and to be subsequently activated. The latter is sold under the trade name Titanium Trichloride AA. Both compositions contain aluminum chloride as a solid solution in the titanium chloride. To emphasize this point, we adopted the nomenclature used in this and previous papers, e.g., $Al_xTi_yCl_z$, where $x \cong 1$, $y \cong 3$, and $z \cong 12$.

Solvents

Heptane (Phillips) was purified by passing it through silica gel and then distilling it from CaH_2. It was stored over CaH_2 under an atmosphere of nitrogen. Toluene was purified by shaking it with aqueous sulfuric acid (concentrated) several times, washing several times with distilled water, shaking this with aqueous Na_2CO_3 to neutralize the acid, drying with $MgSO_4$, CaH_2, and $LiAlH_4$ (in that order), and finally distilling from $LiAlH_4$. It was also stored over CaH_2 under a nitrogen atmosphere. Chlorobenzene was distilled from CaH_2 and stored similarly.

Heats of Interaction

The thermometric titrations were performed by Dr. W. L. Everson and Mrs. E. M. Ramirez of the Analytical Department. The experimental technique and instrumentation employed is similar to that reported by Everson.[20] A brief description will be given here only.

Donor + $\gamma Al_xTi_yCl_z$-160. To 3.4 mmole γ-$Al_xTi_yCl_z$-160 contained in 50 ml. heptane was added the titrant under a nitrogen atmosphere. Titrant was also added simultaneously to a reference vessel containing heptane only. The temperature difference between the two vessels was recorded as a function of volume of titrant added. In this way the total gram-calories evolved as a result of titrant addition was determined for each donor.

Donor + $ZnEt_2$. The titration was performed similarly, except that $ZnEt_2$ was substituted for the γ-$Al_xTi_yCl_z$-160 component.

Donor Compounds

The following compounds were used as received: azulene (K and K Laboratories or Aldrich Chemical Co.); 4,6,8-trimethylazulene, guaiazulene, fluorene, and fluoranthene (Aldrich Chemical Co.); naphthalene, anthracene, pyrene, durene, pentamethylbenzene, hexamethylbenzene, and hexaethylbenzene (Eastman Chemical Co., white label); dimethylfulvene (K and K Laboratories); PF_3 (Ozark Mahoning Co.); and SO_2 (Matheson). The PF_3 and SO_2 samples were shown by mass spectroscopy to be better than 99% pure.

The following compounds were distilled from a 10:1 mixture of CaH_2 and $LiAlH_4$: 1,4-pentadiene and 1,5-hexadiene (Columbia Organic Chemicals); isoprene (Phillips); 1,3-cyclooctadiene and 1,5-cyclooctadiene

(Cities Service Co.); bicyclo[2,2,1]hepta-2,5-diene, cyclooctatetraene, norbornene, and 2-butyne (K and K Laboratories); 2-methylquinoline (Eastman Chemical Co. or Aldrich Chemical Co.); 2,8-dimethylquinoline (Aldrich Chemical Co.); and quinoline, benzene, and mesitylene (Eastman Chemical Co.).

The following compounds were distilled from KOH: pyridine, 2-ethylpyridine, and 2,4,6-trimethylpyridine (Eastman Chemical Co.); and 2-methylpyridine and 2-propylpyridine (K and K Laboratories).

The following compounds were purified by sublimation: acenaphthene (Eastman Chemical Co.), acenaphthylene (Aldrich Chemical Co.), tetracyanoethylene (L. Light and Co.), and $(C_6H_6)_2Cr$ (Orgmet).

Several compounds were gratefully received from colleagues in this laboratory. These include the cyclopentadienyl compounds of Cr, V, Ni, and Co from Dr. L. H. Slaugh; $(C_6H_5)_2PH$ from Dr. G. A. Kurhajec, tetramethylethylene from Dr. W. Spooncer, 1,3-butadiene from Dr. H. De La Mare, *trans*-cyclooctene and bicyclo[2,2,1]heptene-2 from Dr. M. A. Muhs.

SUMMARY

The acceptor behavior of the active sites of a heterogeneous Ziegler catalyst resembles markedly the behavior that has been observed by others for a host of transition metal compounds. These sites functioned as acceptors for a variety of donor molecules, including Lewis bases, azulenes, mono- and polyolefins, cyclopentadienyl compounds of transition metals, and aromatics. An important difference is that the various sites, which we have postulated to be pentacoordinated exposed titaniums, present different steric fronts to the donor molecules.

On the basis of this and past investigations, we concluded that a variety of sites having different abilities to coordinate and orient the olefin are found on the crystal component of the catalyst. The particular distribution of the various sites was found to depend on the specific catalyst components chosen as well as on reaction conditions. The paths by which site removal and site activation are effected by the different donors are clarified by the present work.

The constructive criticism and encouragement of Dr. E. A. Youngman throughout this work are gratefully acknowledged, as are many discussions with my colleagues, especially Dr. H. V. Holler, Dr. H. E. De La Mare, and Dr. R. H. Bauer. Also acknowledged is the diligent technical assistance of Messrs. D. W. Penhale and P. R. Thompson.

References

1. Boor, J., Jr., *J. Polymer Sci.*, **62,** 5345 (1962).
2. Boor, J., Jr., *J. Polymer Sci.*, **C1,** 237 (1963).
3. Boor, J., Jr., *J. Polymer Sci.*, **C1,** 257 (1963).
4. Boor, J., Jr., and E. A. Youngman, *J. Polymer Sci.*, **B2,** 265 (1964).
5. Boor, J., Jr., *J. Polymer Sci.*, **B3,** 7 (1965).
6. Bawn, C. E. H., and A. Ledwith, *Quart. Rev.*, **16,** 361 (1962).
7. Vesely, K., J. Ambroz, R. Vilim, and O. Hamrik, *J. Polymer Sci.*, **55,** 25 (1961).

8. Quynn, R. G., J. L. Riley, D. A. Young, and D. H. Noether, *J. Appl. Polymer Sci.*, **2,** 166 (1959).

9. Minsker, K. S., and R. P. Chernovskaya, *Proc. Acad. Sci. U.S.S.R.* (*Engl. Transl.*), **147,** 1029 (1962).

10. Coates, G. E., *Organo-Metallic Compounds*, Methuen, London, 1956.

11. Hargitay, B., L. Rodriguez, and M. Miotta, *J. Polymer Sci.*, **35,** 559 (1959).

12. Guy, R. G., and B. L. Shaw, *Advan. Inorg. Chem. Radiochem.*, **4,** 78 (1962).

13. de Liefde Meijer, H. J., M. J. Janssen, and G. J. M. van der Kerk, *Rec. Trav. Chim.*, **80,** 831 (1961).

14. Razuvaev, G. A., and G. A. Domrachev, *Tetrahedron*, **19,** 341 (1963).

15. Heilbronner, E., in *Non-Benzenoid Aromatic Compounds*, D. Ginsburg, Ed., Interscience, New York, 1959, p. 253.

16. Natta, G., *J. Polymer Sci.*, **34,** 21 (1959).

17. Streitwieser, A., Jr., *Molecular Orbital Theory for Organic Chemists*, Wiley, New York, 1961, pp. 37, 173.

18. Coppinger, G. M., private communication.

19. Stevenson, D. P., and G. M. Coppinger, *J. Am. Chem. Soc.*, **84,** 149 (1962).

20. Everson, W. L., *Anal. Chem.*, **36,** 854 (1965).

Résumé

Des donneurs d'électrons de structures différentes ont été incorporés dans le catalyseur de Ziegler, $ZnEt_2$ + γ-$Al_xTi_yCl_z$-160, afin d'éclaircir les processus d'échange de site et d'activation des sites. Les donneurs, qui ont été étudiés dans le présent travail, comprennent les azulénes, des composés insaturés, des aromatiques, les pyridines substituées et les quinolines, ainsi que des composés cyclopentadiényliques du V, Cr, Ni, et Co, $(C_6H_6)_2Cr$, et PF_3. On détermine leur effet sur la polymérisation du propyléne. On trouve que le processus d'échange de site et d'activation de site peut être dû à la participation de beaucoup de donneurs différents. On a noté des différences parmi les types de donneurs. Les observations montrent qu'on trouve sur la surface d'un cristal de cocatalyseur de chlorure de titane, un grand nombre de sites isolés susceptibles de coordiner et d'orienter les α-oléfines à des degrés divers.

Zusammenfassung

Um ein Verständnis der Entaktivierungs- und Aktivierungsprozesse der katalytischen Stellen von Zieglerkatalysatoren zu erreichen, wurden Elektronendonoren verschiedener Struktur in den Zieglerkatalysator $ZnEt_2$ + γ -$Al_xTi_yCl_z$-160 eingebaut. Vie untersuchten Donoren waren: Azulene, ungesättigte Verbindungen, Aromaten, substituierte Pyridine und Chinoline, Cyklopentadienylverbindungen von V, Cr, Ni, und Co, $(C_6H_6)_2Cr$ und PF_3. Ihr Einfluss auf die Polymerisation von Propylen wird bestimmt. Es wird gefunden, dass Entaktivierungs- und Aktivierungsprozesse durch eine Vielzahl venschiedener Donoren bewirkt werden können. Variation unter den Donortypen wurde festgestellt. Die Befunde zeigen, dass sich auf der Kristalloberfläche des Titanchloridcokatalysators isolierte Stellen mit unterschiedlicher Koordinierungs- und Orientierungsfähigkeit für das α-Olefins befinden.

Received July 15, 1964

JOURNAL OF POLYMER SCIENCE: PART A VOL. 3, PP. 1013-1030 (1965)

Polyquinoxalines. II.*

J. K. STILLE, J. R. WILLIAMSON, and F. E. ARNOLD, *Department of Chemistry, State University of Iowa, Iowa City, Iowa*

Synopsis

Five new high molecular weight polyquinoxalines have been prepared by the reactions of combinations of two tetramines, 3,3′-diaminobenzidine (II) and 3,3′,4,4′-tetraminodiphenyl ether (IV), with the three bisglyoxals, 1,4-phenylenediglyoxal (I), 1,3-phenylenediglyoxal (VI), and 4,4′-oxydiphenylenediglyoxal (IX). Solution and melt polymerization techniques afford intermediate molecular weight polymers which can be converted to high molecular weight samples ($\eta_{inh} > 1.0$) by heating at 375°C. under reduced pressure. All the polyquinoxalines have excellent thermal stability both in nitrogen and in air. Of these polymers, poly[2,2′-(4,4′-oxydiphenylene)-6,6′-oxydiquinoxaline] (XI) has the highest solubility in hexamethylphosphoramide (HMP), and films can be cast from intermediate molecular weight (η_{inh} = 0.3–0.7) polymer solutions in HMP. Tough, insoluble films can be obtained by heating the cast films in nitrogen or under reduced pressure to 350–400°C.

INTRODUCTION

In earlier publications[1,2] we had demonstrated that high molecular weight polymers containing the quinoxaline moiety and *p*-phenylene units as the only portions of the polymer chain could be obtained from typical quinoxaline-forming reactions in nearly quantitative conversions. The polyquinoxaline formed from the reaction of 1,4-phenylene-diglyoxal (I) with 3,3′-diaminobenzidine (II), was assigned the structure poly[2,2′-(1,4 phenylene)-6,6′-diquinoxaline] (III) by comparison with model quinoxaline-forming reactions. This polymer, which has a completely conjugated

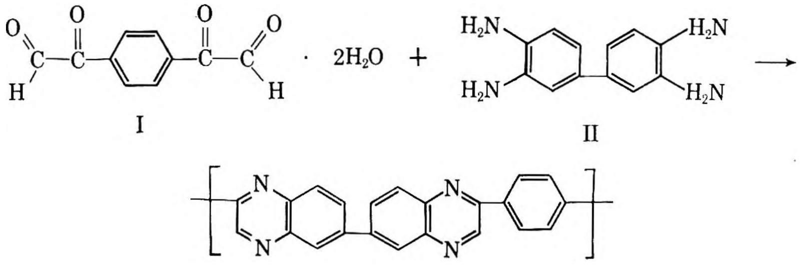

III

---

* Paper presented in part at the Symposium on Ring-Containing Polymers, Polymer Division, 147th Meeting, American Chemical Society, Philadelphia, April 1964, and the Gordon Conference on Polymers, New London, N. H., July 6, 1964.

aromatic polymer chain, showed excellent thermal stability both in air and in nitrogen atmospheres. The temperature at which initial weight loss in either atmosphere occurred was nearly 500°C. or above.

This polyquinoxaline unfortunately has several undesirable physical properties. The polymer is insoluble in common organic solvents and is very difficultly soluble in such solvents as hexamethylphosphoramide. Films of the polymer, even the high molecular weight films, are somewhat brittle.

It was evident that a more flexible polymer chain would be necessary if the problems of solubility and brittleness were to be eliminated in order to obtain a polymer amenable to fabrication. The incorporation of flexible units into the chain would require concomitant stability of the unit if thermal stability in the polymer were to be maintained.

RESULTS AND DISCUSSION

Two structural modifications in the monomers were made initially in order to give some degree of flexibility to the polymer chain. The tetramine, 3,3′-diaminooxydianiline (IV), was employed in polymerizations with 1,4-phenylenediglyoxal (I). Polymerizations of the carbonyl mono-

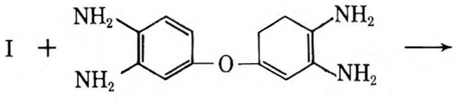

IV

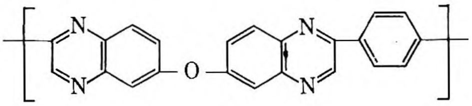

V

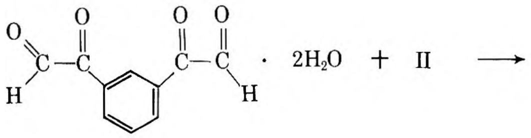

VI

VI

+

IV

↓

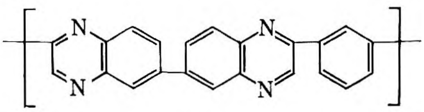

VII

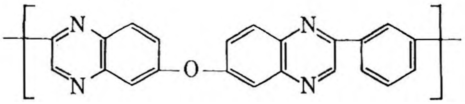

VIII

TABLE I

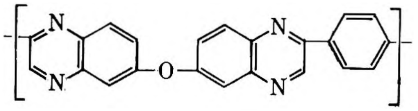

Polymerization conditions			% soluble in			
Solvent	T_1, °C.	T_2, °C.	H_2SO_4	HMP (30°C.)	HMP (200°C.)	[η]
None	225	—	100	60	—	0.20
	225	375		15	25	0.85
HMP (200°C.)	200	—	100	60	—	0.31
	200	375		40	55	1.30

mer, 1,3-phenylenediglyoxal (VI), were carried out with the two available amines, II and IV.

Polymerizations to intermediate molecular weight materials were carried out under nitrogen either in dioxane or hexamethylphosphoramide (HMP) solutions or by melt polymerization in the absence of solvent. Subsequent heating under reduced pressure to 375°C. produced high molecular weight, partially insoluble materials (Tables I and II). The techniques employed for these polymerizations have been previously described.[2]

Note that the structures written for these polymers, and two other polymers, X and XI (discussed later in this paper), are such that the aromatic phenylene units, which are incorporated from the respective bisglyoxals, are attached to the 2- and 2′-positions on the quinoxaline nuclei, rather than on the 3- and 3′-positions, or a mixture of these positions. This has been written by analogy to the polyquinoxaline III, for which there is reasonable evidence[2] for only the 2,2′-isomeric units. The lack of crystallinity in the polyquinoxaline (III) reported by others[3] was offered as evidence for a random structure in this polymer. The suggestion was made that 3- and 3′-phenylene attachment was also taking place. By contrast, our samples of poly-[2,2′-(1,4-phenylene)-6,6′-diquinoxaline] (III) showed reasonable crystallinity (Fig. 1). In fact, one *d* spacing for the polymer, 17 ± 1.0 A. (not shown in Fig. 1) corresponds to a rough calculation of the recurring unit distance, 17 A., for this rodlike polymer.

These polymers (V–VIII) showed greater solubility than poly[2,2′-(1,4-phenylene)-6,6′-diquinoxaline] (III). In particular, poly[2,2′-(1,3-phenylene)-6,6′-oxydiquinoxaline] (VIII), which would be expected to exhibit the highest chain flexibility, demonstrated the greatest solubility. During the polymerization in HMP at 200°C., this polymer did not fall out of solution.

The thermal stabilities of polymers V–VIII (Figs. 2–4) were particularly good, and showed equal or perhaps better stability than III. Complete conjugation in the polymer chain evidently does nothing to improve the stability of the polymer. A polymer chain such as III, which has the opportunity to enjoy complete resonance stabilization, undoubtedly does not, since it would require that every aromatic member of the chain lie in the

TABLE II

	Polymerization conditions			% soluble in			
Polymer	Solvent	T_1, °C.	T_2, °C.	H_2SO_4	HMP (30°C.)	HMP (200°C.)	[η]
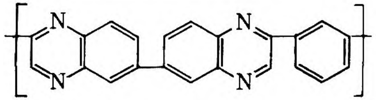	None	225	—	100	75	—	0.25
		225	375		40	75	0.51
	HMP (200°C.)	200	—	100	60	—	0.26, 0.75[a]
		200	375		25	35	2.42
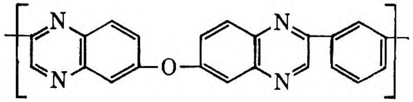	HMP (200°C.)	200	—	100	100	—	0.15
		200	375		45	80	1.76

[a] Viscosities from two different runs.

same plane. This would probably require more energy than that gained from such resonance stabilization. Aromatic ethers show high thermal stability at the ether–oxygen linkage, so it is not surprising that these polymers held up.

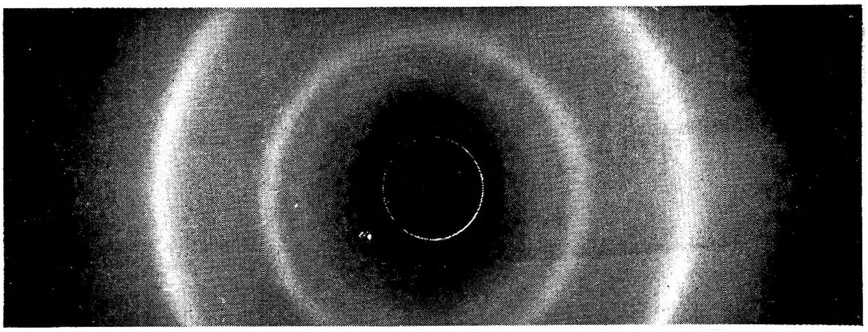

Fig. 1. X-ray powder pattern of poly[2,2′-(1,4-phenylene-6,6′-diquinoxaline].

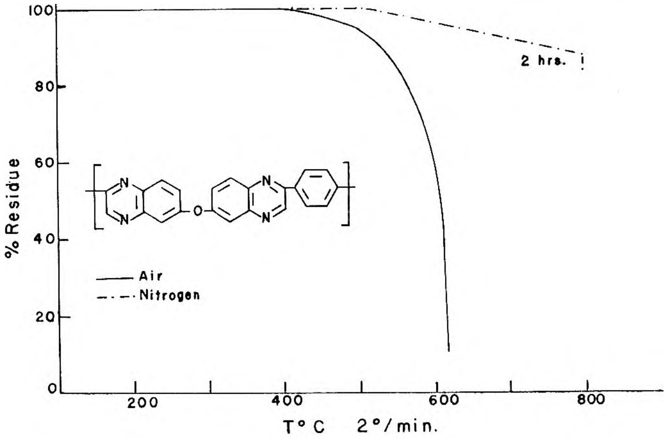

Figure 2.

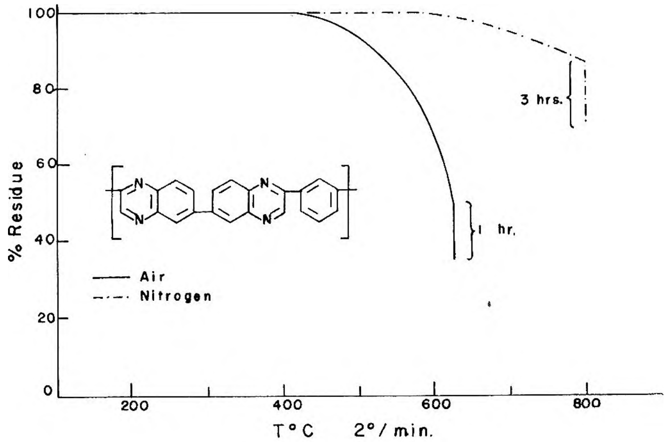

Figure 3.

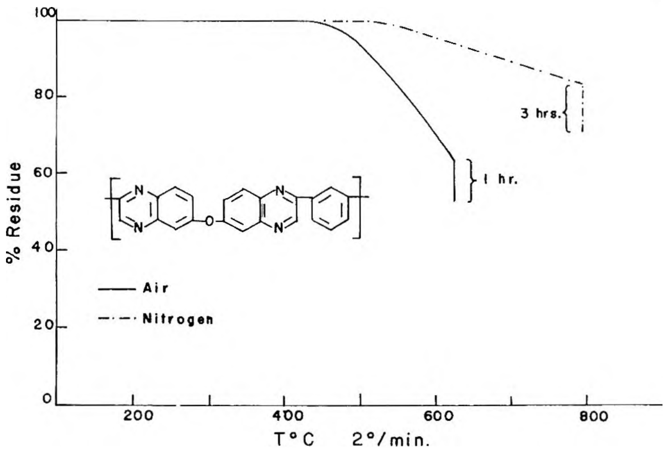

Figure 4.

The difficulty in preparing the best polymers in this series lies in the glyoxal monomer preparation. Unlike the *para* isomer, 1,3-phenylenediglyoxal dihydrate cannot be obtained as a pure crystalline compound. Purification of the oily dihydrate requires a tedious, difficult procedure, and even then the purity of the monomer is in doubt. To overcome this, the carbonyl monomer, 4,4′-diglyoxalyldiphenyl ether (IX) was prepared.

Two quinoxaline polymers, X and XI, were obtained from the polymerization of this diglyoxal with each of the two tetramines

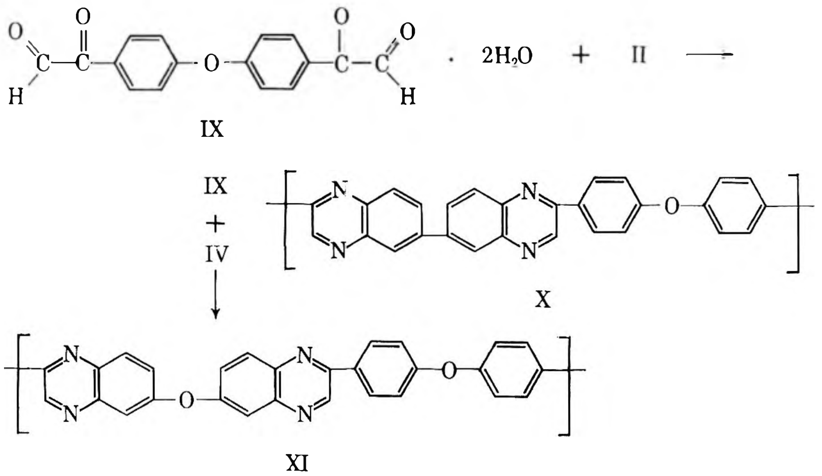

(Tables III and IV). High molecular weight polyquinoxalines could be obtained from any of the methods of polymerization. A study of the course of the reaction for the formation of XI in HMP was made (Table V). The polymerization displayed the characteristics of a condensation polymerization in that a slow build-up of molecular weight was in evidence. In this polymerization, the polymer concentration was about 5 g./100 ml. of HMP, yet no polymer precipitated from solution during the entire course of the reaction. Polymer with an inherent viscosity of 0.23 in HMP has a number-average molecular weight of 5700, or a D.P. of 13 (Fig. 5).

Films of poly[2,2′-(4,4′-oxydiphenylene)-6,6′-oxydiquinoxaline] (XI), which had not been subjected to heating at 375°C. under reduced pressure, could be cast from HMP. The enhanced solubility of this intermediate molecular weight polymer (η_{inh} = 0.34 and 0.72) in HMP allowed concen-

TABLE III

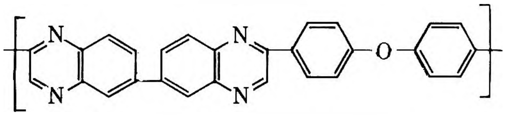

Polymerization conditions			% soluble in			
Solvent	T_1, °C.	T_2, °C.	H_2SO_4	HMP (50°C.)	HMP (200°C.)	[η]
None	250	—	85	75	—	0.23
	250	375	45	35	50	0.92
Dioxane (100°C.)	250	—	100	70	—	0.31
	250	375	100	30	45	0.93
HMP (200°C.)	200	—		100	—	0.23
			60	0		0.90[a]
	200	375	80	25	30	3.2

[a] During this polymerization a small amount of polymer which precipitated had this viscosity in dilute HMP.

TABLE IV

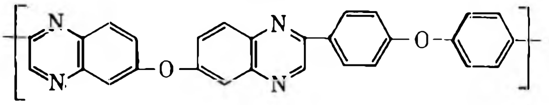

Polymerization conditions			% soluble in			
Solvent	T_1, °C.	T_2, °C.	H_2SO_4	HMP (50°C.)	HMP (200°C.)	[η]
None	250	—	100	85	—	0.56
	250	375	40	40		0.79
Dioxane (100°C.)	250	—	100	80	—	0.24
	250	375	100	45	55	0.40
HMP (200°C.)	250	—	100	100	—	0.20
				0		0.93[a]
	250	375	35	30	35	1.24

[a] During this polymerization, a small amount of polymer which precipitated had this viscosity in dilute HMP.

TABLE V

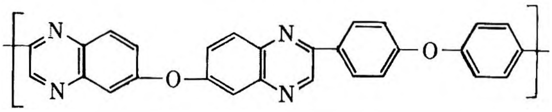

Polymerization conditions		
Time, hr.[a]	T, °C.	η_{inh}
0.5	30	0.099
1.0	100	0.26
2.5	100	0.32
1.0	160	0.34
12.0	160	0.72

[a] Times listed show successive treatment at the respective temperatures. Thus, the reaction was allowed to proceed at 30°C. for 30 min., then the temperature was raised to 100°C. for 3.5 hr., then to 160°C. for 13 hr.

trated polymer solutions. Clear yellow to red films prepared in this manner were somewhat brittle, but could be converted, by heating to 350–400°C. under nitrogen or under reduced pressure, to tough, flexible, translucent films. The resulting polymer was not appreciably soluble in HMP, and the soluble portion of it is a much higher molecular weight polymer (Table IV). The insoluble portion may be crosslinked, but there are no convenient crosslinking sites along the polymer chain so that the insoluble polymer could be linear high molecular weight material. This observation is quite general with all the quinoxaline polymers prepared. The infrared spectra (Fig. 6) of films of this polymer, when first cast, and after heating, show the same characteristic maxima.

Low molecular weight samples of polyquinoxaline XI can be melted under a nitrogen atmosphere. In the melt, further polymerization evidently takes place, since the polymer resolidifies, even on continued heating to 400°C., and the resulting polymer has only taken solubility in HMP. Neither of the

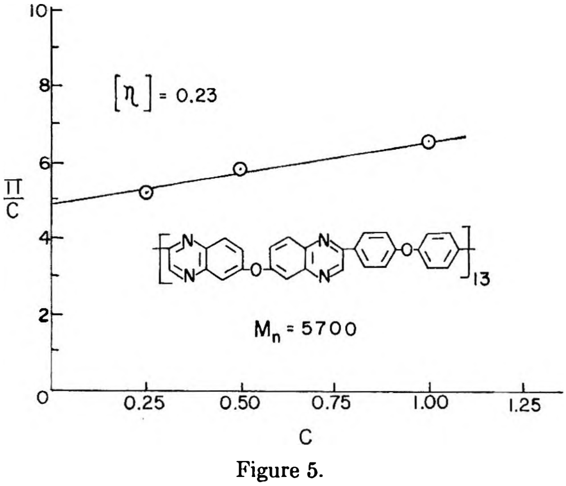

Figure 5.

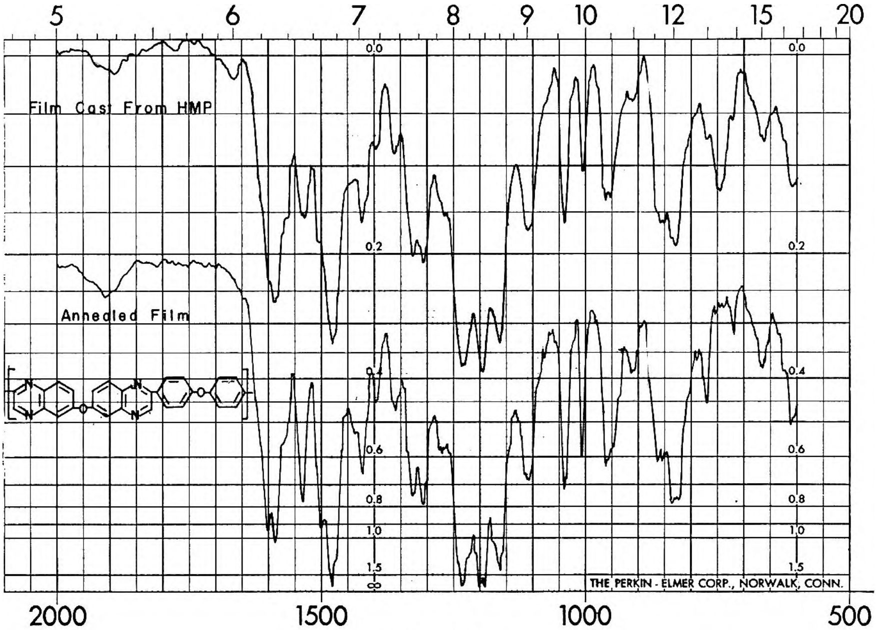

Figure 6.

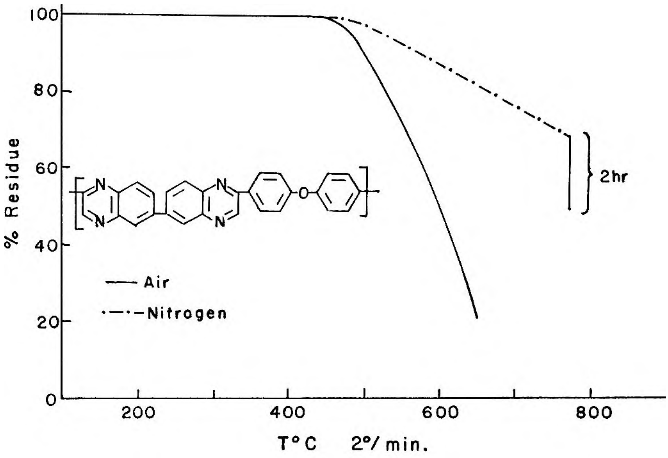

Figure 7.

samples of XI before or after heating to 400°C. showed any crystallinity. By contrast, even low molecular weight samples of poly[2,2′-(1,4-phenylene)-6,6′-diquinoxaline] did not melt.[1,2]

The thermal gravimetric analyses (TGA) of polymers X and XI were very good (Figs. 7 and 8). No sacrifice in thermal stability was made for the sake of solubility. A slightly enhanced stability in XI over that of III, in fact, can be observed. Earlier, we had attributed this to the ability of the more flexible chain to dissipate thermal energy more readily by chain motion, but the difference is sufficiently marginal that no conclusions can be drawn.

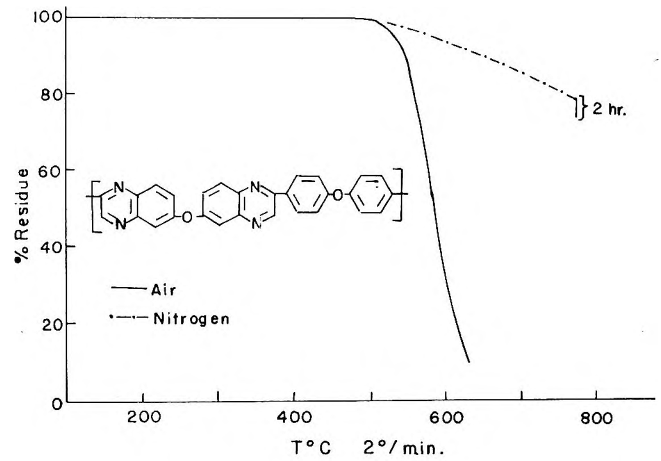

Figure 8.

EXPERIMENTAL

Monomers

3,3′,4,4′-Tetraminodiphenyl ether (IV)

This monomer was prepared from commercial *p*-oxydianiline (Dow Chemical Co.) by following a known procedure.[4] To a solution of 140 g. (0.7 mole) of *p*-oxydianiline in 500 ml. of glacial acetic acid was added dropwise 173 g. (1.6 mole) of acetic anhydride at such a rate to maintain a temperature of 50–60°C. The temperature was maintained at 90–100°C. for an additional hour and the solution was allowed to stand overnight. The precipitate which formed was collected and dried to give 147 g. of 4,4′-diacetyl aminodiphenyl ether, m.p. 227–228.5°C. (lit.:[4] 228–229°C.). The filtrate from the above reaction was poured into 1 kg. of ice, and this precipitate was dried to give an additional 12 g. of acetylated product. The combined yield was 80.5%.

To 700 ml. of acetic anhydride was added 95 ml. of colorless 70% nitric acid at such a rate to maintain a temperature of less than 25°C.[5] After this addition was complete, 75 g. (0.265 mole) of 4,4′-diacetamidodiphenyl ether was added in small portions while the temperature was maintained at 15–20°C. After this addition was complete, the yellow mixture was stirred for 30 min. at room temperature, then poured slowly into 3 liters of a 1:1 mixture of ice and water. The yellow precipitate was dried to give a quantitative yield of 3,3′-dinitro-4,4′-diacetamidodiphenyl ether, m.p. 210–213°C. (lit.:[4] 211–214°C.).

To a slurry of 199 g. (0.53 mole) of 3,3′-dinitro-4,4′-diacetamidodiphenyl ether in 1.3 liters of methanol was added dropwise with vigorous stirring a solution of 84 g. of potassium hydroxide in 300 ml. of methanol. An additional 56 g. of potassium hydroxide was added and the mixture was stirred for 3 hr. The mixture was poured into 2.5 liters of water, and the orange precipitate was collected by filtration. The filtrate was poured into 3 liters of water to give additional material. The combined precipitates, m.p. 174–177°C. (lit.:[4] 175.5–178.5°C.) were recrystallized from 95% ethanol to give 130 g. (84.5%) of 3,3′-dinitro-4,4′-diaminodiphenyl ether, m.p. 178.5–179.5°C.

To a vigorously stirred solution of 240 g. of stannous chloride dihydrate in 500 ml. of concentrated hydrochloric acid was added 46.4 g. (0.16 mole) of 3,3′-dinitro-4,4′-diaminodiphenyl ether in small portions at such a rate as to maintain a temperature of 60–70°C. for an additional 3 hr. The mixture was cooled to −10°C., and the pink precipitate was collected by filtration. The tetrahydrochloride salt was dissolved in 300 ml. of hot water, and 300 ml. of concentrated hydrochloric acid was added. Cooling produced white needles of the tetrahydrochloride salt which were collected and pressed dry under a stream of nitrogen. The tetrahydrochloride was dissolved in water, and this solution was added dropwise to a vigorously stirred solution of 60 g. of sodium hydroxide in 300 ml. of deoxygenated water which was cooled in an ice bath. The grey-white precipitate (45 g.) was collected by filtration under nitrogen, washed with cold water, and dried to yield 31 g. (84%) of product. The tetramine was stored in the dark under a nitrogen atmosphere in the presence of solid potassium hydroxide until ready for use. Just prior to use, this compound was obtained in a highly pure form by sublimation at 159–175°C./0.1 mm. Recrystallization from deoxygenated methanol always produced pink or light brown crystals in 60–70% yields. The sublimation technique always produced pure white tetramine in 80% yields, and any contamination from tin salts was eliminated.

1,3-Diacetylbenzene

The monomer precursor, 1,3-diacetylbenzene, was prepared especially for use in this work by a procedure which was a modification of the one reported[6] for the preparation of methyl ketones from the reaction of acid chlorides with diethyl malonate and subsequent hydrolysis and decarboxylation. From 121 g. (0.6 mole) of commercial isophthaloyl dichloride which had been recrystallized from hexane was produced 30 g. (34%) of 1,3-diacetylbenzene, b.p. 112–120°C./0.3 mm., m.p. 31–32°C. (lit.:[6] b.p. 150–155°C./15 mm., m.p. 31–32°C.). The NMR spectrum of this compound showed a ratio of methyl to phenyl hydrogens of 3:2. The infrared spectrum showed strong absorption at 1700 cm.$^{-1}$ (C═O stretching).

1,3-Phenylenediglyoxal (VI)

To a dioxane solution of 33.3 g. (0.3 mole) of selenium dioxide, 8 ml. of water, and 4 drops of concentrated hydrochloric acid at 70°C. was added 24.3 g. (0.15 mole) of 1,3-diacetylbenzene in 50 ml. of dioxane. The reaction mixture was stirred at the reflux temperature for 8 hr., during which time selenium metal precipitated and was finally removed by filtration. Complete evaporation of dioxane under reduced pressure left a tacky residue which was extracted with two 500-ml. portions of boiling water to give an orange solution. This solution became yellow after cooling and filtering but turned orange upon standing in the cold. To this aqueous solution of

1,3-diacetylbenzene dihydrate was added 2–4 ml. of a 25% lead acetate solution, and the precipitated lead selenite was removed by filtration. Into this almost colorless filtrate was bubbled hydrogen sulfide gas until lead sulfide no longer precipitated. After filtration the clear, light yellow aqueous solution was taken to dryness under reduced pressure at room temperature to yield a yellow, tacky oil.

ANAL. Calcd. for $C_{10}H_{10}O_6$ (dihydrate): C, 53.10%; H, 4.57%. Found: C, 53.01%; H, 4.88%.

The infrared spectrum of this compound showed strong OH and carbonyl absorption at 3400 and 1700 cm.$^{-1}$, respectively. This compound was reported[7] to be a yellow oil which polymerized upon heating.

A solid yellow powder was produced from this oil by stirring and extracting it with both ether and acetone. In both cases the elemental analysis found agrees with that calculated for the monohydrate. This solid material was used in three polymerizations.

4,4′-Diacetyldiphenyl Ether

The monomer precursor, 4,4′-diacetyldiphenyl ether, was prepared in a 63% yield by the Friedel-Crafts acetylation of diphenyl ether in a tetrachloroethylene solvent.[8] The pure product, recrystallized from 95% ethanol, had m.p. 98–99°C. (lit.:[8] b.p. 213–217°C./0.3–0.5 mm.).

4,4′-Oxydiphenylenediglyoxal Dihydrate (IX)

This monomer was prepared by the same selenium dioxide procedure as reported for 1,4-phenylenediglyoxal dihydrate.[1,2] Upon cooling the filtrate from the reaction mixture, crude product precipitated. Recrystallization from a dioxane–water (2:1) mixture afforded a pure white solid (45.7%), m.p. 118–120°C. (dec.) (lit.:[3] 122°C.).

ANAL. Calcd. for $C_{16}H_{14}O_7$ (dihydrate): C, 60.38%; H, 4.43%. Found: C, 60.61%; H, 4.37%.

Model Compounds

In addition to the five model compounds previously prepared in the polyquinoxaline study,[2] three new quinoxaline model compounds have been prepared by the same general quinoxaline forming condensation reaction. The ultraviolet spectra for these compounds appear in Table VI.

1,3-Di(2-quinoxalyl)benzene (XII)

To a 15-ml. dioxane solution containing 1.0 g. (0.009 mole) of *o*-phenylenediamine was added 10 ml. of a dioxane solution containing 0.5 g. (0.002 mole) of the oil, 1,3-phenylenediglyoxal dihydrate. After removal of one-half of the solvent under diminished pressure, the solid precipitate which formed was collected and recrystallized from 95% ethanol to afford 0.0305 g. (14%) of light yellow crystals, m.p. 202–203°C. (lit.:[7] m.p. 202–203°C.).

TABLE VI

	λ, mμ	$\epsilon \times 10^{-3}$
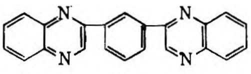 XII	280 353	40.90 39.20
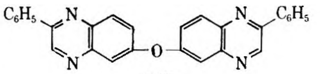 XIII	260 348	70.00 27.30
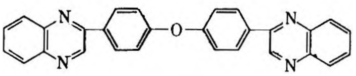 XIV	258 347	15.75 20.40

2,2′-Diphenyl-6,6′-oxydiquinoxaline (*XIII*)

To 1.0 g. (0.004 mole) of 3,3′,4,4′-tetraminodiphenyl ether in 10 ml. of oxygen-free water was added 1.3 g. (0.0087 mole) of phenylglyoxal hydrate at 70°C. This mixture was heated for 1 hr. The precipitate was collected, recrystallized from 95% ethanol, and dried to afford 0.877 g. (47%) of light yellow product, m.p. 223–224.5°C.

ANAL. Calcd. for $C_{28}H_{18}O$: C, 79.90%; H, 4.23%; N, 13.15%. Found: C, 78.89%; H, 4.24%; N, 13.10%.

4,4′-Di(2-quinoxalyl)diphenyl Ether (*XIV*)

To 10 ml. of an aqueous solution of 0.1296 g. (0.0012 mole) of *o*-phenylenediamine was added 0.1901 g. (0.006 mole) of 4,4′-oxydiphenylenediglyoxal dihydrate (IX) in 10 ml. of water at 75°C. A precipitate immediately formed and the mixture was heated for 1 hr., after which time the light yellow solid was collected, washed with hot water and 95% ethanol, and dried to afford 0.1246 g. (55%) of nearly white product, m.p. 165–166°C. (lit.:[3] m.p. 172°C.).

ANAL. Calcd. for $C_{28}H_{18}N_4O$: C, 78.90%; H, 4.23%; N, 13.15%. Found: C, 78.40%; H, 4.23%; N, 13.05%.

Polymers

Polymerizations to form polyquinoxalines were carried out both in hexamethylphosphoramide and dioxane solvents and in the melt state in the absence of solvent. All polymerizations were carried out in a nitrogen atmosphere or under reduced pressure. After the first-stage initial polymer-forming reaction, either in solvent or in the melt state, the moderate molecular weight polymers were all subjected to a second-stage heating cycle (375°C.) to produce higher molecular weight polymers. In each case the polymers were heated under reduced pressure in a rotating flask to which had been added two 8 mm. diameter steel ball bearings to facilitate mixing. In all cases the polymers were obtained in nearly quantitative yields. In the first-stage polymerizations the polymers are yellow or light-colored powders and those from the second-stage heating are without exception red or black powders. In all cases exactly equimolar amounts of monomers were employed.

Poly[2,2'-(1,4-phenylene)-6,6'-oxydiquinoxaline] (V)

Hexamethylphosphoramide Polymerization To 1.1736 g. (0.00509 mole) of 3,3',4,4'-tetraminodiphenyl ether (IV) in 20 ml. of HMP was added a solution of 1.1528 g. of 1,4-phenylenediglyoxal dihydrate (I) in 20 ml. of HMP. The mixture became dark red immediately, and external heating was carried out with an oil bath. The temperature was slowly increased, and at 100°C. the red solution became cloudy; after 5 min. a red brown precipitate appeared. Heating was continued and the temperature was finally maintained at 195°C. for 3 hr., after which time the precipitate was collected, washed with methanol, and dried to yield 1.5325 g. of a dark yellow powder. To the HMP filtrate was added 200 ml. of methanol and a red-orange precipitate was formed which was subsequently collected, washed with methanol, and dried. During this drying the material formed into a black, tarry, plastic mass which, when exposed to air for several weeks, became brittle and crumbled. A portion of the polymer that had precipitated from HMP was heated to 375°C. under reduced pressure and became very black.

Dioxane Polymerization. To a solution of 0.7127 g. (0.00309 mole) of IV in 30 ml. of purified dioxane was added 0.7000 g. of I in 30 ml. of dioxane. The solution became yellow but no precipitate formed upon mixing of the solutions. Heating was started and continued until the reflux temperature was reached without any further change in the appearance of the mixture. No solid had formed after heating for 6 hr. The dioxane was removed under reduced pressure to yield a yellow powder in a quantitative yield. This material was heated to 250°C. under nitrogen and did not change in physical appearance.

ANAL. Calcd. for $(C_{22}H_{12}N_4O)_n$: C, 75.89%; H, 3.45%. Found: C, 75.39%; H, 3.92%.

This material was heated to 375°C. to yield a black powder.

Melt Polymerization. To 1.9909 g. (0.00865 mole) of IV was added 1.9565 g. of I. The two powdered monomers were mixed thoroughly and then heated in a rotating flask. When the bath temperature reached 100°C., the powders formed a white lumpy mass; between 100°C. and 150°C. the mass started to become discolored, and water vapor was observed to condense near the top of the reaction flask. At 150°C. the mass had melted and resolidified in a matter of a few minutes. No further change was noted until the polymer became dark red at 225°C. The final product which had been heated to 250°C. for 1 hr., was a dark red powder and was obtained in quantitative yield. A portion of this polymer (1.8627 g.) was treated in the second-stage heating cycle at 375°C. Some sublimation of white material was noticed during this heating.

Poly[2,2′-(1,3-phenylene)-6,6′-diquinoxaline] (*VII*)

Hexamethylphosphoramide Polymerization. A solution of 0.6722 g. (0.00314 mole) of 3,3′-diaminobenzidine (II) and 0.7096 g. of 1,3-phenylenediglyoxal dihydrate (VI) in 30 ml. of HMP initially formed a red solution, and no precipitate was observed when this solution was heated for 6.5 hr. at 195–200°C. After cooling, and on the addition of 200 ml. of methanol, a tan precipitate was collected and dried to yield 1.7477 g. of polymer. A portion of the polymer was treated in the heating cycle in the usual manner. At 300°C. the material turned black but never melted, and heating was continued to 375°C. The final polymeric product was a black powder.

Melt Polymerization. To 0.7310 g. (0.00338 mole) of II was added 0.7526 g. of VI, and the two solids were mixed and heated slowly to 250°C. At 120°C. water was observed near the top of the reaction flask, and at 150°C. the powders became yellow. At 250°C. the material was brown. No further change in the material was observed as heating was continued for 4 hr.

ANAL. Calcd. for $(C_{22}H_{12}N_4)_n$: C, 79.50%; H, 3.61%. Found: C, 80.05%; H, 4.87%.

A portion of this material which was heated to 375°C. under reduced pressure (0.5 mm.) for 1 hr. was a black powder.

Poly[2,2′-(1,3-phenylene)-6,6′-oxydiquinoxaline] (*VIII*)

To a solution of 0.6177 g. (0.00268 mole) of 3,3′,4,4′-tetraminodiphenyl ether (IV) in 15 ml. of HMP was added 15 ml. of a solution of 0.6066 g. of 1,3-phenylene-diglyoxal dihydrate (VI). The solution became red, but no precipitate formed. The temperature was maintained at 195–200°C. for 4 hr. during which time there was no visible change in the mixture. After cooling, 200 ml. of methanol was added, and the orange precipitate that formed was collected and dried to yield 1.0955 g. of polymer. A portion (0.7315 g.) was heated in the usual manner to 375°C. to yield a black powder. A residue always remained in the elemental analysis combustion.

ANAL. Calcd. for $(C_{22}H_{12}N_4O)_n$: C, 75.89%; H, 3.45%. Found: C, 71.10%; H, 4.88%.

Poly[2,2′-(4,4′-oxydiphenylene)-6,6′-diquinoxaline] (*X*)

Hexamethylphosphoramide Polymerization. To a solution of 0.642 g. (0.00282 mole) of 3,3′-diaminobenzidine (II) in 20 ml. of HMP was added 0.9000 g. of 4,4′-oxydiphenylene-diglyoxal dihydrate (IX) in 20 ml. of HMP. A red solution was immediately produced, but no precipitate formed at this time or while heating of the solution was carried out. The temperature was maintained at 195–200°C. overnight, and a film was observed to have formed on the resin pot. After cooling, this material was collected, washed with methanol, and dried under reduced pressure to give 0.4240 g. of a red film. To the HMP filtrate was added 200 ml. of methanol to give a yellow precipitate which was dried to give a yellow powder. The powder and the film together represented a quantitative yield of polymer. Upon heating to 375°C. in the usual manner the film became black and brittle, but no melting of this material was observed.

Dioxane Polymerization. To a solution of 0.5378 g. (0.00251 mole) of II in 50 ml. of dioxane was added 0.8000 g. of IX in 50 ml. of dioxane. After heating for 30 min. (85°C.) a yellow precipitate was observed. The mixture was maintained at the reflux temperature overnight and the dioxane was removed by evaporation to afford a quantitative yield of polymer. Heating this material to 250°C. under nitrogen for 3 hr. did not change its physical appearance. A portion that was heated in the usual manner to 380°C. became dark brown and expanded in volume at 300°C. and after 15 min. became powdery again.

Melt Polymerization. To 0.4371 g. (0.00243 mole) of II was added with mixing 0.6504 g. of IX. The powders were heated to 200°C. and at 120°C. they began to stick to the glass but were still white. Evolution of water was observed. At 130°C. some discoloration started to take place and at 150°C. all the material had adhered to the glass. Heating at 200°C. for 1.25 hr. resulted in a darkening of the polymer, and the final product was a quantitative yield of dark brown powder. A portion of this material was heated to 375°C. and some softening was observed at 260°C., but the final product was black and fluffy and could be ground into a powder. Some sublimation was observed during this heating cycle.

Poly[2,2′-(4,4′-oxydiphenylene)-6,6′-oxydiquinoxaline] (*XI*)

Hexamethylphosphoramide Polymerization. To a solution of 0.9366 g. (0.00406 mole) of 3,3′,4,4′-tetraminodiphenyl ether (IV) in 20 ml. of HMP was added 1.2944 g. of 4,4′-oxydiphenylenediglyoxal dihydrate (IX) in 30 ml. of HMP. The solution became red, but no precipitate formed until the mixture had been heated at 195–200°C. for 2 hr.; at this time a small amount precipitated from the red solution. The HMP solution was added to 200 ml. of methanol and the resulting yellow precipitate was collected and dried to afford 2.04 g. of polymer. A portion of this polymer was heated to 375°C. under reduced pressure.

A second polymerization was run in which aliquots of the solution were withdrawn periodically and the polymer was precipitated from solution to follow the course of the polymerization (Table V).

Dioxane Polymerization. To a solution of 1.0389 g. (0.00451 mole) of IV in 30 ml. of dioxane was added a solution of 1.4354 g. of IX in 40 ml. of dioxane. The solutions became yellow, and after the reflux temperature had been maintained for 45 min., yellow material precipitated from the solution. Heating was continued for 2 hr. more, after which time the dioxane was evaporated to yield 2.2049 g. of polymer. This powder was heated to 250°C. under nitrogen. Heating in the usual manner at 375°C. for 2.5

hr. produced a black polymer. The analytical sample of this polymer was obtained from the solid residue that remained after the solvent had been completely evaporated. This material was 100% soluble in chloroform.

ANAL. Calcd. for $(C_{23}H_{16}N_4O_2)_n$: C, 76.30%; H, 3.64%; Found: C, 75.71%; H, 4.69%.

Melt Polymerization. To 1.3502 g. (0.00197 mole) of IV was added 0.6269 g. of IX. The materials were mixed and slowly heated and at 120°C. they started to discolor and stick to the flask. Evolution of water was observed. At 150°C. the mixture started to melt and then resolidified; at 200°C. the mixture was black. After cooling, a portion of this polymer was heated to 375°C. At 220°C. it became soft and adhered to the flask; after heating for 1 hr. under reduced pressure at 375°C. the black polymer had to be scraped from the glass reaction flask.

Physical Properties

Films were cast from HMP solutions of polymer by floating the solution on a layer of mercury and evaporating the solvent in a circulating hot air oven and subsequently heating at 100°C. under reduced pressure. The films of poly[2,2′-(4,4′-oxydiphenylene)-6,6′-oxydiquinoxaline] were yellow to red and transparent. Heating this film at 400°C. under nitrogen produced a tough, translucent film. Infrared spectra of these films are shown in Figure 6.

The inherent viscosity of each polymer was taken in a hexamethylphosphoramide solution. The dilute solutions ranged in concentration from 0.8 to 0.1 g./100 ml.

The molecular weight of a dimethylformanide solution of poly[2,2′-(4,4′-diphenyl ether)-6,6′-oxydiquinoxaline] was determined. The instrument used for this determination was a Mechrolab Model 501 high-speed membrane osmometer. The membrane was an S&S cellulose (super dense). The solution concentrations of 1.0, 0.5, and 0.25 g./l. of DMF were employed. Counter readings of the reference value for solvent were 18.34, 18.69, 18.28. Because the polymer diffused through the membrane, the original counter reading for the polymer solutions decreased with time. These changes were plotted against time and a straight line was extrapolated to zero time to obtain the true osmotic pressure before any polymer diffusion had taken place. The difference between this value and the reference value for the pure solvent represented the osmotic pressure for the polyquinoxaline solutions. The value of 4.85 in Figure 5 was used in the Van't Hoff equation to give a number-average molecular weight of 5700 (D.P. 13). The inherent viscosity of this polymer was 0.23 in HMP. The polymer sample employed in this determination was obtained from the dioxane polymerization before heating of the sample to 225°C.

X-ray diffraction patterns on finely ground polymer samples were obtained by use of copper Kα radiation. A sample of poly[2,2′-(1,4-phenylene)-6,6′-diquinoxaline] (III), which had been prepared in refluxing dioxane and then heated to 225°C. under nitrogen showed *d* spacings (Fig. 1) at 17 ±1, 12.45, 7.70, 5.92, 3.48, and 2.04 A. This same sample, which had been heated to 375°C. under reduced pressure showed *d* spacings at 17 ± 1, 13.47, 5.95, and 3.50 A. Two samples of poly[2,2′-(4,4′-oxydiphenylene)-6,6′-oxydiquinoxaline] (XI), one of which was prepared in HMP (Table V, η = 0.72) and the other of which was this same sample subsequently heated to 400°C. under nitrogen for 10 min., showed little or no crystallinity.

The authors would like to thank Dr. C. S. Marvel and Dr. R. T. Foster for the detailed procedure for the preparation of the tetramine monomer, 3,3′,4,4′-tetraminodiphenyl ether. We are very grateful to Norman Baenziger and Mr. Wm. L. Duax for the x-ray patterns.

References

1. Stille, J. K., and J. R. Williamson, *J. Polymer Sci.*, **B2**, 209 (1964).
2. Stille, J. K., and J. R. Williamson, *J. Polymer Sci.*, **A2**, 3867 (1964).
3. DeGaudemaris, G., and B. Sillion, *J. Polymer Sci.*, **B2**, 203 (1964).
4. Marvel, C. S., and R. T. Foster, private communication.
5. Bandwell, F. G., and E. W. Garbish, *J. Am. Chem. Soc.*, **82**, 3588 (1960).
6. Bowman, J., *J. Chem. Soc.*, **1950**, 323.
7. Ruggli, P., and W. Theiheimer, *Helv. Chim. Acta*, **24**, 899 (1941).
8. Smith, C. M., U. S. Pat. 2,903,461 (1959).

Résumé

Cinq nouvelles polyquinoxalines de haut poids moléculaire ont été préparées par les réactions de combinaison de deux tétramines, la 3,3′-diaminobenzidine (II) et le 3,3′,4,4′-tétraminodiphényléther (IV) avec les trois bis-glyoxals, le 1,4-phényléne-di-glyoxal (I), le 1,3-phénylénediglyoxal (VI) et le 4,4′-oxydiphénylénediglyoxal (IX). Les techniques de polymérisation en solution et à l'état fondu fournissent des polymères de poids moléculaire intermédiaire qui peuvent être convertis en échantillons de haut poids moléculaire (η_{inh} > 1.0) en chauffant à 375°C. sous pression réduite. Toutes les polyquinoxalines ont une excellente stabilité thermique, aussi bien dans l'azote qu' à l'air. De ces polyméres, le poly [2,2′-(4,4′-oxydiphényléne)-6,6′-oxydiquinoxaline] (XI) posséde la plus grande solubilité dans l'hexaméthylphosphoramide (HMP) et des films peuvent être coulés à partir de solutions dans le HMP du polymére de poids moléculaire intermédiaire (η_{inh} = 0.3–0.7). On peut obtenir des films durs, insolubles en chauffant les films coulés, sous azote ou sous pression réduite à 350–400°C.

Zusammenfassung

Fünf neue hochmolekulare Polychinoxaline wurden durch Kombinationsreaktionen von zwei Tetraminen, 3,3-Diaminobenzidin (II) und 3,3′,4,4′-Tetraminidiphenyläther (IV), mit den drei Bis-glyoxalen 1,4-Phenylendiglyoxal (I), 1,3-Phenylendiglyoxal (VI) und 4,4′-Oxydiphenylendiglyoxal (IX) dargestellt. Lösungsund Schmelzpolymerisation liefert Polymere mit intermediären Molekulargewichten, welche durch Erhitzen auf 375° unter vermindertem Druck in hochmolekulare Stoffen (η_{inh} > 1,0) umgewandelt werden können. Alle Polychinoxaline besitzen in Stickstoff und in Luft eine ausgezeichnete thermische Stabilität. Von diesen Polymere besitzt Poly 2,2′-(4,4′-oxydiphenylen)-6,6′-oxydichinoxalin (XI) die höchste Löslichkeit in Hexamethylphosphramid (HMP) und aus Lösungen von Polymeren mit mittlerem Molekulargewicht (η_{inh} = 0,3–0,7) in HMP können Filme gegossen werden. Feste, unlösliche Filme können durch Erhitzen der gegossenen Filme in Stickstoff oder unter vermindertem Druck auf 350–400°C erhalten werden.

Received July 20, 1964

JOURNAL OF POLYMER SCIENCE: PART A VOL. 3. PP. 1031-1036 (1965)

Copolymerization of Methyl Methacrylate with Unsaturated Esters of Granular Starch

C. E. BROCKWAY, *Research Center, A. E. Staley Manufacturing Company, Decatur, Illinois*

Synopsis

Methyl methacrylate readily copolymerizes with methacrylate ester groups present at a degree of substitution of about 0.1 in granular starch. This is shown by (*1*) over 50% grafting efficiency by initiation with azoisobutyronitrile; (*2*) higher grafting efficiency with than without the methacrylate groups when initiation is by peroxide; (*3*) crosslinked structure of the copolymers obtained; (*4*) crosslinks which persist in the PMMA recovered after acid hydrolysis to remove starch. By the same set of criteria, maleate half-ester groups in granular starch copolymerize with methyl methacrylate hardly at all.

INTRODUCTION

A previous paper of this series[1] has presented evidence that when methyl methacrylate is grafted to granular corn starch by initiation with hydrogen peroxide plus activator, grafting occurs primarily as a result of attack on starch by hydroxyl radicals. No significant number of radical sites is generated on starch by transfer with growing poly(methyl methacrylate) (PMMA) chains. Richards[2] drew the same conclusion regarding the mechanism of grafting vinyl monomers to cellulose by initiation with peroxide.

Additional work pertinent to the susceptibility of polysaccharides to chain transfer has been published. By studies of chain transfer constants of model carbohydrates,[3] Machell and Richards showed that cellulose and other polysaccharides should be very poor transfer agents, although Chaudhuri and Hermans[4] reported grafting of styrene to cellulose acetate by chain transfer. Kwei and Eirich reported grafting of vinyl pyrrolidone to dextran by chain transfer,[5] although the chain transfer constant of dextran was found to be very small.[6] Various means have been reported for making polysaccharides more amenable to grafting. For cellulose these have included derivatization with radical-generating groups such as peroxy or azo,[7,8] with substituents such as thiol[4,9] or amino[9] groups which are more susceptible than cellulose itself to chain transfer, and with copolymerizable groups such as allyl ether[10-13] or unsaturated ester[14,15] groups. Of these various approaches, the only one to date reported for starch is peroxidation by ozonization.[16,17]

This paper reports the grafting of methyl methacrylate to granular starches containing methacrylate or maleate ester groups.

EXPERIMENTAL

Preparation of Starch Esters

Starch methacrylate was prepared from unmodified granular corn starch and methacrylic anhydride by the method of Caldwell.[18] About 1000 g. (dry basis) of unmodified starch, slurried in 1600 ml. of distilled water, was maintained at about 10°C. during gradual addition of 123 g. of methacrylic anhydride (Borden Chemical Co.). The pH was maintained at about 9 by concurrent incremental addition of aqueous sodium hydroxide. After all the anhydride was added, the pH was allowed to rise to 7 for a few minutes of additional stirring. After thorough washing with water, the granular product was air-dried at room temperature, blended, and the moisture content determined. Saponification values indicated a degree of substitution of methacrylate groups of 0.12; this corresponds to a methacrylate ester group for each 8 to 9 glucose units.

Starch maleate half-ester was prepared similarly. Because of the tendency of the derivatized product to swell in water, filtration was simplified by use of a water–methanol mixture. The product is presumably the sodium salt of the maleate half-ester of starch. An analytical sample was converted to the free carboxy form by treatment with excess nitric acid followed by thorough washing. Determination of acid and saponification numbers yielded values of 0.15 and 0.10, respectively, for the degree of substitution of maleate ester groups.

Procedures

Polymerizations, recovery of product, and determination of grafting efficiency were carried out as previously described.[19]

RESULTS

Starch Methacrylate

Typical runs are summarized in Table I. Polymerizations initiated by hydrogen peroxide plus activator proceeded much as they do with underivatized starch. Temperatures spontaneously rose from the initial 30°C. to a maximum near 40°C. within 10–15 min. With AIBN (azobisisobutyronitrile), heat was applied to maintain the desired temperature of 50°C., and there was no detectable temperature rise. Small amounts of starchy materials, usually less than 1 g., appeared in the aqueous filtrate. In only one instance (run 35D-103) did detectable PMMA appear in the filtrate.

Positive evidence for grafting by way of copolymerization with pendant methacrylate groups is provided by runs 35D-103 and 35D-106, in which

TABLE I
Starch Methacrylate[a]

Run	D.S. of ester on starch	Initiator level, mmole/mole glucose[b]	Conversion of monomer, %	Grafting efficiency, %[c]
13D-61	None[d]	10/1/0	100	88
35D-96	0.12	10/1/0	100	97
13D-60	None[d]	100/1/10	100	72
35D-102	0.12	100/1/10	100	92
35D-103	0.12	AIBN-5[e]	31	54
35D-106	0.12	AIBN-50[e]	88	67

[a] All runs with 50 g. of methyl methacrylate/100 g. of starch (dry basis); polymerizations run for about 3 hr. at 30–39°C. except as noted. All reactants added at the start of the polymerization cycle.

[b] H_2O_2/ferrous ammonium sulfate/ascorbic acid except for the AIBN runs.

[c] Expressed as per cent of PMMA not removed from the granular product by the two successive extractions with 1,2-dichloroethane.

[d] Control run with underivatized, unmodified starch.

[e] Polymerization run at 50–52°C.

grafting efficiencies of over 50% were realized. It has been previously shown[1] that with underivatized starch, AIBN induces high conversion of methyl methacrylate but with little or no grafting. Additional evidence for copolymerization is provided by the peroxide-initiated runs; significantly higher grafting efficiency is realized in the presence than in the absence of the pendant methacrylate groups. The much higher grafting efficiency on starch methacrylate with peroxide than with AIBN suggests, as would be expected, that the peroxide causes grafting by direct attack on the starch as well as by way of copolymerization with pendant unsaturation.

Additional evidence for grafting by copolymerization is provided by the comparative solubilities of the granular products listed in Table I. Products 13D-60 and 13D-61 readily dissolved on heating at 1.3% solids in dimethyl sulfoxide at 110°C. for a few minutes. No other product in Table I was soluble under these conditions; only slight swelling occurred on prolonged heating. This is the expected result, provided that any significant fraction of the polymerizable groups attached to the starch actually undergo either homo- or copolymerization. However, homopolymerization of the pendant groups would not be expected in the presence of a considerable molar excess of monomeric methyl methacrylate.

Acid hydrolysis of the grafted product would not be expected to remove methacrylate units in the polymer from the glucose units to which they are esterified, because of the well-known resistance of polymeric methacrylate esters toward acid saponification.[19–21] However, acid hydrolysis in dilute aqueous medium should ultimately separate each glucose unit from other attached glucose units. Thus, the PMMA recovered by acid hydrolysis should not itself be crosslinked. Surprisingly, the PMMA recovered from all products in Table I except 13D-60 and 13D-61 would swell but not dissolve in 1,2-dichloroethane. Whether this is due to incomplete hydrolysis of the starch, to acid-catalyzed intercondensation of glucose residues attached to PMMA, or to occasional attachment of more than one methacrylate ester group to the same glucose unit has not been established. The very fact of this insolubility is further evidence of the attachment of the PMMA chains to the carbohydrate material.

Maleate Half-Ester of Starch

Table II shows a series exactly parallel to that of Table I except that the starch substrate is now the maleate half-ester. Polymerizations of methyl methacrylate went much more slowly and to lower conversions than under corresponding conditions with either starch methacrylate or underivatized starch. The starch maleate tends to give an extremely viscous slurry in water, especially after the onset of polymerization, and in most runs it was necessary to add sodium sulfate in order to minimize swelling tendency of the starch granules. Even so, 5 g. or more of starch material typically showed up in the aqueous filtrate, along with a much smaller amount of PMMA.

The data of Table II clearly show that little copolymerization occurs between the methyl methacrylate and the maleate half-ester groups. This is indicated by the following considerations:

(*1*) Little or no grafting occurs with AIBN initiation, even at high monomer conversions.

(*2*) With peroxide initiation, grafting efficiency is the same or even lower than that which is shown to occur in the absence of the maleate ester groups.

TABLE II
Maleate Half-Ester of Starch[a]

Run	D.S. of ester of starch	Initiator level, mmole/mole glucose[b]	Conversion of monomer, %	Grafting efficiency, %[c]
13D-61	None[d]	10/1/0	100	88
35D-98	0.13	10/1/0	66	89
13D-60	None[d]	100/1/10	100	72
35D-101[e]	0.13	100/1/10	91	59
35D-100[e]	0.13	AIBN-5[f]	27	12
35D-104[e]	0.13	AIBN-50[f]	91	0

[a] All runs with 50 g. of methyl methacrylate/100 g. starch (dry basis); polymerizations run for about 3 hr. at 30–39°C. except as noted. All reactants added at the start of the polymerization cycle.

[b] H_2O_2/ferrous ammonium sulfate/ascorbic acid except for the AIBN runs.

[c] Expressed as per cent PMMA not removed from the granular product by the two successive extractions with 1,2-dichloroethane.

[d] Control run with underivatized starch.

[e] Sodium sulfate (50 g., anhydrous basis) included in the charge to avoid excessive thickening of the slurry during polymerization.

[f] Polymerization run at 50–52°C.

(3) When heated in dimethyl sulfoxide, the granular products in some instances almost completely dissolve, in others become highly swollen. The fact of partial insolubility suggests a minor amount of copolymerization, since if none whatsoever occurred, the product should be completely soluble.

(4) The PMMA recovered by acid hydrolysis of the granular product is completely soluble in 1,2-dichloroethane.

Comparison of this behavior with copolymerization of methyl methacrylate and simple maleate esters is difficult because of the scarcity of published data. A recent review of copolymerization parameters[22] lists only one instance in which methyl methacrylate (M_1) has been copolymerized with a maleate diester, and none involving a maleate half ester. With diethyl maleate (M_2), the r_1 and r_2 values of 20 and 0, respectively, indicate that the product of copolymerization would practically amount to homopolymer of methyl methacrylate. From the available Q and e values for methyl and ethyl acid maleate,[22] calculations by means of the equations of Alfrey and Price[23] yield the values for copolymerization with methyl methacrylate (M_1) shown in Table III.

TABLE III

M_2	r_1	r_2
Methyl acid maleate	40	0.004
Ethyl acid maleate	0.94	0.30

On this basis, the methyl ester would be expected to copolymerize hardly at all, the ethyl ester readily. But the Q and e values of the half-esters are based on such limited data that the significance of the calculated r values is questionable.

References

1. Brockway, C. E., and K. B. Moser, *J. Polymer Sci.*, **A1**, 1025 (1963).
2. Richards, G. N., *J. Appl. Polymer Sci.*, **5**, 539 (1961).
3. Machell, G., and G. N. Richards, *J. Chem. Soc.*, **1961**, 3308.
4. Chaudhuri, D. K. R., and J. J. Hermans, *J. Polymer Sci.*, **51**, 373 (1961).
5. Shen, K. P., and F. R. Eirich, *J. Polymer Sci.*, **53**, 81 (1961).
6. Kwei, K. P. S., and F. R. Eirich, *J. Phys. Chem.*, **66**, 828 (1962).
7. Schwab, E., V. Stannet, and J. J. Hermans, *TAPPI*, **44**, 251 (1963).
8. Richards, G. N., *J. Appl. Polymer Sci.*, **5**, 553 (1961).
9. Richards, G. N., *J. Appl. Polymer Sci.*, **5**, 558 (1961).
10. Lagache, M., M. Chateau, and J. Pomey, *Compt. Rend.*, **251**, 2353 (1960).
11. Tonami, H., *Sen-i Gakkaishi*, **14**, 100 (1958).
12. French Pat. 1,211,269 (to Regie nationale des usines Renault).
13. Japanese Pat. 3499/62 (to Teikoku Rayon Co.).
14. Faraone, G., G. Parasacco, and C. Cogrossi, *J. Appl. Polymer Sci.*, **5**, 16 (1961).
15. Berlin, A. A., and T. A. Makarova, *J. Gen. Chem. U.S.S.R.*, **21**, 1383 (1951).
16. Kargin, V. A., P. V. Koslov, N. A. Plate, and I. I. Konoreva, *Vysokomolekul. Soedin.*, **1**, 114 (1959).

17. Kargin, V. A., N. A. Plate, and E. P. Rebinder, *Vysokomolekul. Soedin.*, **1,** 1547 (1959).
18. Caldwell, C. G., U. S. Pat. 2,461,139 (February 8, 1949).
19. Brockway, C. E., *J. Polymer Sci.*, **A2,** 3721 (1964).
20. Glavis, F. J., *J. Polymer Sci.*, **36,** 547 (1959).
21. Ide, F., *Kogyo Kagaku Zasshi,* **64,** 1489 (1961).
22. Young, L. J., *J. Polymer Sci.*, **54,** 411 (1961).
23. Alfrey, T., Jr., and C. C. Price, *J. Polymer Sci.*, **2,** 101 (1947).

Résumé

Le méthacrylate de méthyle copolymérise facilement avec des groupements esters méthacryliques présents à un degré de substitution d'environ 0.1 dans de l'amidon en grains. On le montre par (*1*) un rendement de greffage supérieur à 50% par initiation avec l'azoisobutyronitrile; (*2*) une efficacité de greffage plus élevée en présence des groupements méthacryliques qu'en leur absence, lorsque l'initiation est effectuée par un peroxyde; (*3*) une structure ramifiée des copolymères obtenus; (*4*) des pontages qui persistent dans le PMMA recupéré après hydrolyse acide pour èliminer l'amidon. Par le même ensemble de critéres, les groupements hémi-esters maléiques dans l'amidon en grains copolymérisent avec le méthacrylate de méthyle.

Zusammenfassung

Methylmethacrylat copolymerisiert leicht mit Methacrylatestergruppen, die in granulierter Stärke zu einem Substitutionsgrad von etwa 0,1 vorhanden sind. Dies wird bewiesen durch (*1*) mehr als 50% Aufpfropfungsausbeute bei Start mit Azoisobutyronitril; (*2*) höhere Aufpfropfungsausbeute bei Gegenwart als bei Abwesenheit der methacrylatgruppen bei Start mit Peroxyd; (*3*) Vernetzte Struktur der erhaltenen Copolymeren; (*4*) Vernetzungen, welche in den nach saurer Hydrolyse zur Entfernung der Stärke rückgewonnene PMMA vorhanden sind. Die gleichen Kriterien zeigen, dass Maleathalbestergruppen in granulierter Stärke mit Methylmethacrylat kaum copolymerisieren.

Received July 22, 1964

JOURNAL OF POLYMER SCIENCE: PART A VOL. 3, PP. 1037-1044 (1965)

Solvent Effects in Anionic Copolymerization

KENNETH O'DRISCOLL and ROBERT PATSIGA, *Department of Chemistry, Villanova University, Villanova, Pennsylvania*

Synopsis

The monomer pair styrene–*p*-methylstyrene has been anionically copolymerized in the presence of benzene and tetrahydrofuran. The results of these copolymerizations lead to the proposal of a comprehensive mechanism which is consistent with these and other known facts of anionic propagation in both vinyl and diene polymerizations. The essence of the proposed mechanism is that solvent or monomer can complex the positive counterion. Another monomer can then add to the complex or, in the case of the monomer-complexed counterion, a rearrangement can occur which incorporates the complexed monomer into the chain as the last unit.

INTRODUCTION

The use of anionic polymerization has been of considerable interest in recent years particularly because of the stereoregularity of the resultant polymers and also because of the variety of graft, block, and random copolymers which can be prepared anionically. Nevertheless, the detailed mechanism of the propagation step has remained relatively obscure. Stearns and Forman[1] suggested the possibility of a cyclic transition state to explain the stereochemistry of isoprene homopolymerization with a lithium counterion. Medvedev and co-workers[2] have postulated the formation of a π-complex between the monomer and the positive counterion of the chain in order to explain copolymerization behavior in diene–vinyl systems. These two suggestions are not at all contradictory, since the complex formation would presumably precede the transition state which determines the stereochemistry.

Most of the attention has centered on diene polymerization and diene–vinyl copolymerization. Szwarc and Smid[3] have studied copolymerizations of various pairs of vinyl monomers in tetrahydrofuran (THF), but little else has been reported on strictly vinyl, anionic copolymerization in THF or other solvents. It is therefore difficult to explain in a coherent fashion the various observations of solvent effects on copolymerization reactivity ratios or on polymer stereoregularity.

In this paper we present some new data on the anionic copolymerization of styrene and *p*-methylstyrene in benzene. These data, together with other literature data, have led us to propose a mechanism for anionic propagation which we believe is consistent with all of the known facts of homopolymerization and copolymerization by homogeneous anionic systems. Anticipating the formal presentation of the results, we are proposing that addition of vinyl or diene monomers to organoalkali chain ends can proceed via two mechanisms: (*1*) direct addition of monomer to an ion pair wherein the positive counterion is complexed by either solvent or another monomer molecule or, (*2*) formation of a π-complex between the entering monomer and the positive counterion, followed by bond formation between the negative chain end and the complexed monomer.

EXPERIMENTAL

Materials

The monomers, styrene and *p*-methylstyrene, were purified by preliminary drying over calcium hydride, followed by distillation at a reduced pressure of nitrogen. The monomers were then transferred to the polymerization flask by syringe injection. Solvents were distilled in nitrogen atmosphere and then stored over calcium hydride. Durene was given three melt-cool cycles in vacuum and then dissolved in benzene for transfer to the polymerization flask by syringe injection. Butyllithium (15% solution in heptane) was kindly given to us by the Foote Mineral Company.

Polymerization Technique and Rate Measurement

Polymerizations were conducted at 30°C. under an atmosphere of helium. To avoid interference in the rate measurements by the initiation step, a "living polymer" solution in benzene was first prepared. This was accomplished by adding increments of styrene to a butyllithium solution of desired concentration until at least 75% of the butyllithium had been consumed. This was determined by a spectrophotometric analysis of the styryl anion, or "living end" concentration, [L. E.].[4]

During polymerization, sampling was accomplished by forcing volume increments of the polymerizing mixture from the reaction flask by a positive pressure of helium. Polymerization in the samples was immediately terminated by adding them to a benzene–methanol solution. Residual monomer content in the samples was determined by programmed temperature gas chromatography with the use of a 6-ft. column packed with 15% silicone rubber on diatomaceous earth. Experimental error in monomer concentration [M] was approximately ±2%.

RESULTS

When styrene and *p*-methylstyrene were copolymerized, the plots of log monomer concentration versus time exhibited a straight line within experimental error. These plots are shown in Figure 1.

It has previously been shown[1] that combining the steady-state assumption employed in free radical copolymerization kinetics and the observed

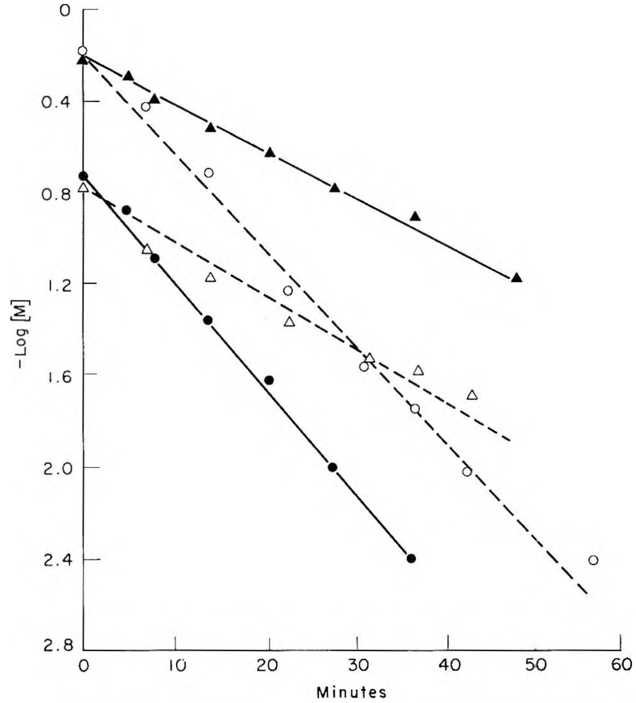

Fig. 1. Pseudo first-order behavior in copolymerization in benzene: (- -) 0.63M styrene (○) with 0.17M *p*-methylstyrene (△), [L.E.] = 0.036M; (——) 0.18M styrene (●) with 0.60M *p*-methylstyrene (▲), [L.E.] = 0.041M; $r_1 = 1/r_2 = 2.5$.

kinetic facts in anionic homopolymerization, the disappearance of monomers during anionic copolymerization can be expressed by:

$$-d[M_1]/dt = k_{11}[M_1^-]^{1/2}[M_1] + k_{21}[M_2^-]^{1/2}[M_1]$$

$$-d[M_2]/dt = k_{22}[M_2^-]^{1/2}[M_2] + k_{12}[M_1^-]^{1/2}[M_2]$$

The fact that the plots in Figure 1 follow a straight line indicates:

$$\frac{-d \ln [M_i]}{dt} = k_{ii}[M_i^-]^{1/2} + k_{ji}[M_j^-]^{1/2} = \text{constant}$$

Under our experimental conditions the sum: $[M_i^-]^{1/2} + [M_j^-]^{1/2}$ does not vary by more than ±10% throughout more than 90% of the polymerization and can therefore be considered constant, especially for the initial 50% or so of conversion. This means, then, for the above relationship to be true: $k_{ii} = k_{ji}$. Thus, styrene and *p*-methylstyrene constitute a monomer pair for which $k_{11} = k_{21}$ and $k_{22} = k_{12}$.

The effect of a small concentration of tetrahydrofuran (THF) on the copolymerization behavior of this monomer pair is shown in Figure 2. The curvature of the plots suggests that even in the presence of a small amount of THF the kinetics have been altered to the extent that the condition $k_{ii} = k_{ji}$ is no longer true.

It is conceivable, however, that the rate constants in each of the several solvation states that Worsfold and Bywater have shown to exist[6] are not dependent on the chain end. This possibility can be disproved by the following considerations:

We define an equilibrium constant for the solvation of a chain end

$$(M_i^-)_{n-1} + \text{THF} \overset{K_i^n}{\rightleftharpoons} (M_i^-)_n$$

and for the propagation reaction

$$(M_i^-)_n + M_j \xrightarrow{k_{ij}^n} (M_j^-)_n$$

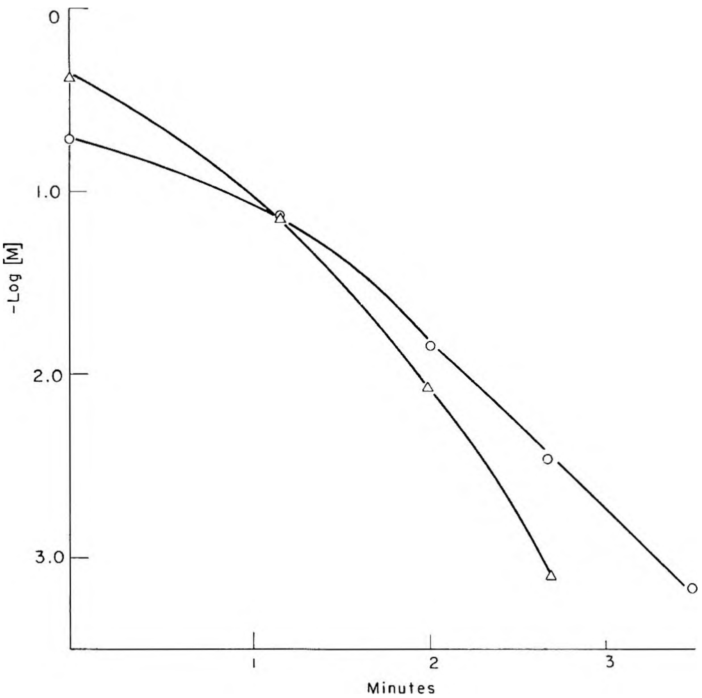

Fig. 2. Lack of pseudo first-order behavior in copolymerization in benzene containing 0.034M THF: 0.45M styrene (○) with 0.18M p-methylstyrene (△), [L.E.] = 0.032M.

The rate of disappearance of monomer M_i would then be given as

$$-d[M_i]/dt = [M_i]\sum_{n=0}^{n}(k_{ii}^n[M_i^-]_n + k_{ii}^n[M_j^-]_n)$$

In these equations n denotes the number of THF molecules solvating the alkali metal counterion of chain end $(M_i^-)_n$. We wish to examine the possibility that, if $k_{ii}^n = k_{ji}^n$ for all n, then a curved plot such as Figure 2 can still be observed. We will do so by assuming that k_{ii}^n does equal k_{ji}^n, and also that there is the equally likely identity, $K_i^n = K_j^n$. Using these assumptions we have

$$
\begin{aligned}
-d \ln [\mathrm{M}_i]/dt = {} & [\mathrm{M}_i^-]_0\{k_{ii}^{(n=0)} + k_{ii}^{(1)}K_i^{(1)} + k_{ii}^{(2)}K_i^{(1)}K_i^{(2)} + \ldots\} \\
& + [\mathrm{M}_j^-]_0\{k_{ji}^{(n=0)} + k_{ji}^{(1)}K_j^{(1)} + k_{ji}^{(2)}K_i^{(1)}K_i^{(2)} + \ldots\} \\
= {} & ([\mathrm{M}_i^-]_0 + [\mathrm{M}_j^-]_0)(k_{ii}^{n=0} + k_{ii}^{(1)}K_i^{(1)} \\
& + k_{ii}^{(2)}K_i^{(1)}k_i^{(2)} + \ldots)
\end{aligned}
$$

The right-hand side of this equation is constant if the sum of the uncomplexed chain end concentrations is constant.

It can readily be shown that

$$([\mathrm{M}_i^-]_0 + [\mathrm{M}_j^-]_0) = \sum_{n=0}^{n} ([\mathrm{M}_i^-]_n + [\mathrm{M}_j^-])\bigg/\left(1 + \sum_{n=0}^{n} K_i^n\right) = \text{constant.}$$

Therefore curved plots of ln $[\mathrm{M}_i]$ versus time could not occur. From the above we can affirm that $k_{ii}^n \neq k_{ji}^n$ in THF.

DISCUSSION AND CONCLUSIONS

Any detailed mechanism of the anionic propagation reaction must explain the following well established facts.

(*a*) In styrene–diene copolymerizations the monomer reactivity ratios change markedly with solvent.[2,7] In THF, the monomer reactivities are as expected from homopolymerization behavior, but a reversal of reactivity is observed as one proceeds through less basic ethers to hydrocarbons.

(*b*) This reversal of reactivity correlates completely with the change in polyisoprene microstructure in the same solvents.[7]

(*c*) Stereoregularity of homogeneous, anionic vinyl polymerization is grossly affected by solvent.[8]

In addition to the above, a satisfactory mechanism must explain the data in this paper and that of Szwarc and Smid.[3]

(*d*) The monomer reactivity ratios for styrene–*p*-methylstyrene are slightly changed in going from THF to benzene. However, they do not at all undergo the reversal of reactivity mentioned in point (*a*) above.

(*e*) For the same pair, $k_{11} = k_{21}$ and $k_{22} = k_{12}$ in benzene. In THF this is not so. For other monomer pairs with more different electronegativities, the disparity is even more pronounced.[3]

The contrast between points (*a*) and (*d*) is most striking, but let us begin instead with a consideration of point (*e*). It may be interpreted to mean that, in a noncomplexing solvent such as benzene, the monomer cannot discriminate between the two possible carbanions to which it can add. The presence of THF, however, causes a monomer such as styrene to show a preference for a *p*-methylstyryl carbanion over a styryl carbanion. An oversimplification of these facts might state that in benzene all carbanions are the same, while, in THF they are different. This is obviously untrue. What is more likely is that in benzene a common moiety of the two different chain ends is controlling the rate of addition of monomer, while in THF the monomer is adding to two different ion pairs. The only thing the two different chain ends have in common is the metal counterion. Therefore we propose that the positive counterion of a chain end can form a π-complex with a monomer (whether vinyl or diene) or it can form a σ- or π-complex with solvent (depending on the nature of the solvent); as shown in eqs. (1) and (2).

$$\tfrac{1}{2}(\mathrm{M_a^-Li^+})_2 \rightleftharpoons M_a^-\mathrm{Li}^+ - \begin{cases} \xrightleftharpoons{\mathrm{M_b}} \mathrm{M_a^-(Li\cdot M_b)^+} & (1)\\ \xrightleftharpoons{\mathrm{S}} \mathrm{M_a^-(Li\cdot S)^+} & (2)\end{cases}$$

Here the subscripted M's refer to various monomer units which may or may not be the same chemically.

The monomer-complexed ion pair can then rearrange to incorporate the complexed monomer unit into the chain

$$\mathrm{M_a^-(Li\cdot M_b)^+} \rightarrow \mathrm{M_aM_b^-Li^+} \qquad (3)$$

or another monomer unit can simply add to the monomer-complexed ion pair

$$\mathrm{M_a^-(Li\cdot M_b)^+} + \mathrm{M_c} \rightarrow \mathrm{M_aM_c^-(Li\cdot M_b)^+} \qquad (4)$$

In a similar fashion the solvent-complexed ion pair can directly add a monomer to the ion pair.

$$\mathrm{M_a^-(Li\cdot S)^+} + \mathrm{M_d} \rightarrow \mathrm{M_aM_d^-(Li\cdot S)^+} \qquad (5)$$

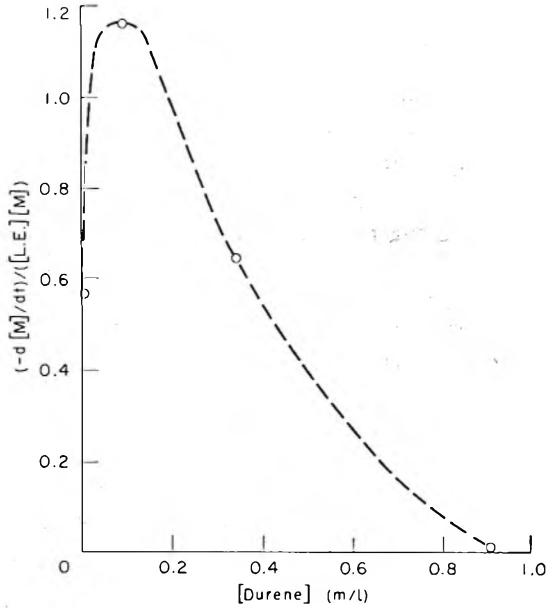

Fig. 3. Effect of durene on apparent rate constant for homopolymerization of styrene, 0.7M in benzene, [L.E.] = 0.02M.

This sequence of reactions completely explains point (*e*), and is consistent with point (*d*). It can also explain the apparent paradox in points (*a*) and (*d*): a diene such as isoprene or butadiene is a far stronger π-complexing agent than styrene[9] and would polymerize via reactions (1) and (3). In the presence of THF the polymerization reaction would be via reactions (2) and (5), and the higher reactivity of styrene (as exhibited in homopolymerization) could show itself.

The completely different characters of the rearrangement reaction (2) and the addition reactions (4) and (5) suggest that the steric requirements of the transition states would be quite different and therefore the stereochemistry of the products would be different [point (*c*)]. The ability of monomer to compete with solvent in complex forming equilibria of reactions (1) and (2) explains point (*b*).

As a test of the proposed mechanism, one could predict that a nonpolymerizable, π-complexing agent such as durene should have a marked effect on polymerization. We have performed a series of experiments with various durene concentrations in benzene, polymerizing $0.7M$ styrene in benzene at a constant chain end concentration of 0.021 mole/l. The results are shown in Figure 3. The slight elevation of the apparent rate constant at low durene concentration may be interpreted as due to an increase in the number of dissociated chain ends. Further increase in durene results in a depression of rate due to reaction sequence (2) and (5) being followed with a relatively weak complexer. It is notable that durene is exhibiting behavior similar to that of THF,[6] a strong σ-complexer.

The mechanism we have proposed is seen to be consistent with the known facts about anionic polymerization. Most of the parts of this mechanism have been proposed separately by others to explain one isolated fact or another, and we therefore acknowledge the contributions of numerous workers to this coherent mechanism.

Support of this work by the Petroleum Research Fund, administered by the American Chemical Society, is greatly appreciated.

References

1. Stearns, R. S., and L. E. Forman, *J. Polymer Sci.*, **41**, 381 (1959).
2. Spirin, Yu. L., A. A. Arest-Yakubovich, D. K. Polyakov, A. R. Gantmakher, and S. S. Medvedev, *J. Polymer Sci.*, **58**, 1181 (1962).
3. Smid, J., and M. Szwarc, *J. Polymer Sci.*, **61**, 31 (1962).
4. O'Driscoll, K. F., J. E. Clark, and E. Ricchezza, *J. Polymer Sci.*, in press.
5. O'Driscoll, K. F., and I. Kuntz, *J. Polymer Sci.*, **61**, 19 (1962).
6. Bywater, S., and D. J. Worsfold, *Can J. Chem.*, **40**, 1564 (1962).
7. Rogers, C. E., and A. V. Tobolsky, *J. Polymer Sci.*, **40**, 73 (1959).
8. Bawn, C. E. H., and A. Ledwith, *Quart. Rev.*, **16**, 361 (1962).
9. Ludvig, E. B., A. R. Gantmakher, and S. S. Medvedev, *Vysokomolekul. Soedin.*, **1**, 1333 (1959).

Résumé

On a copolymérisé anioniquement le styréne avec le *p*-méthylstyréne en présence de benzéne et de tétrahydrofuranne. Les résultats de ces copolymérisations conduisent à la présentation d'un mécanisme compatible avec d'autres faits connus de la propagation anionique dans les polymérisations vinylique et diénique. Dans le mécanisme proposé le solvant ou le monomére peuvent complexer le contre-ion positif. Un autre monomére peut alors s'additionner au complexe ou, dans le cas du contre-ion complexé au monomére, un réarrangement peut avoir lieu, qui incorpore le monomére complexé dans la chaîne.

Zusammenfassung

Das Monomerenpaar Styrol-*p*-Methylstyrol wurde in Gegenwart von Benzol und Tetrahydrofuran anionisch copolymerisiert. Die Ergebnisse dieser Copolymerisation führen zur Aufstellung eines amfassenden Mechanismus, der mit den vorliegenden und anderen bekannten Tatsachen beim anionischen Wachstum bei der Vinyl- und Dienpolymerisation konsistent ist. Die wesentlichen Punkte des vorgeschlagenen Mechanismus bestehen in der Annahme einer Komplexbildung zwischen Lösungsmittel oder Monomeren mit dem positiven Gegenion. Ein weiteres Monomeres kann sich dann an den Komplex addieren oder es kann, im Falle des mit dem Monomeren komplexierten Gegenions, eine Umlagerung auftreten, welche das komplexierte Monomere in die Kette als letzten Baustein einbaut.

Received May 27, 1964
Revised August 24, 1964
Revised September 30, 1964

JOURNAL OF POLYMER SCIENCE: PART A VOL. 3, PP. 1045-1061 (1965)

Stress-Cracking of Polyethylene Examined from the Viewpoint of Critical Strain

L. H. TUNG, *Petrochemicals Research Laboratory, The Dow Chemical Company, Midland, Michigan*

Synopsis

Stress-cracking in polyethylene has been examined from the viewpoint of critical strain based on a proposed theory for the formation of the cracks. Stress-cracking under constant load and constant strain was determined experimentally at 60°C. on a 3.5 melt index high-density polyethylene. A critical strain of 1.95% associated with a critical relaxation time of 90 min. was found for the sample. Good agreement was found between the theory and experiments made in Igepal CO 630. Some disagreements between the theory and experiments made in air were attributed to the rate of propagation of the cracks.

I. INTRODUCTION

The phenomenon of environmental stress-cracking in polyethylene has long been recognized. As the term implies when polyethylene is placed in a certain type of environment, usually surface-active liquids, it fails in a brittle manner at stresses below the yield or ultimate stress of the sample. The failure occurs after the sample has been under stress for a duration, the length of which depends on the magnitude of the stress, the nature of the environment, temperature, and the molecular weight of the sample. Complex stresses were first thought to be essential to induce stress cracking.[1] Later it was found that uniaxial stresses alone were enough to produce stress-cracking in polyethylene.[2-6] Gaube's[3] data show further that stress-cracking can be induced in air and water, which are considered to be inactive environments for stress-cracking. It appears then that stress-cracking in polyethylene is similar to fatigue of the material under static loads; the complex stresses and active environments merely accelerate the failure.

A few attempts have been made to elucidate the mechanism of stress-cracking. Hopkins et al.[7] and later Gaube[3] attributed the effect to the blocking action created by a preferential lateral glide of polyethylene crystallites along the 110 plane preventing ready orientation of the crystallites in the direction of the stress. Isaksen et al.[6] observed that minor small fissures occurred first throughout the sample before failure. The active environment then induced fracture at the site of fissures in the boundary between drawn and undrawn matter and thus prevented extensive cold-drawn of the fibrous materials linked across these fissure sites. These views explain why stress-cracking does not occur in polypropylene and the role of active environments. The delayed action of the formation of the fissures which is presumably the first stage of stress-cracking is, however, still a mystery.

Though much progress has been made, some controversial points still exist on the fine structure of polymer crystallized from melts. Until these points are resolved the detailed mechanism of stress-cracking is likely to remain obscure. In the present work we shall attempt to examine the phenomenon from the viewpoint of critical strain hoping to shed some light on the mechanism of stress-cracking before the fine structure of the polymer is completely understood.

The concept of critical strain is chosen because it worked well for the brittle failure of metals[8] before the dislocation theory of crystalline sites was advanced and it seems to receive support from several sets of published data.[3,4,9] The second reason will be elaborated in the next section.

II. THEORY

The deterioration of mechanical strength of a material under stress must come from one of two sources: (*1*) propagation of flaws already extant in the sample; (*2*) formation of new flaws under stress. Contrary to earlier findings, Carey[2] and later Isaksen et al.[6] observed that stress-cracking of polyethylene was not notch-sensitive. We may thus discredit the propagation of existing flaws as the primary cause. To account for the formation of new flaws we propose that chain slipping is the cause and a strain criterion may be used to correlate chain slipping with the formation of flaws.

A simple mechanical model of two Maxwell elements in parallel as shown in Figure 1 may be used to illustrate our hypothesis. We assume that for each dashpot there is a limit of travel beyond which the element will no longer be capable of sustaining any stress. When a stress greater than the yield strength is applied the limits of travel of both dashpots are exceeded. If the applied stress is below the yield strength, the piece will not fail im-

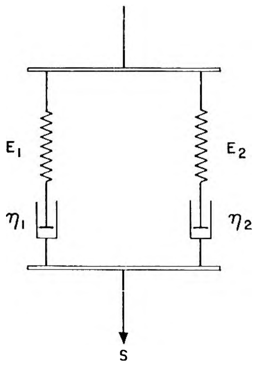

Fig. 1. Simple two-element mechanical model.

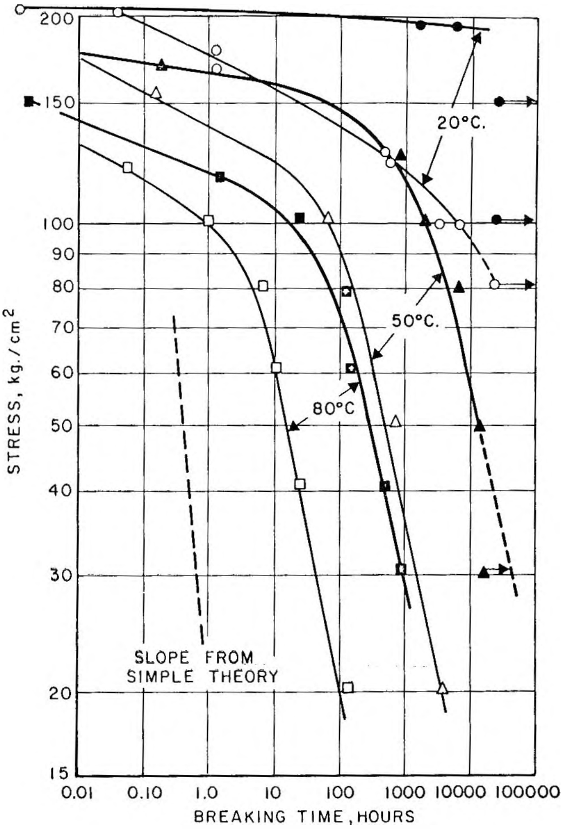

Fig. 2. Stress-cracking data of Gaube[3] on high-density polyethylene: (□) relative specific viscosity 2.5–3, 80°C. in water; (■) relative specific viscosity 4–5, 80°C. in water; (△) relative specific viscosity 2.5–3, 50°C. in water; (▲) relative specific viscosity 4–5, 50°C. in water; (○) relative specific viscosity 2.5–3, 20°C. in air; (●) relative specific viscosity 4–5, 20°C. in air.

mediately. The displacement of the dashpot of the element with shorter relaxation time will proceed at a higher rate than that of the other element. After a period of loading it will exceed its limit of travel and cause stress concentration on the other element leading to cracks and failures. Thus it should be possible to use the viscous strain of the element with shorter relaxation time as a criterion for stress-cracking.

Several sets of stress-crack data under uniaxial stress seem to support such a view. Figure 2 is a reproduction of Gaube's data[3] of high-density polyethylene on a log-log scale. A characteristic of these data is that the portions of the curves representing brittle failures are parallel straight lines for measurements made with samples of different molecular weight and at different temperatures. It can be shown that for the simple mechanical model in Figure 1, the strain ϵ_1 of the dashpot 1 is

$$\epsilon_1 = \frac{St}{\eta_1 + \eta_2} + \frac{S\tau}{\eta_1}\left(\frac{E_1}{E_1 + E_2} - \frac{\eta_1}{\eta_1 + \eta_2}\right)\left(1 - \exp\left\{\frac{t}{\tau}\right\}\right) \quad (1)$$

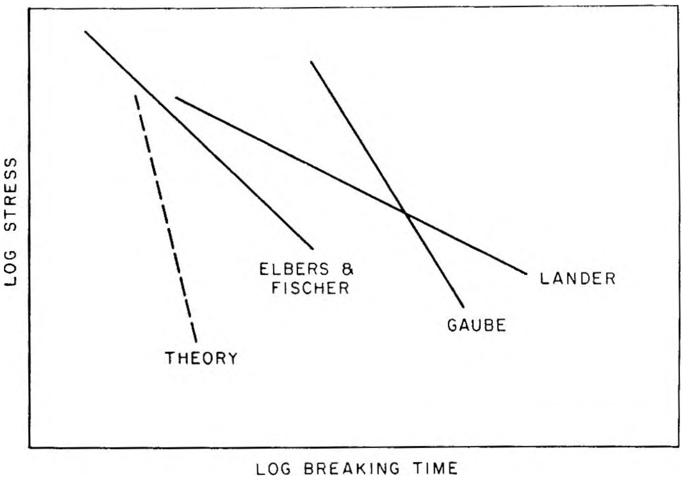

Fig. 3. Comparison of various sets of stress-cracking data.

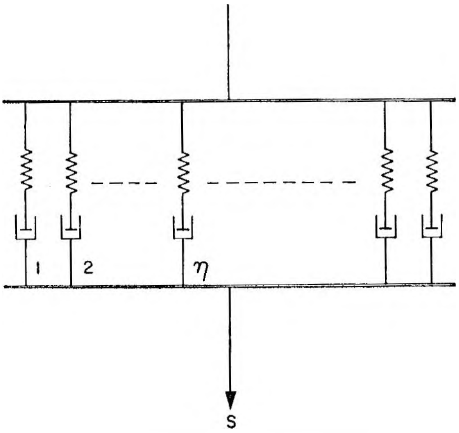

Fig. 4. Maxwell-Wiechert mechanical model.

where S is the total constant stress, E_1 and E_2 are the tensile modulis of springs 1 and 2, respectively, η_1 and η_2 are the viscosities of dashpots 1 and 2 respectively, and

$$\tau = \frac{(1/E_1) + (1/E_2)}{(1/\eta_1) + (1/\eta_2)}$$

When the time of loading t is small in comparison to the overall relaxation time τ, higher terms in the expansion of the exponential can be neglected and

$$S = \epsilon_1\eta_1[(E_1 + E_2)/E_1](1/t) \qquad (2)$$

Now a particular value of ϵ_1 can be considered as the critical strain or the limit of travel for the dashpot. The relationship between S and t in eq.

(2) is thus a straight line on a log-log plot with a slope of -1. This slope is independent E_1, E_2, ϵ_1, η_2, which are related to the temperature of measurement and the molecular weight of the sample. The slope of -1 is shown by the dotted line in Figure 2.

The uniaxial stress stress-cracking data of Elbers and Fischer[4] and Lander,[9] when replotted on a log-log scale, also approximate parallel straight lines in agreement with eq. (2), although the slopes of these lines are different from -1 and different from one another. Figure 3 shows a comparison of the different slopes.

Additional support for the critical strain hypothesis can be derived from the activation energy of the stress-cracking process. If we consider stress-cracking as a rate process and plot breaking time versus the reciprocal of the absolute temperature at a given stress, the above three sets of data all yield an activation energy of approximately 28 kcal./mole. Faucher[10] reported an activation energy of 30 kcal./mole for stress relaxation of polyethylene. Since the present model also involves stress relaxation as the rate-controlling process, the close agreement between the two values is additional support for the critical strain hypothesis.

To compare the hypothesis more quantitatively with experiments we shall use the more realistic Maxwell Wiechert model shown in Figure 4. We shall assume that the strain ϵ_n of the nth dashpot is critical. Let γ be the total strain of the system and $\dot{\gamma}$ its time derivative, then

$$d\gamma/dt = \dot{\gamma} = (dS_n/dt)(1/E_n) + (1/\tau_n E_n)S_n \tag{3}$$

$$d\epsilon_n/dt = S_n/\tau_n E_n \tag{4}$$

$$S = \sum_i S_i \tag{5}$$

where S_n, τ_n, and E_n are the stress, the relaxation time, and tensile modulus of the nth element respectively. The total strain, γ, and also its time derivative, $\dot{\gamma}$, can be considered as functions of time; thus from eq. (3)

$$S_n = \exp\left\{-\int_0^t \frac{1}{\tau_n}\,dt\right\} \int_0^t \exp\left\{\int_0^t \frac{1}{\tau_n}\,dt\right\} E_n\dot{\gamma}(t)dt + C\exp\left\{-\int_0^t \frac{1}{\tau_n}\,dt\right\} \tag{6}$$

When $t = 0$, $C = S_n$ and $S_n = \gamma_0 E_n$, where γ_0 is the total initial strain. Equation (6) now becomes

$$S_n = \exp\{-t/\tau_n\}\, E_n \int_0^t \exp\{t/\tau_n\}\, \dot{\gamma}(t)dt + E_n\gamma_0 \exp\{-t/\tau_n\} \tag{7}$$

Substituting the expression for S_n in eq. (4) and performing the integration, we have

$$\epsilon_n = (1/\tau_n)\int_0^t \exp\{-t/\tau_n\}\left[\int_0^t \exp\{t/\tau_0\}\, \dot{\gamma}(t)dt\right] dt + \gamma_0(1 - \exp\{-t/\tau_n\}) \tag{8}$$

The function $\dot{\gamma}(t)$ is the time derivative of the creep curve which can be determined experimentally.

In the experimental work creep measurements will be carried out to break at different stress levels. The time derivative of the creep curve will be substituted into eq. (8). The integration will be carried out from zero to break time. The purpose is to determine whether a value of τ_n can be found to give a constant ϵ_n for the creep data measured at different stress levels. A constant-strain stress relaxation experiment will also be carried out by using specimens prepared from the same sample. Under such conditions

$$\epsilon_n = \gamma_0(1 - \exp\{-t/\tau_n\}) \tag{9}$$

We shall examine whether the set of ϵ_n and τ_n obtained from creep measurement will fit eq. (9) for relaxation data conducted to breaking time at various constant strain γ_0.

III. CREEP MEASUREMENTS

Experimental Method

The creep apparatus is shown in Figure 5. The lower part of the apparatus was inserted in a 25 × 250 mm. test tube. The test tube was four-fifths submerged in a constant temperature bath during measurement. The strain of the specimen was measured by a linear differential transformer the output of which after rectification and suitable amplification was fed to a Sanborn Twin-Viso recorder for the initial portion of the creep. Long-term creep was recorded on a conventional millivolt recorder.

A sample of 3.5 melt index high-density polyethylene was used throughout the present work. The sample was compression-molded to a thickness of approximately 0.020 in. The specimens were cut from the molded sheet and annealed 24 hrs. at the measuring temperature, 60°C., before use.

Superposition Test

The viscoelastic behavior of semicrystalline polymer is known to be nonlinear. For example, Faucher[10] observed that at 40°C., a high-density polyethylene, Marlex 50, deviated significantly from linearity at strains larger than 0.5%. Since we have assumed a linear viscoelastic model, it is important to know the extent of deviation from linearity for the present sample.

Faucher's test for linearity was based on experiments conducted at constant rate of strain. We shall use the creep superposition test described by Leaderman.[11] In the test a long-duration creep is carried out with a properly conditioned sample. The long-duration creep curve is then compared with the creep curve obtained under cyclic loading. In the cyclic loading the same load is applied on the same sample for a short time period t_1. The load is then removed and then reapplied at $2t_1$, removed at $3t_1$,

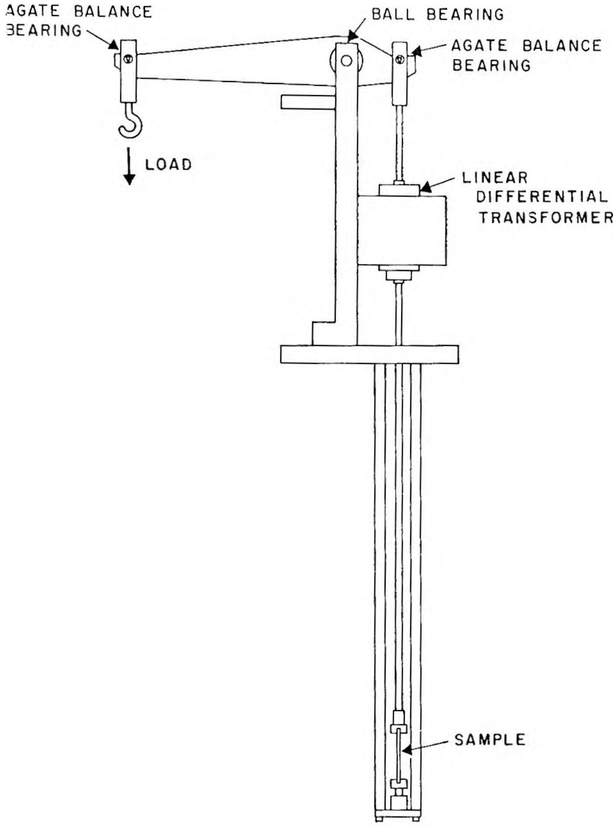

Fig. 5. Creep apparatus.

reapplied at $4t_1$, etc. If the strain obtained from the long-duration creep agrees with that calculated by the Boltzmann superposition principle from the cyclic loading, then the sample exhibits linear viscoelasticity.

The specimen used in the present test was cut into a rectangular shape 0.25 in. wide and 1.5 in. long. The portion exposed between the two sample clamps was 1 in. Air was used as the environment. Similar to observations made by Leaderman on many filamentous materials, polyethylene underwent an apparently permanent elongation as the load was first applied and no further significant permanent deformation was observed in subsequent loadings of the same magnitude. Such a process is called mechanical conditioning by Leaderman. Figure 6*a* shows the creep curve of the initial three cyclic loadings, 10 min. loading followed by 10 min. recovery. The load corresponds to a stress of 450 psi. After the third loading the specimen was allowed to recover overnight. An unrecoverable strain of 0.17% was observed. The same loading cycle was repeated the second day (Fig. 6*b*). The unrecoverable strain increased to 0.21%. A two-cycle loading, 15 min. loading and 15 min. recovery, was made the third day. The unrecoverable strain now remained at 0.21%. A long-duration loading strain again remained at 0.21%. Figure 6c shows the creep curves of the two last loadings. The circles shown in the figure indicate the calculated strain from the cyclic loading by using the Boltzmann superposition

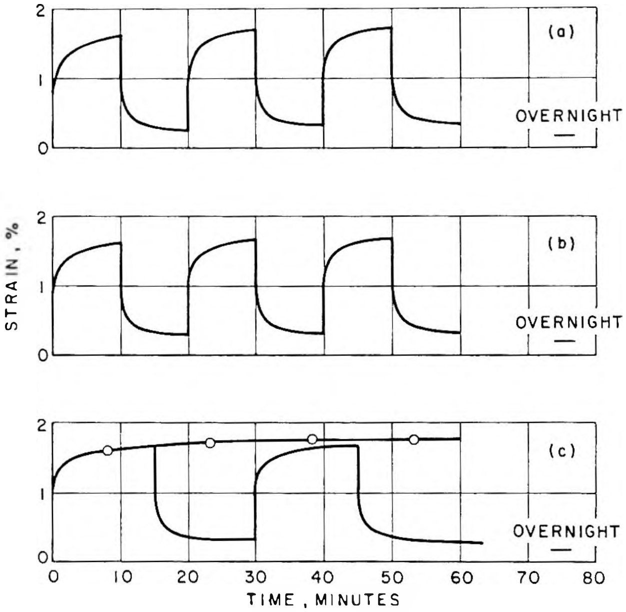

Fig. 6. Superposition test at 450 psi.

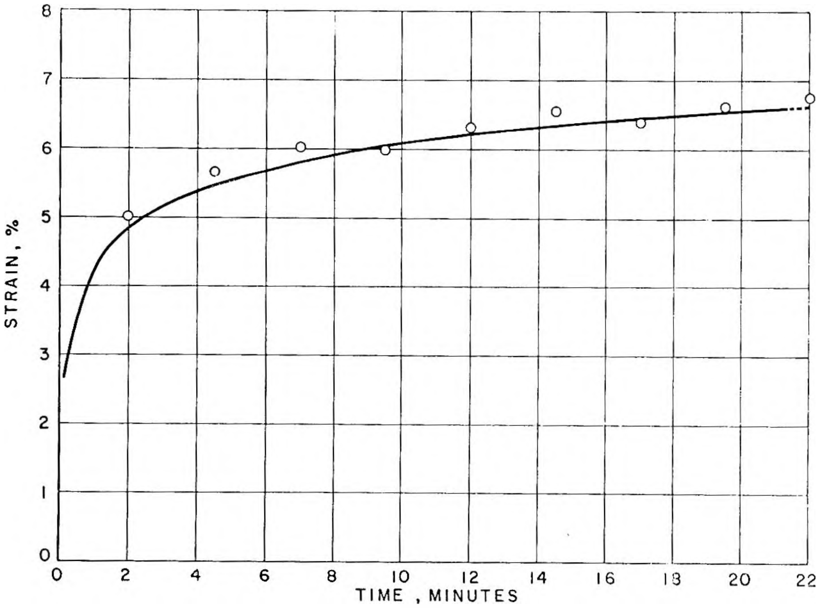

Fig. 7. Superposition test at 900 psi.

principle. The agreement is excellent. Thus, after mechanical conditioning the sample behaves quite linearly.

A second test was made at a stress of 900 psi. The specimen was first loaded continuously for 30 min. for mechanical conditioning. The overnight unrecoverable strain was found to be 1.10%. The next day the specimen was loaded for two cycles of 7.5 min. loading and 7.5 min. recovery. The unrecoverable strain increased to 1.21%. On the third day the sample was loaded for the long-duration creep. It broke, however, after 21 min. of loading. Figure 7 shows the long-duration creep curve. The circles indicate the strains calculated from the cyclic loading. The agreement is less impressive than that at 450 psi, but the behavior is still close to linear. The total strain is about 6.5%.

Creep Rupture Measurements

In spite of the advantage demonstrated in the superposition test, specimens were not mechanically conditioned in the creep rupture measurement. Tests made have shown that the extent of mechanical conditioning has a profound influence on the breaking time of the samples. In order to avoid this influence the specimens were annealed at the measuring temperature 60°C. and then used directly. Rectangular specimens were found to break prematurely at the grips of the clamps during preliminary runs. Dumbbell specimens were subsequently used. The straight portion of the specimen was $^{13}/_{16}$ in. long. The distance between the clamps was still maintained at 1 in. Figure 8 shows three creep curves. The stress was 825 psi. The

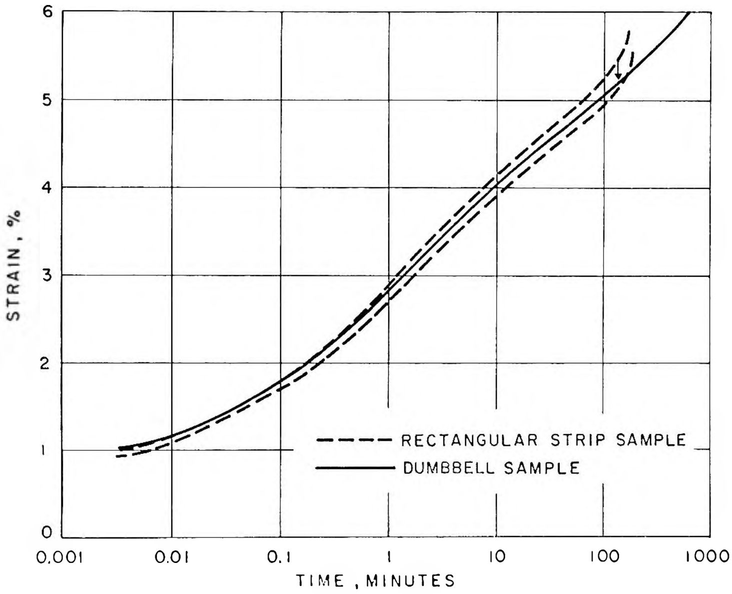

Fig. 8. Comparison of creep curves obtained with rectangular strip specimen and dumbbell specimen.

gage length for all three curves was 1 in. The two duplicate runs made with rectangular strip specimens give the average reproducibility of the present measurements. The creep curve of the dumbbell specimen is shown to agree with those made with rectangular specimens. Similar agreement was found at stresses smaller than 825 psi. However, at 900 psi, the rectangular specimens gave consistently larger strains.

Figure 9 shows creep curves measured at four different loads. The solid lines represent runs made in air, and the dotted lines represent runs made in 25% Igepal CO 630 (an alkylated aryl polyether alcohol) in water solution. All the curves shown in the figure are averages of two repeat runs except the two creep curves in air at 825 psi and 450 psi. The creep curves at these two stresses agree with the creep curves made with rectangular strip specimens.

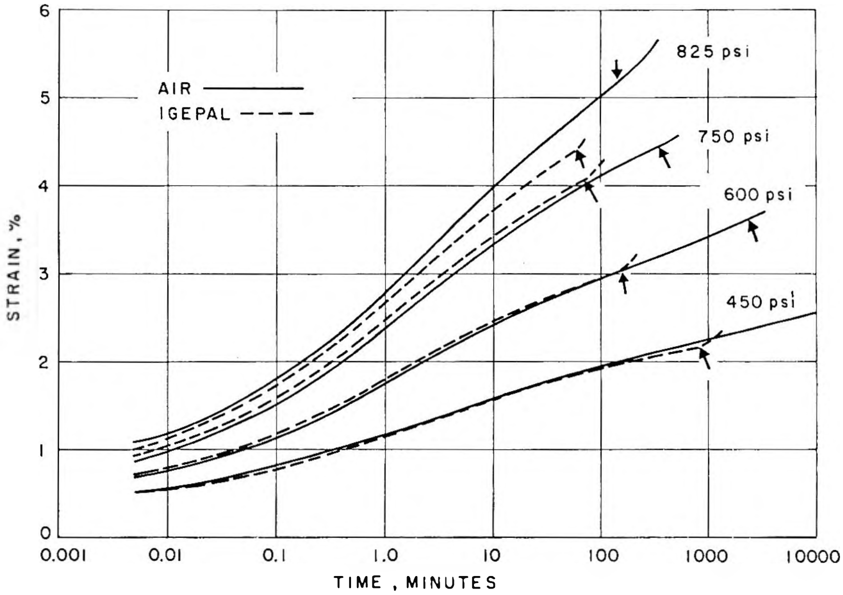

Fig. 9. Creep curves of 3.5 melt index high-density polyethylene.

The breaking time of the runs was taken as the point where the slope of the creep curve began to deviate from the slightly concave curvature. The arrows in Figures 8 and 9 indicate the breaking point of the runs.

The creep curves measured in Igepal do not differ from those measured in air. The largest deviation between the two sets of creep curves is at 825 psi. The discrepancy there is barely larger than the reproducibility shown in Figure 8.

The creep curves shown in Figure 9 are not proportional to the stresses. Omission of mechanical conditioning undoubtedly contributed to this deviation from linear viscoelasticity. As a result, a single creep function cannot be used to represent all the creep curves.

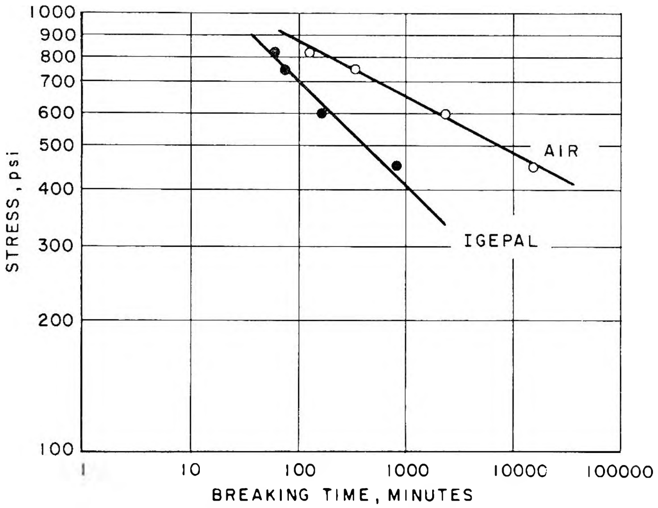

Fig. 10. Stress vs. breaking time of 3.5 melt index high-density polyethylene.

Figure 10 shows breaking time plotted against stress on log-log scale. The data again can be approximately correlated by straight lines. The slope of the line representing runs made in Igepal agrees closely with that of the line correlating Elber and Fischer's[4] data shown in Figure 3. The slope of the other line representing runs made in air, agrees closely with that of the line of Lander's[9] data shown in Figure 3. The slope of Gaube's data[3] was steeper. Gaube observed that runs made in wetting agent and in nonactive environment gave the same slope, a result different from the present data.

Calculation of Critical Strain

The initial portions of the creep curves shown in Figure 9 can be correlated by the equation used by Findley and Khosla[12] for polyethylene:

$$\gamma = \gamma_0 + mt^n \tag{10}$$

TABLE I

Parameters γ_0, m, and n for Creep Curves below 1 Min.

Stress, psi	Environment	γ_0	m	n
450	Air	0.15	1.03	0.200
450	Igepal	0.15	1.00	0.195
600	Air	0.20	1.56	0.219
600	Igepal	0.20	1.60	0.214
750	Air	0.25	2.16	0.236
750	Igepal	0.25	2.25	0.227
825	Air	0.275	2.52	0.224
825	Igepal	0.275	2.36	0.227

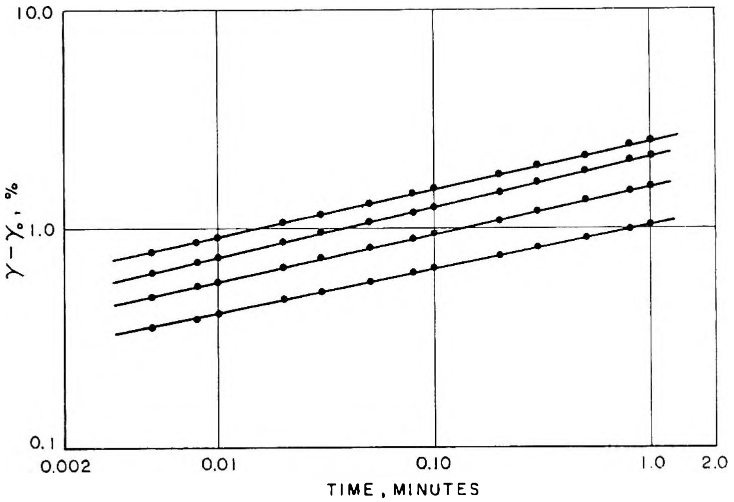

Fig. 11. Curve fitting of the creep curves determined in air with the Findley-Khosla equation. Points in the figure were read from the creep curves.

Figure 11 shows $\gamma - \gamma_0$ versus t on a semilog plot of the runs made in air. Table I shows the values of the parameters γ_0, m, and n for the eight curves shown in Figure 9.

TABLE II
Parameters A and B for Creep Curves above 1 Min.

Stress, psi	Environment	Time interval, min.	A	B
450	Air	1–10	1.18	0.182
		10–100	1.27	0.143
		100–16500	1.29	0.139
450	Igepal	1–10	1.15	0.191
		10–100	1.26	0.143
		100–820	1.38	0.117
600	Air	1–10	1.76	0.286
		10–100	1.89	0.230
		100–2400	1.95	0.217
600	Igepal	1–10	1.80	0.290
		10–170	1.96	0.221
750	Air	1–10	2.41	0.408
		10–100	2.57	0.339
		100–340	2.69	0.304
750	Igepal	1–10	2.50	0.412
		10–76	2.69	0.330
825	Air	1–10	2.80	0.530
		10–135	2.99	0.447
825	Igepal	1–10	2.64	0.477
		10–61	2.83	0.395

The initial strains γ_0 determined through eq. (10) are shown to be proportional to the stress applied. The elastic tensile modulus calculated from γ_0 and the stresses is 300,000 psi.

The creep curves above 1 min. are approximated by straight-line segments on the semilog plot; each segment covers a decade of time increment. Such a segment is represented by the equation

$$\gamma = A + B \log t \tag{11}$$

The parameters A and B determined for these segments are summarized in Table II.

The integration of the first term in eq. (8) was carried out numerically by Gauss' method[13] on a computer. The entire creep curve was integrated in segments by substituting the above empirical equations into eq. (8). A sixteen-term polynomial was used in the Gauss' numerical method for each segment. The empirical equation (11) can also be integrated analytically by series expansion. The results obtained from the two methods of integration agreed to the sixth significant number; much more accurate than

TABLE III

Calculated ϵ_n of Creep Rupture Runs made in Igepal

τ_n, min.	ϵ_n at various stresses 450 psi	600 psi	750 psi	825 psi	Avg. ϵ_n	Standard deviation
50	1.90	2.56	2.68	2.59	2.43	0.31
60	1.90	2.48	2.45	2.33	2.29	0.23
70	1.90	2.39	2.25	2.12	2.16	0.18
80	1.89	2.30	2.08	1.94	2.05	0.16
90	1.89	2.21	1.93	1.78	1.95	0.16
100	1.89	2.12	1.80	1.65	1.86	0.17
300	1.73	1.10	0.75	0.66	1.06	0.42
500	1.47	0.73	0.47	0.41	0.77	0.42

TABLE IV

Calculated ϵ_n of Creep Rupture Runs made in Air

τ_n, min.	ϵ_n at various stresses 450 psi	600 psi	750 psi	825 psi	Avg. ϵ_n	Standard deviation
80	2.29	3.29	3.93	3.56	3.27	0.61
90	2.32	3.29	3.89	3.38	3.22	0.57
100	2.31	3.29	3.83	3.21	3.16	0.55
125	2.35	3.28	3.68	2.85	3.04	0.50
150	2.38	3.28	3.51	2.55	2.93	0.48
175	2.38	3.28	3.34	2.30	2.83	0.49
200	2.38	3.28	3.18	2.10	2.73	0.51
250	2.38	3.28	2.87	1.78	2.58	0.56
300	2.38	3.26	2.61	1.54	2.45	0.62
400	2.38	3.24	2.19	1.21	2.26	0.72
500	2.38	3.21	1.88	1.00	2.12	0.80

required by the precision of present data. The analytical method was more tedious, hence not used.

Table III gives the calculated values of ϵ_n at several relaxation times τ_n for runs made in Igepal.

At a relaxation time of 90 min. the strain ϵ_n is nearest to a constant value. The standard deviation is just slightly larger than the reproducibility of the creep curve.

The values of ϵ_n calculated for the runs made in air are, however, much more scattered. Although the standard deviation is at a minimum when $\tau_n = 150$ min. and $\epsilon_n = 2.93$, the later value can hardly be looked upon as a constant. The calculated results are shown in Table IV.

IV. STRESS RELAXATION MEASUREMENTS

The stress relaxation apparatus is shown in Figure 12. The apparatus is similar to the creep apparatus. A Daytronic force transducer was used to measure the stress. The strain was applied to the specimen by loading the beam rapidly with a large weight. This is done by initially supporting the weight on a laboratory jack. The jack is then lowered by pulling a string prewound on the handle of the jack. The size of the strain is set by the

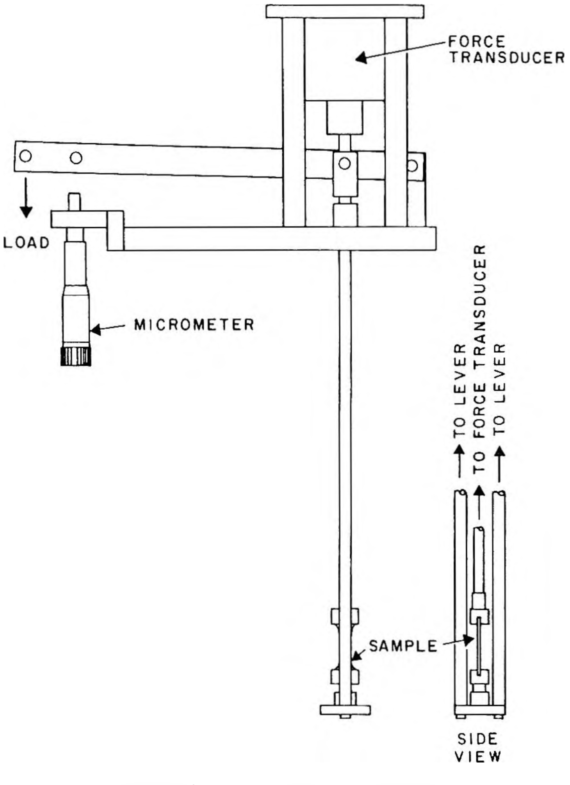

Fig. 12. Stress relaxation apparatus.

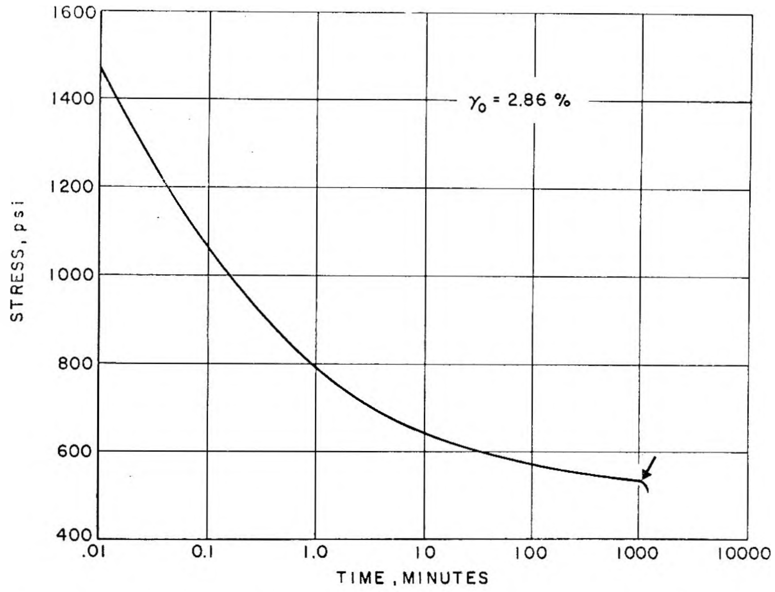

Fig. 13. Stress relaxation curve of 3.5 melt index high-density polyethylene.

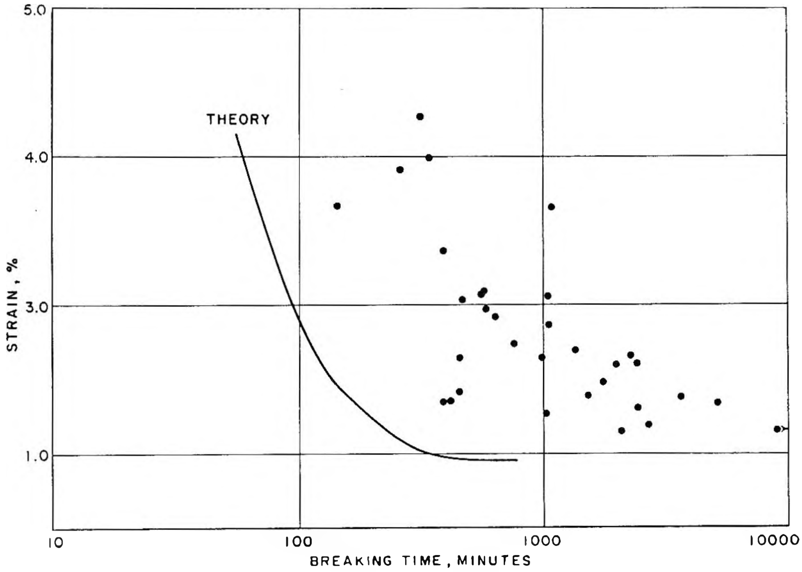

Fig. 14. Strain vs. breaking time of 3.5 melt index high-density polyethylene.

micrometer stop. The actual strain produced is, however, measured by a linear differential transformer (not shown) mounted directly on the supporting rods of the lower sample clamp.

All the stress relaxation runs were made in Igepal. Figure 13 shows a typical stress relaxation curve. The arrow indicates the breaking time.

The breaking times versus strains of the stress relaxation runs are shown in Figure 14. The results are extremely scattered, and it is impractical to use them to solve for ϵ_n and τ_n from eq. (9). The curve shown in Figure 14 is that calculated from eq. (9) by using $\tau_n = 90$ and $\epsilon_n = 1.95$. The only agreement between theory and these experiments is perhaps the prediction that no sample will break if γ_0 is below ϵ_n. One run made at 2.15% strain tested over a week without breaking. Thus it is probable that at strains below 1.95% specimens will remain unbroken for an unlimited amount of time.

V. DISCUSSION

A reason for the scattering of experimental data is probably the lack of rigid control of the thermal history of the specimens used. The specimens were compression-molded in a conventional steam-heated press. After the pressure was applied the mold was rapidly cooled by the circulation of cold water through the plates of the press. The cold water valve was turned fully open rapidly; the exact flow rate and the temperature of the water were not closely controlled. We have found that when the cold water flow rate was deliberately altered, a large deviation in the creep curve was observed. This indicates that the creep curves are sensitive to the fine structure of the polymer. Thus the agreement shown in Figure 9 between the creep curves made in Igepal and air supports the observation of Isaksen et al.[6] that the stress-cracking agents do not alter the structure of the polymer but merely prevent cold drawing of the fibrous material linked across the cracks.

Section III and IV show that there is only limited agreement between theory and experimental results. However, this difficulty can probably be explained by our inability to detect the cracks before some time was consumed in the propagation of these cracks.

According to Isaksen et al.[6] the propagation of the cracks is slower in air than in stress-cracking active environment. The large disagreement between theory and measurements made in air can be accounted for by the influence of the slow crack propagation rate. The rate of propagation of cracks must vary directly with the applied stress as it is shown by Isaksen et al. that the process of cold drawing is involved. We would, therefore, expect to see a larger difference between the breaking time in Igepal and that in air at lower stresses. Figure 10 shows exactly such an effect.

One would also expect the rate of propagation of cracks to be slower in stress relaxation measurements than in creep measurements. At constant total stress any crack formation will shift the stress to a smaller cross-sectional area and thus create a larger stress for the uncracked material, whereas at constant strain no such increase of stress is possible. This effect could be the explanation for the stress relaxation rupture data shown in Figure 14. The experimental breaking times are all longer than that predicted by theory.

Good agreement between the theory and experiments exists for creep measurements made in Igepal where the influence of propagation rate of cracks is small. The standard deviation of the constancy of the critical strain ϵ_n is shown to be in the same order of magnitude as the reproducibility of the creep measurements, in spite of the fact that the specimens were not mechanically conditioned. The agreement of the critical strain ϵ_n calculated from the creep rupture measurements with the critical strain observed for the stress relaxation rupture measurements also strongly supports the validity of the theory.

The author wishes to thank J. A. Moffitt for his help in preparing the computer program for numerical integration.

References

1. Howard, J. B., *SPE J.*, **15**, 397 (1959).
2. Carey, R. H., *Ind. Eng. Chem.*, **50**, 1045 (1958).
3. Gaube, E., *Kunststoffe*, **49**, 446 (1959).
4. Elbers, F., and F. Fischer, *Kunststoffe*, **50**, 485 (1960).
5. Doll, H., and O. Plajer, *Kunststoffe*, **51**, 358 (1961).
6. Isaksen, R. A., S. Newman, and R. J. Clark, *J. Appl. Polymer Sci.*, **7**, 515 (1963).
7. Hopkins, I. L., W. O. Baker, and J. B. Howard, *J. Appl. Phys.*, **21**, 206 (1950).
8. Seely, F. B., and J. O. Smith, *Advanced Mechanics of Materials*, Wiley, New York, 1952.
9. Lander, L. L., *SPE J.*, **16**, 1329 (1960).
10. Faucher, J. A., *Trans. Soc. Rheol.*, **3**, 81 (1959).
11. Leaderman, H., *Elastic and Creep Properties of Filamentous Materials and Other High Polymers*, The Textile Foundation, Washington, D. C., 1943, p. 160.
12. Findley, W. N., and G. Khosla, *SPE J.*, **12**, 20 (1956).
13. Margenau, H., and G. M. Murphy, *The Mathematics of Physics and Chemistry*, 2nd Ed., D. Van Nostrand, Princeton, N. J., 1956.

Résumé

On étudie le crevassement du polyéthyléne sous tension pour déterminer la déformation critique. On se base sur une théorie qui permet d'expliquer la farimation des crevasses. On a étudié à 60°C le crevassement sous charge constante et sous déformation constante. On a utilisé un polyéthyléne de haute densité d'indice de fusion 3.5. On a trouvé une déformation critique de 1.95% associée à un temps de relaxation critique de 90 minutes. On a trouvé un bon accord entre théorie et expériences faites sur Igepal CO 630. Un certain désaccord entre la théorie et les expériences faites à l'air, a été attribué à une vitesse anormale de propagation des crevasses.

Zusammenfassung

Die Spannungs-Rissbildung in Polyäthylen wurde vom Gesichtspunkt der kritischen Verformung auf Grundlage einer für die Rissbildung vorgeschlagenen Theorie unter sucht. Die Spannungs-Rissbildung wurde bei konstanter Belastung und Verformung experimentell bei 60°C. an einem Polyäthylen hoher Dichte mit Schmelzindex 3,5 bestimmt. Für die Probe wurde eine kritische Verformung von 1,95% mit einer kritischen Relaxationszeit von 90 Minuten gefunden. Versuche an Igepal CO630 standen in guter Übereinstimmung mit der Theorie. Gewisse Widersprüche zwischen Theorie und Versuch wurden der Wachstumsgeschwindigkeit der Risse zugeschrieben.

Received July 13, 1964
Revised August 17, 1964

JOURNAL OF POLYMER SCIENCE: PART A VOL. 3, PP. 1063-1067 (1965)

Rates of Sulfonation of Polystyrenes Crosslinked with Pure *p*-, 2:1/*m*:*p*-, and Commercial Divinylbenzenes

RICHARD H. WILEY and T. K. VENKATACHALAM, *Department of Chemistry, University of Louisville, Louisville, Kentucky*

Synopsis

Data for the rates of sulfonation of polystyrene crosslinked with 2, 4, and 8% pure *p*-, 2:1/*m*:*p*-, and commercial divinylbenzenes at 60 and 80°C. have given activation energies varying from 11,520 to 40,190 cal./mole. Rates are lowest and activation energies highest for the *p*-divinylbenzene crosslinked structures. This is attributed to differences in rates of diffusion through the different types of network structures and is consistent with previously noted decreased swelling ratios for the *para* crosslinked types.

Bead copolymers prepared from styrene crosslinked with pure *m*- and *p*-divinylbenzenes (DVB) and mixtures of these have been found to vary significantly in their swelling ratios in both the unsulfonated and sulfonated forms.[1] The *p*-DVB crosslinked copolymers and resins swell less than do those crosslinked with *m*-divinylbenzene and mixtures of *meta* and *para* isomers. This may also be related to a modification in the rates of diffusion-controlled processes within the differently crosslinked structures. It is not unreasonable to expect that the copolymer beads obtained with the use of different crosslinking agents may sulfonate at different rates. This investigation was undertaken to determine the conditions under which such a differentiation might be observed and to obtain quantitative comparisons of rates of sulfonation for the differently crosslinked structures.

For this study we have measured the increase in capacity with time to determine the rate of sulfonation. The feasibility of this approach was indicated in an observation by Pepper[2] that there is an observable change of capacity with increasing time of sulfonation. Concentrated sulfuric acid has been used as the sulfonating agent. The copolymer beads were swollen in ethylene dichloride prior to sulfonation. Preliminary experiments established that with 0.5% benzoyl peroxide initiator rates of sulfonation at 60 and 80°C. were suitable for rate studies. At 2% initiator concentration and 80 or 100°C., there was no differentiation in rates.

EXPERIMENTAL

Materials

Bead copolymers of styrene, crosslinked with 2, 4, and 8 mole-% of different divinylbenzenes were prepared in the presence of 0.5% benzoyl peroxide initiator as previously described.[1] The monomers were obtained and purified as previously described.[1,3] Commercial divinylbenzene (Dow) was used after distillation to remove inhibitor.

Sulfonation Procedure

About 5 g. of copolymer beads in the 20–30 mesh range were preswollen in 100 ml. of distilled ethylene dichloride for 15 hr. and the excess dichloride removed by vacuum filtration on a sintered glass Buchner funnel. Concentrated sulfuric acid (20 ml., 96.2%) was used to flush the swollen beads through a wide, long-stemmed funnel into a 250-ml., three-necked, round-bottomed flask containing 130 ml. of the same acid maintained at the specified temperature in an oil bath. The flask was fitted with a stirrer and an air condenser closed with a silica gel drying tube. After checking that all the beads were in the acid, stirring was started and the speed was so regulated that all the beads were dispersed under the surface of the liquid. The same approximate speed, as determined with a tachometer, was maintained in the sulfonation of different samples.

Samples of the beads were taken out at regular intervals and diluted with decreasing strengths of sulfuric acid and finally with distilled water as previously[1] described. The total capacity of the beads at different times of sulfonation was also determined by the method used previously.

DISCUSSION

The 0.5% initiated resins crosslinked with 4 and 8% *p*-DVB show significantly decreased rates of sulfonation at 60 and 80°C. as compared to rates for resins prepared with a 2:1 mixture of *meta* and *para* isomers (2:1/*m*:*p*-) and commercial divinylbenzenes. The data are given in Table I and II. The decreased rates at 80°C. are apparent in the 4% *p*-DVB resins in the first 20 min. and in the 8% resins over a 4-hr. time span. In the 60°C. measurements the rate is noticeably lower for the 4% *p*-DVB resins up to 3 hr., and a decrease is also apparent in the 2% *p*-DVB resins. Also, the 2 and 4% 2:1/*m*:*p*-DVB resins react more slowly than do the commercial DVB resins at 60°C.

Activation energy values calculated from plots of the 60 and 80°C. rate data (0.5% initiator) are given in Table III. The calculations are based on the slopes in the initial linear region and give values of 11,520–40,190 cal./mole. The activation energies increase with increasing amounts of crosslinking divinyl compound. As with rates of exchange, such an increase indicates that a diffusion controlled process is involved. Furthermore, the fact that the largest increase in E_A is observed for resins with the *p*-divinylbenzene crosslinkage is consistent with previously noted[1] decrease in swelling ratios for the unsulfonated and sulfonated *para* crosslinked resins. Both of these observations are attributable to a decreased permeability of the *p*-divinylbenzene crosslinked structure with its presumed clustering of crosslinkages. Other evidences of diffusion control

TABLE I
Rates of Sulfonation at 60°C. of Polystyrene Crosslinked with Various Divinylbenzene Samples (0.5% Initiator)

Divinyl, mole-%	Time, min.	Capacity of samples crosslinked with DVB, meq./g.		
		C-DVB[a]	p-DVB[b]	2:1/m:p-DVB[c]
2	10	0.38	—	—
2	20	1.12	0.66	0.48
2	30	1.98	1.51	1.38
2	40	2.87	2.27	2.29
2	60	4.15	3.53	3.69
2	80	4.82	4.39	4.54
2	100	5.15	4.89	4.92
2	120	5.31	5.34	5.38
4	15	0.67	—	0.12
4	30	1.68	0.52	0.85
4	45	2.84	1.06	1.52
4	60	3.58	1.55	2.04
4	75	4.33	2.15	2.70
4	90	4.54	2.50	3.04
4	120	5.02	3.68	4.19
4	150	5.23	4.32	4.80
4	180	5.27	5.31	5.35
8	45	0.464	—	0.497
8	90	1.19	—	1.04
8	135	1.84	—	1.52
8	180	2.54	0.197	2.10
8	270	4.27	—	3.35
8	360	5.07	0.256	5.05
8	540	—	0.364	—
8	1440	—	0.707	—

[a] C-DVB, commercial divinylbenzene (Dow).

[b] p-DVB, pure p-divinylbenzene.

[c] 2:1/m:p-DVB, 2:1 mole ratio *meta:para* isomer mixture as separated by vapor-phase chromatography from C-DVB.

of the sulfonation, such as rate alterations with different resin particle sizes and altered agitation, are under study. The available data indicate that the sulfonation process can be improved in terms of uniformity and performance specifications if a pure divinylbenzene isomer is used to establish the crosslinked network.

The alternative to diffusion control of the rate of sulfonation is a chemical reaction rate control. The E_A values for the resins are, however, considerably higher than those obtained for various aromatic hydrocarbons. For m-xylene, toluene, and benzene sulfonated in nitrobenzene with concentrated sulfuric acid the activation energies are 6400, 6790, and 7500 cal./mole.[4] It is also recognized[5] that sulfonation of the various dialkylbenzenes proceeds at different rates. The *para* isomer sulfonates least readily of the three. The increase in activation energy, and decreased

TABLE II
Rates of Sulfonation at 80°C. of Polystyrene Crosslinked with Various Divinylbenzene Samples (0.5% Initiator)

Divinyl, mole-%	Time, min.	Capacity of samples crosslinked with DVB, meq./g.		
		C-DVB	*p*-DVB	2:1/*m*:*p*-DVB
2	5	0.498	0.833	1.08
2	10	2.20	2.33	2.43
2	15	3.47	3.37	3.44
2	20	4.22	4.15	4.07
2	25	4.81	4.78	4.53
2	30	5.07	5.00	4.87
2	40	5.31	5.26	5.27
2	60	5.35	5.33	5.35
4	5	0.53	0.098	0.669
4	10	1.88	0.598	1.48
4	15	2.76	1.51	2.23
4	20	3.45	2.48	2.77
4	30	4.43	3.52	3.61
4	40	4.90	4.16	4.33
4	60	5.25	4.98	4.94
4	90	5.26	5.39	5.35
8	15	1.03	0.296	1.12
8	30	2.16	0.54	2.32
8	60	4.11	1.02	3.94
8	90	4.97	1.34	4.80
8	120	5.14	1.99	5.13
8	150	5.18	2.41	5.20
8	180	5.25	—	5.23
8	240	5.25	4.01	5.23

TABLE III
Activation Energies for Sulfonation of Polystyrenes Crosslinked with Various Divinylbenzenes

	Activation energies for various degrees of crosslinking, cal./mole[a]		
Divinylbenzene	2 mole-% DVB	4 mole-% DVB	8 mole-% DVB
C-DVB	11,520	14,350	18,130
p-DVB	14,140	21,840	40,190
2:1/*m*:*p*-DVB	11,740	15,390	20,803

[a] Values from initial linear slopes of rate of sulfonation data at 60 and 80°C. for resins prepared with 0.5% dibenzoyl peroxide initiator.

rate, for the sulfonation of the copolymer beads containing enhanced amounts of the *para* crosslinking structures are qualitatively in accord with this decreased reactivity of the *para* structure. The rather substantial (2.8-fold) increase from 14,140 cal./mole to 40,190 cal./mole accompanying the increase from 2 to 8% *p*-divinylbenzene appears, however, to be more than can be attributed to this degree of structural alteration. There is at most but 8% of disubstituted benzene nuclei present. Linear extrapolation to 100% *p*-divinylbenzene indicates an unrealistically high value for the activation energy. These considerations do not seem to be in accord with a chemical reaction rate control of the sulfonation process for the resins.

This study was supported in part by the Atomic Energy Commission under Contracts AT-(40-1)-229 and AT-(40-1)-2055 between the University of Louisville and the Atomic Energy Commission. Final preparation of the manuscript was completed during tenure of one of us (RHW) as a visiting professor in the Graduate Division of the City University of New York.

References

1. Wiley, R. H., J. K. Allen, S. P. Chang, K. E. Musselman, and T. K. Venkatachalam, *J. Phys. Chem.*, in press.
2. Pepper, K. W., *J. Appl. Chem. (London)*, **1**, 124 (1951).
3. Wiley, R. H., and R. M. Dyer, *J. Polymer Sci.*, **A2**, 3153 (1964).
4. Stubbs, F. J., C. D. Williams, and F. N. Hinshelwood, *J. Chem. Soc.*, **1948,** 1065.
5. Clarke, H. T., and E. R. Taylor, *J. Am. Chem. Soc.*, **45,** 830 (1923).

Rèsumè

Les résultats obtenus pour les vitesses de sulfonation du polystyrène ponté au moyen de 2,4-divinylbenzène et de 8% de *para*divinylbenzéne pur, d'un mèlange 2/1 *meta-para* et de divinylbenzéne commercial à 60 et 80° ont donné des énergies d'activation variant de 11.520 à 40.190 calories par mole. Les vitesses sont les plus faibles et les énergies d'activation les plus élevées, pour le *para*-divinylbenzéne à structure pontée. Ceci est attribué aux différences de vitesse de diffusion à travers les différents types de structures réticulaires et ceci est compatible avec les rapports décroissant des groupements observés antérieurement pour les types *para*-pontés.

Zusammenfassung

Die Sulfonierungsgeschwindigkeit von mit 2,4 und 8% reinem *para*-, 2:1/*m:p*- und handelsüblichem Divinylbenzol vernetztem Polystyrol bei 60° und 80°C lieferte Akivierungsenergien von 11, 520 bis 40, 190 cal/Mol. Die niedrigsten Geschwindigkeiten und höchsten Aktivierungsenergien treten bei den *para*-Divinylbenzol-vernetzten Strukturen auf. Dieser Umstand wird auf Unterschiede bei der Diffusion durch die verschiedenen Neztwerkstrukturtypen zurückgeführt und steht mit dem früher festgestellten kleineren Quellungsgrad *para*-vernetzter Typen in Übereinstimmung.

Received July 15, 1964
Revised October 8, 1964

JOURNAL OF POLYMER SCIENCE: PART A VOL. 3, PP. 1069-1077 (1965)

Localized Deformation of Lamellar Polyethylene Crystals

D. H. RENEKER, *Engineering Materials Laboratory, Engineering Research Division, Engineering Department, E. I. du Pont de Nemours & Company, Inc., Wilmington, Delaware*

Synopsis

The mechanical and morphological properties of lamellar crystals of polyethylene were studied by deliberately deforming the crystals with a localized strain of known direction and amplitude. In most of the experiments the deformation was achieved by placing the polymer crystals on a thin, brittle, electron-transparent substrate which was supported by a plastic film. Elongation of the plastic film cracked the brittle substrate, and the polyethylene crystals either broke or were converted into fibers and drawn across the cracks. The breaking and drawing properties of the crystal are related to the orientation of the crystal with respect to the crack and to the intersection of fold domains by the crack. Localized deformation of crystals in suspension by ultrasonic irradiation and by other means is discussed.

Introduction

This paper describes an experimental method for producing and observing localized deformations in lamellar crystals, as well as some results of applying the method to crystals of polyethylene.

Examples of lamellar polymer crystals which were mechanically drawn or broken in the course of handling have been shown by Geil[1a] and by Lindenmeyer.[2] Other work describes crystals that were deformed by scratching with a needle,[3] by collapsing or folding from a suspension onto a flat substrate,[3,4] and by shearing between glass plates.[5] It is generally observed that the lamellar crystals break along lines parallel to the growth faces and draw into fibers (or "fibrils") when separated along other lines. The polymer molecules in the lamellar crystal are converted from a folded conformation to a fiber conformation. An abrupt transition region ("neck") distinguishes localized drawing from the more homogeneous processes which may occur during the deformation of lamellar crystals embedded in a bulk polymer,[6,7] or in gutta-percha,[5b] or supported by a uniformly drawn substrate.[8] However, localized drawing is observed[1b] under suitable conditions during deformation of bulk polymers which adopt a lamellar morphology during crystallization from the melt.

Experimental Method

The important morphological details of lamellar polymer crystals have been summarized by Geil.[1a] A 25-μ-thick sheet of Mylar polyester film was placed in a stretcher of the sort shown in Figure 1. A layer of graphite of a thickness suitable for use as a substrate in electron microscopy was evaporated onto the film. A few drops of a suspension of crystals were distributed evenly over the graphite and the liquid allowed to evaporate. This left the crystals firmly attached to the graphite layer. As the plastic film was stretched a small amount (<1% strain), the graphite cracked at 5–15 μ intervals. The intervals were smaller for thin layers of graphite. The cracks spread across the sample at a rate too high to follow and reached a width of the order of 0.1 μ. As stretching continued to strains of 5–20%, the initially formed cracks became wider, and more cracks were formed. The strain rate to which a polymer crystal was subjected was therefore initially high as the crack formed and then decreased as more cracks formed at higher elongations. The film contracted laterally and caused the graphite layer to buckle or corrugate, with the corrugations lying parallel to the draw direction. The large and highly localized deformation of the part of the polymer crystals over the crack frequently caused the lamellar crystals to be converted to fibers, as shown schematically in Figure 1.

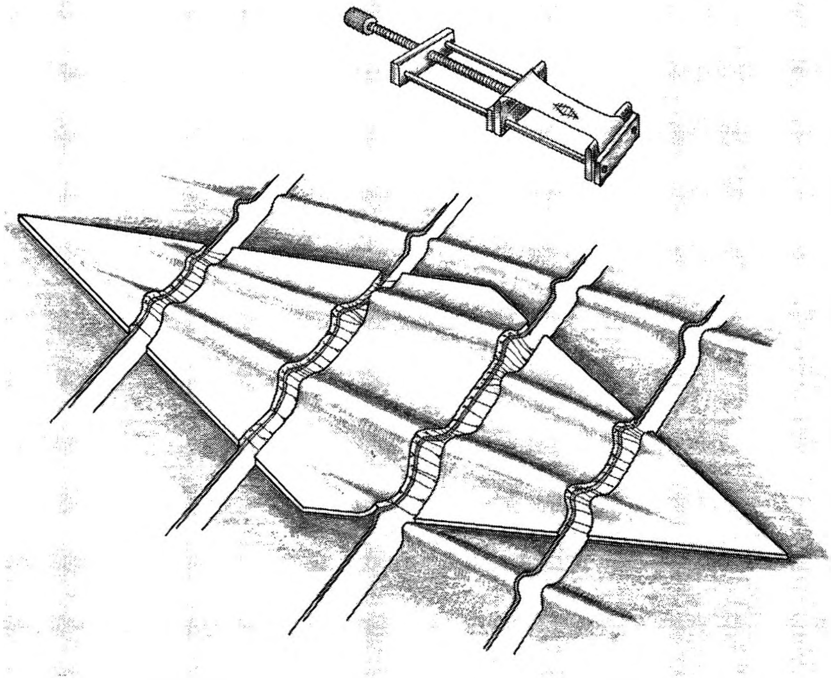

Fig. 1. Sketch showing the method used to produce a localized deformation of a lamellar crystal. The size of the crystal on the stretcher is exaggerated.

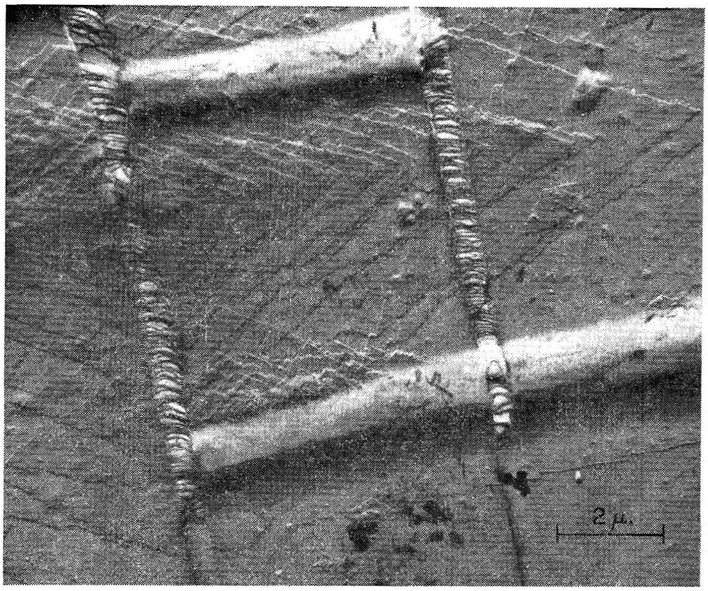

Fig. 2. Crystals which were locally drawn. The crystals were shadowed with chromium at an angle of $\tan^{-1} {}^5/_7$ from the lower right so the corrugations appear as nearly horizontal black and white bands. In the original micrograph very thin fibers were evident in the regions one lamella thick at the bottom of both cracks.

After the deformation process was completed, the crystals (still held on the film in the stretcher) were shadowed with chromium from a direction normal to the draw direction. After shadowing, the crystals and the carbon substrate were stripped from the film with polyacrylic acid and mounted on the specimen grid of an electron microscope for observation. Figure 2 shows an area containing crystals which range from one to about 25 lamellae in thickness, drawn by the above technique.

Results

The polyethylene used for this series of experiments was an essentially linear, high molecular weight, low melt index Alathon resin. The crystals were precipitated from a dilute solution of tetrachloroethylene by slow cooling. The crystals were pyramidal[3,9] and, therefore, underwent a shearing or rotational deformation to be flattened on the flat graphite layer. The results indicate that the common orientation of folds in each fold domain was retained even after the pyramidal crystal had collapsed.

In fold domains where the crack in the graphite substrate was parallel to the growth face, the crystal separated with the formation of only a few fibers which usually did not extend across the crack. If the same crack was followed across a fold-domain boundary into a domain with differently oriented folds, many fibers were drawn across the crack. Figure 3 shows an example of a crack intersecting the tip of a lamellar crystal. The crack made an angle of 28° with the [100] fold-domain boundary. The $\{110\}$

fold planes of polyethylene made an angle of 33.4° with the same fold-domain boundary. On the left of the fold-domain boundary where the crack is nearly parallel to the growth face, the crystal separated with no fibers crossing the crack. On the right, a number of closely spaced fibers were drawn across the crack.

In the part of the crack shown in Figure 3 which lies to the left of the fold-domain boundary, a few small stubs formed along the upper edge of the crack. The stubs probably resulted from the fact that the crack was not exactly parallel to the fold planes.

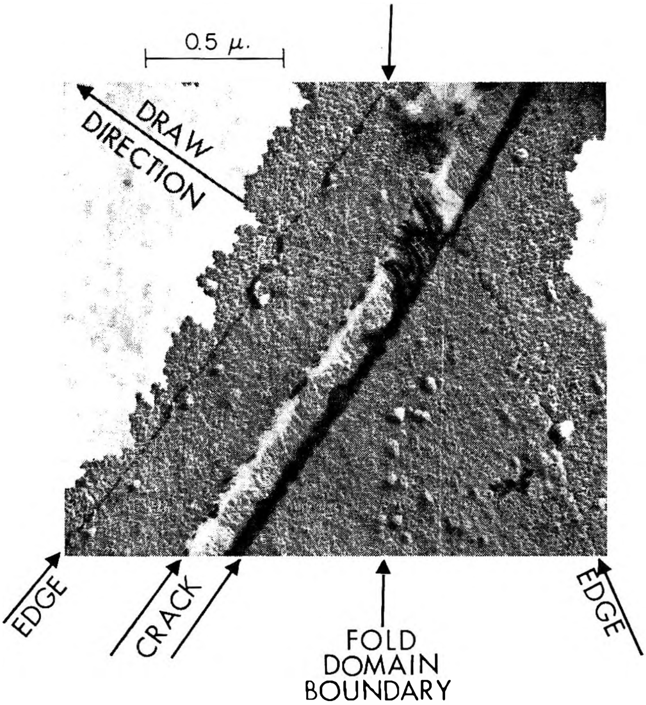

Fig. 3. A region of polyethylene crystal intersected by a crack which runs nearly parallel to a growth face and crosses a fold-domain boundary. Fibers were drawn across the crack in the right fold domain, but not in the left. The chromium shadow material was lost from the upper left corner of the area shown.

Figure 4 shows the arrangement of the folds at the top surface of a flat lamellar crystal with $\{110\}$ growth faces. The molecular axes are normal to the plane of the crystal. The crystal is separated into two parts by a crack. In the upper left fold domain, the crystallographic planes containing the crack and the molecular axes are connected only by van der Waal's forces, so the crystal can separate easily in this fold domain. In the adjacent fold domains the same planes are connected by the much stronger covalent bonds in the folds. The polymer molecules are stripped off the face of the crystal and drawn across the crack in these fold domains.

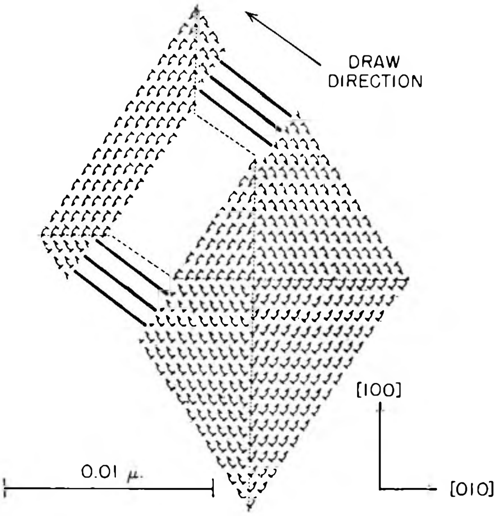

Fig. 4. Diagram showing the structure of a lamellar polyethylene crystal viewed from the top in a direction parallel to the chain axis. The plane of the carbon zig zag is indicated by the short straight lines. The molecular folds at the top of the crystal are shown as curved lines connecting adjacent molecules. Localized drawing of the crystal is indicated along a crack parallel to the growth face in the second quadrant. The presence of folds which cross the crack causes the crystal to be drawn in the first and third quadrants. In the second quadrant no molecules extend across the crack and the crystal fails without drawing into fibers. Note that the crack in the second quadrant is slightly narrower than the length of the fibers in the first and third quadrants. This change in crack width can be used to estimate the draw ratio.

Figure 5 shows a larger area of the same crystal shown in Figure 3. In the lower left corner of the figure occasional fibers were drawn across the crack. These fibers resulted from the interaction of the crack with the small fold-domain boundaries[4] associated with the slightly dendritic growth face.

In most cases superposed lamellae necked and drew in the same region. A few exceptions to this rule were observed, and one such exception is shown in Figure 6. A lower magnification view showing the growth faces of the lamella in contact with the substrate indicates that there were three lamellae in the area above the crack and that the *b* axis of the crystal was parallel to the fibers. Drawn fibers associated with each of the three lamellae can be distinguished at the top edge of the crack. A relative sliding motion of intact lamellae occurred to produce the thumb-shaped region of undrawn crystal, indicated by the star. The black shadow line (indicated by the two arrows) suggests that the lamella in contact with the graphite underwent a homogeneous reduction in thickness in the area between the black line and the upper edge of the crack. Such a homogeneous change in thickness could occur, for example, if the angle between the molecular axis and the plane of the substrate decreased (i.e., the molecular segments tilted) as a result of the deformation.

Fig. 5. A lower magnification view of the crystal shown in Figure 3. Fibers drawn across the crack in the lower left part of the figure result from the presence of small fold domains associated with the growth faces of the dendrites.

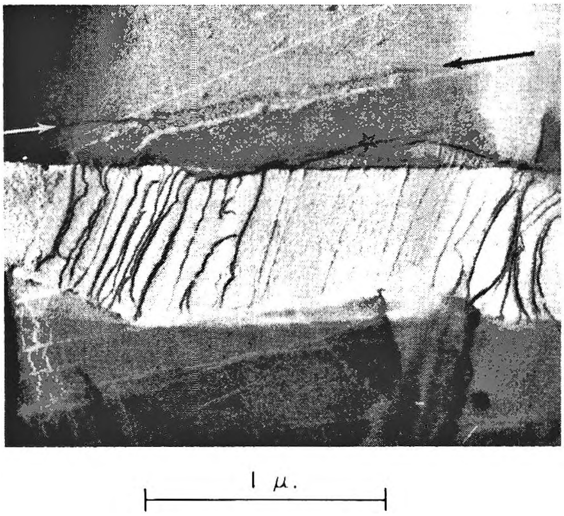

Fig. 6. Region where three superposed lamellae were drawn.

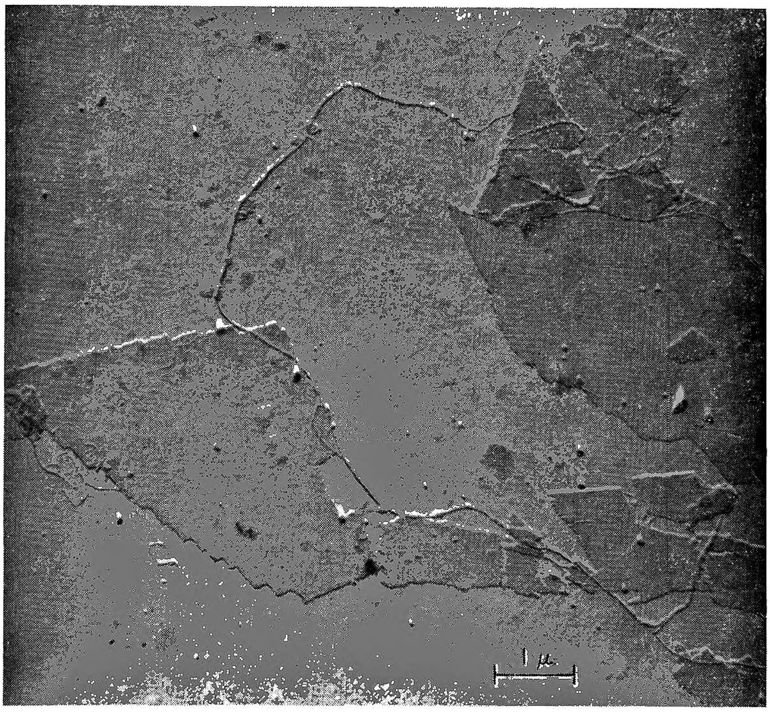

Fig. 7. Lamellar polyethylene crystal broken and drawn by ultrasonic irradiation in a tetrachloroethylene suspension at room temperature. The crystal has broken along [110] planes which are parallel to growth faces, but has drawn into fibers when the breaks are in a different direction. The parts of the broken crystal in the figure are held together by the fibers.

The smallest fibers in Figure 6 (below the star) were less than 50 A. in diameter and, therefore, contained fewer than 130 polyethylene molecules in any cross section. It is interesting to note that the lengths of the individual molecules in these small fibers ranged from one tenth the fiber length to about equal the fiber length.

It is possible to define a draw ratio as the ratio of the length of the fiber to the length (measured in the draw direction) of the part of the lamellar crystal which is converted into fibers. Assuming that the molecules are completely extended, the draw ratio would have a value of l/d, where l is the thickness of the crystal and d is the spacing of the lattice planes perpendicular to the draw direction. For a polyethylene crystal 0.01 μ thick, the draw ratio necessary to completely unfold the molecules would range from 24 for the draw direction normal to nongrowth face $\{110\}$ planes to 14 for the draw direction parallel to the $\vec{a}$ axis. The micrographs are sufficiently detailed to permit estimates of the draw ratio to be made in a few cases. These estimates range between 4 and 20.

Some other procedures for producing localized deformation of polymer crystals were investigated. Polyethylene crystals were deformed into fibers and also broken along planes parallel to growth faces by ultrasonic cavitation bubbles produced in the suspension liquid at room temperature. Figure 7 shows a crystal which was subjected to high intensity 90-kcycle ultrasonic irradiation at room temperature. At temperatures near, but below the dissolving temperature, crystals in suspension were converted into beaded fibers by ultrasonic irradiation, gentle stirring, air bubbles, splashing, passage through an atomizer or other similar treatments. The beaded fibers appeared to consist of "beads" or "frills" of polymer in folded chain crystals connected by short lengths of drawn fiber. A number of micrographs[1c,1d,10-12] showing such "beaded" structures in polyethylene and polyoxymethylene have been published. In all cases the possibility of stirring existed while the crystals were in a warm suspension, although other explanations for the beaded structures were advanced.

Conclusions

Localized deformation produced by the cracks in a strained brittle layer provides a useful way of investigating the mechanical properties of lamellar crystals of polymers. Fold domains in which the fold planes are parallel to the crack break without drawing fibers, while adjacent but differently oriented fold domains are drawn into fibers. The transition region between the lamellar crystal and the fibers is complicated and abrupt, being approximately as long as the crystal is thick. The crystals neck laterally or "unravel" to form fibers. The fibers show a tendency to cohere, particularly in regions where several lamellae are superposed. Sliding of superposed lamellae and homogeneous changes in thickness of lamellae may occur.

Modifications of the experiment should provide more information about the mechanical properties of lamellar crystals and other small objects. The crystals will be subjected to a different kind of strain than that studied above if, for example, narrow cracks in the brittle layer are formed before the crystals are deposited, if the brittle layer is prepared with some more complicated pattern, or if the film is stretched in two directions simultaneously.

R. B. MacLaughlin assisted with most of these experiments. Figure 1 was prepared by Werner Yllo.

References

1. Geil, P. H., *Polymer Single Crystals,* Interscience, New York, 1963, (a) see Figs. VII-28, VII-29, also VII-38; (b) pp. 432, 436–438; (c) p. 470; (d) p. 446.
2. Lindenmeyer, P. H., *J. Polymer Sci.*, **C1**, 5 (1963).
3. Reneker, D. H., and P. H. Geil, *J. Appl. Phys.*, **31**, 1916 (1960).
4. Geil, P. H., and D. H. Reneker, *J. Polymer Sci.*, **51**, 569 (1961).
5. Fischer, E. W., in *Polymer Single Crystals*, P. H. Geil, Interscience, New York, 1963, (a) p. 104; (b) p. 442.
6. Speerschneider, C. J., and C. H. Li, *J. Appl. Phys.*, **33**, 1871 (1962).
7. Geil, P. H., F. R. Anderson, B. Wunderlich, and T. Arakawa, *J. Polymer Sci.*, **A2**, 3707 (1964).
8. Geil, P. H., *J. Polymer Sci.*, **A2**, 3813 (1964).

9. Niegisch, W. D., and P. R. Swan, *J. Appl. Phys.*, **31**, 1906 (1960).
10. Bassett, D. C., and A. Keller, *Phil. Mag.*, **7**, 1553 (1962).
11. Hirai, N., H. Kiso, and T. Yasiu, *Kobunshi Kagaku*, **19**, 64 (1962).
12. van der Heijde, H. B., *Nature*, **199**, 798 (1963).
13. Kobayashi, K., to be published.

Résumé

On a étudié les propriétés mécaniques et morphologiques de lamelle de polyéthyléne en déformant les cristaux par une déformation localisée dont on connait la direction et l'intensité. Dans la plupart des expériences, on provoque la déformation en placant les cristaux de polymère sur un support mince, cassant transparent aux électrons, supporté par un film plastique. L'allongement du film plastique rompt le substrat-cassant, les monocristaux se cassent ou sont transformés en fibres ou filés entre les fentes. Les propriétés de rupture et d'étirage du cristal dépendent de l'orientation du cristal par rapport à la fente et de l'intersection du domaine de repliement avec la fente. On discute aussi de la déformation des cristaux par des ultrasons et par d'autres moyens.

Zusammenfassung

Die mechanischen und morphologischen Eigenschaften von lamellaren Polyäthylenkristallen wurden durch absichtliche Deformation der Kristalle mit einer lokalisierten Beanspruchung von bekannter Richtung und Amplitude untersucht. Bei den meisten Versuchen wurde die Deformation durch Aufdringung der Polymerkristalle auf ein dünnes, sprödes, elektronendurchlässiges Substrat erreicht, welches durch einen Kunststoffilm getragen wurde. Eine Dehnung des Kunststoffilms führte zur Rissbildung in dem sproden Substrat, wobei die Polyäthylenkristalle entweder zusammenbrachen oder in Fasern umgewandelt und entlang der Risse gedehnt wurden. Die Bruch- und Dehnungseigenschaften des Kristalls stehen zu seiner Orientierung zum Riss und zur Durchsetzung von Faltungsbereichen durch den Riss in Beziehung. Die lokalisierte Deformation von Kristallen in Suspension durch Ultraschall und andere Mittel wird diskutiert.

Received June 19, 1964
Revised August 31, 1964

JOURNAL OF POLYMER SCIENCE: PART A VOL. 3, PP. 1079–1106 (1965)

Proton Magnetic Resonance Study on the Structures of Phenol–Formaldehyde Resins

JAMES C. WOODBREY, HAROLD P. HIGGINBOTTOM, and HARRY M. CULBERTSON,* *Plastics Division, Research Department, Monsanto Company, Springfield, Massachusetts*

Synopsis

Because of their commercial importance, the reaction sequences and structures of resins produced when phenol reacts with formaldehyde have been studied by numerous different chemical and physical methods. Many details concerning these reactions and complex chemical structures are still not entirely understood. Most of the experimental methods used have yielded only qualitative information. Many of these methods have been applicable only to the lower molecular weight portions of soluble prepolymers. The present work describes proton magnetic resonance (PMR) methods which yield detailed and quantitative number-average structures for any soluble phenol-formaldehyde resin. It is shown that benzyl-type hemiformals make substantial contributions to the structures of many resoles and that these functionalities exhibit relatively high stability under certain conditions of initial cure. The structures of several resins are discussed in terms of certain aspects of reactions which occurred during the resin syntheses. These reactions include hydroxymethylations and condensations yielding diphenylmethane-type and dibenzyl ether-type bridges. To define the mechanisms and rates of the various reactions at different temperatures and under different catalytic conditions, a much more detailed study is required. Potentially, the PMR methods described can provide most of the necessary quantitative data.

Phenol–formaldehyde polymers, the first entirely synthetic resins to be developed commercially, have been the subject of a large number of investigations during the last 50 years. The chemical reactivity and structures of these resins are still much less than perfectly understood.[1] This testifies to the complexity of these systems and to the ingenuity of earlier workers who developed many useful materials, frequently on purely empirical grounds. Complexity and, in many instances, chemical reactivity have been impeding factors to the elucidation of structures in the common types of soluble prepolymer mixtures. Ideally, it would be desirable to determine the structure and concentration of each component formed when phenol, formaldehyde and their derivatives react under any set of conditions. Since this is not always feasible or even possible by existing methods, one must resort to determining the amounts of various functional groups present. These groups most commonly include methylene or ether

---

* Present address: Monsanto Chemicals (Australia) Ltd., Melbourne, Australia.

bridges joining adjacent phenolic nuclei at the *ortho* or *para* positions and reactive hydroxymethyl groups on similar ring locations.

Chemical methods have been applied to the measurements of total hydroxymethyl[2] and ether-bridge[3] contents in phenolic resins, without regard to the number and positions of these groups in relation to the number of phenolic nuclei and the positions of phenolic hydroxyl groups. Infrared spectrophotometry has been used to detect vibrational absorptions characteristic of certain functional groups; e.g., hydroxymethyl groups,[4] and average degree and position of substitution on the phenolic rings.[4–6] Infrared spectroscopy has been one of the few useful methods applicable to the study of structures of insoluble, cross-linked phenolics.[7] Most of the results from the infrared methods are, however, only qualitative. Paper chromatographic techniques, as applied by Freeman,[8] Reese,[9] and others, have been of value in studying the very early stages of reaction sequences. Concentrations of the various hydroxymethylated phenols and some of the dinuclear components may be determined by these latter methods. Recently, vapor-phase chromatographic (VPC) methods have been used to determine the concentrations of specific mononuclear components in resole prepolymers, which were deactivated by acetylation prior to analysis.[10] X-ray studies have yielded information on the geometrical arrangements of some of the lower molecular weight, crystalline resin components.[1] The type and amount of information obtainable by any single experimental method is quite limited. A specific method is often not applicable to all types and molecular weight ranges of even soluble resins. Further, most of the methods are not quantitative or are of questionable accuracy.

High-resolution proton magnetic resonance (PMR) on soluble novolac prepolymers has yielded direct measurements on the relative amounts of methylene bridges located at different positions on the phenolic rings.[11] The present work was undertaken to explore the applicability of PMR to structural determinations on the more complex resole-type resins. Results obtained describe in detail the number-average structures of many different types of these materials. Certain functionalities are shown to contribute much more than expected to the overall structures of certain prepolymers and their partially cured products. The relationship of structural results to certain aspects of chemical reactions are discussed.

EXPERIMENTAL

Materials Used

Most of the model compounds examined were prepared in this laboratory, while the rest were the gift of Professor W. J. Burke of the Arizona State University. All of the resins examined were prepared from phenol and formalin or paraformaldehyde via the usual methods of acid or base catalysis in the temperature range of 60–90°C. Preparative data on some of the resins studied are summarized in Table I. The acetylated materials were obtained from the freeze-dried parent hydroxy compounds, via treatment

TABLE I
Preparations of Selected Novolacs and Resoles

Sample designations	Catalyst and pH	Initial F/P[a] and source of formaldehyde	Treatment of resin after synthesis, before freeze-drying
Novolacs			
I[b]	HCl, < 3	0.40, PA[c]	Dried *in vacuo* at elevated temp.
I(Ac)[d]	"	"	Same resin as above
II	"	0.66, PA	Dried *in vacuo* at elevated temp.
II(Ac)	"	"	Same resin as above
Resoles			
IN[e]	Lime, 8–10	~1, F[c]	N[e]
IN(Ac)	"	"	Same resin as above
IIN	NaOH, 8–10	~2.5, F	N
IIN(Ac)	"	"	N
IIN(HTAc)[f]	"	"	N
IIIN(Ac)	Lime, 8–10	"	N
IIIHB(Ac)[g]	"	"	HB[g]
IIIa, HB	"	"	Same, pH = 4, 60°C. cure *in vacuo* 12 hr., HB
IIIaHB(Ac)	"	"	Same resin as above
IIIbHB	"	"	Same +85°C., cure *in vacuo*, 25 min. more, HB
IIIbHB(Ac)	"	"	Same resin as above
IIIcHB	"	"	Same +95°C. cure *in vacuo*, 5 min. more, HB
IIIcHB(Ac)	"	"	Same as above
IVHB (Ac)	NH_3,6–8	~1.3, F	HB
IVaHB(Ac)	"	"	Same +105°C. cure, 1 atm., 5 min., HB
IVbHB(Ac)	"	"	Same +105°C. cure, 1 atm., 15 min. more, HB
IVcHB(Ac)	"	"	Same +105°C. cure, 1 atm., 20 min. more, HB
V(Ac)	NaOH, > 12	~2.5, F	None

[a] Formaldehyde to phenol ratio initially charged.

[b] Common Roman numerals designate samples derived from same prepolymer.

[c] PA designates paraformaldehyde and F designates formalin.

[d] (Ac) designates samples acetylated near 0°C. in dilute pyridine solutions.

[e] N designates samples neutralized, $5 < \text{pH} < 7$, at low temperature just prior to freeze-drying.

[f] (HTAc) designates the one sample acetylated at higher temperature in a boiling acetic acid-anhydride mixture.

[g] HB designates samples made highly basic, pH > 12, at low temperature just before freeze-drying.

with acetic anhydride in dilute pyridine solutions near 0°C., followed by addition of water, extraction with ether, and washing with dilute mineral acid, dilute bicarbonate, and water. Water-insoluble products were thoroughly dried, and excess solvent was removed via distillation. Identifications and purities of most of the nonacetylated model compounds were confirmed via melting-point determinations. Purities of most of the acetylated model compounds were confirmed via VPC.[10]

Certain model compounds were not isolated in pure form. Thus, PMR data on methylene glycol and polyoxymethylene oligomers, $HO(CH_2O)_xH$, $x = 1, 2, 3, \ldots$, were obtained from solutions of 50 wt.-% formalin in acetone. The PMR shift assignments for these species are confirmed by the appropriate hydroxyl-to-methylene proton spin-spin multiplicities in the absence of complete hydroxyl-proton exchange averaging (see Appendix I Table A-I). Complex mixtures of the corresponding diacetates were obtained via low-temperature acetylation of 50 wt.-% formalin with excess acetic anhydride in excess pyridine. PMR analyses of these acetate mixtures, and therefore their spectral assignments, were confirmed via VPC component analyses. Similarly, data on benzyl-type hemiformals were obtained from products resulting from the heating of slightly basic, excess benzyl alcohol with paraformaldehyde and from the freeze-drying of slightly basic solutions of saligenin in excess formalin (see Results and Discussion).

To prevent advancement of resole-type resins after synthesis, all treatments of these materials were performed near 15°C. or below. Each was stored in a sealed tube under Dry Ice before analysis. Basic resoles were neutralized to pH 5–7 and freeze-dried prior to dissolution in acetone and spectral analysis. The basic materials were not sufficiently soluble in acetone after freeze-drying. Most resoles had to be freeze-dried before analysis or acetylation, to remove the substantial amounts of water and unreacted formaldehyde frequently present. Freeze-drying of neutral or acidic resole mixtures also removes substantial amounts of free phenol, whereas no phenol is lost upon freeze-drying the basic mixtures. Thus, for samples which were subsequently acetylated, the prior neutralization step was not only unnecessary but undesirable. To prevent loss of free phenol from such samples, they were frequently made highly basic ($pH > 12$) at low temperature just prior to the freeze-drying treatment. Novolacs were dissolved directly in solvent and analyzed.

Spectrometric Procedures

Most of the PMR data were obtained with a Varian Associates model A-60 spectrometer operating at an applied radiofrequency (rf) of 60 Mcycles/sec.

Sample temperatures were about 30°C., except for some of the more advanced, acetylated polymers, where higher temperatures were used to insure total solubility. Chemical-shift data were taken from spectra obtained at sweep rates in the range from 1 to 2 cycles/sec./sec. and applied rf fields in the range of about 0.02–0.2 mgauss. The PMR integral data were taken electronically, with sweep rates in the range from 10 to 20 cycles/sec./sec. and applied rf fields in the range of 0.1–0.2 mgauss. In taking the PMR integrals for the various absorption lines, care was taken to make corrections, where possible, for contributions due to spinning side bands and satellites arising from $\mathbf{H}$–C^{13} spin-spin interactions. Results presented are the averages based on five or more independent determinations of the PMR integrals. The errors shown are standard deviations from these averages. All chemical-shift data are reported as δ values, ppm of the applied field downfield from internal (*ca.* 0.5 vol.-% dissolved) tetramethylsilane (TMS). These data were all obtained from dilute solutions in precision 5 mm. O.D., thin-walled Pyrex sample tubes. Data for most of the nonacetylated materials were obtained from dilute solutions in dry acetone. Some of the results on nonacetylated model compounds and on novolacs were obtained from dilute solutions in dry pyridine and/or dry dimethyl sulfoxide (DMSO). Data on acetylated materials were obtained from dilute solutions (*ca.* 5–22 vol.-%) in carbon tetrachloride or deuteriochloroform.

RESULTS AND DISCUSSION

In the syntheses of phenol–formaldehyde resins, numerous different general types of reactions have been established.[1] Among these are hydroxymethylations of phenol and variously substituted phenolic rings.

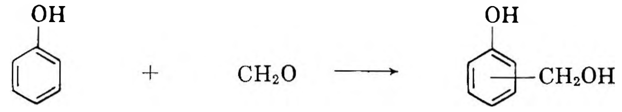

I II

(1)

The hydroxymethylated phenols, II, may participate in complex equilibria with hemiformals and polyformals, some of which are shown in eqs. (2)–(4).

III

(2)

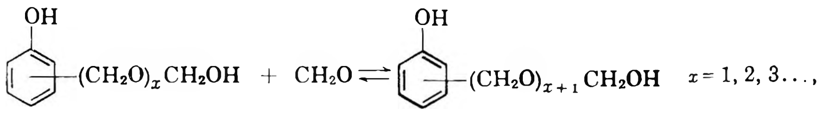

IV

(3)

$$\underset{\text{V}}{HO(CH_2O)_xH} + CH_2O \rightleftharpoons HO(CH_2O)_{x+1}H \qquad x = 1, 2, 3\ldots, \qquad (4)$$

These reactions are also accompanied by condensation type reactions, which lead to diphenylmethane-type methylene bridges (e.g. structures VI) and dibenzyl ether-type bridges (e.g., structures VII).

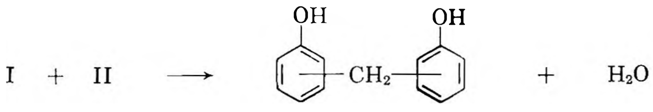

VI

(5)

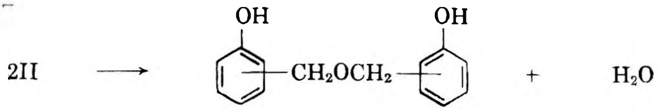

VII

(6)

$$VII \longrightarrow VI + CH_2O \qquad (7)$$

Though the mechanisms and specific rates of many of these reactions are known to be markedly dependent on factors such as pH, type of catalyst, and temperature,[1] most of these effects and the resin structures thus controlled still have not been quantitatively established. The results given below thoroughly describe the number-average structures of various resins and yield some new information on the relative importance of some types of reactions under certain conditions.

Spectral Assignments

Aside from the usual complex spin-spin multiplets from coupled protons on substituted aromatic rings, the spectra are not observably complicated by proton-proton spin interactions. The origins of lines observed in the spectra of the polymers are assigned on the basis of chemical-shift data for the model compounds. Shift data for the nonacetylated materials are tabulated in Appendix I, Table A-I, and those obtained from dilute solutions in acetone are illustrated in Figure 1*a*. These shifts are much more concentration and temperature dependent than the corresponding results for the acetylated model compounds, which are tabulated in Appendix I, Table A-II, and illustrated in Figure 1*b*. Much of this dependence of chemical shifts on concentration and temperature is due to hydrogen bonding and hydroxyl proton-exchange effects, which are not entirely detrimental. For example, the desired shift differences observed between methylene protons of *o*- and *p*-hydroxymethyl groups are primarily due to strong intramolecular hydrogen bonding between *o*-hydroxymethyl and phenolic hydroxyl groups. As shown in Appendix I and Figure 1*b*, these corresponding shift differences in the acetylated materials are much smaller, primarily because of the absence of hydrogen bonding. Resonance positions of hydroxyl protons are markedly variable, depending on the type, concentration and temperature. Lines due to phenolic hydroxyl protons in dry novolac–acetone solutions were usually in the region from about 8.67 to 7.75 ppm. After neutralization and freeze-drying, hydroxyl proton exchange in resoles could usually be adjusted, by addition of small amounts of water or deuterium oxide, so that all of the hydroxyl protons would resonate in the region from about 6.42 to 5.58 ppm, as shown in Figures 2*a* and 3*a*.

In an earlier study, it was indicated that PMR spectra of nonacetylated novolacs in acetone solutions could reveal the relative amounts of methylene bridges located *ortho*, *ortho'*, *ortho*, *para'*, and *para*, *para'* to phenolic hydroxyl groups on flanking aromatic rings.[11] Reexamination of the earlier

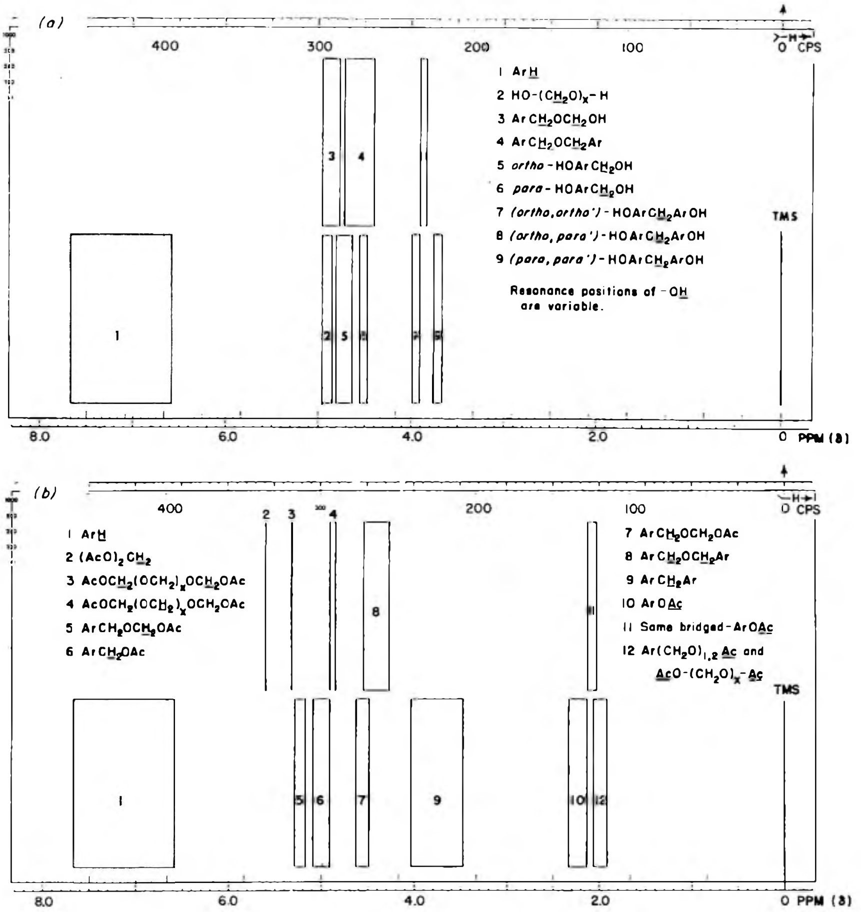

Fig. 1. PMR chemical-shift regions for (*a*) different functional groups of freeze-dried, nonacetylated phenol–formaldehyde resins in dilute solutions in acetone, and (*b*) different functional groups of acetylated phenol–formaldehyde resins in dilute solutions in carbon tetrachloride.

chemical-shift data, most of which are tabulated in Appendix I, Table I-A, shows that such measurements should be possible in *o*-chlorophenol–formaldehyde novolacs or in low molecular weight novolacs, where sufficiently narrow resonance lines are achieveable. Because of their proximity, the methylene proton resonances due to *o,o'*- and *o,p'*-methylene bridges could not be resolved in any of the many novolacs examined during the present work. This was true even for several novolacs examined by PMR at 100 Mcycles/sec., where shift differences (in dimensional units) are $^5/_3$ times larger than those at 60 Mcycles/sec.

Preliminary results indicate that better resolution among the differently located methylene bridges in novolacs may be obtained from dilute, dry solutions in pyridine. This might be expected, since the additional ring currents due to pyridine in phenolic hydroxyl–pyridine hydrogen bonds

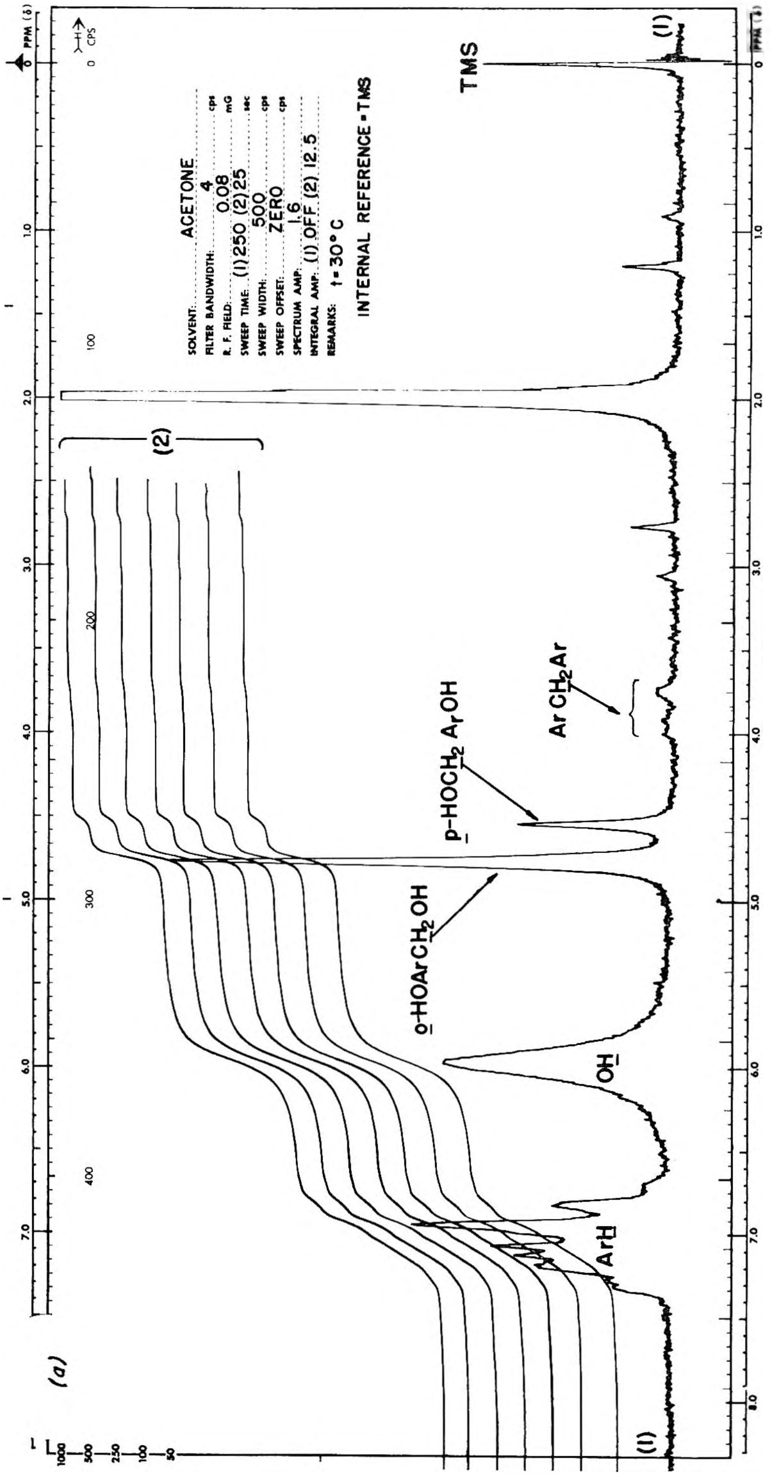
(a)
PPM (δ)
CPS
0
100
200
300
400
1.0
2.0
3.0
4.0
5.0
6.0
7.0
8.0
1000
500
250
100
50
SOLVENT: ACETONE
FILTER BANDWIDTH: 4 cps
R. F. FIELD: 0.08 mG
SWEEP TIME: (1) 250 (2) 25 sec
SWEEP WIDTH: 500 cps
SWEEP OFFSET: ZERO cps
SPECTRUM AMP: 1.6
INTEGRAL AMP: (1) OFF (2) 12.5
REMARKS: t = 30° C
INTERNAL REFERENCE = TMS
TMS
(1)
(2)
Ar CH2 Ar
p-HOCH2 ArOH
o-HOArCH2OH
OH
ArH

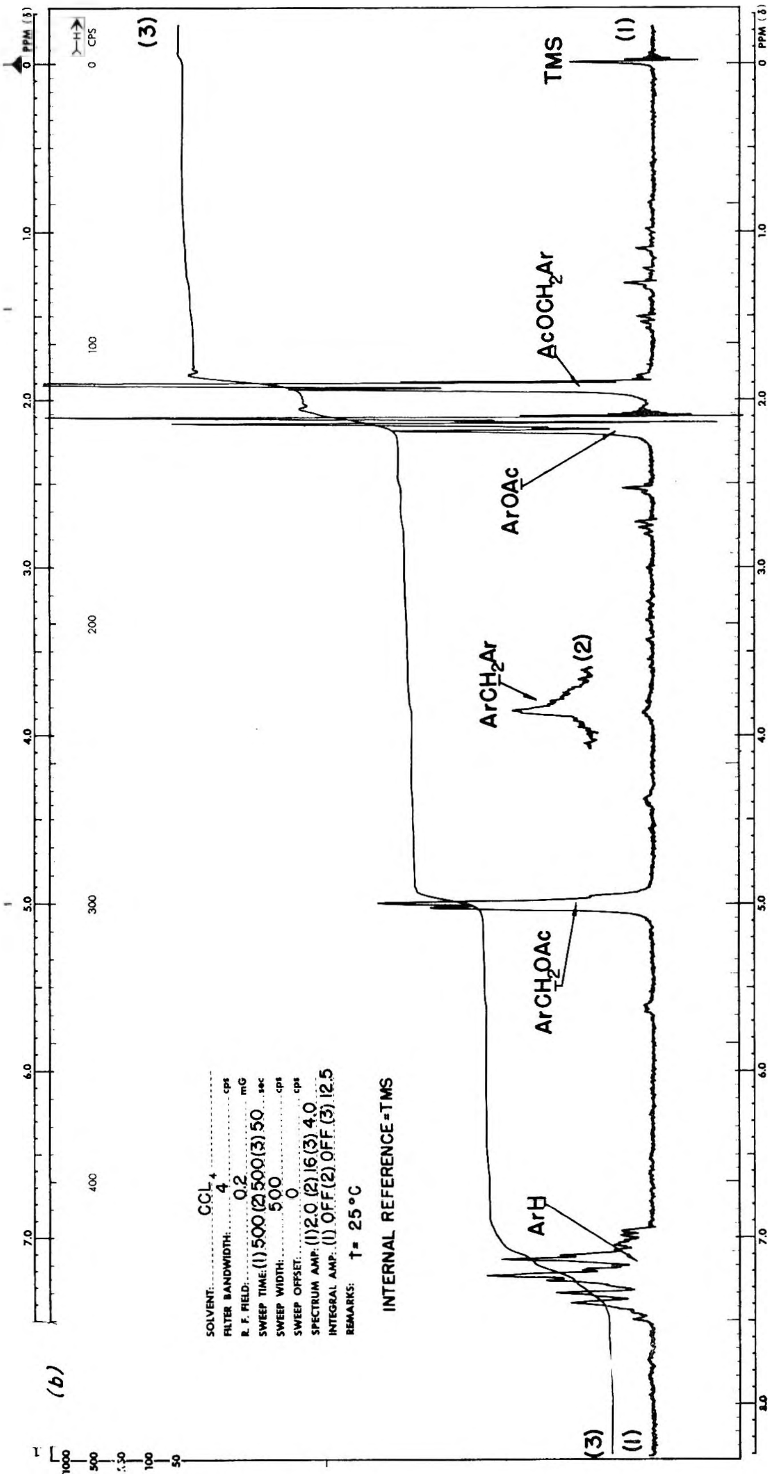

Fig. 2. PMR spectra of (*a*) Resole IN and (*b*) Resole IN(Ac).

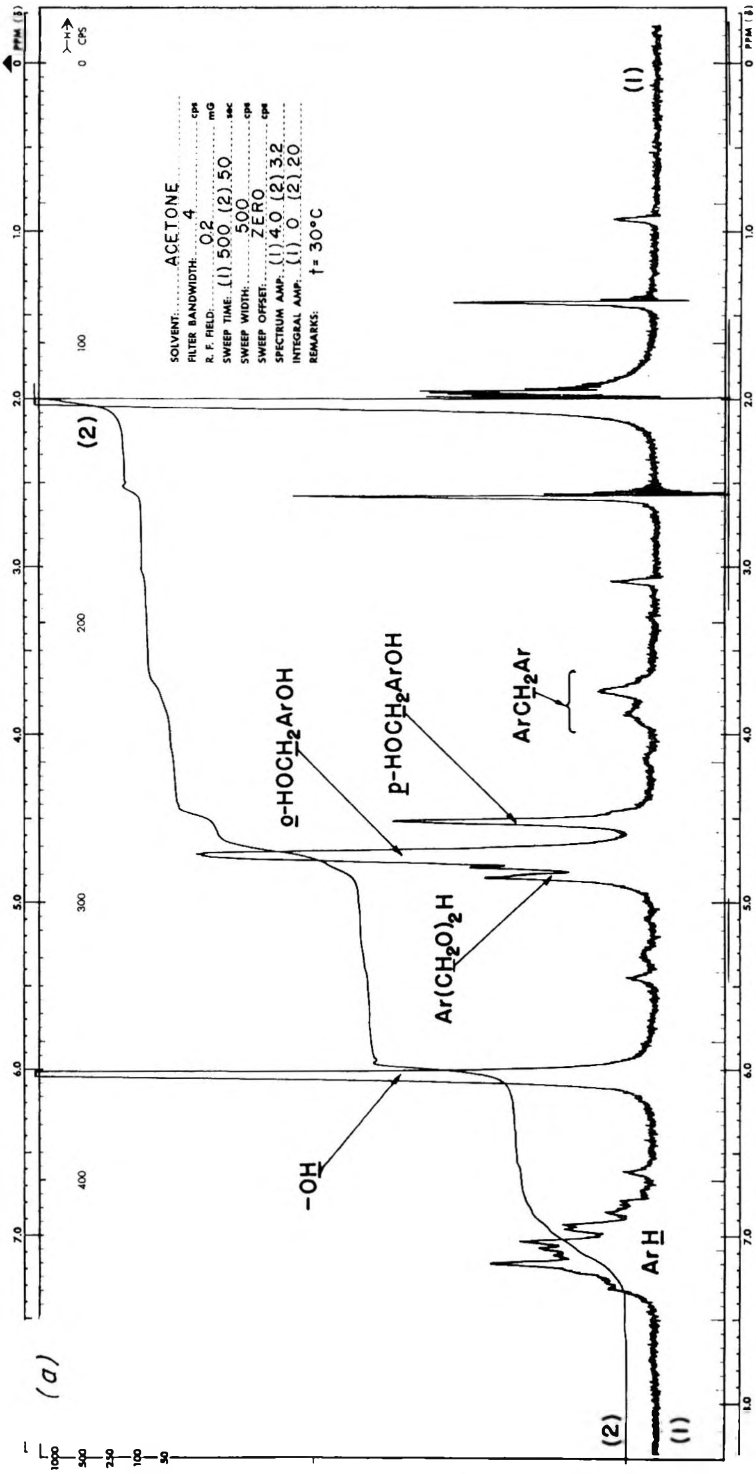
(a)
SOLVENT: ACETONE
FILTER BANDWIDTH: 4 cps
R. F. FIELD: 0.2 mG
SWEEP TIME: (1) 500 (2) 50 sec
SWEEP WIDTH: 500 cps
SWEEP OFFSET: ZERO cps
SPECTRUM AMP: (1) 4.0 (2) 3.2
INTEGRAL AMP: (1) 0 (2) 20
REMARKS: t = 30°C
o-HOCH2ArOH
p-HOCH2ArOH
ArCH2Ar
Ar(CH2O)2H
-OH
ArH
(1)
(2)
PPM (δ)
CPS
0
100
200
300
400
1.0
2.0
3.0
4.0
5.0
6.0
7.0
8.0
1000
500
250
100
50

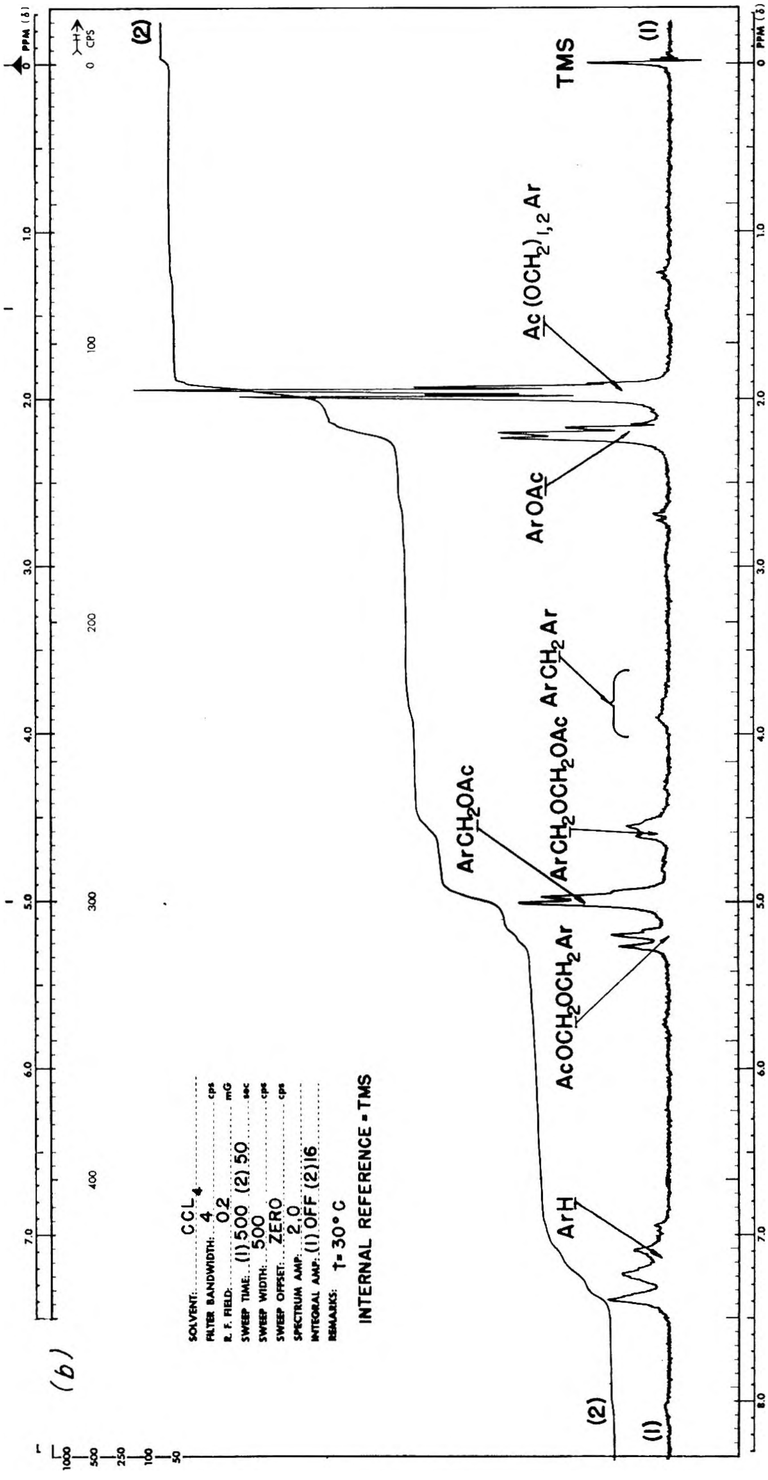

Fig. 3. PMR spectra of (*a*) Resole IIN and (*b*) Resole IIN(Ac).

should have specific shielding effects on the differently located bridge protons. Another possible indication of the relative amounts of differently located bridges in novolacs is the observation that, in sufficiently dry acetone solutions, the resonances due to phenolic hydroxyl protons are frequently split into three or more groups of lines. These indications still need to be confirmed or rejected by additional chemical-shift data on appropriate model compounds.

The assignments for methylene protons in benzyl-type hemiformals, such as structures III, and the corresponding assignments for the acetates, require further explanation. In spectra of freeze-dried, nonacetylated resoles, lines observed in the 4.95–4.77 ppm region cannot arise from unreacted formaldehyde species (V), which have coincident chemical shifts. These species, and benzyl-terminated polyformals (e.g., IV), are all removed from resole solutions upon freeze-drying; i.e., the equilibria (3) and (4) are easily pulled to the left. This is shown by the absence of lines characteristic of the acetylated species in spectra of acetylated resins which contained large excesses of added free formaldehyde before freeze-drying. Spectra of these freeze-dried, nonacetylated resins showed substantial absorption in the 4.95–4.77 ppm region. Additional evidence for the removal of formaldehyde and the polyformals upon freeze-drying was obtained from VPC component analyses of similarly treated acetylated resoles.[10] The methylene protons of phenyl-type hemiformals, diphenyl-type formals, quinone methides, and benzodioxanes may also be excluded as possible origins for the lines observed in the 4.95–4.77 ppm region of many freeze-dried, nonacetylated resoles. These species would all give resonances at lower fields. Methylene protons of dibenzyl-type formals, $C_6H_5CH_2OCH_2OCH_2C_6H_5$, might possibly give resonance lines in the appropriate region, but these species were not found in any of the acetylated resins examined. Benzyl-type hemiformals are present in the acetylated materials derived from freeze-dried, nonacetylated resins having resonances in the 4.95–4.77 ppm region. (The possible conversion, upon acetylation, of dibenzyl-type formals to acetylated benzyl-type hemiformals cannot be excluded. This seems unlikely however, since the acetylations were performed in pyridine solutions near 0°C. Such treatment did not cleave the ether bridges in the dibenzyl ether-type model compounds examined.)

Acetylated benzyl-type hemiformals in acetylated resins give two equally intense groups of lines in the 5.28–5.17 and 4.63–4.47 ppm regions, as shown in Figure 3*b*. These two groups of lines are due to the methylene protons of the acetoxymethyl ends and the benzyl ends, respectively, of the acetylated benzyl-type hemiformal groups. Identical observations were made on both the nonacetylated and acetylated products obtained from benzyl alcohol and paraformaldehyde and from saligenin and formalin (see Experimental and Appendix I). VPC on the acetates of these and of complex resole mixtures shows that the acetylated hemiformals have retention times only slightly longer than the corresponding nonhemiformalated parents.[10] Quantitative VPC component analyses on low molecular weight acetylated resoles are in good agreement with number-average structures, as determined by the PMR methods described below.

Resin Structures

The structures of the polymers studied varied greatly. Novolacs contained methylene-bridged phenolic nuclei only. Spectra of these materials are not shown. Structures of the resoles fell into three different general types. Some contained methylene-bridge and hydroxymethyl functionalities only. Figure 2 shows that Resole IN is of this type.* In addition to these groups, most resoles contained benzyl-type hemiformals. Resole IIN is of this type, as shown by Figure 3. A few resoles contained dibenzyl ether-type bridges, methylene bridges, hydroxymethyl groups, and, in some instances, benzyl-type hemiformals also. Examples of this type of resin are Resoles IIIaHB, IIIbHB and IIIcHB, whose spectra are shown in Figure 4.† Because of the overlap among chemical shifts for some of the groups, the relative amounts of hydroxymethyl groups and dibenzyl ether-type bridges cannot be established on the basis of spectra of the nonacetylated resins alone. For resins containing both of these functionalities, quantitative analyses must be performed on the acetylated materials. When dibenzyl ether-type bridges are absent, as indicated by spectra of the acetates, then the relative amounts of the other functional groups present may be determined from spectra of either the acetylated or the nonacetylated resin. In any case, the locations of functional groups on the aromatic rings are shown much more clearly by spectra of the hydroxy materials than by the spectra of the acetates.

To describe the number-average structures of nonacetylated resins void of ether bridges, it is convenient to define the following ratios: R_A = average number of aromatic ring protons per aromatic ring; R_{HF} = average number of benzyl-type hemiformal groups per aromatic ring; R_{HM} = average number of hydroxymethyl groups per aromatic ring; R_{MB} = average number of diphenylmethane-type methylene bridges per aromatic ring; r_{HM} = ratio of the number of *o*-hydroxymethyl groups to the number of *p*-hydroxymethyl groups; r_{MB} = ratio of the number of *p,p'*-methylene bridges to the number of *o,o'*- plus *o,p'*-methylene bridges. The calulations of these ratios from the PMR integral data are described in Appendix IIA. Provided that bridges do not bond aromatic rings into cyclic structures, then the average number of aromatic rings per molecule $\bar{n}$ and the number-average molecular weights of the nonacetylated resins, $\bar{M}_n$(OH), may also be calculated. These calculations are also described in Appendix IIA. To describe the number-average structure of any of the

---

* The strong line near 2.00 ppm in the spectra of nonacetylated materials is due to acetone. Weaker undesignated lines are either spinning side bands, satellites due to H-C^{13} spin-spin interactions or small amounts of residual ethyl ether.

† The hydroxyl proton resonances in Figure 4*A* are very broad. Some of these resonances are in the region of about 4.17–5.42 ppm, while the others are in the region of about 8.67–10.33 ppm.

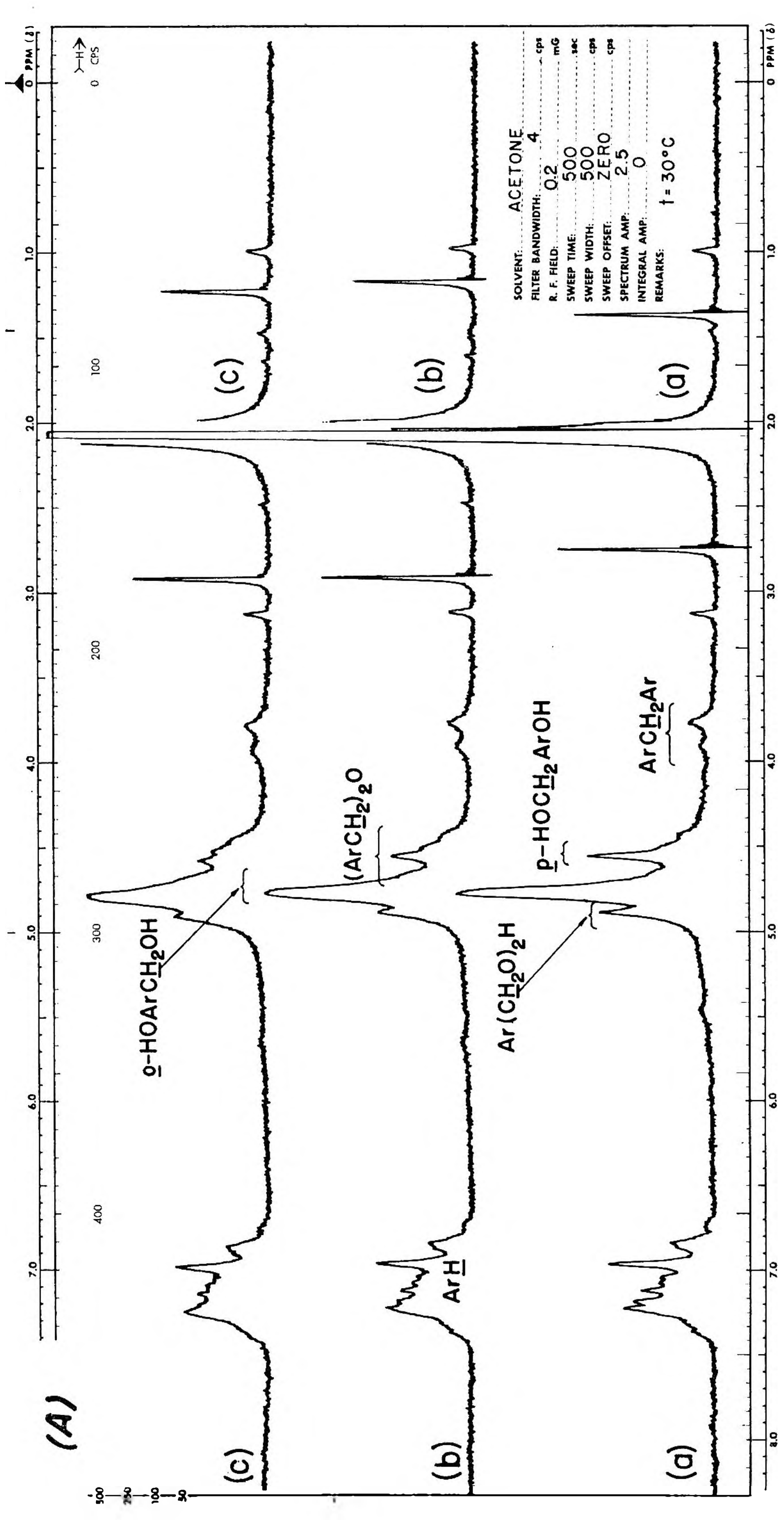
(A)
(a)
(b)
(c)
ArH
Ar(CH2O)2H
o-HOArCH2OH
(ArCH2)2O
p-HOCH2ArOH
ArCH2Ar
SOLVENT: ACETONE
FILTER BANDWIDTH: 4 cps
R. F. FIELD: 0.2 mG
SWEEP TIME: 500 sec
SWEEP WIDTH: 500 cps
SWEEP OFFSET: ZERO cps
SPECTRUM AMP: 2.5
INTEGRAL AMP: 0
REMARKS: t = 30°C
PPM (δ)
0
1.0
2.0
3.0
4.0
5.0
6.0
7.0
8.0
CPS
0
100
200
300
400
500
250
100
50

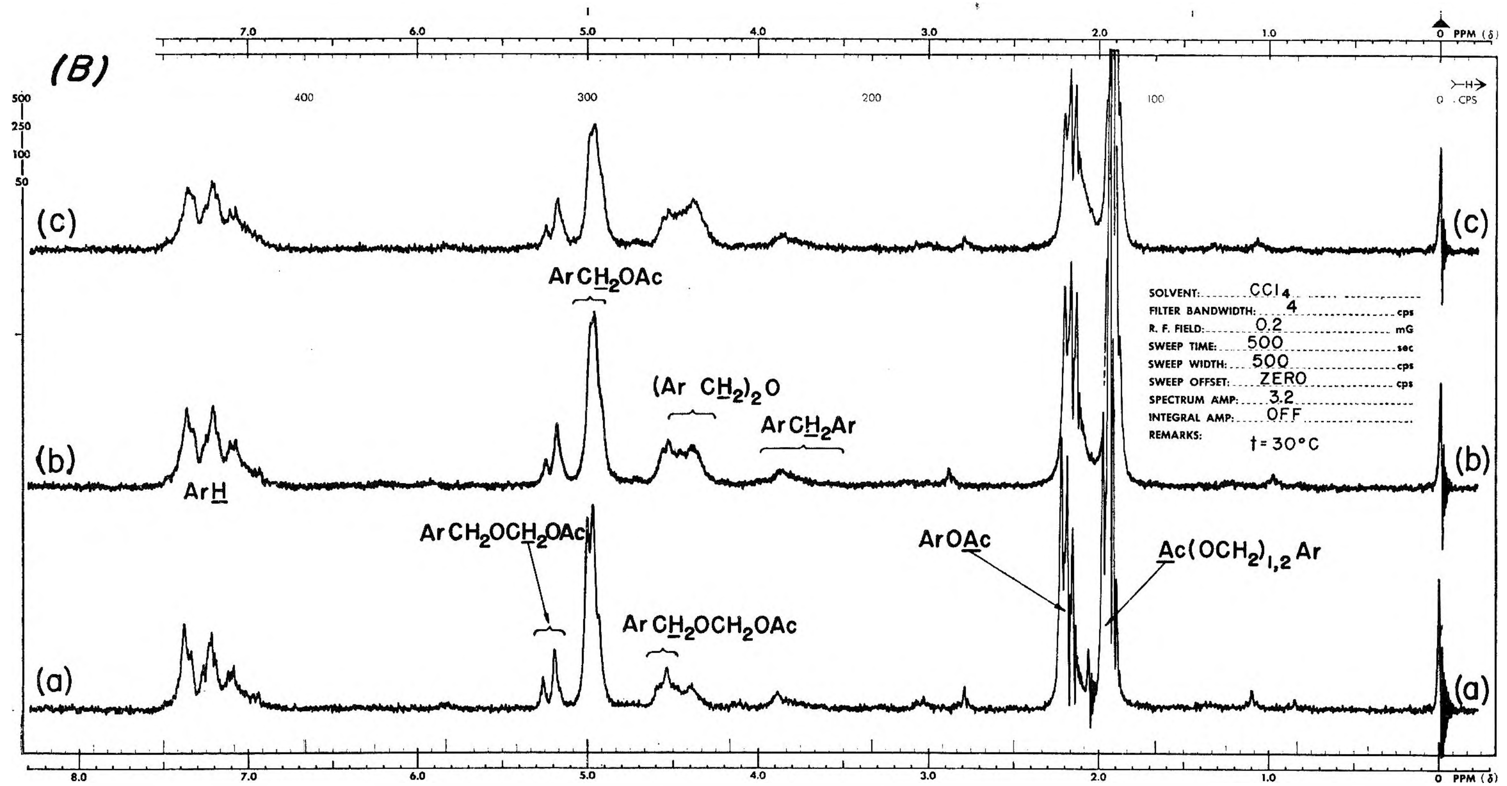

Fig. 4. PMR spectra of (*A*a) Resole IIIaHB; (*A*b) Resole IIIbHB, (*A*c) Resole IIIcHB; (*B*a) Resole IIIaHB(Ac); (*B*b) Resole IIIbHB(Ac); (*B*c) Resole IIIcHB(Ac).

soluble acetylated resins, it is convenient to use the quantities R_A, R_{MB}, and $\bar{n}$ defined above, plus the ratios defined as follows: R_{AHF} = average number of acetylated benzyl-type hemiformal groups per aromatic ring; R_{AM} = average number of acetoxymethyl groups per aromatic ring; R_{EB} = average number of dibenzyl ether-type bridges per aromatic ring. The calculations of these ratios from the PMR integral data are described in Appendix IIB, along with the equations for $\bar{n}$ and the number-average molecular weight for the acetylated resin $\bar{M}_n$ (Ac).

By using the above methods, the structures of resins may now be described on a more quantitative basis. Table II shows the results obtained on Novolacs I and II and their corresponding acetates.

TABLE II
Number-Average Structures of Novolacs I and II and the Corresponding Acetates, Novolacs I(Ac) and II(Ac)[a]

	Novolac I[b]	Novolac I(Ac)[c]	Novolac II[b]	Novolac II(Ac)[c]
R_A	3.74 ± 0.04	3.85 ± 0.09	3.43 ± 0.04	3.70 ± 0.02
R_{MB}	0.66 ± 0.01	0.64 ± 0.02	0.78 ± 0.01	0.79 ± 0.015
$\bar{n}$	2.94 ± 0.10	2.78 ± 0.15	4.55 ± 0.21	4.75 ± 0.34
$\bar{M}_n$(OH)	300 ± 10	284 ± 16	470 ± 23	492 ± 37
$\bar{M}_n$(Ac)	423 ± 13	400 ± 23	661 ± 31	692 ± 51
r_{MB}	0.5		0.45	

[a] The values of R_{HF}, R_{HM}, R_{AHF}, R_{AM}, and R_{EB} were zero.
[b] These results were based on A_1, as calculated from eq. (AII-1).
[c] These results were based on A_6, as calculated from eq. (AII-10).

The relative molecular weights of these materials are in good agreement with the formaldehyde/phenol (F/P) ratios charged. Due to loss of free phenol during the syntheses and purifications, values of F/P in the final resins are higher than the charged values. The experimental errors shown in Table II may be reduced substantially, either by the averaging of more PMR integrals, or by performing the analyses on more concentrated solutions. It should be emphasized, however, that the calculations of $\bar{n}$ and $\bar{M}_n$ (Appendix II) assume the absence of cyclic structures. This assumption may become invalid for some higher molecular weight resins that are still soluble. Also, due to the nature of the equations for $\bar{n}$, (AII-8) and (AII-17), the errors accompanying determinations of this quantity and $\bar{M}_n$ increase greatly with increasing bridging contents. The ratio r_{MB} = 0.5 for novolac I is much higher than the value 0.096 calculated for a trinuclear novolac on the basis of equal reactivity for the *ortho* and *para* positions. This contrast, and the value r_{MB} = 0.45 for novolac II, show that reactions at the *para* positions are, overall, about five times faster under acidic conditions than those at the *ortho* positions. This same trend has been qualitatively indicated by the work of Finn and James.[12]

The results for Resole IN and its corresponding acetate are shown in Table III. Because of a small residual amount of acetic acid in Resole

IN(Ac), the results in the right-hand column of Table III are slightly low. Comparison of the results for Resoles IN and IN(Ac) shows that the low-temperature acetylation procedure is accompanied by conversion of hydroxyl groups to their corresponding acetates only. No other modifications of the resin structure, e.g., further bridge formations such as reactions (5) and (6) are indicated. A more general proof for no modification of basic resin structures upon low-temperature acetylation was obtained from VPC and PMR examinations on all of the acetylated model compounds listed in Appendix I. The results for Resoles IIN(Ac) and IIN(HTAc) in Table IV show that high-temperature acid-catalyzed acetylation cleaves benzyl-type hemiformals, thereby, converting these functionalities to

TABLE III

Number-Average Structures of Resole IN and the Corresponding Acetate, Resole IN(Ac)[a]

	Resole IN[b]	Resole IN(Ac)[c]	Resole IN(Ac)[d]	Resole IN(Ac)[e]
R_A =	3.48 ± 0.07	3.46 ± 0.05	3.52 ± 0.02	3.34 ± 0.05
R_{HM} =	1.31 ± 0.02			
R_{AM}		1.27 ± 0.02	1.29 ± 0.0[illegible]	1.23 ± 0.03
R_{MB} =	0.094 ± 0.01	0.093 ± 0.008	0.094 ± 0.007	0.089 ± 0.008
$\bar{n}$ =	1.103 ± 0.012	1.102 ± 0.009	1.103 ± 0.008	1.098 ± 0.009
$\bar{M}_n$(OH)	148 ± 3			
$\bar{M}_n$(Ac)	255 ± 5	252 ± 4	254 ± 3	247 ± 4
r_{HM}	4.18			
r_{MB}	1.44			

[a] The values of R_{HF}, R_{AHF}, and R_{EB} were zero.

[b] These results were based on A_1, as calculated from eq. (AII-1).

[c] These results were based on A_6, as measured experimentally.

[d] These results were based on A_6, as calculated from eq. (AII-10).

[e] These results were based on A_6, as calculated from eq. (AII-11).

TABLE IV

Number-Average Structures of Resole IIN(Ac) and Resole IIN(HTAc)[a]

	Resole IIN(Ac)	Resole IIN(HTAc)
R_A	2.63 ± 0.03	2.5 ± 0.1
R_{AHF}	0.31 ± 0.01	None
R_{AM}	1.57 ± 0.02	1.90 ± 0.07
$R_{AHF} + R_{AM}$	1.88 ± 0.03	1.90 ± 0.07
R_{EB}	None	None
R_{MB}	0.28 ± 0.04	0.28 ± 0.03
$\bar{n}$	1.39	1.39
$\bar{M}_n$(Ac)	396[b]	390

[a] These results were based on A_6, as calculated from eq. (AII-10).

[b] Vapor-phase osmometry gave the value $\bar{M}_n(\mathrm{Ac}) = 395$ for this sample.

TABLE V
Number-Average Structures of Resole IIIN(Ac) and Resole IIIHB(Ac)[a]

	Resole IIIN(Ac)	Resole IIIN(Ac), less 1.97 wt.-% phenyl acetate	Resole IIIHB(Ac)	Resole IIIHB(Ac), less 6.49 wt.-% phenyl acetate
R_A	2.72 ± 0.03	2.60 ± 0.03	2.95 ± 0.03	2.57 ± 0.03
R_{AHF}	0.24 ± 0.01	0.25 ± 0.01	0.31 ± 0.02	0.37 ± 0.02
R_{AM}	1.63 ± 0.02	1.72 ± 0.02	1.41 ± 0.02	1.65 ± 0.02
$R_{AHF} + R_{AM}$		1.97 ± 0.03		2.01 ± 0.04
R_{EB}	None	None	None	None
R_{MB}	0.18 ± 0.01	0.19 ± 0.01	0.16 ± 0.02	0.19 ± 0.02
$\bar{n}$	1.25	1.23	1.19	1.23
$\bar{M}_n$(Ac)	352	354	324	357

[a] These results were based on A_6, as calculated from eq. (AII-10). The phenyl acetate concentrations were determined by VPC methods described elsewhere.[10]

acetoxymethyl groups.* The effect of pH on loss of free phenol accompanying freeze-drying is shown in Table V.

These results indicate that increasing the pH of Resole III shifted the equilibria (2) further to the right. Otherwise, the structures of Resoles IIIN(Ac) and IIIHB(Ac), less phenyl acetate, are the same. Virtually no phenol is lost upon freeze-drying highly basic resoles.

The value of $r_{HM} = 4.18$ in Table III shows that in Resole III hydroxymethylation at the *ortho* positions was much faster than at the *para* positions. Similar results for resoles IIN and IIaHB are Revealed by Figures 3*a* and 4*Aa*, respectively. These values of r_{HM} are considerably higher than those approximated from the rate constants determined by Freeman and Lewis[13] for NaOH catalysis at 30°C. and higher pH. This was true for all the resoles examined, even though lime catalysis leads to values of r_{HM} about 1.3 times larger than those obtained from NaOH catalysis. Since all the resoles studied in this present work were made in the region 60–80°C., these variations may result from substantial differences in energies of activation and/or from the dependence of the relative rates on pH in the range from about 8 to 13. The value of $r_{MB} = 1.44$ in Table III shows that, under basic conditions, *para, para'* condensation is much faster than the *ortho, ortho'* and *ortho, para'* condensations combined. Though a similar trend was found under acidic catalysis, the dependence of these relative rates on pH and temperature is still ill defined. The results in Tables III, IV, and V also show that methylene-bridged structures appear much earlier in the sequence of reactions than indicated by the data of Freeman and Lewis. These variations may result from large differences in the ener-

---

* A pyridine-bisulfite reagent has been shown to pull equilibria (2) to the left quantitatively, thereby converting benzyl-type hemiformals to the corresponding benzyl alcohols without further resin modifications.[10]

gies of activation for the hydroxymethylation and condensation reactions, and/or from substantial dependence of one or both of these rates on pH in the range of about 8–13.

The substantial amounts of acetylated benzyl-type hemiformals shown in Tables IV and V are of particular interest. These functional groups were found to be present in many resole prepolymers. The relatively high stability of benzyl-type hemiformals has been unappreciated by earlier investigators. Apparently, these species have not been isolated or even detected by other methods used in the study of resole structures.[1] Figure 4 shows the PMR spectra of Resole III after it had been neutralized to pH 4 and cured *in vacuo* at different temperatures for different times (see Table I). The number-average structures of these products, shown in Table VI, reveal that benzyl-type hemiformals are remarkably stable under the conditions of cure used. These structures do not *appear* to be as stable at higher pH and temperatures, as revealed by the results in Table VII. These latter data show that the small hemiformal content of the original Resole

TABLE VI

Number-Average Structures of Resoles IIIaHB(Ac), IIIbHB(Ac), and IIIcHB(Ac)[a]

	Resole IIIaHB(Ac)	Resole IIIbHB(Ac)	Resole IIIcHB(Ac)
R_{A}	2.77 ± 0.05	2.74 ± 0.05	2.77 ± 0.08
R_{AHF}	0.30 ± 0.02	0.30 ± 0.03	0.29 ± 0.02
R_{AM}	1.44 ± 0.05	1.13 ± 0.04	0.97 ± 0.05
R_{EB}	0.09 ± 0.01	0.20 ± 0.01	0.26 ± 0.02
R_{MB}	0.15 ± 0.01	0.22 ± 0.02	0.22 ± 0.02
$\bar{n}$	1.33	1.71	1.95
$\bar{M}_n$(Ac)	366	443	485

[a] These results were based on A_6, as calculated from eq. (AII-10).

TABLE VII

Number-Average Structures of Resoles IVHB(Ac), IVaHB(Ac), IVbHB(Ac), and IVcHB(Ac)[a]

	Resole IVHB(Ac)	Resole IVaHB(Ac)	Resole (IVbHBAc)	Resole IVcHB(Ac)
t, min.[b]	0	5	20	40
R_{A}	3.36 ± 0.02	3.29 ± 0.08	3.23 ± 0.03	3.10 ± 0.07
R_{AHF}	0.073 ± 0.007	None	None	None
R_{AM}	0.658 ± 0.008	0.60 ± 0.07	0.53 ± 0.02	0.46 ± 0.01
R_{EB}	0.032 ± 0.006	0.043 ± 0.005	0.059 ± 0.006	0.079 ± 0.007
R_{MB}	0.42 ± 0.01	0.51 ± 0.01	0.56 ± 0.01	0.64 ± 0.03
$\bar{n}$	1.83	2.25	2.59	3.59
$\bar{M}_n$(Ac)	361[c]	420	476	646

[a] These results were based on A_6, as calculated from eq. (AII-10).

[b] The original prepolymer, Resole IV, was cured *t* minutes in a circulating air oven at 105°C.

[c] Vapor-phase osmometry gave the value $\bar{M}_n(\mathrm{Ac}) = 372$ for this sample.

IV is completely lost on cure at 105°C. for 5 min. Most of the decrease in stability of hemiformals, on curing Resole IV as compared to that observed for Resole III, may be attributed to a marked increase in the rates of hydroxymethylations on changing pH from 4 to about 7. Some of the observed effects are due to the smaller concentration of hemiformal-stabilizing hydroxymethyl groups and to the greater concentration of unreacted ring positions in Resole IV. The presence of hemiformals must, in any case, have an important influence on condensation reactions during prepolymer synthesis and subsequent cure. These effects, and the contributions hemiformals have made to the results of earlier studies, still need to be explored experimentally. Certain factors are worth mentioning. The presence of hemiformals must interfere with both infrared and hydrogen bromide methods for detecting dibenzyl-type ethers in resoles. Benzyl-type hemiformals titrate as free formaldehyde with hydroxylamine.

In agreement with earlier work,[9] the formation of dibenzyl ether-type bridges is found to be markedly dependent on pH. These species are absent from all of the more basic resoles (Tables III, IV, and V). As shown in Table VII, the small amount of ether bridges present in the less basic (pH 6–8) Resole IV increase slowly but steadily on curing this material. Table VI shows that ether-bridge formation accounts for most of the advancement of Resole III at pH 4. The contributions these condensations make to reaction sequences under acidic conditions still need to be examined. Indeed, the mechanisms and specific rates of most of the different reactions in phenol–formaldehyde systems still need to be determined by quantitative experimental data obtained with different catalysts at different temperatures and pH. The PMR methods described above provide the capability for obtaining most of the desired data. These methods have the advantage that they provide quantitative results on any soluble material. Fortunately, many resins remain soluble to surprisingly high molecular weight. For example, the completely soluble Resole V(Ac) yielded the following PMR results: $R_A = 2.05 \pm 0.03$, $R_{AM} = 1.03 \pm 0.02$, $R_{MB} = 0.98 \pm 0.04$, and $R_{AHF} = R_{EB} = 0$. Even though $\bar{n}$ and $\bar{M}_n$ are indeterminate from these PMR results, the R values for such a resin may still be very informative. By using the value $\bar{M}_n$ (Ac) ≈ 3500, estimated from vapor-phase osmometry, the value $\bar{n} \sim 15.8$ is approximated. This yields $R_{MB} \approx 0.94$, which is in good agreement with the value determined directly by PMR. This result, plus the solubility of Resole V(Ac), suggests that this material has very few cyclic or crosslinked structures.

SUMMARY AND CONCLUSIONS

PMR spectra of model compounds have provided spectral assignments for the following functional groups in phenol-formaldehyde resins: benzyl-type hemiformals, hydroxymethyl groups, dibenzyl ether-type bridges, and diphenylmethane-type methylene bridges. Using these assignments, the PMR spectra of soluble resins provide measurements of the ratio of *o*-hydroxymethyl to *p*-hydroxymethyl groups and the ratio of *p,p'*- to *o,o'*- plus *o,p′*-methylene bridges. In the absence of ether bridges, these measurements and those for the average number of each functional group per aromatic ring, the average number of aromatic rings per molecule, and the number-average molecular weights become quantitative. Similarly, spectra of acetylated model compounds have provided assignments for the various functional groups in acetylated resins. The spectra of acetylated materials yield quantitative results for the average number of each of the functional groups, including ether bridges, per aromatic ring, the average number of aromatic rings per molecule, and the number-average molecular weights. Potentially, these methods can provide most of the much desired quantitative data needed to define mechanisms and rates of the various possible reactions under different catalytic conditions and at different temperatures.

Using these PMR methods, results of this present work have shown that low-temperature acetylation of resoles is not accompanied by further condensation or hydroxymethylation reactions. Overall hydroxymethylation and condensation to form *p,p′*-methylene bridges were found to be much faster, both under acidic and basic conditions, than the corresponding reactions leading to *o,o′*- and *o,p′*-methylene bridges. Substantial amounts of benzyl-type hemiformals were found in many resoles. These functional groups, usually thought to be highly unstable, exhibited unexpectedly high stability under some conditions of initial cure. The formation of dibenzyl ether-type bridges is markedly dependent on pH. These structures were not found at all under highly basic conditions, but their formation accounted for most of the advancement in one resole at pH 4. The dependence of these condensations, as well as other reactions, on pH and temperature still need to be defined more quantitatively.

APPENDIX I

Chemical Shift Data on Some Model Compounds for Phenol–Formaldehyde Resins

Chemical-shift data for nonacetylated and acetylated materials are tabulated in Tables A-I and A-II, respectively.

APPENDIX II

Calculations of Number-Average Structures from the PMR Integral Data

A. Nonacetylated Materials

For nonacetylated resins not containing dibenzyl-ether-type bridges, the various PMR integrals A_i are defined as follows: A_1 = relative number of phenolic hydroxyl protons, ArO**H**, 8.67–7.75 ppm, for novolacs in dilute, dry acetone solutions; not directly measureable for resoles; A_2 = relative number of aromatic ring protons, Ar**H**, 7.67–6.58 ppm; A_3 = relative

TABLE A-I
Nonacetylated Materials

Material	Shift, ppm[a]
$HOC\mathbf{H}_2OH$	4.95 (an approximate 1:3:1 triplet, partially exchange-averaged, J = 0.7 cycles/sec.)[b]
$HOC\mathbf{H}_2(OCH_2)_xOC\mathbf{H}_2OH$	4.90 (an approximate 1:1 doublet, slightly exchange-averaged, J = 1.1 cycle/sec.)[b]
$HOCH_2(OC\mathbf{H}_2)_xOCH_2OH$	4.85[b]
$Ar(C\mathbf{H}_2O)_2H$	4.95–4.77[c]
o-$HOC_6H_4C\mathbf{H}_2OH$	4.88–5.13[d]
$4,6\text{-}(CH_3)_2\text{-}2\text{-}(HOC\mathbf{H}_2)\text{-}C_6H_2OH$	4.78, 5.13[d]
$4\text{-}(CH_3)\text{-}2,6\text{-}(HOC\mathbf{H}_2)_2\text{-}C_6H_2OH$	4.63[e]
$2,6\text{-}(HOC\mathbf{H}_2)_2\text{-}C_6H_3OH$	4.80
$2\text{-}Cl\text{-}4,6\text{-}(HOC\mathbf{H}_2)_2\text{-}C_6H_2OH$	6 = 4.63
$2,4,6\text{-}(HOC\mathbf{H}_2)_3\text{-}C_6H_2OH$	2,6 = 4.77, 4.90,[d] 4.57[e]
$[3\text{-}(HOC\mathbf{H}_2)\text{-}2\text{-}(HO)\text{-}C_6H_5]_2CH_2$	4.97,[d] 4.65[e]
$[3,5\text{-}(HOC\mathbf{H}_2)_2\text{-}4\text{-}(HO)\text{-}C_6H_2]_2CH_2$	5.00[d]
p-$HOC_6H_4CH_2OH$	4.55, 4.92[d]
$2,6\text{-}(CH_3)_2\text{-}4\text{-}(HOC\mathbf{H}_2)\text{-}C_6H_2OH$	4.47, 4.90[d]
$2\text{-}Cl\text{-}4,6\text{-}(HOC\mathbf{H}_2)_2\text{-}C_6H_2OH$	4 = 4.53
$2,4,6\text{-}(HOC\mathbf{H}_2)_3\text{-}C_6H_2OH$	4 = 4.50, 4.90,[d] 4.57[e]
$C_6H_5C\mathbf{H}_2OH$	4.58–4.43[f]
$(C_6H_5CH_2)_2O$	4.47, 4.48[f]
$[2\text{-}(HO)\text{-}C_6H_4C\mathbf{H}_2]_2O$	4.72, 5.12[d]
$[4\text{-}(HO)\text{-}C_6H_4C\mathbf{H}_2]_2O$	4.40, 4.58[d]
$[3,5\text{-}(CH_3)_2\text{-}2\text{-}(HO)\text{-}C_6H_5C\mathbf{H}_2]_2O$	4.67, 4.55[f]
$[2\text{-}(HO)\text{-}C_6H_4]_2C\mathbf{H}_2$	3.98[g]
$[3\text{-}(CH_3)\text{-}2\text{-}(HO)\text{-}C_6H_3]_2C\mathbf{H}_2$	3.95[g]
$[3\text{-}(HOCH_2)\text{-}2\text{-}(HO)\text{-}C_6H_3]_2C\mathbf{H}_2$	3.83,[d] 3.92[e]
$2,6\text{-}[2\text{-}(HO)\text{-}C_6H_4C\mathbf{H}_2]_2\text{-}C_6H_3OH$	3.97[g]
$2,6\text{-}[5\text{-}Cl\text{-}2\text{-}(HO)\text{-}C_6H_4C\mathbf{H}_2]_2\text{-}C_6H_3OH$	3.95[g]
p-Chlorophenol–formaldehyde novolac; *o,o′*-methylene bridges	3.97[g]
Dehalogenated *p*-chlorophenol–formaldehyde novolac; *o,o′*-methylene bridges	3.93[g]
o-Chlorophenol–formaldehyde novolac; *o,o′*-methylene bridges	4.00[g]
Dehalogenated *o*-chlorophenol–formaldehyde novolac; *o,o′*-methylene bridges	3.90[g]
$[2\text{-}(HO)\text{-}C_6H_4]\text{-}C\mathbf{H}_2\text{-}[4\text{-}(HO)\text{-}C_6H_4]$	3.90[g]
$[3,5\text{-}Cl_2\text{-}2\text{-}(HO)\text{-}C_6H_2]\text{-}C\mathbf{H}_2\text{-}[3\text{-}Cl\text{-}4\text{-}(HO)\text{-}C_6H_3]$	3.85[g]
$2,4\text{-}[4\text{-}(HO)\text{-}C_6H_4C\mathbf{H}_2]_2\text{-}C_6H_3OH$	2 = 3.83[g]
o-Chlorophenol–formaldehyde novolac; *o,p′*-methylene bridges	3.85[g]
Dehalogenated *o*-chlorophenol–formaldehyde novolac; *o,p′*-methylene bridges	3.83[g]
$[4\text{-}(HO)\text{-}C_6H_4]_2C\mathbf{H}_2$	3.77[g]
$[3\text{-}(CH_3)\text{-}4\text{-}(HO)\text{-}C_6H_3]_2C\mathbf{H}_2$	3.70[g]
$[3,5\text{-}(HOCH_2)_2\text{-}4\text{-}(HO)\text{-}C_6H_2]_2C\mathbf{H}_2$	4.00[d]
$[3,5\text{-}(CH_3)_2\text{-}4\text{-}(HO)\text{-}C_6H_2]_2C\mathbf{H}_2$	3.67
$2,4\text{-}[4\text{-}(HO)\text{-}C_6H_4C\mathbf{H}_2]_2\text{-}C_6H_3OH$	4 = 3.72[g]

TABLE A-I (*continued*)

Material	Shift, ppm[a]
o-Chlorophenol–formaldehyde novolac; p,p'-methylene bridges	3.72[g]
Dehalogenated o-Chlorophenol–formaldehyde novolac; p,p'-methylene bridges	3.70[g]
Trioxane	5.00[f]
m-$\mathrm{HOC_6H_4\mathbf{CH_2}OH}$	4.63
$\mathrm{2,6\text{-}(\mathbf{CH_3})_2\text{-}4\text{-}(HOCH_2)\text{-}C_6H_2OH}$	2.45[d]
$\mathrm{4\text{-}(\mathbf{CH_3})\text{-}2,6\text{-}(HOCH_2)_2\text{-}C_6H_2OH}$	2.22[e]
$\mathrm{4,6\text{-}(\mathbf{CH_3})_2\text{-}2\text{-}(HOCH_2)\text{-}C_6H_2OH}$	4 = 2.22,[d] 6 = 2.38[d]
$\mathrm{[3,5\text{-}(\mathbf{CH_3})_2\text{-}2\text{-}(HO)\text{-}C_6H_2CH_2]_2O}$	2.17,[f] 2.18[f]
$\mathrm{[3,5\text{-}(\mathbf{CH_3})_2\text{-}4\text{-}(HO)\text{-}C_6H_2]_2CH_2}$	2.18

[a] Chemical shifts are for the protons designated by bold-face type. Chemical shifts for the aromatic ring protons were in the range from about 6.58–7.67 ppm. Sample concentrations were between 5 and 25 wt.-% model compound in dry acetone, except where designated to be otherwise.

[b] Data obtained from a 10 vol.-% solution of 50 wt.-% formalin in acetone. The shifts and proton exchange rates were markedly dependent on temperature and the formaldehyde:water:acetone ratios.

[c] Data obtained from dilute acetone solutions of products resulting from the heating of slightly basic excess benzyl alcohol with paraformaldehyde and from the freeze-drying of a slightly basic solution of saligenin in excess formalin.

[d] Data taken from solutions which were 15 wt.-% model compound in dry pyridine.

[e] Data taken from solutions which were 15 wt.-% model compound in dry DMSO.

[f] Data taken from solutions which were 15 wt.-% model compound in carbon tetrachloride.

[g] Results of Hirst et al.[11] Their data have been converted from the low-field $C^{13}\mathbf{H}_3$ line of acetone as their primary reference to internal TMS as the secondary reference, by taking their primary reference as 188 cycles/sec. on the secondary reference scale at 30°C. and ν_0 = 60 Mcycles/sec.

number of methylene protons in benzyl-type hemiformal groups, $\mathrm{Ar(\mathbf{CH_2}O)_2H}$, 4.95–4.76 ppm; A_4 = relative number of methylene protons in o-hydroxymethyl groups, o-$\mathrm{HOAr\mathbf{CH_2}OH}$, 4.80–4.63 ppm; A_5 = relative number of methylene protons in p-hydroxymethyl groups, p-$\mathrm{HOAr\mathbf{CH_2}OH}$, 4.55–4.47 ppm; A_6 = relative number of methylene protons in o,o'- and in o,p'-diphenylmethane-type methylene bridges, o,o'- plus o,p'-$\mathrm{HOAr\mathbf{CH_2}ArOH}$, 3.98–3.83 ppm; A_7 = relative number of methylene protons in p,p'-diphenylmethane-type methylene bridges, p,p'-$\mathrm{HOAr\mathbf{CH_2}ArOH}$, 3.77–3.67 ppm.

The value of A_1, which is also the relative number of aromatic rings, cannot be measured experimentally for resoles, because of exchange among the phenolic and other types of hydroxyl protons present. Because of small amounts of water usually present in novolacs, the values of A_1 measured for these resins are usually too high. The values of A_1 are, therefore, most reliably obtained via calculation from other experimental integrals; viz.

$$A_1 = (1/5)[A_2 + (A_3/4) + (1/2)(A_4 + A_5) + A_6 + A_7] \qquad \text{(AII-1)}$$

TABLE A-II
Acetylated Materials

Material	Shift, ppm[a]
$(AcO)_2C\mathbf{H}_2$	5.60[b]
$AcOC\mathbf{H}_2(OCH_2)_xOC\mathbf{H}_2OAc$	5.32–5.30[b]
$AcOCH_2(OC\mathbf{H}_2)_xOCH_2OAc$	4.90–4.85[b]
$ArCH_2OC\mathbf{H}_2OAc$	5.28–5.17[c]
$C_6H_5C\mathbf{H}_2OAc$	5.10–5.05
$AcOC_6H_4C\mathbf{H}_2OAc$:	
ortho	5.03–5.02
meta	5.08–5.03
para	5.05–5.02
$2,4\text{-}(CH_3)_2\text{-}6\text{-}(AcOC\mathbf{H}_2)\text{-}C_6H_2OAc$	4.93
$2,6\text{-}(CH_3)_2\text{-}4\text{-}(AcOC\mathbf{H}_2)\text{-}C_6H_2OAc$	4.90
$2,6\text{-}(AcOC\mathbf{H}_2)_2\text{-}C_6H_3OAc$	5.02–4.98
$2,4\text{-}(AcOC\mathbf{H}_2)_2\text{-}C_6H_3OAc$	5.00
$2,4\text{-}(AcOC\mathbf{H}_2)_2\text{-}6\text{-}Cl\text{-}C_6H_2OAc$	2,4 = 5.00
$2,4,6\text{-}(AcOC\mathbf{H}_2)_3\text{-}C_6H_2OAc$	2,6 = 5.00–4.97 4 = 5.07–5.03
$[3,5\text{-}(AcOC\mathbf{H}_2)_2\text{-}4\text{-}(AcO)\text{-}C_6H_2]_2CH_2$	4.92
$ArC\mathbf{H}_2OCH_2OAc$	4.63–4.48
$(C_6H_5C\mathbf{H}_2)_2O$	4.53–4.48
$[3,5\text{-}(CH_3)_2\text{-}2\text{-}(AcO)\text{-}C_6H_2C\mathbf{H}_2]_2O$	4.27
$[3,5\text{-}(CH_3)_2\text{-}2\text{-}(HO)\text{-}C_6H_2C\mathbf{H}_2]_2O$	4.55
$[2\text{-}(AcO)\text{-}C_6H_4C\mathbf{H}_2]_2O$	4.40
$[4\text{-}(AcO)\text{-}C_6H_4C\mathbf{H}_2]_2O$	4.45
$[5\text{-}Cl\text{-}2\text{-}(AcO)\text{-}C_6H_3]_2C\mathbf{H}_2$	3.75
Acetylated *o,o′*-bridged novolac; methylene bridges	3.73
$[4\text{-}(AcO)\text{-}C_6H_4]_2C\mathbf{H}_2$	3.87
$[3,5\text{-}(AcOCH_2)_2\text{-}4\text{-}(AcO)\text{-}C_6H_2]_2C\mathbf{H}_2$	3.93
$\mathbf{Ac}OC_6H_5$	2.13
$\mathbf{Ac}OC_6H_4CH_2OAc$:	
ortho	2.27–2.18
meta	2.25–2.18
para	2.25–2.15
$2,4\text{-}(CH_3)_2\text{-}6\text{-}(AcOCH_2)\text{-}C_6H_2O\mathbf{Ac}$	2.18
$2,6\text{-}(CH_3)_2\text{-}4\text{-}(AcOCH_2)\text{-}C_6H_2O\mathbf{Ac}$	2.20
$2,6\text{-}(AcOCH_2)_2\text{-}C_6H_3O\mathbf{Ac}$	2.30–2.23
$2,4\text{-}(AcOCH_2)_2\text{-}C_6H_3O\mathbf{Ac}$	2.33
$2,4\text{-}(AcOCH_2)_2\text{-}6\text{-}Cl\text{-}C_6H_2O\mathbf{Ac}$	2.30
$2,4,6\text{-}(AcOCH_2)_3\text{-}C_6H_2O\mathbf{Ac}$	2.30 to 2.25
$[5\text{-}Cl\text{-}2\text{-}(\mathbf{Ac}O)\text{-}C_6H_3]_2CH_2$	2.20
$[4\text{-}(\mathbf{Ac}O)\text{-}C_6H_4]_2CH_2$	2.05
$[3,5\text{-}(AcOCH_2)_2\text{-}4\text{-}(\mathbf{Ac}O)\text{-}C_6H_2]_2CH_2$	2.23
$[4\text{-}(\mathbf{Ac}O)\text{-}C_6H_4CH_2]_2O$	2.15
$[2\text{-}(\mathbf{Ac}O)\text{-}C_6H_4CH_2]_2O$	2.10
$[3,5\text{-}(CH_3)_2\text{-}2\text{-}(\mathbf{Ac}O)\text{-}C_6H_2CH_2]_2O$	2.28
Acetylated *o,o′*-bridged novolac, **AcO**Ar	2.03
$C_6H_5CH_2O\mathbf{Ac}$	2.08 to 2.05
$AcOC_6H_4CH_2O\mathbf{Ac}$:	2.00–1.95
ortho	2.00–1.95
meta	2.05–1.97
para	2.03–1.97

TABLE A-II (*continued*)

Material	Shift, ppm[a]
$2,6\text{-}(CH_3)_2\text{-}4\text{-}(\mathbf{AcOCH_2})\text{-}C_6H_2OAc$	1.97
$2,6\text{-}(\mathbf{AcOCH_2})_2\text{-}C_6H_3OAc$	2.02–1.95
$2,4\text{-}(\mathbf{AcOCH_2})_2\text{-}C_6H_3OAc$	2 = 1.97, 4 = 2.00
$2,4\text{-}(\mathbf{AcOCH_2})_2\text{-}6\text{-}Cl\text{-}C_6H_2OAc$	2 = 1.97, 4 = 2.03
$2,4,6\text{-}(\mathbf{AcOCH_2})_3\text{-}C_6H_2OAc$	2,6 = 2.00–1.97 4 = 2.07–2.00
$[3,5\text{-}(\mathbf{AcOCH_2})_2\text{-}4\text{-}(AcO)\text{-}C_6H_2]_2CH_2$	1.93
$2,4\text{-}(CH_3)_2\text{-}6\text{-}(\mathbf{AcOCH_2})\text{-}C_6H_2OAc$	1.92
$Ar(CH_2O)_2\mathbf{Ac}$	1.98–1.92[c]
$(\mathbf{AcO})_2CH_2$	2.05–2.03[b]
$\mathbf{AcO}(CH_2O)_x\mathbf{Ac}$, $x > 1$	2.05–2.00[b]
$2,6\text{-}(\mathbf{CH_3})_2\text{-}4\text{-}(AcOCH_2)\text{-}C_6H_2OAc$	2.08
$[3,5\text{-}(\mathbf{CH_3})_2\text{-}2\text{-}(AcO)\text{-}C_6H_2CH_2]_2O$	2.07–2.13
$2,4\text{-}(\mathbf{CH_3})_2\text{-}6\text{-}(AcOCH_2)\text{-}C_6H_2OAc$	4 = 2.05, 2 = 2.23
$m\text{-}(\mathbf{AcO})_2C_6H_4$	2.10

[a] Chemical shifts for the aromatic ring protons were in the range of 6.58–7.67 ppm. Sample concentrations were between 5 and 25 vol.-% model compound in carbon tetrachloride.

[b] Data obtained from the products resulting from low-temperature acetylation of 50 wt.-% formalin in excess pyridine and excess acetic anhydride. Assignments were confirmed via VPC component analyses.[10]

[c] Data obtained from the acetates of products resulting from the heating of slightly basic, excess benzyl alcohol with paraformaldehyde and from the freeze-drying of slightly basic solutions of saligenin in excess formalin. Assignments were confirmed by VPC component analyses.[10]

The following ratios, defined in the text, may then be calculated from the above integrals:

$$R_A = A_2/A_1 \tag{AII-2}$$

$$R_{HF} = A_3/4A_1 \tag{AII-3}$$

$$R_{HM} = (A_4 + A_5)/2A_1 \tag{AII-4}$$

$$R_{MB} = (A_6 + A_7)/2A_1 \tag{AII-5}$$

$$r_{HM} = A_4/A_5 \tag{AII-6}$$

$$r_{MB} = A_7/A_6 \tag{AII-7}$$

Provided that methylene bridges do not bond the aromatic rings into cyclic structures, then the average number of aromatic rings per molecule $\bar{n}$ may be calculated from

$$\bar{n} = (1 - R_{MB})^{-1} \tag{AII-8}$$

and the number-average molecular weight, $\bar{M}_n(OH)$, is given by

$$\bar{M}_n(OH) = \bar{n}[89 + R_A + 61R_{HF} + 31\,R_{HM} + 14R_{MB}] \tag{AII-9}$$

B. Acetylated Materials

For acetylated resins, the various PMR integrals A_i are defined as follows: A_1 = relative number of aromatic ring protons, Ar**H**, 7.67–6.58 ppm; A_2 = relative number of methylene protons in acetoxymethyl ends of benzyl-type hemiformal acetates, $ArCH_2OC\mathbf{H}_2OAc$, 5.28–5.17 ppm; A_3 = relative number of methylene protons in acetoxymethyl groups, $ArC\mathbf{H}_2$-OAc, 5.08–4.90 ppm; A_4 = relative number of methylene protons in benzyl ends of benzyl-type hemiformal acetates, $ArC\mathbf{H}_2OCH_2OAc$, 4.63–4.48 ppm, plus those in dibenzyl-ether-type bridges, $(ArC\mathbf{H}_2)_2O$, 4.55–4.27 ppm; A_5 = relative number of diphenylmethane-type methylene protons, $ArC\mathbf{H}_2Ar$, 4.03–3.42 ppm; A_6 = relative number of methyl protons in acetoxyphenyl groups, ArO**Ac**, 2.33–2.13 ppm, some with bridged rings, 2.13–2.03 ppm; A_7 = relative number of methyl protons in acetoxymethyl groups, $Ar(CH_2O)_{1,2}\mathbf{Ac}$, 2.07–1.92 ppm.

The value of A_6, which is three times the relative number of aromatic rings, may be measured experimentally in the lower-molecular-weight resins. In higher molecular weight resins, the resolution between methyl protons in acetoxyphenyl groups and those in acetoxymethyl groups becomes poor. Fortunately, the value of A_6 may be calculated from

$$A_6 = (3/5)[A_1 + (1/2)(A_3 + A_4) + A_5] \qquad \text{(AII-10)}$$

or from

$$A_6 = (A_6 + A_7) - (3/2)(A_2 + A_3) \qquad \text{(AII-11)}$$

The acetylated resins frequently contain small amounts of acetic acid impurity, which leads to too high a value for A_7. When A_6 is not resolveable from A_7 in such resins, then eq. (AII-10) provides the sole means for obtaining A_6. The following ratios, defined in the test, may then be calculated from the above integrals, potentially in three independent ways.

$$R_A = 3A_1/A_6 \qquad \text{(AII-12)}$$

$$R_{AHF} = 3A_2/2A_6 \qquad \text{(AII-13)}$$

$$R_{AM} = 3A_3/2A_6 \qquad \text{(AII-14)}$$

$$R_{EB} = 3(A_4 - A_2)/4A_6 \qquad \text{(AII-15)}$$

$$R_{MB} = 3A_5/2A_6 \qquad \text{(AII-16)}$$

In the absence of cyclic structures, the values of $\bar{n}$ are given by

$$\bar{n} = (1 - R_{EB} - R_{MB})^{-1} \qquad \text{(AII-17)}$$

and the number-average molecular weights of the acetylated resins, $\bar{M}_n(\mathrm{Ac})$, are calculated from

$$\bar{M}_n(\mathrm{Ac}) = \bar{n}\,[131 + R_A + 103R_{AHF} + 73R_{AM} + 44R_{EB} + 14R_{MB}] \qquad \text{(AII-18)}$$

The authors thank Messrs. A. A. Bibeau and J. R. Ripley and Miss Virginia Lyons for assisting with some of the experimental work. We also thank Mr. Bibeau for writing a computer program to calculate results from the raw PMR data and Professor W. J. Burke for the gift of several model compounds and for copies of spectral data described by reference 11.

References

1. Megson, N. J. L., *Phenolic Resin Chemistry*, Academic Press, New York, 1958; R. W. Martin, *The Chemistry of Phenolic Resins*, Wiley, New York, 1956.

2. Martin, R. W., *Anal. Chem.*, **23**, 883 (1951).

3. Lilley, H. S., and D. W. J. Osmond, *J. Soc. Chem. Ind.* (*London*), **66**, 425 (1947).

4. Richards, R. E., and H. W. Thompson, *J. Chem. Soc.*, **1947**, 1260.

5. Bender, H. L., *Mod. Plastics*, **30**, No. 6, 136 (1953).

6. Burke, W. J., S. H. Ruetman, and H. P. Higginbottom, *J. Polymer Sci.*, **38**, 513 (1959).

7. Conley, R. T., and J. P. Bieron, *Appl. Spectry.*, **1**, 82 (1961); *J. Appl. Polymer Sci.*, **7**, 103, 107 (1963); R. T. Conley, in *Proceedings of the Battelle Symposium on Thermal Stability of Polymers*, Battelle Memorial Institute, Columbus, Ohio, Dec. 1963.

8. Freeman, J. H., *Anal. Chem.*, **24**, 955, 2001 (1959).

9. Reese, J., *Kunststoffe*, **45**, 137 (1955).

10. Higginbottom, H. P., H. M. Culbertson, and J. C. Woodbrey, *Anal. Chem.*, submitted for publication.

11. Hirst, R. C., W. J. Burke, and D. M. Grant, paper presented before the Pittsburgh Conference on Analytical Chemistry and Applied Spectroscopy, Pittsburgh, Pa., March 1962, *J. Polymer Sci.*, in press.

12. Finn, S. R., and J. W. James, *Chem. Ind.* (*London*), **1954**, 1252.

13. Freeman, J. H., and C. W. Lewis, *J. Am. Chem. Soc.*, **76**, 2080 (1954).

Résumé

A cause de leur importance commerciale, les étapes de la réaction et les structures des résines produites lorsque le phénol réagit avec le formaldéhyde ont été étudiées par différentes méthodes chimiques et physiques. De nombreux détails concernant ces réactiones et les structures chimiques complexes ne sont pas encore entiérement compris. La plupart des méthodes expérimentales employées fournissent seulement une information qualitative. Beaucoup de ces méthodes ne sont applicables que pour les fractions de prépolymères solubles de faible poids moléculaire. Ce présent travail décrit les méthodes de résonance magnétique nucléaire (PMR) qui fournit des structures moyennes en nombre d'une façon quantitative et détaillée pour toute résine phénol-formaldéhyde soluble. On montre que les hémiformals de type benzyle apportent une contribution substantielle aux structures de nombreux résoles et que ces fonctionnalités présentent une stabilité relativement élevée dans certaines conditions du traitement initial. Les structures de plusieurs résines sont discutées sur la base de certains aspects de réactions qui ont lieu durant les synthéses de résines. Ces réactions comprennent les hydroxyméthylations et les condensations produisant des ponts de type diphénylméthane et dibenzyl-éther. Pour définir les mécanismes et les vitesses des diverses réactions à des températures différentes et dans des conditions catalytiques différentes, une étude beaucoup plus détaillée est nécessaire. Potentiellement les méthodes PMR décrites peuvent fournir le plus de données quantitatives nécessaires.

Zusammenfassung

Wegen ihrer technischen Bedeutung wurden die bei der Reaktion von Phenol mit Formaldehyd auftretenden Reaktionsfolgen und gebildeten Harzstrukturen mit verschiedenen chemischen und physikalischen Methoden untersucht. Viele Einzelheiten dieser Reaktionen und komplexen chemischen Strukturen sind noch immer nicht ganz klar. Die meisten angewendeten Versuchsmethoden haben nur eine qualitative Information geliefert. Viele dieser Methoden konnten nur auf den niedermolekularen Anteil der löslichen Vorpolymeren angewandt werden. In der vorliegenden Arbeit werden protonmagnetische Resonanz-(PMR)-methoden beschrieben, welche detaillierte und quantitative Zahlenmittelstrukturen für ein beliebiges lösliches Phenolformaldehydharz liefern. Es wird gezeigt, dass Hemiformale von Benzyltyp einen wesentlichen Beitrag zur Struktur vieler Resole bilden und dass diese Funktionalität eine verhältnissmäsig hohe Stabilität unter gewissen Anfangshärtungsbedingungen aufweist. Die Struktur einiger Harze wird auf Grundlage gewisser Aspekte der Reaktionen, welche während der Harzsynthese auftreten, diskutiert. Zu diesen Reaktionen gehören Hydroxymethylierungen und Kondensationen, die zu Brücken vom Diphenylmethantyp und Dibenzyläthertyp führen. Um den Mechanismus und die Geschwindigkeit der bei verschiedenen Temperaturen und unter verschiedenen katalytischen Bedingungen auftretenden Reaktionen festzulegen, ist eine viel mehr in die Einzelheiten gehende Untersuchung notwendig. Grundsätzlich können die beschriebenen PMR-Methoden die meisten der notwendigen quantitativen Daten liefern.

Received July 6, 1964
Revised September 9, 1964

JOURNAL OF POLYMER SCIENCE: PART A VOL. 3, PP. 1107–1125 (1965)

Dye-Sensitized Photopolymerization. I. Polymerization of Acrylamide in Aqueous Solution Sensitized by Methylene Blue–Triethanolamine System

CATHERINE S. HSIA CHEN,* *Central Research Division, American Cyanamid Company, Stamford, Connecticut*

Synopsis

The polymerization of aqueous acrylamide induced by visible light in the presence of methylene blue–triethanolamine as the sensitizing system has been investigated. The polymerization was found to follow a nonsteady-state kinetic scheme. The rate was proportional to the first power of the absorbed light intensity and approximately proportional to the initial monomer concentration. The rate passed through a maximum as a function of the initial dye concentration. The molecular weights of the polymers were in the range of one million. The molecular weights were independent of the absorbed light intensity, essentially directly proportional to the initial monomer concentration, and decreased logarithmically with the initial dye concentration. Both spectroscopy and polymerization behavior suggest that the monomeric form of the dye is a photosensitizer while the associated form is a chain terminator. The kinetic chains were terminated unimolecularly, and the molecular weights were governed by a chain transfer process.

INTRODUCTION

Dye-sensitized photopolymerization was reported first by Bamford and Dewar[1] for styrene, by Oster and co-workers[2–7] for acrylamide and other vinyl monomers, and by other investigators.[8–11]

In Oster's system, a photoreducible dye and a weak reducing agent were used in the monomer solution. The reducing agent was so chosen that it reduced the dye only with the aid of the extra energy from the light absorption. An appropriate amount of oxygen was essential for the initiation of polymerization. The mechanism for the free radical formation proposed was as shown in eqs. (1)–(4):

$$D + RH_2 \xrightarrow{\text{Dark}} \text{No reaction} \tag{1}$$

$$D \xrightarrow{\text{Light}} D^* \tag{2}$$

$$D^* + RH_2 \longrightarrow LD + R^\bullet \tag{3}$$

$$LD + O_2 \longrightarrow SD\cdot + OH\cdot \tag{4}$$

---

* Present address: Summit Research Laboratories, Celanese Corporation of America, Summit, New Jersey.

where D and D* represent the dye and the light excited dye, respectively; LD represents the leuco dye, RH_2 the reducing agent, R^0 the oxidized form of the reducing agent, and SD the semidye or the semiquinone form of the dye. However, Shepp, Chaberek, and MacNeil[10] found that, with the acrylamide–thionine system, a reducing agent was not necessary if oxygen was carefully excluded from the system. The proposed mechanism is represented in eqs. (5) and (6)

$$D \xrightarrow{\text{light}} D^* \tag{5}$$

$$D^* + OH^- \longrightarrow SD\cdot + OH\cdot \tag{6}$$

Dye-sensitized photopolymerization usually proceeds very rapidly. In addition, high quantum yields are obtained. For example, in the acrylamide–riboflavin system, Oster, Oster, and Prati[4] reported a quantum yield of monomer consumption $\phi_m = 4.9 \times 10^3$. For another example, in the acrylamide–thionine system in the absence of oxygen, Shepp, Chaberek, and MacNeil[10] obtained quantum yields ranging from $\phi_m = 1.6 \times 10^2$ to 3.8×10^3.

In these laboratories, a study of dye-sensitized photopolymerization has been undertaken in the hope of further improving both the rates and the quantum yields of the polymerization. Some of our initial results are reported in this series of communications. The first paper is concerned with some fundamental aspects of visible light-induced polymerization of aqueous acrylamide in air sensitized by a methylene blue–triethanolamine system.

EXPERIMENTAL

Light Source

A 250-watt General Electric infrared lamp with a reflector was used. A fixed distance of $5^3/_4$ in. from the envelope of the lamp to the surface of the solution was employed. Different intensities of the incident light were achieved by varying the voltage by means of a Variac. The lamp was calibrated against a tungsten lamp with standard color temperature by means of a Beckman DK-2A spectrophotometer using an integrating sphere. The spectral energy distribution of the lamp at a distance of $5^3/_4$ in. at wave numbers ($\bar{\nu}$) 1400–24500 cm.$^{-1}$ (wavelengths λ = 4000–7700 A.) is shown in Figure 1 for 110 v.; $^1/_2$ and $^1/_4$ the intensity were obtained by changing to 95 and 80 v., respectively. In one series of experiments an interference filter (Bausch and Lomb λ peak = 663 mμ; transmission = 40%; half width = 11 mμ) was used to obtain essentially monochromatic light.

Materials

Acrylamide (American Cyanamid Company) was recrystallized twice from methanol and was dried in vacuum. Methylene blue (Fisher bio-

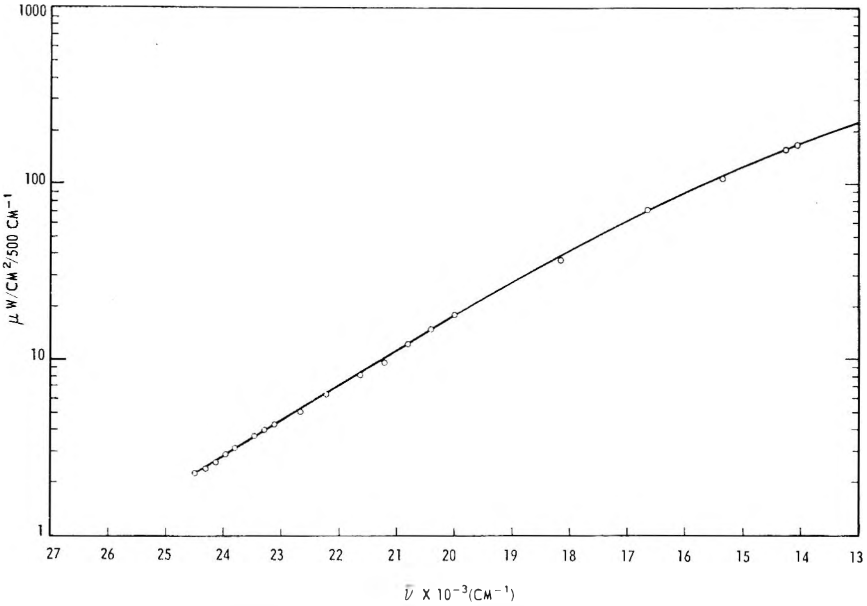

Fig. 1. Spectral energy distribution of the light source. G. E. Infrared lamp with reflector, 250 w. Distance = $5^3/_4$ in.

logical stain) and triethanolamine (Eastman, white label) were used without further purification.

Spectroscopy

Absorption spectra (optical density versus wavelength) of the dye solutions were ascertained by using a Cary Model 14 spectrophotometer. They were replotted as extinction coefficient versus wave number for more convenient presentation and comparison. Observations of the fading of the dye were also performed by use of the Cary 14 spectrophotometer. The decrease of the peak absorption at 665 mμ with time of exposure was followed. Complete fading was indicated when the optical density at 665 mμ decreased to zero.

Polymerization

Aqueous acrylamide solutions of definite molar concentrations, each containing $2.0 \times 10^{-2}M$ triethanolamine, were prepared in volumetric flasks. Methylene blue solutions, 100 times the final molar concentrations employed in polymerizations, were prepared in separate volumetric flasks. A 50-ml. open cylindrical cell, 4 cm. in diameter, was used as the polymerization vessel. A 10-ml. portion of an acrylamide–triethanolamine solution was pipetted into the cell. The thickness of the solution was 0.8 cm. The cell was centered underneath the lamp and immersed in a constant temperature bath (0°C. or 25 ± 0.1°C.). While in the dark, 0.1 ml. of a methylene blue solution was pipetted into the cell. After stirring and allowing the solution to attain temperature equilibrium, the lamp was switched on for a predetermined interval of time. Immediately after switching off the light, the polymer formed was precipitated in excess methanol and collected on a sintered glass filter. The per cent polymerization was determined gravimetrically. The molecular weights of the polymers were determined by measuring the intrinsic viscosities of the polymers in $1N$ NaCl solution at 30°C. Weight-average molecular weights ($\bar{M}_w$) were calculated from the relationship determined in these laboratories.[12]

$$[\eta]_{1N\ \mathrm{NaCl}}^{30} = 3.73 \times 10^{-4}(\bar{M}_w)^{0.66} \tag{7}$$

Energy Absorption

The total energy absorbed by a methylene blue solution was calculated by integrating the area under the absorption spectrum between wave numbers 24000 and 13000 cm.$^{-1}$. The energy absorbed in each 500 cm.$^{-1}$ was ascertained by means of the absorption spectrum and the spectral energy distribution of the light source (Fig. 1). The total energy absorbed (mw./cm.^{2}) was taken as the sum of the energy between 24000 and 13000 cm.$^{-1}$ at the thickness of the cell used. It was then converted to the total energy absorbed (milliwatts) corresponding to the size of the polymerization cell (12.57 cm.^{2} × 0.8 cm.). Energy absorption was ascertained in the above-described manner for several concentrations of methylene blue between 0.1×10^{-5} and $100 \times 10^{-5}M$.

When the interference filter was used, spectra of the filter alone and the filter plus a solution containing $7.0 \times 10^{-5}M$ methylene blue and $7M$ acrylamide were obtained. The solution was of the actual concentrations of the dye and acrylamide employed in this series of polymerization experiments. Energy absorbed in each case was calculated in the same manner as described above. The difference between the two values was taken as the energy absorbed by the solution.

Quantum Yields

Quantum yields were calculated for the polymerization experiments where the interference filter was used. One quantum energy, $E = h\nu = hc/\lambda$ was calculated, based on $\lambda = 663$ mμ, to be 2.997×10^{-12} ergs. The quantum yields in monomer consumption (ϕ_m) were calculated as the number of monomer molecules consumed per one quantum of light absorbed. The quantum yields in polymer formation (ϕ_p) were calculated as the number of polymer molecules formed per one quantum of light absorbed. The values for ϕ_p were actually obtained by dividing ϕ_m by $\bar{M}_n$ of the polymers.

RESULTS AND DISCUSSION

Polymerization Rates

The conversion versus time curves for the polymerization of 1, 2, 4, and $7M$ acrylamide solutions ($7.0 \times 10^{-5}M$ methylene blue–$2.0 \times 10^{-2}M$

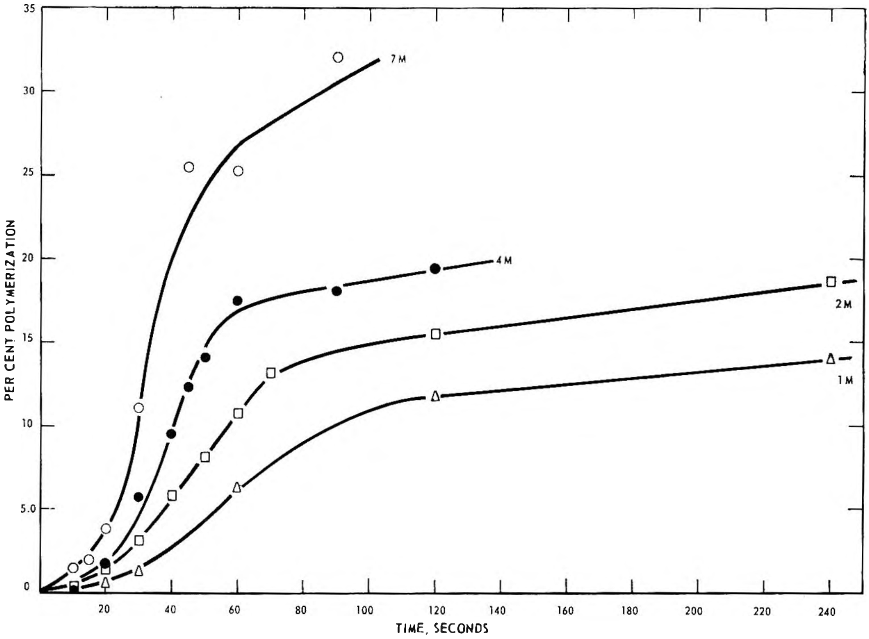

Fig. 2. Polymerization of acrylamide solutions of different concentrations at 25°C.; [methylene blue] = $7.0 \times 10^{-5}M$ [triethanolamine] = $2.0 \times 10^{-2}M$.

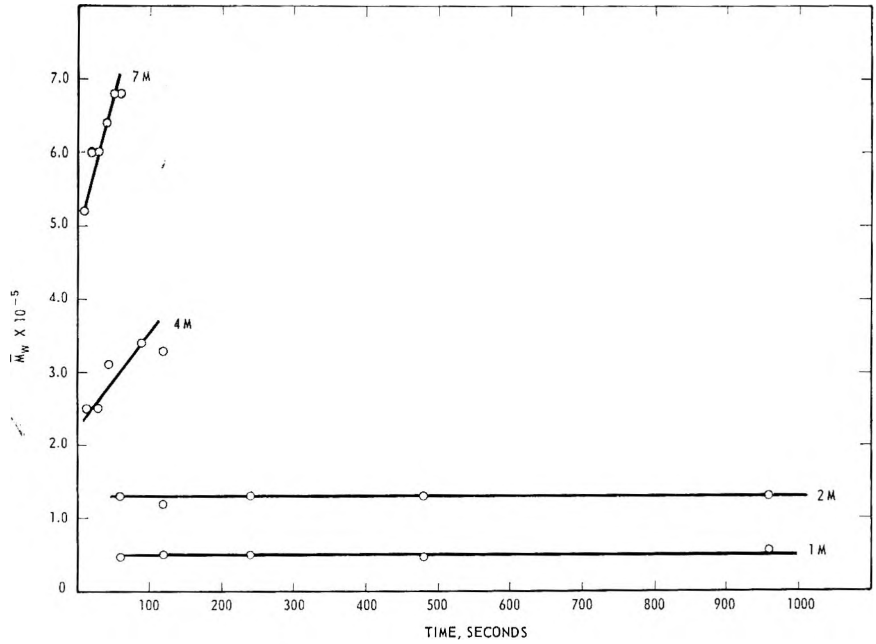

Fig. 3. Molecular weights of polymers obtained under conditions of Figure 2.

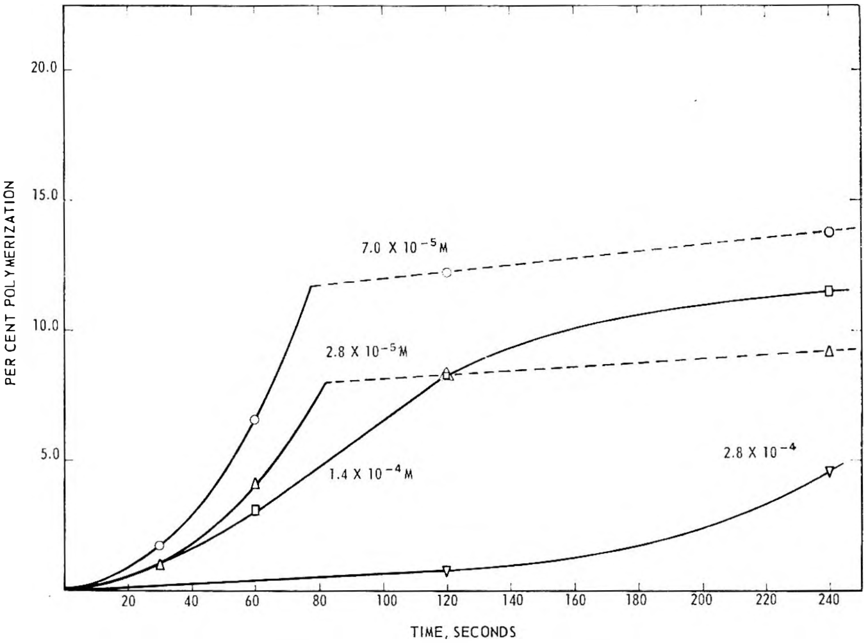

Fig. 4. Polymerization of 1M acrylamide sensitized by different amounts of methylene blue at 0°C.; [triethanolamine] = $2.0 \times 10^{-2}M$.

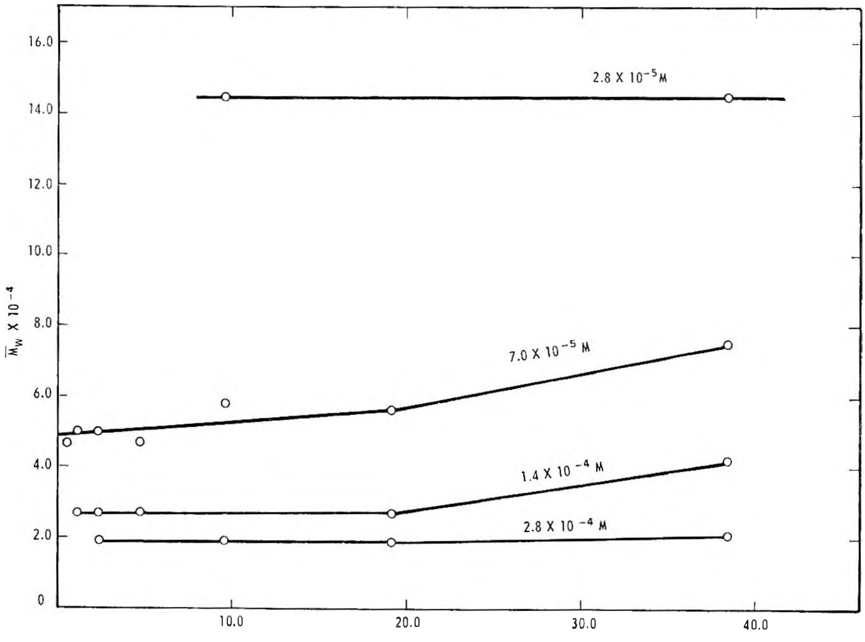

Fig. 5. Molecular weights of polymers obtained under conditions of Figure 4.

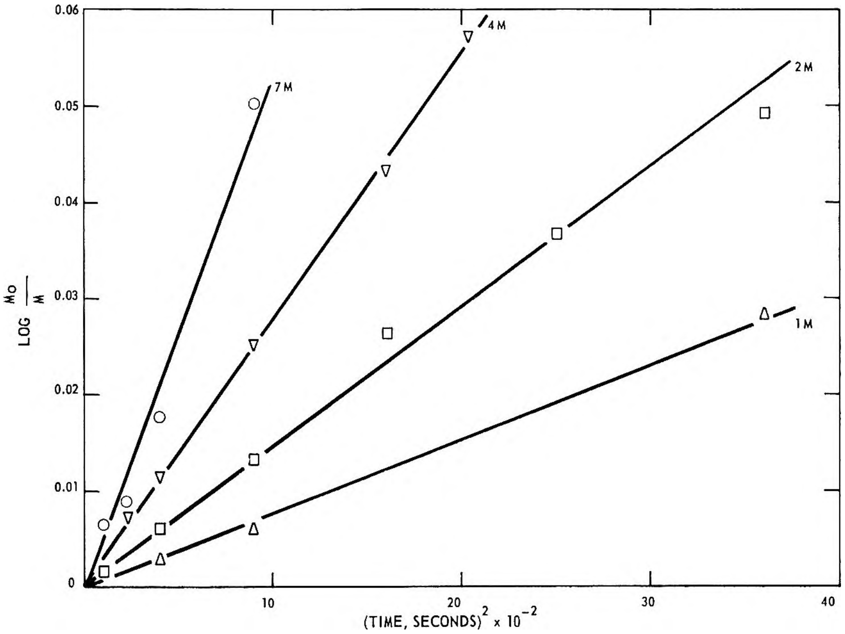

Fig. 6. Rates of photopolymerization at 25°C. of acrylamide at different monomer concentrations; [methylene blue] = $7.0 \times 10^{-5}M$, [triethanolamine] = $2.0 \times 10^{-2}M$.

triethanolamine) at 25°C. are recorded in Figure 2 and the molecular weights of the polymers in Figure 3. The results of the polymerization of $1M$ acrylamide–$2.0 \times 10^{-2}M$ triethanolamine at 0°C. as a function of the concentration of methylene blue are represented in Figure 4 and the molecular weights of the polymers are shown in Figure 5. The polymerization kinetics are quite complicated. The initial nonlinear portion of the curves represents the polymerization before the complete fading of methylene blue while the latter linear portion represents that after fading. It should be noted that before fading of the dye, the rate actually increases with time. In the rate expression,

$$-dM/dt = k_p[\mathrm{M}][\mathrm{R}\cdot] \tag{8}$$

where [M] is the monomer concentration, k_p is the rate constant for propagation, and $[\mathrm{R}\cdot]$ is the radical concentration, if it is assumed that k_p is a constant, the increase in rate with time can be attributed only by an increase in $[\mathrm{R}\cdot]$. Thus, if $[\mathrm{R}\cdot] \propto t$, the rate can be expressed as the following:

$$-dM/dt = Kt[\mathrm{M}] \tag{9}$$

or

$$\log [\mathrm{M}_0]/[\mathrm{M}] = (K/4.606)t^2 \tag{10}$$

where $[M_0]$ is the initial monomer concentration, $[M]$ is the remaining monomer concentration, t is the polymerization time, and K is a proportionality constant including initiation, propagation, functions of dye concentration, and light intensity. The factor represented by K is obviously complex since, even with constant initial dye concentration and constant incident light, the dye fades as polymerization proceeds and the system in turn absorbs less light. However, when the initial part of the nonlinear portions of the curves in Figures 2 and 4 are replotted as log $[M_0]/[M]$ against t^2, sets of straight lines are obtained as represented in Figures 6 and 7, respectively. The slopes are values for $K/4.606$ and represent the rates of polymerization.

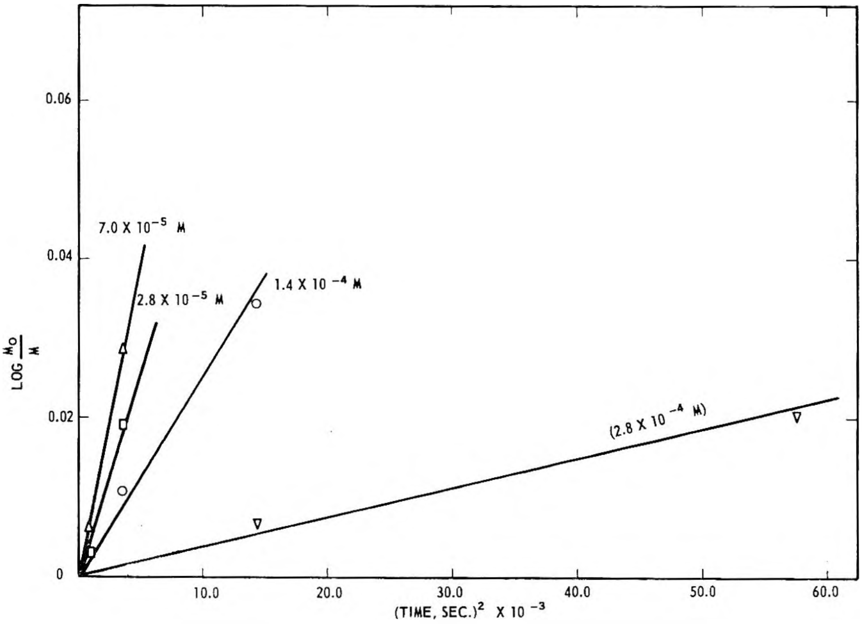

Fig. 7. Rates of photopolymerization at 0°C. of acrylamide at different concentrations of methylene blue; [triethanolamine] = $2.0 \times 10^{-2}M$.

The molecular weights of the polymers were observed to remain essentially unchanged with time (Fig. 5 and two lower curves in Fig. 3) or to increase somewhat with time in more concentrated acrylamide solutions (two upper curves in Fig. 3). This indicates that chain transfer might be taking place. Alcohols are known to be good chain transfer agents for the polymerization of acrylamide; triethanolamine, $N(CH_2CH_2OH)_3$, used here thus might serve both as a reducing agent for the dye and as a chain transfer agent for the polymerization of acrylamide. In more concentrated solutions, the medium becomes quite viscous as the polymerization proceeds. The increase in molecular weight could be explained by the increasing viscosity of the medium and a resultant decrease in the rate of diffusion of the chain transfer agent to the growing polymer chains.

It should be mentioned that except for the induction period which Oster, Oster, and Prati[4] obtained in the acrylamide–riboflavin system in air, the shape of the curves obtained in the present work before the fading of dye is similar to theirs. As should be expected, the curves differ from those reported by Shepp, Chaherek, and MacNeil for the acrylamide–thionine system in the absence of a reducing agent and oxygen.

Effects of the Concentration of Methylene Blue

Effect on Light Absorption. The absorption spectra of methylene blue solutions in water at four molar concentrations are depicted in Figure 8. There are two peaks in the absorption spectrum of methylene blue in the visible region: $\lambda_{max} \simeq 610$ and 665 mμ (or $\nu \simeq 16400$ and 15040 cm.$^{-1}$). These represent two forms of the dye molecules. In unbuffered solutions, the relative intensities of the two peaks vary with the concentration of the dye. The four spectra depicted in Figure 6 are so chosen that such variation is indicated clearly. Other spectra of methylene blue in water and alcohol and those in the presence of various electrolytes can be found in the literature.[13] It has been known for a long time[14–17] that the absorption spectra of the majority of organic dyestuffs in aqueous solution do not obey Beer's law. The deviation from Beer's law is accounted for by the hypothesis of a reversible dimerization and "polymerization" of the dye molecules. The peak at the higher wavelengths (α band) represents the monomeric dye molecules while that at the lower wavelength (β band) represents the associated dye molecules. In Figure 9 the following results are plotted: (*1*) the total energy absorption (circles), (*2*) the extinction coefficients of the peak at $\lambda \simeq 610$ mμ (ϵ_{610}, squares) and (*3*) the extinction coefficients of the peak at $\lambda = 665$ mμ (ϵ_{665}, triangles), as a function of the concentration of methylene blue. It is shown that ϵ_{610} increases with the concentration of methylene blue (squares), but on the other hand ϵ_{665} first increases with the concentration of methylene blue, reaching a maximum at 1×10^{-5}–$4 \times 10^{-5}M$. It then decreases with increasing concentration (triangles). However, it is significant that the total energy absorption, obtained by means of area integration, increases with the concentration of methylene blue (circles).

Effect on Polymerization. The relationship between the rates of polymerization, taken as the slope of the straight lines of log [Mo]/[M] versus t^2 plots, and the concentration of methylene blue is represented in Figure 10 for 0 and 25°C. and [acrylamide] = 1 and 7*M*. In the same figure also are shown the corresponding molecular weights. The polymerization rate varied in the similar way as the ϵ_{665} absorption. The rate of polymerization first increased with the concentration of methylene blue, reaching a maximum at between 5×10^{-5} and $6 \times 10^{-5}M$; it then decreased with the dye concentration and no polymerization took place at a concentration of $84 \times 10^{-5}M$ at 0°C. Similar behavior for rate of polymerization has been observed in other cases of dye-sensitized polymerization.[4,8,10] It has been suggested that a higher concentration of dye molecules may quench the

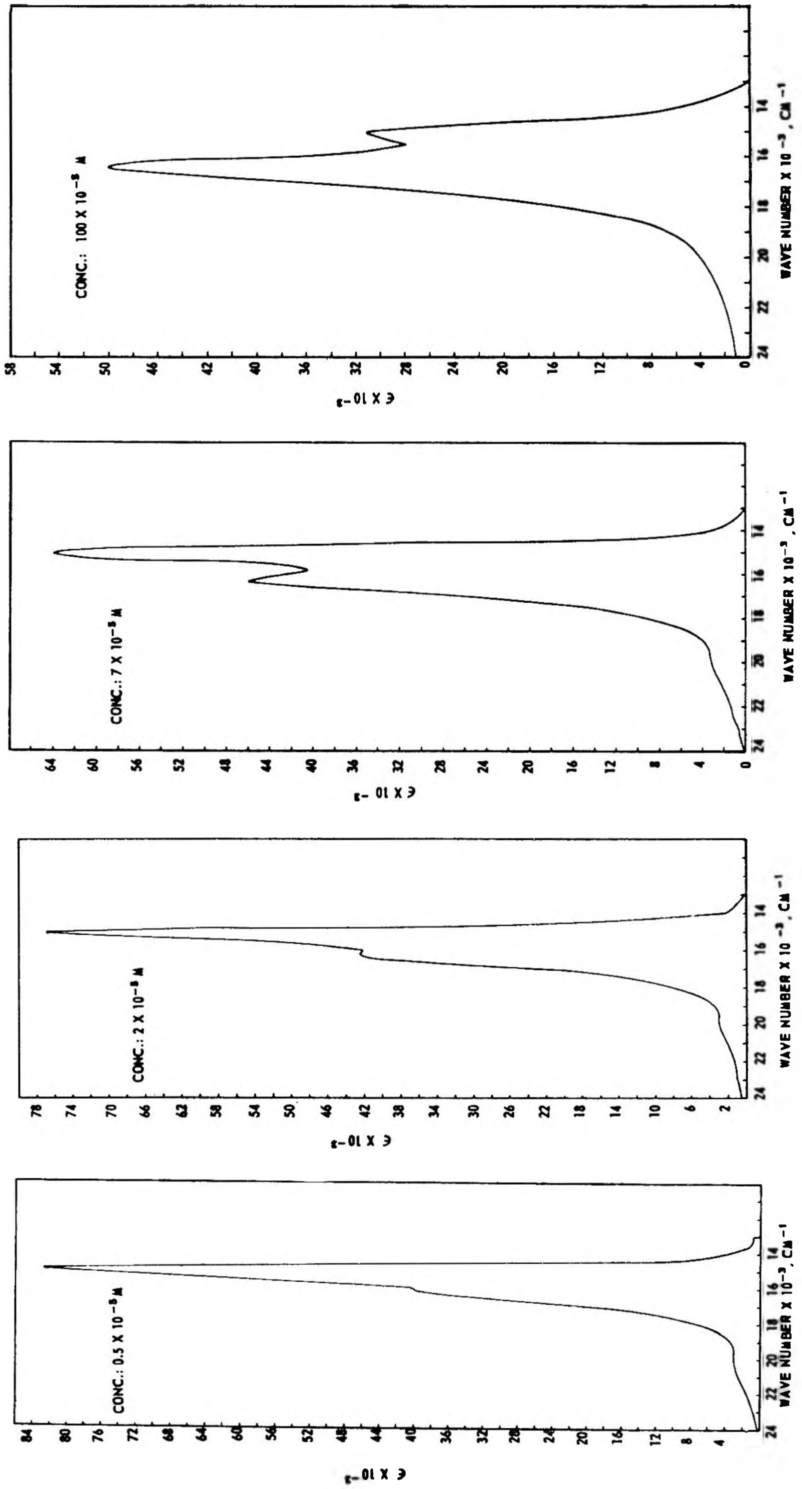

Fig. 8. Absorption spectra of methylene blue solutions.

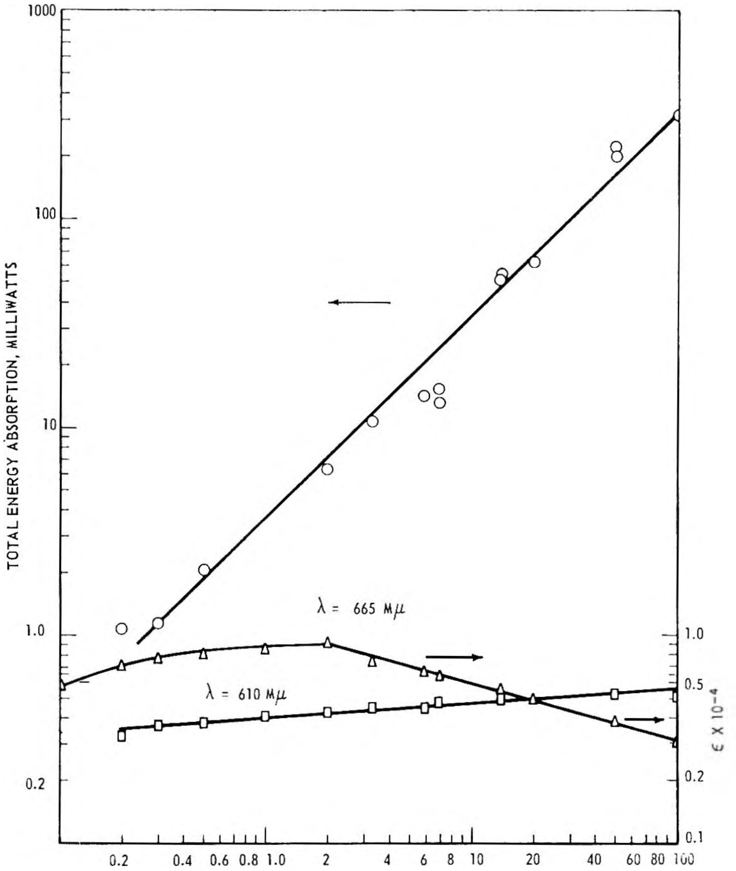

Fig. 9. Plots of ϵ_{665}, ϵ_{610}, and total energy absorption as a function of methylene blue concentration.

triplet state, thus depressing the initiation of polymerization. However, our results show that the molecular weight of the polymers decreases logarithmically with the concentration of methylene blue. This indicates that high concentrations of dye also terminate the polymer chains. Methylene blue in the concentration range 0.1–10% has been used as an inhibitor for polymerization.

Based on our observations both in spectroscopy (Fig. 9) and in polymerization (Fig. 10), the following interpretation is suggested: the monomeric form of methylene blue (λ_{max} = 665 mμ) is a photosensitizer, while the associated form (λ_{max} = 610 mμ) is a chain terminator, probably by degradative chain transfer, and is eventually an inhibitor for polymerization. This interpretation is in accordance with the facts that (*1*) the polymerization rate changes with the dye concentration in a similar manner to ϵ_{665} or the rate increases with the concentration of the monomeric form of the dye; (*2*) the molecular weight decreases with the increase of ϵ_{610} as the dye solution becomes more concentrated. In other words, both

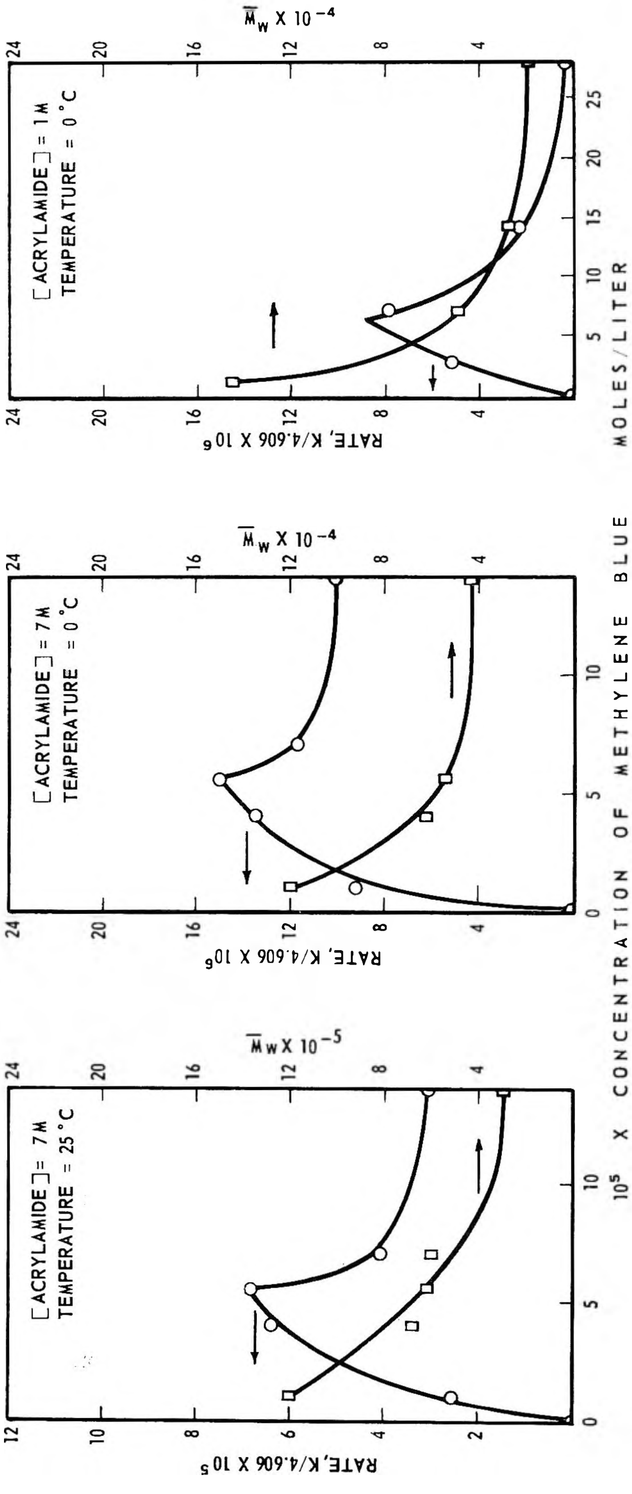

Fig. 10. Effect of methylene blue concentration on the polymerization at [triethanolamine] = 2.0 × $10^{-2}M$. (○) rate; (□) molecular weight.

the rate and the molecular weight decrease with the increase in concentration of the associated form of the dye. It is then understandable that beyond a certain concentration of methylene blue, where the associated form (terminator) becomes predominant, no polymerization takes place.

Since the total energy absorption increases with the dye concentration, that the maximum rate of polymerization occurred between 5×10^{-5} and $6 \times 10^{-5}M$ instead of between 1×10^{-5} and $4 \times 10^{-5}M$ might be attributed to a balance between the concentration of the monomeric form of the dye and the total energy absorption. Thus there would be a closer similarity between the quantum yield–concentration and the ϵ_{665}–concentration plots.

Effects of the Concentration of Acrylamide

Effect on Photobleaching of Methylene Blue. The results for the dependence of photobleaching of methylene blue–triethanolamine on the concentration of acrylamide are recorded in Figure 11 (circles). The rate of

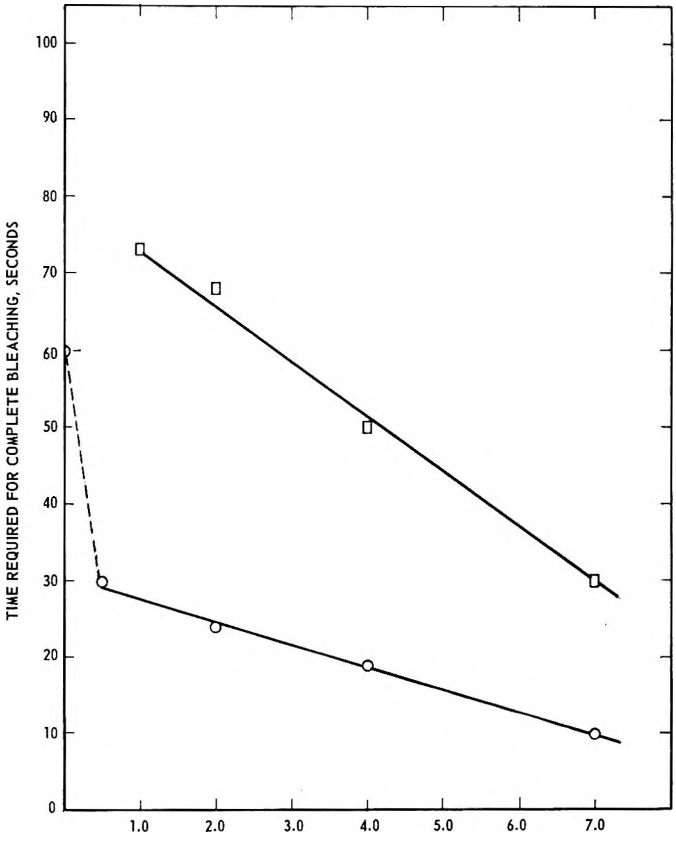

Fig. 11. Photobleaching of methylene blue as a function of acrylamide concentration: (○) [methylene blue] = $2.8 \times 10^{-5}M$, [triethanolamine] = $2.0 \times 10^{-2}M$, using near infrared in Cary 14 spectrophotometer at 25°C.; (□) taken from polymerization data at 25°C. in Figure 2.

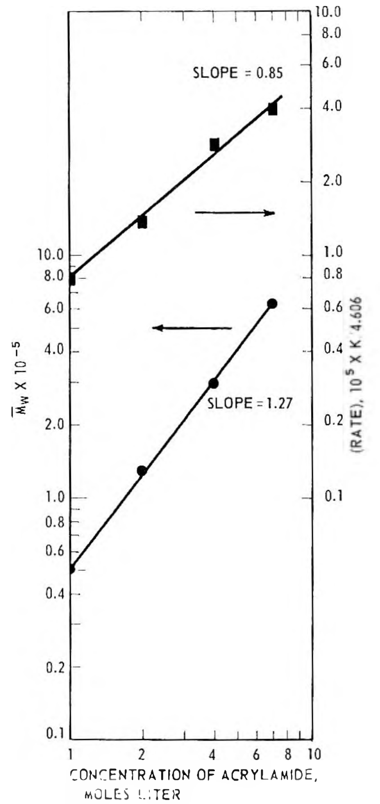

Fig. 12. Effect of concentration of acrylamide on the polymerization at [methylene blue] = $7.0 \times 10^{-5}M$, [triethanolamine] = $2.0 \times 10^{-2}M$, temperature = 25°C.: (■) rate; (●) M_w.

bleaching increases with the concentration of acrylamide. The time required for complete bleaching of the dye decreased to half when $1M$ acrylamide was added to methylene blue–triethanolamine solution. From [acrylamide] = $1M$ to $7M$, the time required for complete bleaching decreased linearly, however, at a lesser speed. No induction time for fading was observed in any case. In addition, it was observed in actual polymerization experiments (summarized in Fig. 2) that the time required for complete fading of the dye decreased with increasing acrylamide concentration also. They are represented as the squares in Figure 11; again a linear relationship between the rate of bleaching and the concentration of acrylamide is indicated. These results suggest that acrylamide participates in the bleaching of methylene blue, logically by displacing the equilibrium when the radicals are removed in initiating the polymer chains.

Effect on Polymerization. Both the rates of polymerization and the molecular weights of the polymers increase with the acrylamide concentration. The rates are obtained from the slopes of the straight lines in Figure 2 and the molecular weights are the average values taken from Figure 3.

As depicted in Figure 12, the squares represent a plot of log rates versus log [acrylamide], while the circles represent that of log molecular weights versus log [acrylamide]; respective slopes of 0.85 and 1.27 are calculated. These results indicate that, in essence, both the rate and the molecular weight are directly proportional to the concentration of acrylamide.

Effect of Light Intensity

The results for the polymerization of 7*M* acrylamide at 25°C. at three different light intensities (1:1/2:1/4) are summarized in Table I. They are plotted as log $[M_0]/[M]$ versus $(\text{time})^2$ in Figure 13. Again the rates are represented by the values $K/4.606$ obtained as the slopes of the straight lines. The relationship of the rates and light intensity is derived as rate $\propto$ $[\text{light intensity}]^{1.0}$. The molecular weights do not seem to be affected greatly by the light intensity (Table I). Based on the first-order dependence of the light intensity it can be concluded that the termination of the kinetic chains is unimolecular. This agrees with the proposition that a terminator is present, since in its absence free radical polymerization is terminated by combination (bimolecular termination) and the rate would depend on the square root of the light intensity. With regard to the molecular weight, in homogeneous kinetics, when the termination is unimolecular, it follows that the molecular weight is independent of the light

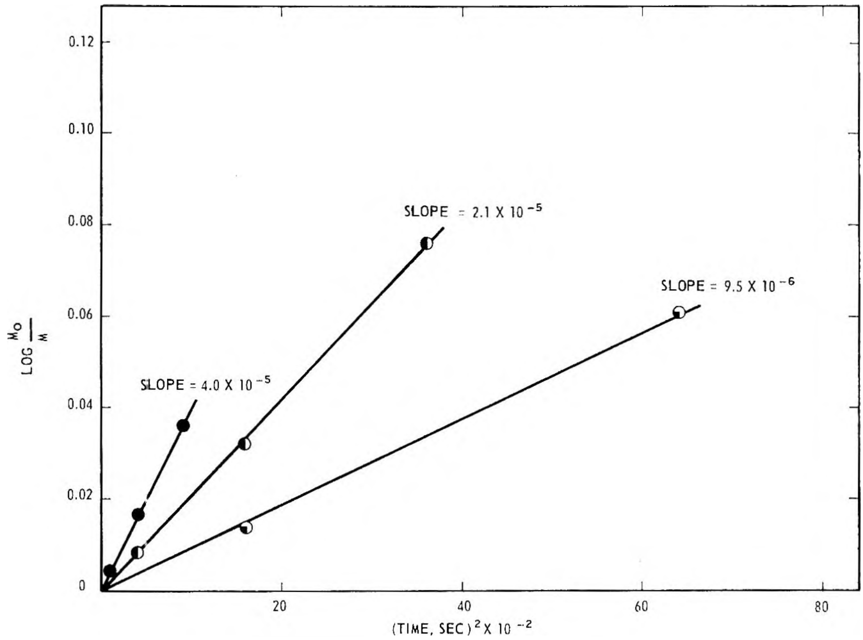

Fig. 13. Rates of polymerization of 7*M* acrylamide at 25°C. at [methylene blue] = $7.0 \times 10^{-6}M$, [triethanolamine] = $2.0 \times 10^{-2}M$, and various relative light intensities: ●:◐: ◐ = 1:½:¼.

TABLE I
Polymerization of Acrylamide at Different Light Intensities[a]

Relative light intensity	Time of exposure, sec.	Polymer, %	30°C. [η] 1N NaCl, dl./g.	$\bar{M}_w \times 10^{-5}$	Remarks
4	10	0.96	2.1	5.2	
	20	3.81	—		
	30	8.00	—		Blue color completely faded
	45	25.3	2.7	7.8	
	60	25.22	—		
	90	31.98	2.7	7.8	
2	20	1.90	2.1	5.2	Became very viscous
	40	7.19	2.4	6.4	
	60	16.12	3.0	9.0	Blue just faded
	80	19.37	—		
	120	26.78	2.8	8.0	
1	40	3.10	3.0	9.0	
	80	12.96	—		
	120	38.77	3.3	10.5	Blue faded

[a] [Acrylamine] = 7M; [Methylene blue] = 7.0 × $10^{-5}M$; [Triethlanolamine] = 2.0 × $10^{-2}M$; temperature 25°C.; light source: G. E. reflector infrared, 250 w. at 110, 95, and 80 v.; distance, 5¾ in.

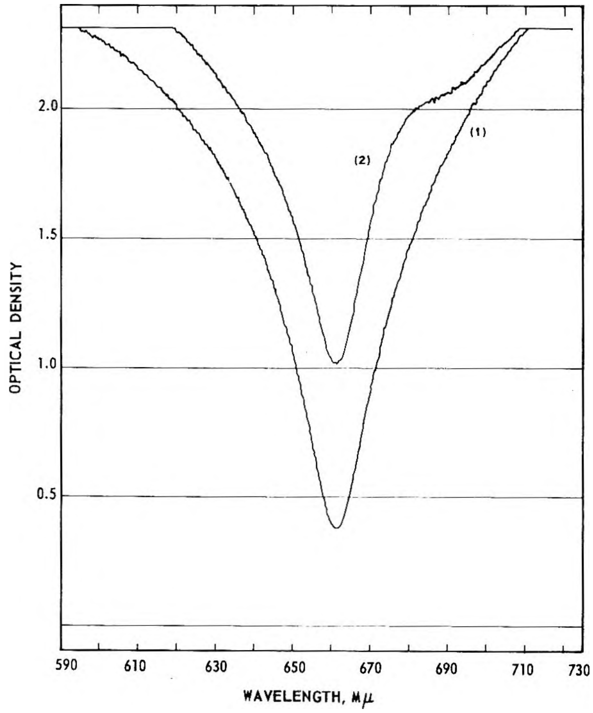

Fig. 14. Spectra of an interference filter (*1*) with and (*2*) without a solution containing 7.0 × 10^{-5} methylene blue and 7M acrylamide.

TABLE II

Polymerization of Acrylamide Induced by Monochromatic Light[a]

Time of exposure, sec.	Energy absorbed, quanta[b]	Polymerization, %	Monomer molecules polymerized	30°C. [η] 1N NaCl, dl./g.	$\bar{M}_w \times 10^{-5}$	$\bar{M}_n \times 10^{-4}$	Quantum yields[c]	
							Monomer	Polymer
60	5.66×10^{17}	0.75	3.16×10^{22}	3.3	10.5	1.48	5.59×10^{2}	0.0038
120	1.132×10^{18}	1.43	6.03×10^{22}	3.3	10.5	1.48	5.32×10^{2}	0.0036
180	1.70×10^{18}	5.47	2.31×10^{23}	3.3	10.5	1.48	1.36×10^{3}	0.0092
240[d]	2.26×10^{18}	14.52	6.12×10^{23}	3.6	10.9	1.53	2.70×10^{3}	0.0176

[a] [Acrylamide] = 7M; [methylene blue] = $7.0 \times 10^{-5}M$; [triethanolamine] = $2.0 \times 10^{-2}M$; temperature 25°C.; interference filter: $\lambda_{\text{peak}} = 663$ mμ; transmission = 40%; half width: 11 mμ; light source: G.E. reflector infrared, 250 w., 110 v.; distance: $5^3/_4$ in.; energy absorbed by the system 2826.14 μw. or 28261.4 ergs/sec.

[b] Based on initial dye concentration. Since the dye was fading as the polymerization proceeded, the actual energy absorption decreases with time of exposure.

[c] For the reason stated in footnote b, the actual quantum yields should be increasingly higher with increased time of exposure.

[d] At the end of 240 seconds, the solution was still blue, but gel-like.

intensity. Since the present polymerization follows nonsteady-state kinetics, the nearly constant molecular weight obtained at different light intensities can probably be as suggested above attributed to a chain transfer process.

Quantum Yields

The quantum yield was calculated for a representative polymerization in which an interference filter was used. The spectra of the interference filter with and without a solution containing $7.0 \times 10^{-5}M$ methylene blue and $7M$ acrylamide are shown in Figure 14. Since the absorption spectrum of the filter was symmetrical, the effective wavelength was taken as the peak wavelength (663 mμ). The results are given in Table II. The quantum yield increases with reaction time until the dye is completely faded. The energy absorbed here is based on the initial dye concentration. The actual quantum yields are increasingly higher with increased time of exposure.

CONCLUSION

In this investigation, employing a methylene bue–triethanolamine system as the sensitizer for photopolymerization of aqueous acrylamide in air, quantum yields of $\phi_m = 5.6 \times 10^2$ to 2.7×10^3; $\phi_p = 3.8 \times 10^{-3}$ to 1.76×10^{-2}, have been obtained. It has been concluded that in aerobic polymerization of acrylamide, the monomeric form of methylene blue is a photosensitizer and the associated form is a chain terminator. Based on this concept, further work has been undertaken to increase the rates and quantum yields of dye-sensitized photopolymerizations by increasing the ratio of the monomeric form to the associated form of the dye. The results will be discussed in subsequent communications.

It is a pleasure to acknowledge the experimental assistance in spectroscopy of Messrs. D. Bell and J. Koren and for the helpful discussions of Dr. R. F. Stamm.

References

1. Bamford, C. H., and M. J. S. Dewar, *Nature*, **163**, 214 (1949).
2. Oster, G., *Nature*, **173**, 300 (1954).
3. Oster, G., *Phot. Eng.*, **4**, 173 (1956).
4. Oster, G. K., G. Oster, and A. Prati, *J. Am. Chem. Soc.*, **79**, 595 (1957).
5. Oster, G., U. S. Pat. 2,850,445 (1958); U. S. Pat. 2,875,045 (1959).
6. Oster, G., *Phot. Sci. Eng.*, **4**, 237 (1960).
7. Oster, G., U. S. Pat. 3,097,096 (1963).
8. Koizumi, M., and A. Watanabe, *Bull. Chem. Soc. Japan*, **28**, 136 (1955); A. Watanabe, and M. Koizumi, *ibid.*, **28**, 141 (1955); A. Watanabe, *ibid.*, **32**, 557 (1959); F. Takemura, *ibid.*, **35**, 1073, 1078 (1962).
9. LuValle, J. E., A. Leiffer, P. H. Dougherty, and M. Koral, *J. Phys. Chem.*, **66**, 2403 (1962).
10. Shepp, A., S. Chaberek, and R. MacNeil, *J. Phys. Chem.*, **66**, 2563 (1962).
11. Troppet, S., G. Delzenne, and G. Smets, *J. Polymer Sci.*, **A2**, 1539 (1964); G. Delzenne, S. Troppets, W. Dewinter, and G. Smets, *J. Polymer Sci.*, **A2**, 1069 (1963); G. Delzenne, S. Troppet, and G. Smets, *J. Polymer Sci.*, **55**, 767 (1961).

12. *New Product Bulletin,* No. 34, American Cyanamid Co., New York, June 1955.
13. Michaelis, L., *J. Phys. Colloid Chem.*, **54,** 1 (1950).
14. Holmes, W. C., *Ind. Eng. Chem.*, **16,** 35 (1924).
15. Rabinowitsch, E., and L. F. Epstein, *J. Am. Chem. Soc.*, **63,** 69 (1941).
16. Scheibe, G., *Kolloid-Z.*, **82,** 1 (1938).
17. Sheppard, S. E., *Rev. Modern Phys.*, **14,** 303 (1942).

Résumé

On a étudié la polymérisation de l'acrylamide en solution aqueuse, induite par la lumiére visible en employant le systéme bleu de méthyléne-triéthanolamine comme sensibilisateurs. La cinétique de la polymérisation n'est pas stationnaire. La vitesse est directement proportionnelle á l'intensité de la lumiére absorbée et á peu prés proportionnelle á la concentration initiale en monomére. La vitesse en fonction de la concentration initiale en colorant passe par un maximum. Le poids moléculaire des polyméres était de l'ordre du million. Les poids moléculaires sont indépendants de l'intensité de la lumiére absorbée mais directement proportionnels á la concentration initiale en monomére, et diminuent d'une façon logarithmique avec la concentration initiale en colorant. Sur la base des résultats spectroscopiques et du comportement de la polymérisation, on suggére que la forme monomérique du colorant agit comme photosensibilisateur, tandis que la forme associée provoque la terminaison de la chaîne. Les chaînes cinétiques sont terminées par un processur monomoléculaire et les poids moléculaires sont gouvernés par un processus de transfert de chaîne.

Zusammenfassung

Die durch sichtbares Licht mit Methylenblau- Triäthanolamin als Sensibilisatorsystem angeregte Polymerisation von wässrigem Acrylamid wurde untersucht. Die Polymerisation verlief nach einem nicht stationären kinetischen Schema. Die Geschwindigkeit war der ersten Potenz der Intensität des absorbierten Lichtes und angenähert der Anfangskonzentration des Monomeren proportional. Die Geschwindigkeit ging als Funktion der Anfangsfarbstoffkonzentration durch ein Maximum. Das Molekulargewicht der Polymeren lag im Bereich von einer Million. Das Molekulargewicht war von der Intensität des absorbierten Lichtes unabhängig, im wesentlichen zur Anfangsmonomerkonzentration direkt proportional und nahm mit der Anfangsfarbstoffkonzentration logarithmisch ab. Sowohl die spektroskopischen Befunde als auch das Polymerverhalten sprechen dafür, dass die monomere Form des Farbstoffes ein Photosesibilisator ist, während die assizoerte Form kettenabbrechend wirkt. Der Abbruch der kinetischen Ketten verlief monomolekular, die Molekulargewichte wurden durch Kettenübertragungen bestimmt.

Received June 16, 1964

JOURNAL OF POLYMER SCIENCE: PART A VOL. 3, PP. 1127-1136 (1965)

Dye-Sensitized Photopolymerization. II. Enhanced Sensitization by Combination of a Cationic and an Anionic Dye

CATHERINE S. HSIA CHEN,* *Central Research Division, American Cyanamid Company, Stamford, Connecticut*

Synopsis

In dye-sensitized photopolymerization of the redox type, enhanced rates and quantum yields of polymerization were achieved by employing suitable combinations of a cationic and an anionic dye. The enhancement could be attributed to the more reactive new species of the sensitizing dye molecules produced as a result of an interaction between the cationic and the anionic dyes. In a combination of two cationic dyes where practically no interaction between the dyes was indicated, essentially no effect on the polymerization was observed.

INTRODUCTION

In the previous communication,[1] it was concluded that in the photopolymerization of aqueous acrylamide sensitized by a methylene blue–triethanolamine system, the monomeric form of methylene blue ($\lambda_{\max} = 665$ mμ) is a sensitizer while the associated form ($\lambda_{\max} \simeq 610$ mμ) is a terminator. It would follow that conditions which perturb the equilibrium between the two forms of the dye, thus changing the relative amounts of each form existing in the solution also, would influence the polymerization behavior.

The primary purpose of this series of investigations is to increase the rate of dye-sensitized photopolymerization. This can be accomplished simultaneously by (*1*) increasing the number of quanta of light absorbed per unit time and (*2*) by increasing the quantum yields for polymerization. Many means have been reported by which one can alter the relative intensities of the α band (representing the monomeric form) and the β band (representing the associated form) of organic dyestuffs, for example, by the addition of an electrolyte.[2] Thus, it appeared that the added electrolyte might advantageously be a second dyestuff which absorbs in a different region of the visible spectrum from the first dye.

It is known that double- or multiple-charged dyes seldomly associate in solution.[2] Also it is anticipated that there should be interaction between

---

* Present address: Summit Research Laboratories, Celanese Corporation of America, Summit, New Jersey.

a cationic and an anionic dye. As a consequence, it is expected that when a combination of two such dyes is used as the sensitizer, the polymerization behavior should deviate from that when either dye is used alone, in a manner which depends on the type of interaction. Methylene blue (I), a mono charged cationic blue dye,

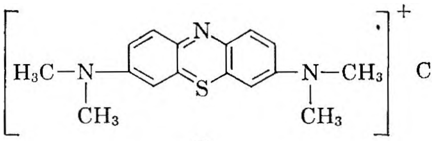

I

and eosin Y (II), a double-charged anionic red dye,

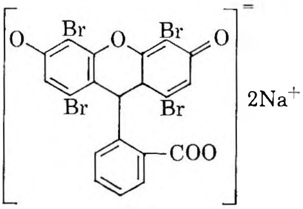

II

were chosen for this investigation. The results of both spectroscopic and polymerization experiments are described in this communication.

EXPERIMENTAL RESULTS AND DISCUSSION

The experimental procedures were essentially the same as described in the previous paper.[1] Eosin Y used was Fisher biological stain. All polymerizations were performed with the use of $7M$ acrylamide and $2 \times 10^{-2}M$ triethanolamine.

Combination of a Cationic and an Anionic Dye

7.0×10^{-5}M Methylene Blue and 3.0×10^{-5}M Eosin Y

Spectroscopy. A comparison of the absorption spectra of aqueous solutions of (*1*) $7.0 \times 10^{-5}M$ methylene blue alone, (*2*) $3.0 \times 10^{-5}M$ eosin Y alone, and (*3*) a mixture containing $7.0 \times 10^{-5}M$ methylene blue and $3.0 \times 10^{-5}M$ eosin Y in a 5 mm. cell is shown in Figure. 1. Additional experimental data derived from the spectra are summarized in Table I. Figure 1 shows that the spectrum for the mixture differs significantly from the spectra for individual dyes. In the region corresponding to the methylene blue absorption (550–750 mμ), the following aspects are noteworthy: (*a*) the absorption was shifted towards longer wavelengths, (*b*) the original peak at $\lambda = 665$ mμ which now was found at 667 mμ was depressed, (*c*) the original peak at $\lambda = 612$ mμ became less distinct and almost shoulder-like to the peak at $\lambda = 667$ mμ. The maximum absorption of this shoulder was at 620–625 mμ, and in the mixture it was calculated that $\epsilon_{667}/\epsilon_{625} =$

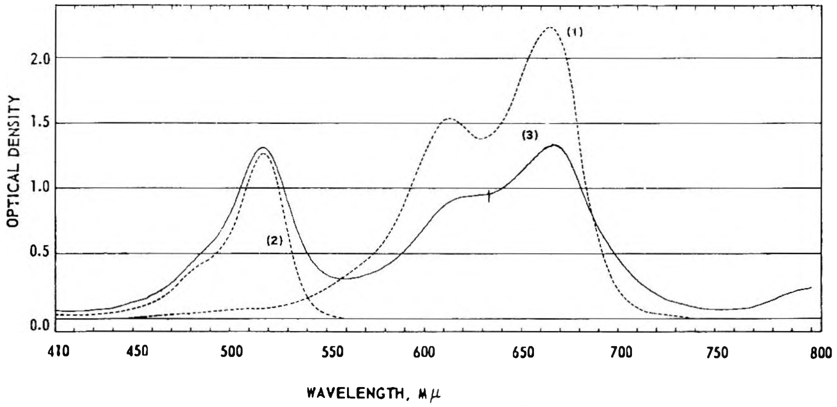

Fig. 1. Absorption spectra of (*1*) 7.0 × $10^{-5}M$ methylene blue, (*2*) 3.0 × $10^{-5}M$ eosin Y, and (*3*) 7.0 × $10^{-5}M$ methylene blue + 3.0 × $10^{-5}M$ eosin Y. Cell thickness = 5 mm.; temperature = 25°C.

1.52 as compared to $\epsilon_{665}/\epsilon_{612} = 1.47$ obtained for methylene blue alone. In the region corresponding to eosin Y absorption (450–550 mμ), no great

TABLE I

Polymerizations Sensitized by Methylene Blue and Eosin Y at [Acrylamide] = 7.0*M*, Triethanolamine = 2.0 × $10^{-2}M$

Temp., °C.	Dye concn. × 10^5, *M* Methylene blue	Dye concn. × 10^5, *M* Eosin Y	Peak absorption, $\epsilon \times 10^{-4}$ Methylene blue	Peak absorption, $\epsilon \times 10^{-4}$ Eosin Y	Total energy absorption (400–770 mμ), mw.	Polymerization $10^5 K$ 4.606	Polymerization $\bar{M}_w \times 10^{-5}$
25	0	3.0		$\epsilon_{518} = 8.40$	1.68	0.62[a]	6.4
	7.0	0	$\epsilon_{665} = 6.49$ $\epsilon_{612} = 4.41$ $\frac{\epsilon_{665}}{\epsilon_{612}} = 1.47$		13.0	4.02	7.8
	7.0	3.0	$\epsilon_{667} = 3.83$ $\epsilon_{625} = 2.52$ $\frac{\epsilon_{667}}{\epsilon_{625}} = 1.52$	$\epsilon_{518} = 8.77$	16.7	14.30	5.5
0	0	3.0				0.26[b]	4.5
	7.0	0				1.01	6.0
	7.0	3.0				6.78	5.2
25	0	6.0		$\epsilon_{518} = 10.1$	2.9	1.24[a]	2.5
	7.0	6.0	$\epsilon_{673} = 2.16$ $\epsilon_{635} = 1.61$ $\frac{\epsilon_{673}}{\epsilon_{635}} = 1.34$	$\epsilon_{518} = 10.1$	16.5	3.62	—
0	3.5	0				1.30	0.7
	3.5	3.0				1.41	—

[a] After an induction period of 15 sec.

[b] After an induction period of 30 sec.

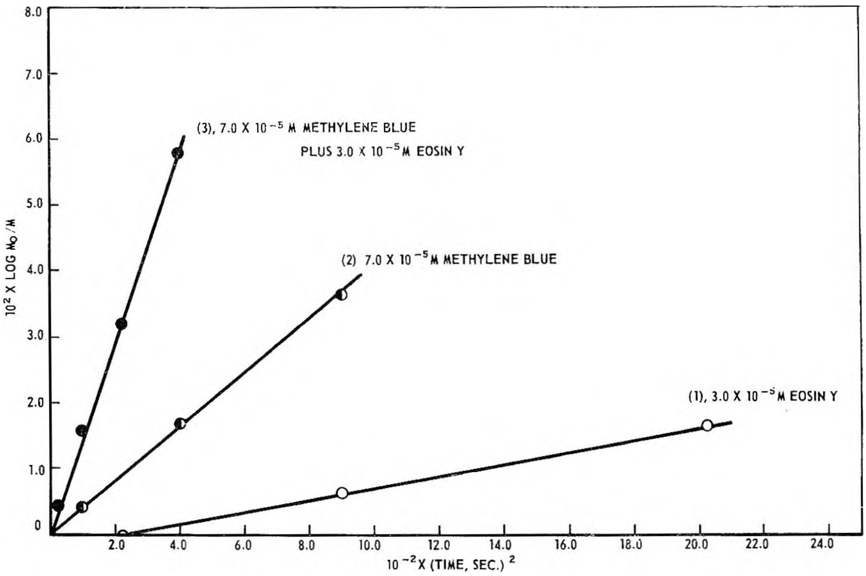

Fig. 2. Polymerization of $7M$ aqueous acrylamide at 25°C. Sensitized by (*1*) $3.0 \times 10^{-5}M$ eosin Y, (*2*) $7.0 \times 10^{-5}M$ methylene blue, and (*3*) $7.0 \times 10^{-5}M$ methylene blue + $3.0 \times 10^{-5}M$ eosin Y. [Triethanolamine] = $2.0 \times 10^{-2}M$.

change was indicated; the shoulder at $\lambda_{max} = 480$ mμ, representing the associated form of eosin Y molecules, appeared to be less pronounced in the dye mixture.

It is reasonable to ascribe these results to an interaction between the two dyes in the mixture which results in an increase in the relative amounts of the monomeric form to the associated form of methylene blue molecules. Even more important perhaps was the indication that the nature of the association between the dye molecules was changed, since the β peak was shifted to a longer wavelength by 10 mμ. The interaction between the two dyes was shown also by their absorption spectra in the ultraviolet region (200–400 mμ) which will be discussed in a subsequent paper. The total energy absorbed (400–770 mμ) by the polymerization system was somewhat higher when the dye mixture was employed than the sum of energy absorbed when each individual dye of the corresponding concentration was present (16.67–14.72 mw.). This is a result of the shift of absorption to the longer wavelengths where the output of our light source[1] is higher.

Polymerization. The results for the polymerizations are represented in Figure 2 for (*1*) $3.0 \times 10^{-5}M$ eosin Y, (*2*) $7.0 \times 10^{-5}M$ methylene blue, and (*3*) $7.0 \times 10^{-5}M$ methylene blue plus $3.0 \times 10^{-5}M$ eosin Y. The slope representing the initial rates ($K/4.606$) of polymerization together with the molecular weights of the polymers are recorded in Table I. It should be noted that when eosin Y was employed, an induction period was observed and the rate of polymerization was small. The low rate of

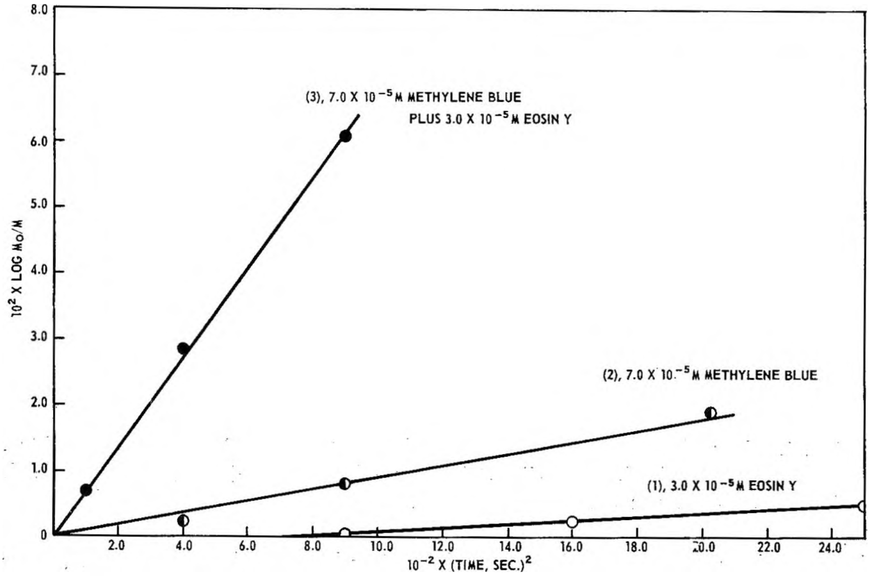

Fig. 3. Polymerization of $7M$ aqueous acrylamide at 0°C. sensitized by (*1*) $3.0 \times 10^{-5}M$ eosin Y, (*2*) $7.0 \times 10^{-5}M$ methylene blue, and (*3*) $7.0 \times 10^{-5}M$ methylene blue $+ 3.0 \times 10^{-5}M$ eosin Y. [Triethanolamine] $= 2.0 \times 10^{-2}M$.

polymerization sensitized by $3.0 \times 10^{-5}M$ eosin Y could be attributed to the small amount of energy absorbed by the system (Table I). The rate of polymerization with the dye mixture as the sensitizer was considerably higher than the expected additive rates when the two individual dyes of corresponding concentrations was employed. The rate was 3.5-fold higher than that when methylene blue alone was employed. The enhanced rate cannot be accounted for by the small increase in energy absorption by the system (Table I). More logically it can be attributed to either or both of the above-mentioned factors: namely, (*a*) a higher ratio of the monomeric form to the associated form of the methylene blue molecules and (*b*) a different nature or degree of association among methylene blue molecules in the dye mixture. Thus, the overall resulting species act as a more efficient photosensitizer in the present system. Since in the dye mixture the increase in energy absorption is far less than the increase in rate of polymerization, this implies that the quantum yields of polymerization are increased accordingly.

It is noteworthy that in spectrum *3* in Figure 1, the absorption started to increase at 750 mμ. However, it was ascertained experimentally that radiation above 750 mμ (Wratten filter No. 87) did not induce polymerization.

The enhanced rate which resulted when a mixture of $7.0 \times 10^{-5}M$ methylene blue and $3.0 \times 10^{-5}M$ eosin Y was employed as the sensitizer was further confirmed by carrying out the polymerizations at 0°C. The results are recorded in Figure 3 and Table I. Here a six- or sevenfold

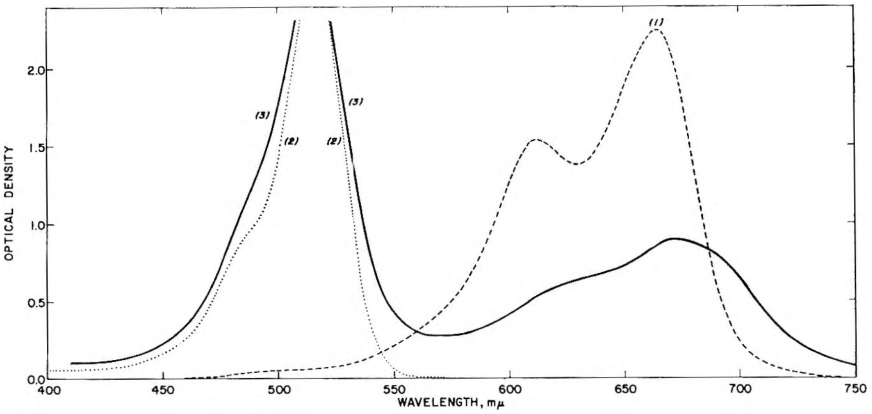

Fig. 4. Absorption spectra of aqueous solutions of (*1*) 7.0 × $10^{-5}M$ methylene blue. (*2*) 6.0 × $10^{-5}M$ eosin Y, and (*3*) 7.0 × $10^{-5}M$ methylene blue + 6.0 × $10^{-5}M$ eosin Y. Cell thickness = 5 mm.; temperature = 25°C.

increase in rate was obtained. This higher increase in rate at 0°C. over that at 25°C. could indicate that the interaction between the two dyes was temperature dependent also.

When eosin Y was present lower molecular weight polymers were obtained.

*7.0 × 10^{-5}*M *Methylene Blue and 6.0 × 10^{-5}*M *Eosin Y*

In the above-described experiments the charge equivalent ratio of methylene blue to eosin Y was greater than but close to one (7.0 × 10^{-5}: 6.0 × 10^{-5}). In order to observe the effects of the presence of excess eosin Y in a combination of the two dyes, a mixture of 7.0 × $10^{-5}M$ methylene blue and 6.0 × $10^{-5}M$ eosin Y was employed as the sensitizer for the polymerization. Here the ratio in charge equivalents, methylene blue: eosin Y = 7.0 × 10^{-5}:12 × 10^{-5}, is considerably less than one. The results are discussed below.

Spectroscopy. Figure 4 represents a comparison of the spectra of (*1*) 7.0 × $10^{-5}M$ methylene blue, (*2*) 6.0 × $10^{-5}M$ eosin Y, and (*3*) a mixture of 7.0 × $10^{-5}M$ methylene blue and 6.0 × $10^{-5}M$ eosin Y. Other data are recorded in Table I. Again interaction between the two dyes was indicated. The absorption spectrum of the mixture deviated greatly from those of the individual dyes at the same concentrations. In the region corresponding to the methylene blue absorption (550–750 mμ), the original peaks at λ = 665 mμ and λ = 612 mμ approached one broad band with the peak absorption at λ = 673 mμ and a slight shoulder at λ = 635 mμ. These changes not only indicated that methylene blue molecules existed as different species from those in the single dye solution, but also could suggest that they differ from those in the above dye mixture which contained less eosin Y. However, the exact nature of the species is yet to be ascertained.

As in the case discussed above, the absorption in the region corresponding to eosin Y (450–550 mμ) was not affected greatly; the shoulder at $\lambda_{max} =$ 480 mμ again disappeared in the dye mixture. Also, the total energy absorbed by the system was again slightly higher when the mixture was employed (Table I).

Polymerization. The polymerization data are presented in Table I. When the mixture contained $7.0 \times 10^{-5}M$ methylene blue and $6.0 \times 10^{-5}M$ eosin Y the rate was comparable to but slightly lower than that when $7.0 \times 10^{-5}M$ methylene blue alone was employed (4.0:3.6). In contrast to the above-described cases there was no enhancement in the power of sensitization. This result could be attributed to the different states which the methylene blue molecules were in, as indicated by the absorption spectra described above (Fig. 4). On the other hand, when eosin Y was used as the sensitizer, an induction period for polymerization was observed. In addition, the molecular weights of the polymer decreased with its increasing concentration (Table I). These observations suggest that another factor which would lower the rate of polymerization could arise from the possible inhibiting nature of eosin Y when it is present in excess of methylene blue.

Similar results were obtained when the polymerizations were carried out at 0°C. with the use of (*1*) $3.5 \times 10^{-5}M$ methylene blue alone or (*2*) $3.5 \times 10^{-5}M$ methylene blue and $3.0 \times 10^{-5}M$ eosin Y as the sensitizer. Here, again, eosin Y was in excess (ratio in equivalents: methylene blue: eosin Y = 3.5:6.0), and again no enhancement of rate of polymerization was observed, as shown in Table I (1.30:1.41).

These results are significant, for they point out that only suitable concentration ratios of a cationic and an anionic dye can result in the enhancement of sensitizing power for polymerization.

Combination of Two Cationic Dyes

Figure 5 depicts a comparison of the absorption spectra of aqueous solutions of (*1*) $7.0 \times 10^{-5}M$ methylene blue, (*2*) $8.66 \times 10^{-5}M$ acridine orange, and (*3*) a mixture of $7.0 \times 10^{-5}M$ methylene blue and $8.66 \times 10^{-5}M$ acridine orange, in a 5-mm. cell. Other data derived from the spectra are summarized in Table II. No substantial change was observed in the spectrum of the mixture as compared to the spectra of the individual dyes. This observation indicates that there is a very little interaction between the two dyes. Since acridine orange (III) is another cationic dye,

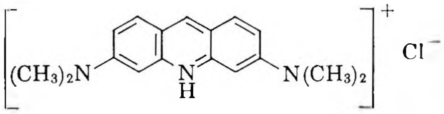

III

the lack of interaction between it and methylene blue is not surprising.

TABLE II
Polymerizations at 25°C. Sensitized by Methylene Blue and Acridine Orange at [Acrylamide] = 7.0M, [Triethanolamine] = 2.0 × $10^{-2}M$

Dye concn. × 10^6, M		Peak absorption, $\epsilon \times 10^{-4}$		Total energy absorption, (400–770 mμ), mw.	Polymerization	
Methylene blue	Acridine orange	Methylene blue	Acridine orange		$10^5 K$ 4.606	$\bar{M}_w \times 10^{-5}$
7.0	0	$\epsilon_{665} = 6.49$ $\epsilon_{612} = 4.41$ $\frac{\epsilon_{665}}{\epsilon_{612}} = 1.47$		13.0	4.02	7.8
0	8.66		$\epsilon_{491} = 1.0$	0.85	0[a]	
7.0	8.66	$\epsilon_{665} = 6.37$ $\epsilon_{612} = 4.36$ $\frac{\epsilon_{665}}{\epsilon_{612}} = 1.46$	$\epsilon_{491} = 1.69$	15.6	4.70	8.0

[a] No polymerization and no fading after 90 sec.

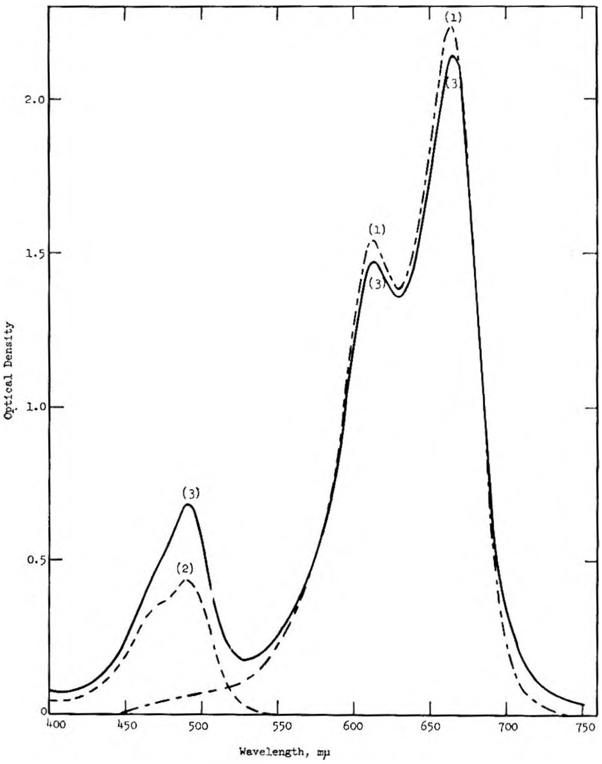

Fig. 5. Absorption spectra of (*1*) 7.0 × $10^{-5}M$ methylene blue, (*2*) 8.66 × $10^{-5}M$ acridine orange, and (*3*) 7.0 × $10^{-5}M$ methylene blue + 8.66 × $10^{-5}M$; acridine orange. Cell thickness = 5 mm.; temperature = 25°C.

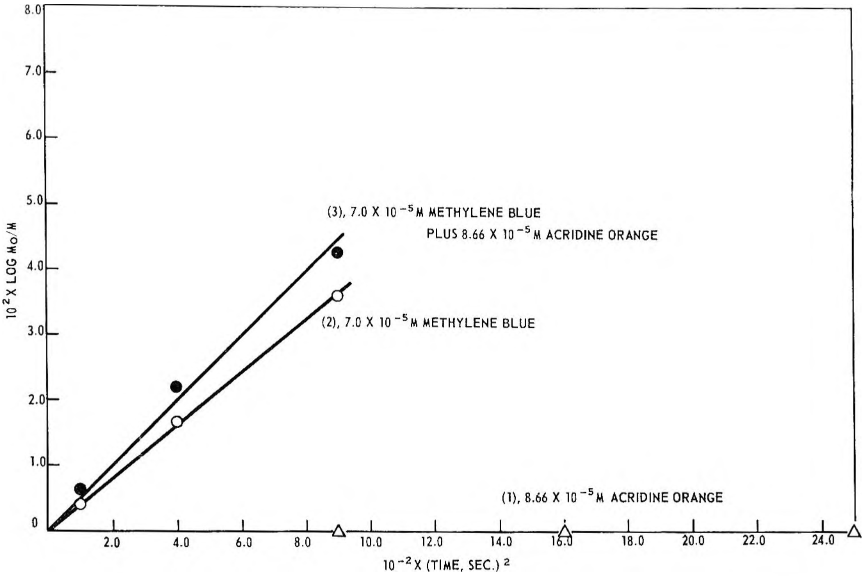

Fig. 6. Polymerization of $7M$ aqueous acrylamide at 25°C. sensitized by (*1*) 8.66 × $10^{-5}M$ acridine orange, (*2*) 7.0 × $10^{-5}M$ methylene blue, and (*3*) 7.0 × $10^{-5}M$ methylene blue + 8.66 $10^{-5}M$ acridine orange.

The results for polymerizations are summarized in Figure 6 and Table II. Acridine orange itself did not induce any polymerization in 90 sec. It appeared quite inert under the experimental conditions employed, since no fading of the dye was observed in that period also. When acridine orange was used in combination with methylene blue, there was no substantial change in the rate of polymerization compared with that when methylene blue alone was employed. Also, the presence of acridine orange had no effect on the molecular weights of the polymers. The methylene blue molecules acted as a sensitizer quite independently of the acridine orange molecules during the polymerization, as was indicated by the absorption spectra in Figure 5.

CONCLUSION

The above results and discussion lead to the conclusion that, in the dye-sensitized photopolymerization of the redox type, increased rates and quantum yields of polymerization can be accomplished by employing suitable combinations of a cationic and an anionic dye. The enhanced rates and quantum yields can be attributed to the more reactive new species of the sensitizing dye molecules produced as a result of an interaction between the cationic and the anionic dyes. As pointed out previously,[1] in a single dye system the active species were the monomeric form of the dye molecules. However, in the more complicated mixed dye systems, as in the present cases, they could be of a more complex nature as evidenced by the absorption spectra. The exact species which are resulted from ionic interaction of the two dyes have yet to be identified. In a combination of two cationic dyes where practically no interaction between the dyes was indicated, essentially no effect on the polymerization was observed.

It is a pleasure to acknowledge the experimental assistance in spectroscopy of Miss M. J. Mursick and Mr. D. Bell.

References

1. Chen, C. S. H., *J. Polymer Sci.*, **A3**, 1107 (1965).
2. Michaelis, L., *J. Phys. Colloid Chem.*, **54**, 1 (1950).

Résumé

Au cours de la photopolymérisation de type rédox, initiée par des colorants, on a augmenté la vitesse et le rendement quantique de la polymerisation par l'utilisation d'un mélange approprié de colorants cationique et anionique. Cet accroissement peut être attribué á l'augmentation de réactivité de la nouvelle espéce de molécule colorante initiatrice engendrée par interaction entre les colorants cationique et anionique. On n'a observé aucun effet notable sur la polymérisation lors de l'utilisation d'un mélange de deux colorants cationiques entre lesquels aucune interaction n'avait pratiquement été décelée.

Zusammenfassung

Bei der farbstoff-sensibilisierten Photopolymerisation vom Redoxtyp wurde durch Verwendung geeigneter Kombinationen eines kationischen und eines anionischen Farbstoffes eine Erhöhung der Geschwindigkeit und der Quantenausbeute der Polymerisation erreicht. Die Erhöhung konnte auf die durch Wechselwirkung zwischen dem kationischen und dem anionischen Farbstoff gebildete reaktivere neue Form des sensibilisierenden Farbstoffmoleküls zurückgeführt werden. Bei einer Kombination zweier kationscher Farbstoff, wo praktisch keine Wechselwirkung zwischen den Farbstoffen zu erkennen war, wurde kein wesentlicher Einfluss auf die Polymerisation beobachtet.

Received June 16, 1964

JOURNAL OF POLYMER SCIENCE: PART A VOL. 3, PP. 1137–1154 (1965)

Dye-Sensitized Photopolymerization. III. Structural Effects of Thiazine Dyes

CATHERINE S. HSIA CHEN,* *American Cyanamid Company, Stamford, Connecticut*

Synopsis

Photopolymerization of aqueous acrylamide was investigated by use of mixtures of thiazine dyes with different structural features and triethanolamine as sensitizers. New methylene blue N (I), with two electron-donating methyl groups in the 2- and 10-positions, and methylene green (III), with an electron-withdrawing nitro group in the 2-position of methylene blue (II, 3,9-bisdimethylaminophenazothionium chloride) were employed. Induction periods for polymerization were observed for both I and III; the kinetics thereafter were of similar nature to those reported for II.[1] The lengths of the induction period were in the order of III > II > I. The rate of polymerization and the quantum yield were in the order of III > II > I. In combination with an anionic dye (eosin Y) in an equivalent ratio of 7:6, spectroscopy indicated interaction between both I and eosin Y and III and eosin Y, III–eosin Y interaction was of similar nature to II–eosin Y interactions, but to a lesser extent. Interaction between I and eosin Y, however, was of a different nature. Results in polymerization showed that enhancement in rate was observed for III–eosin Y but not for I–eosin Y. The order of enhancement was thus II > III > I.

INTRODUCTION

In previous investigations[1,2] it was found that methylene blue molecules associated to a higher degree in more concentrated aqueous solutions and the degree of association had definite effects on the polymerization behavior of aqueous acrylamide when methylene blue–triethanolamine was used as the photosensitizer. It was also found that addition of eosin Y to aqueous methylene blue solutions resulted in changes in the electronic structure of the methylene blue molecules through interaction, and, when a suitable combination of the two dyes was used as the sensitizer, enhanced rates of polymerization was achieved. These findings have demonstrated that the sensitizing power of methylene blue is dependent on the electronic structure of its molecules. However, thus far the changes in the electronic structure have been induced by changes in physical or environmental conditions. In this investigation, a change in electronic structure of the dye molecules was brought about by chemical substitution on the thiazine nucleus. The

---

* Present address: Summit Research Laboratories, Celanese Corporation of America, Summit, New Jersey.

objective was to study the effect of this structural change on the ability of the dyes as photosensitizers for polymerization.

In addition to methylene blue (II), two other commercially available thiazine dyes were chosen for comparative studies; these were: new methylene blue N (I), with two electron-donating methyl groups, and methylene green (III), with an electron-withdrawing nitro group.

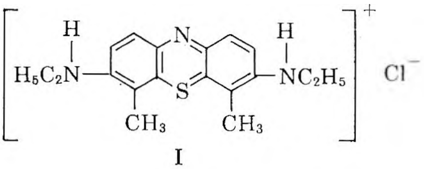

I

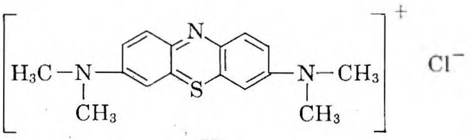

II

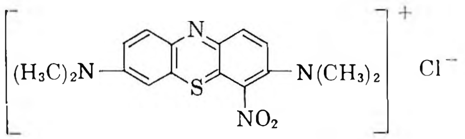

III

This communication reports the polymerizations of aqueous acrylamide sensitized by new methylene blue N–triethanolamine and methylene green–triethanolamine and presents a comparison among the three thiazine dyes investigated.

EXPERIMENTAL RESULTS AND DISCUSSION

The experimental procedures were essentially the same as described previously.[1,2] New methylene blue N and methylene green were of the biological stain grade (Allied Chemical Corporation). All polymerizations were performed with the use of $7M$ aqueous acrylamide and 2×10^{-2} M triethanolamine at 25°C.

Polymerization Kinetics

Induction Period. In contrast to the results obtained with the methylene blue–triethanolamine system[1] and similar to those observed for riboflavin by Oster, Oster, and Prati,[3] induction periods were observed for both the new methylene blue–triethanolamine and the methylene green–triethanolamine systems when they were used as photosensitizers. As shown in Figure 1 and Table I, the induction period decreased with increasing absorbed light intensity. This was shown by its decrease with increasing dye concentration (Fig. 1) and with decreasing intensity of the

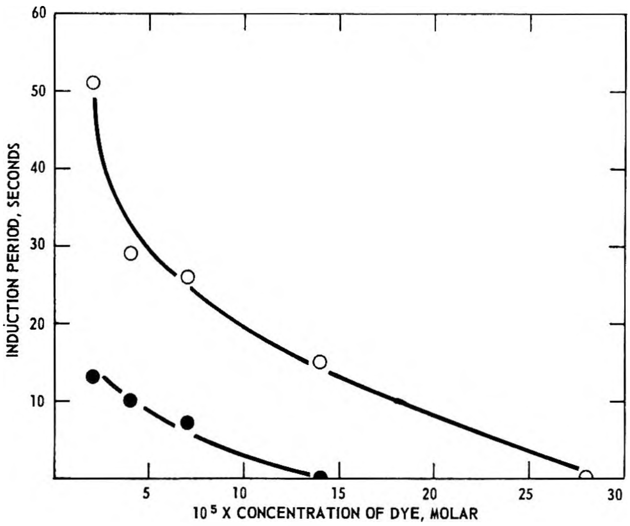

Fig. 1. Induction period as a function of dye concentration: (○) methylene green; (●) new methylene blue N.

incident light (Table I). Furthermore, considerably longer induction periods existed for methylene green than for new methylene blue N. Thus, among the three thiazine dyes investigated, the lengths of the induction period were in the following order: III > I > II.

Rates and Molecular Weights. The conversion versus time curves after the induction period followed the same nonsteady-state pattern as described for methylene blue.[1] As represented in Figures 2 and 3 for polymerization employing different concentrations of new methylene blue N and methylene green, respectively, straight lines were obtained when log $[M_0]/[M]$ was plotted against t^2 for the initial stages of the polymerizations. The slopes were the values for $K/4.606$ which represented the rates of polymerization. The intercepts with the x axis provided another means to ascertain the lengths of the induction period in addition to the experimental observations.

TABLE I
Dependence on Light Intensity

Dye	Relative light intensity	Induction period, sec.	$\frac{K}{4.606}$	Avg. $\bar{M}_w \times 10^{-5}$	Dependence on light intensity
Methylene green	4 (110 v.)	26	8.64×10^{-6}	8.72	
	2 (95 v.)	38	5.12×10^{-6}	9.57	Rate $\propto I^{0.92}$
	1 (80 v.)	67	4.61×10^{-7}	9.57	$\bar{M}_w \propto I^0$
New methylene blue N	4	7	8.33×10^{-5}	5.77	Rate $\propto I^{1.3}$
	2	10	3.73×10^{-5}	8.26	$\bar{M}_w \propto I^{-0.3}$
	1	21	1.33×10^{-5}	9.10	

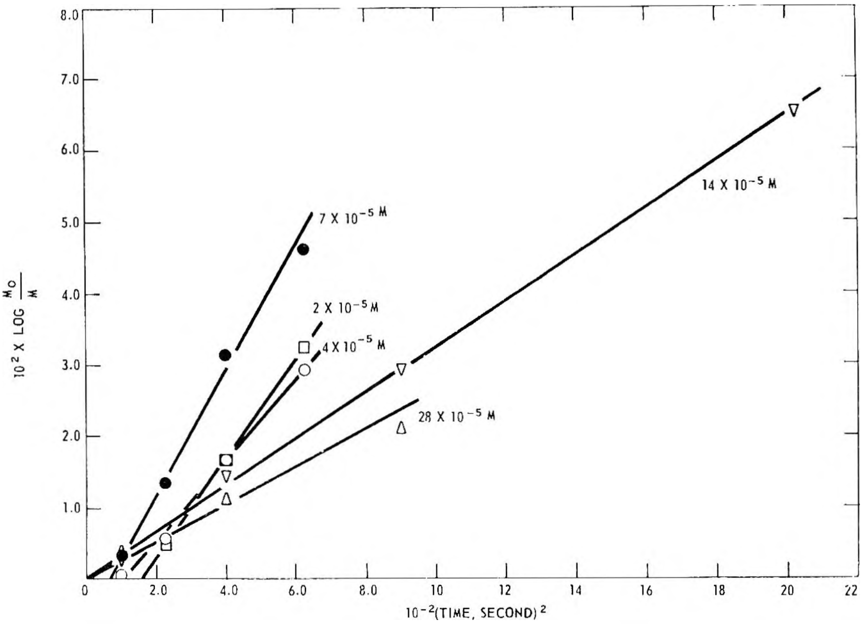

Fig. 2. Polymerization rates as a function of the concentration of new methylene blue N.

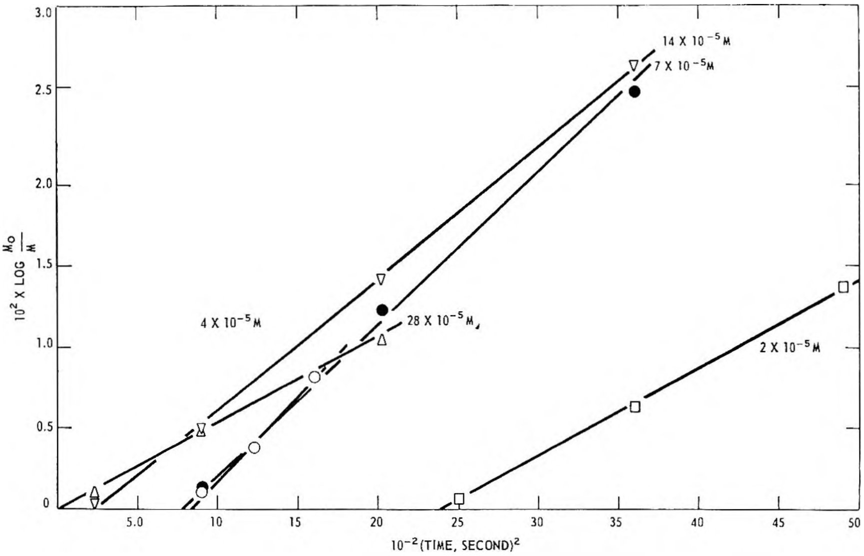

Fig. 3. Polymerization rates as a function of the concentration of methylene green.

The molecular weights of the polymers are summarized in Figures 4 and 5 for new methylene blue N and methylene green, respectively. In both cases, at higher dye concentrations, the molecular weights increased gradually with time (or conversion) and at lower dye concentrations they increased more rapidly with time. As mentioned previously in the case of methylene blue[1] this increase in molecular weight with polymerization time might be attributed to an increase in viscosity of the medium during the polymerization. At lower dye concentrations, higher molecular weights

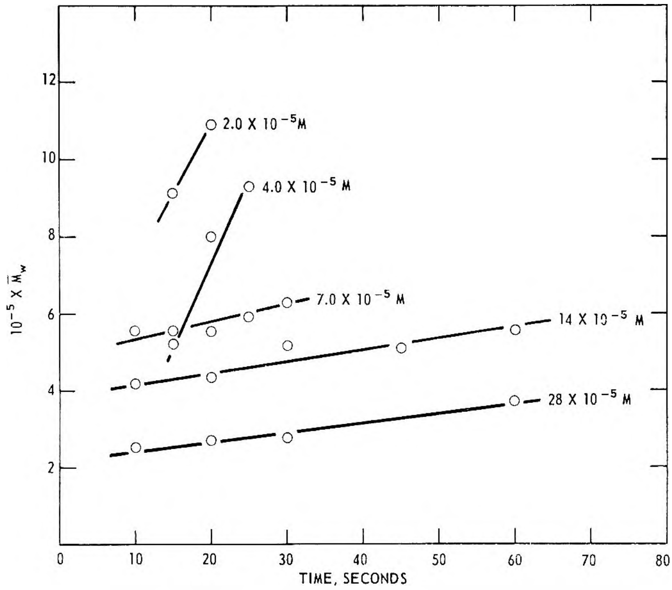

Fig. 4. Molecular weights of polymers as a function of the concentration of new methylene blue N.

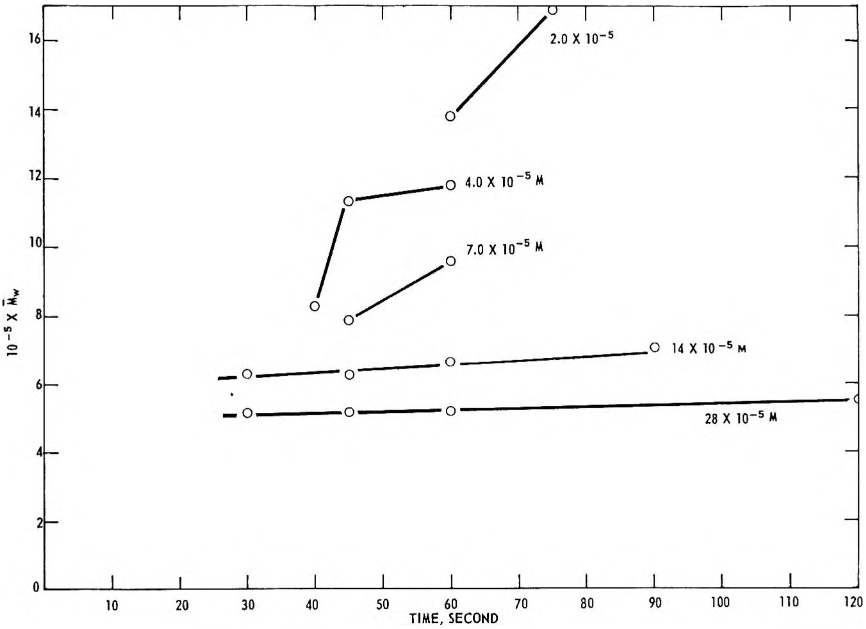

Fig. 5. Molecular weights of polymers as a function of the concentration of methylene green.

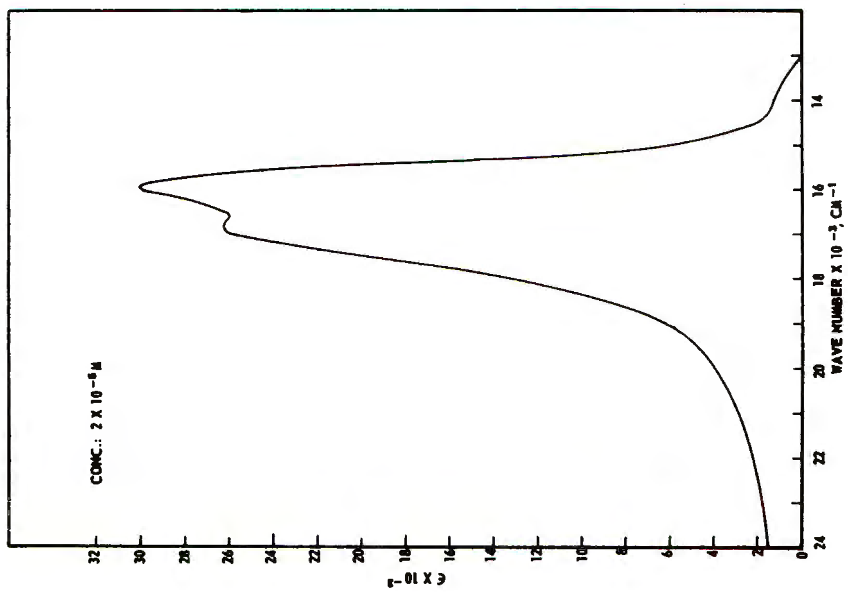
CONC.: 2 X 10⁻⁵ M
ε X 10⁻³
0
2
4
6
8
10
12
14
16
18
20
22
24
26
28
30
32
WAVE NUMBER X 10⁻³, CM⁻¹
24
22
20
18
16
14

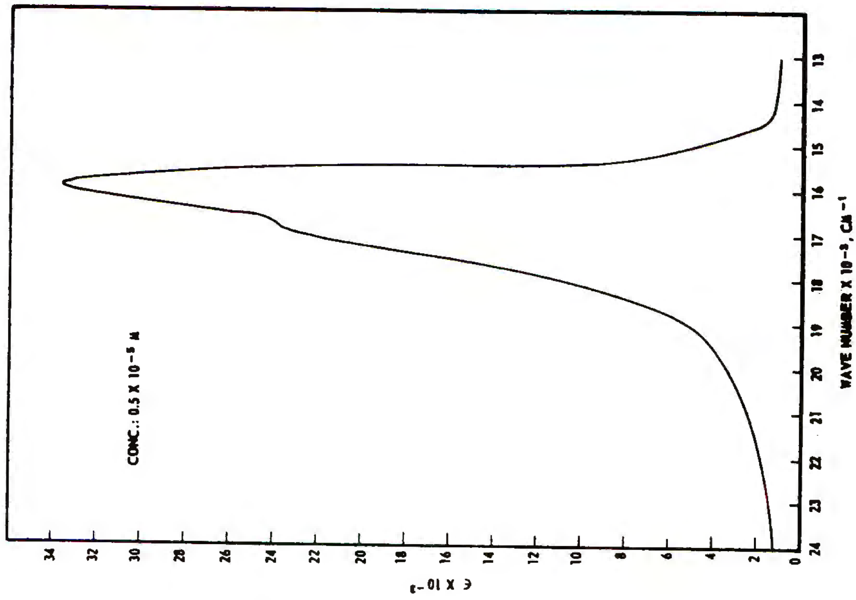
CONC.: 0.5 X 10⁻⁵ M
ε X 10⁻³
0
2
4
6
8
10
12
14
16
18
20
22
24
26
28
30
32
34
WAVE NUMBER X 10⁻³, CM⁻¹
24
23
22
21
20
19
18
17
16
15
14
13

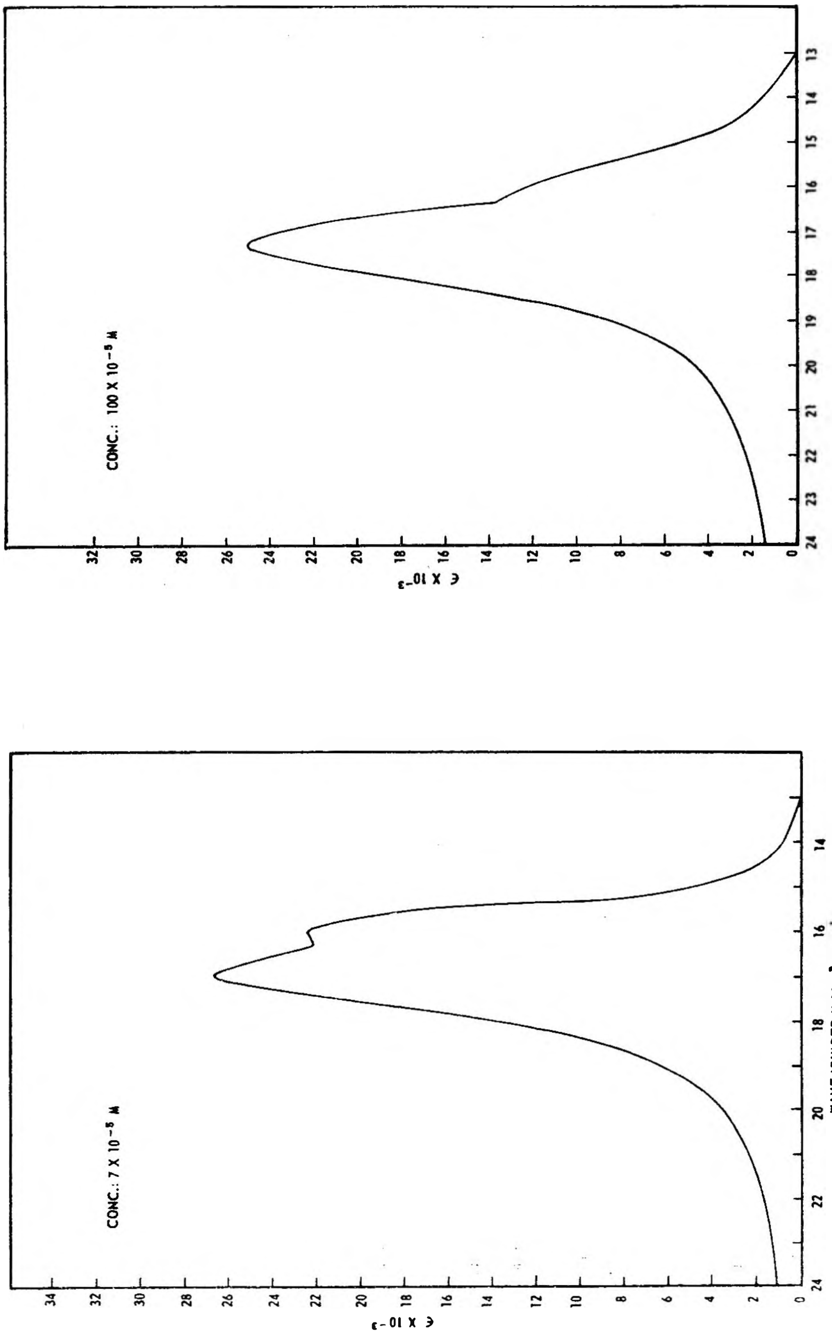

Fig. 6. Absorption spectra of aqueous solutions of new methylene blue N at different concentrations.

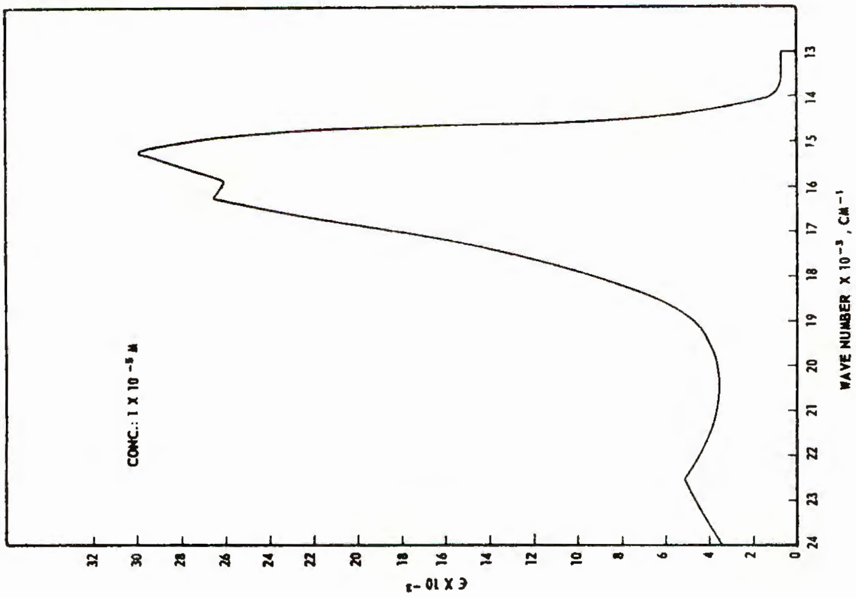
CONC.: 1 X 10 ⁻⁵ M
ε X 10⁻³
0
2
4
6
8
10
12
14
16
18
20
22
24
26
28
30
32
24
23
22
21
20
19
18
17
16
15
14
13
WAVE NUMBER X 10⁻³ , CM⁻¹

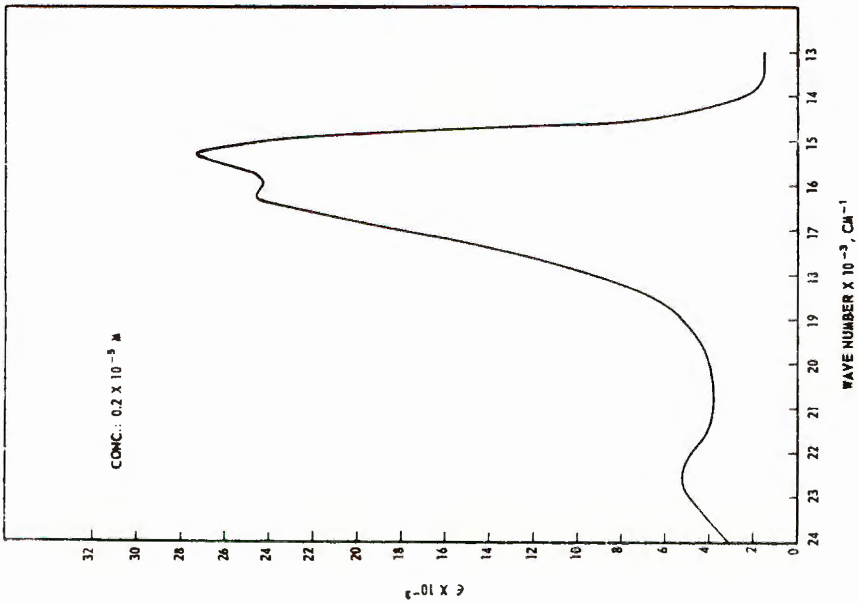
CONC.: 0.2 X 10⁻⁵ M
ε X 10⁻³
0
2
4
6
8
10
12
14
16
18
20
22
24
26
28
30
32
24
23
22
21
20
19
13
17
16
15
14
13
WAVE NUMBER X 10⁻³, CM⁻¹

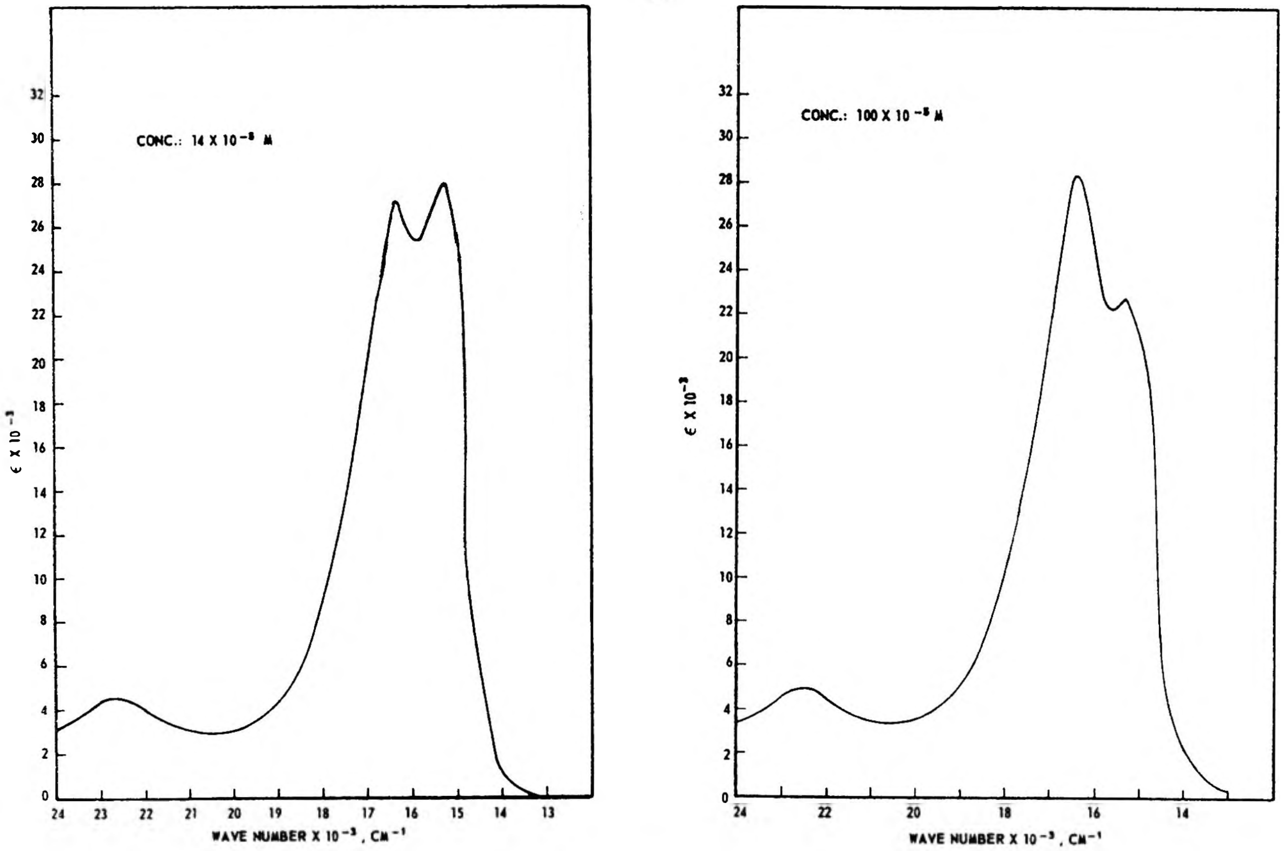

Fig. 7. Absorption spectra of aqueous solutions of methylene green at different concentrations.

were obtained; therefore, the medium became more viscous during the polymerization and, as a result, the molecular weights increased more rapidly.

Dependence on Light Intensity. The data for polymerizations employing three different light intensities are recorded in Table I for methylene green and new methylene blue N. In both cases the rates were approximately proportional to the first power of the light intensity. The molecular weights were independent of the light intensity in the case of methylene green; however, they increased with decreased intensity in the case of new methylene blue N.

Effect of the Dye Concentration

Spectroscopy. The absorption spectra of new methylene blue N and methylene green each at four representative concentrations covering a range of 0.2×10^{-5} to $100 \times 10^{-5}M$ are depicted in Figures 6 and 7, respectively.

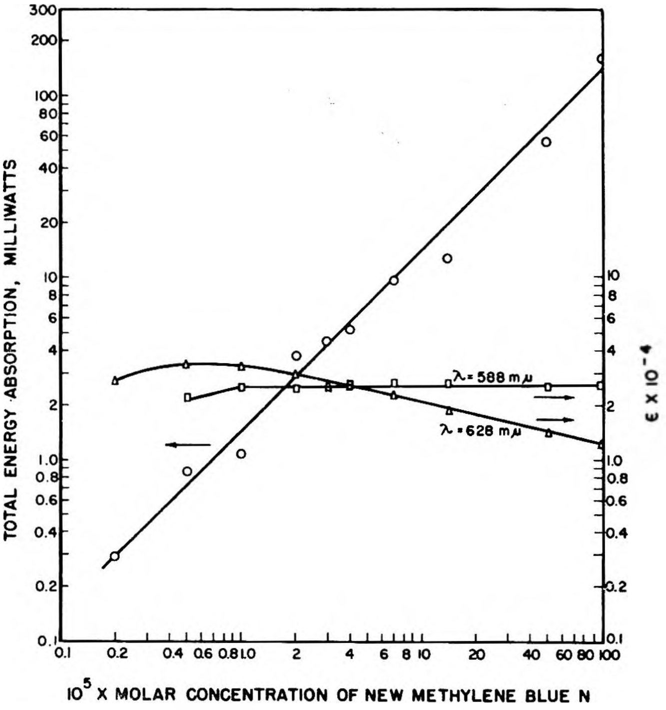

Fig. 8. ϵ_{628}, $\epsilon_{\sim 588}$ and total energy absorption as a function of the concentration of new methylene blue N.

In each case the relative intensity of the α to the β peak changed with the total concentration of the dye. It is noteworthy that by comparing the spectra of the three dyes at the same concentrations, the case of association of the molecules was in the order: I > II > III.

In Figures 8 and 9 the following curves are plotted for new methylene blue and methylene green, respectively: (*1*) the total energy absorption (circles), (*2*) $\epsilon_{\alpha\text{peak}}$ (triangles: 628 mμ for new methylene blue N and 655 mμ for methylene green) and (*3*) $\epsilon_{\beta\text{peak}}$ (squares: ~588 mμ for new methylene blue and ~610 mμ for methylene green) vs. the dye concentration. The results are similar to those discussed for methylene blue,[1] and the differences are self-evident on comparing the three plots.

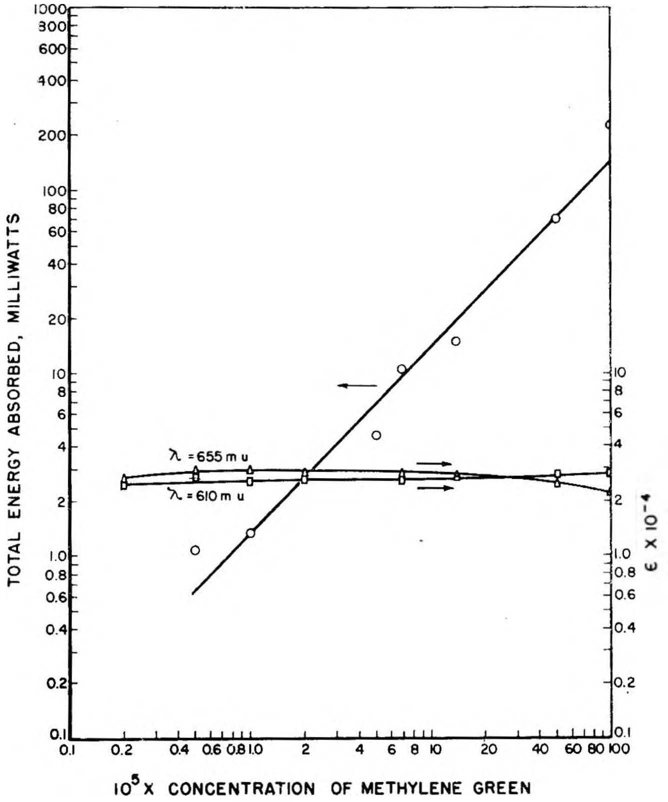

Fig. 9. ϵ_{655}, $\epsilon_{\sim 610}$ and total energy absorption as a function of the concentration of methylene green.

Polymerization. The relationship between the rates of polymerization (represented by $K/4.606$, open circles) and the concentration of the dye are presented in Figure 10 for both new methylene blue N and methylene green. In the same figure the corresponding molecular weights are also shown (solid circles). As was observed for methylene blue,[1] in both cases the polymerization rates passed through a maximum, and the molecular weights of the polymers decreased with the increase in concentration of the dye. These results again supported the conclusion that the single molecules of the dye were the photosensitizer while the associated ones the terminator.

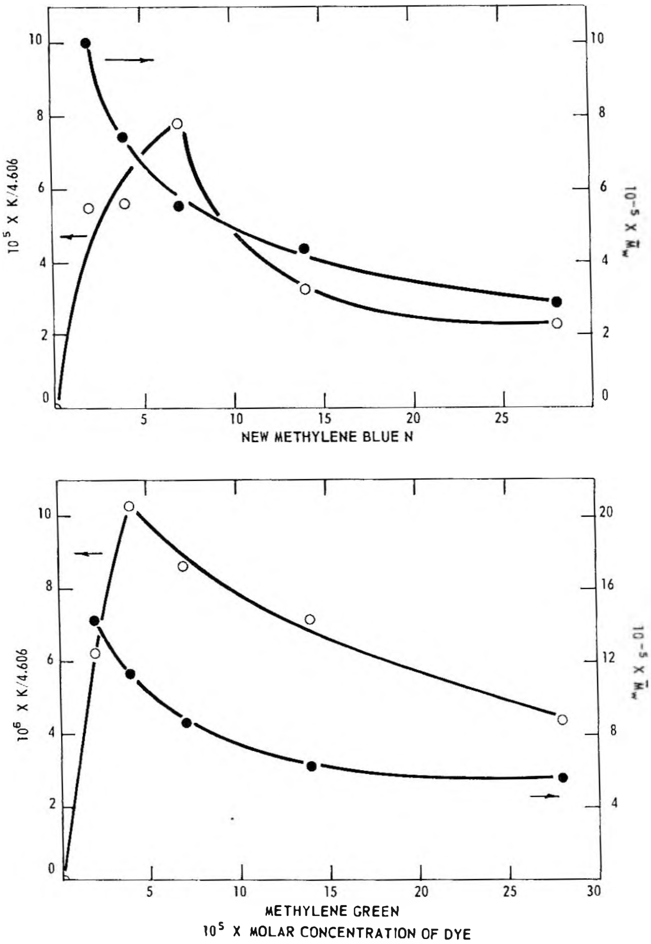

Fig. 10. Rates and molecular weights of polymerization of 7*M* acrylamide as a function of dye concentration.

Effect of the Structural Features of the Thiazine Dyes on the Polymerization

Rates and Molecular Weights. A comparison of the rates of polymerization and the molecular weights of the polymers is displayed in Figure 11. On the left side the values of $K/4.606$ divided by the number of milliwatts of energy absorbed (representing a comparison of quantum yields), taking into account the induction periods and on the right side the molecular weights (average value of those represented in Figs. 4 and 5 for each dye concentration) are plotted against dye concentration. Apparently the quantum yield increases in the order: III < II < I. These results suggest that when thiazine dyes are used as photosensitizer of the redox type, nuclear substitution of electron-donating groups is activating, while that of electron-withdrawing groups is deactivating. It then follows that

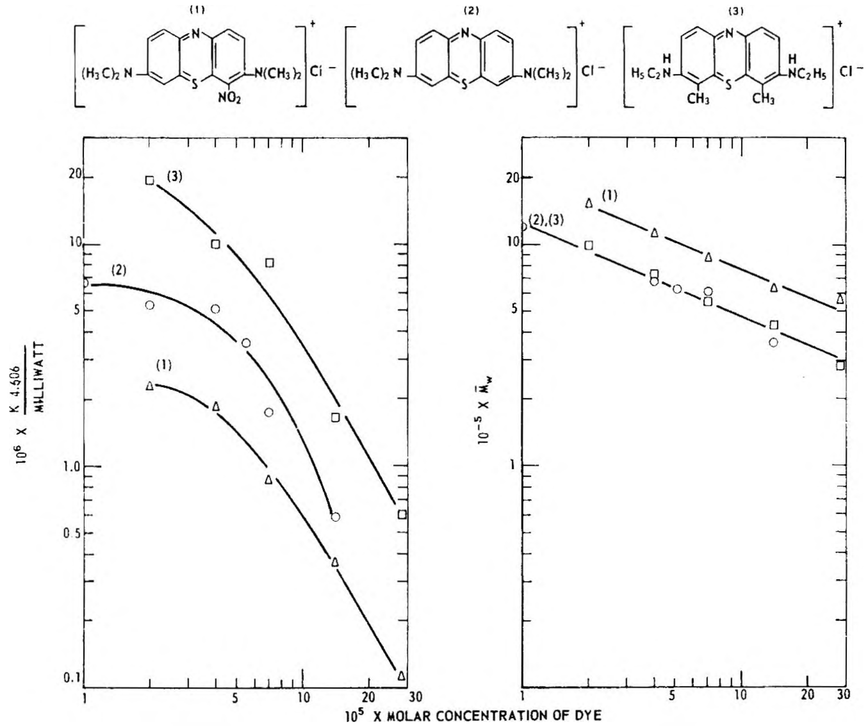

Fig. 11. Comparison of polymerizations of 7*M* acrylamide sensitized by three thiazine dyes.

substitution with even stronger electron-donating groups, e.g., a dimethoxy derivative (IV),

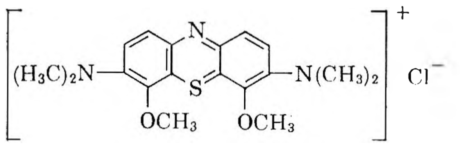

should result in more powerful photosensitizers than the methyl-substituted new methylene blue N now available.

The molecular weights of the polymers obtained when new methylene blue N was used as the sensitizer were the same as those obtained with methylene blue, while the molecular weights were invariably higher when methylene green at the same concentrations was used.

Sensitization with an Anionic Dye–Eosin Y Combination

Spectroscopy. The absorption spectra of aqueous solutions of (*1*) 7.0 × $10^{-5}M$ new methylene blue N and (*2*) a mixture of 7.0 × $10^{-5}M$ new methylene blue N and 3.0 × $10^{-5}M$ eosin Y are depicted in Figure 12 and those of (*1*) 7.0 × $10^{-5}M$ methylene green and (*2*) a mixture of 7.0 × $10^{-5}M$ methylene green and 3.0 × $10^{-5}M$ eosin Y in Figure 13. Among

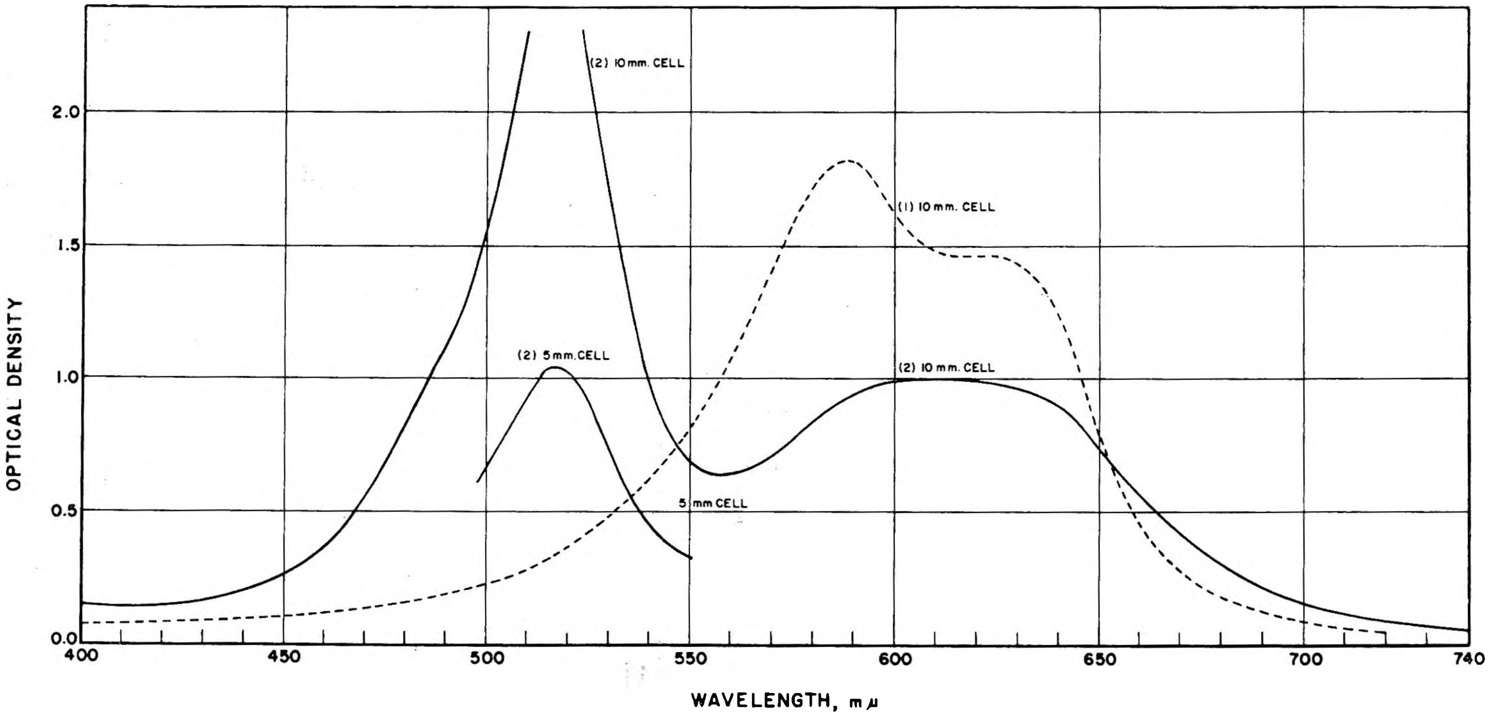

Fig. 12. Absorption spectra of aqueous solutions of (*1*) 7.0 × $10^{-5}M$ new methylene blue N and (*2*) a mixture of 7.0 × $10^{-5}M$ new methylene blue N and 3.0 × $10^{-5}M$ eosin Y. Cell thickness: 5 mm. and 10 mm.

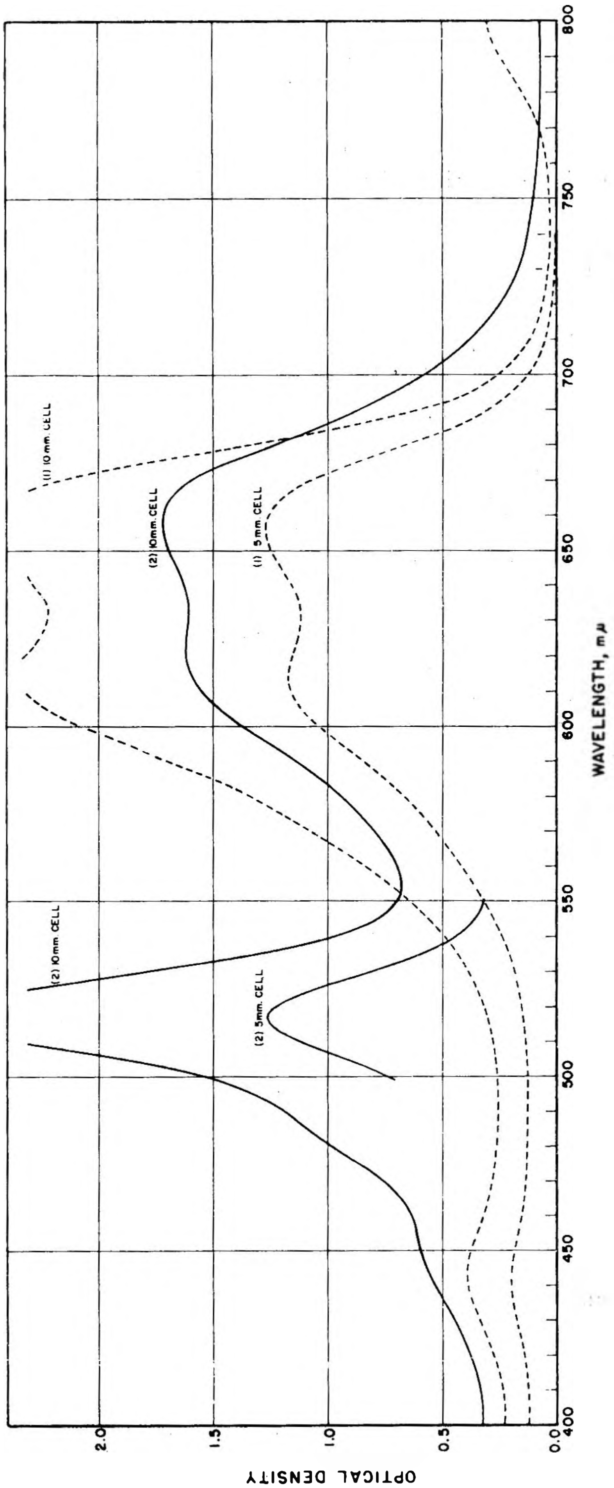

Fig. 13. Absorption spectra of aqueous solutions of (*1*) 7.0 × $10^{-5}M$ methylene green and (*2*) a mixture of 7.0 × $10^{-5}M$ methylene green and 3.0 × $10^{-5}M$ eosin Y. Cell thickness: 5 mm. and 10 mm.

the three dyes, at the specified concentrations the extent of interaction with eosin Y is in the following order: new methylene blue N > methylene blue > methylene green. In the case of new methylene blue N both the α and the β peaks combined into a depressed broad band in the mixture. In the case of methylene green the changes in absorption in the mixture were similar to those described for methylene blue–eosin Y[2] except to a lesser degree.

Polymerization. A comparison of polymerizations employing mixtures of $7.0 \times 10^{-5}M$ new methylene blue N–$3.0 \times 10^{-5}M$ eosin Y and $7.0 \times 10^{-5}M$ methylene green–$3.0 \times 10^{-5}M$ eosin Y with other pertinent data is summarized in Table II. Enhancement in rate was observed with $7.0 \times 10^{-5}M$ methylene green–$3.0 \times 10^{-5}M$ eosin Y (1.9-fold), although to a lesser extent than with $7.0 \times 10^{-5}M$ methylene blue–$3.0 \times 10^{-5}M$ eosin Y (3.5-fold). Furthermore, the induction period decreased somewhat. On the other hand, comparable rates were observed for $7.0 \times 10^{-5}M$ new methylene blue N–$3.0 \times 10^{-5}M$ eosin Y and $7.0 \times 10^{-5}M$ new methylene blue N alone. The latter results resembled what was observed previously for the $7.0 \times 10^{-5}M$ methylene blue–$6.0 \times 10^{-5}M$ eosin Y system.[2] There also, drastic interaction between the two dyes was indicated by the fact that the α and the β peaks of methylene blue approached one broad band; however, essentially no change in the rate of polymerization was observed. While these observations are very interesting, sensible explanations await the identification of the initiating species and the elucidation of the initiation.

TABLE II

Polymerizations Sensitized by Combinations of Cationic and Anionic Dyes

Sensitizer	Induction period, sec.	$\frac{K}{4.606} \times 10^{-5}$	$\bar{M}_w \times 10^{-5}$	Rate ratio: $\frac{\text{cationic + anionic dyes}}{\text{cationic dye alone}}$
$7.0 \times 10^{-5}M$ new methylene blue N	7	8.33	5.74	
$7.0 \times 10^{-5}M$ new methylene blue N + $3.0 \times 10^{-5}M$ eosin Y	7	8.20	5.99	~1
$7.0 \times 10^{-5}M$ methylene green	26	0.86	8.71	
$7.0 \times 10^{-5}M$ methylene green + $3.0 \times 10^{-5}M$ eosin Y	21	1.63	8.83	1.90
$7.0 \times 10^{-5}M$ methylene blue	0	4.02	6.0–7.8	
$7.0 \times 10^{-5}M$ methylene blue + $3.0 \times 10^{-5}M$ eosin Y	0	14.30	5.5	3.5

CONCLUSION

In this investigation it has been shown that chemical substitution on the thiazine nucleus definitely has an influence on the ability of the dye to function as a photosensitizer. The above-described results seem to indicate that election-donating groups activate while electron-withdrawing groups deactivate the dye molecule. On the other hand, both types of substitution introduce an induction period for polymerization. In mixtures with an anionic dye, the nature of the substitution also influences the nature of interaction which in turn influences the rate of polymerization.

Among the three thiazine dyes, although new methylene blue N produces the higher rate and quantum yield, it also introduces a small induction period for polymerization. In addition, there is no enhancement in rate of polymerization when it is used in combination with eosin Y. Therefore, as summarized in Figure 14, the most efficient sensitizer for aqueous systems so far investigated has been 7.0 × $10^{-5}M$ methylene blue–3.0 × $10^{-5}M$ eosin Y–2.0 × $10^{-2}M$ triethanolamine.[2] Based on the available results, it is anticipated that more efficient sensitizing systems can be found by further systematic investigations.

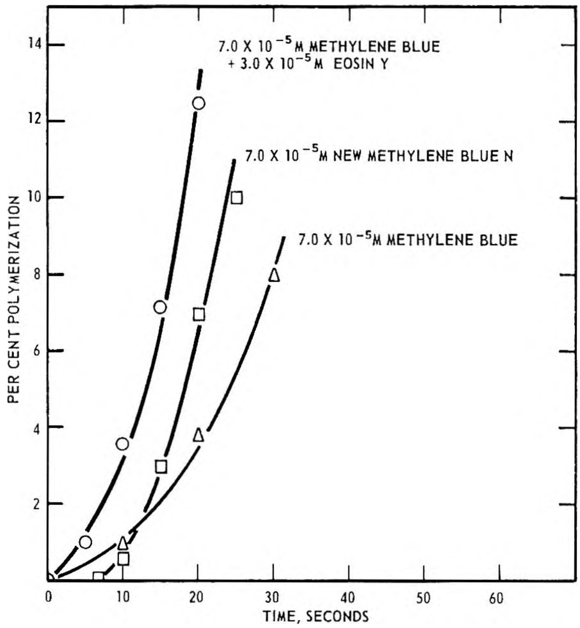

Fig. 14. Direct comparison of the three most effective sensitizers for aqueous acrylamide found in this series of investigations.

The experimental assistance of Miss J. Mursick and Mrs. D. Bell with spectroscopy and Mrs. Ruth Fiala with viscosity measurements is greatly appreciated.

References

1. Chen, C. S. H., *J. Polymer Sci.*, **A3**, 1107 (1965).
2. Chen, C. S. H., *J. Polymer Sci.*, **A3**, 1127 (1965).
3. Oster, G. K., G. Oster, and A. Prati, *J. Am. Chem. Soc.*, **79**, 595 (1957).

Résumé

La photopolymérisation de l'acrylamide en solution aqueuse a été étudiée en employant des mélanges de colorants thiaziniques de structures différentes et de triéthanolamine comme sensibilisateurs. On a utilisé le "bleu de méthylène N" (I) avec deux groupes méthyles électro-donneurs dans les positions 2 et 10, et le "vert de méthylène" (III) avec un groupe nitré électrocapteur dans la position 2 du bleu de méthylène (II, chlorure de 3,9-bisdiméthylaminophénazothionium). On observe des périodes d'induction pour la polymérisation de I et de III; ensuite les cinétiques sont de nature semblable á celles décrites pour II. Les durées des périodes d'induction sont dans l'ordre III > II > I. La vitesse de polymérisation et le rendement quantique sont dans l'ordre III > II > I. En combinaison avec un colorant anionique—l'éosine Y dans une proportion équivalente de 7:6, des mesures spectroscopiques indiquent une interaction entre I et l'éosine Y, et entre III et l'éosine Y. L'interaction entre III et l'éosine Y est semblable à celle entre II et l'éosine Y, mais moins forte. Cependant, l'interaction entre I et l'éosine Y est d'une nature différente. Les résultats de polymérisation montrent que la vitesse augmente pour III–éosine Y, mais pas pour I–éosine Y. L'ordre d'augmentation de vitesse est donc II > III > I.

Zusammenfassung

Die Photopolymerisation von wässrigem Acrylamid wurde unter Verwendung von Thiazinfarbstoffen verschiedener Struktur und Triäthanolamin als Sensibilisator untersucht. Neumethylblau N (I) mit zwei Elektrondonator- Methylgruppen in der 2- und 10- Stellung, und "Methylgrün" (III) mit einer elektronenentziehenden Nitrogruppe in der 2- Stellung von Methylenblau (II, 3,9-Bisdimethylaminophenazothioniumchlorid) wurden verwendet. Bei I und III wurden Induktionsperioden der Polymerisation beobachtet; danach erwies sich die Kinetik der für II mitgeteilten als ähnlich. Die Länge der Induktionsperiode lag in der Reihenfolge III > II > I. Die Polymerisationsgeschwindigkeit und die Quantenausbeute lag in der Reihenfolge III > II > I. In Kombina. tion mit einem anionischen Farbstoff- Eosin Y in einem Äquvalentverhältnis von 7:6, liess die Spektroskopie eine Wechselwirkung zwischen I und Eosin Y sowie zwischen III–Eosin Y erkennen. Die Wechselwirkung zwischen III und Eosin Y war von ähnlicher Natur, aber geringerem Ausmass wie II–Eosin Y. Die Wechselwirkung zwischen I und Eosin Y war jedoch von anderer Natur. Die Polymerisationsergebnisse zeigten, dass für III–Eosin Y, jedoch nicht für I–Eosin Y Beschleunigung auftrat. Die Reihenfolge der Beschleunigung war daher II > III > I.

Received June 16, 1964

JOURNAL OF POLYMER SCIENCE: PART A VOL. 3, PP. 1155-1170 (1965)

Dye-Sensitized Photopolymerization. IV. Enhanced Rates of Polymerization of Acrylamide in Ethylene Glycol, Sensitized by Thiazine Dyes with Triethanolamine

CATHERINE S. HSIA CHEN,* *Central Research Division, American Cyanamid Company, Stamford, Connecticut*

Synopsis

The polymerization of acrylamide, in ethylene glycol, induced by visible light, with methylene blue–triethanolamine as the sensitizing system, was found to follow a steady-state kinetic scheme after an induction period. The rate was proportional to the half power of the absorbed light intensity and to the second power of the initial monomer concentration. In an experimentally convenient range of dye concentration the rate increased with the dye concentration. The molecular weights of the polymers were in the range of 3.0×10^4–2.5×10^5; they were insensitive to the absorbed light intensity; they increased with the initial monomer concentration and decreased with the initial dye concentration. The induction period was inversely proportional to the first power of the light intensity. Polymerization in the ethylene glycol systems was found to proceed at considerably faster speed than in the aqueous systems. The faster polymerization was attributed primarily to the fact that methylene blue at all concentrations employed existed principally in the monomeric form in the ethylene glycol systems. New methylene blue N–triethanolamine and methylene green–triethanolamine also were investigated as the sensitizing systems for the polymerization of acrylamide in ethylene glycol. Similar results as with methylene blue–triethanolamine were obtained.

INTRODUCTION

It has been reported that one of the means for alteration of the relative intensities of the α and the β bands of organic dyestuffs is to change the nature of the solvent.[1] For instance, in alcohols the α-band is more pronounced than in water, indicating that the dye molecules are less associated in alcohols than in water. It has also been ascertained experimentally that methylene blue in methanol and ethylene glycol exists primarily in the unassociated form. Based on the hypothesis[2] that the monomeric form of the dye is a photosensitizer and the associated form is a terminator, methylene blue in these solvents should serve as a more efficient photosensitizer than in water. As a consequence, a more efficient polymerization process would be predicted. Thus an investigation of the polymeriz-

---

* Present address: Summit Research Laboratories, Celanese Corporation of America, Summit, New Jersey.

ation of acrylamide in these solvents and a comparison with the corresponding aqueous systems should yield information which would further assess the above hypothesis. For this purpose, ethylene glycol can be distinguished from methanol as the solvent in the following ways. In methanol, the polymer precipitates out during the polymerization, thus rendering the process heterogeneous. In addition, only very low molecular weight polyacrylamide is produced in methanol, for it is an extremely efficient chain-transferring agent for the polymerization of acrylamide. Ethylene glycol is a waterlike solvent which dissolves both acrylamide and polyacrylamide. Therefore, the system will remain homogeneous throughout the polymerization as is the case with water. This enables convenient comparison between the aqueous and the ethylene glycol systems. The results and conclusions are described in this communication.

EXPERIMENTAL RESULTS AND DISCUSSION

Ethylene glycol (Fisher Certified Reagent) was used in place of water. Other experimental procedures were the same as described previously.[2]

Methylene Blue System

Absorption Spectra In Ethylene Glycol

Figure 1 depicts two representative spectra of methylene blue in ethylene glycol of the concentrations $6.88 \times 10^{-5}M$ and $96 \times 10^{-5}M$, respectively. These spectra differed from those in aqueous solutions of comparable molar concentrations[2] in the following manner: (*1*) the α-peak was predominant, the β-peak appearing only as a shoulder; (*2*) the relative intensity of the α and the β peaks remained unchanged with the concentration, and (*3*) Beer's law was obeyed. It was thus indicated that the ethylene glycol, methylene blue existed primarily as unassociated molecules, even up to a relatively high concentration of $1 \times 10^{-3}M$. Also, it was ascertained that acrylamide up to a concentration of $7M$ did not alter the absorption spectrum.

Polymerization Kinetics

Rate, Molecular Weight, and Induction Period. Figures 2 and 3 are plots of per cent polymerization versus time, up to the complete fading of methylene blue. Differences from the aqueous methylene blue–triethanolamine systems[2] were observed. In the present investigation when ethylene glycol was used as the solvent, an induction period for polymerization was observed, and thereafter the per cent polymerization was linear with time. The length of the induction period decreased with the increase of the absorbed light. This was shown by its decrease with the increase of methylene blue concentration (triangles, Fig. 4), and with the increase of the incident light intensity (Table II). The induction could be attributed

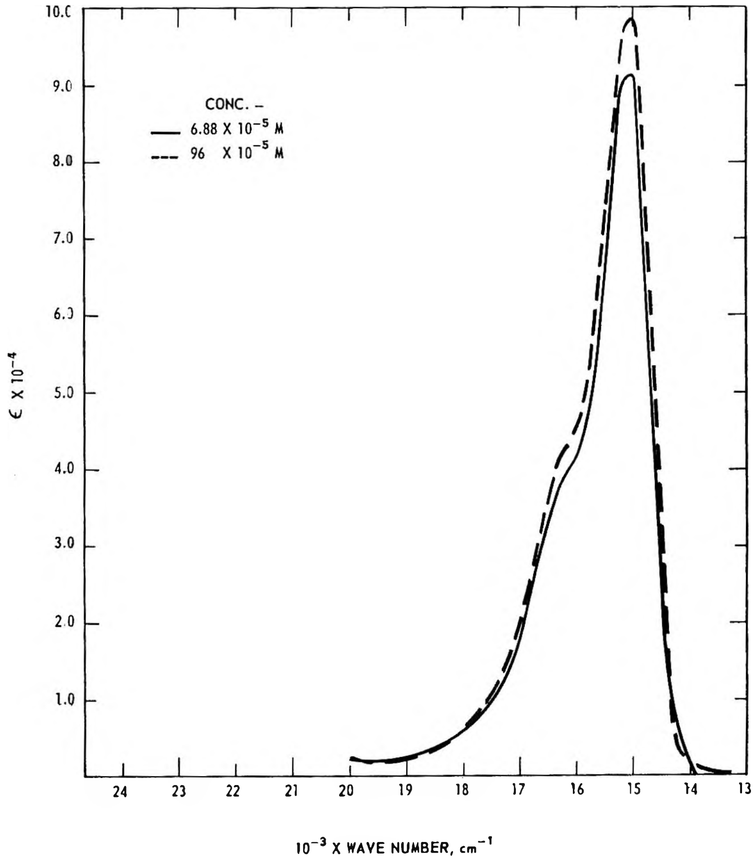

Fig. 1. Absorption spectra of methylene blue in ethylene glycol: (——) 6.88×10^{-6} M 1; (- - -) $96 \times 10^{-5}M$

to the amount of oxygen present in the polymerization system, as described by Oster and co-workers.[3] The optimum amount of oxygen should then be dependent on the system, such as the nature of the dye, the solvent, the solubility of oxygen in the solvent and others. Minimization or complete elimination of the induction period should be feasible upon further investigation.

The rates of polymerization were calculated as the slope of the straight lines (per cent polymerization per second) by means of the least squares method. They were then converted to moles of acrylamide consumed per liter per second. The molecular weights of the polymers obtained in this investigation were lower than those obtained or the corresponding aqueous systems since ethylene glycol was a more powerful chain transferring agent for the polymerization of acrylamide.

Effect of Acrylamide Concentration. The results on polymerizations of 1, 2, 4, and $7M$ acrylamide at a concentration of $6.88 \times 10^{-5}M$ methylene blue are presented in Figure 2 and Table I. It was found that the rate of

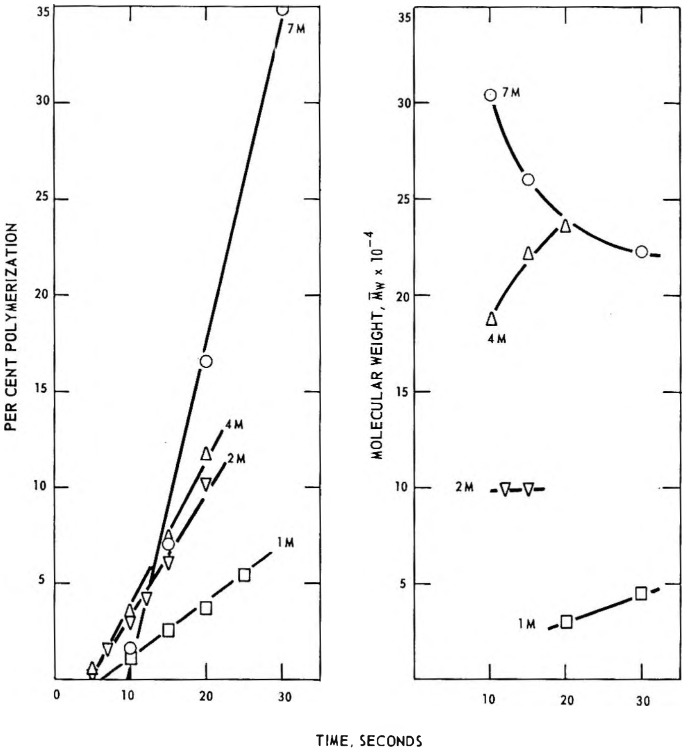

Fig. 2. Polymerization at 25°C. as a function of acrylamide concentration. [Methylene blue] = $6.88 \times 10^{-5} M$.

monomer consumption was approximately proportional to the second power of the initial monomer concentration. The molecular weight of the polymers increased rapidly with the monomer concentration up to $4M$ acrylamide; thereafter, the increase became gradual.

Effect of the Dye Concentration. The data for the polymerizations of $2M$ acrylamide at methylene blue concentrations in an experimentally practical range are presented in Figure 3. The results derived from the data are shown in Figure 4. Unlike the observations for the aqueous system in

TABLE I

Polymerization of Acrylamide in Ethylene Glycol at Different Concentrations[a]

[Acrylamide], M	Induction period, sec.	Rate $\times 10^2$, mole/l./sec.[b]	Avg. $\bar{M}_w \times 10^{-4}$
1.0	6	0.28	3.74
2.0	5	1.16	10.1
4.0	5	2.99	21.5
7.0	10	11.92	24.6

[a] [Methylene blue] = $6.88 \times 10^{-5} M$; [triethanolamine] = $2.0 \times 10^{-2} M$; temp. = 25 ± 0.1°C.

[b] Rate $\propto$ [acrylamide]^2.

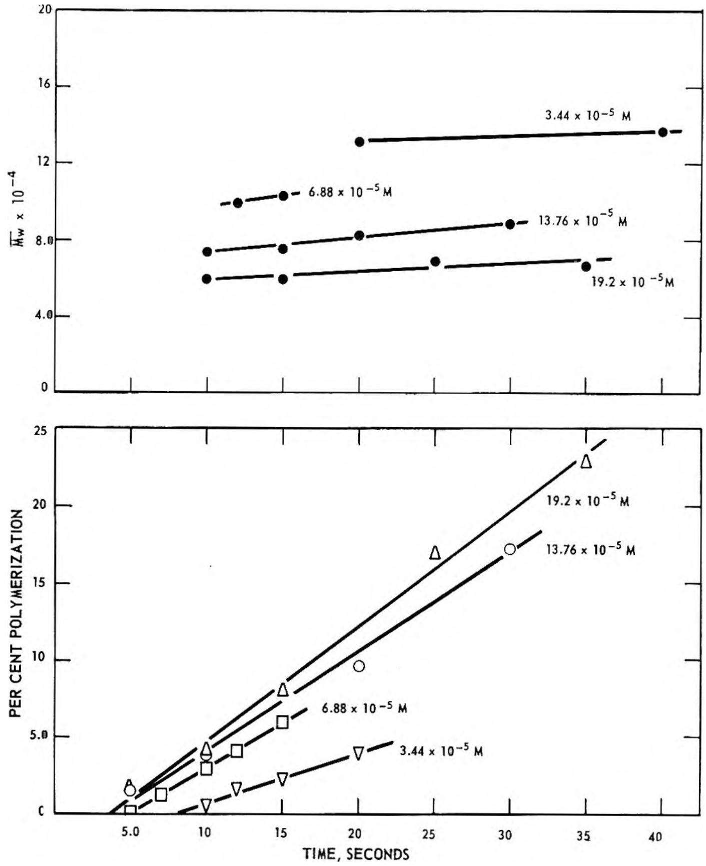

Fig. 3. Polymerization of $2M$ acrylamide as a function of the methylene blue concentration at 25°C.

a similar range of methylene blue concentrations,[2] the rate of polymerization increased with the dye concentration instead of passing through a maximum. This could be attributed to the relatively unassociated state of the methylene blue molecules in ethylene glycol as discussed above. However, the absolute initial amount of the associated molecules (terminator) would increase as the dye concentration increased, therefore, a linear relationship between the rate and the total dye concentration should not be expected. As was observed (circles in Fig. 4), the increase in rate of polymerization became more gradual at higher methylene blue concentrations. It should be anticipated that the rate would eventually decrease at even higher dye concentration.

The molecular weight of the polymers decreased with the increase in methylene blue concentration (squares, Fig. 4). A relationship of $\bar{M}_w$ α[methylene blue]$^{-1.4}$ was derived. Since the chain transfer to ethylene glycol or triethanolamine should not be affected by the concentration of methylene blue, the lower molecular weights at higher dye concentrations

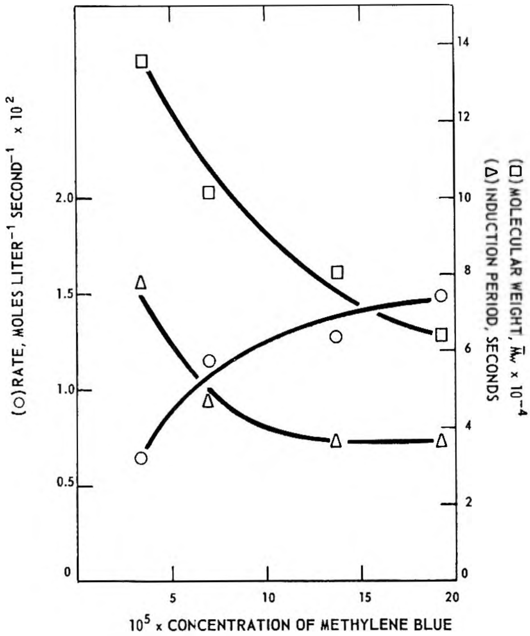

Fig. 4. Plots of (○) rate, (□), $\bar{M}_w$, and (Δ) induction period as a function of the concentration of methylene blue. Temp. = 25°C.; [acrylamide] = $2M$; [triethanolamine] = $2.0 \times 10^{-2}M$.

could be attributed to shorter kinetic chain lengths which resulted from (*1*) higher rate of initiation and termination and possibly (*2*) higher concentration of the associated molecules of the dye (terminator).

Effect of the Light Intensity. The results employing three different light intensities (1:1/2:1/4) at [methylene blue] = $6.88 \times 10^{-5}M$ are compared in Table II. The rate of polymerization was found to be approximately proportional to the half power (0.4) of the light intensity, suggesting essentially a bimolecular termination. This result was in contrast to the unimolecular termination observed for the corresponding aqueous system[2] and again supported the hypothesis that the associate molecules of the dye was a terminator.[1] Since in the present ethylene glycol system,

TABLE II
Dependence on Light Intensity[a]

Relative light intensity	Induction period, sec.	Rate × 10^3, mole/l./sec.	$M_w \times 10^{-4}$	Dependence on light intensity (I)
4 (110 v.)	5	11.6	10.1	Rate ∝ $I^{0.4}$
2 (95 v.)	7	8.21	10.1	$\bar{M}_w \propto I^{\sim 0}$
1 (80 v.)	19	6.77	9.3	Induction period ∝ I^{-1}

[a] [Acrylamide] = $2M$; [triethanolamine] = $2.0 \times 10^{-2}M$; temp. = 25 ±0.1°C.; [methylene blue] = $6.88 \times 10^{-5}M$.

at a concentration of $6.88 \times 10^{-5}M$ methylene blue, only a low concentration of the associated dye molecules were present, therefore the termination of the kinetic chain was essentially by the combination of two propagating polymer chains.

The molecular weight of the polymers was independent of the light intensity and was controlled by chain transfer processes.

Other Thiazine Dyes

For comparison, new methylene blue N and methylene green were also investigated in ethylene glycol. The structures of these thiazine dyes are given elsewhere.[4] Figure 5 depicts absorption spectra of $1.04 \times 10^{-3}M$ new methylene blue N and $1.02 \times 10^{-3}M$ methylene green as indicated. In the case of new methylene blue N even at this high concentration the β peak is barely detectable, indicating practically no association among the dye molecules. In the case of methylene green the β peak is more prominent, however, far less than that of the corresponding aqueous solution.[4]

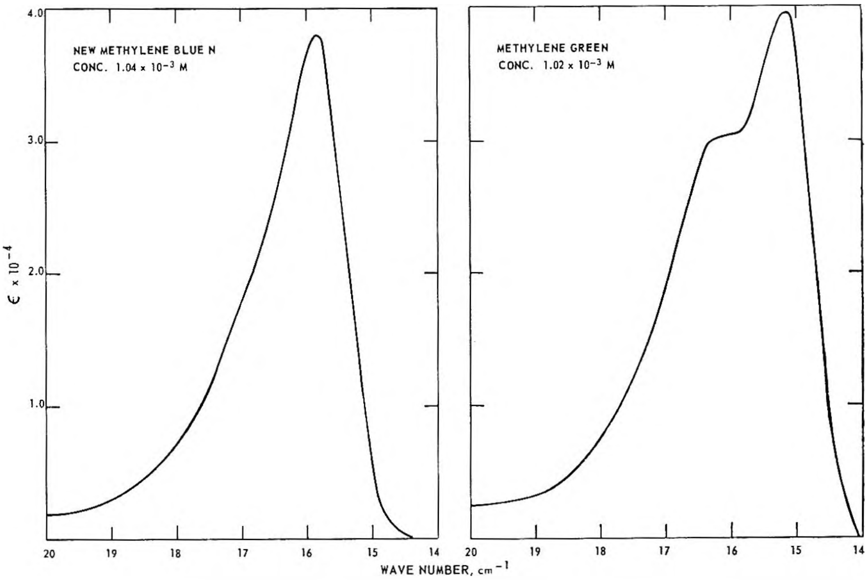

Fig. 5. Absorption spectra of new methylene blue N and methylene green in ethylene glycol.

The results of polymerization of $7M$ acrylamide in ethylene glycol at 25°C. photosensitized by $7.0 \times 10^{-5}M$ new methylene blue N–$2.0 \times 10^{-2}M$ triethanolamine and $7.0 \times 10^{-5}M$ methylene green–$2.0 \times 10^{-2}M$ triethanolamine, respectively, are summarized in Table III. As was described for methylene blue, in both cases the polymerization was characterized by an induction period and a steady-state kinetic scheme thereafter.

TABLE III
Polymerization of Acrylamide in Ethylene Glycol Sensitized By Methylene Green and New Methylene Blue N[a]

Dye	Induction period, sec.	Rate × 10^2, mole/l./sec.	Avg. $\bar{M}_w \times 10^{-5}$
New methylene blue N	7	8.69	4.14
Methylene green	19	1.76	4.41

[a] [Dye] = 7.0 × $10^{-5}M$; [triethanolamine] = 2.0 × $10^{-2}M$; [acrylamide] = $7M$; temp. = 25 ± 0.1°C.

Comparison between the Ethylene Glycol and the Aqueous Systems

Figure 6 shows a direct comparison of the polymerizations of $7M$ acrylamide at 25°C. with the use of (*1*) 6.88 × 10^{-5} methylene blue–2.0 × $10^{-2}M$ triethanolamine (triangles), (*2*) 7.0 × $10^{-5}M$ new methylene blue N–triethanolamine (squares), and (*3*) 7.0 × $10^{-5}M$ methylene green–2.0 × $10^{-2}M$ triethanolamine (circles) in ethylene glycol and in water.

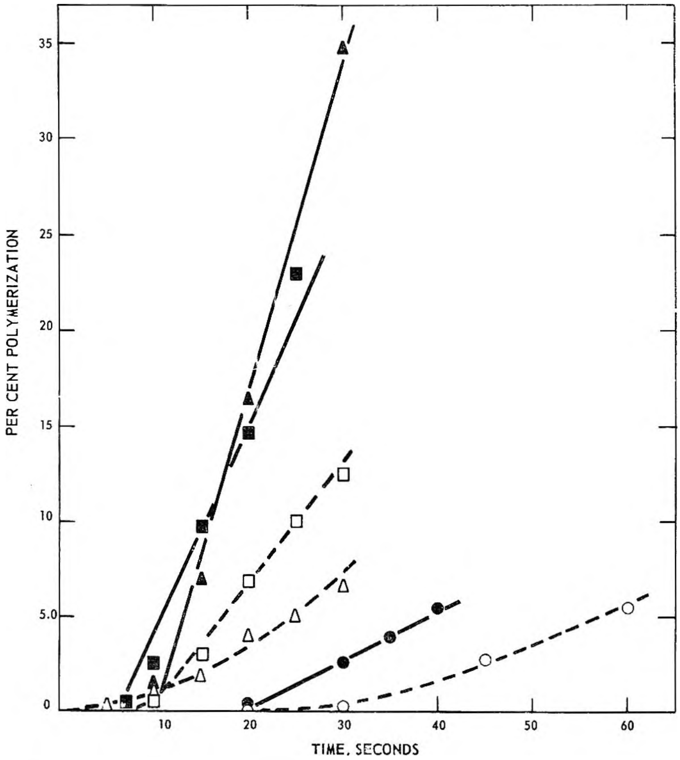

Fig. 6. Polymerization of $7M$ acrylamide at 25°C.; direct comparison between (- -) aqueous and (—, —) ethylene glycol systems: (△, ▲) methylene blue; (□, ■) new methylene blue; (○, ●) methylene green.

In all three cases, aside from the differences in the kinetics described, the polymerization proceeded faster in ethylene glycol than in water. The faster polymerization, so far, has been attributed to the relatively unassociated state of the dye molecules in ethylene glycol, however, another important factor, the viscosity of the medium, also should be considered. It has been reported for the riboflavin–acrylamide system[3] that the rate of polymerization was proportional to the one-half power of the viscosity of the medium. The viscosity dependence of rate was determined in glycerol–water mixture. In our investigation, changing from the aqueous system to ethylene glycol system was also accompanied by a manyfold increase in viscosity. The results on the effect of the viscosity of the medium in our investigation will be discussed in the next section.

The Factor of Viscosity

An aqueous system having similar viscosity to the ethylene glycol system was made up by dissolving an appropriate amount of poly(ethylene

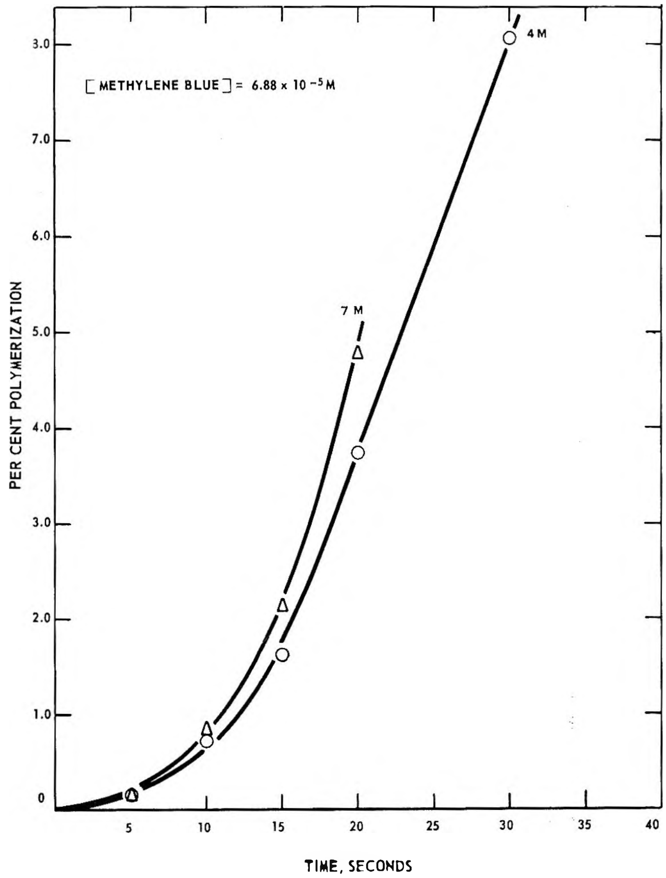

Fig. 7. Polymerization of acrylamide in aqueous polyethylene oxide solution.

TABLE IV

Comparison Between Photopolymerization of Acrylamide in Aqueous and Ethylene Glycol Systems: Comparable and Different Viscosities

Medium	[Acrylamide], M	Absolute viscosity at 25°C., cpoise	α peak $\epsilon \times 10^{-4}$, mole/l./cm.	β peak $\epsilon \times 10^{-4}$, mole/l./cm.	K (log [Mo]/[M]/t^2)	Rate, mole/l./sec.	Avg. $\bar{M}_w \times 10^{-5}$
Water	4	1.54	$\epsilon_{665} = 6.49$	$\epsilon_{612} = 4.41$	2.81		2.94
Water and poly-(ethylene oxide)	4	16.7	$\epsilon_{665} = 7.50$	$\epsilon_{612} = 5.43$	4.12		2.70
Ethylene glycol	4	16.3	$\epsilon_{665} = 9.13$	shoulder: 610–630 mμ		2.99×10^{-2} (5 sec. induction period)	2.15
Water	7	2.27	$\epsilon_{665} = 6.49$	$\epsilon_{612} = 4.41$	4.02		6.93
Water and poly-(ethylene oxide)	7	16.7	$\epsilon_{665} = 7.50$	$\epsilon_{612} = 5.43$	5.41		4.53
Ethylene glycol		16.0	$\epsilon_{665} = 9.42$	shoulder: 610–630 mμ		1.19×10^{-1} (10 sec. induction period)	2.46

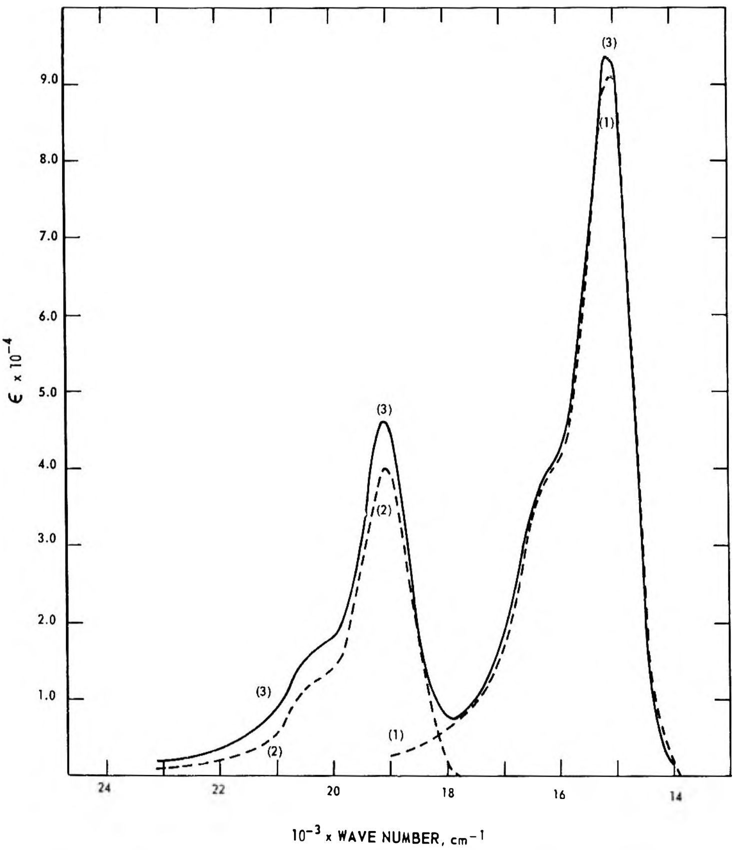

Fig. 8. Comparison of the absorption spectra of ethylene glycol solutions of (*1*) 7.0 × $10^{-5}M$ methylene blue, (*2*) 3.0 × $10^{-5}M$ eosin Y, and (*3*) a mixture of 7.0 × $10^{-5}M$ methylene blue + 3.0 × $10^{-5}M$ eosin Y.

oxide) in water (Polyox WSR-35). In the visible region, the shape of the absorption spectrum of 7.0 × $10^{-5}M$ methylene blue in this aqueous poly(ethylene oxide) solution was found to be the same as that in pure water with the exception that the overall absorption was somewhat greater (Table IV). Polymerizations of both 4*M* and 7*M* acrylamide in this polyethylene oxide solution were investigated. In these systems, methylene blue molecules were in the similar state to those in water, but in this case the viscosity was comparable to that of the ethylene glycol system. As shown in Figure 7, the polymerization was found to follow the nonsteady-state kinetics observed for the aqueous systems.[2] The rates were represented as the slopes of the log $[M_0/M]$ versus t^2 plots. A comparison of the aqueous, the aqueous poly(ethylene oxide), and the ethylene glycol systems are summarized in Table IV. When the two aqueous systems, with and without poly(ethylene oxide), were compared, if we were to attribute the difference in rate of polymerization only to the difference in the initial viscosity of the medium, the following relationships would be derived: rate

$\propto$ [viscosity]$^{0.16}$ for 4*M* acrylamide and rate $\propto$ [viscosity]$^{0.15}$ for 7*M* acrylamide. On the other hand, the higher rates observed for the poly(ethylene oxide) systems could also be attributed to the somewhat higher energy absorption by these systems. Therefore, it could be concluded that in our investigation the effect of the initial viscosity of the rate of polymerization was small. The above results thus suggested that the different type of kinetics and the enhancement in rate of the photopolymerization in ethylene glycol were primarily due to the more favorable electronic state of the methylene blue molecules in that solvent.

Sensitization in Combination with Eosin Y

Based on the fact that molecules of a single thiazine dye are unassociated in a solvent like ethylene glycol, it is anticipated that there should be little or no interaction between the molecules of two dyes such as methylene blue and eosin Y. Spectroscopic results supported this prediction. As indicated in Figure 8, in ethylene glycol virtually no interaction was present in a solution of $7.0 \times 10^{-5}M$ methylene blue and $3.0 \times 10^{-5}M$ eosin Y. As was the case for a single dye solution, the molecules of both dyes simply behave independently of others present.

The results for polymerization sensitized by (*1*) $7.0 \times 10^{-5}M$ methylene blue, (*2*) $3.0 \times 10^{-5}M$ eosin Y, and (*3*) their mixture are compared in Figure 9. The polymerization sensitized by $3.0 \times 10^{-5}M$ eosin Y (circles)

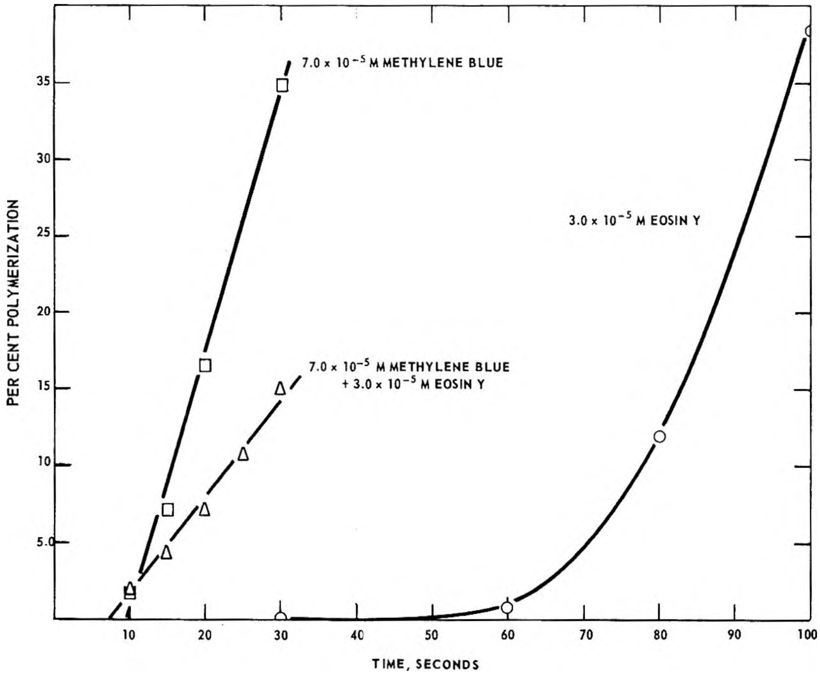

Fig. 9. Comparison of polymerization of 7*M* acrylamide in ethylene glycol at 25°C. with methylene blue, eosin Y, and their mixture as sensitizers.

TABLE V

Quantum Yields in Polymerization of 7*M* Acrylamide in Ethylene Glycol[a]

Dye	$E(= h\nu)$, ergs/quantum	Energy absorbed, quantum/sec.[b]	Irradiation time, sec.	No. of molecules converted	$\overline{\text{DP}}$	Quantum yield	
						ϕ_m	ϕ_p
Methylene blue (λ = 663 mμ)	2.997×10^{-12}	1.0804×10^{17}	10	6.334×10^{20}	4.28×10^{3}	5.86×10^{2}	0.137
			15	2.943×10^{21}	3.66×10^{3}	1.82×10^{3}	0.497
			20	6.962×10^{21}	2.76×10^{3}	3.22×10^{3}	1.17
			30	1.465×10^{22}	3.17×10^{3}	4.52×10^{3}	1.43
New methylene blue N (λ = 633 mμ)	3.139×10^{-12}	3.5792×10^{16}	7	2.444×10^{20}	8.83×10^{3}	9.76×10^{2}	0.111
			10	1.100×10^{21}	5.79×10^{3}	3.07×10^{3}	0.530
			15	4.126×10^{21}	4.66×10^{3}	7.68×10^{3}	1.65
			20	6.068×10^{21}	4.78×10^{3}	8.48×10^{3}	1.78
			25	9.705×10^{21}	4.96×10^{3}	1.09×10^{4}	2.20

[a] Temperature = 25°C.; [triethanolamine] = $2.0 \times 10^{-2}M$.

[b] Based on initial dye concentration, became increasingly less as the dye faded with irradiation time.

proceeded with a relatively long induction period but thereafter quite rapidly. The polymerization sensitized by a mixture of $7.0 \times 10^{-5}M$ methylene blue and $3.0 \times 10^{-5}M$ eosin Y (triangles) followed the same kinetics as described for methylene blue alone; however, it proceeded at a slower speed. It became apparent that, in the ethylene glycol system, eosin Y within its induction period for polymerization actually hindered the polymerization sensitized by methylene blue also.

Quantum Yields

Quantum yields were calculated for the polymerizations sensitized by $6.88 \times 10^{-5}M$ methylene blue and $7.0 \times 10^{-5}M$ new methylene blue N. Since the spectra of both dyes were nearly symmetrical (Figs. 1 and 5), white light was used, and the peak wave-length was used as λ in $E = h\nu = hc/\lambda$. The energy absorbed by the system was again obtained by area integration based on the spectral distribution of the lamp[2] and the absorption spectra in ethylene glycol (Figs. 1 and 5). It had been ascertained that the concentration of acrylamide (up to $7M$) does not alter the spectrum of methylene blue in ethylene glycol. The results are tabulated in Table V. The values for quantum yields were calculated with the induction periods included. Again, it should be pointed out that the energy absorbed was based on the initial dye concentration; the actual quantum yields were increasingly higher with increasing time, since the energy absorbed became increasingly less as the dye faded.

CONCLUSION

In ethylene glycol, thiazine dyes are present primarily in the unassociated form throughout the concentration range of interest (up to $1 \times 10^{-3}M$). When they are used as the photosensitizers together with triethanolamine for the polymerization of acrylamide, the polymerizations follow, after an induction period, a steady-state kinetics, and the chains are terminated bimolecularly. These observations differ from the nonsteady-state kinetics and unimolecular termination for the polymerizations in the corresponding aqueous systems. By direct comparison between the polymerizations of the aqueous and the ethylene glycol systems under otherwise indentical experimental conditions it is concluded that polymerizations take place at considerably faster rates in ethylene glycol (Fig. 6). The faster rate of polymerization is attributed to the relatively unassociated state of the dye molecules and is not due to the higher viscosity of the ethylene glycol system. The bimolecular termination in ethylene glycol is attributed to the essential absence of a terminator which has been proposed to be the associated form of the dye and is present in the aqueous systems. These results lend further support to the hypotheses that (*1*) the power of sensitization of thiazine dyes is dependent on the electronic state of the molecules which in turn is susceptible to the change of the environment and

(*2*) the monomeric form (unassociated form) of the dye is a photosensitizer while the associated form is a terminator.

This series of preliminary investigations has served to demonstrate some of the factors which affect the dye sensitized photopolymerization. Among the systems investigated thus far, the most efficient initiation is produced by methylene blue and new methylene blue N in ethylene glycol. It is anticipated that further improvements can be made on the ethylene glycol systems by performing one or all of the following: (*1*) addition of a suitable antioxidant so as to diminish or to eliminate the induction period, (*2*) coupling methylene blue or new methylene blue N with another amine or weak reducing agent at an optimal concentration so as to increase the efficiency of initiation, and (*3*) addition of a suitable promotor for the polymerization. However, in the present systems the primary photochemical reaction is not a chain reaction, therefore, the maximum quantum yield in initiation is unity. For polymerization processes far more efficient than the present ones, a primary photochemical reaction which involves a chain process will probably have to be considered.

References

1. Michaelis, L., *J. Phys. Colloid Chem.*, **54**, 1 (1950).
2. Chen, C. S. H., *J. Polymer Sci.*, **A3**, 1107 (1965).
3. Oster, G. K., G. Oster, and A. Prati, *J. Am. Chem. Soc.*, **79**, 596 (1957).
4. Chen, C. S. H., *J. Polymer Sci.*, **A3**, 1137 (1965).

Résumé

La polymérisation de l'acrylamide dans l'éthyléne glycol, induite par la lumiére visible en utilisant le systéme bleu de méthyléne-triéthanolamine comme sensibilisateur, suit un schéma cinétique stationnaire aprés une période d'induction. La vitesse est proportionnelle á la racine carrée de l'intensité de la lumiére absorbée et au carré de la concentration initiale en monomére; de plus, elle augmente avec la concentration en colorant. Les poids moléculaires des polyméres sont d'environ 3.0 × 10^4 á 2.5 × 10^5: ils sont indépendants de la lumiére absorbée, augmentent avec la concentration initiale en monomére et diminuent avec la concentration en colorant. La période d'induction est inversément proportionnelle à l'intensité de la lumiére. La polymérisation est beaucoup plus rapide dans l'éthyléne glycol que dans l'eau. Ceci est attribué au fait que le bleu de méthyléne se trouve principalement sous forme monomérique dans l'éthyléne glycol, aux concentrations employées. Des sensibilisateurs tels que le bleu de méthyléne N–triéthanolamine et vert de méthyléne triéthanolamine ont été employés pour la polymérisation de l'acrylamide dans l'éthyléne glycol. On a obtenu des résultats semblables á ceux obtenus avec le systéme bleu de méthyléne–triéthanolamine.

Zusammenfassung

Die durch sichbares Licht mit Methylenblau- Triäthanolamin als Sensibilisatorsystem angeregte Polymerisation von Äcrylamid in Athylenglykol folgte nach einer Induktionsperiode einem kinetischen Schema mit stationärem Verlauf. Die Geschwindigkeit war der Wurzel aus der Intensität des absorbierten Lichtes und dem Quadrat der Endkonzentration des Polymeren proportional. In dem experimentell bequem zugänglichen Bereich der Farbstoffkonzentration nahm die Geschwindigkeit mit der Farbstoffkonzentration zu. Das Molekulargewicht der Polymeren lag im Bereich von 3.10^4 bis $2{,}5.10^5$; es war von der absorbierten Lichtintensität unabhängig, es nahm mit der Anfangsmonomerkonzentration zu und mit der Anfangsfarbstoffkonzentration ab. Die Induktionsperiode war der Lichtintensität umgekehrt proportional. Die Polymerisation verlief in Äthylenglykol mit beträchtlich höherer Geschwindigkeit als im wässrigen System. Die raschere Polymerisation wurde primär dem Umstand zugeschrieben, dass in Äthylenglykol Methylenblau bei allen verwendeten Konzentrationen hauptsächlich in der monomeren Form vorlag. Weiters wurden Neumethylenblau *N*–Triäthanolamin und Methylengrün–Triäthanolamin als Sensibilisatorsystem für die Polymerisation von Acrylamid in Äthylenglykol untersucht. Es wurden ähnliche Ergebnisse wie bei Methylenblau–Triäthanolamin erhalten.

Received June 16, 1964

JOURNAL OF POLYMER SCIENCE: PART A VOL. 3, PP. 1171-1184 (1965)

Thermal Degradation of Poly(methyl Methacrylate) in a Closed System*

J. E. CLARK and H. H. G. JELLINEK, *Department of Chemistry, University of Windsor, Windsor, Ontario, Canada*

Synopsis

The thermal degradation of poly(methyl methacrylate) has been studied with unfractionated and fractionated polymer samples over a temperature range of 275–400°C. in a closed system by a new technique. Kinetic data have been obtained at temperatures about 100°C. higher than was possible previously. The results are compared with those obtained in open systems. Two main degradation reactions are operative. It is shown that the energies of activation for these reactions do not vary with polymer chain length in accordance with what is to be expected from the usually assumed depolymerization mechanisms. The termination reactions are diffusion-controlled. Hydrogenation by Adam's catalyst and bromination of the polymers have only moderate effects on the rate of degradation.

The thermal degradation of poly(methyl methacrylate) in high vacuum has been studied by a number of workers.[1-3] Also an investigation in a closed system at relatively low temperatures and under small pressures has been carried out.[4] It seems to be well established that for polymers prepared in bulk or concentrated benzene solutions with benzoyl peroxide as catalyst two major reactions take place on degradation. The first reaction is due to initiation at chain ends, which carry double bonds, with subsequent depolymerization and second-order terminations if the polymer chains are sufficiently long. The second slower reaction, having a higher energy of activation than the first one, consists either of chain end initiation of chains having no double bond ends or random initiation, with subsequent depropagation and second-order termination.

In previous work, the first reaction had to be studied either at such low temperatures that the second reaction became very slow, or if higher temperatures were employed, the first reaction became so fast that a large proportion of it was over before measurements could be started. The present work is concerned with an attempt of extending kinetic data for both reactions to temperatures for which no data have yet been published. A new technique, which was described in a previous publication,[5] has been developed for this purpose based on the use of an automatically recording

---

* Presented at the Symposium on Thermal Stability of Polymers, Battelle Memorial Institute, Columbus, Ohio, Dec. 5–6, 1963.

quartz spoon reaction vessel. Kinetic data could be obtained up to 400°C.; an improved version of this apparatus which will be described in a later publication, allows kinetic data for the second reaction to be obtained up to 450°C. Part of the work will be reported here, without a detailed kinetic analysis of the experimental data.

EXPERIMENTAL

Apparatus and Procedure

The apparatus consisted of a quartz spoon reaction vessel automatically recording gas pressures developed in the reaction vessel during degradation. It was described in detail in a previous publication.[5] The gauges had sensitivities of the order of 0.035 cm./atm.; pressures of 1 mm. Hg could be ascertained readily. In all cases, a 20-mg. portion of polymer deposited in the form of a thin film from acetone solution on the walls of the reaction vessel was taken for each experiment. The time necessary to heat the reaction vessel to the desired temperature was not more than 30 sec.

Materials

The following polymer samples were used in the investigation; they were prepared from Rohm and Haas monomer, purified as described previously:[5] sample I: 70 g. monomer in 60 g. benzene plus 0.5 g. benzoyl peroxide, polymerized at 80°C. for 3 hr., conversion 50%, $[\eta] = 0.50$ dl./g., $\bar{M}_v = 104{,}000$ obtained from $[\eta] = 4.85 \times 10^{-5}\bar{M}_v^{0.8}$; sample II: 100 g. monomer plus 0.5 g. benzoyl peroxide, polymerized at 80°C. for 30 min. under a nitrogen atmosphere, 75% conversion, $[\eta] = 0.98$ dl./g., $\bar{M}_v = 241{,}000$; sample III (compare also previous paper[5]): 100 g. monomer plus 0.5 g. benzoyl peroxide, polymerized at 60°C. for 30 min., 5% conversion, $[\eta] = 2.01$ dl./g., $\bar{M}_v = 591{,}000$; Sample IV: similar procedure as for sample III, $[\eta] = 2.28$ dl/g., $\bar{M}_v = 691{,}000$.

Sample IV was fractionated (acetone plus methanol) into nine fractions all designated by F with $F_1(\bar{M}_v = 1{,}360{,}000)$, $F_5(\bar{M}_v = 669{,}000)$, F_9 $(\bar{M}_v = 111{,}500)$.

RESULTS

Energies of Activation

Sample III was degraded over a range of temperatures from 275 to 400°C. The degradation curves, except the one for 275°C., were given in the previous paper.[5] They show that for the fast reaction useful results could still be obtained at 400°C. for the first reaction, whereas Brockhaus and Jenckel[2] could not obtain any results for this reaction above 300°C., as the time for heating their reaction vessel was about 15 min. Similar remarks hold true for Madorsky's work.[3] The fact that two reactions are operative

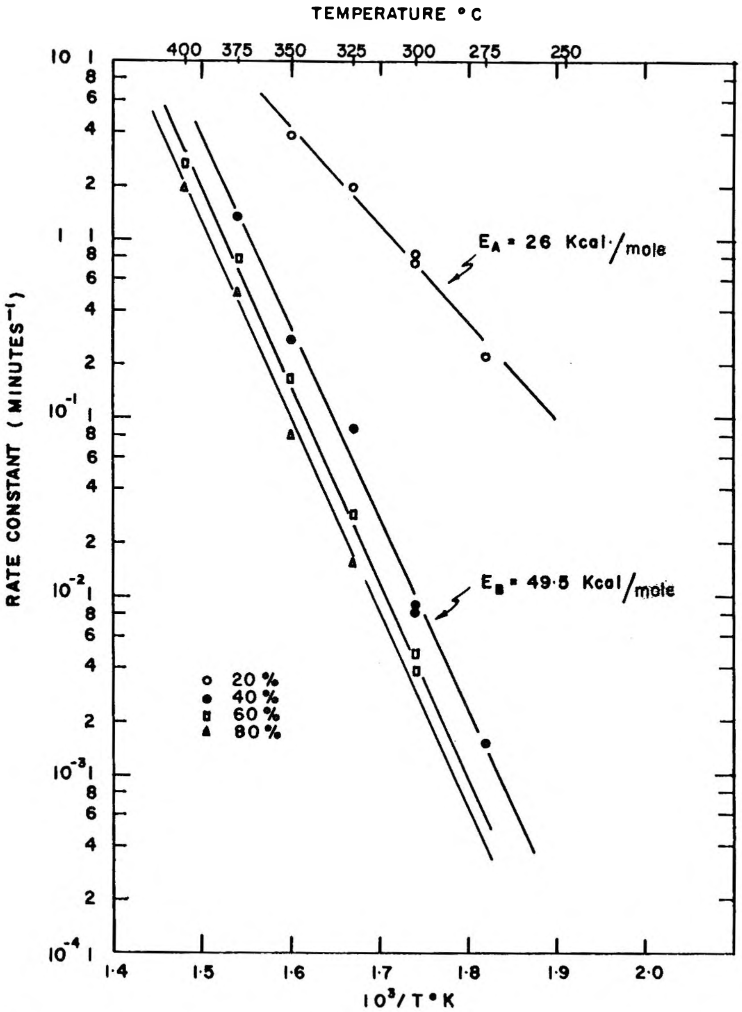

Fig. 1. Energies of activation E_A and E_B for the slow and fast reaction, respectively.

is clearly brought out by plotting the rate of gas formation against the amount of gas or the percentage conversion to gas.

Energies of activation were obtained for various percentages of conversion by plotting the respective $d\left(\frac{dn}{dt}\right)/dn$ values against the reciprocal absolute temperatures. For the fast reaction, an Arrhenius equation is obtained (see Fig. 1):

$$k_{A,20\%} = 6.0 \times 10^9 e^{-26000/RT} \text{ min.}^{-1}$$

and for the slow reactions the Arrhenius equations are (see Fig. 1)

$$k_{B,40\%} = 4.9 \times 10^{16} e^{-49500/RT} \text{ min.}^{-1}$$

$$k_{B,60\%} = 3.0 \times 10^{16} e^{-49500/RT} \text{ min.}^{-1}$$

$$k_{B,80\%} = 1.4 \times 10^{16} e^{-49500/RT} \text{ min.}^{-1}$$

The actual rate constants are given in Table I.

TABLE I
Rate Constants for the Fast Reaction (k_A) and the Slow Reaction (k_B) in the Pyrolysis of PMMA III at Various Temperatures

Temp. at which k measured, °C.	$k_{A,20\%}$, min.$^{-1}$	k_B, min.$^{-1}$		
		40%	60%	80%
275	0.225	0.0015		
300				
(20 mg.)	0.850	0.009	0.005	—
(40 mg.)	0.750	0.008	0.004	—
325	2.00	0.089	0.029	0.015
350	3.80	0.275	0.164	0.078
375	—	1.350	0.790	0.510
400	—	—	2.700	1.960

Percentage of Rapidly Degrading Polymer and Initial Rates as Functions of Chain Lengths

Polymer samples I, II, III, IV, F_1, F_5, and F_9 were degraded at 350°C.; the respective rate constants are given in Table II. The rate constants for the slow reactions are also given in Table II.

TABLE II
Rate Constants for the Fast Reaction (k_A) and the Slow Reaction (k_B) in the Pyrolysis of Various PMMA Samples at 350°C.

PMMA	$k_{A,20\%}$, min.$^{-1}$	k_B, min.$^{-1}$			P_v[a]
		40%	60%	80%	
I	4.56	0.810	0.110	0.048	1040
II	4.55	0.810	0.110	0.052	2410
III	3.80	0.275	0.165	0.080	5910
IV	4.64	0.105	0.080	0.060	6915
F_1	4.02	0.100	0.065	0.035	13,600
F_5	4.16	0.250	0.120	0.070	6690
F_9	4.08	0.100	0.065	0.035	1115

[a] P_v = viscosity-average chain length.

The amount of fast degrading polymer was obtained by linear extrapolation of the fast reaction to zero rate of monomer formation. Some typical curves are given in Figures 2 and 3, where the rate of monomer formation is plotted against the amount of monomer produced or percentage conversion to monomer. The extrapolated values in percentage of the original sample as a function of the reciprocal viscosity-average chainlength P_v are shown in Figure 4. Some of Brockhaus and Jenckel's[2] results obtained at 300°C. are also given in Figure 4.

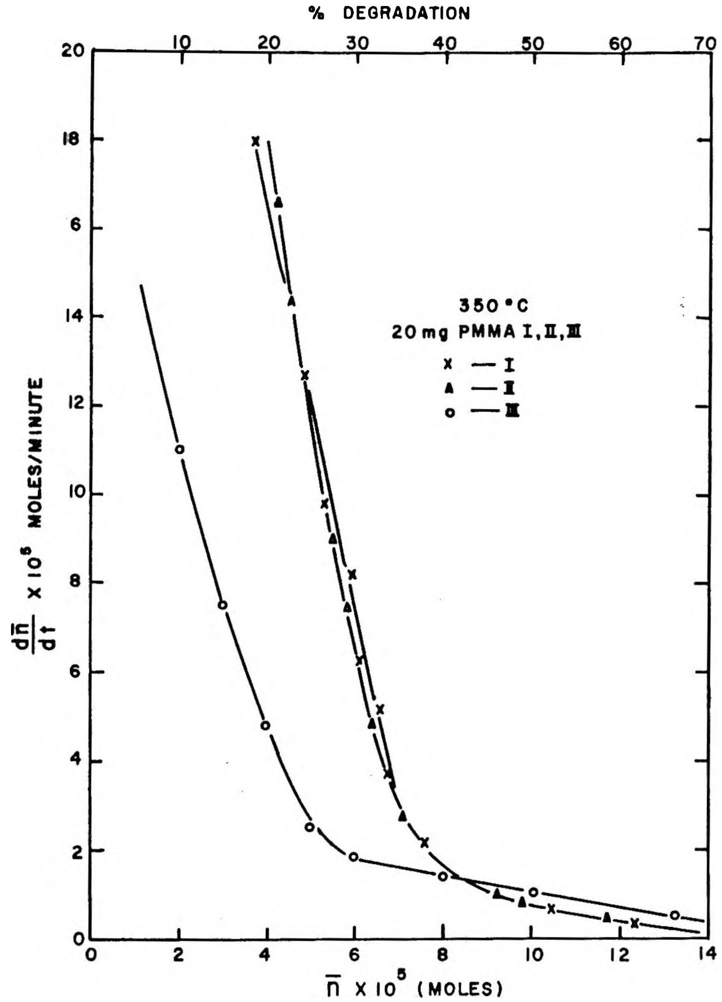

Fig. 2. Rate of monomer (gas) formation vs. monomer (gas) produced for samples I, II, and III at 350°C.

The initial rates of monomer production were also obtained by extrapolation, assuming that the fast reaction obeys the following empirical equation over its entire range,

$$dm_1/dt = -k_A m_1 + \text{constant} \tag{1}$$

where constant = $k_A\, m_{1,\,\text{final}}$. The initial rates are expressed in moles of monomer/base mole/minute. The curve is shown in Figure 5.

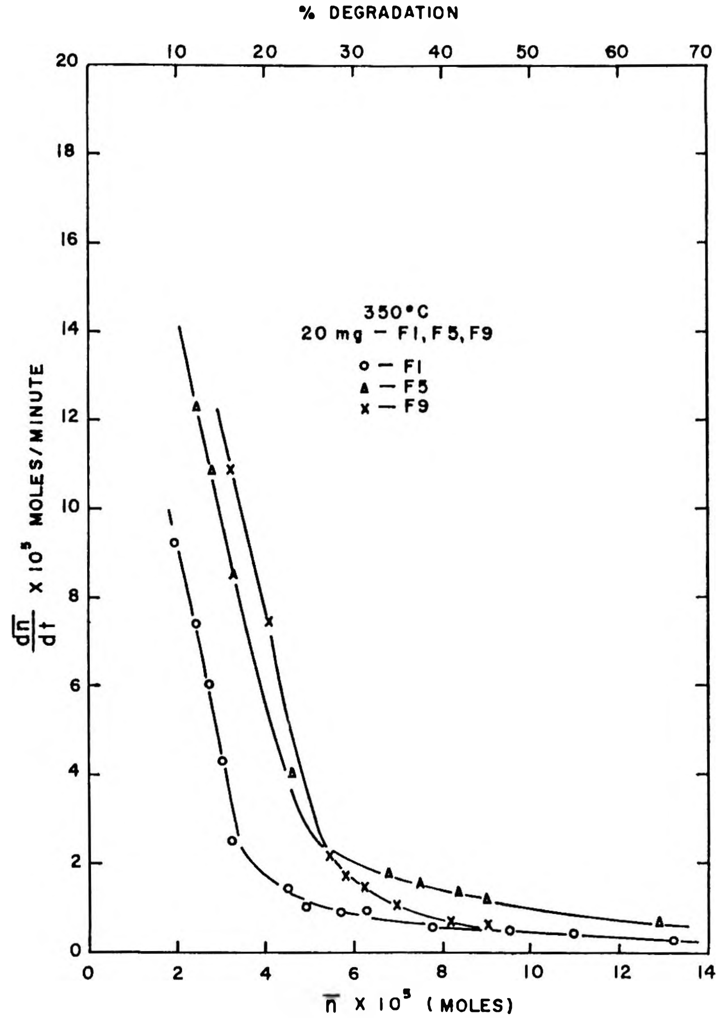

Fig. 3. Rate of monomer (gas) formation vs. monomer (gas) produced for fractionated samples F_1, F_5, and F_9.

Hydrogenation

Attempts were made to hydrogenate the double bonds at the chain ends. Adams catalyst (National Lead Company, New York) and 10% palladium on activated charcoal were used. Adams catalyst was found to be more effective and the experiments described below were carried out with this catalyst. First, monomer was hydrogenated in chloroform solution in the presence of Adams catalyst (2 ml. monomer, 28 ml. chloroform, 0.20 g. catalyst, 5 mm. Hg, room temperature, 90 min.). The hydrogen was quantitative, and the infrared spectrum was identical with that of methylisobutyrate. Hydrogenation of sample IV was then attempted, leading to the hydrogenated samples H_5 and H_6. H_5 and H_6 were obtained by treating

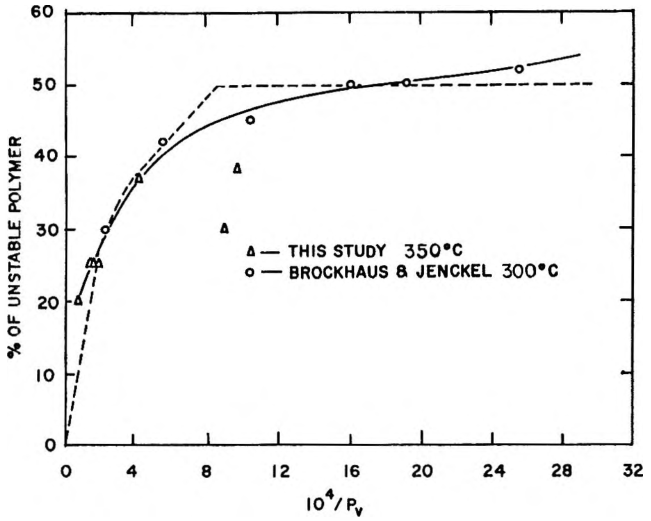

Fig. 4. Values extrapolated to zero rate of monomer formation in percentage of the original sample as a function of the reciprocal viscosity-average chain length at 350°C. and Brockhaus and Jenckel's values for 300°C. Dashed line see text.

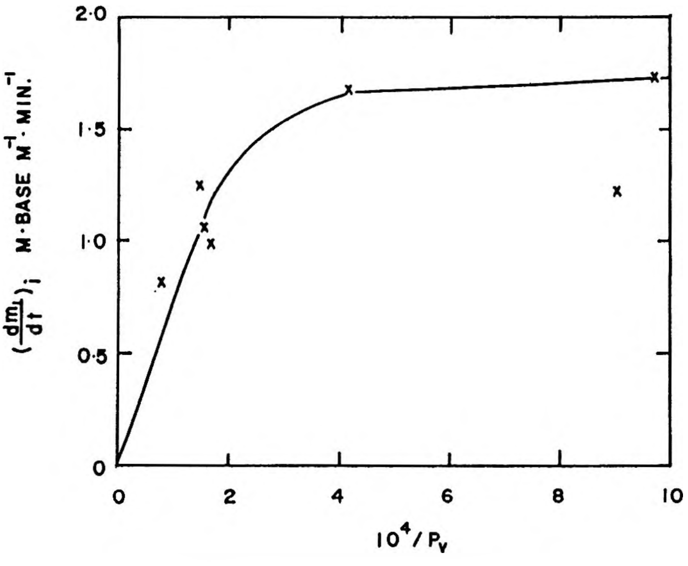

Fig. 5. Initial rates of monomer formation as a function of reciprocal viscosity-average chain lengths at 350°C.

IV in chloroform solution (H_5: 0.50 g. polymer, 25 ml. chloroform, 0.20 g. catalyst, 15 mm. Hg, 2 hr., room temperature; H_6: same procedure but 4 hr.). The degradation curves of the hydrogenated and untreated polymer (average curve, standard deviations are indicated) are given in Figure 6.

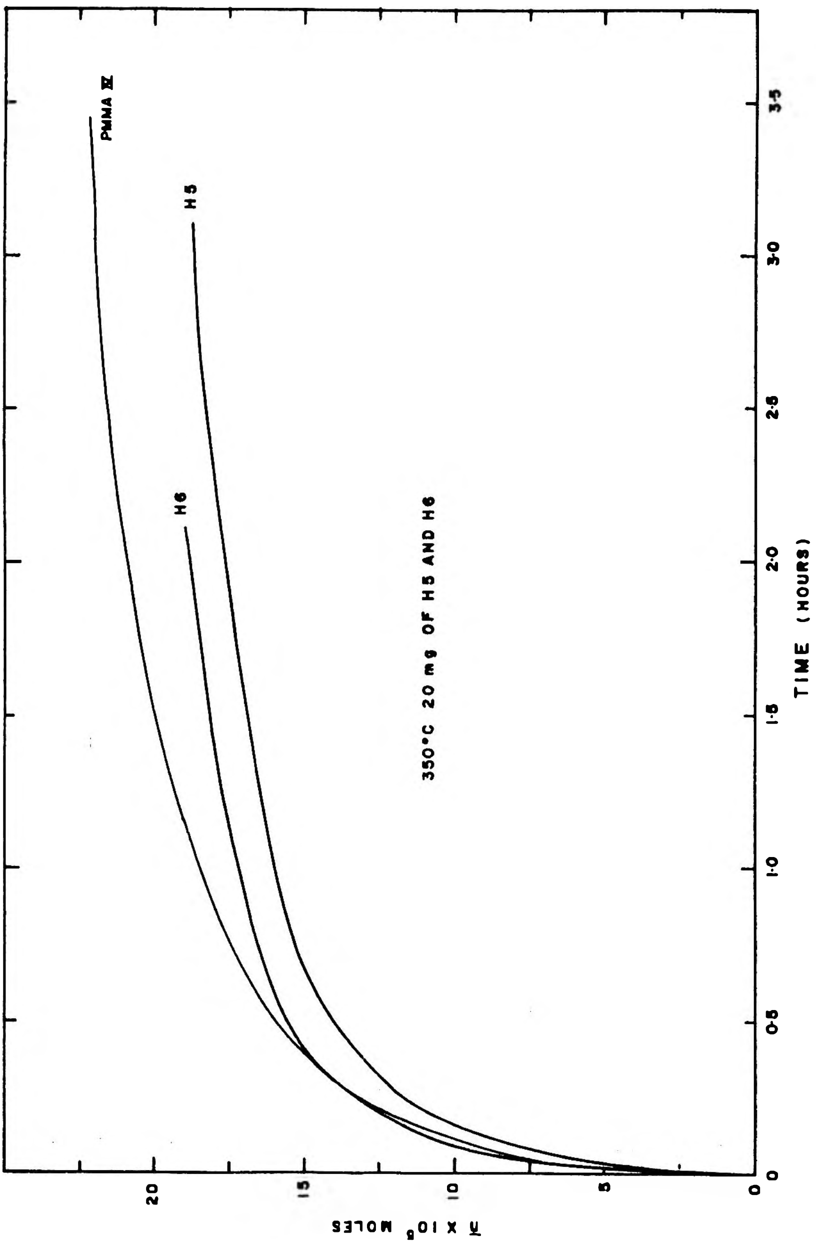

Fig. 6. Degradation curves for untreated and hydrogenated polymer (sample IV) at 350°C.

Bromination

Bromination was attempted in chloroform and glacial acetic acid solutions. However, no marked changes in the degradation curves were obtained, although the percentage of fast degrading polymer obtained by extrapolation to zero-rate monomer formation decreased somewhat.

DISCUSSION

Fast Reaction

It is by now well established[1-3] that the fast part of the degradation is due to the breakdown of chains having double bonds at one of their ends. The reaction consists of chain end initiation, depropagation with a fairly long kinetic chainlength and second order termination.

The experimental results will be discussed without going into a detailed kinetic analysis at this stage of the work, as, for instance, Gordon[6] has done. It is clear that the temperature range for kinetic analysis has been extended by another 50–100°C. by the method employed in this work.

The rate of monomer formation of the fast reaction can be represented over an appreciable extent by a straight line relationship,

$$dm_1/dt = -k_A m_1 + C \tag{2}$$

where k_A is a constant of proportionality and C a constant. If it is assumed that the reaction can be extrapolated to its beginning and end, then $C = k_A m_{1,e}$, where $m_{1,e} = m_0 f_e$ is the final amount of monomer produced from the fast reaction when $dm_1/dt = 0$; m_0 is the initial number of moles of monomer contained in the polymer sample and f_e the fraction $m_{1,e}/m_0$ of the sample degraded to monomer. The initial rate of monomer formation is then given by:

$$(dm_1/dt)_i = k_A m_{1,e} = k_A m_0 f_e \tag{3}$$

From kinetic considerations[7] it follows that the initial rate of monomer formation, for the case where the initial chain length P_0 of a homogeneous polymer sample is smaller than the kinetic chainlength ϵ, is given by:

$$(dm_1/dt)_i = k_i m_0 f_i \tag{4}$$

where k_i is the rate constant for initiation and f_i is the fraction of initial chains having one double bond chain end. Hence, for $P_0 < \epsilon$, the experimental rate constant k_A is given by,

$$k_A = (f_i/f_e)k_i \tag{5}$$

If $P_0 > \epsilon$, one obtains:[7]

$$(dm_1/dt)_i = k_d(k_i/k_t)^{1/2}(1/P_0)^{1/2}(V_m)^{1/2}m_0 f_i \tag{6}$$

where k_d and k_t are the rate constants for depropagation and termination, respectively, and V_m is the volume of one base mole of polymer at the reaction temperature. Hence, for this case:

$$k_A = k_d(k_i/k_t)^{1/2}(V_m)^{1/2}(1/P_0)^{1/2}(f_t/f_e) \tag{7}$$

f_e and V_m will not change appreciably with temperature in contrast to the rate constants.

Thus it is to be expected that the apparent energy of activation for k_A will change with increasing chainlength from

$$E_{\text{app}} = E_t$$

to

$$E_{\text{app}} = E_d + (E_i/2) - (E_t/2)$$

Due to the high viscosities of the reaction media, E_t will usually be diffusion controlled. If this were not the case $E_t \cong 0$. It is surprising to find that the apparent energy of activation seems to be independent of chainlengths. There is as yet no satisfactory explanation for this behavior.

Grassie and Melville[1] found 31,000 ± 1000 cal./mole for number-average chain lengths ranging from 360 to 5000. Madorsky[3] found 33,000 cal./mole for a number-average chain length 1500; Brockhaus and Jenckel[2] found 27,000 ± 1000 cal./mole for viscosity-average chain lengths 390 and 4260, respectively; our work gives 26000 cal./mole for a viscosity-average chain length of 5910.

On the basis of the mechanism outlined above, E_{app} could only remain constant if $E_d - (E_t/2)$ happened to be equal to $E_i/2$. In a recent note, Grassie[8] discussed the energy of activation for this reaction; Ivin[9] obtained the heat of polymerization $\Delta H_{gc} = 21.4$ kcal./mole from polymer–monomer equilibria. By assuming the energy of activation for the polymerization reaction to be 5 kcal./mole., the energy of activation for the depropagation reaction becomes $E_d = 26.4$ kcal./mole. For this value and Cowley and Melville's[10] apparent energy of activation of 8 kcal./mole for photodegradation, a value of 37 kcal./mole is obtained for the energy of activation of the termination reaction. This high value indicates that the termination reaction is diffusion-controlled. Cowley and Melville had already pointed out that the termination reaction for photodegradation was diffusion-controlled; however, their reaction was carried out below 200°C. If it were assumed that,

$$E_d - (E_t/2) = E_i/2 = 16.5 \text{ kcal./mole}$$

a value of $E_t = 19.8$ kcal./mole results for $E_{\text{app}} = 33$ kcal./mole.

The initial rates of monomer formation for the fast reaction as a function of the reciprocal viscosity-average chain length (actually, number-average chain lengths should be taken, which will be approximately half of the viscosity-average values) give a curve (sec Fig. 5) as expected from eqs. (4) and (6). However, whether the initial rate for larger chain lengths is actually proportional to $P_0^{-1/2}$ cannot be ascertained from the available data. A similar curve was obtained previously from Grassie's data at a lower temperature.[7] Thus there do not seem to be any essential differences whether the reaction is carried out in an open or closed system.

The type of curve shown in Figure 4, where the fraction of the rapidly degraded material extrapolated to zero rate of monomer formation is plotted against the reciprocal viscosity-average chain length, is also to be expected from such a mechanism. As chains degrade, assuming disproportionation as termination reaction, half of the chains are terminated at each stage with single bonds and the other half with double bonds. The type of curve expected from such a mechanism can be derived without going into a detailed kinetic analysis as follows.

If n_0 is the initial number of chains in a homogeneous polymer sample of chainlength P_0, $n_0 f_i$ the number of chains having one double bond chain end, and ϵ the kinetic chainlength, then the amount of monomer produced at the end of the reaction (provided only chains with double bond chain ends degrade) is given by eqs. (8)–(11).

For $P_0/\epsilon \geqq 2$:

$$m_1 = \epsilon n_0 f_i \left[1 + \sum_{n=1}^{b} (1/2^n) \right] + n_0 f_i \, (1/2^{b+1}) P_r \tag{8}$$

As $n_0 = m_0/P_0$, where m_0 is the number of base moles contained in the polymer sample, one obtains,

$$m_1/m_0 f_i = (\epsilon/P_0) \left[1 + \sum_{n=1}^{b} (1/2^n) \right] + (1/2^{b+1}) \, (P_r/P_0) \tag{9}$$

Here b is the number of initiations per original chain which lead to zips of length ϵ and P_r is the residual chain length after these zips have taken place. The sum converges rapidly to one.

For $P_0/\epsilon \leqq 2$:

$$m_1/m_0 f_i = (1/P_0)[\epsilon + 1/2(P_0 - \epsilon)] \tag{10}$$

For $\epsilon \geqq P_0$:

$$m_1/m_0 = f_i \tag{11}$$

The general result represented by eq. (9) can also be obtained in the following way.

If a_i = number of initiated chains, a_t = number of terminated chains, n_B = number of chains with double bond ends, then $\epsilon a_i = m_1$ and $n_B = n_0 f_i - 1/2 a_t$; steady-state conditions give $a_t = a_i$, hence $n_B = f_i n_0 - 1/2 m_i/\epsilon$.

At the end of the reaction $n_B = 0$; hence $n_0 f_i = 1/2 m_1/\epsilon$ or

$$m_1/m_0 f_i = 2\epsilon/P_0$$

which is identical with eq. (9), provided the chain length is relatively large compared with ϵ.

For combination as termination process, one obtains (provided that no chain has more than one double bond), eqs. (12) and (13).

For $P_0 \geq \epsilon$:

$$m_1 = n_0 f_i$$

or

$$m_1/m_0 f_i = \epsilon/P_0 \qquad (12)$$

For $P_0 < \epsilon$:

$$m_1/m_0 = f_i \qquad (13)$$

The same equations are valid for first-order termination, provided stable chain ends are formed.

The dotted line in Figure 4 was drawn by using eqs. (9), (10), and (11) with $\epsilon = 1.17 \times 10^3$.

Slow Reaction

The slow reaction has an appreciably higher energy of activation than the fast one: Madorsky[3] found 55 kcal./mole for $\bar{P}_n = 51{,}000$; Brockhaus and Jenckel[2] give 49.5 ± 3 kcal./mole for $\bar{P}_v = 4260$ and 44.2 ± 3 kcal./mole for $\bar{P}_v = 390$; our value is 49.5 kcal./mole for $\bar{P}_v = 5910$.

The apparent energy of activation in this case is given by eqs. (14) and (15).

For $P_0 > \epsilon$:

$$E_{\text{app}} = E_d + (E_i/2) - (E_t/2) \qquad (14)$$

For $P_0 < \epsilon$:

$$E_{\text{app}} = E_i \qquad (15)$$

E_i should be given by the apparent energy of activation of 44.2 kcal./mole found for the short-chain sample investigated by Brockhaus and Jenckel[2] ($\bar{P}_v = 390$).

If $E_d = 26.4$ kcal./mole is taken for the depropagation reaction as before and 49.5 kcal./mole as apparent energy of activation for long chains, an energy of activation is obtained for the termination reaction which is near 0 kcal./mole. This does not agree at all with the value deduced from the slow reaction for the same type of termination reaction. This discrepancy has as yet to be explained.

The question arises as to the mode of initiation for the slow reaction. If this were chain end initiation, eqs. (4) and (6) would be applicable. In such a case, the rate constant k_B given in Table II should be independent of chainlength as long as the kinetic chainlength is larger than the polymer chains. For the case where $P_0 > \epsilon$, the rate constants should decrease with polymer chain length. From the data so far available (see also Brockhaus and Jenckel's[2] data) a definite decision cannot be made.

For random initiation and $\epsilon > P_0$, the initial rate of monomer formation is given by,

$$(dm_1/dt)_i = k_i m_0 (P_0 - 1) \qquad (16)$$

and the rate constants should increase with polymer chain length. For $P_0 > \epsilon$ and second-order termination,

$$(dm_1/dt)_t = k_d(k_i/k_t)^{1/2}(V_m)^{1/2}m_0 \tag{17}$$

The rate constants k_B should be independent of chain length. Here again, data are as yet not extensive enough to allow a definite decision to be made. Gordon[6] assumed chain end initiation for his detailed kinetic analysis. Notwithstanding all available experimental data or deductions from kinetic analysis, conclusive evidence will only be obtained from measurements of chain lengths during degradation of samples where the chains containing double bonds have been eliminated beforehand. It would lead too far to discuss here the interesting work by Bywater[4] carried out with fractionated polymer samples, which did not contain polymer molecules with double bond chain ends. It must also be pointed out that if termination by disproportionation were to take place, double bond chain ends will be produced continuously during the degradation.

The hydrogenated and brominated samples show only a small decrease in rate of monomer formation. It is likely that for heterogeneous catalysis, as used here for the hydrogenation, it will only happen rarely that the condition is fulfilled for double bond chain ends just to make contact at a reactive site of the catalyst. As far as bromination is concerned, the high temperature used during degradation probably decomposes the bromides formed.

It is gratefully acknowledged that this work was made possible by a grant from the National Research Council of Canada.

References

1. Grassie, N., and H. W. Melville, *Proc. Roy. Soc.* (*London*), **A199**, 1, 14, 24, 39, 949 (1950); see also N. Grassie and E. Vance, *Trans. Faraday Soc.*, **49**, 184 (1953).
2. Brockhaus, A., and E. Jenckel, *Makromol. Chem.*, **18/19**, 262 (1956).
3. Madorsky, S. L., *J. Polymer Sci.*, **11**, 491 (1953); see also S. L. Madorsky, *J. Res. Natl. Bur. Sta.*, **62**, 219 (1959).
4. Bywater, S., *J. Phys. Chem.*, **57**, 879 (1953).
5. Jellinek, H. H. G., and J. E. Clark, *Can. J. Chem.*, **41**, 355 (1963).
6. Gordon, M., *J. Phys. Chem.*, **64**, 19 (1960).
7. Jellinek, H. H. G., *Degradation of Vinyl Polymers*, Academic Press, New York, 1955, p. 46.
8. Grassie, N., *J. Polymer Sci.*, **B1**, 551 (1963).
9. Ivin, K., *Trans. Faraday Soc.*, **51**, 1273 (1955).
10. Cowley, P. R. E. J., and H. W. Melville, *Proc. Roy. Soc.* (*London*), **A210**, 461 (1951).

Résumé

Une nouvelle technique a permis l'étude en systéme fermé de la dégradation thermique du poly-méthacrylate de méthyle avec des échantillons fractionnés et non-fractionnés dans un domaine de températures de 275–400°C. Des renseignements cinétiques ont été obtenus á des températures de 100°C supérieures à ce qui était possible auparavant. Les resultats sont comparés avec ceux obtenus en système ouvert. Deux réactions principales de dégradation entrent en jeu. Il apparaît que l'énergie d'activation pour ces réactions ne varie pas avec la longueur de chaîne, ceci en accord avec ce qui peut être attendu des mécanismes de dépolymérisation généralement adoptés. Les réactions de terminaison sont contrôlées par diffusion. L'hydrogénation à l'aide du catolyseur d'Adam et la bromuration des polyméres n'ont que des effets modérés sur la vitesse de dégradation.

Zusammenfassung

Der thermische Abbau von Polymethylmethacrylat wurde an unfraktionierten und fraktionierten Polymerproben im Temperaturbereich von 275–400°C in einem geschlossenen System nach einem neuen Verfahren untersucht. Kinetische Daten wurden bei um etwa 100°C höheren Temperaturen erhalten als es früher möglich war. Die Ergebnisse werden mit den in offenen Systemen erhaltenen verglichen. In der Hauptsache sind zwei Abbaureaktionen wirksam. Es wird gezeigt, dass die Aktivierungsenergie dieser Reaktionen in Übereinstimmung mit dem, was man nach dem üblicherweise angenommenen Depolymerisationsmechanismus erwarten sollte, nicht von der Polymerkettenlänge abhängt. Die Abbruchsreaktionen sind diffusionskontrolliert. Hydrierung mit dem Adam- Katalysator sowie Bromierung der Polymeren haben nur geringen Einfluss auf die Abbaugeschwindigkeit.

Received July 6, 1964

JOURNAL OF POLYMER SCIENCE: PART A VOL. 3, PP. 1185–1193 (1965)

Graft Copolymerization onto Cellulose by the Ceric Ion Method

YOSHIO IWAKURA, TOSHIKAZU KUROSAKI,* and YOHJI IMAI,
Department of Synthetic Chemistry, The Faculty of Engineering,
University of Tokyo, Japan

Synopsis

Styrene was polymerized in ceric salt–alcohol redox systems and hydroxyl endgroups on the polystyrene obtained were characterized quantitatively by the spectrophotometric determination of the polymer treated with *p*-phenylazophenyl isocyanate. A series of polymerizations of acrylamide initiated in redox systems of ceric salt and various alcohols was studied as a model system for graft copolymerization onto cellulose. From studies of the rate of polymerization it was shown that the grafting was likely to occur at hemiacetal and 1,2-glycol units. The cellulose–styrene graft copolymer was isolated from the reaction products by a selective extraction technique and characterized by acetolysis of the cellulose backbone. The graft copolymers obtained were found to be a mixture of block and graft copolymers.

INTRODUCTION

Grafting of vinyl monomers onto cellulose by the ceric ion method has been studied by various investigators.[1–5] We also have reported previously the grafting of glycidyl methacrylate onto cellulose.[6] However, the mechanism of grafting and the structure and composition of graft copolymers have not clearly been elucidated. The polymerization of vinyl monomers by ceric ion–alcohol systems has been studied in connection with the initiation mechanism of grafting.[7,8]

The present work was undertaken to establish a clear picture of the cellulose graft copolymerization by the ceric ion method. The initiation mechanism of grafting has been studied by means of model compounds. The cellulose–styrene graft copolymers have been separated and characterized.

RESULTS AND DISCUSSION

Endgroup Determination of Polystyrene Initiated by Oil-Soluble Ceric Salt–Alcohol Redox Systems

The polymerization of styrene initiated by oil-soluble ceric salt–alcohol redox systems has been reported previously as a model system for cellulose graft copolymerization.[6]

---

* Present address: Research Laboratory of Resources Utilization, Tokyo Institute of Technology; Tokyo; Japan.

The initiation mechanism of reaction between alcohols and ceric salt has been written generally as follows:

$$\mathrm{Ce^{IV} + RCH_2OH \rightleftharpoons B \rightarrow Ce^{III} + R\dot{C}HOH\ (or\ RCH_2O\cdot)}$$

where B represents the ceric–alcohol complex, and $\mathrm{R\dot{C}HOH}$ (or $\mathrm{RCH_2O\cdot}$) a free radical. However, the existence of a free radical $\mathrm{R\dot{C}HOH}$ or $\mathrm{RCH_2O\cdot}$ has never been confirmed definitely. The previous results showed that the rate of polymerization decreases in the order: 1,2-glycol > primary- > secondary- > tertiary alcohols. The very slow rate of polymerization with *tert*-butyl alcohol suggested the little possibility of formation of $\mathrm{R{-}\overset{|}{\underset{|}{C}}{-}O\cdot}$.

When the polymerization is initiated by $\mathrm{R\dot{C}HOH}$ radical, the resulting polystyrene should have a hydroxyl group. In the previous paper, the hydroxyl group has been demonstrated by molecular weight increase of polystyrene after treating it with diisocyanate. In this work, a novel spectrophotometric method has been developed by using the reactive dye of I for further quantitative determination of the hydroxyl endgroup of polymer.

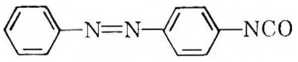

I

The polystyrene was treated with I at 100–110°C. in toluene in the presence of catalytic amounts of triethylenediamine. The polymer was precipitated in methanol. The colored polymer was purified by passing a benzene solution of the polymer through an aluminum oxide column to remove unreacted dyes. The extinction coefficient for *p*-phenylazophenyl carbamyl group was determined spectrophotometrically on the model com-

TABLE I

Number-Average Molecular Weight Estimated by Endgroup Determination

Sample	Initiator	$\bar{M}_n \times 10^{-4}$[a]	$\bar{M}_v \times 10^{-4}$
A	2,3-Butanediol–oil-soluble ceric salt	11.0	12.0[b]
B	Ethyl alcohol–oil-soluble ceric salt	18.0	8.3[b]
C	$\mathrm{H_2O_2{-}Fe^{++}}$	42	30[b]
D[c]	Phenylisopropyl potassium (anionic polymerization)	4.8	4.8[d]
E[c]	Phenylisopropyl potassium	3.8	4.0[d]

[a] Number-average molecular weight obtained by spectroscopic determination of the polymer treated with *p*-phenylazophenyl isocyanate.

[b] Molecular weight calculated from the intrinsic viscosity based on data of Alfrey et al.[9] $[\eta] = 1.2 \times 10^{-4} Mn^{0.70}$.

[c] Obtained by anionic polymerization and terminated with ethylene oxide.

[d] Molecular weight calculated from the intrinsic viscosity based on the data of Morton et al.[10] $[\eta] = 1.46 \times 10^{-4} M_w^{0.69}$.

pound, *p*-phenylazophenyl butylurethane ($C_6H_5-N=N-C_6H_4NH$-$COOC_4H_9$). Both the model compound and the colored polymer obtained showed an absorption maximum at 442 mμ in toluene. This absorption band was used for the analysis. The number-average molecular weights ($\bar{M}_n$) determined by this method are given in Table I in comparison with the molecular weights determined by viscosity measurements. The $\bar{M}_n$ was calculated by assuming that polystyrenes A, B, D, and E each contain one hydroxyl endgroup and polystyrene C contains two. Polystyrenes C, D, and E were used to check the accuracy of this method.

Polymerization of Acrylamide Initiated by Ceric Nitrate–Model Compounds Redox Systems

In order to study the initiation mechanism of grafting, a series of polymerization of acrylamide was carried out in aqueous redox systems of ceric nitrate and various model compounds. The model compounds studied were II–IX.

CH_3CH_2OH
II

$(CH_3)_2CHOH$
III

$(CH_3)_3COH$
(IV)

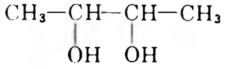

$$\underset{\displaystyle OH}{CH_3-\underset{|}{CH}}-\underset{\displaystyle OH}{\underset{|}{CH}}-CH_3$$

V

$CH_3CH_2CH_2CHO$
VI

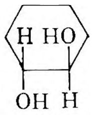

VII

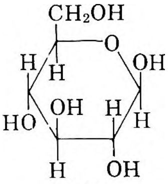

VIII

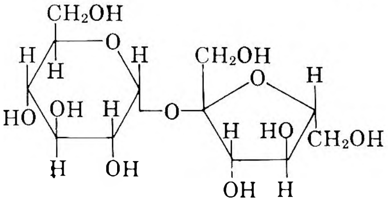

IX

The experiments were carried out in a stream of nitrogen at 25°C. Samples were withdrawn at various times and the polyacrylamide was precipitated in methanol. Figure 1 shows the monomer conversion as a function of time and indicates that the glucose–ceric salt and 2,3-butanediol–ceric salt redox systems were very effective initiators. *trans*-1,2-Cyclohexanediol (VII) is more suitable than 2,3-butanediol (V) as a model compound, because the cyclohexanediol is similar to 1,2-glycol unit of cellulose molecule in its cyclic and 1,2-glycol structure.

Glucose (VIII) which contains a hemiacetal unit, is the most effective reducing agent among the model compounds chosen. This consideration may lead to the conclusion that the grafting occurs most easily at a hemiacetal unit in the end of the cellulose molecule. This result is in accord with the speculation of Terasaki et al.[11] given in the oxidation mechanism of cellulose by ceric salt. Moreover, considering the considerable effectiveness of model compounds containing a 1,2-glycol unit, the grafting

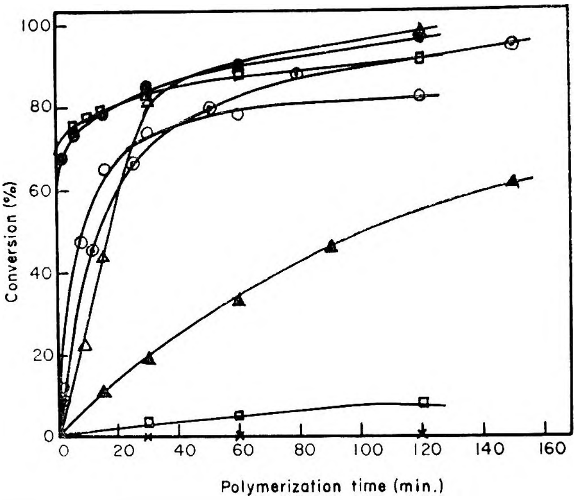

Fig. 1. Polymerization of acrylamide initiated by model compounds–ceric ammonium nitrate: (●) glucose; (□) 2,3-butanediol; (O) *trans*-1,2-cyclohexanediol; (⊙) *n*-butyraldehyde; (△) saccharose; (▲) ethyl alcohol; (■) isopropyl alcohol; (×) *tert*-butyl alcohol. Ceric nitrate, 2.5 × 10^{-3} mole/l., HNO_3, 2.5 × 10^{-3} mole/l.; acrylamide, 0.7 mole/l.; model compound, 0.1 mole/l.

also would occur to some extent at the 1,2-glycol unit. It would seem that the structure of graft copolymers consists of a mixture of block-type and graft-type structures.

Preparation of the Cellulose–Styrene Graft Copolymers

Cellulose–styrene graft copolymers were prepared in a manner similar to that described by Ide.[12] The results of graft copolymerization are given in Table II.

The reaction products probably consist of graft copolymer, unreacted cellulose, and homopolystyrene. The separation of true graft copolymer from the mixture was carried out according to the method of selective ex-

TABLE II
Grafting of Styrene onto Bemberg Rayon[a]

No.	Styrene, ml.	Water, ml.	Cellulose, g.	Wt. of polymerization product, g.
I	10	50	2.000	5.791
II	5	25	0.200	1.085
III	5	25	0.400	1.982
IV	5	25	0.600	3.294
V	5	25	0.800	3.476
VII[b]	5	14.6	0.200	0.736

[a] Concentration of ceric ammonium nitrate, 4.0 × 10^{-3} mole/l.; 60°C.; 20 hr.
[b] Polymerization was carried out in the presence of 0.4 ml. of carbontetrachloride.

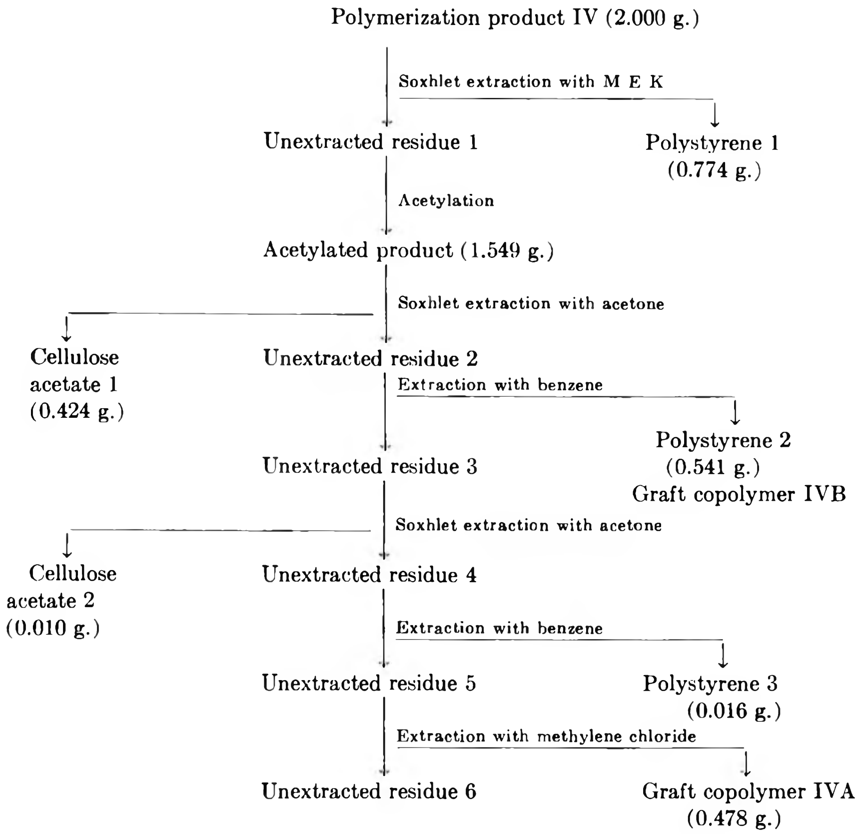

Fig. 2. Separation of graft copolymers from polymerization product IV.

traction adopted by Hachihama et al.,[13] with a few modifications. Methyl ethyl ketone and cuprammonium solution were chosen as solvents for selective extraction, because methyl ethyl ketone was highly effective for extraction of polystyrene. Alternating extractions of the graft copolymers by these two solvents were repeated. However, the weight of graft copolymers decreased continuously without reaching a constant weight. This is probably due to an oxidative degradation of cellulose chains in the cuprammonium solution. The experiment shows difficulty of treating the graft copolymer in its original form. Then, the acetylation of the graft copolymer was made to convert cellulose to a soluble form, according to the method given in the literature.[14] The nongrafted homopolystyrene was removed as much as possible by extracting it with methyl ethyl ketone by means of a Soxhlet apparatus and the unextracted residue was subjected to acetylation. Alternating extractions of the acetylated graft copolymers with benzene and acetone were repeated until no further precipitate was obtained on pouring the benzene extracts into methanol and the acetone extracts into water, respectively. Finally, the true graft copolymer was extracted with methylene chloride. The product extracted with benzene as described above also was characterized as graft copolymer which was different from the methylene chloride extracts. A typical example of the procedure is illustrated in Figure 2.

Characterization of the Separated Graft Copolymers

In order to isolate and characterize the polystyrene side chains of the graft copolymers, acetolysis of the cellulose backbone was carried out by the method of Kobayashi.[14] The composition of the graft copolymers could be determined by elemental analysis as well as by weighing the samples before and after the acetolysis. The molecular weight was determined by viscosity measurement for the grafted polystyrene chains obtained by acetolysis. The results obtained are summarized in Table III, where the numbers of polystyrene branches grafted on a cellulose chain were calculated by assuming that no degradation occurred during the graft polymerization and acetylation.

TABLE III
Composition of Cellulose–Styrene Graft Copolymers

Graft copolymer	Method of determination of composition[a]	Composition				Number of polystyrene chains per cellulose chain
		Cellulose, wt.-%	Polystyrene, wt.-%	Cellulose, mole-%	Polystyrene, mole-%	
IVA	A	8.4	91.6	43.3	56.7	1.3
IVA	B	9.9	90.1	48.4	51.6	1.1
IVB	B	5.9	94.1	33.9	66.1	2.0
III	A	12.0	88.0	49.2	50.8	1.0

[a] A, acetolysis; B, elemental analysis.

Table IV gives the results of the molecular weight determination of the nongrafted homopolystyrene and the grafted polystyrene. The molecular weights of the homopolymers are considerably higher than those of the

TABLE IV
Molecular Weights of Grafted Polystyrene and Homopolystyrene

No.	Polymer	$[\eta]$[a]	Mol. wt. $\times 10^{-5}$[b]
IVA	Grafted polystyrene	1.35	6.1
IVB	Graft copolymer	5.20	—
IVB	Grafted polystyrene	2.05	11
IV	Homopolystyrene	2.58	15
III	Grafted polystyrene	1.20	5.2
VII	Grafted polystyrene	0.31	0.75
VII	Homopolystyrene	0.59	1.9
I	Homopolystyrene	2.78	17

[a] Determined in toluene at 30°C.

[b] Calculated from $[\eta] = 1.2 \times 10^{-4} M^{0.70}$.

grafted polystyrene. It has been reported in many instances[15-17] of different grafting systems that the chain lengths of the homopolymer are equal to or less than those of the grafted branches. It seems that the interesting results obtained here are characteristic of the ceric ion method and that they can be explained by an inherent mechanism of chain termination in this system.

EXPERIMENTAL

Materials Used

The alcohols and styrene were purified as described earlier.[6] *trans*-1,2-Cyclohexanediol was prepared by the method given in the literature.[18] Glucose and saccharose, reagent grade, were used without further purification. The ceric ammonium nitrate, reagent grade, was dissolved in $1N$ nitric acid and the stock solution, $0.1N$ in ceric nitrate, was used to prepare the polymerization recipes. Commercial acrylamide was recrystallized two times from benzene–chloroform, m.p. 84.5°C. *p*-Phenylazophenyl isocyanate was prepared according to the method described in the patent literature[19] and recrystallized from benzene, m.p. 97–98°C. *p*-Phenylazophenyl butylurethane was prepared from *p*-phenylazophenyl isocyanate and *n*-butyl alcohol, and recrystallized from *n*-hexane, m.p. 128–129°C.

ANAL. Calcd. for $C_{17}H_{19}N_3O_2$; C, 68.69%; H, 6.40%; N, 14.14%. Found: C, 68.62%; H, 6.49%; N, 14.26%.

Determination of Hydroxyl Endgroups by *p*-Phenylazophenyl Isocyanate

To a round-bottomed flask were added 0.2 g. of the polystyrene having hydroxyl group, approximately 20 mg. of *p*-phenylazophenyl isocyanate, 1 mg. of triethylenediamine, and 20 ml. of toluene. The solution was heated at 100–110°C. for 7 hr. and was then poured into methanol. The colored polymer precipitate was dissolved in benzene, purified by passing the solution through an aluminum oxide column, and eluted with benzene. The purification was repeated until the polymer gave a constant extinction. The extinction of the solution of polymer in toluene was measured at 442 mμ on a Hitachi Model EPS-2 spectrophotometer. The extinction coefficient for the determination of *p*-phenylazophenyl carbamyl group was obtained on the model compound, *p*-phenylazophenyl butylurethane, and estimated to be 3.6 l./g. cm. The number-average molecular weight ($\bar{M}_n$) was calculated from the equation:

$$\bar{M}_n = 1.07 \times 10^3\, wf/(A_s - A_p)$$

where A_s is the measured extinction of colored polymer, A_p the correction for background absorption of original colorless polymer, w the concentration of sample in grams per liter, and f the number of endgroups of a polymer molecule (1 or 2).

Polymerization of Acrylamide

Acrylamide, alcohol, and distilled water were placed together in a three-necked flask equipped with a reflux condenser and a gas inlet tube. The flask was thermostatted at 25°C. After nitrogen was bubbled through the solution for 30 min., the polymerization was started by adding the ceric nitrate solution by means of a pipet. Samples were pipetted in at various times, and the polymer was precipitated in methanol containing a small amount of hydroquinone, filtered, and dried under vacuum.

Grafting of Styrene onto Cellulose

The graft copolymers were prepared by the method given in the literature.[12] Bemberg rayon (D.P. = 450) was used as a cellulose. The polymerization was carried out at 60°C. for 20 hr.

Acetylation and Acetolysis of Cellulose–Styrene Graft Copolymers

The experiments were carried out by the method of Kobayashi.[14]

Acetylation. About 1.5 g. of the graft copolymer was weighed accurately to the milligram into a 100 ml. round-bottomed flask. To the flask was added 15 ml. of a solution consisting of acetic anhydride (4.7 g.), benzene (11.7 g.) and concentrated sulfuric acid (11.5 mg.). The mixture was warmed at 40°C. for 5–6 hr. The polymer swelled markedly. It was collected on a glass filter, washed many times with methanol, dried *in vacuo* and weighed.

Acetolysis. A 0.4-g. portion of the acetylated graft copolymer was dissolved in a mixture of benzene (5 g.), acetic anhydride (5 g.), and concentrated sulfuric acid (0.35 g.). The solution was warmed at 50°C. for 40 hr. After the reaction was completed, the solution was poured into methanol. The precipitate was dissolved in methylene chloride and reprecipitated with methanol. The polymer obtained was dried *in vacuo* and weighed.

References

1. Mino, G., and S. Kaizerman, *J. Polymer Sci.*, **31,** 242 (1958).
2. Kaizerman, S., G. Mino, and F. Meinhold, *Textile Res. J.*, **32,** 136 (1962).
3. Richard, G. N., *J. Appl. Polymer Sci.*, **5,** 539 (1961).
4. Ide, H., *Kogyo Kagaku Zasshi,* **64,** 213, 764, 1489, 1676 (1961); *ibid.*, **65,** 82, 88 (1962).
5. Iwai, S., T. Kakurai, and T. Noguchi, *Seni Gakkaishi,* **19,** 547 (1963).
6. Iwakura, Y., T. Kurosaki, K. Uno, and Y. Imai, *J. Polymer Sci.*, **C4,** 673 (1964).
7. Mino, G., S. Kaizerman, and E. Rasmussen, *J. Polymer Sci.*, **38,** 393 (1959); *J. Am. Chem. Soc.*, **81,** 1494 (1959).
8. Katai, A. A., U. Kulshrestha, and R. H. Marchessault, *J. Polymer Sci.*, **C2,** 403 (1963).
9. Alfrey, T., A. Bartovics, and H. Mark, *J. Am. Chem. Soc.*, **65,** 2319 (1943).
10. Morton, M., T. E. Helminiak, S. D. Gadkary, and F. Bueche, *J. Polymer Sci.*, **57,** 471 (1962).
11. Terasaki, I., and M. Matsuki, *Seni Gakkaishi,* **18,** 147 (1962).

12. Ide, H., *Kogyo Kagaku Zasshi*, **65**, 88 (1962).
13. Sumitomo, H., and Y. Hachihama, *Kogyo Kagaku Zasshi*, **66**, 1508 (1963).
14. Kobayashi, Y., *J. Polymer Sci.*, **51**, 359 (1961).
15. Mori, Y., Y. Minoura, and M. Imoto, *Makromol. Chem.*, **25**, 1 (1958).
16. Cooper, W., G. Vaughan, S. Miller, and M. Fielden, *J. Polymer Sci.*, **34**, 651 (1958).
17. Huang, R. Y. M., B. Immergut, H. Immergut, and W. H. Rapson, *J. Polymer Sci.*, **A1**, 1257 (1963).
18. *Organic Syntheses*, Coll. Vol. 3, 217.
19. Hilger, J., II, 1701, *Chem. Zentr.*, **1932**.

Résumé

On a polymérisé le styrène par un système redox sel cérique–alcool, et on a dosé spectrophotométriquement les groupements hydroxyliques terminaux en traitant le polymère par l'isocyanate de *p*-phénylazophényle. L'étude de la polymérisation de l'acrylamide, initiée par divers systèmes redox sel cérique-divers alcools, a été effectuée, ces polymérisations devant servir de modèle pour l'étude de la copolymérisation par greffage sur la cellulose. Au départ de mesures de vitesses de polymérisation, on a montré que le greffage semblait avoir lieu au niveau des unités hémi-acétals et 1,2-glycols. Le copolymère greffé cellulose–styrène, isolé des produits de réaction par une technique d'extraction sélective, a été caractérisé par l'acétolyse du squelette de la cellulose. Les copolymères greffés se sont avérés être un mélange de copolymères greffés et à blocs.

Zusammenfassung

Styrol wurde in einem Cersalz–Alkohol-Redoxsystem polymerisiert und die Hydroxylendgruppe des erhaltenen Polystyrols durch spektrophotometrische Bestimmung des mit *p*-Phenylazophenylisocyanat behandelten Polymeren quantitativ charakterisiert. Eine Reihe von Acrylamidpolymerisationen bei Startung in einem Redoxsystem aus Cersalzen und verschiedenen Alkoholen wurde als Modellsystem für Pfropfcopolymerisation auf Zellulose untersucht. Die Untersuchung der Polymerisationsgeschwindigkeit zeigte, dass die Aufpfropfung wahrscheinlich an Hemiacetal- und 1,2-Glycoleinheiten stattfindet. Das Zellulose-Styrol-Pfropfcopolymere wurde aus dem Reaktionsgemisch durch ein selektives Extraktionsverfahren isoliert und durch Acetolyse der Zellulosehauptkette charakterisiert. Das erhaltene Pfropfcopolymere erwies sich als eine Mischung von Block- und Pfropfcopolymeren.

Received May 29, 1964
Revised July 1, 1964

JOURNAL OF POLYMER SCIENCE: PART A VOL. 3, PP. 1195-1219 (1965)

Spherulitic Crystallization. Part I. "Odd-Even" Polyamides: Nylon 56 and Nylon 96

J. H. MAGILL,* *Research Department, British Nylon Spinners Ltd., Pontypool, Monmouthshire, England*

Synopsis

Nylon 56 and nylon 96 polymers have been shown to crystallize in a number of spherulitic forms which are primarily dependent on the crystallization temperature. A variety of structural types have been reconciled within a general pattern of spherulitic crystallization behavior peculiar to "odd-even" polyamides. Spherulite growth rates and spherulite morphology presented for most of these structures follow a consistent pattern. Crystalline platelets exhibiting single-crystal properties have been grown from the melts of these polymers. The morphology of these platelets and spherulites is discussed in relation to the "transition stage" between single crystals and spherulites.

INTRODUCTION

Spherulitic crystallization in polyamides has been the subject of recent papers in the literature. Nylon 66, nylon 610, and nylon 6 have been studied from the morphological aspect by use of both optical[1-5] and electron microscopy as well as x-ray methods.[6-13] Crystallization and spherulitic growth rates for nylon 6, nylon 66, and nylon 610 have also been measured.[14-19] The effect of melt conditions and additives on the crystallization behavior of nylon 6 have also been examined.[20]

The present paper deals with optical properties and rates of spherulitic growth and is only a facet of a more extensive study embracing more than twenty polyamides of a variety of chemical and physical structures. The two polymers reported in this paper are believed to be typical of the series comprising "odd-even" polyamides; i.e., polymers in which the diamine and dicarboxylic acid molecular constituents have odd and even numbers of carbon atoms, respectively, in the structural polymer unit. The spherulitic crystallization behavior of odd-even polyamides has been mentioned previously in the literature,[21,22] and a few infrared studies[10,23,24] and limited x-ray work[8,10,22] have also appeared on odd-even polymers. The present account reveals some novel features concerning the overall crystallization behavior in films and fibers of nylon 56 and nylon 96.

---

* Present address: Mellon Institute, Pittsburgh, Pa.

EXPERIMENTAL

Polymers

The nylon 56 and nylon 96 polymers were prepared by Dr. M. H. Bride. They were free from delustrant (TiO_2) and had the characteristics shown in Table I.

TABLE I

Polymer	Optical m.p., °C.[a]	Inherent viscosity	Amine endgroups, μeq./g.	Carboxyl endgroups, μeq./g.
Nylon 56	258	0.941	70.6	55.9
Nylon 96	242	0.920	35.3	53.5

[a] Melting points were determined optically on spherulitic aggregates prepared from these polymers. The name aggregate refers to the large positively birefringent spherulites grown in the region between the low birefringent zone and the polymer melting point.

Inherent viscosities were measured in a 0.5% (w/v) solution in 90% (w/v) phenol–water. No further classification of these materials was made.

Procedure

Microscopical observations were made on sections of polymer chip mounted in MS 550 silicone oil between thin clean glass cover slips held together by small clips. Samples were immersed for a predetermined period in a thermostatted silicone oil bath held at the fusion temperature ±1°C. After melting, these samples were quickly transferred to another silicone oil bath maintained to within ±0.1°C. of the desired crystallization temperature. Samples were rapidly withdrawn from this bath at different intervals, ranging from a few seconds to several days, and quenched in acetone–solid carbon dioxide to arrest further crystallization. The same procedure was also used for specimens melted and crystallized under pressure by use of an apparatus kindly loaned by Mr. P. H. Harris. All spherulites produced in this work are predominantly two-dimensional, having been grown between glass cover slips to a size where their diameter exceeds their thickness.

Spherulitic growth rates in nylon 96 were determined from a series of specimens maintained for different periods in the crystallization bath. The mean size of the larger spherulites in each of the crystallized samples was plotted as a function of crystallization time (residence time at the crystallization temperature). All specimens were fused at 265°C. for 15 min. before crystallization.

Growth rates in nylon 56 were determined on polymer sections fused at 300°C. for 15 min. on a temperature-controlled hot plate. After melting, samples were crystallized isothermally on a Köfler hot stage thermostatted to ±0.2°C. of the crystallization temperature. The times taken for the periphery of a growing spherulite to pass selected fiducial marks on the graduated microscope eyepiece were noted for the different crystallization temperatures. Growth rate measurements on remelted samples gave reproducible results. In this way, it was established that the fusion conditions were not detrimental to the polymer stability. Spherulites exhibiting zigzag extinction patterns as well as those of low to zero birefringences were examined on a Leitz universal microscope stage. Birefringence measurements were made with the use of a Berek compensator. Some spherulites were studied by x-ray diffraction methods.

Fibers were formed by rapidly withdrawing a glass rod from the molten polymers (under nitrogen). These fibers were subsequently drawn and doubly oriented above room temperature.

RESULTS

Formation of Spherulites from the Melt

Nylon 56. All the spherulites exhibit a positive birefringence with the arms of the Maltese cross parallel and perpendicular to the principal vibrations of the incident polarized light. Well defined spherulites are formed when the molten polymer was allowed to cool in air to room temperature. Isothermal crystallization below 205°C. produces fibrillar-looking spherulites. Nylon 56 spherulites crystallized at a higher temperature (205–210°C.) show a slight distortion of the Maltese cross which is reminiscent of a zigzag extinction pattern. This extinction behavior becomes progressively more distinct and is finally well defined for specimens crystallized in the range 215–226°C. (Fig. 1). When these spherulites are viewed with the analyzer removed, a spiral morphology is observed. The center of the spiral is often rather indistinct. The pitch or spacing of the spiral increases

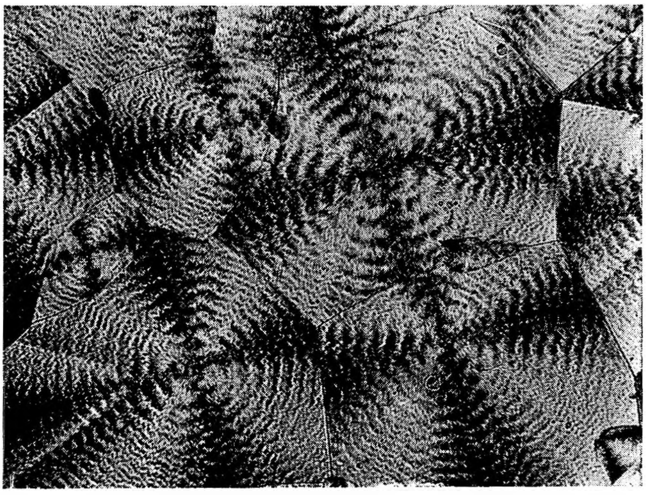

Fig. 1. Nylon 56 positively birefringent spherulites grown by slow cooling from 225°C. downwards after fusing polymer at 300°C. (15 min). × 130.

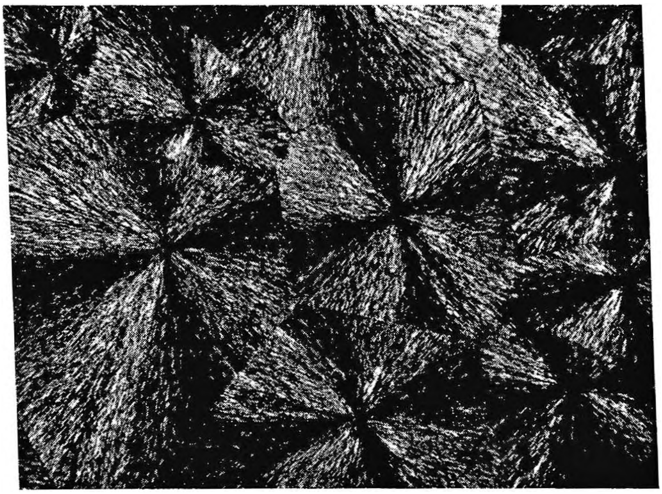

Fig. 2. Nylon 56 spherulites grown at 228°C. after melting polymer at 282°C. (30 min.).

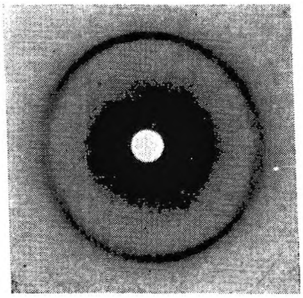

Fig. 3. Microbeam x-ray diffraction pattern from low birefringent nylon 56 spherulite grown at 232°C.

with crystallization temperature and does not change with annealing. Samples fused at 290°C. (30 min.) and crystallized at 215, 220, and 225°C. had average spacings of 30, 47, and 53 μ respectively. At higher temperatures still, the positively birefringent zigzag type structures are eventually replaced by coarser, less well defined spherulites of lower birefringence. These are first evident in the 226°C. crystallized specimens where both these spherulitic morphologies coexist. Orientation "defects" in cooperative twisting of adjacent lamellae or fibrils are apparent in these spherulites. Figure 2 shows the granular-looking spherulites grown at 228°C. which at higher magnification show a twisting lamellarlike composition. The overall birefringence of these positive spherulites is low and their optical melting point was 253–254°C. Structures of lower birefringence (<0.001) can be grown about 232.5°C. (optical melting point about 254°C.). They are not shown here as individual entries since they are difficult to reproduce photographically. However, they are portrayed as dark circular zones associated with the spherulites in Figure 12. Owing to their mottled appearance no detectable change in the overall birefringence was observable when such spherulites were tilted in all orientations with the use of a Leitz universal stage, although fluctuations in local birefringence were evident within areas a few microns in size in these spherulites. Spherulites were tilted as high as 35° with respect to the horizontal plane. Sometimes a few negatively birefringent spherulites are also formed in this same temperature region. Except for the sign of the orientation, they are indistinguishable in appearance from the other spherulites.

Microbeam (50 μ) x-ray examination of 600 μ diameter spherulites grown at 232°C. revealed some orientation in the pattern, as shown in Figure 3. With the beam perpendicular to the plane of the spherulite, a single spacing, approximately 4.18 A., suggestive of a pseudohexagonal unit cell is found. A weaker reflection with a 7.12 A. spacing corresponds to the molecular chain direction and suggests that the (002) does not lie exactly in the plane of the spherulitic film. A randomized sample of this material reveals the following reflections: 4.18 A. (S), 4.35 A. (M), 4.05 A. (M), 3.8 A. (W), and 7.1 A (W). These spacings suggest that both α and γ forms are present, although the γ pseudohexagonal form is the predominant one. An infrared spectrum (by Dr. I. Matsubara) of one of these spherulitic films also showed a strong absorption at 730 cm.$^{-1}$, a weaker band at 590 cm.$^{-1}$, and a still weaker band at 510 cm.$^{-1}$ The spectrum is related to, but is not identical to that for the true γ structure, in keeping with the x-ray diffrac-

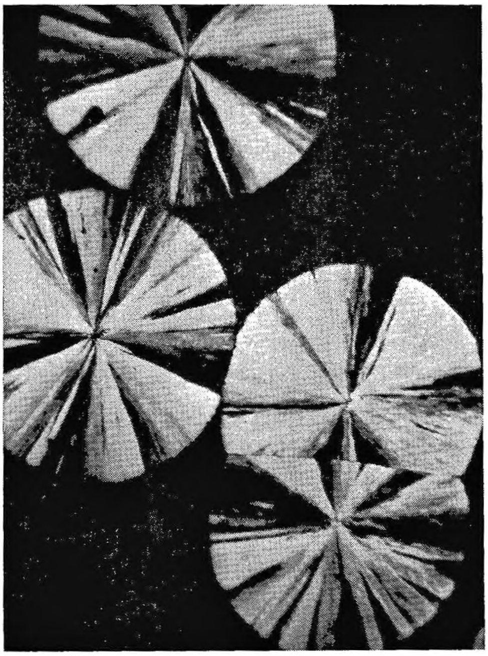

Fig. 4. Positively birefringent spherulitic aggregates of nylon 56 formed at 245°C. after polymer fusion at 280°C. × 60.

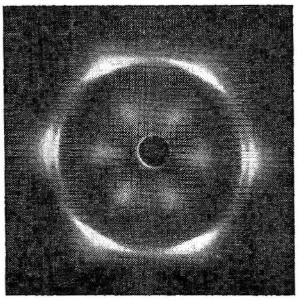

Fig. 5. Microbeam x-ray diffraction pattern of nylon 56 spherulitic aggregate grown at 245°C.

tion measurements. Both these forms are also present in nonoriented polymer chips.

At crystallization temperatures of 233°C. and upwards to near the melting point, spherulitic crystalline aggregates grow as in Figure 4. Above 245°C. they seem to form sporadically in time and have been grown to sizes approaching 6 mm. diameter, having densities (measured in a density gradient column) around 1.14 g./cc. Tilting these samples to large angles on the universal stage reveals some granularity akin to that observed in the lower birefringent spherulites in the extinction direction. These types of spherulites appear positively birefringent when grown in thin films (thickness <20 μ approximately); otherwise they possess irregular optical properties with no well defined Maltese extinction cross in the analyzer and polarizer directions. Figure 4 shows such spherulites of intermediate thickness. Microbeam x-ray photographs (taken with the use of a 100 μ diameter collimator) at five points along the radius of such a spherulite (grown at 245°C. to 3000 μ diameter) indicated that the crystallite orientation was almost invariant except near the center, where the optical properties were ill-defined. One of these patterns is shown in Figure 5. The low-angle reflections for this same sample were diffuse, showing a single order and indicating a spacing of about 120 A.

The photograph resembles that normally obtained with the x-ray beam parallel to the fiber axis of a doubly orientated yarn, except that a double equatorial reflection is present in Figure 5. There is also faint splitting of at least one of the other reflections. Again more than one phase is present in this crystalline aggregate since a rotated sample gave the following *d* spacings: 7.2 A. (VW), 4.35 A. (M), 4.18 A. (S), 4.05 A. (VW), 2.8 A. (VVW), 3.55 A. (VVW), 2.42 A. (VW). The 4.05 A. line is broad and may be a doublet. The (002) plane lies in the plane of the spherulitic film. The γ structure corresponding to the strong 4.18 A. spacing is the predominant one. The α form gives rise to less intense 4.35 and 3.8 A. reflections. In the thin, doubly-oriented yarns of nylon 56, the α structure is predominant. In these fibers, a reversal in the equatorial intensities is found when the x-ray beam is perpendicular or parallel to the direction of deformation in the fiber. Spherulitic films cast from formic acid solution show exclu-

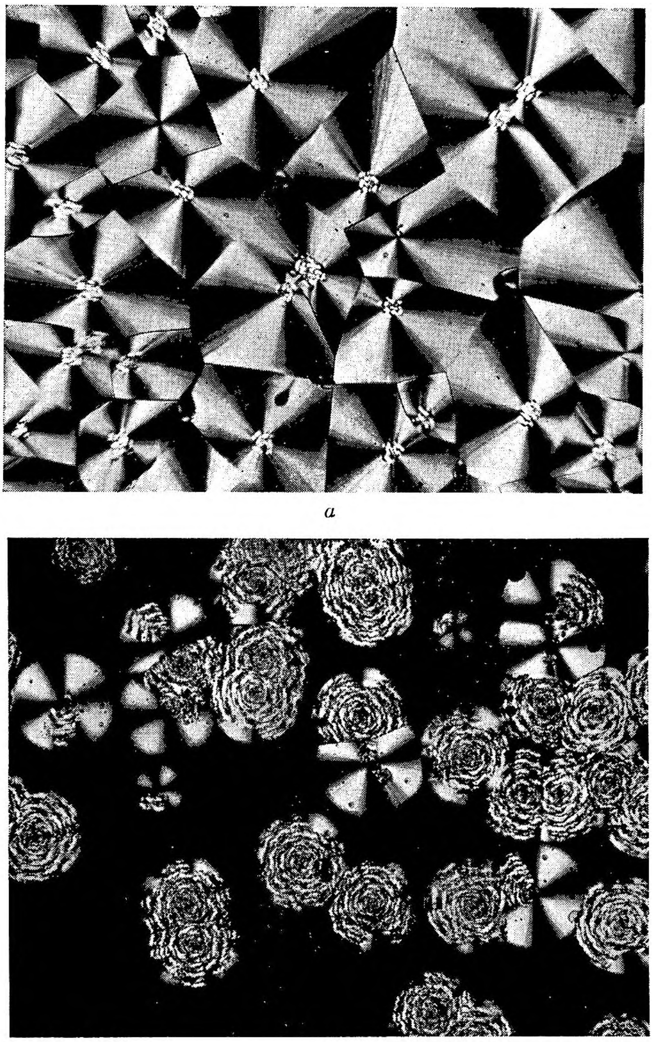

Fig. 6. Nylon 96 spherulites: (*a*) spherulites formed at 210°C. (15 min.) after sample was melted at 270°C. (30 min.); × 150; (*b*) "mixed" spherulites grown at 215°C. after polymer fusion at 270°C. (15 min.), × 187.

sively the α form with d spacing corresponding to 4.35 and 3.75 A., respectively. The spherulites exhibit low negative birefringence.

Nylon 96. The general pattern of spherulitic crystallization in nylon 96 follows a similar trend to that of nylon 56, but there are notable differences. Crystallization at and above approximately 205°C. gives rise to finely ringed positively birefringent spherulites. At still higher crystallization temperatures (210°C.), a coarse zigzag spherulitic structure develops (Fig. 6*a*), and both morphologies coexist within the same spherulite at 215°C. The zigzag composition of these spherulites increases with temperature,

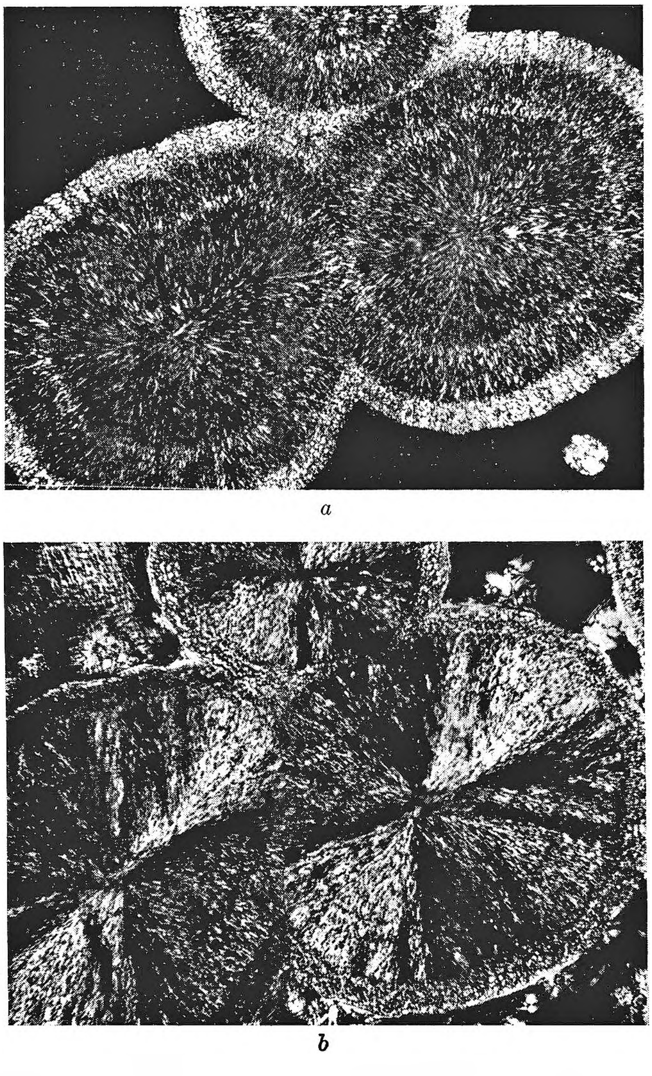

Fig. 7. Nylon 96: (*a*) crystallized stepwise at temperatures 228°C./227°C./226°C./225°C., respectively, with fusion temperature 262°C. (15 min.), × 150; (*b*) spherulites of Figure 7*a* after heating to 232°C., × 150.

and these are depicted before impingement in Figure 6*b* at 215°C. These spherulites have been described as "mixed" spherulites[25] because of the coexistence of two different spherulite types. Growth in the region of 216°C. produces both positive and negative wide ringed spherulites. A 45° extinction pattern is observed in these spherulites. This rare orientation has prevailed several years after its preparation, although moisture penetration has wrought other changes in the morphology of the samples. In polymer samples isothermally crystallized at 217°C., the spherulites are predominantly of the coarse zigzag structure. They melt at 238°C.

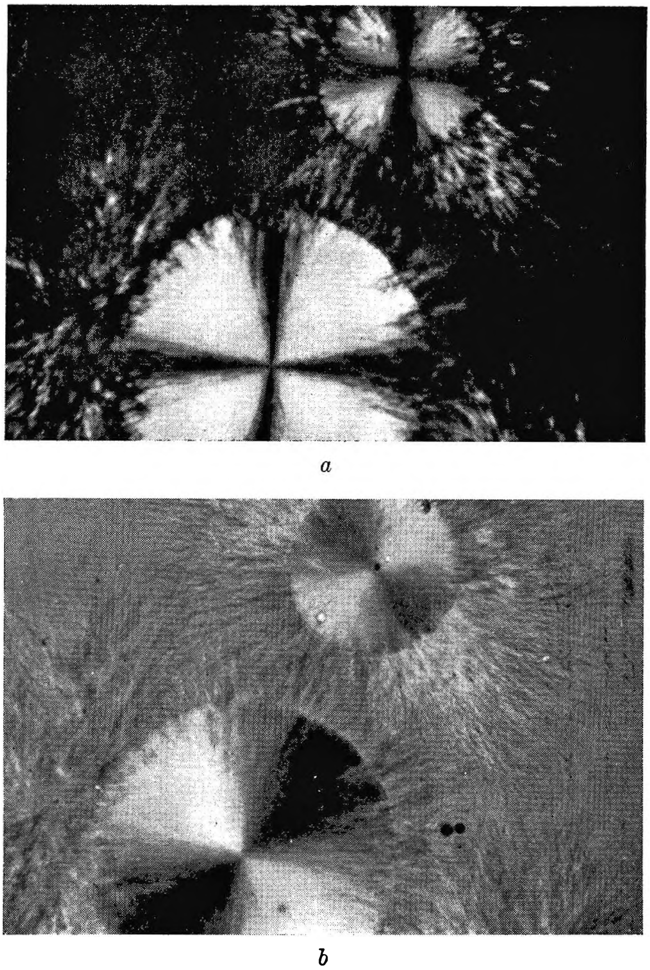

Fig. 8. Different species of spherulites: (*a*) grown in nylon 96 at 230°C. (15 hr.) after fusion at 265°C. (15 min.), × 440; (*b*) same as Fig. 8*a* with $\lambda/4$ wave plate showing up orientation difference and fibrillar overgrowths, × 440.

without change in the sign of the birefringence. The morphological habit is temperature-dependent and can be cycled between both structural forms by raising or lowering the temperature by a few degrees. Universal stage experiments reveal that the extinction pattern associated with this coarse periodic structure is due to a cooperative twisting of crystallites as growth proceeds radially from the center of the spherulite. It is impossible to resolve microscopically any discernible change in the spacings of the fine ringed portions of the structure associated with these mixed spherulites below 215°C. Both coarse and fine ringed features are perceptible within a single spherulite when the analyzer is removed. No detailed measurements were made of the ring spacings, but the coarse rings increased with crystallization temperature. The coarser rings emanate from the spherulite

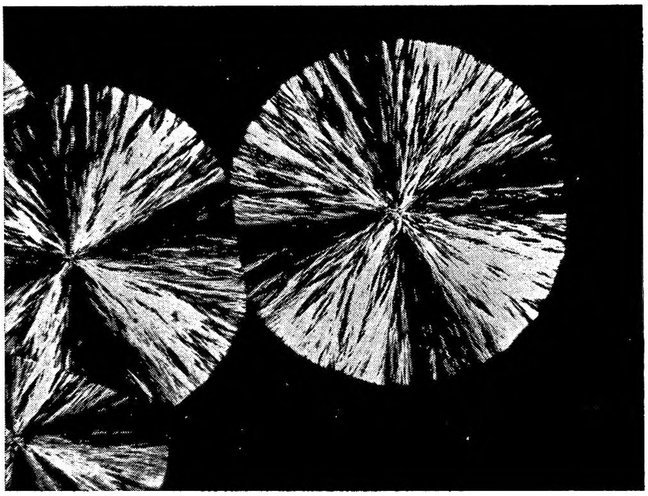

Fig. 9 Nylon 96 positive spherulitic aggregates formed at 235°C. ($16^1/_2$ hr.) after melting polymer at 260°C. (15 min.). × 90.

center in concentric circles or spirals, with left-hand or right-hand twist equally probable.

Uniformly sized granular-looking spherulites of low negative birefringence are simultaneously initiated and grow from the melt at temperatures around 225–229°C. Sometimes faintly positive as well as low birefringent spherulites grow together in this region for thinner samples. The apparent morphology of these structures is a function of the sample thickness. Comparatively thick specimens (~100 μ or more) exhibit a mottled appearance as in Figure 7*a*, while thinner specimens (a few microns or less) show a twisted lamellar habit where the lamellae or fibrils are intricately interwoven at large and varying angles from the radial direction. The observed textures in Figure 7*a* spherulites corresponds to the following stepwise sequence of growth temperatures: 228°C. (30 min.) → 227°C. (20 min.) → 226°C. (15 min.) → 225°C. (10 min.) → quenched at −60°C. The outer overgrowth at 225°C. exhibits a negatively birefringent zone. When this sample was heated to 230–231°C., it became isotropic; on subsequent holding at 232°C. for several hours, crystallization occurred within the original outline with formation of a homogeneous center of low negative birefringence with one discernible ringed overgrowth of higher negative birefringence (see Fig. 7*b*). A granular or mottled type appearance still persisted but it is less dominant than that shown in Figure 7*a*. The optical melting point of this newly formed structure is about 240–242°C. Examination of the lower birefringent samples crystallized in this range reveals no dominant overall orientation.

Spherulitic crystallization in the vicinity of 230°C. is complex. At least three new types of spherulites coexist with these mottled or granular spherulites described above. These are: (*1*) narrow ringed positively birefringent spherulites, periodicity ~1.5 μ; (*2*) negative spherulites smaller in size and

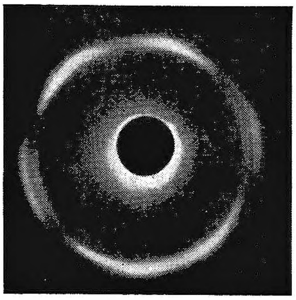

Fig. 10. X-ray microbeam diffraction pattern 150 μ from the center of spherulitic aggregate of nylon 96.

magnitude of the birefringence than (*1*); (*3*) spherulitic aggregates of positive sign simultaneously nucleated and concentrated nearer the edges of the sample. In addition, types (*1*) and (*2*) also grow with whiskerlike overgrowths. These growths are depicted on the spherulites in Figure 8*a*. Figure 8*b* clearly shows the opposing sign of birefringence of these two entities when a $\lambda/4$ plate is used. The smaller spherulite is negatively birefringent. The splinelike overgrowths on the spherulites correspond to the mottled or spline-like spherulites which are just visible in the photograph, impinging on the other structures. The spherulitic aggregates in Figure 9 are the largest species present at 230°C. These spherulitic aggregates (*3*) are about three times larger than the ringed spherulites (*1*) which in turn are just less than twice the size of (*2*). The magnitude of the birefringence for these spherulites is (*3*) > (*1*) > (*2*). The optical melting points are (*1*) 237°C., (*2*) 236°C., and (*3*) 240–242°C., while the splinelike overgrowths become isotropic at 231–232°C.

Only positive spherulite aggregate type structures (Fig. 9) grow between 231°C. and the melting point. These spherulites are comprised of lamellae which are not as coarse as in nylon 56. Around 235°C., these spherulites seem to form sporadically in time from the supercooled melt and have been grown to 1000 μ diameter after crystallization for several days.

A 900 μ diameter spherulite was examined by means of the microbeam x-ray camera, by using a 50 μ as well as a 25 μ diameter collimated beam perpendicular to the plane of the spherulite. Some variation in orientation was noted at different points along the spherulite radius with the 50 μ diameter beam, but these variations appeared to be less pronounced when the smaller beam was used. A typical diffraction pattern obtained at 150 μ from the spherulite center is shown in Figure 10. Further out, at 300 μ from the center, the orientation is improved, since the arcs are shorter. Still, there is more doubling of the strong spots in this photograph than in that of the larger nylon 56 spherulite aggregate (Fig. 5) which it resembles. Double orientation is also strongly featured in this pattern, though it is less perfected than in the nylon 56. A rotated sample containing these spherulites again gave *d* spacings corresponding to both α and γ phases; these are: 4.20 A.(S), 4.35 A. (W), 3.45 A. (VVW), 10.2 A. (VW), 4.05 A. (VW), 2.42 A. (VW), 6.8 A. (VW), and 3.65 A. (VVW). Except for the longer fiber axis repeat distance, a close resemblance is noted to the nylon 56 spherulitic aggregate. Here, too, the molecular or fiber axis is substantially perpendicular to the plane of the film containing the spherulite.

Drawn nylon 96 yarn is comprised mainly of the α form with d spacings at 4.4, 9.2, and 6.1 A., approximately. The single yarn did not give many reflections since it was very thin. However, results seem to correspond with the formic acid cast film which was found to have its main d spacing at 4.35 and 3.75 A., which is characteristic of an α structure. The spherulites grown from solution have a low negative birefringence, similar to that in the nylon 56 specimens.

General Pattern of Crystallization Behavior

The general pattern of spherulitic crystallization for both polyamides is summarized in Figure 11. T_f refers to the highest fusion temperature used, T_m is the polymer melting point, and T_1 and T_2 are the temperatures where structures of zero or low birefringence are formed. The entire range of spherulitic structures for either polymer can be obtained within a single spherulite by controlled cooling of the polymer during its crystallization from the molten state. Figure 12 shows this morphological pattern for nylon 56, ranging from the crystalline aggregate-like spherulitic center through the low birefringent zone to a fibrillar overgrowth found at lower temperatures. No intermediate zigzag extinction pattern (as in Fig. 1) appears between the low birefringent and fibrillar structure here because cooling was too rapid in this instance. The pattern for nylon 96 is illustrated in Figure 13. The center spherulitic aggregate zone is shown surrounded by a narrow zero birefringent overgrowth followed by a wide zig-

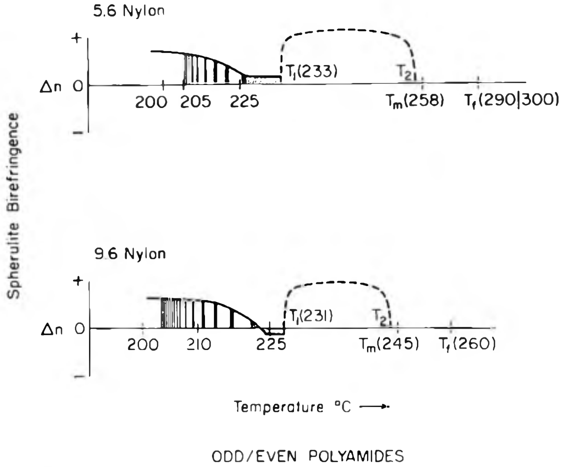

Fig. 11. General simplified spherulitic growth pattern of odd-even polyamides. The birefringence scale is arbitrary.

zag ringed structure. On top of this zero birefringent overgrowth is a fine, fully ringed structure with a faint zigzag Maltese cross. The narrow peripheral overgrowth, which probably grows during quenching, appears fibrillar.

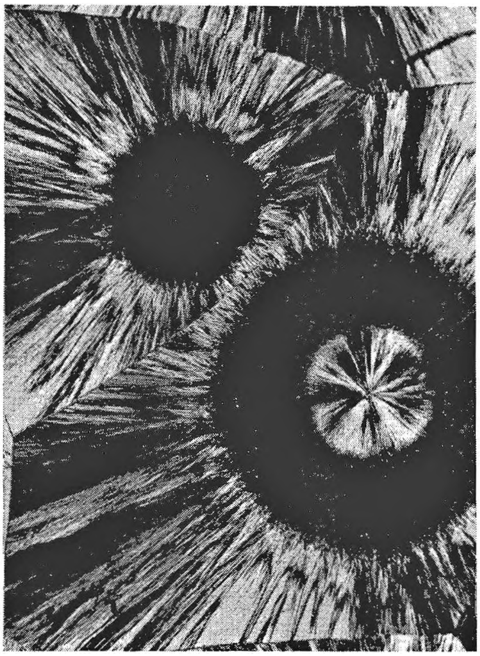

Fig. 12. Nylon 56 spherulites formed on controlled cooling of polymer melted at 280°C. (15 min.), × 80.

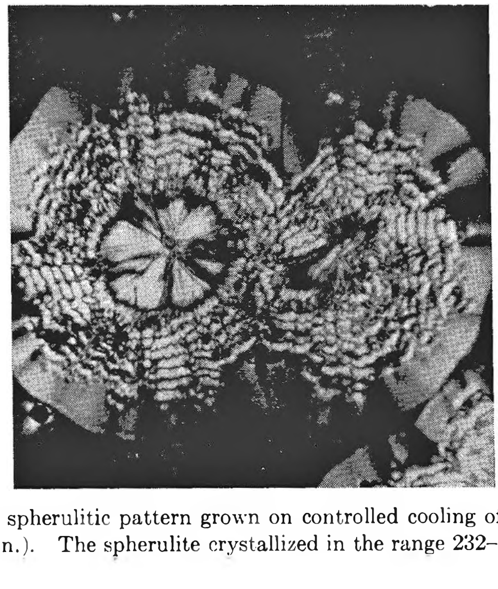

Fig. 13. Nylon 96 spherulitic pattern grown on controlled cooling of sample melted at 260°C. (15 min.). The spherulite crystallized in the range 232–213°C. × 430.

Isotropic Melting Below T_m

Melting can be induced in sections of polymer chip rapidly heated to temperatures between $T_1 + 5°C.$ approximately and the respective optical melting points for both polymers. The precise lower limiting temperature was not determined. The isotropic state of the polymer after this rapid heating was confirmed optically. If the heated specimens are held in this region near T_m, spherulitic crystallization ensues. Positively birefringent spherulites are formed. These are optically identical to the spherulites grown directly from the melt after fusion above T_m, but they are predominantly of equal sizes and are more numerous than the latter. The induction

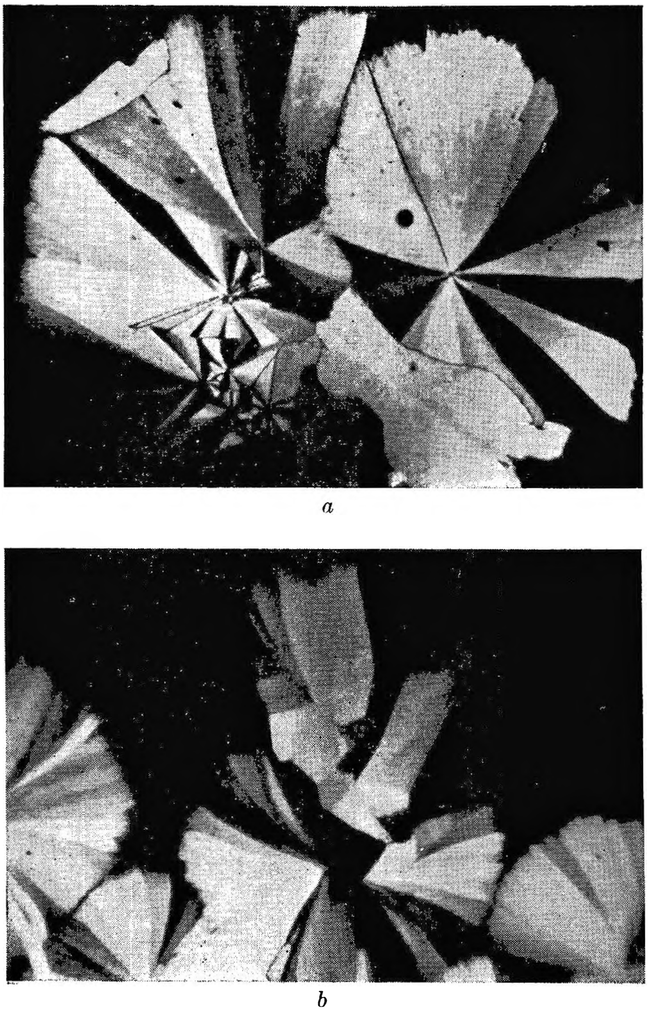

Fig. 14. Nylon 56: (*a*) crystalline platelet arrays formed at 247°C. (127 hr.) after polymer fusion at 280°C. (30 min.), × 100; (*b*) platelets formed at 247°C. after fusing polymer at 290°C. (30 min.), × 150.

time for their appearance is shorter too, so that melting under these conditions leaves residual nuclei. For the same growth temperature, their spherulite growth rates are similar in magnitude to those formed for the different fusion conditions above T_m. Overgrowths can be formed on these spherulites by changing the crystallization temperature, and their morphology is again solely dependent on this growth temperature.

Crystalline Platelet Growth

When spherulitic growth is severely restricted in one dimension either by submitting the molten polymer, in thin film form, to continual pressure during crystallization or by crystallizing a very thin sandwich of polymer, then plateletlike structures result. These structures range in thickness from a few microns downwards and can be grown to several hundred microns in the other two dimensions. Their formation seems peculiar to crystallization temperatures in the range between T_1 and T_2 (Fig. 11) in all classes of polyamides which form spherulite aggregates. They are produced by isothermal crystallization (above T_1) directly from the melt or from the "partially melted" very thin sections heated rapidly to, and held within, a few degrees of the polymer optical melting temperature.[21] Spherulitic arrays composed of wedge-shaped platelets (Fig. 14*a*) and the conformations of platelets in different extinction positions (Fig. 14*b*), illustrate some of these structures obtained in nylon 56. Figure 14*b* shows an

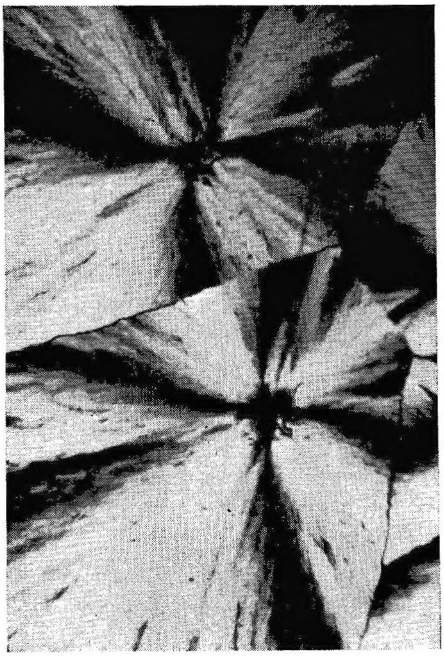

Fig. 15. Nylon 56 spherulites with single-crystal plateletlike centers grown at 245°C., × 100.

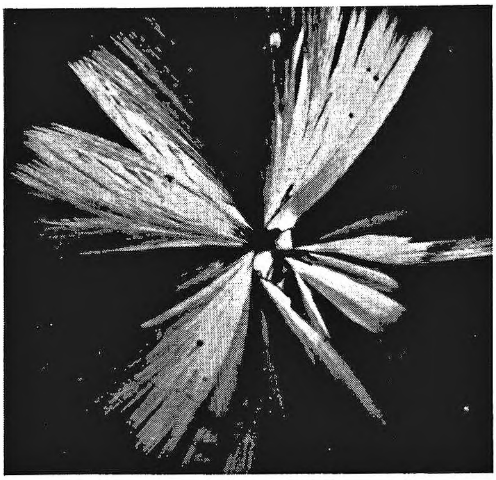

a

b

Fig. 16. Nylon 96 crystalline arrays: (*a*) grown at 236°C. for several days after melting polymer at 264°C. for 15 min., × 90; (*b*) grown at 232°C. for 16 hr. after melting polymer at 260°C. for 15 min., × 245.

intermediate stage of transition between the plateletlike and aggregatelike spherulites when growth occurs in a sample of tapering thickness. In Figure 15 two spherulitic aggregates are depicted with plateletlike centers. These series of photographs are the first direct examples, known to the writer, showing this transition from a single crystal to spherulite array.

The optical properties of these platelets are similar to those of single crystals, in that extinction is obtained on rotation every 90° between crossed polars. Each platelet exhibits a distinct biaxial interference figure when examined chronoscopically with a Bertrand lens between crossed polars. The sign of the birefringence of these crystals is positive and they have large optical axial angles ($2V \sim 60°$ for nylon 56 specimens). It can be deduced from universal stage experiments that the crystallographic or molecular axis, i.e., direction of highest refractive index, γ, is substantially perpendicular to the platelets. The fiber axis repeat distance was about

14.2 A., as found from an x-ray rotation photograph from one of these areas. The refractive index in the growth direction β is greater than that in the α direction at right angles to it. Both α and β lie in the plane of the platelet. Variations in orientation over the platelet become apparent with an increase in platelet thickness. Densities in excess of 1.18 g./cc. are obtained for these platelets which have melting points very dependent on the crystallization temperature at which they were formed.

Growth in thin films of nylon 96 crystalline arrays are shown in Figures 16*a* and 16*b*. The optical behavior of any one of these platelets is again consistent with a single-crystal habit.

On rapidly cooling these spherulitic aggregates and plateletlike structures from their crystallization temperature, fractures develop. The aggregates mostly crack radially. The crystalline platelets show fissures essentially along their length for the wedge-shaped variety of Figure 14*a*. These cracks are readily "healed" on annealing at the temperature of the platelet formation.

Spherulite Growth Rates

The range covered for nylon 56 is 220°–242°C. and included measurements on all spherulite types of Figure 11. A wider range of textures is covered in nylon 96 (200–234°C.), encompassing most of the structure in Figure 11. In the low birefringent range between 225 and 230°C., faintly negatively birefringent spherulites grow at the same rates as their faintly positive birefringent counterpart. At 230°C., only the positively birefringent ringed spherulite (growth rate = 0.21 μ/min.) and the positively birefringent aggregate (growth rate = 0.65 μ/min.) were measured.

In either polymer, when a growing film is quenched to −70°C. and brought up to room temperature, no further growth is observed over periods of several months in the absence of moisture, suggesting that the glass temperature is above 25°C. X-ray diffraction reveals that both polymers can be quenched from the molten state to the glassy state without incipient crystallization on return to room temperature. Only a single amorphous

TABLE II

Temperature, °C.	Radial growth rate G, μ/min.
220.5	104.5
222	83.1
224.5	72.6
226	65.4
230	28.6
235	9.7
236	9.6
239	7.3
240	5.8
242	3.3

TABLE III

Temperature, °C.	Radial growth rate G, μ/min.
200	101.0
203	80.0
205	68.0
207.5	53.8
213	31.9
215	30.0
218	15.4
225	4.8_5
230	0.65, 0.21
231	0.48
234	0.16

halo results. By analogy with other polyamides[26,27] the glass temperature must be in the range 40–60°C.; the presence of moisture lowering this value considerably. T_g was taken at 45°C. in the analysis of the data given in Tables II and III for nylon 56 and nylon 96, respectively.

DISCUSSION

Spherulitic Morphology

Although optical microscopy does not reveal detailed structure in spherulites in the submicron range, it serves to classify these macrostructures. The present work shows that nylon 56 and nylon 96 have much in common throughout the range of spherulitic textures observed (Fig. 11). At the same time, however, there are noteworthy differences. Generally for a given polymer sample, it may be concluded that once the primary nucleus is formed, subsequent growth is primarily governed by the crystallization temperature. The coarser texture of the spherulites becomes more obvious the higher the growth temperature. This is clearly illustrated by the detailed photographs during isothermal growth and by the controlled cooling of crystallizing specimens where the observed morphological features are characteristic of the temperature range studied (see Figs. 12 and 13).

Deductions about the crystallite orientation based on the sign of the birefringence are not straightforward in polyamides,[2] which contain strongly polarizable groups which invariably give rise to a biaxial indicatrix. The presence of more than one crystalline modification within a single spherulite (as found in this work) introduces a further complication. The sign of the birefringence of the spherulite can change, depending on which axis of the unit cell is aligned with its radius and on the relative amounts of each phase present. The present evidence, x-ray and optical, indicates that the (002) plane in the crystalline aggregate lies essentially in the plane of the spherulite film, but some variations in orientation occur on going out along the radius in thick samples. The refractive index in the radial direction is larger than in the transverse direction in these spherulites. This tendency for a crystallographic plane to lie parallel to the surface has been noted by Mann and Roldan[7] for the crystalline aggregates of nylon 66 and nylon 610. The crystallite orientation is better defined in odd-even polymer spherulites, though an unequivocal assignment of the reflections cannot be made at this stage. However, with the help of the present observations on crystalline aggregates and platelets, and preliminary refractive index measurements on doubly oriented fibers, it is believed that the equatorial reflections (Figs. 5 and 10) are from (010) planes. It is assumed here that the crystal plane which is rotated into the plane of the flattened oriented sample is the hydrogen-bonded plane as found by Bunn[11] for nylon 66. The other reflection(s), approximately 60° removed from the equatorial ones, is associated with (100) and (110) planes in both polyamides. As already indicated, both diffraction patterns resemble those generally found for doubly-oriented yarn. The noted doubling of some reflections can be attributed to (*1*) twisting lamellae which are smaller in nylon 96 than in nylon 56, and/or (*2*) the presence of two crystal phases. Initially it was thought that (*1*) provided a satisfactory explanation because the doubling of strong spots is greatest for nylon 96 spherulites which provide greater facility for lamellar twisting because of their narrower lamellae. However this effect is now considered to be secondary. The presence of two crystallographic structures is believed to be the prime influence now.

The zero- or low-birefringent spherulites suggest a randomized or branched structure. In very thin samples the interwoven lamellae or fibrils must have restricted orientation perpendicular to the plane of the spherulite. The overall structure in the thicker spherulites does not show significant orientation changes because areas which extinguish in one orientation are compensated for by other regions which become suitably oriented on the universal stage—the overall effect is one of invariant average orientation within the spherulite. The small orientation within the spherulite (Fig. 3) revealed by x-ray patterns can be attributed to local changes in the area covered by the beam. These changes are not necessarily representative of the overall spherulite. Although the evidence is not definitive at this stage, the low birefringence value (<0.001) suggests that the spherulite orientation must be close to random in thick samples. Following just below the zero-birefringent region, the zigzag extinction pattern is reconciled with an in-phase twisting biaxial indicatrix about an oblique plane. The amplitude of this zigzag decreases as the growth temperature decreases. The observation on the 45° extinction cross in nylon 96 spherulites formed about 216°C. arises from destructive interference between opposing crystallite orientations where the ends of the zigzag in adjacent quadrants overlap. This blurring is more apparent the further away from the center of the spherulite, where synchronization of the twist is diminished, probably due to misalignment of one of the optic axes in the biaxial indicatrix with the principal vibration direction of the microscope. This 45° extinction has been observed in other polyamides for a different reason[7] (double orientation effect).

The absence of periodic extinction patterns at the lower temperatures, must be due to noncoordinated twisting in adjacent fibrils or lamellae so that only a straight extinction cross corresponding with the principal vibration of the microscope results. The finer texture, faster growth rates, and higher viscosity at these lower crystallization temperatures all act to the detriment of a well-coordinated spherulitic texture. With some exceptions (next section) these observations on spherulite morphology can be accounted for by the Keith and Padden phenomenological theory[31] of spherulitic growth. The widths of fibrils and lamellae decrease and the onset of branching becomes more profuse the lower the crystallization temperature in accordance with this theory.

In general, the texture of nylon 56 is coarser than that in nylon 96 spherulites. This is particularly obvious at temperatures where aggregates grow in thin films (see Figs. 4 and 9). Another difference between these polymers arises at 230°C., where, in nylon 96, several different spherulites coexist simultaneously. Anomalous bulk crystallization rates using dilatometric or density balance method, may be expected at this temperature because of the complexity of the system. Just below this temperature the sign of the spherulite birefringence in the low birefringent zones is not the same for both polymers. In nylon 96 "mixed" spherulites[25] grow, whereas a single zigzag extinction pattern is found in nylon 56 specimens. No explanation can be forwarded for these morphological differences at this stage.

The solution-grown spherulites are believed to have rotational symmetry about their radial *a* axis while the *c* axis is substantially tangential to this direction.

Single-Crystal Platelets

These structures are peculiar to polyamide polymers which form aggregates and they are observed only in very thin samples. The platelets are well oriented and must be layered on top of each other to a depth of several crystal step heights in the thicker specimens since the low angle measurements suggest values around 120 A. The single-crystal nature of these platelets is beyond dispute, for electron diffraction studies have shown diffraction spots out to five or six orders.[21] The fact that they grow in the thin area of a tapered sample concomitantly with crystalline aggregates suggests that they are only a thickness modification of the aggregates. The influence of the containing cover glasses on the sample may have some orienting effect during crystal growth, especially in the thinner regions of the sample, but definite conclusions on this point must await further experimentation with thin polymer films on different substrates. Different stages of the transition in morphology from the platelets to the aggregates are shown in Figures 14–16. These observations are not readily explicable on the basis of the Keith and Padden theory.[31] Aggregates and lamellar platelets grown at the same temperature should have identical textures.

Furthermore, the extent or protrusion of the crystallization front into the melt (during growth) cannot be reconciled with lamellar width. At any rate this identity would only hold precisely if the growth front was spherical. The fact that a stable growth front can persist out to large distances in the presence of polymer impurity species of low molecular weight (since these polyamides have $\bar{M}_w/\bar{M}_n$ around 2) may be due to the fact that such species do not have a profound influence on texture because they are highly crystallizable. If this is so, then theory and experimental may be partly reconciled by assuming that spherulitic aggregates are comprised of these lamellar single crystals (as stated previously[21]). The aggregates, because of their thickness, entertain splaying or disordering of the platelets giving less well ordered structures. An array of such platelets (Figs. 14 and 16) must represent the transition stage between the single crystal and the polycrystalline spherulite.

The fact that these emanating wedge-shaped sections can proceed to a spherulitic habit either at their growth temperature, or by lowering this temperature, suggests that spherulitic growth must proceed with a lower free energy than the plateletlike crystal growth. Very thin platelets grow more slowly than spherulitic aggregates at the same temperature. The large anisotropy of surface free energies (i.e., end fold versus lateral surface free energy) and the magnitude of the unit cell in polyamides facilitate such a morphological changeover so that spherulites rather than single crystals are the predominant structure except at small supercoolings. These observations support the Fullman-Sears hypothesis[29,30] of spherulite growth. The number of intercrystalline lamellar boundaries in the polymer crystal arrays is usually six or greater. Splaying and twisting of such lamellar arrays result in a less ordered texture which is a spherulite. The transition stage is well substantiated in Figures 14, 15, and 16. The polycrystalline configurations increase as the growth temperature is lowered since more interlamellar boundaries are generated.

Analysis of Growth Rate Measurement

The spherulite growth model forwarded by Hoffmann[32] was used in examining the experimental results of both polymers. The growth rate G is given by the eq. (1):

$$G = G_0 \exp\{-\Delta F_\eta^x/RT\} \exp\{-\Delta G^x/RT\} \quad (1)$$

where G_0 is essentially constant and ΔG^x varies at ΔT^{-1} for two-dimensional surface nucleation and ΔT^{-2} for three-dimensional nucleation. Embodied in the second exponential term is the thermodynamic driving force for crystal formation. For coherent two-dimensional lamellar growth, this term becomes

$$\exp\{-4b_0\sigma\sigma_e T_m^2/\Delta h_f k(T^2\Delta T)\}$$

where σ_e = end fold surface free energy, σ = lateral surface free energy, k = Boltzmann's constant, Δh_f = heat of fusion of the crystal, b_0 = mono-

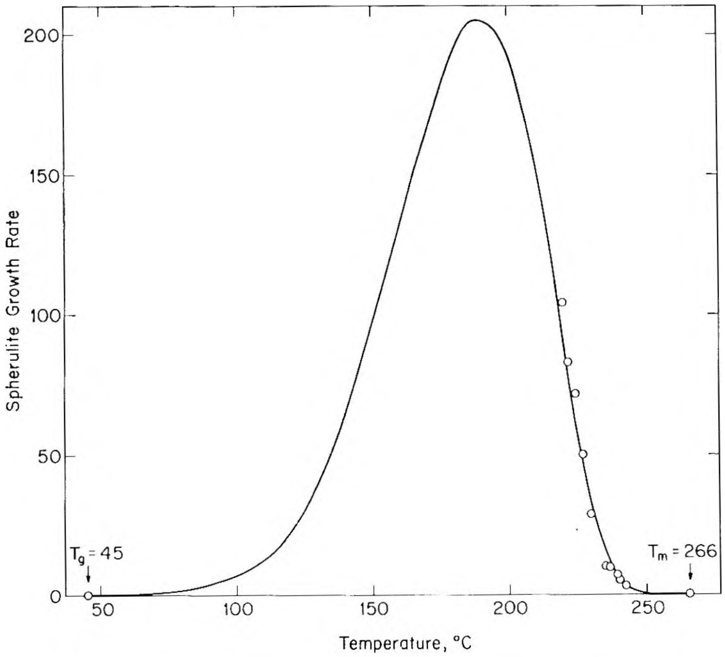

Fig. 17. Spherulite growth rate (μ/minute) vs. crystallization temperature (theoretical curve) fitted to experimental points for nylon 56.

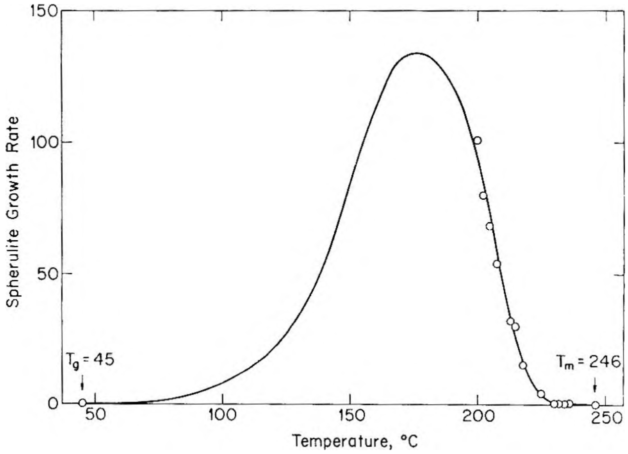

Fig. 18. Spherulite growth rate (μ/minute) vs. crystallization temperature (theoretical curve) fitted to experimental points for nylon 96.

layer thickness, T_m = thermodynamic melting point, and $\Delta T = T_m - T$. The first exponential term of eq. (1) contains the temperature-dependent free energy of activation $\Delta F_\eta^{\ddagger} = C_1T/(C_2 + T - T_g)$ derived from the Williams, Landel, and Ferry (WLF) equation[33] for polymer systems.[32] This term describes the segmental jump rate process from the melt to the crystallization front. The constants $C_1 = 4.12 \times 10^3$ and $C_2 = 51.6$ are believed to be universal constants. This jump rate preponderates from T_g up to the maximum ($T_{\max}$) in the G–T plot illustrated in Figures 17 and 18. Above $T_{\max}$, the nucleation expression is more important.

The experimental results for both polymers were fitted by computer to this theoretical equation. The results fit the ΔT^{-1} law better than the ΔT^{-2} law, so that three-dimensional nucleation can be excluded. From work on other polyamides[26,27] and evidence in this work, T_g was taken as 45°C. T_m and C_2 were varied in a realistic manner during this curve-fitting process until an acceptable fit to the data was obtained. The fact that reasonable agreement between experiment and theory exists does not mean that the model is the correct one. It must be pointed out that the data are not extensive enough to provide an adequate test of the theory. Other work of the writer[36] covering a very extensive range of polymer molecular weights and temperatures suggests that this simple approach is inadequate and that neither C_1 nor C_2 (in the first exponential term of the growth equation) can be treated as constants. The true reference temperature does not appear to be T_g, but some temperature below it. There is evidence which justifies this approach. The molecular parameters governing the crystallization behavior are listed in Table IV.

TABLE IV

Polymer	T_m, °C.	T_g, °C.	Δh_f, ergs/cm.^{3} of repeat unit	G_0, μ/min.	C_2	B	$\sigma\sigma_e$, ergs^2/cm.^{4}	$T_{\max}/T_m$
Nylon 56	266	45	18.8×10^8	3.38×10^7	105	208	325	0.85
Nylon 96	246	45	$18.8 \times 10_8$	1.77×10^7	110	164	256	0.87

The polymer melt density in the region of the melting point was assumed unity in deriving Δh_f on the basis of a value of 45 cal./g. as the heat of fusion. The nylon 56 corresponds to 9.55 kcal./mole repeat units and for nylon 96 it is equivalent to 12.07 kcal./mole repeat units. These values are in keeping with results on other polyamides.[35]

A schematic drawing of the crystalline lattices in these polyamides indicates that both the parallel or antiparallel packing of molecular chains insures comparable hydrogen bonding in the polymer crystal. The difference in the $\sigma\sigma_e$ values in Table IV must come about because of a difference in σ rather than σ_e, since the number of hydrogen bonds per unit length of folded molecular chain is greater for nylon 56. Chain folding is likely to be equally facile in either polymer. In any case, the $\sigma\sigma_e$ values here are lower than that found for nylon 6 (480 erg^2/cm.^{4}) where an antiparallel packing of chains occurs in melt-crystallized samples.[17] The ratio $t_{\max}/t_{m}$ is almost identical for both polyamides in this paper. Favorable comparison is found with nylon 6 (0.82)[17] and nylon 66 (~0.79)[15] as well as for other types of polymers.[28] This parameter must be inherently associated with polymer crystallization. Polymers with the same melting points often have different configurational chain complexities. However, seldom can definite conclusions be made about polymer crystallization rates in this context.

CONCLUSIONS

(1) For the odd-even polyamides a general pattern of spherulite morphology is followed over the crystallization range studied.

(2) For a given polymer, the spherulitic texture is governed by the crystallization temperature—the higher this temperature, the coarser the fibrils or lamellae comprising the spherulites.

(3) Isothermal spherulitic growth rates from "partially melted" isotropic polymer proceeds at the same rate as in samples crystallized directly from the melt. The induction time for nucleation of these spherulites is much longer, and the nucleation density lower, in samples melted above T_m.

(4) The calculated growth rate parameters agree within an order of magnitude for both polymers.

(5) Spherulitic crystallization at the higher temperature stems from an array of single crystal platelets. An agglomeration of such platelets represents the "transition state" between the single crystal and the true spherulite.

(6) Spherulite growth proceeds with a lower free energy than crystalline platelet growth.

(7) Plateletlike structures are only prevalent in polyamides which can form spherulitic aggregates in the region just below T_m.

(8) The molecular chain axis is predominantly perpendicular to these single platelets. This orientation, more or less, persists in the crystalline aggregates so that the (002) plane of the unit cell must lie in the plane of the polymer film.

(9) The ratio of the temperature of maximum growth rate to the polymer melting point is essentially a constant.

(10) Solution-crystallized spherulites in nylon 56 and nylon 96 are negatively birefringent.

The author thanks Mr. C. Mumford for assistance with the experimental details. He is also indebted to Dr. S. S. Pollack and Mr. H. Bevan for x-ray measurements. Gratitude is also expressed to Dr. Pollack for helpful discussion and to Mr. Bob Anderson for computer calculations.

References

1. Khoury, F., *J. Polymer Sci.*, **26**, 373 (1957).
2. Cannon, C. G., F. P. Chappel, and J. I. Tidmarsh, *J. Textile Inst.*, **54**, T210 (1963).
3. Brenschede, W., *Kolloid-Z.*, **114**, 35 (1959).
4. Lindergren, C. R., *J. Polymer Sci.*, **50**, 181 (1961).
5. Keller, A., *J. Polymer Sci.*, **17**, 291 (1955).
6. Keller, A., *J. Polymer Sci.*, **17**, 351 (1955).
7. Mann, J., and L. Roldan, *J. Polymer Sci.*, **60**, 1 (1962).
8. Kinoshita, Y., *Makromol. Chem.*, **33**, 1 (1959).
9. Roldan, L. G., and H. S. Kaufman, *J. Polymer Sci.*, **B1**, 603 (1963).

10. Miyake, A., *J. Polymer Sci.*, **44,** 223 (1960).
11. Bunn, C. W., and E. V. Garner, *Proc. Roy. Soc.* (*London*), **A189,** 39 (1947).
12. Vogelsong, D. C., *J. Polymer Sci.*, **A1,** 1055 (1963).
13. Geil, P. H., *Polymer Single Crystals*, Vol. 5, Interscience, New York, 1963, p. 274.
14. Hartley, F. D., F. W. Lord, and L. B. Morgan, *Ricerca Sci.* (*Suppl.*), **25A** 577 (1955).
15. Magill, J. H., *Polymer,* **2,** 221 (1961).
16. Burnett, B. B., and W. F. McDevit, *J. Appl. Phys.*, **28,** 1101 (1957).
17. Magill, J. H., *Polymer,* **3,** 43 (1962); *ibid.*, **3,** 663 (1962).
18. Inoue, M., *J. Polymer Sci.*, **55,** 753 (1961).
19. McLaren, J. V., *Polymer,* **4,** 175 (1963).
20. Inoue, M., *J. Polymer Sci.*, **A1,** 2013 (1963).
21. Magill, J. H., and P. H. Harris, *Polymer,* **3,** 252 (1962).
22. Slichter, W. P., *J. Polymer Sci.*, **36,** 259 (1959).
23. Terenzi, J. F., Jr., *Dissertation Abstr.*, **20,** 3538 (1960).
24. Cannon, C. G., *Spectrochim. Acta,* **16,** 302 (1960).
25. Magill, J. H., *Res. Develop.* (*London*), **11,** 30 (1962).
26. Chappel, F. P., M. F. Culpin, R. G. Gosden, and T. C. Tranter, *J. Appl. Chem.* (London), **14,** 12 (1964).
27. Champetier, G., and J. P. Pied, *Makromol. Chem.*, **44/46,** 64 (1961).
28. Mandelkern, L., *Crystallization of Polymers*, McGraw-Hill, New York, 1964, p. 264.
29. Fullman, R. L., *Acta Met.*, **5,** 638 (1957).
30. Sears, G. W., *J. Phys. Chem.*, **65,** 1738 (1961).
31. Keith, H. D., and F. J. Padden, *J. Appl. Phys.*, **34,** 2409 (1963).
32. Hoffman, J. D., and J. D. Weeks, *J. Chem. Phys.*, **37,** 1723 (1962).
33. Williams, M. L., R. F. Landel, and J. D. Ferry, *J. Am. Chem. Soc.*, **77,** 3701 (1955).
34. Miller, A. A., *J. Polymer Sci.*, **A1,** 1857 (1963).
35. Dole, M., and B. Wunderlich, *Makromol. Chem.*, **34,** 29 (1959).
36. Magill, J. H., *J. Appl. Phys.*, **35,** 3249 (1964).

Résumé

On a montré que les polymères du nylon 5,6 et du nylon 9,6 cristallisent dans un certain nombre de formes sphérulitiques qui dépendent principalement de la température de cristallisation. Plusieurs types de structures ont été incorporés dans un schéma général du comportement de cristallisation sphérulitique, particulièrement pour les polyamides "pair-impair". Les vitesses de croissance des sphérulites et la morphologie des sphérulites de la plupart de ces structures suivent un schéma convenable. Des plaquettes cristallines présentant des propriétés de monocristaux ont été formées à partir de ces polymères fondus. La morphologie de ces plaquettes et sphérulites est discutée relativement à l'étape de transition entre les monocristaux et les sphérulites.

Zusammenfassung

Nylon-5,6- und Nylon-9,6-Polymere kristallisieren in einer Anzahl sphärolithischer Formen, welche primär von der Kristallisationstemperatur abhängen. Eine Vielzahl von Strukturtypen wurde innerhalb eines allgemeinen Schemas des den "ungerade-gerade"-Polyamiden eigentümlichen Sphärolithkristallisationsverhalten miteinander in Einklang gebracht. Die Sphärolithwachstumsgeschwindigkeiten und die für die meisten Strukturen angegebene Sphärolithmorphologie folgen einem konsistenten Schema. Kristalline Plättchen mit Einkristalleigenschaften wurden aus der Schmelze dieser Polymeren gezogen. Die Morphologie dieser Plättchen und Spharolithe wird in bezug auf den "Übergangszustand" zwischen Einkristallen und Sphärolithen diskutiert.

Received August 20, 1964
Revised October 15, 1964

JOURNAL OF POLYMER SCIENCE: PART A VOL. 3, PP. 1221-1226 (1965)

Dilute Solution Properties of Nylon 66 Dissolved in 2,2,3,3-Tetrafluoropropanol

P. R. SAUNDERS, *Chemstrand Research Center, Inc., Durham, North Carolina*

Synopsis

Light-scattering and viscosity measurements have been made on dilute solutions of nylon 66 dissolved in 2,2,3,3-tetrafluoropropanol. The polyelectrolyte behavior of polyamides in carefully distilled solvent is due to traces of water in the solvent. If care is taken to exclude water, 2,2,3,3-tetrafluoropropanol is a nonionic solvent for nylon 66. The polyelectrolyte effects of nylon 66 in the wet solvent can be repressed by the addition of sodium trifluoroacetate. The action of the sodium trifluoroacetate is to immobilize the water molecules in solution rather than to act as an electrostatic screen. Molecular weights estimated from the light-scattering data and the relation between intrinsic viscosity and second virial coefficient are identical with the results based on measurements in the solvent system formic acid–water–sodium formate.

The study of polyamides in dilute solution is complicated by the fact that the polymer molecules are electrically charged in all the commonly used solvents.[1,2] In these circumstances, care must be exercised to ensure that molecular parameters, deduced on the basis of viscosity and light-scattering studies, are not invalidated by polyelectrolyte effects.[3] These difficulties would be avoided if a solvent for polyamides existed, which would dissolve them in a nonionized condition.

2,2,3,3-Tetrafluoropropanol is a good solvent for polyamides. The low value of the dissociation constant for the alcoholic proton, 4.6×10^{-12}, suggests that there will be little tendency to protonate the polymer. The low refractive index of this solvent, 1.32, would lead to a high sensitivity for light-scattering measurements of solutions of polyamides. However, Beachell and Carlson[4] have reported that polyamides dissolved in this solvent exhibit strong polyelectrolyte effects as demonstrated by the characteristically sharp increase in reduced specific viscosity with increasing dilution. These authors found it necessary to add 0.2 moles/l. of sodium trifluoroacetate to the solution before reasonable viscosity and light-scattering data could be obtained. The effect of adding salt was attributed to the electrostatic screening of the polymeric charges. This rather surprising result has been investigated further in this work.

EXPERIMENTAL

An unfractionated sample of nylon 66 was used throughout this work. On the basis of endgroup determinations the number-average molecular weight was 17,000. Light-scattering results[6] in formic acid-water-potassium chloride gave a weight-average molecular weight of 32,000.

Technical grade 2,2,3,3-tetrafluoropropanol was obtained from the Organic Chemicals Department, E. I. du Pont de Nemours & Co. What is apparently an azeotropic mixture of water and fluoroalcohol distilled over at 92°C., and the bulk of the distillate came over in the range 106.5–108°C. NMR measurements indicated that this distillate also contained traces of water. Dry fluoroalcohol was produced by adding the very hygroscopic salt, sodium trifluoroacetate, to the distillate and then redistilling. In these circumstances, the boiling point was constant at 108°C. The NMR spectra were obtained on a Varian DP60 instrument.

Values of intrinsic viscosity were based on measurements in Cannon-Fenske viscometers at 25°C. Flow times were greater than 100 sec. and kinetic energy corrections were not applied.

Light-scattering measurements were performed at 25°C. in a Brice-Phoenix photometer, with the use of incident unpolarized monochromatic light of wavelength 4358 A. The photometer was modified to permit use of the scattering cell assembly described by Dandliker and Kraut.[5] Solutions and solvent were freed from suspended matter by passage through a fine grade sintered glass filter, followed by ultracentrifugation at 50,000*g* for 90 min. For the polymer studied here, $\bar{M}_w$ <50,000, the dissymmetry of scattering was not expected to differ appreciably from unity, and only the 90° intensities were observed. The photometer was calibrated with the Cornell standard polystyrene as reference, the excess turbidity of a solution of 0.5 g./100 ml. toluene being taken to be 3.51×10^{-3} cm.$^{-1}$.

Differential refractive indices were measured at 25°C. in a Brice-Phoenix differential refractometer calibrated by means of sucrose solutions.

RESULTS AND DISCUSSION

Viscosity

The reduced specific viscosity of nylon 66 dissolved in distilled 2,2,3,3-tetrafluoropropanol is shown in Figure 1 as a function of the polymer concentration. Below a concentration of 0.1 g./100 ml., the reduced viscosity increases sharply with further dilution, in manner characteristic of a polyelectrolyte. The presence of sodium trifluoroacetate in solution results in the elimination of the increase in reduced viscosity with dilution, and it becomes possible to extrapolate to an intrinsic viscosity value. This agrees with the results of Beachall and Carlson. The effect on the intrinsic viscosity of nylon 66, of adding various amounts of sodium trifluoroacetate to the solvent is shown in Table I.

Within experimental error, the intrinsic viscosity is independent of the concentration of salt present in solution. This is a very illuminating result because if the effect of the electrolyte is to screen the polymeric charges,

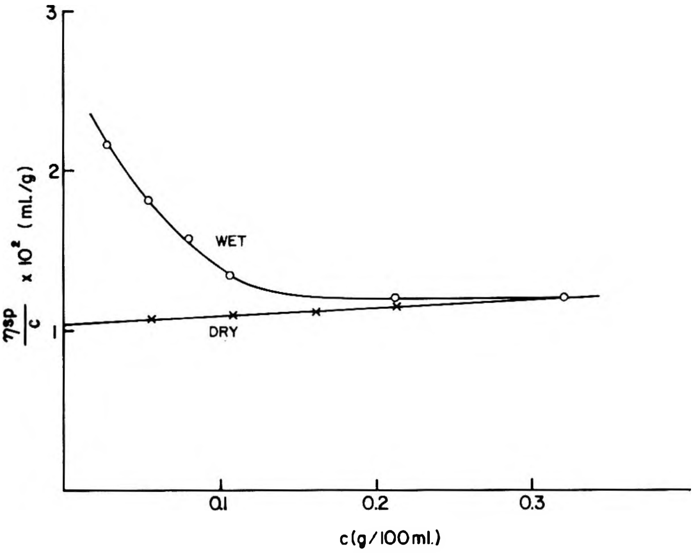

Fig. 1. Reduced specific viscosity of nylon 66 dissolved in wet and dry 2,2,3,3-tetrafluoropropanol as a function of polymer concentration.

the intrinsic viscosity will be dependent on the ionic strength of the solvent. The results, in combination with the fact that sodium trifluoroacetate is extremely hygroscopic leads one to suspect that the action of the electrolyte is to immobilize water molecules in the polymer solutions and that in some way this inhibits the protonation of the polymer molecules.

This conclusion was further supported when viscosities were measured in pure dry fluoroalcohol. Use was made of the hygroscopic nature of sodium trifluoroalcohol by distilling fluoroalcohol from a solution of the salt, in which case water was eliminated from the distillate. The intrinsic viscosity of the polymer in the pure distillate was 1.05, which is identical with that measured in the wet solvent containing sodium trifluoroacetate. This means that 2,2,3,3-tetrafluoropropanol dissolves nylon 66 in a nonionic state.

The influence of traces of water on the ionization of 2,2,3,3-tetrafluoropropanol was investigated via nuclear magnetic resonance. The absorption spectra of the F^{19} nuclei for the wet and dry solvents are shown in Figure 2. The dry spectrum is obtained when the fluoroalcohol is distilled from a mixture containing sodium trifluoroacetate. It is exactly what

TABLE I

Concn. of sodium trifluoroacetate, *M*	Intrinsic viscosity (dl./g.)
0.01	1.05
0.025	1.06
0.05	1.06
0.1	1.06
0.2	1.06

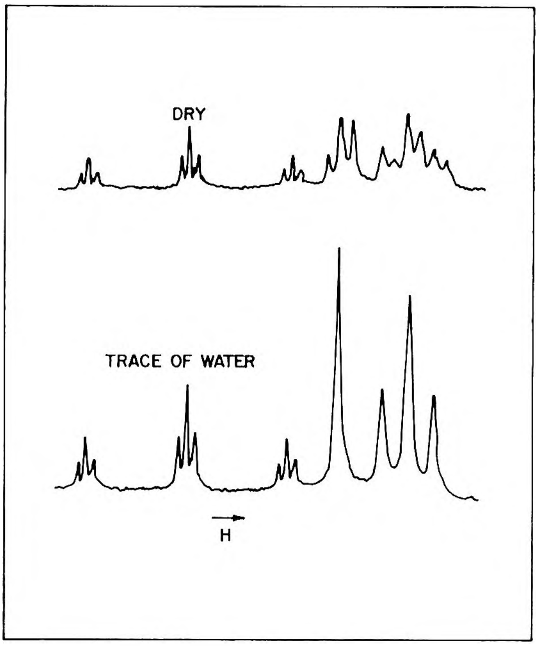

Fig. 2. Influence of water on the NMR absorption spectrum of the F^{19} nuclei of 2,2,3,3-tetrafluoropropanol.

would be expected for pure undissociated fluoroalcohol. The wet spectrum is produced by distilled fluoroalcohol and also when a trace of water is added to the dry solvent. When water is present, the alcoholic proton is exchanging rapidly, which results in two modifications of the NMR spectrum. First, the absorption band for the alcoholic proton is not split into a triplet by the α protons. Second, the absorption band for the α protons is split into a triplet by the adjacent fluorine atoms but each component of the triplet is not split into a doublet by the alcoholic proton. Thus, NMR provides an internal double check on the conclusion that traces of water cause a large increase in the ionization of 2,2,3,3-tetrafluoropropanol.

Light Scattering

The light-scattering data for nylon 66 in dry fluoroalcohol and also for fluoroalcohol containing 0.1 mole/l. of sodium trifluoroacetate are shown in Figure 3. The two sets of data are identical within experimental error and show no signs of a polyelectrolyte effect. The value of weight-average molecular weight obtained from the extrapolated data, $M_w = 32{,}000$, is in complete agreement with the value obtained for the same polymer measured in the solvent system formic acid–water–potassium chloride.[6] Further, the function $\sqrt{HC/\tau}$ is a linear function of polymer concentration, which shows that the third virial coefficient has a finite value.

The intrinsic viscosity $[\eta]$ and the second virial coefficient A_2 are for a given molecular weight both a measure of the average linear dimensions

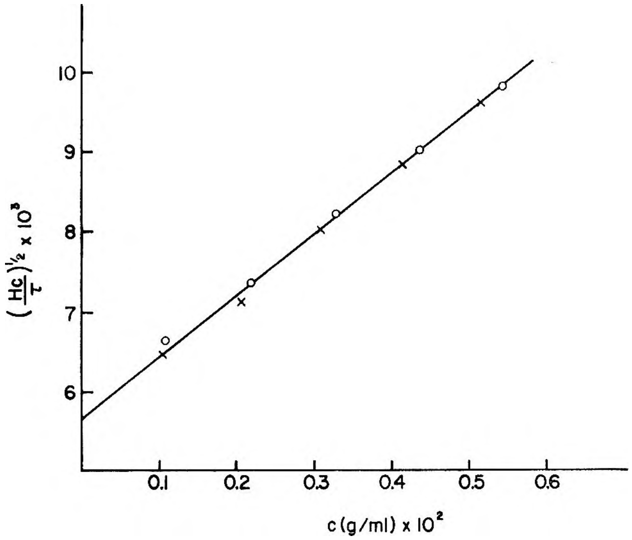

Fig. 3. Light scattering of nylon 66 in 2,2,3,3-tetrafluoropropanol: (O) dry solvent; (×) Wet solvent containing 0.1 mole/l. of sodium trifluoroacetate.

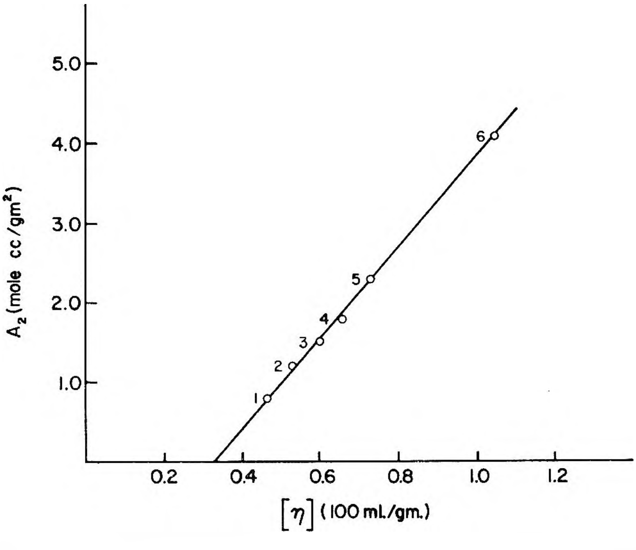

Fig. 4. Relation between intrinsic viscosity [η] and second virial coefficient A_2 for nylon 66 in various solvents: (*1*) 75% $HCHO_2$ 0.5*M* $NaCHO_2$; (*2*) 80% $HCHO_2$, 0.5*M* $NaCHO_2$; (*3*) 85% $HCHO_2$, 0.5*M* $NaCHO_2$; (*4*) 90% $HCHO_2$, 0.5*M* $NaCHO_2$; (*5*) 98% $HCHO_2$, 0.5*M* $NaCHO_2$; (*6*) 2,2,3,3-tetrafluoropropanol.

of the molecules in solution. As these dimensions are changed, by changing the solvent, there will be a unique relation between these two parameters. The results for nylon 66 in tetrafluoropropanol are plotted in Figure 4 together with results for the same polymer in a variety of solvents containing formic acid–water–sodium formate. The results all fall on a straight line, although the fluoroalcohol is a much better solvent than any of the others. The present results also confirm the conclusion, reached earlier,[7] that nylon 66 is not a polyelectrolyte when dissolved in aqueous formic acid containing excess sodium formate.

If the relation between A_2 and $[\eta]$, reported by Krigbaum,[8] is applied to these data, a value for the universal constant Φ can be estimated. $\Phi = 2.5 \times 10^{21}$ is close to the accepted mean value of 2.2×10^{21}. In conclusion, it has been demonstrated that nylon 66 dissolved in pure dry 2,2,3,3-tetrafluoropropanol is in a nonionic state. This result will be of considerable value in avoiding the problems associated with polyelectrolyte effects in other solvents. The excellent agreement between the viscosity and light-scattering data for nylon 66 in the two different solvent systems leads to increased confidence in the interpretation of the results.

I wish to thank W. C. Lawrence of these laboratories for the NMR spectra and their interpretation.

References

1. Schaefgen, J. R., and C. F. Trivisonno, *J. Am. Chem. Soc.*, **74**, 2715 (1952).
2. Fendler, H. G., and H. A. Stuart, *Makromol. Chem.*, **25**, 159 (1957).
3. Saunders, P. R., *J. Polymer Sci.*, **43**, 273 (1960).
4. Beachell, H. C., and D. W. Carlson, *J. Polymer Sci.*, **40**, 543 (1959).
5. Dandliker, W. B., and J. Kraut, *J. Am. Chem. Soc.*, **78**, 2380 (1956).
6. Saunders, P. R., *J. Polymer Sci.*, **57**, 131 (1962).
7. Saunders, P. R., *J. Polymer Sci.*, **A2**, 3755 (1964).
8. Krigbaum, W. R., *J. Polymer Sci.*, **18**, 315 (1955).

Résumé

On a effectué des mesures de diffusion lumineuse et de viscosité sur des solutions diluées de nylon 66 dans le 2,2,3,3-tétrafluoropropanol. Le comportement polyélectrolytique des polyamides dans un solvant soigneusement distillé est dû aux traces d'eau dans le solvant. Si on prend spoin d'éliminer l'eau, le 2,2,3,3-tétrafluoropanol est un solvant non ionique pour le nylon 66. L'effet polyélectrolytique du nylon 66 dans le solvant mouillé peut être supprimé par addition de trifluoroacétate de sodium. Le rôle du trifluoroacétate de sodium est d'immobiliser les molécules d'eau en solution plutôt que d'agir comme un écran électrostatique. Les poids moléculaires obtenus par diffusion lumineuse ainsi que la relation entre la viscosité intrinsèque et le second coefficient du viriel, sont identique aux résultats obtenus avec le système acide formique–eau–formiate de sodium comme solvant.

Zusammenfassung

Lichtstreuungs- und Viskositätsmessungen wurden an verdünnten Lösungen von Nylon 66 in 2,2,3,3-Tetrafluorpropanol ausgeführt. Das Polyelektrolytverhalten von Polyamiden im sorfältig destillierten Lösungsmittel wird durch Spuren von Wasser im Lösungsmittel verursacht. Bei sorgfältigem Wasserausschluss ist 2,2,3,3-Tetrafluorpropanol ein nichtionisches Lösungsmittel von Nylon 66. Die Polyelektrolyteffekte von Nylon 66 im feuchten Lösungsmittel können durch Zusatz von Natriumtrifluoracetat unterdrückt werden. Die Wirkung des Natriumtrifluoracetat besteht in einer Immobisierung der Wassermoleküle in Lösung und nicht in einer elektrostatischen Abschirmung. Die durch Lichtstreung bestimmten Molekulargewichte und die Beziehung zwischen Viskositätszahl und zweitem Virialkoeffizienten sind mit den Ergebnissen von Messungen im Lösungsmittelsystem Ameisensäure–Wasser–Natriumformiat identisch.

Received August 10, 1964
Revised November 10, 1964

JOURNAL OF POLYMER SCIENCE: PART A VOL. 3, PP. 1227–1244 (1965)

Study of Hydrocarbon-Soluble Organometallic Catalysts. I. Correlations between Catalytic Activity and Electric Conductivity of $Al(C_2H_5)_3$–$Ti(OC_4H_9)_4$ Catalysts in the Synthesis of Stereoregular Polyacetylene

I. V. NICOLESCU and EM. ANGELESCU, *Faculty of Chemistry, University of Bucharest, Bucharest, Rumania*

Synopsis

The correlation between the catalytic activity of the system $Al(C_2H_5)_3$–$Ti(OC_4H_9)_4$ and its electrical conductivity in stereospecific polymerization was investigated. The activity of the catalyst was evaluated for varying molar ratios of Al/Ti (in the range of 0.75–6) and reaction temperatures (in the range of −78 to +70°C.) by means of the velocity of absorption of the acetylene. The ionic state of the catalytic complex may be assessed on the basis of electrical conductivity measurements. The electrical conductivity of the pure state of the two catalyst components is in the range of 10^{-12} or 10^{-10} (ohm-cm.)$^{-1}$ while that for the catalyst complex is of the order of 10^{-8} (ohm-cm.)$^{-1}$. The experimental data prove the existence of a correlation between the velocity of reaction, the composition of the catalyst complex, and the electrical conductivity. The values obtained for the activation energy of the electrical conductivity correlate with the energy required to break the complex ion aggregate of the catalyst and therefore with the activity of the catalyst.

INTRODUCTION

For the synthesis of stereoregular polyacetylene, Natta and co-workers[1] used hydrocarbon (*n*-heptane)-soluble organometallic catalytic systems obtained by the interaction of aluminum alkyls with titanium alcoholates, namely: $Al(C_2H_5)_3$–$Ti(OC_3H_7)_4$ (I), $Al(C_6H_{13})_3$–$Ti(OC_4H_9)_4$ (II), as well as $Li(C_5H_{11})$–$Ti(OC_3H_7)_4$ (III).

The best results as regards the highest yield in solid polymer are obtained with catalytic systems I and II when the catalytic components in a Al/Ti molar ratio between 1.4 and 2.5 and the reaction is carried out at temperatures between 45 and 75°C.

Infrared spectra and x-ray diffraction studies indicate that the resulting polyacetylenes possess a high degree of crystallinity and a *trans* configuration. Hence it follows that these catalytic systems show a good activity and selectivity as to the orientation of this polyaddition towards a stereoregular macromolecular structure. Such catalytic systems were also used in the stereospecific polymerization of acetylene by Kambara and Hatano.[2] The catalyst system based upon $Al(C_2H_5)_3$ and $Ti(OC_4H_9)_4$ was also used in our acetylene polymerization studies[3] undertaken at the same time as those of Kambara and Hatano.

As shown by the numerous studies reported in the literature, hydrocarbon-soluble catalytic systems of the Ziegler-Natta type, successfully used in many stereospecific polymerization reactions, offer some advantages over insoluble organometallic catalysts.[4–6] Among the most frequently employed we may mention catalyst systems based on aluminum alkyls and titanium alcoholates or titanium chloroalcoholates,[6] those based upon $Al(C_2H_5)_3$ and vanadium acetylacetonates,[4] those based upon AlR_3 and chromium acetylacetonate,[7,8] or those made up from cobalt compounds and $AlCl(C_2H_5)_2$.[9]

The differences in activity of the catalysts with respect to polymer yield, molecular weight of the polymers, or degree of crystallinity are, on the whole, conditioned by: the chemical structure and the valence state of the components, the molar ratio between the components of the catalytic systems, and the temperature, duration, and the reaction medium.

It is usually rather difficult to give a theoretical explanation of the influence exerted by the factors determining the activity of the catalysts, as well as for the differences in activity of the same catalyst, as a function of different molar ratios between the components of the catalytic system.

In current research practice the optimum molar ratio between the catalytic components or the optimum reaction temperature corresponding to the maximum activity of the catalytic system is determined empirically by a great number of experiments. There have been as yet few investigations carried out on the physical factors which would define the fundamental state of catalyst responsible of the higher or lower catalytic activity and which would thus provide a means of establishing correlations between physical properties of the organometallic catalytic complex and the mechanism of the process.

In heterogeneous catalysis the fundamental state of solid catalysts—semiconductive oxides, reduced metals, alloys, etc.—is investigated by means of the electric conductivity, magnetic susceptibility, thermoelectrical effect, electron spin resonance, etc.

The necessity of establishing correlations between the physical properties of the catalysts and their activity becomes therefore more and more imperative in the heterogeneous catalysis. With a view of furthering this research in the field of soluble Ziegler-Natta catalytic systems we deemed it interesting and useful to investigate certain correlations between physical properties of these catalytic systems and their activity in the stereospecific polymerization process.

RESULTS AND DISCUSSION

Considering, in accordance with the hypothesis of Natta and co-workers,[10] that the stereospecific polymerization reaction catalyzed by organo me-

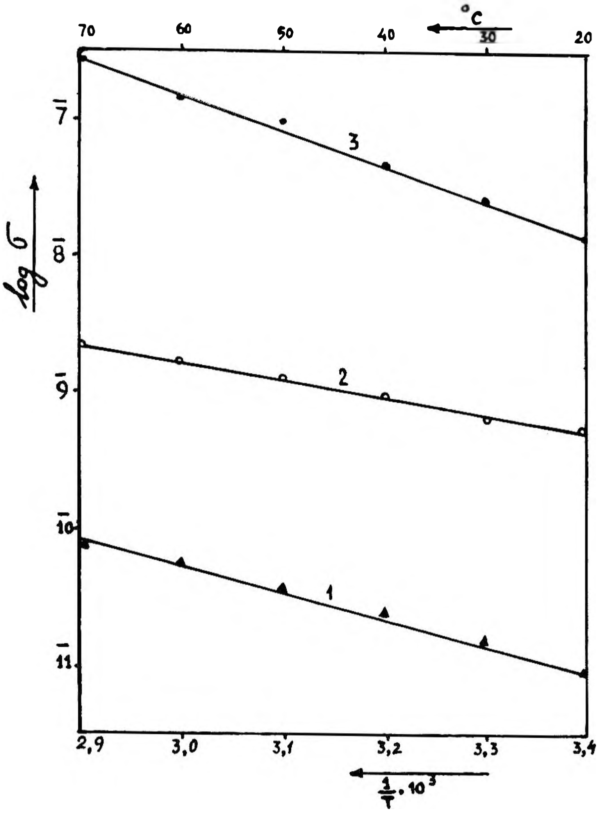

Fig. 1. Electric conductivity as a function of temperature: (*1*) $Ti(OC_4H_9)_4$; (*2*) $Al(C_2H_5)_3$; (*3*) $Al(C_2H_5)_3$–$Ti(OC_4H_9)_4$, Al/Ti ratio = 1.

tallic systems proceeds according to a coordinated-ionic mechanism, we may suppose the catalytic system acts in the form of a complex coordinated ion of various degrees of ionization. The degree of ionization of the catalytic complex represents the energetic state of the complex which ensures in the first stage the polarization of the monomer molecule, followed by the interchange of electrons between the catalyst and the polarizated molecule of the monomer. In this way the polarization contributes towards bringing the molecules near the active bond, towards their penetration into this bond, and thus the activation energy of the transition state decreases.[11]

Our investigations were based on the supposition that this ionizing state of the catalytic system, which to a great extent brings about its activity, can be estimated by electric conductivity measurements. Indeed, by determining the electric conductivity of the components of the system $Al(C_2H_5)_3$ and $Ti(OC_4H_9)_4$, then that of a mixture of these components in the molar ratio Al/Ti = 1, we obtained the values shown in Figure 1. The electric conductivity was represented therein as log σ against $1/T \times 10^3$.

By examining these results one may notice some interesting facts. (*a*) The pure catalytic components exhibit low values of electric conductivity, of the order of 10^{-12} and 10^{-10} (ohm-cm.)$^{-1}$ at 20°C., whereas the catalytic complex formed by interaction of $Al(C_2H_5)_3$ with $Ti(OC_4H_9)_4$ possesses a much higher electric conductivity, namely $\sigma = 10^{-8}$ (ohm-cm.)$^{-1}$, that is, two or four orders of magnitude greater. (*b*) The electric conductivity increases in every case with increasing temperature in the investigated range of 20–70°C. (*c*) Electric conductivity values plotted as log σ against $1/T \times 10^3$ result in straight lines, which permits a calculation of the activation energies of electric conductivity.

These experimental findings point out, in the first place, the existence of a ionized state of the catalytic system, demonstrating that this fundamental property of soluble-type organometallic catalysts may be determined by electric conductivity measurements and may represent a criterion in the estimation of the catalytic activity of such catalysts. In the second place these results provide an additional argument in favor of the hypothesis according to which, in the case of soluble catalytic systems too, the catalyst is in truth a complex ion originating from the interaction of the catalytic components, and the mechanism of reaction is probably here also a coordinated ion mechanism as in the case of the classical catalysts of the Ziegler-Natta type.

In order to support these observations it seemed necessary to investigate the activity of soluble-type catalytic systems and to attempt to correlate the results of a conductometric study with the behavior of this type of catalyst in a stereospecific polymerization reaction. For this purpose we chose the soluble catalytic system mentioned above, $Al(C_2H_5)_3$–$Ti(OC_4H_9)_4$, and investigated its activity and specificity in the stereospecific polymerization reaction of acetylene. This reaction is of interest for the synthesis of organic semiconductors. Moreover, a specification as manifold as possible of the practical conditions for the activation (polarization) of the acetylene molecule would also afford a possibility of synthetizing dienes, various polymers, and copolymers, etc.

In connection with our endeavor, as already mentioned, that of establishing correlations between the degree of ionization of the catalytic complex as represented by the electric conductivity values and the activity of the catalyst, we considered the activity of the catalytic system as varying mainly with the composition (the varying Al/Ti ratio of the components) and with the temperature of reaction. The evaluation of the catalytic activity was effected by determining the yield of solid polymer and the relative crystallinity of the polymer at various Al/Ti ratio values as at various polymerization temperatures.

We shall report first our results concerning the variation of the activity of the above-mentioned catalytic system as depending on the Al/Ti ratio of the catalytic components at various reaction temperatures and then the results obtained in the electric conductivity investigation of the same catalysts.

Activity of the $Al(C_2H_5)_3$–$Ti(OC_4H_9)_4$ Catalyst in the Polymerization of Acetylene

Acetylene polymerization reactions were carried out in an apparatus allowing the introduction of exactly measured amounts of the catalytic components. A medium of inert gas was used, namely purified and dried argon, and the solvent was redistilled and dried (on metallic sodium) *n*-heptane. In all polymerization experiments a constant feeding of 12 l./hr. acetylene was employed. Acetylene was purified and dried. The reaction time was maintained constant throughout these experimental polymerizations. The amount of catalyst too was taken uniformly in every instance as 2% of the total volume of reactants.

We investigated thus the activity of the catalytic system for various Al/Ti molar ratios between 0.75 and 6. The experimental data recorded in Table I and Figure 2 show that in polymerizations carried at a constant temperature but at various Al/Ti ratio of the catalytic components, there exists a maximum yield in solid acetone-inextractible polyacetylene corresponding to a molar ratio Al/Ti = 1 in the catalyst sample used in the process.

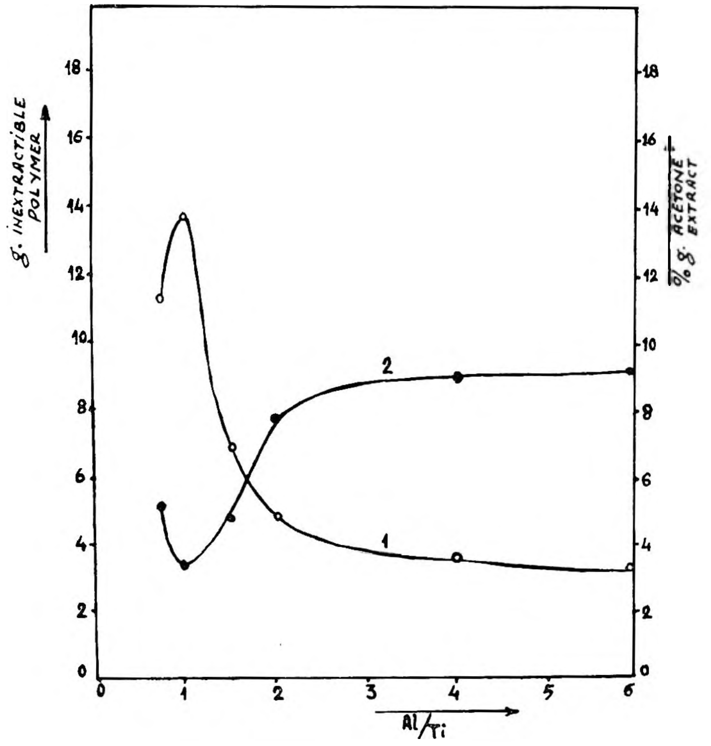

Fig. 2. Variation of the yield of inextractible polyacetylene and extractible products as a function of the Ti/Al ratio in the catalytic components: (*1*) inextractible polymer; (*2*) acetone extract.

TABLE I
Polymerization of Acetylene with an $Al(C_2H_5)_3$–$Ti(OC_4H_5)_4$ Catalyst[a]

Al/Ti ratio	Acetylene, l. Introduced	Acetylene, l. Reacted	Wt. total polymer, g.	Acetone extract wt., g.	Acetone extract % by weight in total polymer	Wt. acetone-insoluble polymer, g.
0.75	48.300	10.850	11.987	0.589	5.15	11.40
1.00	48.450	13.150	14.150	0.480	3.40	13.67
1.50	48.125	7.250	7.388	0.338	4.80	7.05
2.00	47.925	5.500	5.174	0.404	7.80	7.05
4.00	47.725	4.800	4.035	0.335	9.05	3.70
6.00	48.550	3.925	3.716	0.336	9.30	3.38

[a] Conditions: Polymerization temperature, 70°C.; solvent, 100 cm.^{3} *n*-heptane: polymerization time, 4 hr.; total catalyst per volume in reaction, 2%; acetylene feed, 12 l./hr.; extraction time, 8 hr.

In the case of Al/Ti molar ratios higher than 2, the variations in the polyacetylene yield are small. A remarkable fact is that if the maximum yield in solid polymer is found at an Al/Ti molar ratio of 1, the yield of the acetone-extractible products at the same molar ratio of the catalytic components is minimum, and afterwards it increases in the same time with decreases of the yield solid polyacetylene and thus it increases in the same way as the Al/Ti ratio increases. The extraction of soluble components from the polyacetylenes obtained was carried out with acetone over 2 periods of 8 hr.

We also wished to determine whether catalytic systems prepared with different Al/Ti ratio of catalytic components, have different activities and selectivities. A minimum catalytic activity, as against the quantity of inextractible polymer produced, may be ascribed to catalysts having Al/Ti molar ratios >2, which direct unselectively the polymerization reaction, resulting in polymerized products of a high degree of molecular weight dispersity.

Thus, catalytic systems of Al/Ti > 2 are not selective; they promote approximatively to the same extent both the formation of inextractible polyacetylene of high molecular weight and side reactions resulting in low molecular weight, acetone-extractible products. In an analogous manner we may assume, in the case of a catalyst with Al/Ti = 1, a maximum selectivity, because here the high yield of inextractible polyacetylene and the minimum yield of extractible polymer indicate that the reaction is directed in such a way that high molecular weight chain growth is preferentially promoted.

As regards the influence of the total amount of catalyst on the polyacetylene yield, it may be found from Table II and Figure 3, that in the case of catalytic amounts higher than 2% of the total volume in reaction the resulting quantities of polyacetylene are practically constant, whereas in polymerization processes with less than 2% of the catalyst, the solid

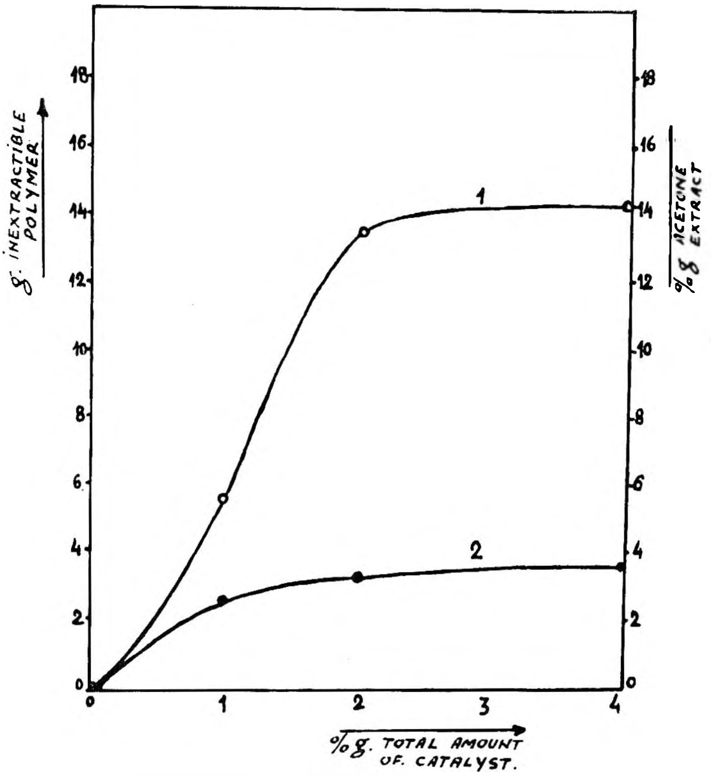

Fig. 3. Variation of polyacetylene and extractible product yield as a function of the total amount of catalyst: (*1*) inextractible polymer; (*2*) acetone extract.

polymer yield is considerably diminished. This fact should be explained by assuming that the impurities present in the solvent or in the monomer are added on the catalyst, shutting off and partially deactivating a certain amount of catalytic complex.

The yield of extractible products varies in the same manner, which demonstrates to a great extent the reproductible character of experiments

TABLE II

Polymerization of Acetylene with an $Al(C_2H_5)_3$–$Ti(OC_4H_9)_4$ Catalyst[a]

Total catalyst per reaction volume, %	Acetylene, l.		Wt. total polymer, g.	Acetone extract		Wt. acetone-insoluble polymer, g.
	Introduced	Reacted		Wt., g.	% per total polymer	
1	47.900	6.300	5.85	0.150	2.70	5.70
2	48.450	13.150	14.15	0.480	3.40	13.67
4	48.125	13.650	14.86	0.560	3.75	14.30

[a] Conditions: Al/Ti = 1; polymerization temperature, 70°C.; solvent, 100 cm.^{3} *n*-heptane; polymerization time, 4 hr.; acetylene feed, 12 l./hr.; extraction time, 8 hr.

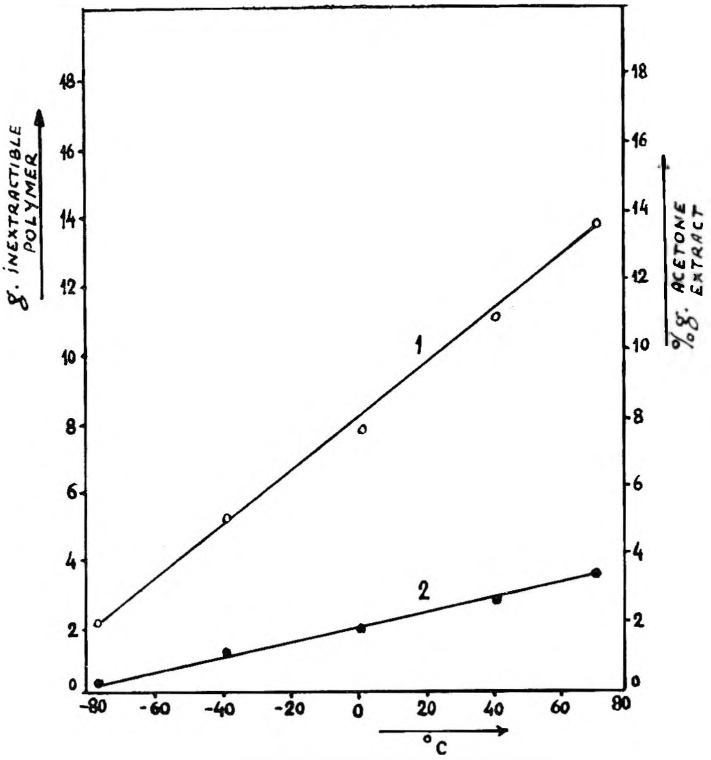

Fig. 4. Variation of polyacetylene and extractible product yield as a function of the temperature of polymerization: (*1*) inextractible polymer; (*2*) acetone extract.

carried out with the same catalyst under identical working conditions. These findings induced us to choose as an optimum catalyst concentration an amount corresponding to 2% of the total volume in reaction.

Having thus established the fact that a catalytic system prepared by the interaction of $Al(C_2H_5)_3$ and $Ti(OC_4H_9)_4$ and containing the catalytic

TABLE III

Polymerization of Acetylene with an $Al(C_2H_0)_3iTi(OC_4H_7)_3$ Catalyst[a]

Polymerization temperature, °C.	Acetylene, l.		Wt. total polymer, g.	Extraction extract		Wt. acetone-insoluble polymer, g.
	Introduced	Reacted		wt., g.	% per total polymer	
70	48.450	13.150	14.15	0.480	3.40	13.67
40	48.275	10.675	11.25	0.300	2.75	10.95
0	48.550	7.400	7.85	0.150	1.95	7.70
−40	48.125	4.575	5.20	0.060	1.12	5.14
−78	47.725	3.200	2.10	0.008	0.40	2.09

[a] Conditions: Al/Ti = 1; solvent, 100 cm.^{3} *n*-heptane; polymerization time, 4 hr.; amount of catalyst per total reaction volume, 2%; acetylene feed, 12 l./hr. extraction time, 8 hr.

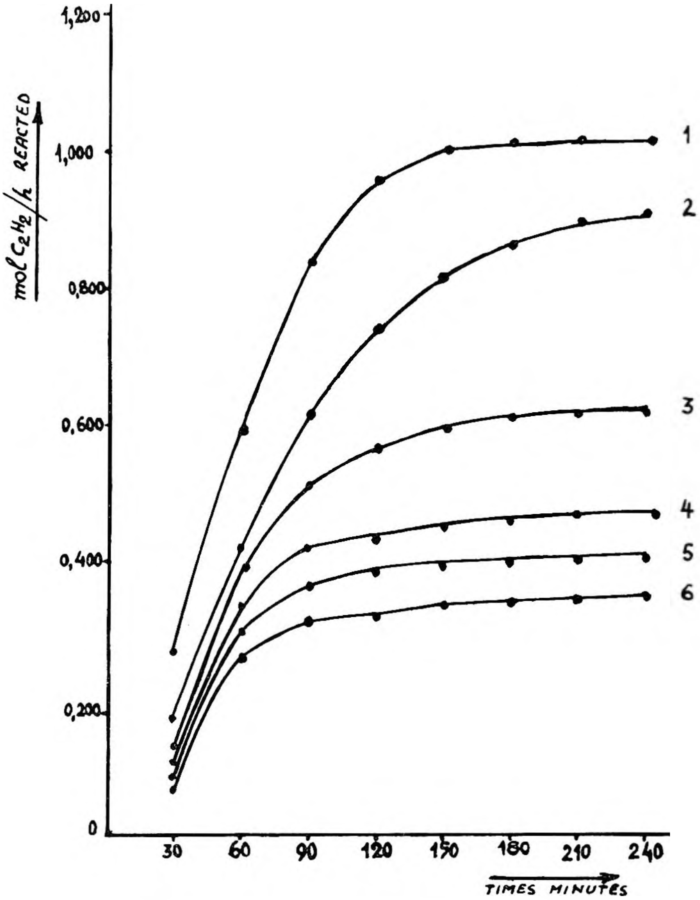

Fig. 5. Overall velocity of the polymerization reaction of acetylene with $Al(C_2H_5)_3Ti(OC_4H_9)_4$ catalyst: (*1*) Al/Ti = 0.75; (*2*) Al/Ti = 1; (*3*) Al/Ti = 1.5; (*4*) Al/Ti = 2; (*5*) Al/Ti = 4; (*6*) Al/Ti = 6. Temperature, 70°C.; solvent, 100 cm.^{3} *n*-heptane; acetylene feed, 12 l./hr.

components in the Al/Ti molar ratio of 1 has an optimum activity, we carried on the polymerization experiments at various reaction temperatures over the range from +70°C. to −78°C. Experimental data included in Table III and Figure 4 show that the polyacetylene yield decreases with decreasing polymerization temperature, reaching its lowest value at a temperature of −78°C. At the same time it can be ascertained that the percentage extractible products diminishes in the same way as does the total polymer yield. We consider worth mentioning the fact that polyacetylene obtained in experimental polymerization processes carried out at low temperatures is almost free of extractible products, exhibits a high degree of crystallinity and is different in appearance from the black, powdery polyacetylenes resulting from operations at higher polymerization temperatures. These low-temperature polymers soak up

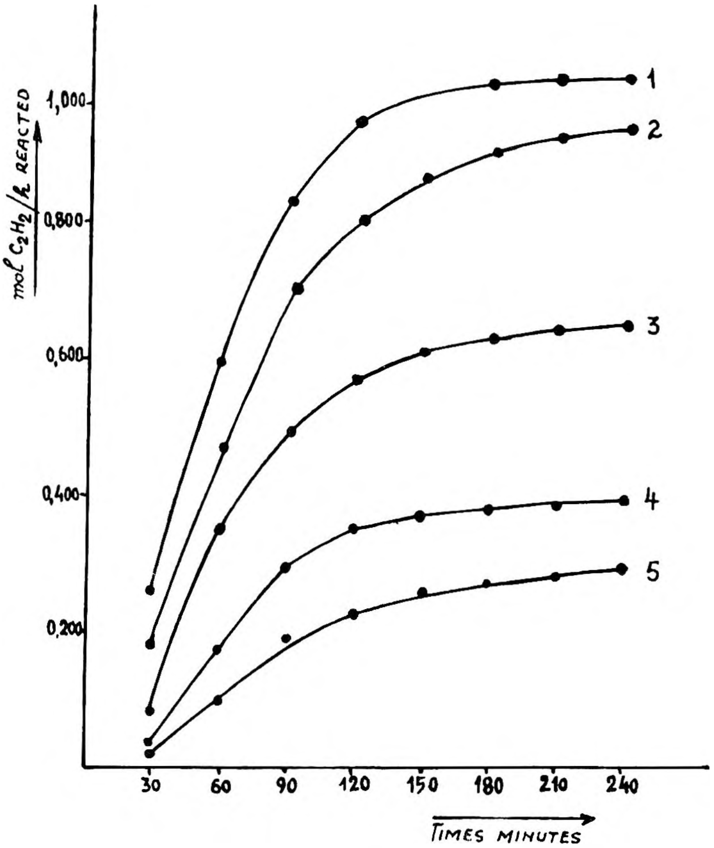

Fig. 6. Absorption reaction isotherms of acetylene at: (*1*) 70°C.; (*2*) 40°C.; (*3*) 0°C.; (*4*) −40°C.; (*5*) −78°C. Catalyst, $Al(C_2H_5)_3$–$Ti(OC_4H_9)_4$, Al/Ti = 1; solvent, 100 cm.^{3} *n*-heptane; acetylene feed, 12 l./hr.

large quantities of solvent, attaining thus elasticity, which is lost again after removal of the solvent; after removal of solvent these polymers are hard but breakable black masses.

Similar results are also obtained on determining the activity of catalytic systems as a function of the Al/Ti molar ratio and the temperature by following the overall velocity of the process expressed as moles acetylene transformed per hour. In the case of polymerization experiments carried out at a temperature of 70°C., the experimental results were as recorded in Figure 5.

The process may be adequately characterized also by drawing up the absorption-reaction isotherms of acetylene in the case of the catalytic system of molar ratio Al/Ti = 1 and in various polymerization temperature conditions, as shown in Figure 6.

From these isotherms it may be seen that a very slow increase occurs after approximately 120 min. in the polymerization with different Al/Ti ratios at a constant temperature (Fig. 5). One may suppose that the formation of solid polymer causes a deactivation of the catalyst and hampers the solubilization of acetylene in the liquid phase.

The same holds true for the influence of polymerization temperature on the velocity of the process at a constant molar ratio between the catalytic components (Fig. 6). From these experimental data it follows that the catalytic system of maximum activity with respect to the production of acetone-insoluble polymers corresponds to an Al/Ti molar ratio of 1 and a reaction temperature of 70°C. (Fig. 7).

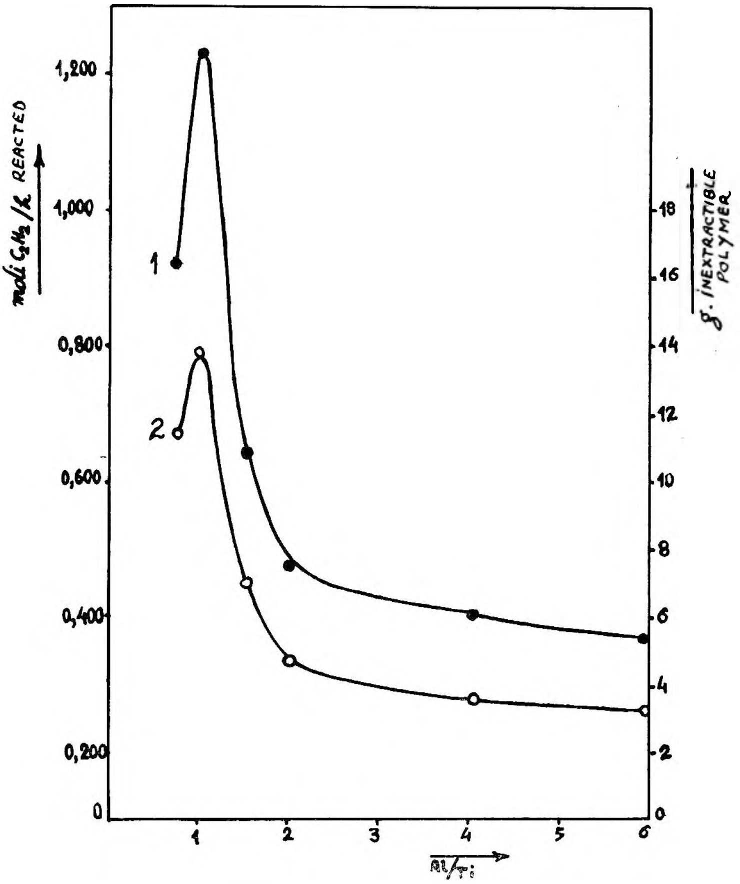

Fig. 7. Variation of inextractible polymer yield by comparison with the total acetylene absorption vs. the composition of the catalyst: (*1*) total C_2H_2 reacted; (*2*) weight inextractible polymer. Reaction temperature, 70°C.

The study of the relative crystallinity of polyacetylenes produced constitutes the subject of a separate note.[12] It is shown therein that there exists a certain proportionality between the activity of the catalyst with respect to the optimum polymer yields and the degree of crystallinity. The catalytic system with Al/Ti = 1 is able to produce polyacetylenes of highest crystallinity. Depending on the temperature at which the poly-

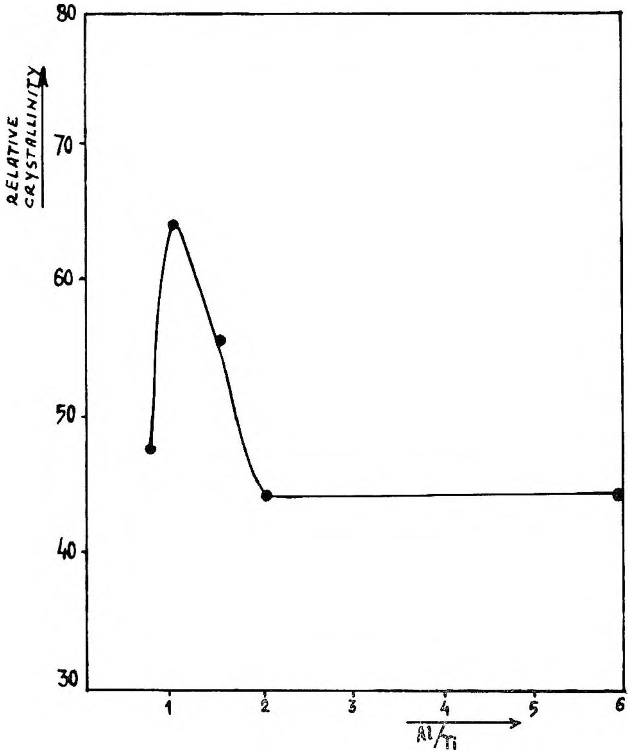

Fig. 8. Variation of the relative crystallinity of polyacetylene as a function of the Al/Ti molar ratio. Catalyst, $Al(C_2H_5)_3$–$Ti(OC_4H_9)_4$; polymerization temperature, 70°C.; solvent, 100 cm.^{3} *n*-heptane; acetylene feed, 12 l./hr.

merization process is conducted the crystallinity varies, increasing with decreasing reaction temperature (Figs. 8 and 9).

There exists a direct correlation between activity and stereospecificity of the catalyst; the latter on its composition expressed by the Al/Ti molar ratio of the components. It seems on the other hand that such a correlation does not exist as regards the reaction velocity. We cannot state precisely whether this observation represents just a peculiarity, an "anomaly" of the investigated system, or constitutes a more general aspect of this matter.

Investigation of the Electric Conductivity of the Catalytic System $Al(C_2H_5)_3$–$Ti(OC_4H_9)_4$

The electric conductivity of this catalytic system was measured by means of a specially built cell, equipped with platinum electrodes and allowing the introduction of the catalytic components in an inert gas atmosphere. The cell was thermostatted with paraffin oil. Electric conductivity determinations were achieved by measuring the resistivity with the aid of a Tesla BM 283 terra-ohmmeter bridge at a cell feeding current of 100 v. No secondary electrical phenomena were found. The

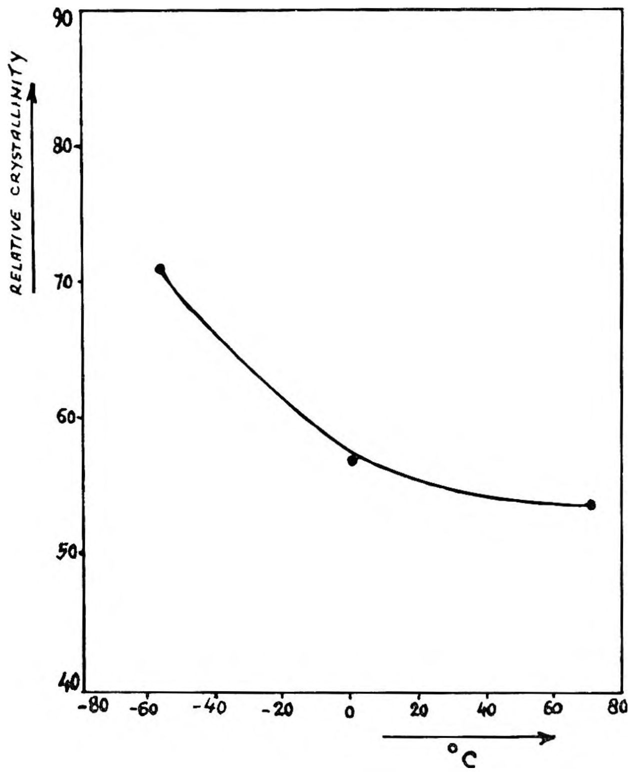

Fig. 9. Variation of the relative crystallinity of polyacetylene as a function of the polymerization temperature. Catalyst, $Al(C_2H_5)_3$–$Ti(OC_4H_9)_4$; Al/Ti = 1; solvent 100 cm.^{3} n-heptane; acetylene feed, 12 l./hr.

conductivity was calculated from the resistivity formula $\sigma = c/\rho$, where c is a constant of the apparatus.

We investigated the electric conductivity of the system $Al(C_2H_5)_3$–$Ti(OC_4H_9)_4$ at Al/Ti molar ratios between 0.75 and 6, in the temperature range of 20–70°C. The results are recorded in Figure 10.

Both from Figures 10 and 11, where conductivity–composition isotherms at temperatures between 40 and 70°C. are represented, it appears that the activity of the catalysts and the reaction velocity differ considerably. The greatest values for electric conductivity are found for the catalytic systems possessing a maximum catalytic activity (when $Al/Ti < 2$). The maximum in electric conductivity corresponds also with the optimum temperature of reaction.

The correlation between catalytic activity and electric conductivity is also illustrated by the data in Figures 12 and 13.

In Figure 12 are shown the variation of the catalytic activity (in terms of weight of polymer obtained) and the electric conductivity, both in dependence on the temperature of reaction, while in Figure 13 a comparison is given between the conductivity–composition and catalytic activity–composition isotherms at a temperature of 70°C. Particularly remarkable is the evident correspondence between the maxima in Figure 11 and the maxima and the general shape of curves in Figure 13. These results permit us to state that in the case of the reaction and of the catalytic system investigated the degree of ionization of the catalyst corresponding to an optimum catalytic activity may be rendered conspicuous and this fact may be determined by means of electric conductivity measurements.

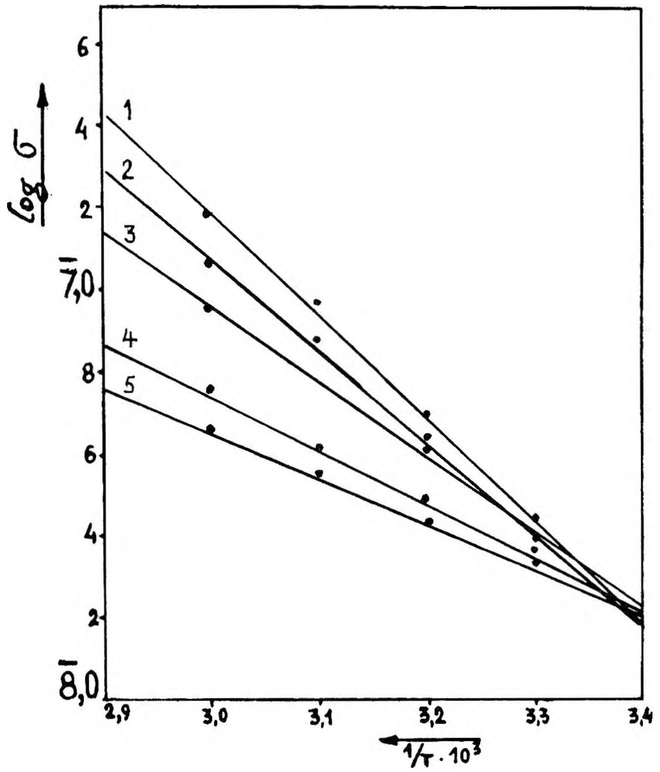

Fig. 10. Dependence of electric conductivity on temperature for the $Al(C_2H_5)_3$–$Ti(OC_4H_9)_4$ catalyst system: (*1*) Al/Ti = 0.75; (*2*) Al/Ti = 1; (*3*) Al/Ti = 1.5; (*4*) Al/Ti = 2; (*5*) Al/Ti = 4; (*6*) Al/Ti = 6.

The existence of a correlation was also established, particularly marked at a temperature of 70°C., between the degree of ionization, the fundamental state of the catalyst, and the catalytic activity variation as a function of the velocity of reaction, as well as of the composition of the catalyst system as determined by the molar ratio of the catalytic components. The electronic state of the catalyst brought about by the interaction of the two catalytic components, which has the capacity of polarizing (activating) the monomer molecule, is in this way made evident and may be estimated quantitatively.

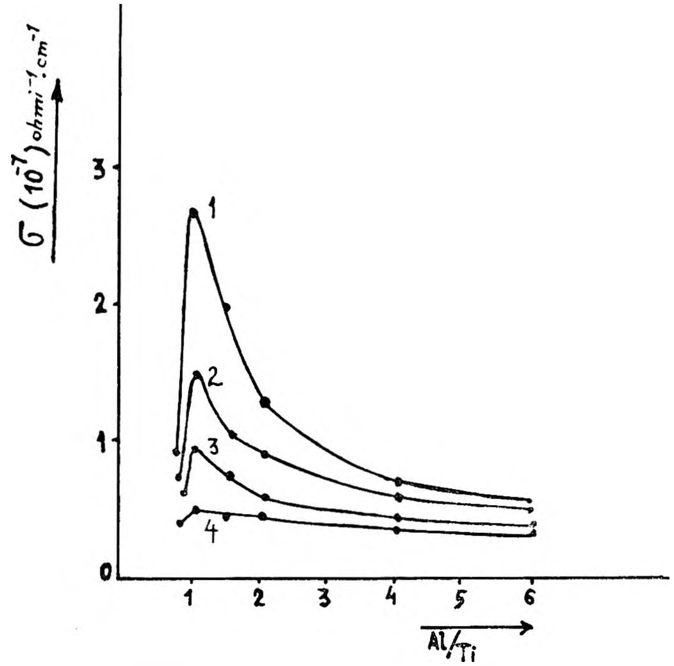

Fig. 11. Conductivity-composition isotherms of the catalyst in the temperature range of 40–70°C.: (*1*) 70°C.; (*2*) 60°C.; (*3*) 50°C.; (*4*) 40°C.

From the electric conductivity values obtained we calculated the activation energies of the electric conductivity for the temperature range of 20–70°C., making use of the known relation:

$$\ln (\sigma_2/\sigma_1) = (E/2kR)[(1/T_1) - (1/T_2)]$$

The values obtained in electron volts were then converted to kilocalories per mole and are thus recorded in Table IV, together with electric conductivity values at 70°C., as well as with those of catalytic system activity (expressed in weight of acetone-inextractible polymer formed).

TABLE IV

Al/Ti	$E_{\text{conduct.}}$, kcal./mole	$\sigma_{70°\text{C.}} \times 10^{-8}$ (ohm-cm.)$^{-1}$	Wt. inextractible polymer, g.
0.75	10.0[a]	8.8	11.40
1.0	11.8	26.6	13.67
1.5	11.4	18.7	7.00
2.0	8.6	13.3	4.77
4.0	6.1	7.1	3.70
6.0	5.7	5.8	3.40

[a] Activation energy of this catalyst was calculated for the temperature range of 50–70°C.

Activation energies of electric conductivity vary in the opposite way as the activation energy and in the same manner at the electric conductivity values in the catalytic systems investigated. The highest values are obtained with the most active catalytic systems (Al/Ti = 0.75–1.5), but subsequently the activation energy of electric conductivity decreases, together with the decreasing catalytic activity and the degree of ionization of the complex. This may be explained by assuming that in the

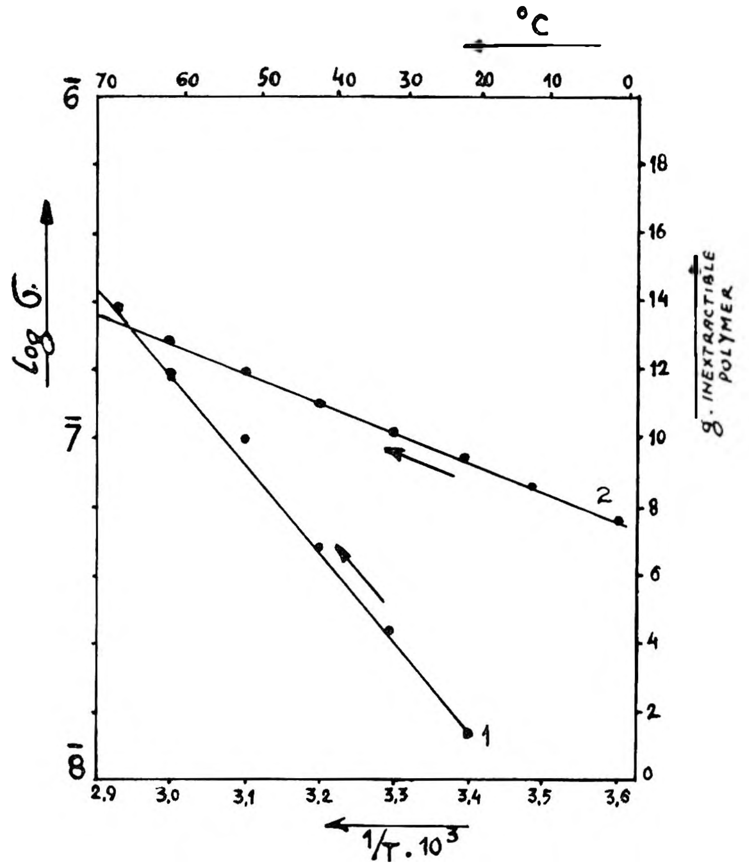

Fig. 12. Dependence of catalytic activity and electric conductivity on the temperature: (*1*) catalytic activity; (*2*) electric conductivity.

catalytic systems of this type the complex ions are present in an associated state (in the form of aggregates), this association being the more powerful the greater the degree of ionization. Under such conditions, the activation energy of electric conductivity would represent precisely the required energy for the dissociation of these complex ion aggregates. In this manner the correspondence found between the high values of the activation energy of electric conductivity and the degree of ionization of the catalytic system can be justified. Future research will show to

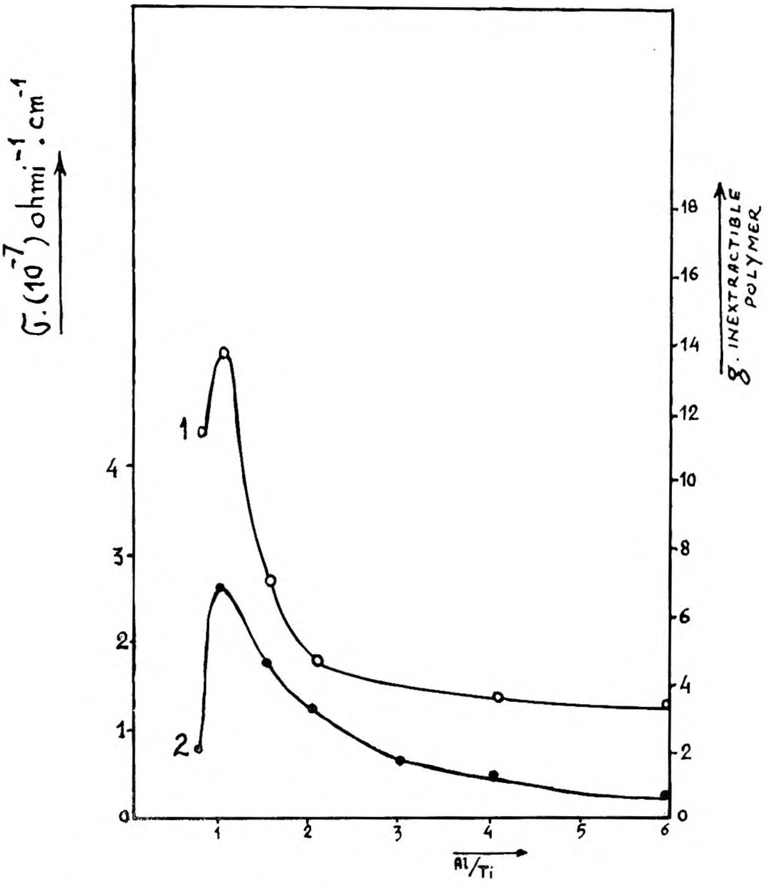

Fig. 13. Correlation between catalytic activity and electric conductivity: (*1*) conductivity–catalyst composition isotherm; (*2*) activity–catalyst composition isotherm.

what an extent these observations are generally valid and thus useful in the estimation of the fundamental state of the soluble Ziegler-Natta catalysts.

References

1. Natta, G., G. Mazzanti, and P. Corradini, *Atti Accad. Nazl. Lincei, Rend. Classe Sci. Fis. Mat. Nat.* [8], **25**, 3 (1958).

2. Kambara, S., and M. Hatano, *Bull. Tokyo Inst. Technol., Spec. No.*, No. 52, 541.64, 10 (1963).

3. Nicolescu, I. V., and Em. Angelescu, paper presented at the Chemistry Session, Cluj, Sept. 1962.

4. Valvassori, A., G. Sartori, and F. Ciampelli, *Chim. Ind. (Milan)*, **44**, 1095 (1962).

5. Kelly, R. J., H. K. Garner, H. E. Haxo, and W. R. Bingham, *Rubber Chem. Technol.*, **35**, 1101 (1962).

6. Natta, G., P. Pino, and G. Mazzanti, *Gaz. Chim. Ital.*, **87**, 570 (1957).

7. Natta, G., L. Porri, P. Corradini, and D. Moreno, *Atti. Accad. Nazl. Lincei, Rend. Classe Sci. Fis. Mat. Nat.* [8], **20**, 560 (1956).

8. Natta, G., L. Porri, G. Zanini, and L. Fiore, *Chim. Ind.* (*Milan*), **41**, 526 (1959).
9. Longiave, C., R. Castelli, and G. Croce, Ital. Pat. 592,477.
10. Natta, G., *Chim. Ind.* (*Milan*), **11**, 1207, 1960.
11. Angelescu, Em., *Analele Romîno-Sovietice, Chim.*, **2**, 126 (1963).
12. Angelescu, Em., and I. Gănar, *Analele Univ. Chemie, Bucuresti,* Ser. *Stiint. Nat.*, **42**, 157 (1964).

Résumé

Le point important du présent travail est l'établissement d'une corrélation entre l'activité catalytique d'un système $Al(C_2H_6)_3$–$Ti(OC_4H_9)_4$ et sa conductivité électrique dans les réactions de polymérisation stéréospécifique. On détermine l'activité du catalyseur en fonction du rapport molaire Al/Ti (dans le domaine de 0.75 à 6), en fonction de la température de la réaction, (dans le domaine de −78 à +70°C) et en fonction de la vitesse d'absorption de l'acétylène. On a déterminé l'état ionique du complexe catalytique par des mesures de conductivité électrique. La conductivité électrique des composés du catalyseur à l'état pur se situe dans le domaine de 10^{-12} ohm^{-1} cm^{-1} et 10^{-10} ohm^{-1} cm^{-1} et pour le complexe catalytique on obtient une valuer de l'ordre de 10^{-8} ohm^{-1} cm^{-1}. Les données expérimentales prouvent l'existence d'une corrélation entre la vitesse de réaction, la composition du catalyseur et la conductivité électrique. Les valeurs que nous obtenons pour l'énergie d'activation de la conductivité électrique sont reliées à l'énergie requise pour rompre l'aggrégat ionique complexe du catalyseur et, par conséquent, avec l'activité du catalyseur.

Zusammenfassung

Der Hauptgegenstand der vorliegenden Arbeit ist die Aufstellung einer Beziehung zwischen der katalytischen Aktivität des Systems $Al(C_2H_5)_3$–$Ti(OC_4H_9)_4$ bei der stereospezifischen Polymerisation und seiner elektrischen Leitfähigkeit. Die Aktivität des Katalysators wird gekennzeichnet durch das Molverhältnis Al/Ti (im Bereich von 0,75–6), durch die Reaktionstemperatur (im Bereich von −78 to +70°C.) und die Geschwindigkeit der Absorption des Äthylens. Der ionische Zustand des katalytischen Komplexes wird gekennzeichnet durch elektrische Leitfähigkeitsmessungen. Die elektrische Leitfähigkeit der Katalysatorkomponente im reinen Zustand liegt im Bereich von $10^{-12}\Omega^{-1}$. cm^{-1} und $10^{-10}\Omega^{-1}$. cm^{-1}; für den katalytischen Komplex wurden Werte in der Grössenordnung von $10^{-8}\Omega^{-}$. cm^{-1} erhalten. Die Versuchsergebnisse beweisen das Bestehen einer Beziehung zwischen der Reaktionsgeschwindigkeit, der Zusammensetzung des katalytischen Komplexes und der elektrischen Leitfähigkeit. Die für die Aktivierungenergie der elektrischen Leitfähigkeit erhaltenen Werte stehen in Beziehung zu der zur Abtrennung des komplexen Ionenaggregats vom Katalysator erforderliche Energie und daher auch zu der Aktivität des Katalysators.

Received February 17, 1964

BOOK REVIEWS

N. G. GAYLORD, Editor

Encyclopedia of Polymer Science and Technology. Vol. I. A to Amino Acids, H. F. MARK, N. G. GAYLORD, AND N. M. BIKALES, Editors, Interscience, New York, 1964. xviii + 893 pp., subscription $40.00; single copy $50.00.

The editors of the encyclopedia, of which this is the first volume, have set themselves the formidable task of compounding a comprehensive account of polymer science in a series of articles dealing with all the aspects of the subject. There will be chapters on the chemical processes involved in the making of polymers, both natural and synthetic, on fundamental principles, on properties, on test methods, and on applications. At the same time, this work includes detailed discussions of numerous low molecular weight compounds in as much as these are of importance to polymers. Volume I, for example, contains excellent reviews of the chemistry of acetylene, maleic and fumaric acid, alcohols, amines, and others.

It consists altogether of 31 articles on subjects ranging from Ablative Polymers to Amino Acids, written by 56 experts. With a work of this scope, a judgment must be based on samples taken more or less at random, and the reviewer is indebted to J. K. Lawson and L. H. Peebles, both at the Chemstrand Research Center, for helping him with this task.

A final judgment on the extent to which cross-references are made from one subject to another cannot be made until further volumes have appeared. Much will depend, also, on the general index to the entire encyclopedia when it is finished, and it is to be hoped that a provisional index will be made available from time to time when only part of the entire encyclopedia is completed.

Every reader will, of course, find minor points that are debatable. Some of them are a matter of personal taste; some are genuine errors of facts, or omissions. A reviewer who mentions minor points that could be considered as shortcomings in a work of this nature could well be accused of pettiness. If a few examples are given nevertheless, this is done not so much to criticize but rather because it is an easy way to give the reader some idea of the quality and scope of the articles.

A good example of the high quality of the book is the article on amines, which is well written and quite comprehensive. One even wonders whether the writer did not cover more than was necessary, because he includes a discussion of amides and imides at times. In Table III, Dabco is not listed as a synonym for triethylenediamine although the name Dabco is used later. The description of the reaction between sulfuric acid and ethanolamine on p. 837 is incomplete, because this reaction does not produce ethyleneimine but the inner salt of aminoethyl sulfuric acid, which is subsequently converted to ethyleneimine by the action of strong alkali. On p. 847, no reference is made to high-temperature polymers made from aromatic diamines and dicarboxylic acids, and the stability of polybenzimidazoles given on p. 858 seems over-estimated. These are all minor items, however, and they do not affect the general excellent impression given by this article.

Similar points could be made in connection with the very good articles on acrylic fibers and acrylonitrile polymers. For example, a more detailed discussion of the "collapsed" gel would have been in place on p. 349. Also, in an encyclopedia it is disappointing to find that the table of transfer constants on p. 395 does not include any of the German work. A discussion of the *Q–e* scheme of Alfrey and Price (p. 394) is out of place in the article on polyacrylonitrile, and the same can be said of Bamford's scheme. Nevertheless, the article on this important polymer makes good reading and covers the subject well.

Naturally, not all articles are of equally high standard, and a certain amount of unbalance in works of this kind is inevitable. It was noted, for example, that the chapter on albumins and globulins gives comparatively little information beyond a few generalities. One wonders why this subject is covered in less than 10 pages, as compared to 16 pages on adsorption, 54 on amines, and more than 100 on adhesion and bonding.

However, it is not the occasional inadequacy of coverage that is determinative for a book of this kind, but the enormous body of valuable information that is contained in the almost 900 pages of this volume. The task set by the editors is a gigantic one, but it appears from Volume I that the challenge is well met and that the encyclopedia will become one of the great classics: a source of information and an instrument of teaching for many years to come.

J. J. Hermans

Chemstrand Research Center, Inc.
Durham, North Carolina

Water and Solute–Water Interactions. J. L. KAVANAU, Holden-Day, Inc., San Francisco, 1964, 101 pp., $5.50.

This book forms a unified part of a larger work by Dr. Kavanau entitled *Structure and Function in Biological Membranes* and concerns itself with a review and discussion of measurements and theories in the areas of water structure and solute–water interactions. It starts with a detailed examination of the structure of ice, relates the structure to its various physical properties, and critically compares various models which have been proposed for it. The structure of liquid water is next discussed and four statistical-thermodynamic models are compared. These include the "vacant-lattice-point" models of Forslind and of Samoilov which treat water as a defective expanded ice I structure, and the well-known "flickering-cluster" model by Frank based on the co-operative formation and disappearance of short-lived hydrogen-bonded aggregates. The detailed ice-like structure developed by Némethy and Scheraga is discussed at this point. Finally there are the "water-hydrate" model of Claussen and of Pauling and Marsh, which are derived from the crystalline clathrates of rare gases, halogens and hydrocarbons, and the model of Pople, based on the "bending" or distortion of hydrogen bonds rather than on bond-breaking. This section concludes with a discussion of the properties of liquid deuterium oxide in terms of the Némethy-Scheraga model.

The largest portion of the book deals with the interactions of water with various solutes. The ability of non polar hydrocarbon groups to organize the solvent in their immediate vicinity is described in terms of Frank's "icebergs" and of opposing theories, in particular Eley's. The formation of "soft ice"—water which is oriented around ions by dipole-ion interactions—and its physical consequences are explored. The problem of long-range order (extended ice-sheaths) in the solvent extending out from dissolved polyelectrolytes and proteins is treated in great detail, presumably as an introduction to descriptions of membrane–water interfaces in the larger monograph. The effects of ions on the water structure are developed in terms of the theories of Gurney, Frank, and others. There is a full discussion of "structure-breaking" and "structure-forming" ions, the thermodynamic and spectroscopic evidence for these effects, and a critical discussion of the use of the Born model by various investigators for calculating ion-water interactions. The book ends with a description of the probable effects of the fixed charges of biological interfaces on proton transfer at the interfaces.

In his introduction the author states that he has presented all major viewpoints, with comprehensive literature citations. This is most certainly true. The book is lucidly written and gives an astounding amount of detail in theory and measurement in a very short space.

J. Steigman

Polytechnic Institute of Brooklyn
Brooklyn, New York

JOURNAL OF POLYMER SCIENCE: PART A VOL. 3, NO. 3 (1965)

NOTES

Studies on Graft Copolymers of Methyl Methacrylate with Cellulose Using Pentavalent Vanadium Compounds

We have been able to synthesize graft polymers of cellulose with methyl methacrylate using pentavalent vanadium as initiator. The distinction in our method lies in the fact that the initiation has been carried out with pentavalent vanadium nitrate in solution, prepared by adding hot concentrated ammonium vanadate solution to concentrated nitric acid.

In our experiment a 3.00-g. portion of cellulose (wood pulp, rayon grade) supplied by M/S. Fross-Silk, Germany, was swollen in 250 cc. distilled water. To this was added 25 cc. of methyl methacrylate, and then 10 cc. of vanadium pentanitrate (prepared by adding 3.48 g. of ammonium vanadate in 12.5 cc. of 69% concentrated nitric acid and the whole diluted to 100 cc.) was added, and the whole reaction mixture stirred for 24 hr. at 30°C. The reaction was carried out in an atmosphere of nitrogen. The whole mass was filtered and washed till free from acid. After drying, the cellulose was extracted with 300 cc. benzene for 66 hr. The increase in weight after drying was 1.1200 g., and hence the graft was 37.33%. The grafted cellulose was insoluble in cuprammonium solution.

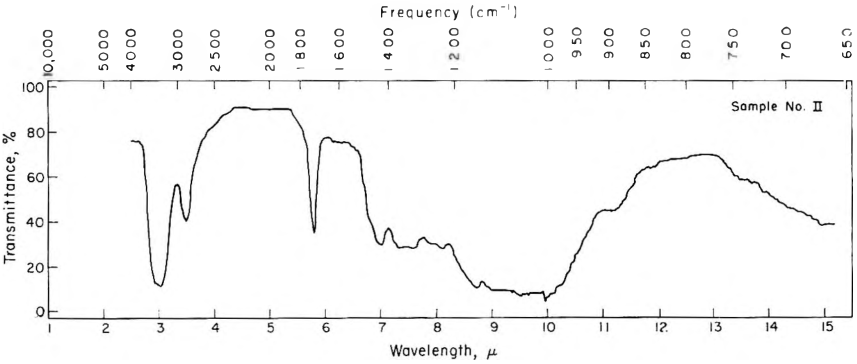

Figure 1.

Infrared spectra of the grafted cellulose (Fig. 1) indicated the presence of ester groups ($COOCH_3$) at 1720 cm.$^{-1}$.

Further studies on grafting by use of vanadium and other oxidation-reduction systems are in progress.

The authors are grateful to the Council of Scientific and Industrial Research for sponsoring this work at this Institute and Dr. A. B. Biswas, National Chemical Laboratory, Poona, for taking the infrared spectrum of the sample.

Harcharan Singh
R. T. Thampy
V. B. Chipalkatti

High Polymer Division
Shri Ram Institute
Delhi, India

Received June 30, 1964